4-6-2017

Uncovering Transcriptional Activators and Targets of HSF-1 in Caenorhabditis elegans

Jessica Brunquell
University of South Florida, jlhoskin@mail.usf.edu

Uncovering Transcriptional Activators and Targets of HSF-1 in *Caenorhabditis elegans*

by

Jessica Brunquell

A dissertation submitted in partial fulfillment
of the requirements for the degree of
Doctor of Philosophy
with a concentration in Cellular and Molecular Biology
Department of Cell Biology, Microbiology, and Molecular Biology
College of Arts and Sciences
University of South Florida

Major Professor: Sandy D. Westerheide, Ph.D.
Brant Burkhardt, Ph.D.
Younghoon Kee, Ph.D.
Cecilia Nunes, Ph.D.

Date of Approval:
March 24, 2017

Keywords: heat shock response, HSF1, heat shock proteins, *C. elegans*, longevity

DEDICATION

I would like to dedicate this work to my parents, William J. Hoskins and Janice A. Hoskins, for their continuous love and support. Also, to my mentor Sandy D. Westerheide for providing me with countless opportunities to advance as a scientist, and for her guidance which contributed to my success. To my husband Andrew J. Brunquell for his whole-hearted understanding, love, and support. Lastly, to my life-long friend Danielle J. DeLaire for her humor, love, and encouragement.

ACKNOWLEDGEMENTS

I would like to acknowledge my committee members: Brant Burkhardt, Ph.D., Younghoon Kee, Ph.D., Cecilia Nunes, Ph.D., and Patrick Bradshaw, Ph.D., as well as my lab mates, for helpful guidance and discussion throughout the duration of my degree. I would also like to especially acknowledge Rachel Raynes, Ph.D., for her mentorship, and the undergraduate students that contributed to this work: Philip Bowers, Stephanie Morris, and Alana Snyder.

TABLE OF CONTENTS

LIST OF TABLES

LIST OF FIGURES

LIST OF ACRONYMS

HSR: Heat shock response
HSF1: Heat shock factor 1
HS: Heat shock
HSP: Heat shock protein
HSE: Heat shock element
AROS: Active regulator of SIRT1
SIRT1: silent mating type information regulation 2 homolog 1
CCAR1: Cell cycle and apoptosis regulator 1
CCAR2 (DBC1): Cell cycle and apoptosis regulator 2
microRNA: miRNA
FUdR: 5-fluoro-2'-deoxyuridine
ESA: Essential for SIRT1 activity
L1: First larval stage
L2: Second larval stage
L3: Third larval stage
L4: Last larval stage
YA: Young adult
YFP: Yellow fluorescence protein
GFP: Green fluorescence protein
EV: Empty vector
RNAi: RNA interference
qRT-PCR: quantitative reverse transcription polymerase chain reaction
NGM: Nematode growth medium
LZ: Leucine zipper
LST-3: Lateral signaling target 3
NLS: Nuclear localization sequence
CH-CDF: Charge hydropathy and cumulative distribution function
CDF: Cumulative distribution function
CH: Charge-hydropathy
CGN: Conservation of Genomic Neighborhood
RNA-seq: RNA sequencing
DAVID: Database for Annotation, Visualization, and Integrated Discovery
NHR: Nuclear hormone receptor
miRNA-seq: microRNA sequencing

ABSTRACT

In order to survive, cells must be able to cope with a variety of environmental stressors. The heat shock response (HSR) is a pro-survival mechanism employed by cells in response to protein denaturing stress, such as heat. Since its discovery in 1960, the heat shock response has been found to be regulated by the transcription factor heat shock factor 1 (HSF1). During periods of increased stress, HSF1 undergoes a multi-step process of activation that involves homotrimerization, DNA-binding, and post-translational regulatory modifications, all of which ultimately function to control the transcription of chaperone genes. These chaperone genes encode molecular chaperone proteins which function to promote survival during stress by restoring protein homeostasis to the cell. Although HSF1 is classically studied for its role in regulating the HSR, HSF1 also has roles in regulating metabolism, development, and longevity. Studies in the nematode *Caenorhabditis elegans* demonstrate the HSF1 homolog, HSF-1, as a global regulator of gene expression that has both stress-dependent and -independent functions. Modulating HSF1 activity therefore has implications beyond stress-induced processes, and has been suggested as a promising therapeutic target for diseases of aging and protein dysfunction.

We were interested in determining regulators of the HSR using *C. elegans* as a model to test for effects on proteostasis and longevity. In these studies, we observed the effects of compound treatment (Chapters 1 and 2), genetic manipulation (Chapters 3 and 4), and

environmental stimuli (Chapters 5 and 6), on the HSR in *C. elegans*. In Chapters 1 and 2, we describe our findings that treatment with the DNA synthesis inhibitor Fluorodeoxyuridine, and treatment with coffee and caffeine, enhance the heat shock response and improve proteostasis in aging worms in an HSF-1-dependent manner. In Chapters 3 and 4, we uncovered that negative regulation of the HSR by the cell cycle and apoptosis regulator CCAR2 is conserved in *C. elegans*, and is mediated by the CCAR2 ortholog, LST-3. We also uncovered that negative regulation of the HSR by LST-3 requires the SIRT1 homolog Sir-2.1, and knockdown of LST-3 via *lst-3* RNAi works through Sir-2.1 to enhance stress-resistance, fitness, proteostasis and longevity. In Chapters 5 and 6, we describe the global impact of HSF-1 in regulating transcriptional processes during a heat stress. The profiling of global HSF-1 mRNA and miRNA targets has allowed us to uncover a heat-dependent and -independent role for HSF-1 in regulating gene expression to impact stress-resistance, proteostasis, and longevity. Altogether, these studies demonstrate the impact of compound treatment, genetic manipulation, and environmental stimuli on the heat shock response, while also uncovering global stress-dependent and -independent roles for HSF-1. This work therefore provides insight into various methods of activating the HSR by modulating HSF-1 activity, and uncovering global HSF-1 target genes, which may be useful for designing therapeutic treatment strategies for diseases of protein dysfunction.

CHAPTER 1. INTRODUCTION

The History of the Heat Shock Response

Ferruccio Ritossa discovered the heat shock response in 1960

In 1960 at the Genetics Institute in Pavia, Ferruccio Ritossa unintentionally discovered the heat shock response (HSR) in *Drosophila melanogaster.* Ritossa was an established investigator in Italy, and chose to perform his studies on nucleic acid synthesis in *Drosophila*. At the time, *Drosophila* was an unpopular model organism, and many scientists thought that studies utilizing the fruit fly for scientific advancement were irrelevant. However, Ritossa chose this model over more popular bacterial models because he considered the fruit fly to be more similar to human studies (1). During his research, one of his colleagues mistakenly increased the incubator temperature where his flies were being kept and Ritossa observed a chromosomal puffing pattern. This increase in puffing suggested an increase in transcriptional activity was occurring in response to increased temperatures. After recreating these conditions with the correct experimental controls, Ritossa was able to successfully repeat what he previously witnessed (2). Although Ritossa grasped the importance of such a transcriptional response, he had difficulty publishing his results, and his manuscript was rejected for lacking biological importance. The study was eventually published in *Experientia* in 1962 (1,3), although years would pass before the biological significance of his findings were grasped by the scientific community.

The discovery of heat shock factor 1

Years after Ritossa discovered the HSR, transcription and translation became the focus of stress-related research. In the 1970's, pulse radiolabeling of mRNA and protein products uncovered changes in transcription and translation rates occurred in response to heat shock (HS) (4-6). These studies revealed a global decrease in transcription and translation during exposure to increased temperatures, with the exception of select genes and their corresponding protein products, which are coined heat shock proteins (HSPs). It was later found that treatment with heat resulted in robust induction of heat shock protein 70 (Hsp70), which is named for its molecular weight of 70 kDa. Studies examining the promoter of *hsp70* identified a series of three inverted repeats of the sequence nGAAn, which is referred to as a heat shock element (HSE) (7-9). The discovery of HSEs ultimately allowed for the identification of the transcriptional regulator of the HSR, the transcription factor heat shock factor 1 (HSF1), via affinity chromatography and biochemical purification of HSE-oligonucleotide bound sepharose beads (10-12). The stress field has since expanded and diverged into two groups, one focused on structural analyses of HSPs, and the other on regulation of the HSR by HSF1.

Heat Shock Proteins and Molecular Chaperones

Heat shock proteins function to promote proteostasis

Many of the *hsp* genes upregulated by HSF1 during stress encode molecular chaperones which function to refold misfolded proteins that accumulate and aggregate during stress. Chaperones recognize the exposed hydrophobic amino acid residues of unfolded proteins, and are therefore capable of interacting with a broad range of misfolded protein substrates (13,14). Although the expression of many chaperone genes are upregulated

upon exposure to protein denaturing stressors, others are constitutively expressed. As such, chaperones are not only important for maintaining proteostasis during stressful insults, but can also assist during de novo protein folding, assembly, transport, and protein clearance (15-18). Overall, the regulation of protein chaperone expression is important for maintaining proteome integrity during and independently of stress.

The chaperone Hsp70 is highly induced upon stress and functions to refold denatured proteins

The Hsp70 class of chaperones are central to the proteostasis network. A constitutive and stress inducible form of Hsp70 is present in the cell, and each function to maintain and restore the quality of the proteome. The constitutive form of Hsp70, Hsc70, is responsible for *de novo* protein folding, while the highly stress inducible Hsp70 functions to prevent proteins from aggregating and misfolding (19). Thus, both the constitutive and stress-inducible forms of Hsp70 function as protein folding catalysts that are responsible for maintaining the proteome.

The structure of Hsp70 plays an important role in mediating its function and protein-protein interactions. Hsp70 is composed of two domains, a conserved nucleotide-binding domain and a variable protein binding domain. The nucleotide-binding domain hydrolyzes ATP, which in turn regulates structural changes in the protein-binding domain (20-22). While in the ATP-bound state, the protein-binding domain acts as a rigid base with a flexible lid that folds back and binds to the nucleotide-binding domain, thus allowing misfolded polypeptide substrates with hydrophobic residues to enter. Upon ATP hydrolysis, the lid detaches from the nucleotide-binding domain, ultimately sequestering

the misfolded polypeptide in order to prevent the aggregation of misfolded protein products. The structure of Hsp70 is therefore essential for its function as a holdase.

In addition to functioning as a holdase, Hsp70 can also refold misfolded proteins and act as a molecular chaperone. Two models exist for the protein refolding capacity of Hsp70. The first kinetic partitioning model suggests that through holdase activity, the free concentration of the misfolded polypeptides are low, and this promotes an environment to allow the protein to refold into its native state. The second local unfolding model suggests that the binding and release of substrates from Hsp70 may function to untangle misfolded regions of the polypeptide, and contribute to the kinetics of protein folding (23). Thus, Hsp70 may function to restore proteostasis during stress by contributing to the kinetics that promote a protein refolding state.

Hsp70 activity is regulated by various protein-protein interactions. For example, Hsp70 typically functions in a complex with J-domain proteins and nucleotide exchange factors to increase binding specificity and strength. J-domain proteins guide Hsp70 to misfolded substrate proteins, while nucleotide exchange factors can control the ATP/ADP bound state of Hsp70. For example, the J-domain protein Hsp40 is a co-chaperone that functions to enhance Hsp70 binding specificity and ATPase activity (24). During basal conditions, nucleotide exchange factors promote substrate release from Hsp70, however during stress, nucleotide exchange factors become denatured thus lose the ability to accelerate substrate release (25,26). Thus, J-domain proteins and nucleotide exchange factors act in conjunction with Hsp70 to modulate binding affinity and client protein binding to promote a protein refolding during stress.

Small HSPs act as holdases to prevent the aggregation of misfolded proteins during stress

Small HSPs are ubiquitous molecular chaperones that can prevent aggregation and denaturation of proteins during periods of increased stress. Small HSPs, which are characterized by their low molecular mass, are the least evolutionary conserved class of molecular chaperones (27,28). The most studied group of mammalian small HSPs is the α-crystallins αA (HspB4) and αB (HspB5), both of which act quickly to shield the cell against the denatured polypeptides. Small HSPs are thus the chaperones that form the first line of defense against protein aggregation and misfolding to promote homeostasis during stress.

The structure of small HSPs is unique in that it contributes to complex formation that promotes the regulation of protein stability through electrostatic interactions (29). Small HSPs have a highly variable N-terminal domain, and an α-crystallin domain in the C-terminal region. The N-terminal region is highly variable between species, however due to the nature of this region to be flexible, it may be involved in stabilizing the formation of oligomers or the recognition and selection of substrate proteins (30-32). Unlike the N-terminal domain, the small C-terminal region is highly-conserved between species and commonly protrudes from formed complexes due to its flexibility (33). This C-terminal extension is essential for chaperone activity in both mammalian Hsp25 and *C. elegans* Hsp-16.2 (34-36). Overall, it is clear that the structure of small HSPs allow for the formation of large complexes which can quickly shield misfolded proteins from the surrounding environment during stress.

HSF1 Structure and Regulation

The domains of HSF1 contribute to transcriptional activity

HSF1 is a multi-domain protein containing a DNA-binding domain, trimerization domains, a regulatory domain, and a transactivation domain (Figure 1.1). The DNA-binding domain of HSF-1 is highly-conserved and conforms to a helix-turn-helix motif (37-39). HSF1 homotrimerizes during stress, and the DNA-binding domain of each monomer recognizes one of the three inverted repeats that compose the HSE in the major groove of the promoter of HSF1 target genes (40). The trimerization domain consists of three hydrophobic heptad repeats A/B/C (HR-A/B/C). The HR-A/B region is responsible for oligomerization during stress, however this can be prevented by the HR-C region which is able to fold back and inhibit the HR-A/B region (41-43). The transactivation domain is targeted by several proteins that regulate transcriptional initiation and elongation (44). The regulatory domain represses HSF1 activation during basal conditions by forming an inhibitory complex with the MAP kinase ERK (45), however this interaction can be prevented by phosphorylation events during stress to allow for HSF1 activation (46,47). The domains of HSF1 are therefore essential for coordinating a balance of HSF1 activity during both stressed and unstressed conditions, ultimately controlling the regulation of the HSR.

HSF1 activity is regulated by phosphorylation

Depending on the cellular environment, HSF-1 activity can be modulated by multiple kinases. There are currently 22 phosphorylation sites that have been identified within HSF1, and some sites are stress-inducible while others are constitutively phosphorylated (48,49). Hyper-phosphorylation of HSF1 during stress is commonly associated with

increased transcriptional activity. For example, phosphorylation of HSF1 by the kinases CK2, CaMKII, PKA, MAPK, and PLK1 promote DNA-binding and the transcriptional activity of HSF1 (50-54). However, phosphorylation of HSF1 by the kinases MK2, and GSK-3β can reduce DNA-binding and transcriptional activity (55,56). Overall, it is clear that phosphorylation is one post-translational modification that can be utilized by the cell to fine-tune HSF1 activity.

HSF1 activity is regulated by acetylation

Acetylases also regulate HSF1 activity depending on the cellular environment. For example, the histone deacetylase HDAC1 associates with the DNA-binding domain of HSF1 to inhibit HSF1 binding to HSEs ultimately decreasing *hsp70* mRNA levels during HS. The deacetylases HDAC7, HDAC9, and SIRT1 associate with the activation domain of HSF1, increase HSF1 binding to HSEs, and enhance *hsp70* mRNA expression during HS (57). Additionally, acetylation of the DNA-binding domain of HSF1 by p300 results in attenuation off of the DNA and transcriptional inactivation (58). However, the deacetylase activity of SIRT1 allows HSF1 to remain in a DNA-bound transcriptional state, thereby enhancing *hsp70* mRNA expression during HS (58). The HSR is thus controlled by regulating HSF1 activity via post-translational modifications.

Summary: The HSF1 activity cycle

The HSR is tightly a regulated response that functions to maintain protein homeostasis during stress and promote survival. HSF1 is a monomer in the cytoplasm during basal conditions, and is kept in an inactive state through associations with Hsp70, Hsp90, and Hsp40 (Figure 1.2a) (59-61). It is thought that in response to protein denaturing stressors, Hsp70, Hsp90, and Hsp40 are titrated away from HSF1 in response to the concentration

of denatured proteins increases (8,62-65). Once HSF1 is released from the Hsp70/40/90 complex, homotrimerization and subsequent translocation into the nucleus allows HSF1 to bind to HSEs in the promoter of *hsp* genes (Figure 1.2b). Transcriptional activation occurs upon hyper-phosphorylation (Figure 1.2c) (52,66), whereas attenuation occurs via acetylation of the DNA-binding domain of HSF1 (Figure 1.2d) (58). The deacetylase activity of SIRT1 promotes the HSR by enhancing DNA-binding (58). Overall, the HSR is a tightly controlled and complex response regulated by a variety of factors in response to protein denaturing stressors.

Sirtuin Activity Regulates the HSR

SIRT1 regulates the mammalian HSR

SIRT1 is a prolongevity factor that can regulate various biological processes including metabolism, cytoprotection, and apoptosis (67). SIRT1 belongs the highly-conserved sirtuin family, where mammals have seven sirtuin family members SIRT1-7 and *C. elegans* have four sirtuin family members Sir-2.1-2.4 (68,69). SIRT1 regulates many diverse biological processes through the deacetylation of target substrates. Some processes regulated by SIRT1 include controlling chromatin structure, apoptosis, and the HSR (67,70,71). Interestingly, SIRT1 enhances mammalian HSF1 activity by extending the DNA-bound state of HSF1 during stress. This method of regulation may be conserved across species, as the *C. elegans* SIRT1 homolog, Sir-2.1, can also regulate HSF-1 and the HSR in the nematode (72). SIRT1 is therefore a highly-conserved regulator of the HSR.

SIRT1 is regulated by AROS and CCAR2

SIRT1 is regulated by various genetic factors depending on the cellular environment. For example, active regulator of SIRT1 (AROS) enhances SIRT1 activity, were as the cell cycle and apoptosis regulator CCAR2 (also known as DCB1) inhibits SIRT1 activity (73,74). AROS was identified as a SIRT1 interacting partner by a yeast two-hybrid screen, whereas CCAR2 was identified as a SIRT1 interacting partner via co-immunoprecipitation (73,75). In both contexts, the acetylation state of p53 was found to be a target of AROS and CCAR2 in response to regulating the deacetylase activity of SIRT1. SIRT1 activity can therefore be regulated by AROS and CCAR2, and may ultimately affect various physiological processes.

CCAR2 inhibits SIRT1 activity

CCAR2 is a large multidomain protein that regulates various cellular pathways through inhibition of SIRT1 activity (76). CCAR2 inhibits SIRT1 by competitively binding to the catalytic domain of SIRT1 and inhibiting deacetylase activity by blocking the essential for SIRT1 activity domain from coming into contact with the deacetylase core (Figure 1.3) (77). This inhibitory interaction is enhanced with several post-translational modifications, including enhanced phosphorylation of CCAR2 on T454, which can stabilize the CCAR2/SIRT1 complex (78,79). Conversely, the CCAR2/SIRT1 interaction is inhibited by acetylation of CCAR2 at K112 and K115 (80,81). The ability of CCAR2 to inhibit SIRT1 activity thus highlights CCAR2 an interesting target to enhance the prolongevity effects of SIRT1.

CCAR2 negatively regulates the HSR

CCAR2 regulates many cellular processes including the HSR. In mammalian cells, overexpression of CCAR2 decreases *hsp70* transcription, HSF1 binding to the *hsp70* promoter, while increasing HSF1 acetylation during HS (67). Conversely, knockdown of CCAR2 enhances *hsp70* mRNA expression in response to HS (67). Thus, the SIRT1 modulator CCAR2 negatively impacts the HSR in mammals.

Genome-wide Studies of the HSR

Various physiological processes are altered in response to HS

Uncovering genome-wide changes in response to HS has been an active area of research in multiple model organisms (82-89). These studies have confirmed that common cellular processes are conserved across species and altered during HS. As expected, HSPs and molecular chaperones are the largest group found to be induced upon HS. Next, the proteolytic system, which can clear misfolded and aggregated proteins from the cell, is also enhanced during HS. DNA and RNA modifying enzymes, metabolic enzymes, kinases, and proteins involved in cellular structure have also been commonly shown to be regulated. These cellular processes appear to be conserved in their regulation, although the genetic composition of each class varies from species to species. Also, the expression kinetics for heat inducible gene transcription is likely highly dependent on the severity and duration of HS, which also vary between datasets. However, it appears that protein chaperones, the proteolytic system, DNA and RNA modifying enzymes, metabolic enzymes, regulatory kinases, and structural integrity proteins may be conserved systems impacted during HS.

Transcription and translation are repressed during HS

In order to prevent newly synthesized proteins from becoming misfolded or aggregated, selective inhibition of transcription and translation occurs during increased periods of heat (90,91). There are multiple mechanisms that may control this phenomenon. First, HSF1 may be an orchestrator of stimulus dependent chromatin conformation. For example, HSF1 decreases the acetylation of core histones in an HDAC1/2 dependent manner, ultimately compacting chromatin and inhibiting transcription (92). Also, transcriptional repression may be mediated by RNA-polymerase II pausing via stress-induced sumoylation of chromatin bound proteins at actively transcribed promoters (93). Thus, multiple mechanisms may play a role in transcriptional repression during HS.

In addition to HS resulting in transcriptional repression, translation is also globally repressed during stress. The mechanisms currently known to halt translation during HS include repression of cap recognition complexes and repression of the initiation factor *eIF2α* (94,95). Recently, ribosome footprint profiling has uncovered a conserved mechanism of translation elongation pausing following a severe HS (96). Interestingly, Hsp70 was found to regulate translation by interacting with elongation factors, ribosomal proteins in the exit tunnel, and with nascent chains (96,97). Thus, repression of translation elongation during stress is a conserved mechanism that may function to prevent the misfolding of newly synthesized polypeptides.

Post-transcriptional changes following HS

microRNAs (miRNAs) are a family of small (19-23 bp), non-coding, and conserved RNA molecules that elicit a complex mechanism of post-transcriptional genetic control by fine-tuning gene expression. miRNAs modulate gene expression by post-transcriptionally

regulating target genes through inhibition of mRNA translation (98) or destabilization of mRNA molecules (99). Over the last decade, HS has been reported to alter miRNA expression in plants, humans, rodents, and more recently in *C*. *elegans* (100,101). In human dermal fibroblast and HeLa cell lines, various miRNAs were shown to be induced and suppressed in response to HS (100,102). Also, a targeted screen in HeLa cells identified 8 miRNAs differentially expressed in response to heat, and found that 7 out of 8 of these heat-induced miRNAs contained at least one HSF1 binding site in their promoters (101). Subsequently, overexpression and silencing of HSF1 was shown to impact miRNA expression. These data therefore suggest a direct regulatory role for mammalian HSF1 in controlling heat-induced miRNA expression.

The HSR in Aging and Disease

Activating the HSR to combat aging

The average life expectancy of the population increases each year resulting in a need to uncover interventions to delay the onset of age-related diseases and decline. The HSR has been implicated to play a role in aging, as the ability of cells to maintain proteostasis deteriorates rapidly during the aging process. Mammalian and non-mammalian models such as human cell culture lines, rat, *Drosophila*, and *C. elegans* show a decreased capacity to mount a response to stress when comparing young vs old animals (103-109). HSF1 may also play an important role during aging, as a reduction in *C. elegans* HSF-1 levels results in decreased lifespan (110,111). Also, neurodegenerative diseases commonly occur later in life when the HSR is dampened (112-114). Thus, activating the HSR is one method suggested to combat aging.

Activating the HSR to combat disease

Many diseases are known to be associated with a malfunction in protein folding, and it is suggested that maintaining the proteome is important for promoting a healthy cellular environment. When the cell cannot cope with increasing levels of misfolded proteins, the formation of toxic protein aggregates can result and lead to a disease state (115). Activating the HSR may therefore be one therapeutic strategy to prevent protein folding diseases by increasing chaperone levels to overcome the build-up of toxic aggregate species.

Small-molecule activators of the HSR

Uncovering pharmalogical activators of the HSR are of interest for diseases of aging and protein dysfunction. Modulators of the HSR often target cellular components responsible for maintaining proteostasis including translation inhibition (puromycin) (116,117), protein folding inhibitors (azetidine 2-carboxylate, canavanine) (118-120), chaperone inhibitors (geldanamycin, radicicol) (121-124), DNA-synthesis inhibitors (fluorodeoxyuridine) (125), and proteasome/protease inhibitors (MG132) (126). Modifying these pathways may enhance proteostasis by decreasing protein turnover or increasing the production of chaperones. However, many pharmalogical activators of the HSR are not therapeutically feasible due to cytotoxicity and bioavailability (127). Therefore, uncovering feasible HSR activators may assist in the design of new potential therapies for aging and diseases of protein conformation.

C. elegans as a Model Organism

An introduction to C. elegans

C. elegans is an advantageous model organism for studying the molecular basis of cellular and physiological processes and how they impact aging and longevity (128). This organism is small in size, has a short life cycle, short life span, transparent anatomy for microscopic analysis, generates a large number of offspring, and has both easy and economic culturing (Figure 1.4) (129,130). The nematode goes through various molts before becoming a progeny producing adult, these include the first, second, third, and fourth larval stages (L1-L4, respectively). *C. elegans* are hermaphroditic and born with sperm, whereas oocytes are produced during adulthood. After adulthood, the typical lifespan of the worm is 20-30 days depending on their growth temperature which typicall ranges from 20°C-25°C. There are numerous resources available for *C. elegans* genetics including a fully sequenced annotated genome, detailed anatomical atlas, cell fate map, an RNAi feeding library for simple gene knockdown, and many available resources on basic biology and behavior. In addition, *C. elegans* is particularly beneficial for our studies as the HSR is highly-conserved in this species, and we are able to observe the effects of manipulating the HSR on aging and longevity.

Longevity studies in C. elegans often implement the use of FUdR

Aging and longevity studies in *C. elegans* provide valuable information on the consequence of genetic or chemical stimuli on lifespan. During longevity studies, separating progeny from adult *C. elegans* is essential to follow the original parental population throughout their lifespan. Rapid progeny development of larval nematodes makes it difficult to separate the parental generation from offspring during aging

experiments. For this reason, the DNA synthesis inhibitor 5-fluoro-2'-deoxyuridine (FUdR) is commonly employed to maintain a synchronous population of nematodes for aging studies (131-133). *C. elegans* embryos undergo rapid cellular divisions, requiring continual DNA synthesis. FUdR inhibits DNA synthesis after it is metabolized into FdUMP (5-fluoro-2′-deoxyuridine 5′-monophosphate) by thymidine kinase. FdUMP subsequently inhibits thymidylate synthase, an enzyme that is essential for pyrimidine biosynthesis (134). As adult nematodes undergo minimal cellular divisions, the standard practice for inhibition of reproduction is to treat synchronous populations of nematodes with FUdR at their last larval stage just before progeny production occurs. This is thought to have a minimal impact on adult nematodes while inhibiting the development of embryos. Adult nematodes are then scored every other day for survivors throughout lifespan. *C. elegans* are therefore advantageous for studying lifespan in response to various treatments due to their short lifespan and the ease of performing lifespan assays.

The HSR is highly-conserved in C. elegans and mediated by HSF-1

The HSR is vital for maintaining cellular function and promoting survival during stress, and regulation of the HSR and HSF1 are highly-conserved from yeast to human. In *C. elegans*, the HSF1 homolog, HSF-1, undergoes similar activation steps. HSF-1 exists as a monomer that homotrimerizes and binds to partially conserved HSEs in the promoter region of *hsp* genes during HS (135). HSF-1 has also been shown to be phosphorylated upon HS, similarly to a mammalian system (135). There are many advantages in utilizing the worm to study the HSR, such as observing the effects of manipulating the HSR and HSF-1 activity on a whole organism. In fact, studies of the HSR in *C. elegans* have identified a cell non-autonomous regulatory process that requires thermosensory neurons

for *hsp* induction, and that activation of the HSR in one tissue can elicit a response in distal tissues (136,137). Moreover, HSF-1 has a non-stress role in promoting longevity and development (111,138). Therefore, studies of the HSR in C. elegans have uncovered a conserved function for HSF1, a cell non-autonomous role for activation of the HSR, and a role for HSF-1 outside of stress responses.

Studies: Uncovering Transcriptional Regulators and Targets of HSF-1 in *C. elegans*

We were interested in testing the effects of various genetic, compound, and environmental stimuli on activation of the HSR by examining various HSF-1 regulated processes such as cytoprotection, longevity, transcription, and proteostasis using *C. elegans* as a model organism (Figure 1.5). Chapters 1 and 2 describe our findings that FUdR, coffee, and caffeine activate the HSR in an HSF-1-dependent manner and improve proteostasis in aging worms. Chapters 3 and 4 describe our findings that the nematode protein LST-3 is an ortholog to mammalian CCAR2, and that negative regulation of the HSR by CCAR2 is conserved in *C. elegans* and is mediated by LST-3. Chapters 5 and 6 describe the genome-wide impact HSF-1 may have in regulating transcriptional processes during HS. By globally profiling HSF-1 mRNA and miRNA targets, we have uncovered heat-dependent and -independent processes controlled by HSF-1. Overall, these studies have found small molecule and genetic regulators of the HSR, while also uncovering stress-dependent and independent roles for HSF-1 in cytoprotection, longevity, transcription, and proteostasis.

Figure 1.1. HSF1 is a multi-domain protein. The domains of HSF-1 are important for regulating transcriptional activity. The DNA binding domain recognizes heat shock elements in the promoter region of heat shock protein genes. The HR-A/B region and the HR-C region control homotrimerization and subsequent transcription initiation. The regulatory domain and the transactivation domain harbor post-translational modification sites that control HSF-1 activity.

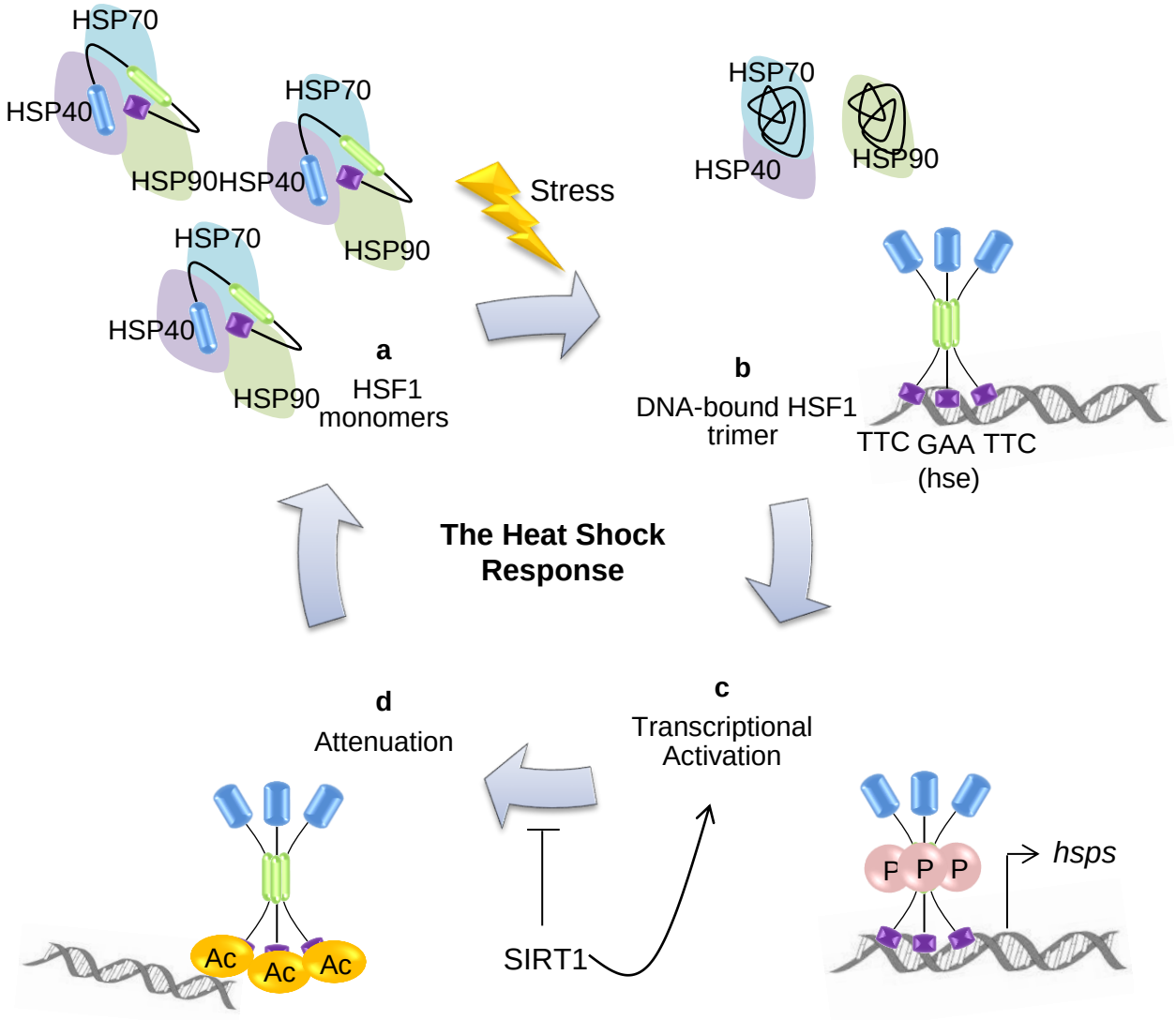

Figure 1.2. The mammalian HSF1 activity cycle. (**a**) Under non-stressed conditions, HSF1 is kept in a monomeric state by HSP70, HSP40, and HSP90, and shuttles between the nucleus and the cytoplasm. (**b**) Upon stress, HSF1 homotrimerizes and binds to heat shock elements which consist of three inverted repeats in the promoter region of HSF1 target genes. (**c**) Transcriptional activation via hyperphosphorylation allows for transcriptional activity and the production of heat shock protein genes, among other HSF1 target genes. (**d**) The HSR is attenuated when acetylation of the DNA-binding domain blocks accessibility of HSF-1 to DNA. The deacetylase SIRT1 deacetylates HSF-1 and subsequently increases the DNA-bound state of HSF-1, thus preventing attenuation and promoting the production of *hsp* genes.

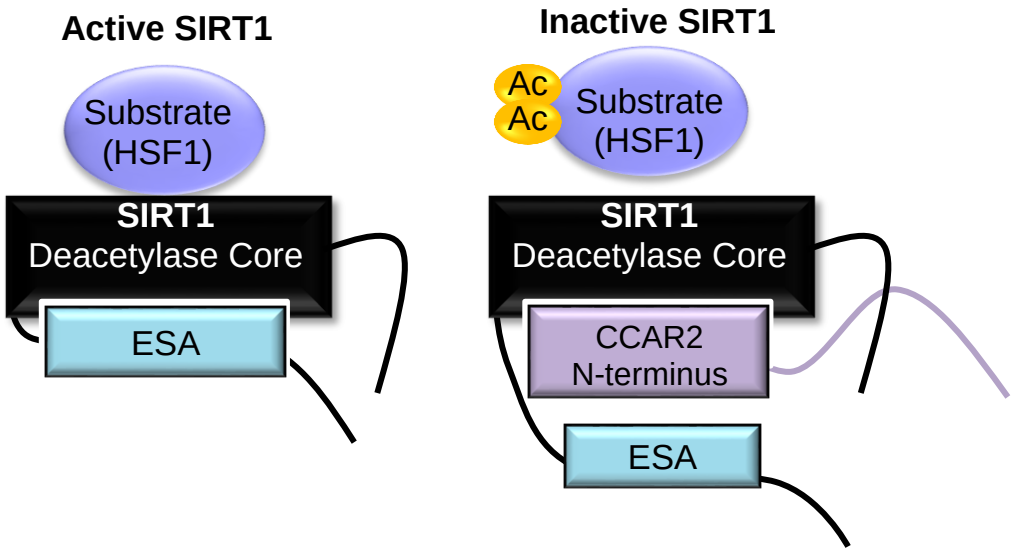

Figure 1.3. CCAR2 negatively regulates SIRT1 activity. When SIRT1 is in its active deacetylase state, the essential for SIRT1 activity domain (ESA) enhances substrate binding by changing the conformation of the deacetylase core, ultimately resulting in deacetylation of target proteins. CCAR2 (also known as DBC1) competitively inhibits the ESA domain from associating with the deacetylase core, resulting in decreased substrate binding and increased acetylation of target proteins.

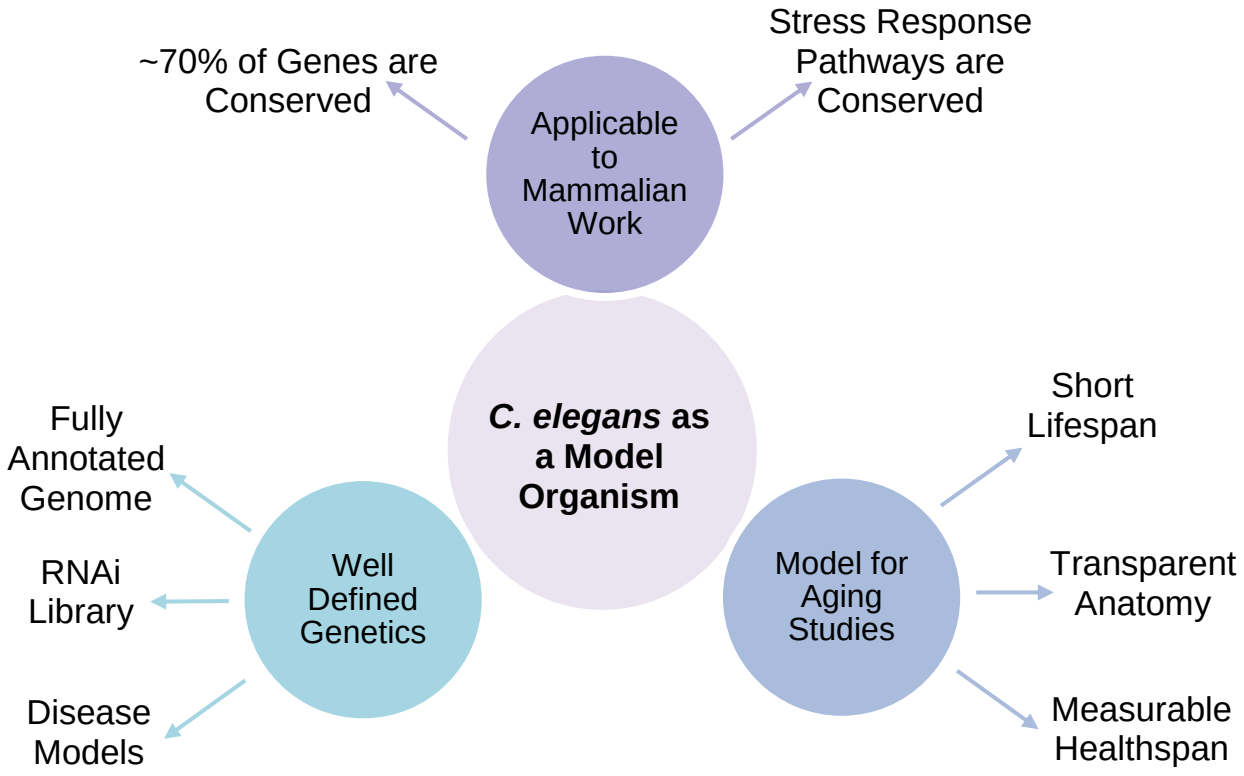

Figure 1.4. *Caenorhabditis elegans* are an ideal model organism. The characteristics that make *C. elegans* a model organism include well defined genetics, translational impact to mammalian systems, and use for aging studies. These attributes combined make this nematode an ideal system for studying the effects of stress responses on the physiology of a whole organism.

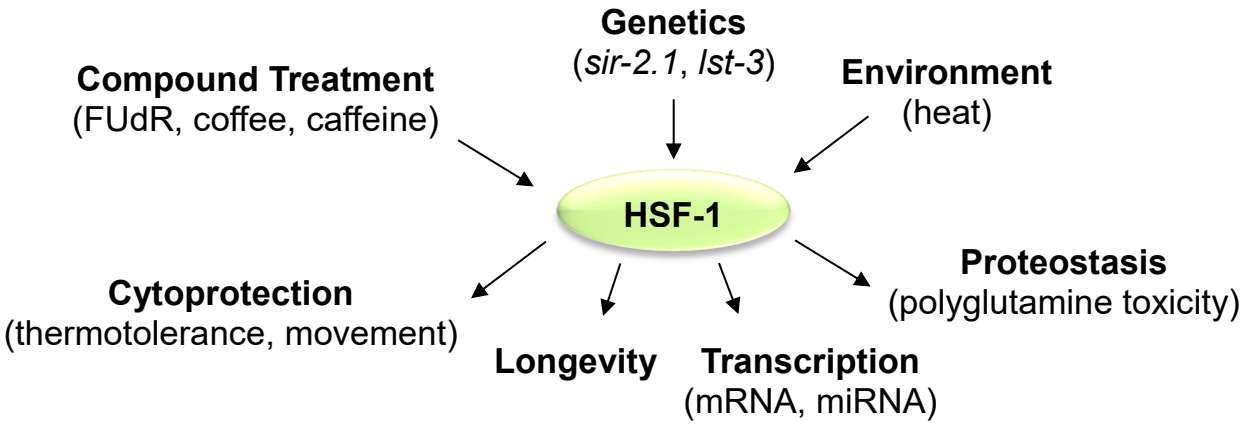

Figure 1.5. Studies: uncovering transcriptional regulators and targets of HSF-1. Using *C. elegans* as a model organism, we tested the effects of compound treatment (Chapters 1 and 2), genetics (Chapters 3 and 4), and environment (Chapters 5 and 6) on various HSF-1-regulated processes including cytoprotection, longevity, transcription, and proteostasis.

CHAPTER 2. FLUORODEOXYURIDINE ENHANCES THE HEAT SHOCK RESPONSE AND DECREASES POLYGLUTAMINE AGGREGATION IN AN HSF-1-DEPENDENT MANNER IN *CAENORHABDITIS ELEGANS*

Authored by Jessica Brunquell, Philip Bowers, and Sandy D. Westerheide

Published in Mechanisms of Ageing and Development: Brunquell, J., et al. (2014). "Fluorodeoxyuridine enhances the heat shock response and decreases polyglutamine aggregation in an HSF-1-dependent manner in Caenorhabditis elegans." Mech Ageing Dev 141-142: 1-4.

Experiments were performed and analyzed by J. Brunquell, or under the guidance of J. Brunquell. J. Brunquell and P. Bowers performed qRT-PCR replicates and polyglutamine aggregate analyses. All data analyses and figures were generated by J. Brunquell. The manuscript was written by J. Brunquell and S.D. Westerheide. See Appendix H for copyright permission.

Abstract

The heat shock response is a prolongevity mechanism employed by cells to maintain proteostasis during stress. This response is conserved in all organisms, and in *Caenorhabditis elegans*, is mediated by the transcription factor heat shock factor 1 (HSF-1). We show here that a compound commonly used to prevent larval development during aging studies in *C. elegans,* 5-fluoro-2'-deoxyuridine (FUdR), enhances heat shock induction of *hsp* mRNA expression in an HSF-1-dependent manner. Treatment with FUdR also decreases age-dependent polyglutamine aggregation in a Huntington's disease

model, and this effect depends on HSF-1 as well. We therefore conclude that FUdR treatment modulates the HSR and proteostasis, and should be used with caution when used to inhibit reproduction during aging studies.

Introduction

The model organism *Caenorhabditis elegans* is frequently used in aging studies due to its rapid lifecycle, short lifespan, and ability to easily obtain a synchronous population. However, the rapid progeny development in this model makes it difficult to separate the parental generation from offspring during aging experiments. For this reason, the DNA synthesis inhibitor 5-fluoro-2'-deoxyuridine (FUdR) is commonly employed to maintain a synchronous population of nematodes in aging studies (131-133).

C. elegans embryos undergo rapid cellular divisions which requires continual DNA synthesis. FUdR is able to inhibit DNA synthesis after it is metabolized into FdUMP (5-fluoro-2′-deoxyuridine 5′-monophosphate) by thymidine kinase. FdUMP subsequently inhibits thymidylate synthase, an enzyme that is essential for pyrimidine biosynthesis (134). As adult nematodes undergo minimal cellular divisions, the standard practice for inhibiting reproduction is to treat synchronous populations of nematodes with FUdR around the L4/young adult (YA) life stage prior to progeny production. This treatment strategy is thus thought to have a minimal impact on adult nematodes while inhibiting the development of progeny.

Recent studies have suggested that FUdR treatment may enhance stress-resistance. For instance, treatment with FUdR increases the lifespan of *gas-1* mitochondrial mutants and *tub-1* fat storage mutants, while also affecting the metabolism of wild-type nematodes (139-141). These recent studies have highlighted the importance of testing the effects of

FUdR on the particular conditions that are going to be used in an experiment prior to its use. We were therefore interested in determining effects on the HSR and proteostasis in response to treatment with FUdR by observing changes in chaperone expression in wild-type worms, and aggregate formation in a *C. elegans* Huntington's disease model.

Results

Standard FUdR treatment enhances hsp mRNA expression

To determine if the HSR is affected by treatment with the standard doses of 100 µM or 200 µM of FUdR given to L4/YA worms, transcript levels of the *hsp-70* genes *C12C8.1* and *F44E5.5* and the *hsp-16.2* gene *Y46H3A.3* were analyzed via qRT-PCR with or without heat shock (HS) and with or without *hsf-1* RNAi as indicated (Figure 2.1). As expected, HS induced *C12C8.1*, *F44E5.5*, and *Y46H3A.3* mRNA expression in an HSF-1-dependent manner. Interestingly, 200 µM of FUdR on its own was able to activate expression of *F44E5.5* mRNA. In addition, treatment with either 100 µM or 200 µM of FUdR enhanced HS induction of this gene and of the *C12C8.1* and *Y46H3A.3* mRNAs. This data indicates that standard FUdR treatment strategies used to inhibit progeny can enhance the HSR and would thus likely affect experimental results.

Low-dose FUdR treatment enhances hsp mRNA expression

We next looked for an alternative FUdR treatment strategy that would inhibit progeny production without impacting the HSR. We found that FUdR doses lower than 100 µM, given at the L4/YA stage, were not effective against preventing progeny development (data not shown). However, a low-dose treatment of 25 µM FUdR effectively inhibited all progeny from hatching if given at the L1 larval stage instead of the typical L4/YA stage. Also, this early treatment condition did not result in developmental defects (Figure A1,

see Appendix A). We were therefore interested in determining the effects of this alternative, low-dose, FUdR treatment strategy on the HSR.

Using low-dose 25 µM FUdR treatment, we again evaluated the transcript levels of *C12C8.1*, *F44E5.5*, and *Y46H3A.3* with or without HS and with or without *hsf-1* RNAi (Figure 2.2). Interestingly, 25 µM FUdR alone induced *C12C8.1*, *F44E5.5*, and *Y46H3A.3* expression in an HSF-1-dependent manner, and the induction of all three mRNAs were enhanced by HS. We were therefore unable to find an FUdR treatment condition that could effectively prevent progeny development while also not activating or enhancing the HSR.

Low-dose and standard FUdR treatment improves proteostasis in a C. elegans Huntington's disease model

As activation of the HSR improves proteostasis, we next tested whether FUdR was able to affect protein aggregation using a *C. elegans* Huntington's disease model. This model expresses 35 polyglutamine tracts fused to YFP (Q35::YFP), where polyglutamine aggregates form in an age-dependent manner (142). We observed that treatment with 25 µM FUdR from the L1 larval stage to day 3 of adulthood, or 200 µM of FUdR from L4/YA stage to day 3 of adulthood, decreased polyglutamine aggregation that was enhanced with HS and in an HSF-1-dependent manner (Figure 2.3a). As a separate approach to aggregate counting, we also quantified aggregate numbers using ImageJ software. The results indicate that blind analysis by hand counting aggregates and ImageJ quantification both reveal a similar trend (Figure 2.3b). Therefore, we conclude that low-dose and standard FUdR treatment strategies promote proteostasis in a *C. elegans* Huntington's disease model.

Discussion

In this study, we have found that various doses and stages of FUdR treatment enhances the HSR and promotes proteostasis in *C. elegans*. We first tested an FUdR treatment strategy commonly used by the *C. elegans* community during lifespan assays (100 µM or 200 µM FUdR from the L4 larval stage through adulthood), and found that hsp mRNA expression enhanced in response to FUdR treatment. We then tested an alternative treatment strategy (25 µM FUdR from the L1 larval stage through adulthood) and found that although this low-dose treatment was able to effectively inhibit progeny development without causing any developmental delays, we still observed induction and enhancement of the HSR in response to treatment. Both standard and low-dose FUdR treatment promoted proteostasis in a *C. elegans* Huntington's disease model. Additionally, each of these observations were found to be dependent on HSF-1. We were therefore unable to find an FUdR treatment strategy that could be used during lifespan assays to effectively inhibit progeny while also not affecting the HSR.

Other studies were published while our work was in progress, confirming that FUdR treatment increases stress-resistance and proteostasis in *C. elegans* (143,144). Although the effect of FUdR on proteostasis was suggested to be independent of HSF-1 (143), our research shows that HSF-1 is required. In this study, we used *hsf-1* RNAi for gene-knockdown, whereas the study that demonstrated independence of HSF-1 used a C-terminally truncated *hsf-1* mutant worm (*sy441*) (145). It is possible that this mutant worm may retain partial HSF-1 activity. Future studies regarding the dependence of HSF-1 on FUdR-mediated induction of the HSR may help determine the role of HSF-1 in regulating this process.

Overall, our data further support a role for FUdR in promoting proteostasis in an HSF-1-dependent manner. These findings confirm FUdR as an activator of the HSR through HSF-1, and highlight that caution should be taken when using FUdR in aging and stress-response studies.

Methods

C. elegans strains and maintenance

The Bristol N2 (wild-type) and Q35::YFP (142) strains were used in this study. All strains were grown at 24°C and maintained on standard nematode growth media (NGM) seeded with the *Escherichia coli* strain OP50. Age synchronization was accomplished by standard 20% hypochlorite treatment and a 24 hour rotation at 220 rpm in M9 buffer at 24°C without food.

RNA interference

Synchronized larval nematodes were placed onto standard NGM plates supplemented with 25 µg/mL ampicillin and 1 mM isopropyl-beta-D-thiogalactopyranoside seeded with either empty plasmid (EV control, L4440) or *hsf-1* RNAi from the Ahringer RNAi library (146). RNAi bacteria were grown for 12 hours and concentrated 20x in order to prevent inadvertent caloric restriction through inhibition of bacterial growth from FUdR treatment. Bacteria were allowed to induce on the plates overnight at room temperature.

Fluorodeoxyuridine treatment

FUdR (Sigma, *cat#* F0503) was diluted in sterile water to obtain a 100 mM stock. FUdR was added as a supplement to RNAi plates at a final concentration of 25 µM, 100 µM, or 200 µM, as indicated.

Heat shock treatment

Nematodes were grown on 100 mm RNAi plates, wrapped in parafilm, and submerged in a 33°C water bath for 30 minutes. For qRT-PCR analysis, animals were allowed to recover for 15 minutes at growth temperature prior to RNA extraction. For aggregate analysis, animals were allowed to recover overnight at growth temperature.

Quantitative RT-PCR

RNA was extracted with TRIzol® reagent (Ambion®, *cat*# 15596-026) by standard protocol, and cleaned up using the RNeasy Kit (Qiagen, *cat*# 74104). RNA was reverse transcribed using a High Capacity cDNA Reverse Transcription Kit (Applied Biosystems, *cat*# 4368814) according to manufacturer's instructions. cDNA was diluted to 50 ng/µl to be used as a template for qRT-PCR performed with the StepOne Plus Real-time PCR system (Applied Biosystems, *cat*# 4376600) using iTaq™ Universal SYBR® Green Supermix (BioRad, *cat*# 1725121) according to manufacturer's instructions. Statistical analysis was performed with GraphPad (GraphPad Software, La Jolla California USA, http://www.graphpad.com) using ANOVA followed by the Bonferroni post-test when an interaction term was significant as indicated by the F statistic.

Protein aggregation assay

Q35::YFP nematodes were grown on control RNAi (EV, L4440) or hsf-1 RNAi plates. Worms without FUdR treatment were picked to new plates daily after first progeny development until day 3 of adulthood was reached. FUdR-treated worms were also picked to new plates daily in order to undergo similar conditions to the control worms. The EVOS fluorescence microscope was used to image each worm after sedation with 10 mM levamisole. Protein aggregation was scored by blind analysis of 50 worms per condition

in independent biological triplicates as previously described (128,173), where any stand-alone GFP aggregate was scored as such. For ImageJ quantification, the color of the fluorescent images was inverted and then adjusted to black and white using Adobe Photoshop© (Adobe Systems Incorporated, San Jose, CA, USA). ImageJ (v. 1.44; http://imagej.nih.gov/ij/) was used to adjust the color threshold of each fluorescent image by the triangle method as a means to set an automatic threshold (178). Particle analysis was used to count and outline each aggregate with the following parameters: Size: 0-Infinity; Circularity: 0.00-1.00; Show: Outlines.

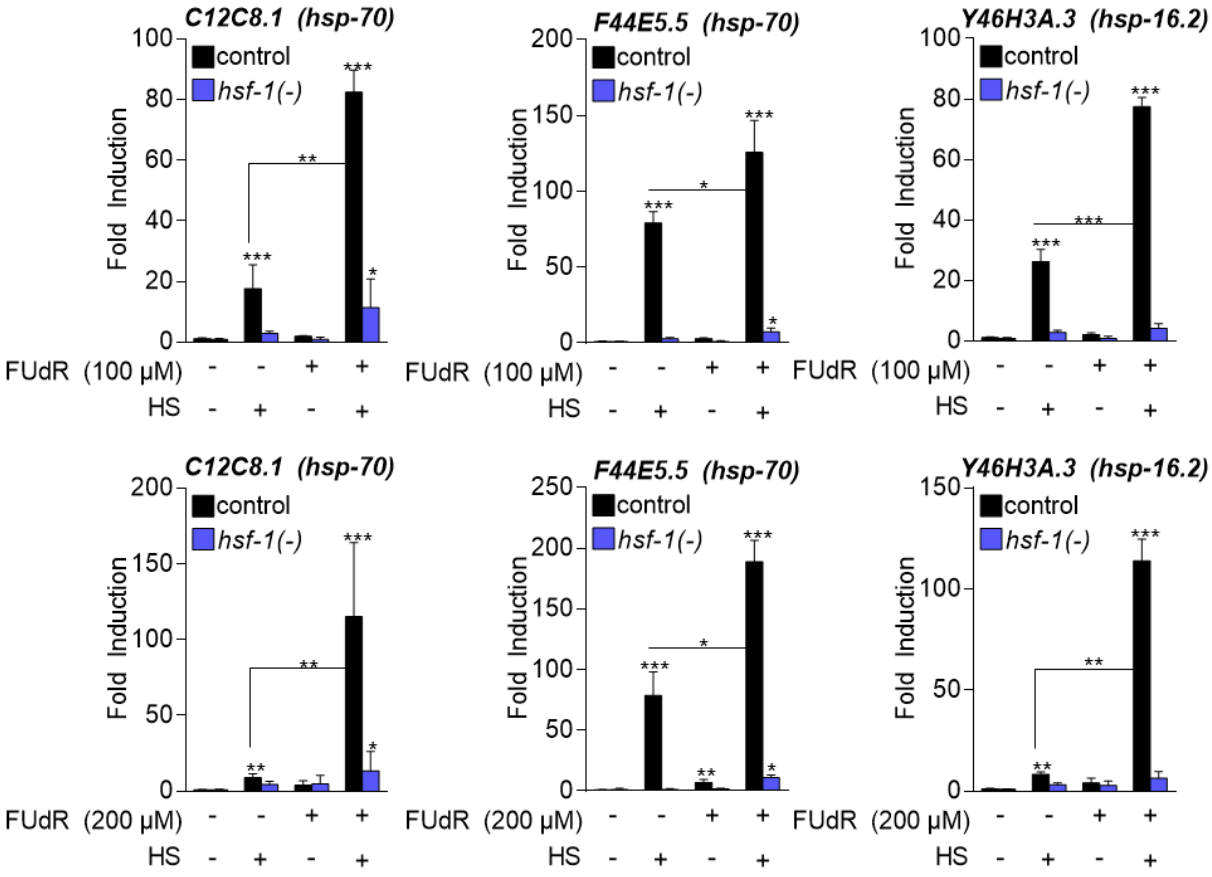

Figure 2.1 Treatment with 100 µM or 200 µM FUdR from the L4/YA stage enhances HS induction of *hsp-70* and *hsp-16.2* mRNA expression in *C. elegans* in an HSF-1-dependent manner. Synchronized nematodes were grown until the L4/YA stage while being fed control RNAi (black bars) or *hsf-1* RNAi [*hsf-1*(-), blue bars] as indicated. After developing to the point just before progeny production, worms were either picked to new plates daily, or transferred to plates containing 100 µM or 200 µM FUdR, to avoid progeny contamination, until collection at day 3 of adulthood. Worms were heat shocked (HS) at 33°C for 30 minutes and allowed a 15 minute recovery before collection. mRNA levels were quantified for the *hsp-70* genes *C12C8.1* and *F44E5.5*, and the *hsp-16.2* gene *Y46H3A.3,* via qRT-PCR. Results are representative of averaged technical duplicates from independent biological triplicates. Statistical analysis was performed using ANOVA followed by Bonferroni's comparison test (*P<0.05, **P<0.01, ***P<0.001).

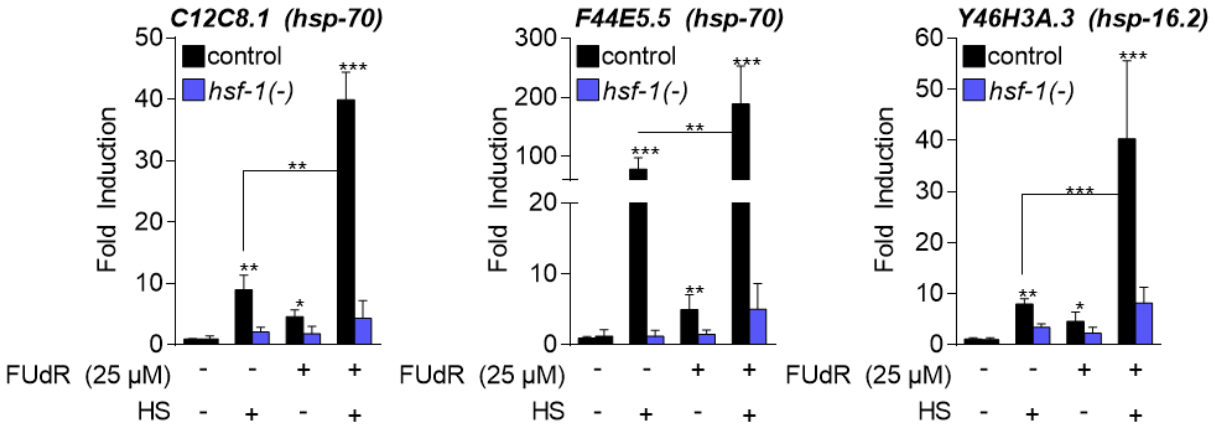

Figure 2.2. Treatment with 25 µM FUdR from the L1 stage enhances HS induction of *hsp-70* and *hsp-16.2* mRNA expression in *C. elegans* in an HSF-1-dependent manner. The same growth and experimental conditions were used as indicated in Figure 2.1, except nematodes were grown on 25 µM FUdR plates from the L1 stage until day 3 of adulthood. Results are representative of averaged technical duplicates from independent biological triplicates. Statistical analysis was performed using ANOVA followed by Bonferroni's comparison test (*P<0.05, **P<0.01, ***P<0.001).

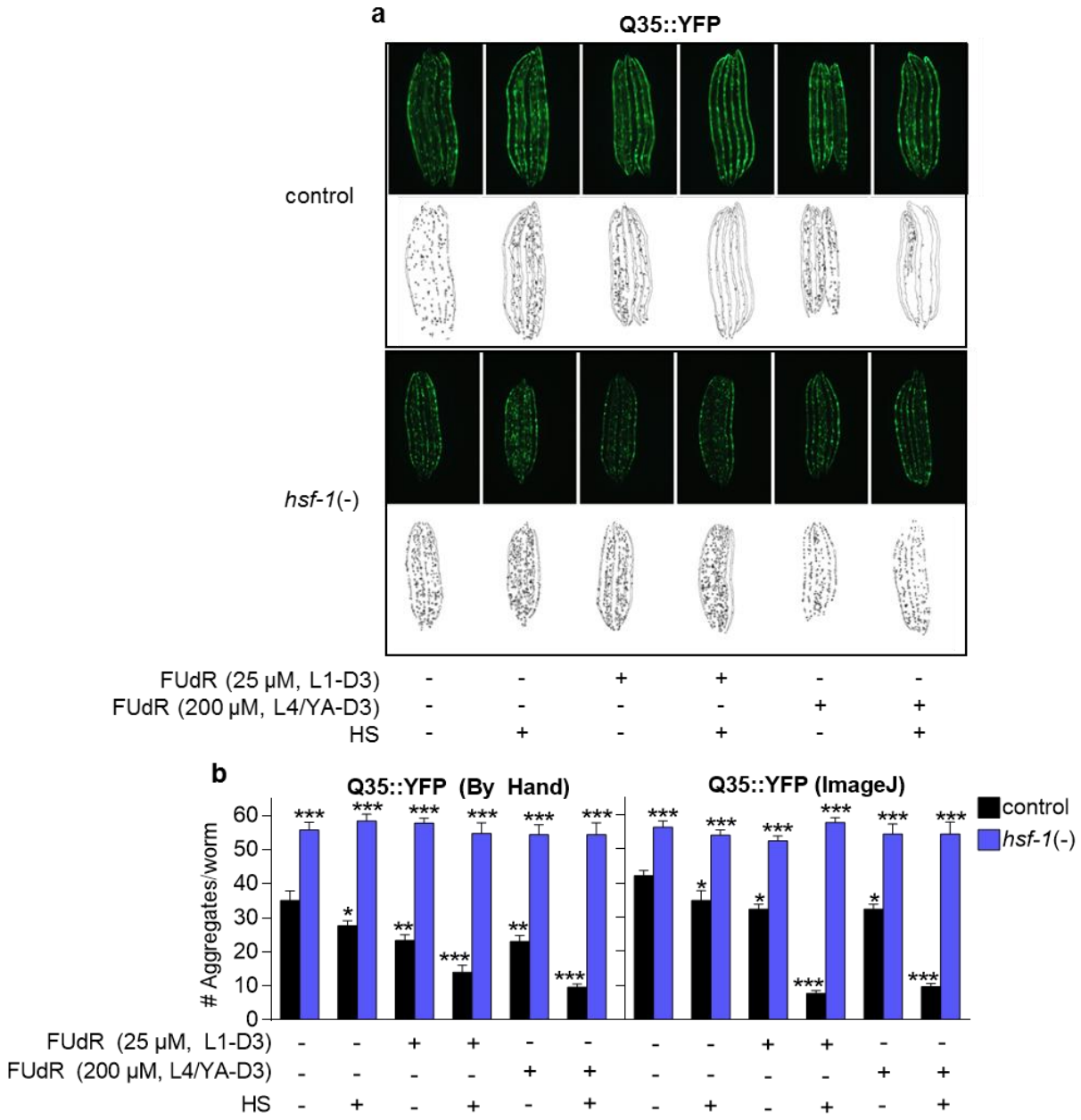

Figure 2.3. Treatment with FUdR decreases polyglutamine aggregation in an HSF-1-dependent manner. 25 µM FUdR was administered at the L1 stage, or 200 µM of FUdR was administered at the L4/YA stage, until day 3 of adulthood using the same growth conditions as described in Figures 2.1 and 2.2. Q35::YFP nematodes were heat shocked at 33°C for 30 minutes and allowed to recover overnight. Images were taken, and aggregates were scored, on day 3 of adulthood (D3). (**a**) Fluorescent images of 5 worms for each condition are shown. The ImageJ outlines of the worms and aggregates are shown below each fluorescent image. (**b**) Quantification of the collective number of aggregates per worm by hand counting and using ImageJ software. Aggregates in 50 worms were counted per each condition based off of the fluorescent images for each treatment condition in biological triplicate. Significance was determined using ANOVA followed by Bonferroni's comparison test (*P<0.05, **P<0.01, ***P<0.001).

CHAPTER 3: COFFEE EXTRACT AND CAFFEINE ENHANCE THE HEAT SHOCK RESPONSE AND PROMOTE PROTEOSTASIS IN AN HSF-1-DEPENDENT MANNER IN *CAENORHABDITIS ELEGANS*

Authored by Jessica Brunquell, Stephanie Morris, Alana Snyder, and Sandy D. Westerheide

Accepted with revisions to Cell Stress & Chaperones.

Experiments were performed and analyzed by J. Brunquell, or under the guidance of J. Brunquell. J. Brunquell, S. Morris, and A. Snyder performed qRT-PCR replicates and polyglutamine aggregate analyses. All data analyses and figures were generated by J. Brunquell. The manuscript was written by J. Brunquell and S.D. Westerheide.

Abstract

As the population ages, there is a critical need to uncover strategies to combat diseases of aging. One method suggested to improve the quality of aging is through moderate consumption of coffee and caffeine. Studies in the soil-dwelling nematode *Caenorhabditis elegans* have demonstrated the protective effects of coffee extract and caffeine in promoting the induction of conserved longevity pathways including the insulin-like signaling pathway and the oxidative stress response. We were interested in determining the effects of coffee and caffeine treatment on the regulation of the heat shock response. The heat shock response is a highly-conserved cellular response that functions as a cytoprotective mechanism during stress, mediated by the heat shock transcription factor

HSF-1. In the worm, HSF-1 not only promotes protection against stress, but is also essential for development and longevity. Induction of the heat shock response has been suggested to be beneficial for diseases of protein-conformation by preventing protein misfolding and aggregation, and as such has been proposed as a therapeutic target for age-associated neurodegenerative disorders. In this study, we demonstrate that coffee is a potent, dose-dependent, inducer of the heat shock response. Treatment with a moderate dose of pure caffeine was also able to induce the heat shock response, indicating caffeine as an important component within coffee for producing this response. The effects that we observe with both coffee and pure caffeine on the heat shock response are both dependent on HSF-1. In a *C. elegans* Huntington's disease model, worms treated with caffeine were protected from polyglutamine aggregates and toxicity, an effect that was also HSF-1-dependent. In conclusion, these results demonstrate caffeinated coffee, and pure caffeine, as protective substances that promote proteostasis through induction of the heat shock response.

Introduction

The average life expectancy of the population increases each year, resulting in a need to uncover interventions to delay the onset of aging-related diseases. Caffeine is a bioavailable compound that is consumed in large quantities worldwide with implications in promoting human healthspan and aging-associated neuropathologies (147). Moderate caffeine consumption has been suggested to promote protection against numerous neurodegenerative disorders including Alzheimer's disease, dementia, and Parkinson's disease (148,149). Additionally, epidemiological studies have correlated moderate caffeine consumption with improved memory (150), and reduced cognitive decline and

mortality (151,152). Thus, moderate caffeine consumption has been suggested to promote healthy aging and longevity in humans.

Studies in the multi-cellular nematode *Caenorhabditis elegans* have demonstrated the positive impact of caffeine on longevity. Caffeine was uncovered as a longevity-promoting substance in a screen aimed at uncovering FDA-approved compounds that could extend the *C. elegans* lifespan (153). The lifespan extension observed in response to caffeine treatment was found to be temperature- and dose-dependent, and mediated in part through the insulin-like signaling pathway (153-155). Additionally, a worm Alzheimer's model treated with caffeinated coffee extract was protected against β-amyloid-induced paralysis, an effect that was found to be dependent on the oxidative stress response factor SKN-1 (156). Taken together, these results suggest that caffeine and coffee treatment may act through conserved longevity pathways to promote healthy aging in *C. elegans*.

The cytoprotective heat shock response (HSR) is a highly-conserved response employed by cells exposed to protein denaturing stressors, such as heat, which functions to maintain proteostasis (157). The mammalian HSR is regulated at the transcriptional level by the transcription factor heat shock factor 1 (HSF1). During stressful insults, HSF1 enhances the expression of heat shock protein (*hsp*) genes which encode chaperone proteins. Chaperones serve multiple cytoprotective functions including the prevention of aggregate formation, promotion of protein folding, and mediation of protein degradation (158,159). Regulation of the HSR by HSF1 is thus an important cytoprotective mechanism utilized during heat stress to promote survival.

While HSF1 is classically studied for its role in regulating the HSR, studies of the *C. elegans* HSF1 homolog, HSF-1, have shown this transcription factor to also be essential for development and longevity (110,111). Knockdown of *hsf-1* in *C. elegans* decreases lifespan and induces rapid aging, while its overexpression increases lifespan (110,111,138). Also, increased expression of *hsp-70* in a *C. elegans* Huntington's disease model protects against protein aggregate formation and its associated toxicity (160). Thus, enhancing HSF-1 activity may promote longevity and proteostasis.

Many diseases of protein quality control, such as neurodegenerative disorders, are associated with the misfolding, aggregation, and accumulation of disease-associated proteins. Neurodegenerative diseases have been associated with a decline of the HSR, and decreased proteome maintenance, during the process of aging (161-163). In order to combat diseases of protein quality control, the identification of compounds that can be harnessed therapeutically to activate the HSR has been an active area of research over the past decade. However, many of the compounds currently known to modulate HSF1 activity are not therapeutically feasible due to cytotoxicity and bioavailability issues (127). Therefore, uncovering alternative HSR activators may assist in the design of new potential therapies for diseases of protein conformation, and aging, such as neurodegenerative disorders.

An interesting characteristic of HSR activators is that they often function synergistically with heat shock (HS) to enhance induction of the HSR. For example, the anti-inflammatory drug indomethacin synergizes with a mild heat stress to increase *hsp* induction (164). Similarly, the triterpenoid celastrol (165), the inflammatory pathway intermediate arachidonic acid (166), the hydroxylamine derivative bimoclomal (167),

caloric restriction (72), and the pyrimidine analog fluorodeoxyuridine (125), can also function synergistically with HS to enhance *hsp* expression compared to treatment with each compound alone. Thus, many currently known HSR activators have synergistic effects on *hsp* expression when combined with a heat stress.

In this study, we demonstrate caffeine as a component in coffee that mediates induction of the HSR in *C. elegans*. Using *hsp-70* as a marker for induction of the HSR, we show a dose-dependent role for caffeine in inducing the HSR alone and together with HS, greater than that of decaffeinated or caffeinated coffee extracts. Furthermore, a *C. elegans* Huntington's disease model was protected from polyglutamine aggregation and toxicity in response to treatment with caffeinated coffee extract, and even more so in response to treatment with a moderate dose of pure caffeine, an effect that is dependent on HSF-1. We therefore conclude that caffeinated coffee and, to a greater extent, caffeine are protective compounds that can induce the HSR and suppress age-associated protein aggregation in *C. elegans*.

Results

Treatment with caffeinated and decaffeinated coffee extract enhances HS-induced hsp-70 promoter activity

To determine the effects of coffee on the HSR, we grew worms on plates supplemented with coffee extract and then assessed *hsp-70* promoter activity by visualizing GFP expression under the control of the HS-inducible *C12C8.1* (*hsp-70*) promoter (p*hsp-70*::GFP) (Figure 3.1). Synchronous p*hsp-70*::GFP nematodes were left untreated (control), or subjected to treatment with decaffeinated or caffeinated coffee extract added at a 10% vol/vol to NGM plates, from the L1 larval stage to the L4 larval stage prior to

treatment with or without a 30 minute HS (Figure 3.1a). As expected, HS treatment of the control showed induction of HS-induced GFP expression as compared to the untreated control. Treatment with caffeinated (3.6 mM caffeine) and decaffeinated (0.032 mM caffeine) coffee extracts both enhanced HS-induced GFP expression as compared to the HS-treated control, with the caffeinated coffee extract having a stronger effect on *hsp-70* promoter activity. To quantify the GFP expression of the fluorescent images in Figure 3.1a, fluorescence intensity was measured for each treatment condition using ImageJ (Figure 3.1b). Treatment with decaffeinated and caffeinated coffee extract increased HS-induced fluorescence intensity 10-fold and 20-fold as compared to the HS-treated control, respectively. Thus, we conclude that components present in decaffeinated coffee can enhance the HSR, while caffeinated coffee further increases this effect, suggesting a role for coffee and caffeine in modulating the HSR.

We were next interested in more closely examining tissue-specific induction of the *hsp-70* promoter in response to treatment with caffeinated coffee extract alone (Figure 3.1c). We observed that *hsp-70* promoter activity was localized to intestinal gut granules. *C. elegans* gut granules are acidic lysosome-like organelles that serve as sites for fat storage and nutrient metabolism (168). These granules fluoresce under ultraviolet light due to the accumulation of glycosylated anthranilic acid, and can be visualized with a DAPI filter (168). Corresponding DAPI images are therefore shown to visualize the location of gut granules. Overlay of the GFP/DAPI images confirmed the localization of GFP expression to these intestinal granules in response to treatment with caffeinated coffee extract. Thus, treatment with caffeinated coffee extract results in tissue specific-

activation of the *hsp-70* promoter in gut granules in the absence of stress, and enhancement of *hsp-70* promoter activity throughout the worm during HS.

Treatment with caffeinated coffee extract enhances hsp-70 mRNA expression greater than that of decaffeinated coffee

We next used qRT-PCR to measure the expression of the endogenous *hsp-70* family members *C12C8.1, F44E5.4*, and *F44E5.5* in response to treatment with caffeinated and decaffeinated coffee extracts (Figure 3.2). Synchronous wild-type worms were left untreated (control), or subjected to treatment with decaffeinated or caffeinated coffee extract (added at a 10% vol/vol to NGM plates) from the L1 larval stage to the L4 larval stage prior to treatment with or without a 15 minute HS. As expected, HS treatment of the control increased the expression of each *hsp-70* family member as compared to the untreated control. Consistent with the results in Figure 3.1, decaffeinated coffee extract did not induce *C12C8.1* mRNA expression upon treatment alone, but was able to enhance HS-induced *C12C8.1* mRNA expression 6-fold as compared to the HS-treated control. Additionally, treatment with caffeinated coffee extract alone induced *C12C8.1* mRNA expression 3-fold, and enhanced HS-induced *C12C8.1* mRNA gene expression 35-fold. We also observed that treatment with caffeinated coffee extract had a stronger effect (13-fold) on *C12C8.1* mRNA expression compared to treatment with decaffeinated coffee extract (Figure 3.2a). A similar trend is also observed for the *hsp-70* family members *F44E5.4* and *F44E5.5* (Figure 3.2b-c). Treatment with caffeinated coffee extract therefore has a stronger effect on inducing *hsp-70* mRNA expression, and enhancing *hsp-70* mRNA expression upon HS, as compared to treatment with decaffeinated coffee

extract. These data thus further suggest a role for caffeine as a component in coffee that can activate the HSR.

Treatment with pure caffeine robustly enhances hsp-70 mRNA expression in a dose-dependent manner

To determine the effects of pure caffeine on the HSR, qRT-PCR was performed for the *hsp-70* family members *C12C8.1, F44E5.4*, and *F44E5.5* in response to treatment with various doses of caffeine (Figure 3.3). Synchronous wild-type worms were left untreated (control), treated with caffeinated coffee, or subjected to treatment with low (0.5 mM, 1 mM), moderate (3.6 mM), and high (5 mM, 10 mM) doses of pure caffeine, from the L1 larval stage to the L4 larval stage prior to a 30 minute HS-treatment. We observed that low and moderate doses of caffeine did not affect the rate of development of the worm, whereas high doses stunted development Figure B1 (see Appendix B). We therefore focused our studies on low and moderate doses of caffeine to avoid changes in the developmental stages of the worms from affecting our data. As expected, HS-treatment increased the induction of each HS-inducible *hsp-70* family member (80-200-fold) as compared to the untreated control. Similar to the trend observed in Figure 3.2, treatment with caffeinated coffee extract alone induced the expression of each *hsp-70* family member (5-20 fold), and enhanced the expression of each *hsp-70* family member when combined with HS (150-300 fold), compared to the respective controls. Interestingly, pure caffeine treatment has a robust, and dose-dependent, effect on *hsp-70* mRNA expression compared to treatment with caffeinated coffee extract. In fact, treatment with 3.6 mM pure caffeine alone induced *C12C8.1* mRNA expression (50-fold) similarly to that of HS (80-fold), indicating caffeine as a strong inducer of the HSR (Figure 3.3a). Additionally,

treatment with 3.6 mM pure caffeine (the amount of caffeine resulting from our caffeinated coffee extract protocol) resulted in the largest enhancement of HS-induced *C12C8.1* mRNA expression, compared to treatment with caffeinated coffee extract and low-dose caffeine treatment. A similar trend is also observed for the *hsp-70* family members *F44E5.4* and *F44E5.5* (Figure 3.3b-c). These data thus demonstrate caffeine as a component in coffee that induces and enhances the HSR.

Induction of hsp-70 mRNA expression in response to treatment with caffeinated coffee extract and moderate caffeine is dependent on HSF-1

We next used qRT-PCR to assess the role of HSF-1 in regulating *hsp-70* mRNA expression in response to treatment with caffeinated coffee extract and pure caffeine. Wild-type worms were either left untreated or subjected to treatment with caffeinated coffee extract, or 3.6 mM pure caffeine, from the L1 larval stage the L4 larval stage prior to treatment with or without a 30 minute HS in the presence of control or *hsf-1* RNAi (Figure 3.4). As expected, HS treatment of the control increased the expression of each *hsp-70* family member as compared to the untreated control in an HSF-1-dependent manner. Consistent with the results in Figure 3.3, treatment with caffeinated coffee extract and 3.6 mM caffeine induced *C12C8.1, F44E5.4*, and *F44E5.5* mRNA expression upon treatment alone, and also collectively with HS (Figure 3.4, black bars). Additionally, the ability of worms to enhance *hsp-70* mRNA expression in response to caffeinated coffee extract and pure caffeine treatment is dependent on HSF-1. Worms fed *hsf-1* RNAi showed a 500-1500-fold decrease in their ability to enhance *hsp-70* mRNA expression upon treatment with caffeinated coffee extract or 3.6 mM caffeine during HS (Figure 3.4,

blue bars). Thus, induction of the HSR in response to caffeinated coffee extract and pure caffeine treatment is dependent on HSF-1.

Caffeinated coffee extract and pure caffeine treatment protect a C. elegans Huntington's disease model against polyglutamine aggregation and toxicity in an HSF-1-dependent manner

We were next interested in testing the effects of caffeinated coffee extract and 3.6 mM pure caffeine on proteostasis by observing protein aggregate formation in a *C. elegans* Huntington's disease model (Figure 3.5). The Huntington's disease model we used harbors 35 polyglutamine repeats fused to YFP under the control of a muscle promoter (Q35::YFP), and develops insoluble protein aggregates in the body wall muscle in an age-dependent manner (142). Synchronous Q35::YFP worms were left untreated (control), or subjected to treatment with caffeinated coffee extract or 3.6 mM pure caffeine from the L1 larval stage until day 3 of adulthood in the presence of control or *hsf-1* RNAi. We observed a decrease in punctate-YFP aggregation upon treatment with caffeinated coffee extract and 3.6 mM pure caffeine, an effect that is dependent on HSF-1 (Figure 3.5a). ImageJ was used on threshold-adjusted images to allow quantification of the number of aggregates per worm for each treatment condition (Figure 3.5b). Treatment with caffeinated coffee extract and 3.6 mM pure caffeine suppressed aggregate formation by a magnitude of 10 and 15 less aggregates per worm, respectively, compared to the control (Figure 3.5b, black bars). The decrease in aggregate formation observed in response to treatment with caffeinated coffee and 3.6 mM pure caffeine was dependent on HSF-1, as worms cultured in the presence of *hsf-1* RNAi did not exhibit a decrease in aggregate formation in response either treatment condition (Figure 3.5b, blue bars).

These data suggest that treatment with caffeinated coffee extract and pure caffeine protects against polyglutamine aggregate formation in a *C. elegans* Huntington's disease model in an HSF-1-dependent manner.

We next assessed the toxicity associated with polyglutamine expansions by observing paralysis in the Huntington's disease model in response to treatment with caffeinated coffee extract or pure caffeine (Figure 3.5c). Synchronous Q35::YFP worms were left untreated (control), or subjected to treatment with caffeinated coffee extract or 3.6 mM pure caffeine from the L1 larval stage until day 5 of adulthood in the presence and absence of *hsf-1* RNAi. Treatment with caffeinated coffee extract reduced paralysis by 25%, while 3.6 mM pure caffeine reduce paralysis by 39%, compared to the control (Figure 3.5c, black bars). The ability of caffeinated coffee extract and 3.6 mM caffeine to reduce paralysis is abolished in the presence of *hsf-1* RNAi, showing dependence on HSF-1 (Figure 3.5c, blue bars). This data correlates to Figure 3.5b, suggesting that the number of aggregates present in the worm may be associated with paralysis. Thus, treatment with caffeinated coffee extract and 3.6 mM pure caffeine decreases polyglutamine aggregate formation and paralysis in an HSF-1-dependent manner in a *C. elegans* Huntington's disease model.

Discussion

In this study, we demonstrate caffeine as a component in coffee that activates the HSR and promotes proteostasis in *C. elegans* (for a summary of results, see Figure 3.6). We observe that treatment with caffeinated coffee extract results in greater activation of the HSR as compared to decaffeinated coffee extract, and find a dose-dependent role for pure caffeine in activating the HSR. Furthermore, we show a central role for HSF-1 in

regulating the response to caffeinated coffee extract and pure caffeine treatment on *hsp-70* mRNA induction. Additionally, treatment with caffeinated coffee extract and a moderate dose of pure caffeine protects against polyglutamine aggregation and toxicity in a *C. elegans* Huntington's disease model in an HSF-1-dependent manner. Overall, this work suggests that caffeinated coffee extract and moderate caffeine consumption may protect against age-associated neurodegeneration by promoting proteostasis through activation of the HSR.

Caffeine is well known for its bioavailability in natural products including coffee, tea, and chocolate (169). The degree of caffeine consumption varies world-wide. The average amount of caffeine consumed in the US is approximately 168 mg per day, the equivalent of two cups of coffee (170). Our data suggests that the effects of caffeine are highly dose-dependent, and that an optimum dose of caffeine can maximize health benefits while decreasing health risks. Our treatment conditions consisted of low (0.5 mM, 1 mM), moderate (3.6 mM), and high-dose (5 mM, 10 mM) chronic caffeine exposure from the first larval stage to the last larval stage of development. Moderate caffeine treatment enhanced the HSR with no developmental delays, whereas high-dose caffeine treatment severely stunted development. We therefore conclude that moderate chronic caffeine consumption may promote proteostasis while avoiding off-target phenotypic effects.

Coffee extract contains many dissolved solutes other than caffeine, including chlorogenic and phenolic acids, aromatic compounds, and diterpene molecules, among others (171-173). Although we demonstrate caffeine as a robust activator of the HSR, our data also suggests other coffee components as modulators of the HSR. Worms treated with decaffeinated coffee extract show a moderate enhancement of HS-induced *hsp-70*

mRNA expression, suggesting a caffeine-independent induction of the HSR. Two diterpene molecules found in coffee extract, cafestol and kahweol, affect the oxidative stress response and protect against neurodegeneration (174,175). Thus, it would be interesting to determine if these compounds, along with other coffee components, also modulate the HSR.

In mammals, the pharmacological effects of caffeine are mediated by stimulation of the central nervous system through non-selective inhibition of neuronal adenosine receptors (176,177). In *C. elegans*, caffeine-mediated lifespan extension was found to be dependent on adenosine signaling (155), suggesting a partially conserved mechanism. Interestingly, the density of serotonergic receptors, and serotonin levels, are increased in response to caffeine intake in mammals (178), while the metazoan HSR is induced through stimulation of serotonergic neurons (179). Therefore, it would be interesting to determine the dependency of adenosine receptors and serotonin signaling in caffeine-mediated induction of the HSR in *C. elegans*.

The metazoan HSR is a highly complex system that employs cell-nonautonomous signaling to maintain proteostasis between tissues (136,137). The release of neuropeptides from neurons, such as serotonin, can act as a signaling mechanism to activate the HSR in distal tissues (179,180). Treatment with caffeinated coffee extract results in unique tissue-specific activation of the *hsp-70* promoter in gut granules, a process that may be elicited through coffee-mediated neurostimulation. Gut granules are located predominately in the intestine and are major sites for fat storage and nutrient metabolism (181-183). The HSR has been linked to the metabolic state of an organism. For example, caloric restriction can synergize with heat to enhance the HSR (72).

Although caffeinated coffee extract treatment does not affect *C. elegans* feeding, or initiate a secondary caloric restrictive response (156), our data suggests that gut granular metabolic processes may influence the HSR. Further investigation into coffee-induced neuronal stimulation, and the effects on tissue-specific *hsp-70* promoter induction, may uncover novel neuronal receptors that mediate cell-nonautonomous signaling.

C. elegans is a powerful model that can be utilized to uncover therapeutic compounds for neurodegenerative diseases. Many of the compounds found to elicit positive responses in *C. elegans* neurodegenerative disease models have a translational impact in mammalian systems (184). Small molecule activators of the HSR have been suggested as possible therapeutic strategies to prevent aggregate-associated neurodegenerative disorders (163,185-187). HSR inducers often function synergistically with one another to enhance induction of the HSR (72,125,165). We can now add coffee extract and caffeine to the list of compounds that induce the HSR alone, and that function synergistically with heat to promote induction of the HSR. Ultimately, this finding may aid in the design of potential therapies for diseases of protein quality control.

Overall, this study demonstrates caffeinated coffee extract and a moderate dose of caffeine as activators of the HSR, both alone, and in combination with HS. Our studies suggest that the genetic mechanisms behind the neuroprotective benefits associated with coffee and caffeine supplementation depend, at least in part, on activation of the HSR and HSF-1. Caffeinated coffee extract and moderate caffeine treatments are promising therapeutic options for age-associated neurodegenerative diseases due to bioavailability and low toxicity. Additionally, caffeine readily crosses the blood-brain barrier, making it an ideal therapeutic candidate for neurodegenerative disorders (188). Caffeinated coffee

extract and caffeine may elicit their protective benefits, in part, through induction of the HSR, thus warranting further studies in mammalian systems.

Methods

C. elegans strains and maintenance

The wild-type N2, p*C12C8.1*::GFP (111), and Q35::YFP (AM140) (142) strains were used in this study. Worms were maintained at 23°C on standard NGM plates seeded with *Escherichia coli* OP50. A synchronous population of nematodes was obtained by standard 20% hypochlorite treatment, and a 24 hour rotation at 220 rpm in M9 buffer without food.

RNAi feeding

Synchronous L1 nematodes were plated onto standard NGM plates supplemented with 25 µg/mL ampicillin and 1 mM isopropyl-beta-D-thiogalactopyranoside seeded with sequence-verified empty vector control RNAi or *hsf-1* RNAi isolated from the Ahringer RNAi library (146).

Heat shock conditions

Synchronous nematodes were grown on plates, wrapped in parafilm, and submerged in a 33°C water bath for either 15 or 30 minutes as indicated. For qRT-PCR, worms were allowed to recover for 15 minutes prior to RNA extraction.

Coffee extract and caffeine media preparation

We performed an aqueous extraction protocol to obtain decaffeinated and caffeinated coffee extract that was developed in the Pallanck laboratory (174). This extraction method was previously determined to contain 0.032 mM caffeine in the decaffeinated coffee extract, and 3.6 mM caffeine in the caffeinated coffee extract (174). Briefly, 18.48 g of

caffeinated and decaffeinated Starbucks House Blend whole bean coffee was ground for 3 minutes, placed into boiling water for 30 minutes, filtered with a French press, and sterilized with a 0.2 µM filter. Coffee extract was then added at a final volume of 10% to plates. The indicated concentrations of pure caffeine (Fisher Scientific, cat# S93153) were added to NGM prior to autoclaving, similarly to Sutphin *et al.* (154). Worms were exposed to each treatment condition from the L1 larval stage until the L4 larval stage for gene expression analyses, until day 3 of adulthood for polyglutamine aggregate analyses, and until day 5 for the paralysis assay.

RNA preparation and cDNA synthesis

Total RNA was extracted using TRIzol® reagent (Ambion®, *cat*# 15596-026) by standard protocol, and purified using RNeasy columns (QIAgen, *cat*# 74104). RNA was reverse transcribed using a High Capacity cDNA Reverse Transcription Kit (Applied Biosystems, *cat*# 4368814) according to manufacturer's instructions. cDNA was diluted to 50 ng/µl prior to being used as a template for qRT-PCR.

Quantitative RT-PCR

qRT-PCR was performed with the StepOne Plus Real-time PCR system (Applied Biosystems, *cat*# 4376600) using iTaq™ Universal SYBR® Green Supermix (BioRad, *cat*# 1725121) according to the manufacturer's instructions. Data analysis was performed according to standard calculations using the comparative Ct method (189). Relative mRNA levels were normalized to *gapdh*, and calculated from independent biological triplicates and technical duplicates.

Fluorescence microscopy and quantification

Worms were collected in 1 mL of M9 buffer, placed onto a glass slide, and anesthetized with 10 mM levamisole prior to imaging. An EVOS fluorescence microscope was used for phase contrast, GFP, and DAPI imaging. Fluorescence intensity was quantified using ImageJ (ImageJ Software, Bethesda Maryland USA, http://imagej.nih.gov/ij/) for 50 worms per treatment condition in independent biological triplicates (190).

Polyglutamine aggregation assay

Synchronous Q35::YFP animals were cultured on control or treatment plates as indicated. Worms were picked daily to new plates until day 3 of adulthood to avoid progeny contamination. At day 3 of adulthood, 5 worms were lined up side by side on a NGM plate spotted with 10 µL of 10 mM levamisole to induce paralysis. Worms were photographed as described above, and ImageJ (ImageJ Software, Bethesda Maryland USA, http://imagej.nih.gov/ij/) was used to apply the triangle method as a means to set an automatic color threshold. Particle analysis was then used to count the number of aggregates of 50 worms per condition in independent biological triplicates (125,190,191).

Paralysis assay

Synchronous Q35::YFP animals were cultured on control or treatment plates as indicated. Worms were picked to new plates daily until day 5 of adulthood to avoid progeny contamination. Paralysis was determined by transferring 100 live worms per condition, in biological duplicates, to a corresponding fresh plate and observing movement within 5 minutes. Worms that did not move within that time frame were scored as paralyzed.

Statistical analyses

Statistical analyses were carried out with GraphPad Software (GraphPad Software, La Jolla California USA, http://www.graphpad.com) using ANOVA followed by the Bonferroni post-hoc test. Error bars are representative of standard deviation between independent biological replicates as indicated.

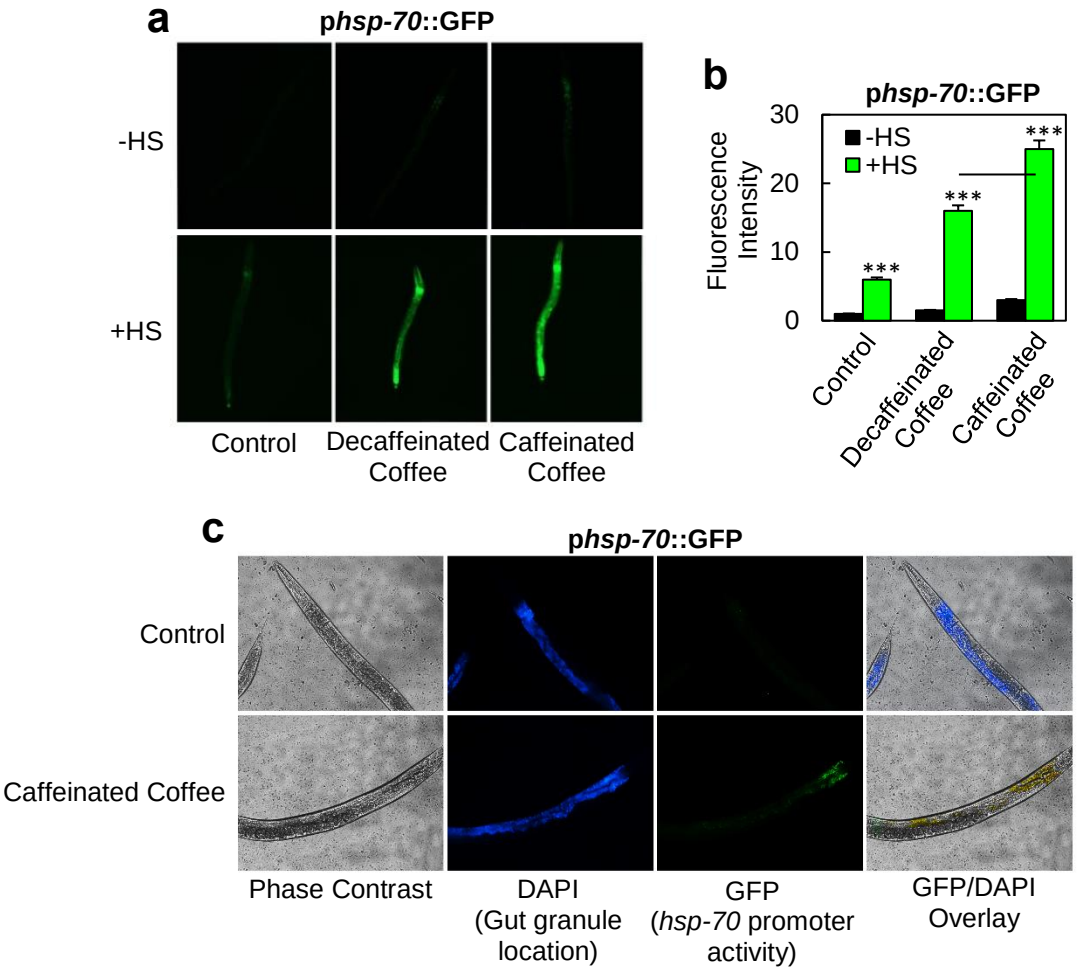

Figure 3.1. Treatment with coffee extract enhances HS-induced *hsp-70* promoter activity. (**a**) Fluorescent images are shown of synchronous p*hsp-70*::GFP nematodes left untreated (control), or subjected to treatment with decaffeinated and caffeinated coffee extract (added at a 10% vol/vol to NGM plates), from the L1 larval stage to the L4 larval stage prior to treatment with or without a 33°C 15 minute heat shock (HS) followed by a 12 hour recovery. (**b**) The GFP intensity of 50 worms given the same treatment conditions in (**a**) was quantified using ImageJ and significance was determined using the Bonferroni post-hoc test compared to the control and between treatment conditions. * $p < 0.05$, *** $p < 0.001$. (**c**) Treatment with caffeinated coffee extract results in localized p*hsp-70*::GFP expression. Phase contrast, DAPI, GFP, and DAPI/GFP overlay images of p*hsp-70*::GFP worms left untreated or subjected to treatment with caffeinated coffee extract are shown in order to compare tissue specific *hsp-70* promoter activation to the location of gut granules.

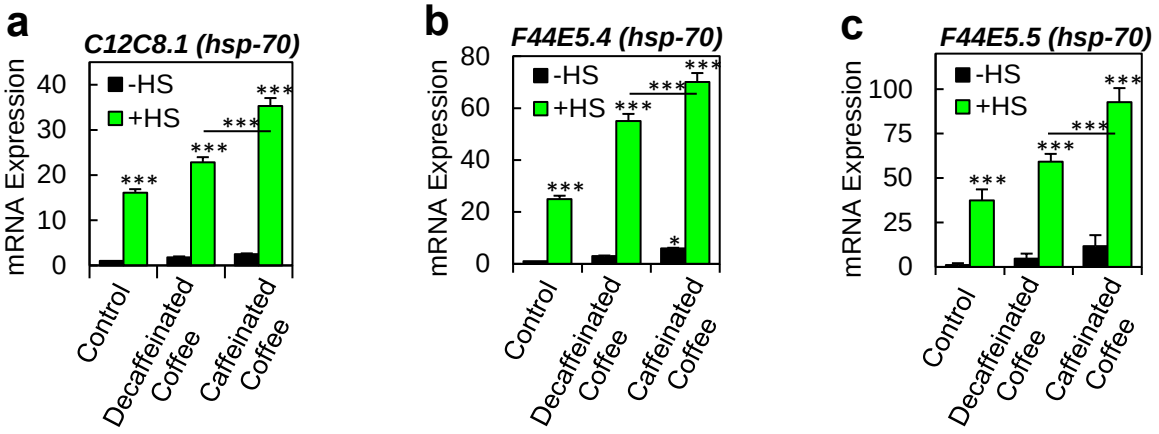

Figure 3.2. Treatment with caffeinated coffee extract enhances *hsp-70* mRNA expression in a dose-dependent manner greater than decaffeinated coffee. (**a-c**) mRNA expression for the *hsp-70* genes *C12C8.1*, *F44E5.4*, and *F44E5.5* was determined with qRT-PCR using synchronous wild-type worms left untreated (control), or subjected to treatment with decaffeinated and caffeinated coffee extract (added at a 10% vol/vol to NGM plates), from the L1 larval stage to the L4 larval stage prior to treatment with or without a 33°C 15 minute heat shock (HS) followed by a 15 minute recovery. Results are representative of technical duplicates from biological triplicates, and significance was determined using the Bonferroni post-hoc test compared to the control and between treatment conditions. * $p < .05$, *** $p < 0.001$.

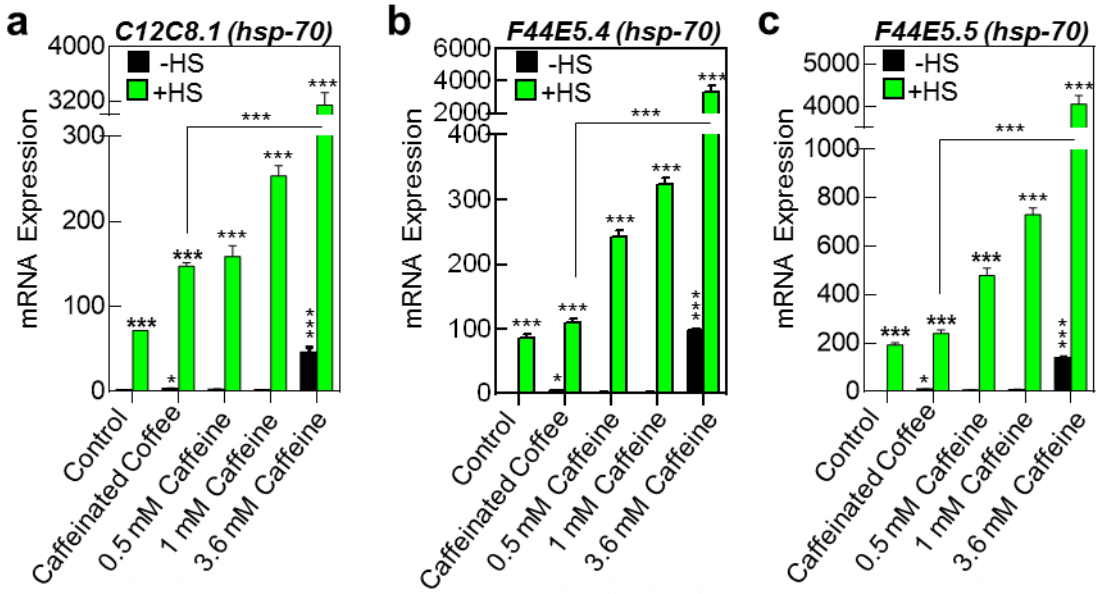

Figure 3.3. Treatment with pure caffeine enhances *hsp-70* mRNA expression greater than caffeinated coffee extract in a dose-dependent manner. (**a-c**) mRNA expression for the *hsp-70 genes C12C8.1, F44E5.4,* and *F44E5.5* was determined with qRT-PCR using synchronous wild-type worms grown on standard plates left untreated (control), and plates supplemented with caffeinated coffee extract (for comparison) or various doses of pure caffeine, as indicated, from the L1 larval stage to the L4 larval stage before treatment with or without a 33°C 30 minute heat shock (HS) followed by a 15 minute recovery. The amount of caffeine previously found to be present in the protocol we used to obtain our caffeinated coffee extract is 3.6 mM. Results are representative of technical duplicates from biological triplicates, and significance was determined using the Bonferroni post-hoc test compared to the control and between treatment conditions. * $p < 0.05$, *** $p < 0.001$.

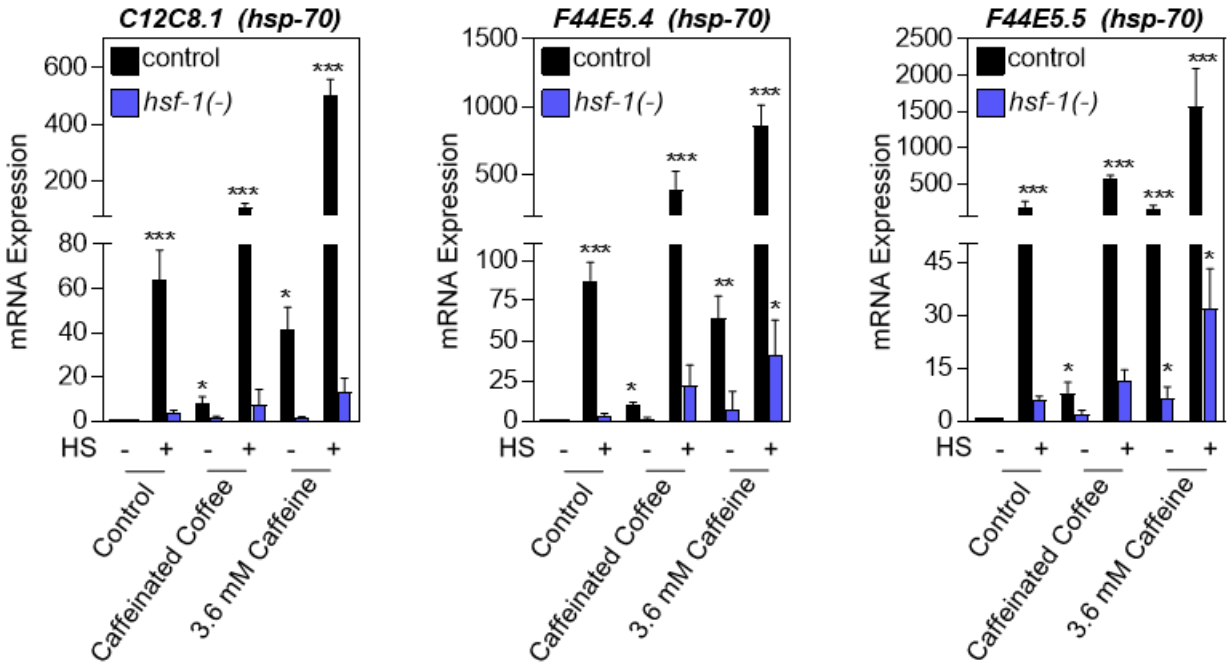

Figure 3.4. Induction of *hsp-70* mRNA expression in response to treatment with caffeinated coffee extract and caffeine is dependent on HSF-1. mRNA expression for the *hsp-70* genes *C12C8.1*, *F44E5.4*, and *F44E5.5* was determined with qRT-PCR using synchronous wild-type worms grown on RNAi plates fed empty vector RNAi (control) or *hsf-1* RNAi to knockdown gene expression. Worms were then left untreated (control) or grown on plates supplemented with caffeinated coffee extract (added at a 10% vol/vol to NGM plates) or 3.6 mM pure caffeine, as indicated, from the L1 larval stage to the L4 larval stage before treatment with or without a 33°C 30 minute HS followed by a 15 minute recovery. Results are representative of technical duplicates from biological triplicates, and significance was determined using the Bonferroni post-hoc test compared to the control and between treatment conditions. * $p < 0.05$, **<0.01, *** $p < 0.001$.

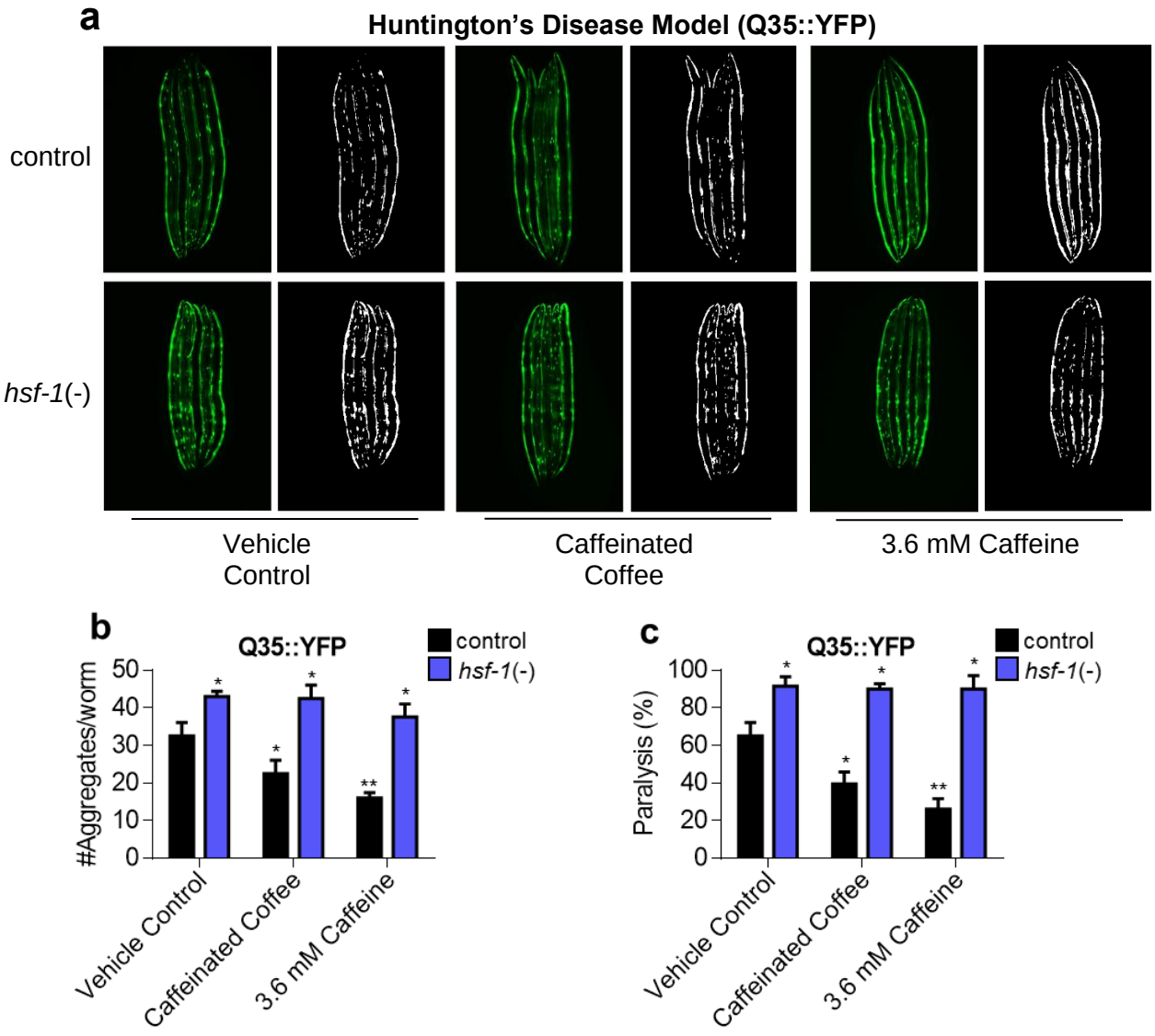

Figure 3.5. Treatment with caffeinated coffee extract and 3.6 mM pure caffeine promotes proteostasis in a *C. elegans* Huntington's disease model in an HSF-1-dependent manner. (**a**) Polyglutamine aggregates in a *C. elegans* Huntington's disease model are suppressed upon treatment with caffeinated coffee extract and caffeine. Fluorescent images and threshold-adjusted images (black and white) are shown of synchronous worms expressing 35 polyglutamine tracts fused to YFP (Q35::YFP) under the control of a muscle promoter that were grown on RNAi plates with empty vector RNAi (control) or *hsf-1* RNAi. Worms were left untreated (control), or subjected to treatment with caffeinated coffee extract (added at a 10% vol/vol to NGM plates) or 3.6 mM pure caffeine from the L1 larval stage until day 3 of adulthood. (**b**) Quantification of polyglutamine aggregates. Aggregates were scored with ImageJ particle analysis using the threshold-adjusted images from (**a**) for 50 worms per condition in biological triplicates. (**c**) Treatment with caffeinated coffee extract and 3.6 mM caffeine prevents paralysis in a *C. elegans* Huntington's disease model. Worms given the same treatment conditions in (**a**) were grown until day 5 of adulthood and a worm was considered paralyzed if no movement was observed in 1 minute for 100 worms per condition in biological duplicates. Significance was determined using the Bonferroni post-hoc test compared to the control and between treatment conditions. * $p < 0.05$, **<0.01.

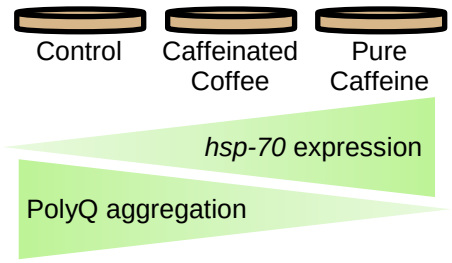

Figure 3.6. Summary of the effects of caffeinated coffee extract and pure caffeine on the heat shock response and proteostasis in *C. elegans*. In this study, we have found that *C. elegans* treated with caffeinated coffee extract and pure caffeine induce *hsp-70* mRNA expression upon treatment alone, and in combination with HS, in an HSF-1-dependent manner. The level of induction of *hsp-70* mRNA expression observed in response to treatment with caffeinated coffee extract and pure caffeine treatment corresponds to the extent of polyglutamine aggregate suppression and paralysis observed in a *C. elegans* Huntington's disease model. We therefore conclude that moderate caffeine consumption may promote proteostasis through induction of the HSR.

CHAPTER 4. DBC1/CCAR2 AND CCAR1 ARE HIGHLY DISORDERED PROTEINS THAT HAVE EVOLVED FROM ONE COMMON ANCESTOR

Authored by Jessica Brunquell, Jia Yuan, Aqeela Erwin, Sandy D. Westerheide, and Bin Xue

Published in Biomedical Research International: Brunquell, J., et al. (2014). "DBC1/CCAR2 and CCAR1 Are Largely Disordered Proteins that Have Evolved from One Common Ancestor." Biomed Res Int 2014: 418458.

Data analyses were performed by J. Yuan, A. Erwin, and B. Xue. J. Brunquell and B. Xue performed figure generation. The manuscript was written by J. Brunquell, S.D. Westerheide, and B. Xue. See Appendix H for copyright permission.

Abstract

Cell cycle and apoptosis regulator 2 (CCAR2, DBC1) is a predominantly nuclear, multi-domain protein, that modulates gene expression by inhibiting several epigenetic modifiers. For example, CCAR2 regulates chromatin remodeling through the inhibition of the deacetylases SIRT1 and HDAC3, and the methyltransferase SUV39H1. CCAR2 shares many highly-conserved protein domains with its paralog cell cycle and apoptosis regulator 1 (CCAR1). In this study, we examined the full-length sequential and structural properties of CCAR2 and CCAR1 from multiple species, and correlated these properties with the evolutionary path of these proteins. Our data confirms that the conserved domains shared between CCAR2 and CCAR1 have similar structures, as well as similar patterns of disorder. Our data suggests that CCAR2 emerged later in evolution than

CCAR1. CCAR2 contains regions that exhibit less conservation across species as compared to the same regions in CCAR1, suggesting a continuously evolving scenario for CCAR2. Additionally, our analyses indicate similarities between CCAR2, CCAR1, and the nematode protein lateral signaling target 3 (LST-3). Altogether, this study suggests that CCAR1 evolved from LST-3, and that CCAR1 underwent a duplication event to evolve into modern day CCAR2. This study provides insight into the structure and evolution of CCAR2 and CCAR1, which may impact future studies on the biological functions of these proteins.

Introduction

Cell cycle and apoptosis regulator 1 (CCAR1) and 2 (CCAR2) are emerging as important regulators of a variety of physiological processes. CCAR2 regulates gene expression by inhibiting the chromatin modifying deacetylases SIRT1 and HDAC3, and the methyltransferase SUV39H1 (73,192-194). As a result, CCAR2 regulates a variety of cellular processes including aging, metabolism, apoptosis, and stress response pathways (67,73,194-197). CCAR2 studies are currently expanding to uncover new interacting partners and roles in other biological processes.

CCAR1 is the paralog of CCAR2 that was originally identified as a mediator of apoptosis in a process that involves sequestration of 14-3-3 and altered expression of multiple cell-cycle regulatory genes (195,196,198). CCAR1 also binds to a mediator complex and enhances the transcription of estrogen receptor and glucocorticoid receptor target genes, while also acting as a co-activator of p53-dependent transcription (199). Additionally, CCAR1 cooperatively binds to CCAR2 and synergistically enhances

estrogen receptor function (200). Thus, similarly to CCAR2, CCAR1 regulates a variety of cellular processes, and functions together with CCAR2 in some cases.

The domains of CCAR2 and CCAR1 are important for their functions. CCAR2 and CCAR1 share many of the same functional domains including an S1-Like domain and a nuclear localization signal (NLS) on the N-terminus, a Leucine zipper (LZ) domain and a Nudix domain that are centrally located, and an EF-Hand domain and coiled-coil segments on the C-terminus (196,200,201). However, experimental evidence regarding the specific functions of the S1-Like, Nudix, and EF-Hand domains for both CCAR2 and CCAR1 have not yet been determined.

The N-terminus of CCAR2 (aa1-264) is the region where most of the currently known protein-protein interactions have been mapped. The S1-Like domain was originally identified in the ribosomal protein S1. Proteins that contain homology to this domain typically have RNA binding capabilities, suggesting evolution from an ancient nucleic acid binding protein (202). The NLS is an important site for regulation via post-translational modifications, where acetylation can disrupt CCAR2 translocation into the nucleus and ultimately inhibit nuclear interactions (203). The LZ is a structural motif that functions as a dimerization domain, and can bind to DNA to regulate gene expression in CCAR2, but it is likely non-functional in CCAR1 (204). CCAR2 interactions with epigenetic modifiers, nuclear receptors, and mRNA splicing components all take place within the N-terminal area (73,192-194,200,203). The CCAR2/SIRT1 interaction has been highly studied due to the important role that CCAR2 plays in inhibiting the epigenetic modifications that are regulated by SIRT1. Conflicting data points to either the LZ of CCAR2 (aa243-264) (73,77,200,205) or the N-terminal amino acids 1-240 as being critical for this interaction

with SIRT1 (203). The N-terminus has therefore been implicated in a majority of CCAR2 regulated processes.

The central region of CCAR2 and CCAR1 contains a Nudix domain that is catalytically inactive due to the absence of key amino acid residues within the catalytic site. However, it has been suggested to play a role in sensing NAD products of the SIRT1 deacetylase reaction (196). The SAP domain, specific to CCAR1, is also centrally located. This domain shares homology with a DNA-binding motif commonly found in a diverse set of nuclear proteins that are typically involved in chromosomal organization (206). The central region of CCAR1 and CCAR1 is therefore not known to be involved in many interactions.

The C-terminus of both CCAR2 and CCAR1 contains an EF-Hand domain and coiled-coil segments. EF-Hand domains bind to calcium ions and regulate gene expression but, similar to the Nudix domain, the EF-Hand of CCAR2 and CCAR1 may not be functional (195). Both proteins also contain a coiled-coil segment in the C-terminus, with an extra coiled-coil segment present in CCAR1. Coiled-coil regions are known to contain important protein interaction motifs (207). The coiled-coil region of CCAR2 has been shown to interact with only one protein thus far, the circadian cycle nuclear receptor Rev-erbα. Overexpression of CCAR2 can enhance the stability and expression of Rev-erbα, ultimately affecting circadian oscillations and metabolism (208). Coiled-coil segments are typically protein interactions motifs, thus there are likely more roles for the C-terminus of both CCAR2 and CCAR1.

The presence of highly-conserved domains shared between CCAR2 and CCAR1 indicates that CCAR2 and CCAR1 may have evolved from one common ancestor. Corresponding to this, an evolutionary connection between CCAR2 and CCAR1 has been

reported in the large ortholog database OrthoDB (209). Also, CCAR2 and CCAR1 are predicted to be intrinsically disordered as demonstrated in the D2P2 database of predicted disordered proteins (210). As shown by previous studies on other proteins (211-220), evolutionary analysis that takes protein intrinsic disorder into account can uncover segments that are critical for protein function (221-223). We were therefore interested in evaluating the detailed evolutionary path that CCAR2 and CCAR1 have taken, and the factors that have influenced their evolutionary path in order to add to the current knowledge base of these two proteins.

In this study, we have predicted the structural properties of CCAR2 and CCAR1, and our findings support the function of both proteins in many protein-protein interactions due to the high occurrence of disordered residues in each protein. Phylogenetic analysis predicts that both CCAR2 and CCAR1 evolved from one common ancestor, the nematode protein LST-3. Collectively, this study provides insight into the future studies of CCAR2 and CCAR1 by evaluating both evolution and structure.

Results

CCAR2 and CCAR1 are intrinsically disordered proteins with a similar domain structure and a similar pattern of predicted intrinsic disorder

Human CCAR2 (hCCAR2) and human CCAR1 (hCCAR1) have ~30% sequence similarity to one other, and share multiple highly-conserved domains. Figure 4.1 shows the sequential locations of the functional domains for both proteins, and indicates the known or predicted functions of the domains, and Table 4.1 lists the predicted or known function of each domain. The sequence alignment of each domain is provided in Figure C1 and Figure C2 (see Appendix C). The size difference between CCAR2 and CCAR1 is

the result of three segments found in hCCAR1 that hCCAR2 lacks, including an elongated N-terminal disordered region, a SAP domain, and an extra coiled-coil segment in its C-terminus (CC1).

In order to compare the similarities in conformational properties between hCCAR2 and hCCAR1, the degree of predicted protein intrinsic disorder of these two proteins were analyzed (Figure 4.2). While 41% of hCCAR2 is composed of disordered residues, 61% of residues are disordered in hCCAR1. As expected, a majority of the functional domains listed in Figure 4.1, including the S1-Like, LZ, Nudix, and EF-Hand, are located in the structured segments of both proteins. The domains that are intrinsically disordered, or have a high degree of structural flexibility as indicated by higher disorder score, are the NLS and coiled-coil segments on hCCAR2 and hCCAR1, as well as the SAP domain that is specific to hCCAR1. The predicted 3D structures of these functional domains indicate that many of these domains are structured and have limited flexibility.

Analysis of the disorder curves on the C-terminal residues (~400aa) of hCCAR2 and hCCAR1 indicates a high degree of similarity on the curve of predicted protein intrinsic disorder in this region, thereby suggesting a similar conformational fluctuation and further functional role (Figure 4.2, shaded region). Corresponding to this finding, a sequence alignment between these two regions shows 30% sequence identity, indicating evolutionary conservation (Figure C3, see Appendix C). The high degree of similarity between the structure of the conserved domains in hCCAR2 and hCCAR1, along with the similarity in the C-terminal region, leads to the presumption that hCCAR2 and hCCAR1 may share a common molecular origin.

In addition to hCCAR2 and hCCAR1, we determined the sequence level of intrinsic

disorder from other species using a CH-CDF plot. We carried out CH-CDF analysis for all of the proteins in our dataset, and found that all CCAR2 and CCAR1 proteins have large negative values (<-0.1) on CDF distance, indicating that these proteins are mostly intrinsically disordered (Figure 4.3). In terms of CH distances, CCAR1 and CCAR2 proteins have varying distributions. Most CCAR1 proteins have a positive CH distance, while all CCAR2 proteins have a negative CH distance. Detailed analysis indicates that many groups have localized distribution on this CH-CDF plot, such as amphibian CCAR1 and bird CCAR1. Mammalian CCAR1 proteins have the broadest distribution on CH distance, followed by CCAR1 proteins from aquatic animals. Compared to mammalian CCAR2 proteins, mammalian CCAR1 proteins are more scattered in the CH-CDF plot, indicating more structural variability. Therefore, based on the algorithms of CH and CDF distance, it can be concluded that most CCAR1 proteins have extra charged residues, while almost all CCAR2 proteins are more structure-prone.

Human CCAR2 shares common ancestry with the nematode CCAR1 ortholog LST-3

To study the evolutionary relationship between CCAR2 and CCAR1, phylogenetic analysis was performed with the CCAR2 homologs and paralogs listed in Table C1 (see Appendix C), and the results are shown in Figure 4.4. Most mammals have evolved to incorporate both CCAR2 and CCAR1 into their genomes (Figure 4.4. purple shaded region). As a comparison, insects and nematodes have only incorporated CCAR1 into their genomes (Figure 4.4. light and dark blue shaded regions). Interestingly, the first known evolutionary appearance of CCAR2 is in zebrafish (Figure 4.4. pink shaded region). This is a clear indication that CCAR2 emerged later than CCAR1. Another

interesting observation is that the nematode LST-3 proteins are more closely related to CCAR1 in lower species, such as insects. These observations have revealed an interesting evolutionary picture of CCAR2/CCAR1/LST-3, where CCAR2 has evolved from CCAR1, and CCAR1 originated from LST-3.

To compare homology between nematode LST-3 and hCCAR2/hCCAR1, a cross-validation between the nematode proteome and the human proteome was performed. Specifically, the nematode *Caenorhabditis elegans* protein LST-3 was aligned against the complete human proteome and the only two significant hits (E value < 1.0e-20) were hCCAR2 and hCCAR1. Conversely, both hCCAR2 and hCCAR1 protein sequences were aligned against the complete *C. elegans* proteome, and the only significant hit was LST-3. This result shows that the only possible ancestor of CCAR2 and CCAR1 in higher species is nematode LST-3.

To further explore the evolutionary path of LST-3, CCAR1, and CCAR2, we compared the full-length sequences of *C. elegans* LST-3, zebrafish CCAR1 (zCCAR1), and zebrafish CCAR2 (zCCAR2), as the first emergence of CCAR2 is in zebrafish. The resulting gapped-disorder curve of this comparison is shown in Figure 4.5. A gapped disorder curve aligns proteins by the shape of the curve based on the disorder score. Instead of presenting the actual sequence similarity, the gapped disorder curve describes the overall similarity of the flexibility of the protein segments, which indicates any evolutionary gaps that may be present between proteins (224-226).

The structural similarities shared between zCCAR2, zCCAR1, and LST-3 include a structured segment present at aa200 (Figure 4.5, shaded area 1), a similar disordered curvature spanning from aa200-400 (Figure 4.5, shaded area 2), the fluctuating peaks

from aa500-600, and the increasingly disordered C-termini beginning at aa1100 and continuing to the end of the proteins (Figure 4.5, shaded area 3). The N-termini of zCCAR2 and LST-3 have two gapped regions (pink lines) that are located immediately before and after the S1-Like domain. zCCAR1 contains two other gapped segments similar to zCCAR2, one near the center of the protein that corresponds to the conserved Nudix domain, and another on the C-terminus that does not correspond to a well-defined functional region. When compared to either zCCAR1 or LST-3, zCCAR2 contains four additional gapped regions, thus indicating a difference of four insertions or deletions throughout evolution. The locations of these insertions and deletions are roughly in line with the gapped segments in the sequence alignment provided in Figure C4 and Figure C5 (see Appendix C).

CCAR2 is more conserved than CCAR1

The conservation of the genomic neighborhood (CGN) of CCAR2 and CCAR1 was calculated for mammals, birds, insects, reptile, amphibians, and fish (Figure 4.6). The CCAR2 gene is not present in birds, insects, or amphibians, but in the species where CCAR2 gene is present, the CGN score of the CCAR2 gene for that species is higher than that of CCAR1. This is another indication that the genomic region surrounding the CCAR1 gene is less conserved than the CCAR2 gene.

Two synteny plots comparing the human and mouse genes for CCAR2 and CCAR1 are illustrated in Figure 4.7. In these plots, more conserved genes can be found in the neighboring region of CCAR2 as compared to CCAR1, also indicating that CCAR2 is more conserved than CCAR1.

CCAR1 appeared before CCAR2 in evolution

To further examine the variability of insertions and deletions in CCAR2 and CCAR1, the amino acid substitution rate of each conserved domain across various groups of species was analyzed (Figure 4.8). The overall mutation rate for CCAR1 is approximately 20% from amphibian to human, while CCAR2 has a relatively high substitution rate of about 50% from insect to mammal and 30% from *Therapsida* to primate. Even after CCAR2 becomes more conserved after *Therapsida*, the substitution rate of various domains in CCAR2 is still approximately 10% higher than that of the corresponding CCAR1 domains. Also, the mutation rate of each domain for CCAR2 in fish is similar to that of insects for CCAR1, indicating a similar trend during the beginning of the evolutionary process between both proteins, with CCAR1 evolving first.

Examination of each domain individually reveals that the evolutionary process has varied between both proteins. Interestingly, the fish CCAR2 protein contains a SAP domain that then disappears from amphibian and onward. The remaining S1-Like, NLS, LZ, Nudix, and CC2 domains continue to have high mutation rates from fish to amphibian, while the EF-Hand domain remains relatively conserved. Variation continues to be observed between all domains until a gradual steadying of mutation rates occurs in *Therapsida* and continues until human.

The mutation rate of each domain in CCAR1 exhibits a different trend. The mutation rate of the S1-Like, LZ, EF-Hand, SAP, NLS, and CC2 domains in CCAR1 varies from insects to fish, while the mutation rate between all domains decreases from fish to amphibian. Limited changes occur from amphibians to mammals in all domains except for the NLS and CC1 domains, where the mutation rate decreases more dramatically.

This is followed by a further increase in mutation rates in all domains from mammals to *Therapsida*, with an eventual leveling off of the mutation rates in humans. This data further supports CCAR1 appearing first in evolution, not only by appearing in insects before CCAR2, but also by becoming conserved much earlier in evolution.

CCAR2 and CCAR1 exhibit similar domain flexibility

To determine if the mutation rate of each domain has affected protein structure and flexibility in the evolutionary process, the average disorder score of each domain across different species was compiled (Figure 4.9). The overall disorder scores between the various domains of CCAR2 and CCAR1 are very similar. The NLS and CC2 domains are disordered in both proteins, while the Nudix, S1-Like, EF-Hand, and LZ are ordered domains. Also, the SAP domain in CCAR2 that is only present in fish is highly disordered, corresponding with the intrinsic disorder of the SAP domain throughout CCAR1 evolution. Even though this overall similarity in structure exists, differences can be seen in the trend of intrinsic disorder across evolution between each domain in CCAR2 and CCAR1. The S1-Like, Nudix, LZ, and EF-Hand domains in CCAR1 tend to become less structured throughout evolution, while in CCAR2 the same domains become more structured.

During the evolutionary process, it appears that some domains underwent a drastic change in structural flexibility that is measured by predicted disorder score. In CCAR2, the S1-Like and LZ domains decreased in structural flexibility from fish to amphibian, whereas the opposite trend is observed in CCAR1. The NLS and CC2 domains of CCAR2 tend to drastically change in structural flexibility where a vibration pattern can be observed, before eventual leveling off into a disordered structure in primates, and carrying over into humans. In CCAR1, structural flexibility has increased in the SAP domain from

fish to amphibian, The NLS domain had a sudden decrease in structural flexibility from mammals to *Therapsida,* before increasing from primate to human.

Discussion

CCAR2 and CCAR1 are emerging as important regulators in a number of cellular pathways. CCAR2 and CCAR1 share a similar domain structure, indicating they may have similar biological functions. The similar domain structure shared between the two multi-domain proteins may also indicate origination from a common ancestor (227). Therefore, it is important to investigate the process by which the functional domains of these two proteins have evolved. We predict here for the first time that CCAR2 and CCAR1 are comprised of mostly intrinsically disordered regions, and that several of the functional domains in these two proteins are intrinsically disordered. These findings provide support for the role of these two proteins in many molecular interactions, as intrinsically disordered regions are frequent sites for protein-protein interactions (228). In our prediction, the extended N-terminus of CCAR1 is much more flexible than that of CCAR2, as denoted by a higher disorder score, which may indicate a unique functional role for this region. Corresponding to this, CCAR1 has recently been shown to have distinct functions apart from CCAR2, such as binding directly to the LZ domain of CCAR2 and synergistically regulating the function of CCAR2 (200). This regulatory ability would require a unique region capable of binding directly to CCAR2, which our analysis suggests may be on the N-terminal domain.

It is often found that two protein paralogs develop throughout evolution from one common ancestor (229). Supporting this notion, our analysis of CCAR2 and CCAR1 from multiple species has established evidence that both proteins have evolved from one

common nematode ancestor, LST-3. We have shown that CCAR1 first appears in insects, while CCAR2 first appears much later in fish. Further supporting this claim is the fact that the CCAR2 protein in fish is the only species in which CCAR2 contains a SAP domain, a domain typically only found in CCAR1 proteins.

The SAP domain is a DNA/RNA binding domain with about 40 amino acids. The core structure of this domain is a two- or three-helix bundle. There are currently two x-ray structures of SAP domains in the PDB, however, in these two x-ray structures, the SAP domains are in complexes with other proteins and RNA. Therefore, these two x-ray structures of SAP domains cannot be used to assess the actual structural flexibility of the SAP domain by itself. There are also several other NMR structures for SAP domains in the PDB database. From these structures, the SAP domain has huge structural flexibility. The RMSD values of structural alignment between these structures from different NMR experiments are very large. Therefore, results from NMR experiments provide evidence that the SAP domain is flexible. In addition, the length of the SAP domain is less than 40 amino acids, indicating that the SAP domain may not have enough hydrophobic interaction by itself. Furthermore, in our prediction, the SAP domain is likely to be in a “dip” indicating a structure-prone tendency, however, this “dip” is flanked by two long disordered regions. Therefore, the possible 3D structural picture of the SAP domain is that this domain forms a small and flexible hydrophobic core, and sits in the middle of a long disordered region. The SAP domain of LST-3 was likely passed on to the fish CCAR2 protein in the early evolutionary history of CCAR2. Other species may not have required this particular domain in CCAR2, and hence continued to evolve without it. All of these

findings combined suggest that LST-3 is the common ancestor, and ortholog, to both CCAR2 and CCAR1.

A gapped disorder plot shows that zCCAR2 contains four additional gapped regions when compared to zCCAR1 and LST-3, indicating that a difference of four insertions/deletions and/or substitutions allowed for the first evolutionary appearance of CCAR2 in zebrafish. As mutation rate is linked to evolution, understanding the mutation rates of these proteins can help to decipher their evolutionary history. We see that CCAR1 emerges earlier in evolution in insects, and that it becomes relatively conserved by the amphibian period, except for the CC1 and the CC2 regions, which were still undergoing evolution. CCAR2, on the other hand, took much longer to become relatively conserved, and still has not yet reached the low mutation rate of CCAR1, indicating the possibility of acquiring new functional roles in the future evolutionary period. CCAR2 becomes relatively conserved in *Therapsida.* Taking into consideration that *Therapsida* appeared about 300 million years later than amphibians, this provides evidence that CCAR2 arose much later in evolution than CCAR1, further supporting the notion that a CCAR1 homolog gave rise to CCAR2 over time.

Domain-level analysis provides yet more information on the correlation between protein flexibility and evolution. The disorder scores for the NLS and CC2 domains in CCAR2 have undergone drastic changes in the evolutionary process. This may indicate the sudden acquisition of a hydrophobic core, and thus an increased protein-binding ability. However, since this new function may not be essential for the species, the acquired hydrophobic binding sites may disappear in the evolutionary process.

The LZ domain of CCAR2 has been implicated in a variety of regulatory processes.

The LZ domain is a heptad repeat of leucine residues, which represents the hydrophobic core of a coiled-coil formed by two different chains. The basic regions next to the LZ domain along the coiled-coil can interact with the major groove of DNA to regulate the process of gene expression. A substitution in heptad repeats from hydrophobic to less-hydrophobic, or hydrophilic and charged residues, will lessen the hydrophobic interaction and distort the structure of the coiled-coil, and thereby prevent DNA binding ability. Therefore, in order to retain the function of the LZ domain, all of the mutations on this domain should be hydrophobic-dominant and thus be more structure-prone with a lower disorder score. In CCAR2, the LZ domain tends to become more structure-prone. Conversely, the LZ in CCAR1 loses structure slightly from insect to fish. It is interesting to see this deviation since CCAR2 first appears in fish. The presence of CCAR2 in fish may have resulted in a decreased requirement for the LZ domain in CCAR1, ultimately affecting the current functional role of the LZ in modern CCAR2 and CCAR1. This same concept is also applicable to each the structured domains as well.

Overall, our data presents new findings on the structure and evolution of CCAR2 and CCAR1. Our findings support the function of both proteins in many protein-protein interactions due to the high occurrence of disordered residues. We have found an unstructured region on the N-terminus of CCAR1 that may be responsible for unique protein interactions independent of CCAR2. Similarly, we have determined that the LZ of CCAR2 may be involved in unique interactions, as the LZ of CCAR1 has become unstructured and possibly non-functional throughout evolution. We see that CCAR1 appeared much earlier in the process of evolution as compared to CCAR2, and that the nematode LST-3 protein may be the common ancestor of CCAR2 and CCAR1. As the

nematode *C. elegans* is a model organism frequently used in experimental biology, this work may help to broaden CCAR2 and CCAR1 studies by demonstrating the important role nematodes have had in the evolution of these two proteins. Specifically, the nematode LST-3 protein may have undergone multiple insertions and deletions to give rise to modern-day CCAR1 and CCAR2.

Methods

CCAR2 homologs and paralogs

BLASTP (230,231) was used to align the human CCAR2 (hCCAR2) protein sequence (UniProt ID: Q8N163) against the entire UniProt database (232). The obtained UniProt hits were filtered using a cutoff alignment score set at 10% of the hCCAR2-hCCAR2 alignment score based on trial and error. The 129 sequences that remained had a minimal sequence similarity of ~30% and a minimal sequence coverage of ~50% as compared to hCCAR2, complying with previous studies (233). After removing redundant sequences using BLASTClust and cutoff of 90% sequence identity, 93 sequences from 65 species were used for analysis (Table C1, see Appendix C). The 65 species include: mammals, birds, reptiles, amphibians, fish, insects, and nematodes. The proteins found include CCAR2, CCAR1, LST-3, and other undefined generic names. In addition, the complete proteomes of human, zebrafish, and *C. elegans* were downloaded from UniProt for comparative studies.

Disorder prediction

PONDR-FIT (234) and PONDR-VLXT (235) were employed to run disorder prediction analysis. The disorder scores from both PONDR-FIT and PONDR-VLXT were used to measure the flexibility of the amino acids in all of the proteins examined. PONDR-FIT is

one of the most accurate disorder predictors as it adopts the meta-predictor strategy. Meta-predictors are prevailing in the field of disorder prediction due to improved accuracy (234,236). Many state-of-the-art disorder predictors are meta-predictors (236-241). PONDR-FIT uses an artificial neural network to optimize the prediction results from six component predictors: PONDR-VLXT (235), PONDR-VSL2 (242,243), PONDR-VL3 (244,245), FoldIndex (246), IUPred (247), and TopIDP (248). PONDR-FIT improves the prediction accuracy significantly in various testing datasets compared to its component predictors (234). PONDR-VLXT is the first generation of disorder prediction software that is specifically designed to detect local flexibility of amino acid sequences. Although PONDR-VLXT is not the most accurate tool, it is still powerful due to its sensitivity to amino acid composition (234,249). PONDR-VLXT has been successfully applied in detecting linear interaction motifs (MoRFs) (250-252), which have proven to be extremely abundant in protein-protein interactions (228,253-255). The values of predicted disorder scores were applied to measure the structural flexibility of proteins and the combination of disorder scores from PONDR-VLXT, PONDR-FIT, and other predictors, has been applied in many studies in order to explore a broad range of biological questions. Examples of these studies include methionine oxidation (224), phosphorylation (256), p53 evolution (233), binding motifs (257), iPS transcription factors (224), PTEN interactions (256), the spliceosome (258), the structural flexibility of viral proteins (224), and evolution across species (257,259). In this manuscript, we have also used predicted disorder scores to measure the structural flexibility of whole protein sequences along with local regions.

CH-CDF analysis

The previously mentioned predictors were used to predict intrinsic disorder at a residue level. Intrinsic disorder can also be measured at the entire sequence level using a Charge-Hydropathy and Cumulative Distribution Function (CH-CDF) plot (239,260). A CH-CDF plot is composed using parameters from both a Charge-Hydropathy (CH) plot (261) and a Cumulative Distribution Function (CDF) plot (262). In each of these two plots, structured proteins and disordered proteins stay in different regions, and can be separated by a linear boundary line. The distance of a protein from the boundary line in each of them (dCH in CH plot and dCDF in CDF plot) describes the tendency of the protein for being structured or disordered. The sign of the distance (positive or negative) shows whether the entire protein is structured or disordered. The performances of these two individual plots are often complementary. Therefore, their combination improves the prediction accuracy at the sequential level to 90% (239,260). In the CH-CDF plot, the directional distance dCH in the CH plot is set as the y-axis, and the directional distance dCDF in the CDF plot is used as the x-axis. As dCH and dCDF both have positive and negative values, the entire CH-CDF plot can be split into four quadrants using dCH=0 and dCDF=0: (1) Q1, dCH>=0 & dCDF>=0; (2) Q2, dCH<0 & dCDF>=0; (3) Q3, dCH<0 & dCDF<0; and (4) Q4, dCH>=0 & dCDF <0. By definition, proteins in Q2 are predicted to be structured. Proteins in Q3 and Q4 are disordered. Proteins in Q1 have excessive charged residues but can be structured.

Three-Dimensional structure prediction

The 3D structure of the structured domains for both human CCAR2 and CCAR1 were built using HHpred (263), RaptorX (264), and I-TASSER (265). Each structured domain

has three predicted structures. The structure with the highest QMean score (266) was selected as the final predicted structure.

Phylogenetic analysis

Mega5 (267) was used to run multiple sequence alignments, and to analyze the phylogeny of the sequences. CLUSTALW was chosen to perform the multiple sequence alignment (default PAM matrix, Gap opening score 10, Gap extension score 0.1). Nearest-neighboring algorithm was selected to analyze the phylogenetic relations among the sequences. The final phylogenetic tree was obtained by bootstrapping 2000 times.

Genome neighborhood analysis

We calculated the conservation of genomic neighborhood (CGN) score (268,269) of both CCAR2 and CCAR1 for selected species, including mammals, birds, insects, reptiles, amphibians, and fish. When calculating the CGN score, all of the genes within a window of two million bases from the center of CCAR2 or CCAR1 of that species were extracted from GeneBank. The number of total genes in the window of the human genome was defined as M_{HS}, the number of common genes between human and another species X was counted as C_X, and then the CGN score of species X was calculated as $CGN_X = C_X / M_{HS}$. The human and mouse gene lists were also used to build a synteny plot (270-272).

Mutation rate analysis

The substitution rate between each group of domains between each species set is calculated as follows: (1) Two groups of sequences were aligned using CLUSTALW. (2) The domain structure of hCCAR1 was used to label the location of similar regions in all of the other sequences. (3) The amino acid of each sequence, on each site within a specific region, in the second group was compared with the amino acid sequence in the

first group. If no match was found, a substitution was recorded for this site. (4) This process was repeated for each group with step (3) for all of the sequences in the second group. The final substitution frequency is S_i for the i-th site. (5) The sum was calculated for all of the substitutions for the sites in the entire region to get the total substitution $\sum S_i$ (i=1,…,L), where L is the number of sites in this region. (6) For example, if there were M sequences in the first group and N sequences in the second group, the final substitution rate would be $\sum S_i / (M*N*L)$.

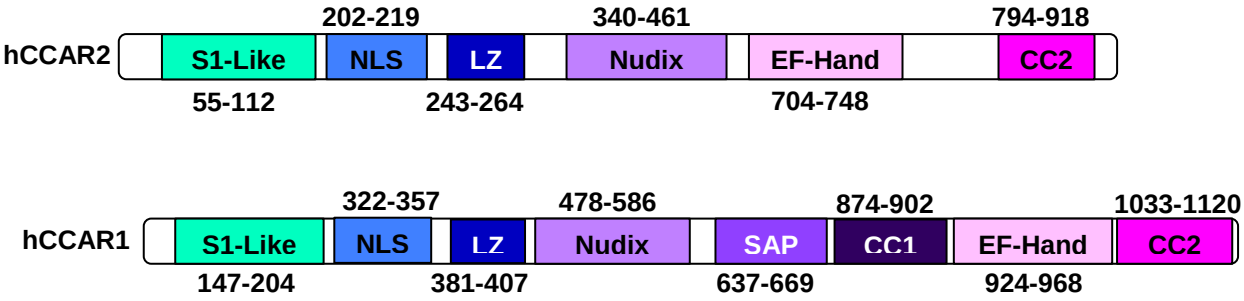

Figure 4.1. Human CCAR2 and CCAR1 are paralogs. The domains for human CCAR2 (hCCAR2) and human CCAR1 (hCCAR1) are depicted along with the amino acid boundaries for each domain.

Table 4.1. The domain function of human CCAR2 and CCAR1.

Domain Name	Domain Function
S1-Like	Homology to an RNA-binding domain.
NLS	Nuclear localization signal. Acetylation of the NLS in CCAR2 regulates nuclear localization.
LZ	Likely non-functional in CCAR1. Regulation of a diverse set of cellular pathways in CCAR2.
Nudix	Catalytically inactive hydrolase domain in CCAR2 and CCAR1. Predicted to function as a sensor in CCAR2 that may bind to NAD metabolites and regulate SIRT1.
SAP	Homology to a putative DNA-binding motif predicted to be involved in chromosomal organization.
EF-Hand	Inactive variant of a calcium dependent regulator of multiple cellular processes.
CC	Predicted protein-protein interaction motif.

The domains for hCCAR2 and hCCAR1 are listed along with their known or predicted function.

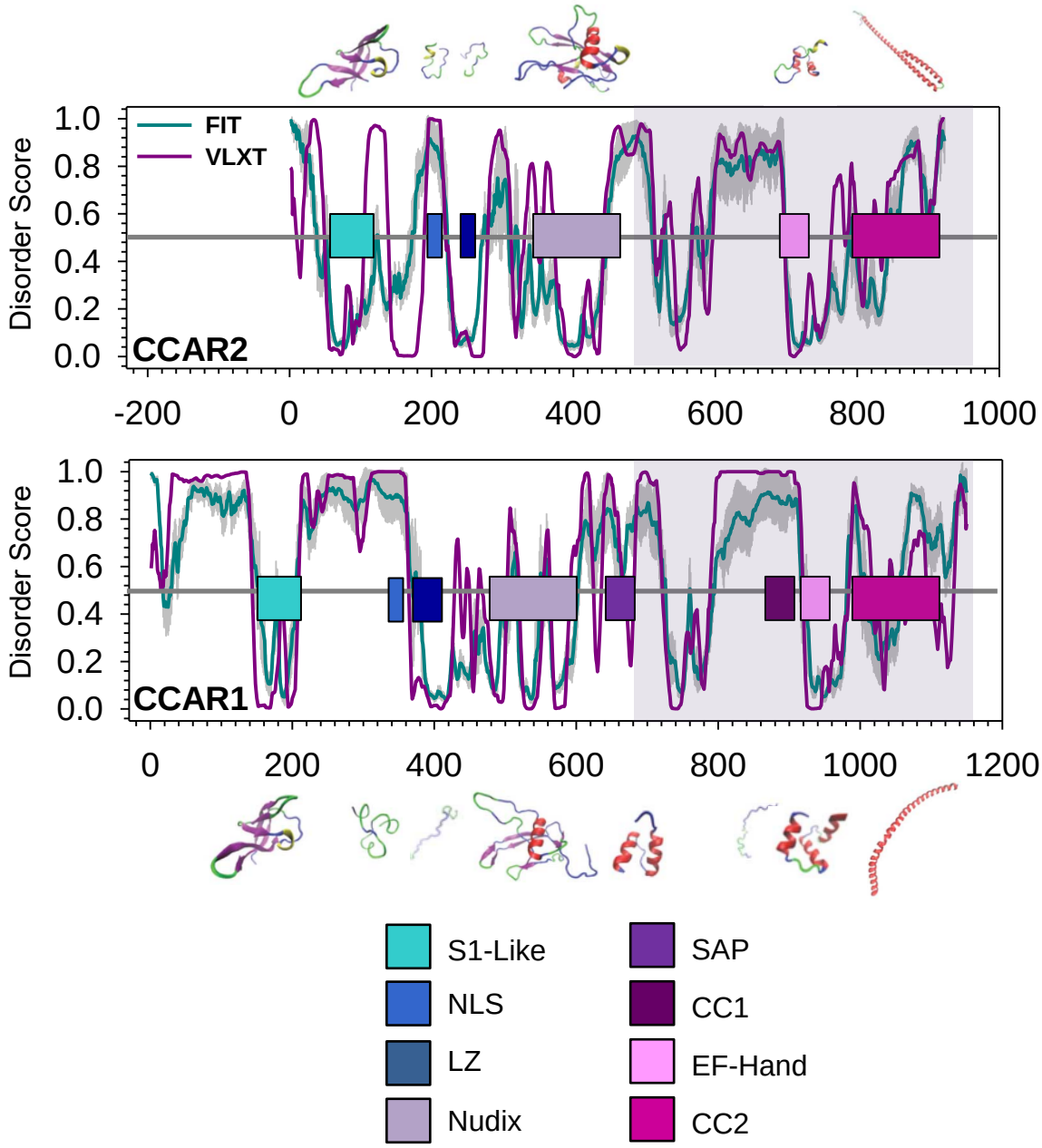

Figure 4.2. Disorder analyses show the domain structure and molecular flexibility of hCCAR2 and hCCAR1. The curves present the disorder score predicted by PONDR-FIT (FIT, dark cyan) and PONDR-VLXT (VLXT, dark pink). The x-axis of human CCAR2 (Hccar2, UniProtID: Q8N163) is shifted by 200 residues in order to align the C-terminus to human CCAR1 (hCCAR1, UniProtID: Q8IX12). The gray shadow behind PONDR-FIT represents the prediction of error. Residues with a score higher than 0.5 are disordered, while residues with a score lower than 0.5 are structured. The horizontal bars are the conserved functional domains identified in both proteins (S1-Like: aqua blue; NLS: medium blue; LZ: dark blue; Nudix: light purple; SAP: medium purple; CC1: dark purple; EF-Hand: light pink; CC2: dark pink). The predicted 3D structures are scaled roughly with their lengths.

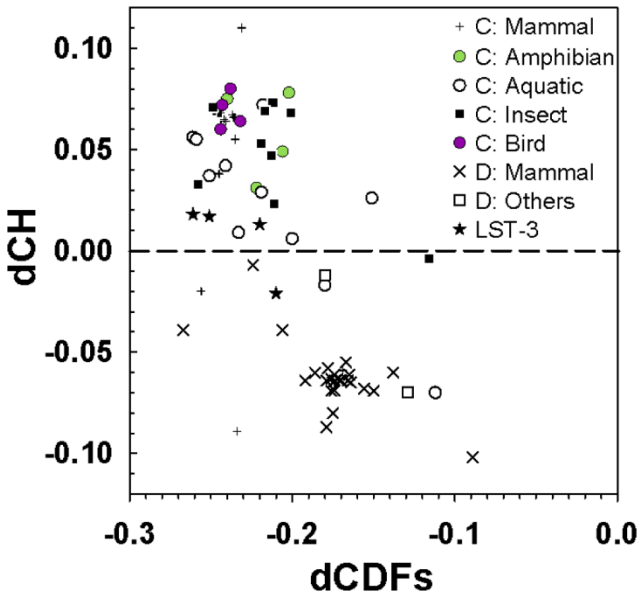

Figure 4.3. CH-CDF analysis for all CCAR2 and CCAR1 proteins. The x-axis and y-axis are the CDF and CH distances, respectively. The CDF distance is calculated from PONDR-VSL2 prediction. All CCAR2 proteins are split into two groups: mammal and others (as denoted by "D" in the legend). All CCAR1 proteins are arranged into six groups, including mammal, amphibian, aquatic animals, insect, and bird (as denoted by "C" in the legend). Nematode LST-3 proteins are in one group.

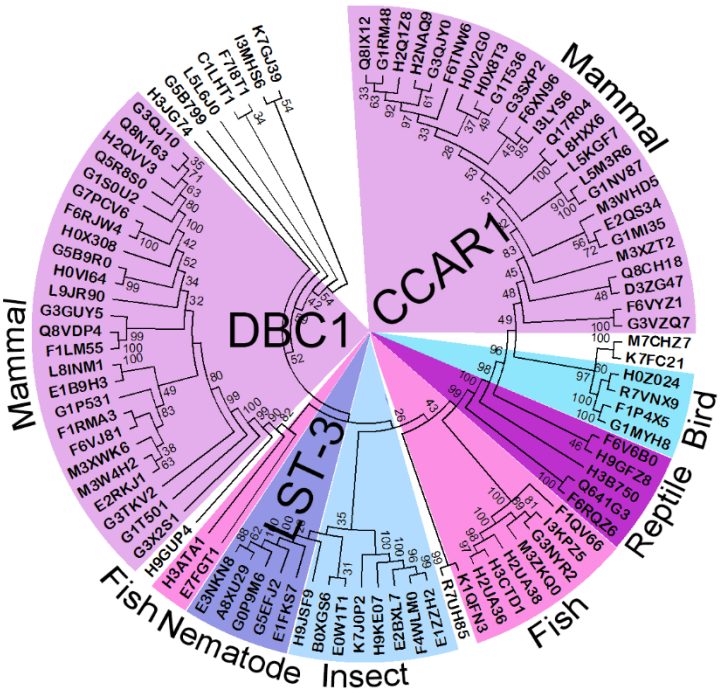

Figure 4.4. Phylogenetic analysis of CCAR2 and CCAR1 homologs. A phylogenetic tree was built for all 93 protein sequences in 65 species as listed in Table C1 using Mega5 software. The dashed lines split the tree into two parts: all CCAR2 proteins are on the left while all CCAR1 proteins are on the right. The nematode LST-3 proteins, although closely related to CCAR1, are categorized into a sub-group of CCAR1. The colored shadows cover several regions that are extensively discussed in the manuscript.

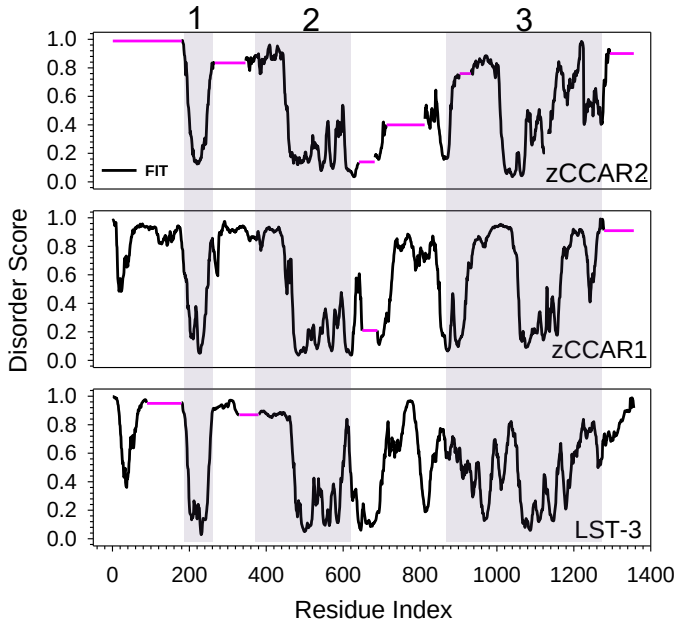

Figure 4.5. Gapped disorder prediction for zCCAR2, zCCAR1, and LST-3. The disorder prediction was analyzed by PONDR-FIT for zebrafish CCAR2 (zCCAR2, UniProt ID: E7FGT1), zebrafish CCAR1 (zCCAR1, UniProt ID: F1QV66), and *C. elegans* LST-3 (UniProt ID: G5EFJ2). Residues with a score higher than 0.5 on the -axis are disordered, while residues with score lower than 0.5 are structured. The -axis represents the amino acid number. The black line represents the disorder prediction, while the pink horizontal lines represent gapped segments. The shaded regions represent similar patterns seen between all three proteins.

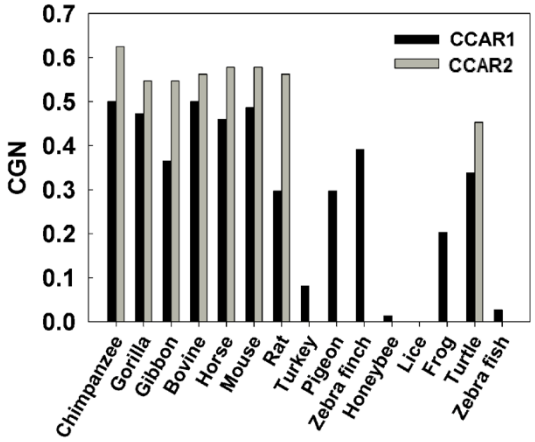

Figure 4.6. CGN score between human and other species for both CCAR1 (black) and CCAR2 (gray). A high CGN score of >0.5 indicates that more than half of the gene neighbors are conserved within 2 Mb and shows conservation of the local chromosomal environment, while a score of <0.5 indicates that less than half of the neighboring genes are conserved.

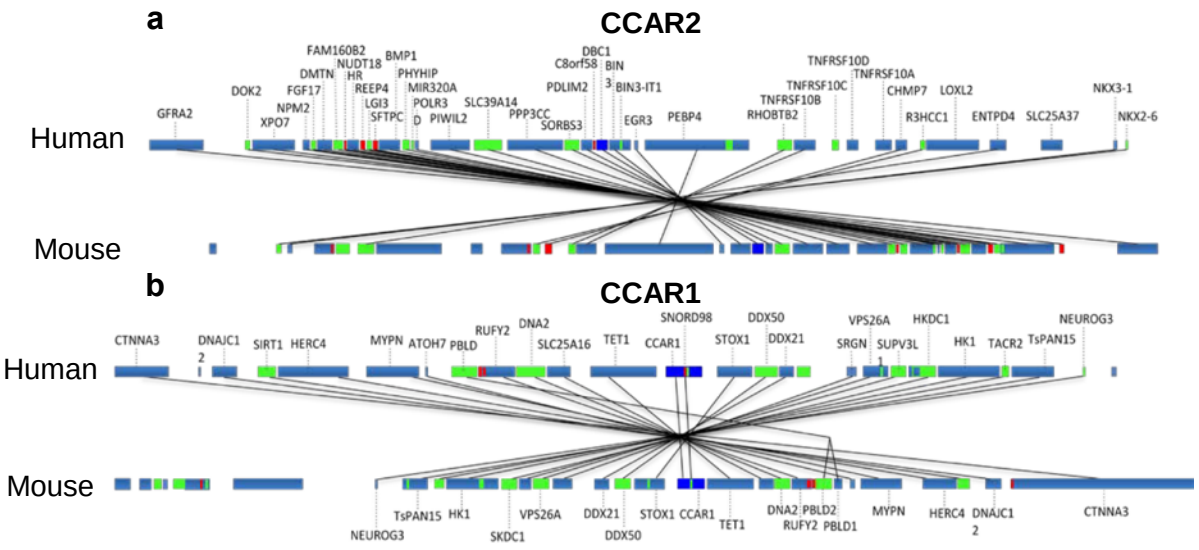

Figure 4.7. Genome neighborhood analysis between human and mouse CCAR2 (a) and CCAR1 (b). The lines connect identical genes from human and mouse, surrounding 2 Mb of either CCAR2 (a) or CCAR1 (b).

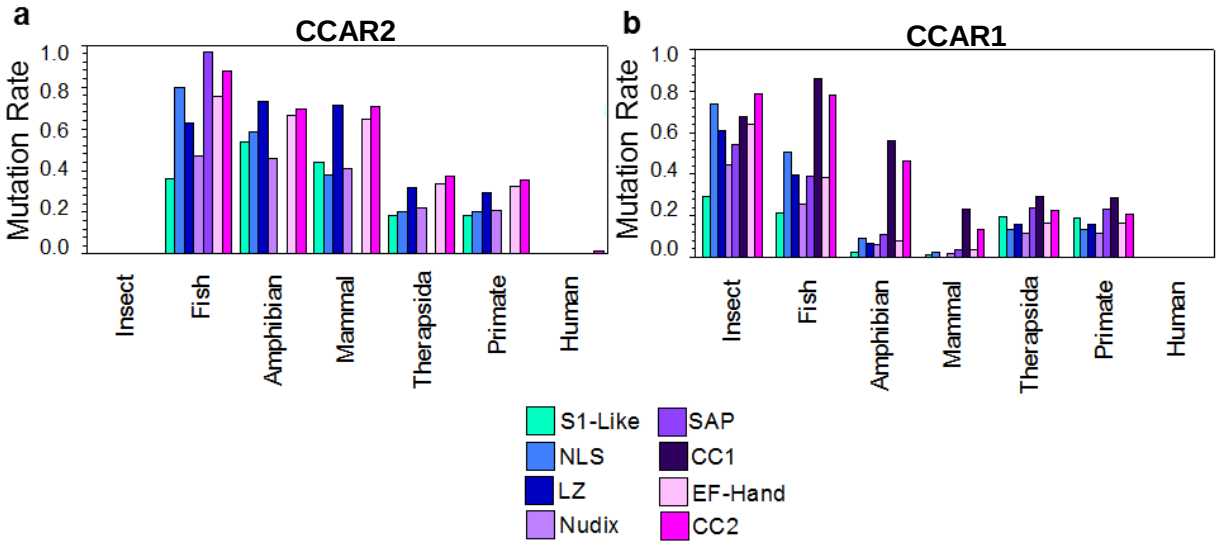

Figure 4.8. The amino acid substitution rates of specific domains among various groups of species for CCAR2 (a) and CCAR1 (b). Based on the sequences in Table C1, human is in one group, all other primates excluding human are in the second group, all other Therapsida excluding primates are in the third group, all other mammals compose the fourth group, amphibians are in the fifth group, fish are in the sixth group, and insects are in the seventh group. Eight domains were analyzed including the S1-Like, NLS, LZ, SAP, CC1, EF-Hand, and CC2 domains.

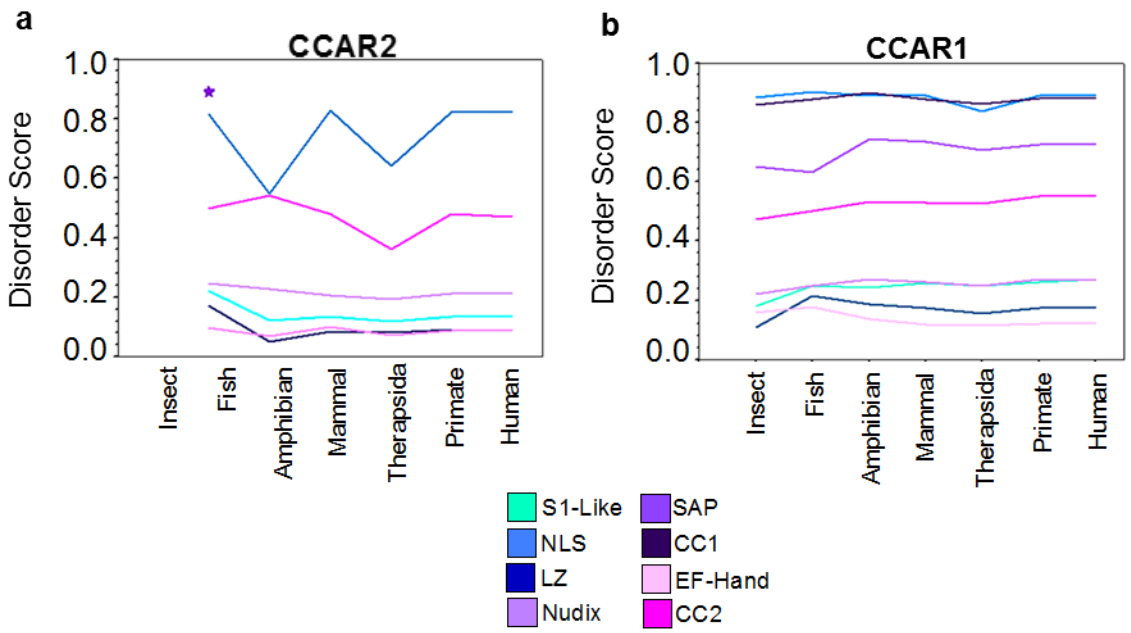

Figure 4.9. The average disorder score for each domain in CCAR2 and CCAR1 across all grouped species. The categorization of domains and species groups is the same as in Figure 4.8. The disorder score for each domain is averaged for all of the sequences in each species group. The original disorder score was predicted by PONDR-FIT.

CHAPTER 5: LST-3 IS A NEGATIVE REGULATOR OF SIR-2.1 AND THE HEAT SHOCK RESPONSE IN *CAENORHABDITIS ELEGANS*

Authored by: Jessica Brunquell, Rachel Raynes, Philip Bowers, Stephanie Morris, Alana Snyder, and Sandy D. Westerheide

All experiments were performed by, or under the guidance of, J. Brunquell. J. Brunquell, P. Bowers, S. Morris, and A. Snyder performed florescent imaging and qRT-PCR replicates. J. Brunquell and S. Morris performed immunoblotting. J. Brunquell and A. Snyder performed polyglutamine aggregate analyses. All data analyses were performed by J. Brunquell. J. Brunquell, R. Raynes, and S.D. Westerheide participated in design of the study. The manuscript was written by J. Brunquell and S.D. Westerheide.

Abstract

Defects in protein quality control during aging are central to many human diseases, and strategies are needed to better understand mechanisms of controlling the quality of the proteome. The heat shock response (HSR) is a conserved survival mechanism mediated by the transcription factor HSF1 which functions to maintain proteostasis. In mammalian cells, HSF1 is regulated by a variety of factors such as the prolongevity factor SIRT1. SIRT1 promotes the DNA-bound state of HSF1 through deacetylation of the DNA-binding domain of HSF1, thereby enhancing the HSR. SIRT1 is also regulated by various factors, including negative regulation by the cell-cycle and apoptosis regulator CCAR2. CCAR2 negatively regulates the HSR, possibly through its inhibitory interaction with SIRT1.

We were interested in studying conservation of the SIRT1/CCAR2 interaction in *Caenorhabditis elegans*, and utilizing this model organism to observe the effects of modulating sirtuin activity on the HSR, longevity, and proteostasis. The HSR is highly conserved in *C. elegans*, and is mediated by the HSF1 homolog, HSF-1. We have uncovered that negative regulation of the HSR by CCAR2 is conserved in *C. elegans* and is mediated by the CCAR2 ortholog, LST-3. This negative regulation requires the SIRT1 homolog Sir-2.1. In addition, knockdown of LST-3 via *lst-3* RNAi works through Sir-2.1 to enhance stress-resistance, fitness, longevity, and proteostasis. This work therefore provides insight into the benefits of enhancing sirtuin activity to promote the HSR, which may allow for the development of new methods to modulate this response for therapeutic purposes.

Introduction

Maintaining the quality of the proteome is essential for cellular homeostasis, and an accumulation of misfolded proteins is a feature of many aging-related diseases (66). A conserved mechanism utilized by the cell to maintain proteostasis is through induction of the cytoprotective heat shock response (HSR). The HSR is regulated by the transcription factor heat shock factor 1 (HSF1). HSF1 functions to protect cells from protein-damaging stress through the transcription of heat-inducible heat shock protein (*hsp*) genes which encode protein chaperones that assist in protein folding and clearance (273-276). Increasing chaperone expression is not only beneficial during stress, but also solubilizes toxic aggregate species in animal models of protein dysfunction diseases (277). Uncovering HSR activators to promote chaperone production is thus an active area of research.

One factor known to modulate the HSR is the sirtuin family member silent mating type information regulation 2 homolog 1 (SIRT1) (57,58,67,278,279). SIRT1 belongs to a family of conserved NAD^+-dependent deacetylases that promotes the HSR and longevity (280,281). Increased expression of SIRT1 enhances the HSR through deacetylation of the DNA-binding domain of HSF1, thereby prolonging its DNA-competent state and allowing for increased transcription of *hsp70* (58). SIRT1 is also essential for maintaining the proteome, as a SIRT1 deficiency results in defective protein quality control mechanisms (282). Enhancing SIRT1 activity may therefore be one strategy for promoting the HSR and proteostasis.

SIRT1 activity is controlled by a number of factors depending on the cellular environment. Active regulator of SIRT1 (AROS) is a positive regulator of SIRT1 that promotes deacetylation of the SIRT1 substrates HSF1 and p53 (67,75). Cell cycle and apoptosis regulator 2 (CCAR2), also known as DBC1, is a negative regulator of SIRT1 that enhances acetylation of p53 and HSF1 (67,73,192). Bioinformatic analyses also suggest the presence of a NAD^+ binding site on CCAR2 that may limit the cellular availability of NAD^+ required for SIRT1 to function (196). The ability of AROS and CCAR2 to modulate SIRT1 activity, and impact the acetylated state of HSF1, also impacts the HSR (67). AROS enhances the HSR by promoting HSF1 binding to the *hsp-70* promoter and enhancing *hsp-70* mRNA expression, whereas CCAR2 dampens the HSR by decreasing HSF1 binding to the *hsp-70* promoter and inhibiting *hsp-70* mRNA expression (67). Thus, sirtuin modulators are able to impact the mammalian HSR.

Caenorhabditis elegans is an ideal model organism for studying the impact of genetics on physiology and longevity. The HSR is highly conserved in *C. elegans* and is mediated

by the HSF1 homolog, HSF-1. HSF-1 has been associated with aging and longevity, as knockdown of *hsf-1* decreases lifespan and induces rapid aging, while its overexpression increases lifespan (110,111,138). Additionally, SIRT1-regulated processes are also conserved in the worm and mediated by Sir-2.1. Worms expressing extra copies of *sir-2.1* exhibit increased longevity (283-285). Also, enhancing *sir-2.1* activity through the induction of caloric restriction enhances the transcription of *hsp-70* (72). Although *C. elegans* does not possess an ortholog to AROS, CCAR2 is conserved in the worm and is referred to as lateral signaling target 3 (LST-3) (76). We were therefore interested in determining if negative regulation of the HSR by the SIRT1 modulator CCAR2 is conserved in the worm, and how this interaction would impact stress-related responses and longevity.

In this study, we have identified LST-3 as a negative regulator of Sir-2.1 and the HSR in *C. elegans.* LST-3 negatively regulates the HSR by modulating *hsp-70* promoter activity, HSF-1 acetylation, and HSF-1 binding to the *hsp-70* promoter during HS. A family of HS-inducible *hsp-70* genes is enhanced during heat shock (HS) in response to *lst-3* RNAi, and this effect is dependent on the deacetylase activity of Sir-2.1. We have also found that modulating Sir-2.1 activity via *lst-3* RNAi promotes stress-resistance, fitness, longevity, and proteostasis. This work thus supports the use of sirtuin modulators as a means to improve proteostasis and promote healthy aging, which may be beneficial for aging-related diseases of protein quality control.

Results

Negative regulation of the HSR by CCAR2 is conserved in C. elegans and mediated by LST-3

To determine if LST-3 negatively regulates the HSR in *C. elegans*, we first tested for effects on transcription driven by the *hsp-70* promoter in response to *lst-3* RNAi (Figure 5.1). To do this, we used a *C. elegans* HS-inducible promoter fusion construct that has the promoter of *hsp-70* (*C12C8.1*) fused to GFP (p*hsp-70*::GFP). This reporter worm was fed control RNAi, *hsf-1* RNAi [*hsf-1*(-)], or *lst-3* RNAi [*lst-3*(-)] from the L1 larval stage to the L4 larval stage prior to treatment with or without a 15 minute HS, followed by a 6 hour recovery (Figure 5.1a). Our RNAi feeding strategy resulted in a 50-fold reduction in *hsf-1* and *lst-3* mRNA levels (Figure D1, see Appendix D). As expected, HS treatment of control RNAi worms resulted in increased GFP expression compared to the untreated control, and this was dependent on HSF-1. Interestingly, *lst-3* RNAi enhanced GFP expression during HS compared to the HS control. To quantify the GFP expression of the fluorescent images, ImageJ was used to measure the fluorescence intensity for each treatment condition (Figure 5.1b). In the RNAi control, HS resulted in a 9-unit increase in fluorescence intensity, which was dependent on HSF-1. When HS was combined with *lst-3* RNAi, the fluorescence intensity increased 20-units. We also analyzed the GFP expression of our reporter worm via immunoblot (Figure 5.1c), followed by quantification of band intensity by ImageJ (Figure 5.1d), and a similar trend was observed. Treatment with HS induced GFP expression 25-units, and HS combined with *lst-3* RNAi resulted in a 50-unit increase in GFP expression. Thus, *lst-3* RNAi increases HS-inducible *hsp-70*

promoter activity by a magnitude of 2x, indicating that LST-3 would normally negatively regulate the HSR.

lst-3 RNAi decreases HSF-1 acetylation and increases HSF-1 binding to the hsp-70 promoter

CCAR2 has previously been shown to affect HSF1 acetylation and DNA-binding in mammalian cells (67). To determine if these functions are also conserved in *C. elegans*, we assessed the effects of *lst-3* RNAi on HSF-1 acetylation and DNA-binding to the *hsp-70* promoter (Figure 5.2). An EQ73 worm strain containing HSF-1 tagged GFP under the control of its own endogenous promoter (HSF-1::GFP) (135) was fed control RNAi or *lst-3* RNAi [*lst-3*(-)] from the L1 larval stage to the L4 larval stage prior to treatment with or without a 15 minute HS. To assess HSF-1 acetylation, immunoprecipitation of HSF-1 using an α-GFP antibody, followed by immunoblotting with an α-acetylated lysine antibody, was performed (Figure 5.2a, top panel). Total HSF-1 levels and resulting IgG bands are also shown as controls (Figure 5.2a, middle and bottom panel, respectively). To quantify the total acetylation levels of HSF-1, ImageJ was used to determine the band intensity of the α-acetylated lysine immunoblot (Figure 5.2b). HS treatment decreased HSF-1 acetylation by 9-units in the RNAi control, whereas *lst-3* RNAi decreased HSF-1 acetylation by 18-units compared to the RNAi control. Furthermore, *lst-3* RNAi combined with HS decreased acetylation by 13-units compared to the HS RNAi control. Thus, *lst-3* RNAi decreases HSF-1 acetylation, therefore suggesting that LST-3 would normally enhance this modification.

We next performed chromatin immunoprecipitation in HSF-1::GFP worms fed control RNAi, *hsf-1* RNAi [*hsf-1*(-)], or *lst-3* RNAi [*lst-3*(-)] from the L1 larval stage to the L4 larval

stage prior to treatment with or without a 15 minute HS (Figure 5.2c-d). To measure HSF-1 binding to the *hsp-70* promoter, we designed primers to encompass a known HSF-1 binding site ~200 bp upstream of the transcription start site in the promoter of the *hsp-70* gene *C12C8.1* (Figure 5.2c), or to a non-specific binding site ~4,100 bp upstream as a control (Figure 5.2d). A diagram of the primer design locations is also shown (Figure 5.2e). As expected, HS increased HSF-1 binding to the *hsp-70* promoter 10-fold, and this binding was abolished upon treatment with *hsf-1* RNAi. Interestingly, *lst-3* RNAi increased HSF-1 binding 5-fold in the absence of HS, and 40-fold during HS, compared to the respective controls. We therefore conclude that LST-3 would normally decrease HSF-1 binding to the *hsp-70* promoter, similarly to CCAR2 in mammalian cells (67).

lst-3 RNAi enhances hsp-70 mRNA expression upon HS in a Sir-2.1-dependent manner

CCAR2 is suggested to negatively regulate the HSR through its inhibitory association with SIRT1 (67). To determine if negative regulation of the HSR by LST-3 in *C. elegans* is mediated through Sir-2.1, we used qRT-PCR to measure the expression of the HS-inducible *hsp-70* family members *C12C8.1*, *F44E5.4*, and *F44E5.5* in wild-type (N2) worms, and in LG339 worms containing a non-functional Sir-2.1 protein (*sir-2.1Δ*), in response to *lst-3* RNAi (Figure 5.3). Synchronous N2 or *sir-2.1Δ* worms were fed control RNAi, *hsf-1* RNAi [*hsf-1*(-)], or *lst-3* RNAi [*lst-3*(-)] from the L1 larval stage to the L4 larval stage prior to treatment with or without a 15 minute HS, followed by a 15 minute recovery. In wild-type worms, HS treatment of the control increased the expression of each *hsp-70* family member in an HSF-1-dependent manner, as expected (Figure 5.3a-c). Consistent with the results in Figure 5.1, *lst-3* RNAi enhanced HS-induced *C12C8.1* mRNA

expression compared to the HS treated control (Figure 5.3a). A similar trend is also observed for the *hsp-70* genes *F44E5.5* and *F44E5.4* (Figure 5.3b-c). Interestingly, the ability of *lst-3* RNAi to enhance HS-induced *hsp-70* mRNA expression was abolished in the *sir-2.1Δ* strain (Figure 5.3d-f). To ensure that these results were specific to Sir-2.1, we also examined Sir-2.3 (a homolog to mammalian SIRT4) by performing the same analyses in a *sir-2.3Δ* strain (RB654) (Figure D2a-c, see Appendix D). The ability of *lst-3* RNAi to enhance *hsp-70* mRNA expression during HS is unaffected in this *sir-2.3Δ* strain. Thus, negative regulation of the HSR by LST-3 is dependent on Sir-2.1.

We were next interested in determining if the deacetylase activity of Sir-2.1 was required for LST-3 to negatively regulate the HSR (Figure D3, see Appendix D). We used a small-molecule selective inhibitor of mammalian SIRT1 deacetylase activity, EX-527, which has also been shown to inhibit Sir-2.1 in *C. elegans* (286,287). First, we assessed *hsp-70* promoter activity by feeding p*hsp-70*::GFP worms control RNAi, or *lst-3* RNAi [*lst-3*(-)] in combination with EX-527, from the L1 larval stage to the L4 larval stage prior to treatment with or without a 15 minute HS, followed by a 6 hour recovery (Figure D3a, see Appendix D). Similar to Figure 5.1, *lst-3* RNAi resulted in enhanced *hsp-70* promoter activity during HS compared to the HS control. Blocking the deacetylase activity of Sir-2.1 upon treatment with EX-527 prevented *lst-3* RNAi from enhancing *hsp-70* promoter activity during HS. This trend was confirmed using qRT-PCR for the *hsp-70* genes *C12C8.1*, *F44E5.5*, and *F44E5.4* (Figure D3b-d, see Appendix D). These data suggest that negative regulation of the HSR by LST-3 is mediated through the deacetylase activity of Sir-2.1.

lst-3 RNAi promotes stress-resistance and fitness in a Sir-2.1-dependent manner

To examine the impact of LST-3 on stress-resistance and fitness, we next assessed survival upon exposure to a lethal HS (thermotolerance) and thrashing in aging worms in response to *lst-3* RNAi (Figure 5.4). Wild-type (N2) or *sir-2.1Δ* worms were fed control RNAi or *lst-3* RNAi [*lst-3*(-)] from the L1 larval stage until day 3 of adulthood, treated with a lethal 42°C 1 hour HS, and survivors were scored 12 hours after the HS. This HS treatment condition resulted in ~50% survival in wild-type worms fed control RNAi, and ~80% survival in wild-type worms fed *lst-3* RNAi (Figure 5.4a). *lst-3* RNAi not only promoted survival during a lethal HS, but also enhanced the fitness of worms that survived the lethal HS which was measured in number of body bends/30 seconds (Figure 5.4b). Wild-type worms fed control RNAi that survived a lethal HS moved at a rate of 20 body bends/30 seconds, whereas worms fed *lst-3* RNAi moved at a rate of 55 body bends/30 seconds. The ability of *lst-3* RNAi to enhance thermotolerance and fitness was dependent on Sir-2.1 (Figure 5.4c-d). *sir-2.1Δ* worms fed *lst-3* RNAi did not show an increase in survival upon exposure to a lethal HS compared to the RNAi control, and exhibited a dramatic decrease in fitness regardless of *lst-3* RNAi treatment. These data therefore suggest that LST-3 would normally reduce stress-resistance and fitness through inhibition of Sir-2.1.

lst-3 RNAi promotes longevity in a Sir-2.1-dependent manner

Next, we performed lifespan assays to assess the impact of LST-3 on longevity (Figure 5.5). Wild-type (N2) or *sir-2.1Δ* worms were fed control RNAi or *lst-3* RNAi [*lst-3*(-)] from the L1 larval stage throughout life. Worms were scored every other day starting at day 1 of adulthood for survival, and scored as dead when non-responsive to poking with a

platinum wire. Wild-type worms fed control RNAi had a median survival of 10 days, and a maximum survival of 18 days, whereas worms fed *lst-3* RNAi had a median survival of 12 days, and a maximum survival of 22 days (Figure 5.5a). The increase in median and maximum lifespan observed in response to treatment with *lst-3* RNAi was dependent on Sir-2.1, as *sir-2.1Δ* worms show a 4 day decrease in longevity when fed *lst-3* RNAi compared to the RNAi control (Figure 5.5b). Thus, LST-3 would normally decrease longevity via inhibition of Sir-2.1.

lst-3 RNAi promotes proteostasis in a C. elegans Huntington's disease model

To observe the impact of LST-3 on proteostasis, we used a *C. elegans* Huntington's disease model to observe polyglutamine aggregate formation and toxicity in response to *lst-3* RNAi (Figure 5.6). The Huntington's disease model used here (AM140) contains 35 polyglutamine repeats fused to YFP under the control of a muscle promoter (Q35::YFP), and develops insoluble protein aggregates in an age-dependent manner in the body wall muscle (142). Synchronous Q35::YFP worms were fed control RNAi, *hsf-1* RNAi [*hsf-1*(-)], or *lst-3* RNAi [*lst-3*(-)] from the L1 larval stage until day 3 of adulthood prior to treatment with or without a 15 minute HS, followed by a 12 hour recovery. Fluorescent images, as well as threshold-adjusted images, are shown (Figure 5.6a). ImageJ was used on the threshold-adjusted images to quantify the number of aggregates per worm for each treatment condition (Figure 5.6b). As expected, *hsf-1* RNAi increased aggregate formation in the absence of HS by 10 aggregates/worm, and in the presence of HS by 12 aggregates/worm, compared to the respective controls. Interestingly, *lst-3* RNAi decreased aggregate formation by 9 aggregates/worm in the absence of HS, and by 12

aggregates/worm during HS, compared to the respective controls. LST-3 would therefore normally decrease proteostasis in a *C. elegans* Huntington's disease model.

We next examined paralysis in the Huntington's disease model in order to assess the toxicity associated with aggregate formation (Figure 5.6c). Synchronous Q35::YFP worms were fed control RNAi, *hsf-1* RNAi [*hsf-1*(-)], or *lst-3* RNAi [*lst-3*(-)] from the L1 larval stage until day 5 of adulthood prior to treatment with or without a 15 minute HS, followed by a 12 hour recovery. As expected, treatment with *hsf-1* RNAi increased the number of paralyzed worms by 19% regardless of HS. Treatment with *lst-3* RNAi decreased the number of paralyzed worms by 12% in the absence of HS, and by 25% during HS. These data suggest that LST-3 would normally antagonize proteostasis and lead to increased aggregate-associated toxicity in a *C. elegans* Huntington's disease model.

To determine if the decrease observed in aggregate formation in response to *lst-3* RNAi may be due to increased *hsp-70* mRNA levels in aging worms, we performed qPCR on day 3 *C. elegans* fed *lst-3* RNAi (Figure 5.6d-f). Interestingly, treatment with *lst-3* RNAi increased the expression of each *hsp-70* family member in the absence of HS, while collectively enhancing *hsp-70* expression when combined with HS. *lst-3* RNAi may therefore prevent age-associated decline of the HSR, and be beneficial for maintaining proteostasis during aging, suggesting LST-3 normally dampens the HSR with age.

Discussion

In this study, we have identified LST-3, a CCAR2 ortholog, as a negative regulator of the HSR in *C. elegans*. We have found that LST-3 modulates *hsp-70* promoter activity, HSF-1 acetylation, and HSF-1-binding to the *hsp-70* promoter during HS. Worms treated with

lst-3 RNAi show an increase in HS-inducible *hsp-70* gene expression that is dependent on Sir-2.1. Additionally, *lst-3* RNAi promotes stress-resistance, thermotolerance, fitness, longevity, and proteostasis, while also preventing an age-dependent decline in the HSR. We therefore conclude that enhancing the HSR by modulating sirtuin activity is one strategy that may be utilized to promote proteostasis and longevity, and may be beneficial for diseases of protein quality control.

Our previous bioinformatics study was the first to suggest LST-3 as an ortholog and common ancestor to mammalian CCAR2 (76). The work performed here is the first to show that the function of mammalian CCAR2 in negatively regulating the HSR is conserved in *C. elegans* and is mediated by LST-3. It would be interesting to determine if other known SIRT1/CCAR2 pathways in mammalian cells, such as the regulation of p53 (192,288), are also conserved in *C. elegans.* This study, combined with future work, could expand *C. elegans* as a model for studying other SIRT1/CCAR2 regulated processes which would be beneficial to assess in a whole organism.

Uncovering compounds that modulate the SIRT1/CCAR2 interaction to promote SIRT1 activity is of interest, as CCAR2 exhibits binding specificity for SIRT1 and not to other sirtuin family members (192). Recently, a carboxamide-based pharmacological scaffold compound, EX-527, was found to prevent the SIRT1/CCAR2 interaction (81). However, this compound also inhibits the deacetylase activity of SIRT1 (287). If new compounds are developed to inhibit SIRT1/CCAR2 binding, while not inhibiting SIRT1 catalytic activity, it would be beneficial to test these small-molecules in *C. elegans* to detect possible effects on growth, reproduction, healthspan, and lifespan. Our work provides a model in which to assess small-molecule regulators of SIRT1/CCAR2 binding,

which may be beneficial for future studies into developing therapeutic strategies to promote SIRT1 activation.

Modulating the HSR by controlling SIRT1 activity is a promising method of promoting proteostasis, as many of the small-molecules known to modulate HSF1 activity are not feasible due to cytotoxicity and bioavailability (127). The likelihood of developing diseases of protein dysfunction, such as neurodegenerative disorders, is increased upon aging, possibly due to induction of the HSR dramatically declining during the aging process (103,104). Activators of the HSR have been suggested as possible therapeutic strategies for these diseases of aging (163,185-187). Our data suggest that modulating Sir-2.1 activity may prevent an age-associated decline in the HSR, and prevent polyglutamine aggregation in a *C. elegans* Huntington's disease model. Therefore, our studies support the use of sirtuin modulators for diseases of protein quality control to promote healthy aging.

In addition to this work providing a new model to study SIRT1/CCAR2 regulated processes, and supporting sirtuin modulators as a means to induce the HSR, we have also uncovered a novel function for LST-3 in negatively regulating the HSR in *C. elegans*. There is currently little known regarding the function of LST-3 in *C. elegans*. LST-3 is involved in a lateral signaling pathway that is part of a group of proteins that regulate vulval development (289). Based on our work, we can now add a function for the highly under characterized LST-3 protein in negatively regulating Sir-2.1 and the HSR. As future work further characterizes the function of LST-3, it will be interesting to see if other stress response pathways are also influenced by this protein.

In conclusion, our work demonstrates the positive effects of promoting the HSR by enhancing Sir-2.1 activity. We have identified LST-3 as a CCAR2 ortholog that maintains a conserved function in negatively regulating the HSR, thereby providing a new model for future CCAR2 studies. It will be interesting to see if future studies find small molecules that interfere with the SIRT1/CCAR2 interaction and promote proteostasis and healthy aging in mammalian systems. This study supports the use of sirtuin modulators to benefit diseases of protein dysfunction, while also uncovering a novel function for LST-3 in regulating the HSR in *C. elegans*.

Methods

C. elegans strains and growth conditions

The following *C. elegans* strains were used in this study: Bristol N2 (wild-type), *sir-2.1Δ (*LG339) (290), *sir-2.3Δ* (RB654) (291), Q35::YFP (AM140) (38), and the *pC12C8.1*::GFP reporter strain (39). All strains were grown at 23°C and maintained on standard nematode growth media (NGM) containing the *Escherichia coli* strain OP50 as a food source. Age synchronization was accomplished by 20% hypochlorite treatment followed by washing and 24 hour incubation in M9 buffer at 23°C at 220 rpm.

RNA interference

Synchronous L1 nematodes were placed onto standard NGM plates supplemented with 25 µg/mL ampicillin and 1 mM isopropyl-beta-ᴅ-thiogalactopyranoside seeded with either HT115 bacteria containing an empty vector (L4440, control), or with sequence verified gene-specific RNAi strains isolated from the Ahringer RNAi library (40). RNAi bacteria was concentrated 10x prior and allowed to induce on the plates overnight at room temperature.

HS treatment

C. elegans were grown on RNAi plates as indicated, wrapped in parafilm, and then submerged in a 33°C water bath for the allotted times. Prior to RNA extraction, animals were allowed to recover for 15 minutes at growth temperature. Prior to GFP analysis, animals were allowed to recover for 8 hours at growth temperature.

EX-527 compound treatment

EX-527 (Sigma, *cat#* E7034) was diluted in DMSO and added to NGM after autoclaving at a final volume of 1 µM. Synchronous worms were grown on vehicle control or EX-527 supplemented plates from the L1 larval stage to the L4 larval stage prior to analyses.

Fluorescence microscopy

Animals were anesthetized with 10 mM Levamisole and photographed using an EVOS fluorescence microscope. Image processing was accomplished using Adobe Photoshop© (Adobe Systems Incorporated). Quantification of fluorescence intensity was performed using ImageJ Software (v. 1.44; http://imagej.nih.gov/ij/).

Immunoblotting

Animals were harvested in Buffer C (20mM HEPES pH 7.9, 25% glycerol, 0.42M NaCl, 1.5 mM MgCl2, 0.2 mM EDT, and 0.5mM DTT) with the addition of Halt™ protease inhibitors (Pierce, *cat#* 78430). Protein was extracted by sonication with a Diagenode Bioruptor 300 for 15 minutes with 30 second pulses. Protein was quantified by Bradford assay, resolved on a 10% SDS-PAGE gel, and transferred to a PVDF membrane. The blot was incubated with anti-GFP polyclonal antibody (Abcam, *cat#* ab290) at a 1:2500 dilution and with anti-Actin (Amersham, *cat#* JLA20-C) at a 1:750 dilution. Quantification of band intensity was performed using ImageJ Software (v. 1.44; http://imagej.nih.gov/ij/)

following the guidelines for analyzing 1-D gels by generating lane profile plots, drawing lines to enclose peaks of interest, and then measuring peak areas using the wand tool.

Quantitative RT-PCR

RNA was extracted with TRIzol® reagent (Ambion®, *cat*# 15596-026) by standard protocol. RNA was reverse transcribed using a High Capacity cDNA Reverse Transcription Kit (Applied Biosystems, *cat*# 4368814) according to the manufacturer's instructions. cDNA was diluted to 50 ng/µl to be used as a template for qRT-PCR performed with the StepOne Plus Real-time PCR system (Applied Biosystems, *cat* # 4376600) using iTaq™ Universal SYBR® Green Supermix (BioRad, *cat*# 1725121) according to the manufacturer's instructions. Data analysis was performed according to standard calculations and normalized to a GAPDH control (41). Results are representative of averaged technical duplicates from independent biological triplicates. Statistical analysis was performed with GraphPad (GraphPad Software, www.graphpad.com) using ANOVA followed by the Bonferroni post-test.

Lifespan analysis

All lifespan assays were performed at 23°C with 100 worms per condition. Animals were transferred to fresh plates daily for 5 days to avoid progeny contamination. Adult worms were scored every other day and counted as dead when no response was observed by gentle poking with a platinum wire. Survivability was plotted using GraphPad Prism v.6 (GraphPad Software, www.graphpad.com) and statistical analysis was done using the Kaplan-Meyer log-rank test.

Thermotolerance and thrashing assay

100 synchronized L1 nematodes were grown on control (L4440) or gene-specific RNAi plates at growth temperature (23°C), transferred to new plates daily until day 3 of adulthood, and then submerged in a 42°C water bath for 1 hour which allowed for a 50% survival rate which is considered lethal. Animals were scored 12 hours later and marked as dead when non-responsive to poking by a platinum wire. Live animals were then scored for fitness by assessing movement when placed into a drop of M9 on a glass slide. Worms were allowed to acclimate to the M9 for 10 seconds, and then body bends were counted for 30 seconds.

Protein aggregation assay

Q35::YFP (AM140) nematodes were synchronized and grown on empty vector (L4440, control) or gene-selected RNAi plates. Worms were picked to fresh plates daily after first progeny development until day 3 of adulthood, and then plates were submerged in a 33°C water bath for 15 minutes and allowed to recover for 12 hours at growth temperature. Protein aggregates were scored in a blind analysis of at least 50 worms per condition in independent biological triplicates as previously described (38), and also by ImageJ analysis.

Paralysis assay

Q35::YFP (AM140) nematodes were synchronized and grown on empty vector (L4440, control) or gene-selected RNAi plates. Worms were picked to fresh plates daily after first progeny development until day 5 of adulthood, and then plates were submerged in a 33°C water bath for 15 minutes and allowed to recover for 12 hours at growth temperature. Paralysis was determined by transferring live worms to a corresponding RNAi plate, and

observing movement within a 2 minute period. Worms that did not move within the timeframe were considered paralyzed.

Acetylation assay

Approximately 13,000 HSF-1::GFP (EQ73) worms were bleach synchronized and placed onto gene-specific RNAi plates until reaching the L4 stage prior to being left untreated or heat shocked as described above. Worms were collected in HLB Buffer [50 mM HEPES-KOH, pH 7.5, 150 mM NaCl, 1 mM EDTA, 0.1% (wt/vol) sodium deoxycholate, 1% (vol/vol) Triton X-100, 0.1% (wt/vol) SDS, Halt™ protease inhibitors (Pierce, *cat*# 78430), 1 μM trichostatin A, 1 μM nicotinamide, and 1 μM EX-527] and homogenized with a Dounce homogenizer prior to centrifugation at 14,000xg for 20 minutes at 4°C. Protein was quantified by Bradford assay, and immunoprecipitation was accomplished using 1 mg protein extract and an anti-GFP polyclonal antibody (Abcam, *cat*# ab290) at a 1:100 dilution. The antibody-protein complex was allowed to form overnight at 4°C with rotation. 50 μL of salmon sperm DNA/protein-A agarose beads (Millipore, *cat*# 16-157) was then added and allowed to incubate for 1 hour at 4°C. The beads were washed 3 times with HLB buffer supplemented with 1 μM trichostatin A, 1 μM nicotinamide, and 1 μM EX-527 before being boiled in Laemeli buffer. The resulting supernatant was then resolved on a 10% SDS-PAGE gel and transferred to a PVDF membrane. The blot was incubated with anti-GFP antibody (Abcam, *cat*# ab290) at a 1:50,000 dilution and with anti-AcK antibody (Cell Signaling *cat*# 9441) at a 1:100,000 dilution.

Chromatin immunoprecipitation procedure and data analysis

Chromatin immunoprecipitation (ChIP) was performed essentially as previously described (292). Where approximately 13,000 HSF-1::GFP (EQ73) worms were bleach

synchronized and placed onto gene-specific RNAi plates until reaching the L4 stage prior to being left untreated or given a 15 minute HS as described above. Worms were collected, cross-linked with 1% formaldehyde, lysed with a homogenizer, and quenched with Glycine before being sonicated with a Diagenode Bioruptor 300 for 10 minutes with 30 second pulses. Protein was quantified and technical triplicates were performed with 2 mg of total protein diluted in HLB buffer [50 mM HEPES-KOH, pH 7.5, 150 mM NaCl, 1 mM EDTA, 0.1% (wt/vol) sodium deoxycholate, 1% (vol/vol) Triton X-100, 0.1% (wt/vol) SDS, and Halt™ protease inhibitors (Pierce, *cat*# 78430)]. 1% of each sample was saved as the input. An anti-GFP polyclonal antibody (Abcam, *cat*# ab290) at a 1:100 dilution, and the IgG antibody was used at a 1:1,000 dilution. The antibody-protein complex was allowed to form overnight at 4°C. 50 µL of salmon sperm DNA/protein-A agarose beads (Millipore, *cat*# 16-157) was added to the diluted supernatant and allowed to incubate for 1 hour at 4°C. The antibody-protein-agarose bead complex was washed 2 times with WB1 (50 mM HEPES-KOH, pH 7.5, 150 mM NaCl, 1 mM EDTA pH 8.0, 1% sodium deoxycholate, 1% Triton X-100, 0.1% SDS and HALT protease inhibitors), WB2 (50 mM HEPES-KOH, pH 7.5, 1 M NaCl, 1 mM EDTA, pH 8.0, 0.1% sodium deoxycholate, 1% Triton X-100, 0.1% SDS and HALT protease inhibitors), WB3 (50 mM Tris-Cl, pH 8.0, 0.25 mM LiCl, 1 mM EDTA, 0.5% NP-40 and 0.5% sodium deoxycholate), and then with 1xTE. The ChIP samples and the input samples were placed at 45°C for 2 hours with the addition of proteinase K buffer/proteinase K. The samples were then reverse cross-linked with an overnight incubation at 65°C, and DNA was purified the next day using a PCR purification kit. qRT-PCR was performed using primers flanking a HS element in the promotor of the *hsp-70* (*C12C8.1*) gene. Percent input was calculated by first adjusting

the raw Ct values of the diluted input to 100% by subtracting 6.644 (log_2 of the dilution factor). The square of the average Ct values of the ChIP samples, subtracted from the adjusted input, was then multiplied by 100 to obtain the percent input.

Statistical Analyses

Statistical analyses were carried out with GraphPad Software (GraphPad Software, La Jolla California USA, http://www.graphpad.com). All error bars are representative of standard deviation between independent biological replicates, as indicated.

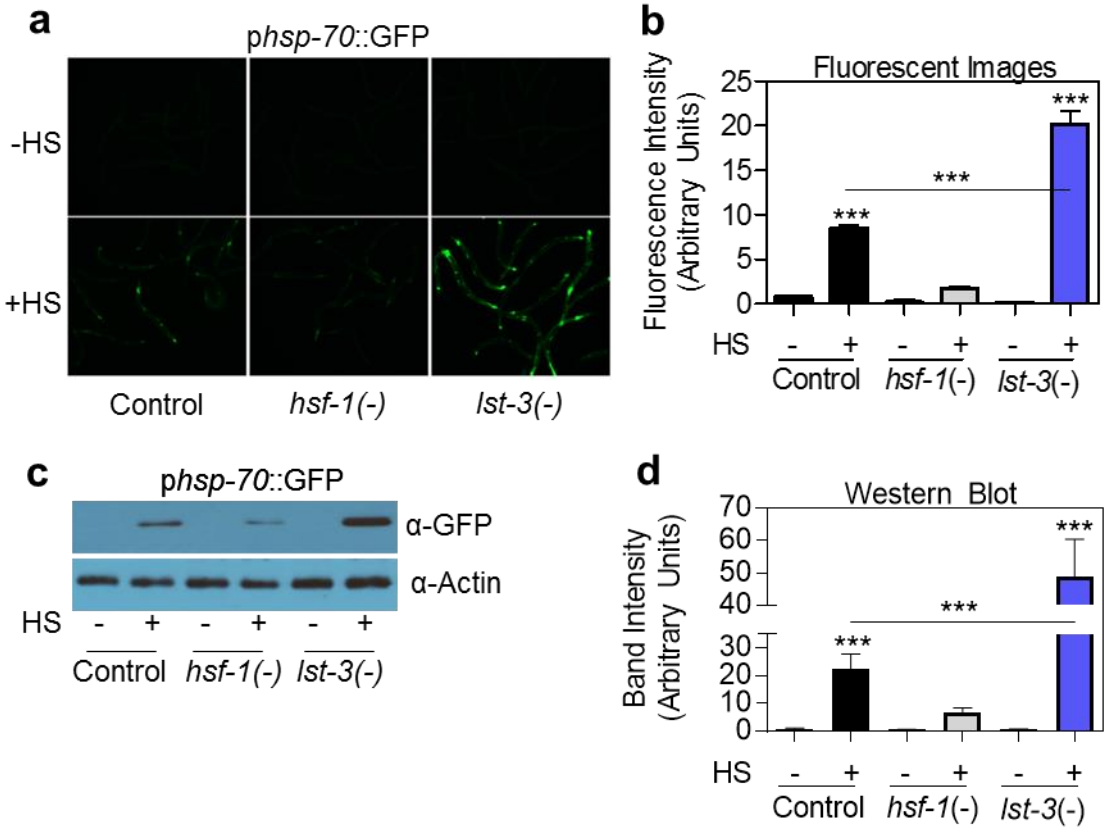

Figure 5.1. *lst-3* RNAi enhances *hsp-70* promoter activity upon HS. (**a**) Fluorescent images are shown of *pC12C8.1*(*hsp-70*)::GFP worms fed control RNAi, *hsf-1* RNAi [*hsf-1*(-)], or *lst-3* RNAi [*lst-3*(-)] from the L1 larval stage to the L4 larval stage prior to treatment with or without a 15 minute 33°C HS, followed by a 6 hour recovery. (**b**) Quantification of GFP intensity for 50 worms/condition for each treatment condition in A was determined using ImageJ. (**c**) GFP protein levels in worms given the same treatment conditions in (**a**) were determined via immunoblotting. (**d**) Quantification of band intensity for the immunoblot in (**c**) was done using ImageJ software and graphed as intensity in arbitrary units. For (**b**) and (**d**), significance was determined using the Bonferroni post-hoc test where *** $p < 0.001$.

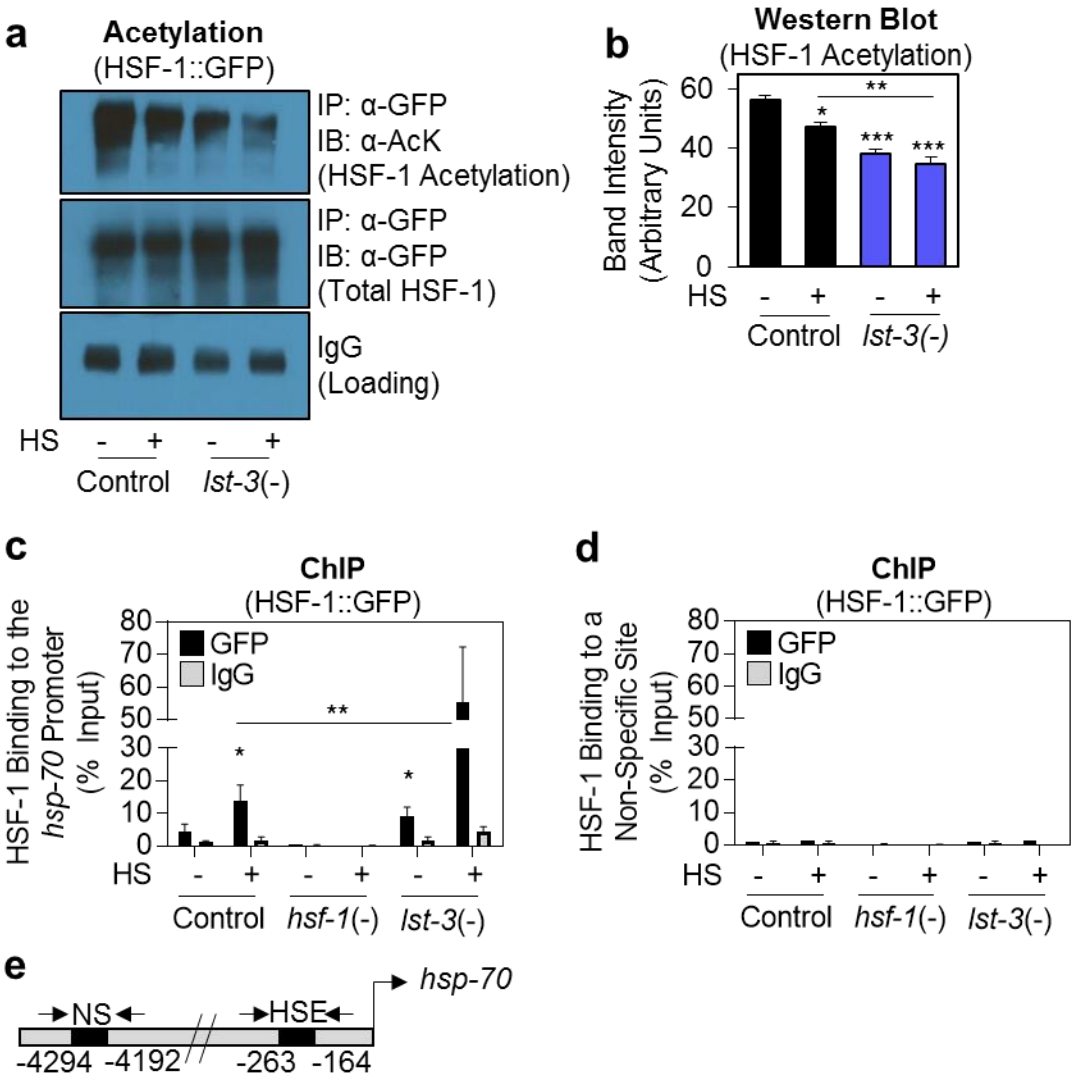

Figure 5.2. *lst-3* RNAi decreases HSF-1 acetylation and increases HSF-1 recruitment to the *hsp-70* promoter. (**a**) Acetylation was assessed in HSF-1::GFP (EQ73) worms were fed control or *lst-3* RNAi [*lst-3*(-)] from the L1 larval stage to the L4 larval stage prior to treatment with or without a 15 minute 33°C HS. HSF-1 was immunoprecipitated (IP) using an α-GFP antibody and acetylation was measured by immunoblotting (IB) and probing with an α-AcK (acetylated lysine) antibody, total HSF-1 levels were measured by probing with an α-GFP antibody. IgG bands are also shown as a loading control. (**b**) Quantification of band intensity for the top panel in A was done using ImageJ software and graphed as intensity in arbitrary units. (**c**) HSF-1 binding to the *hsp-70* promoter was assessed by performing chromatin immunoprecipitation in HSF-1::GFP (EQ73) worms using the same treatment conditions in (**a**), and an α-GFP antibody to immunoprecipitate HSF-1. Binding was assessed via qRT-PCR using primers designed to encompass HS elements in the promoter region of the *C12C8.1* (*hsp-70*) gene. (**d**) HSF-1 binding to a non-specific site ~4kb upstream of the *hsp-70* promoter was assessed by performing chromatin immunoprecipitation using the same conditions in (**c**). (**e**) Primer design schematic used for ChIP. Primers for ChIP were designed to flank the known *C. elegans* HSF-1 binding site (TTCnnGAA) in the promoter of the *hsp-70* gene *C12C8.1* or at a non-specific site ~4kb upstream of the transcription start site. For (**b**) and (**c**), significance was determined using the Bonferroni post-hoc test where * p<.05, ** p< 0.01, *** p< 0.001.

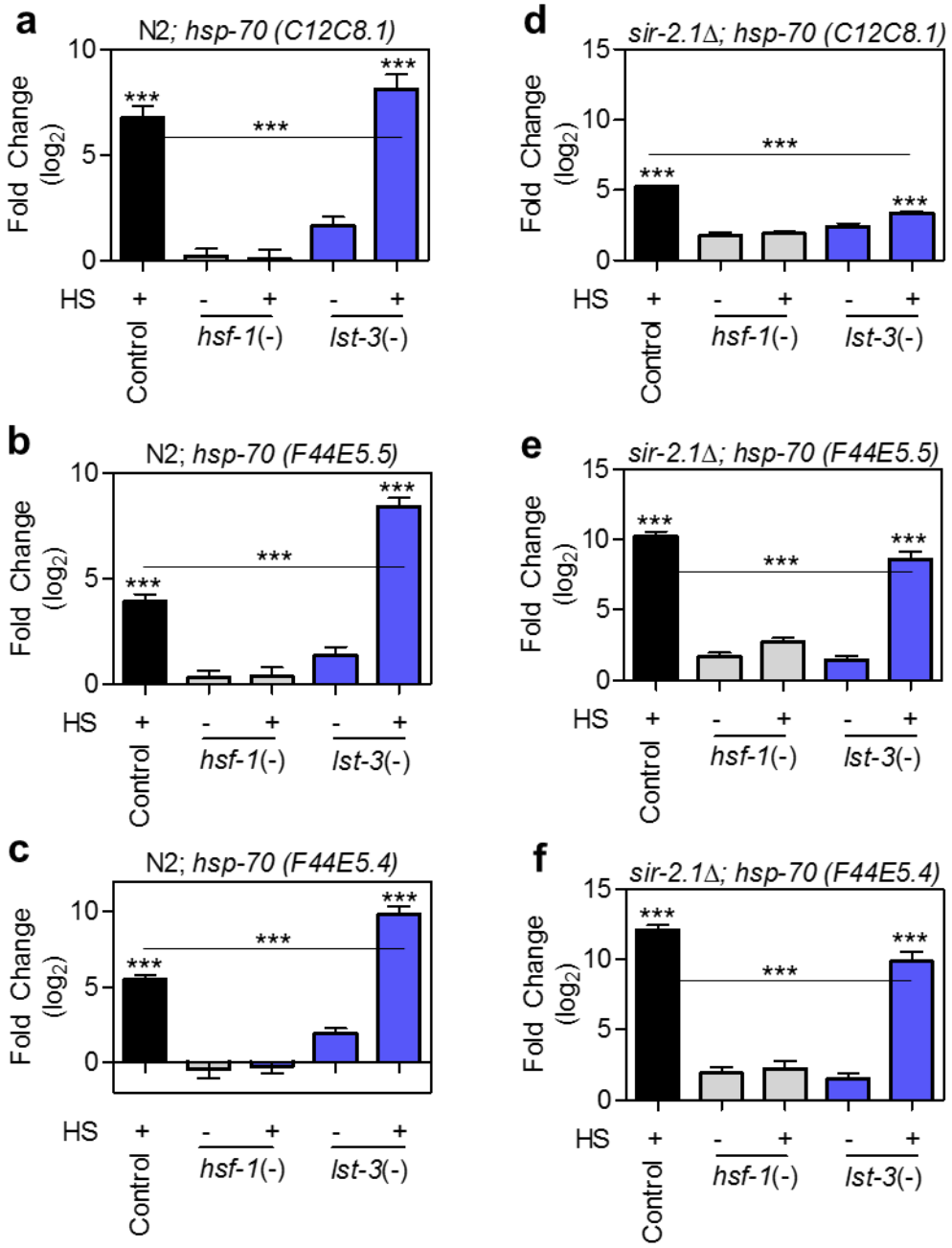

Figure 5.3. *lst-3* RNAi enhances a family of *hsp-70* mRNAs in a *sir-2.1*-dependent manner upon HS. (**a-c**) qRT-PCR was used to measure the expression of the *hsp-70* family members *C12C8.1*, *F44E5.5*, and *F44E5.4* in synchronous wild-type (N2) worms fed control RNAi, *hsf-1* RNAi [*hsf-1*(-)], or *lst-3* RNAi [*lst-3*(-)] from the L1 larval stage to the L4 larval stage prior to treatment with or without a 15 minute 33°C HS followed by a 15 minute recovery. (**d-f**) qRT-PCR was used to measure the expression of the *hsp-70* family members *C12C8.1*, *F44E5.5*, and *F44E5.4* in a *sir-2.1Δ* strain (LG339) given the same treatment conditions in (**a-c**). For (**a-f**), significance was determined using the Bonferroni post-hoc test where * p<.05, ** p< 0.01, *** p< 0.001.

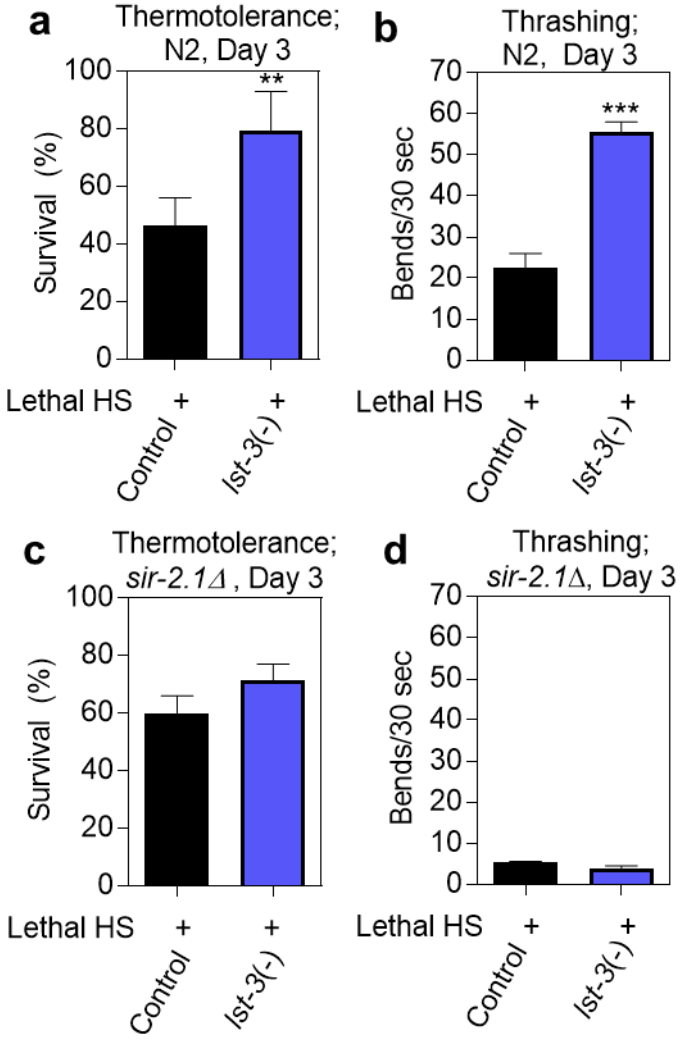

Figure 5.4. *lst-3* RNAi promotes thermotolerance and thrashing in aging worms in a *sir-2.1*-dependent manner. (**a**) Thermotolerance was measured in wild-type (N2) worms fed control RNAi or *lst-3* RNAi [*lst-3*(-)] from the L1 larval stage until day 3 of adulthood prior to treatment with a lethal (50% survival in the control) 42°C 1 hour HS. (**b**) Thrashing was measured as number of body bends/30 seconds for survivors of the lethal HS in (**a**). (**c**) Thermotolerance was measured in *sir-2.1Δ* worms fed control RNAi or *lst-3* RNAi [*lst-3*(-)] from the L1 larval stage until day 3 of adulthood prior to treatment with a lethal 42°C 1 hour HS. (**d**) Thrashing was measured in number of body bends/30 seconds for survivors of the lethal HS in (**c**). For (**a-d**), significance was determined using the Bonferroni post-hoc test where ** $p < 0.01$, *** $p < 0.001$.

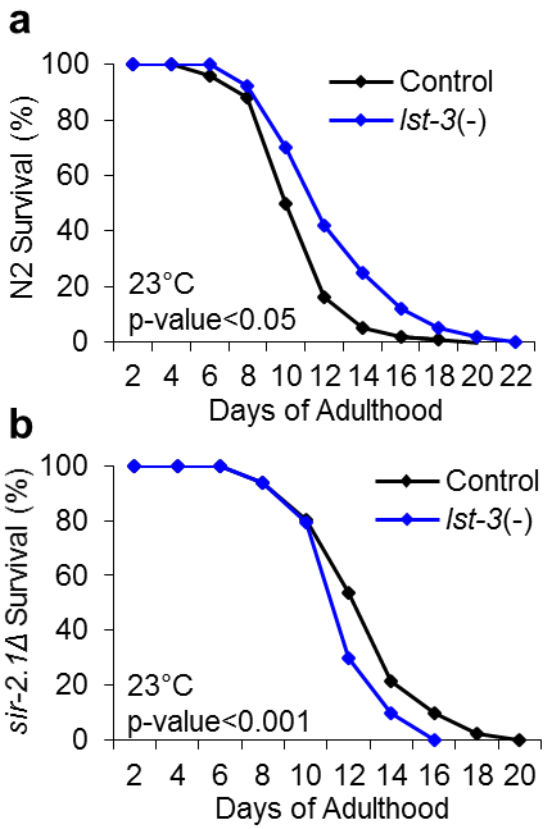

Figure 5.5. *lst-3* RNAi increases longevity in a *sir-2.1*-dependent manner. (**a**) Lifespan analysis was performed at 23°C in wild-type (N2) worms fed control RNAi or *lst-3* RNAi [*lst-3*(-)] throughout lifespan. (**b**) Lifespan analysis was performed at 23°C in *sir-2.1Δ* worms fed control RNAi or *lst-3* RNAi [*lst-3*(-)] throughout lifespan. For (**a-b**), worms were scored every other day for survival, and significance was determined using the Mantle-Cox rank test.

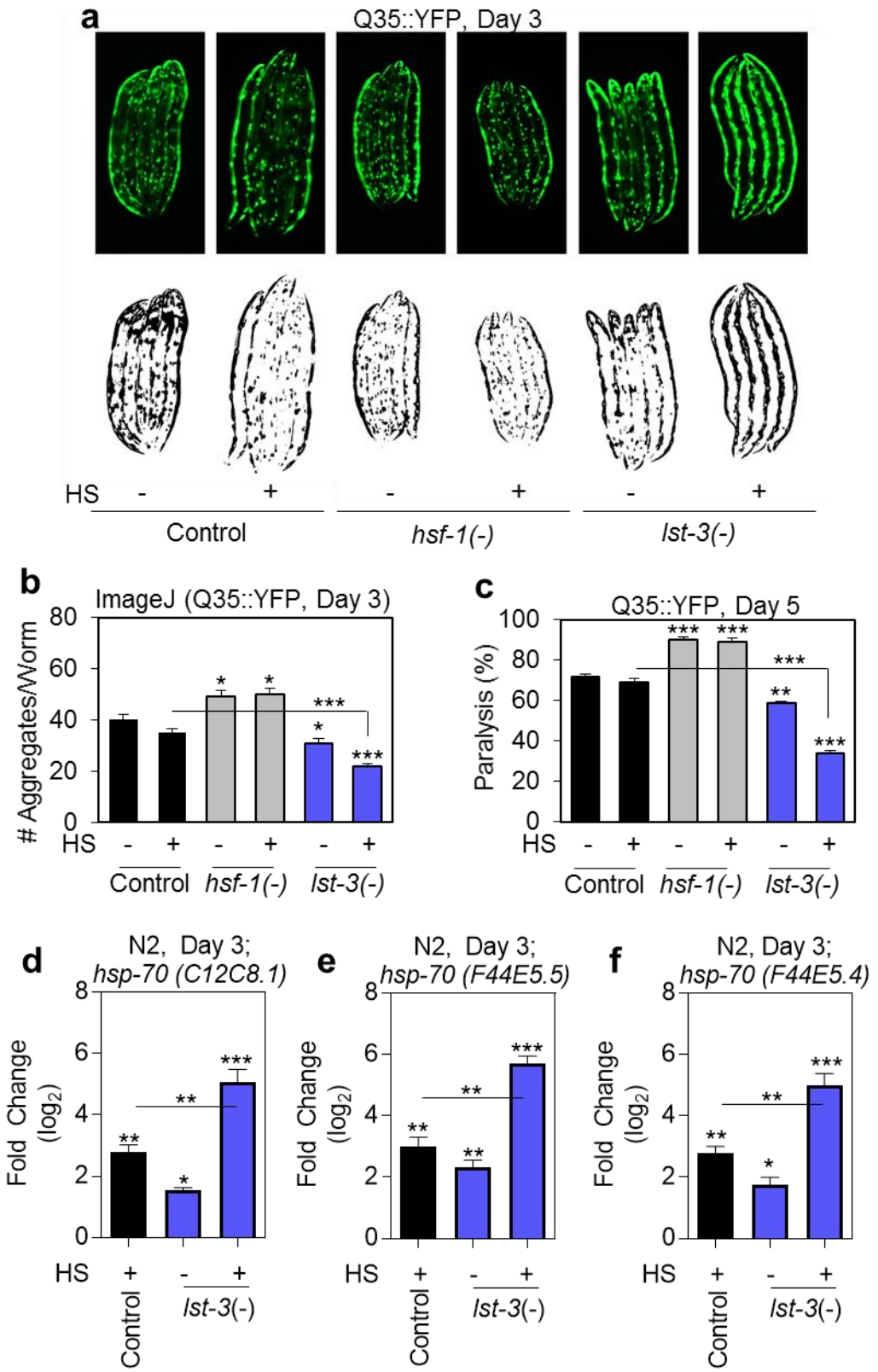

Figure 5.6. *lst-3* RNAi decreases polyglutamine aggregation and paralysis in a Huntington's disease model, and prevents age-related decline of the HSR. (**a**) Fluorescent images of a *C. elegans* Huntington's disease model containing 35 polyglutamine repeats fused to YFP under the control of a--

Figure 5.6. *lst-3* RNAi decreases polyglutamine aggregation and paralysis in a Huntington's disease model, and prevents age-related decline of the HSR (Continued). muscle promoter (Q35::YFP) were fed control RNAi, *hsf-1* RNAi [*hsf-1*(-)], or *lst-3* RNAi [*lst-3*(-)] from the L1 larval stage until day 3 of adulthood prior to treatment with or without a 15 minute HS followed by a 12 hour recovery. Threshold-adjusted images, are shown below the fluorescent images. (**b**) ImageJ was used to quantify the number of polyglutamine aggregates/worm using the threshold-adjusted images from A for 50 worms/condition in biological triplicates. (**c**) Paralysis was measured in Q35::YFP worms were fed control RNAi, *hsf-1* RNAi [*hsf-1*(-)], or *lst-3* RNAi [*lst-3*(-)] from the L1 larval stage until day 5 of adulthood prior to treatment with or without a 15 minute HS followed by a 12 hour recovery. (**d-f**) qRT-PCR was used to measure the expression of the *hsp-70* family members *C12C8.1*, *F44E5.5*, and *F44E5.4* in wild-type (N2) worms given the same treatment conditions in (**a**). For (**b-f**), significance was determined using the Bonferroni post-hoc test where * p<.05, ** p< 0.01, *** p< 0.001.

CHAPTER 6. THE GENOME-WIDE ROLE OF HSF-1 IN THE REGULATION OF GENE EXPRESSION IN CAENORHABDITIS ELEGANS

Authored by: Jessica Brunquell, Stephanie Morris, Yin Lu, Feng Cheng, and Sandy D. Westerheide

Published in BMC Genomics: Brunquell, J., et al. (2016). "The genome-wide role of HSF-1 in the regulation of gene expression in Caenorhabditis elegans." BMC Genomics 17: 559.

All experiments were performed by, or under the guidance of, J. Brunquell. J. Brunquell performed RNA preparation for RNA-sequencing, qRT-PCR replicates for HS and RNAi treatment condition verification, Western blotting, and fluorescent imaging. S. Morris performed qRT-PCR replicates for RNA-seq verification. Y. Lu and F. Cheng contributed to data analyses, normalization of the sequencing data, and dendogram clustering of the samples. J. Brunquell, F. Cheng, and S.D. Westerheide participated in design of the study. The manuscript was written by J. Brunquell and S.D. Westerheide. See Appendix H for copyright permission.

Abstract

The heat shock response, induced by cytoplasmic proteotoxic stress, is one of the most highly-conserved transcriptional responses. This response, driven by the heat shock transcription factor HSF1, restores proteostasis through the induction of molecular chaperones and other genes. In addition to stress-dependent functions, HSF1 has also been implicated in various stress-independent processes. In *C. elegans*, the HSF1

homolog HSF-1 is an essential protein that is required to mount a stress-dependent response, as well as to coordinate various stress-independent processes including development, metabolism, and the regulation of lifespan. In this work, we have performed RNA-sequencing for *C. elegans* cultured in the presence and absence of *hsf-1* RNAi followed by treatment with or without heat shock. This experimental design thus allows for the determination of both heat shock-dependent and -independent biological targets of HSF-1 on a genome-wide level. Our results confirm that *C. elegans* HSF-1 can regulate gene expression in both a stress-dependent and -independent fashion. Almost all genes regulated by HS require HSF-1, reinforcing the central role of this transcription factor in the response to heat stress. As expected, major categories of HSF-1-regulated genes include cytoprotection, development, metabolism, and aging. Within both the heat stress-dependent and -independent gene groups, significant numbers of genes are upregulated as well as downregulated, demonstrating that HSF-1 can both activate and repress gene expression either directly or indirectly. Surprisingly, the cellular process most highly regulated by HSF-1, both with and without heat stress, is cuticle structure. Via network analyses, we identify a nuclear hormone receptor as a common link between genes that are regulated by HSF-1 in a HS-dependent manner, and an epidermal growth factor receptor as a common link between genes that are regulated by HSF-1 in a HS-independent manner. HSF-1 therefore coordinates various physiological processes in *C. elegans*, and HSF-1 activity may be coordinated across tissues by nuclear hormone receptor and epidermal growth factor receptor signaling. This work provides genome-wide HSF-1 regulatory networks in *C. elegans* that are both heat stress-dependent and -independent. We show that HSF-1 is responsible for regulating many genes outside of

classical heat stress-responsive genes, including genes involved in development, metabolism, and aging. The findings that a nuclear hormone receptor may coordinate the HS-induced HSF-1 transcriptional response, while an epidermal growth factor receptor may coordinate the HS-independent response, indicate that these factors could promote non-cell autonomous signaling that occurs through HSF-1. Finally, this work highlights the genes involved in cuticle structure as important HSF-1 targets that may play roles in promoting both cytoprotection as well as longevity.

Background

When organisms are exposed to protein-denaturing stressors such as heat, the heat shock response (HSR) is engaged to manage protein damage and restore proteostasis (157). The HSR is highly-conserved across species and is regulated by the transcription factor heat shock factor 1 (HSF1). During basal conditions, HSF1 exists as a monomer in the cytoplasm and nucleus, and during stress conditions undergoes trimerization and accumulation in the nucleus, where it binds to heat shock elements in the promoters of heat shock protein (*hsp)* genes (293). HSPs primarily act as molecular chaperones which refold the misfolded proteins that accumulate during stress, but they can also have essential functions in protein synthesis, processing, and degradation (294,295). Thus the HSR, and HSPs, play a large role in maintaining organismal proteostasis.

The soil-dwelling, free-living, nematode *Caenorhabditis elegans* is a powerful model organism that has provided insights into the regulation of a number of stress response pathways, including the HSR. HSF-1, the *C. elegans* homolog to mammalian HSF1, contains conserved N-terminal DNA-binding and trimerization domains, as well as a putative transactivation domain at the C-terminus (145). It has recently been shown that

the same activity steps required for mammalian HSF1 activation, including trimerization, hyperphosphorylation, and induction of DNA-binding, are also required for worm HSF-1 activation (135,138).

Studies in *C. elegans* show that HSF-1 plays a central role not only in the HSR, but also in contributing to organismal physiology. HSF-1 is essential to worm viability, as a truncated mutant that lacks the C-terminal putative activation domain is defective in chaperone induction and egg laying, and also has a decreased lifespan (145). In addition, this strain has a temperature-sensitive developmental arrest phenotype, with arrest occurring at the L2-L3 transition (145). Various experiments using *hsf-1* RNA interference (RNAi) have shown that HSF-1 regulates the expression of specific *hsp* genes upon heat shock (HS), and have also implicated a non-stress-induced role for HSF-1 in processes including development, metabolism, and longevity (58,110,111,145,296-299). Interestingly, studies in *C. elegans* have identified the HSR as a cell non-autonomous process that requires thermosensory neurons for *hsp* induction (300). Upon the completion of sequencing of the *C. elegans* genome, over 40 percent of the predicted protein products were found to be significantly conserved in other organisms (301), and many signaling pathways are conserved (302). *C. elegans* is thus an excellent model system for studying the role of HSF-1 in stress responses and other physiological processes in a simple multicellular organism.

In this study, we have performed RNA-sequencing (RNA-seq) with synchronous larval stage L4 wild-type *C. elegans* fed empty vector (EV) control RNAi or *hsf-1* RNAi treated with or without HS. We show that significant numbers of genes are upregulated as well as downregulated by HSF-1 under both conditions. In addition to *hsp* genes, HSF-1 is

required for the regulation of genes involved in a wide variety of cellular processes including cytoprotection, development, metabolism, and aging. Network analysis points to possible routes by which HSF-1 signaling may be coordinated across tissues. A nuclear hormone receptor may coordinate the HS-induced HSF-1 transcriptional response, while an epidermal growth factor receptor may coordinate the HS-independent response. Surprisingly, the top HSF-1-regulated gene category, both with and without heat stress, is cuticle structure. This result, together with other recent studies, thus links regulation of the extracellular matrix to HSF-1, cytoprotection, and longevity.

Results

Experimental set-up for genome-wide analysis of regulation of gene expression by HSF-1

Previous experiments have shown that HSF-1 regulates the expression of specific *hsp* genes upon HS, and have also implicated a non-stress-induced role for HSF-1 in development, metabolism, and longevity (58,110,111,145,296-299). To examine HS-dependent vs. -independent gene regulation by HSF-1 on a genome-wide level, we used whole transcriptome RNA-sequencing. We treated synchronous L1 larval stage nematodes with RNAi against *hsf-1* [indicated as *hsf-1*(-)] or with an EV control plasmid [indicated as *hsf-1*(+)] until the L4 larval stage. At the L4 stage, we then treated nematodes from both groups with or without a 30 minute 33°C HS, as diagrammed (Figure E1a, see Appendix E). Experiments were performed in biological duplicates. The L4 stage was chosen for our studies as this is a time when the response to HS is strong, prior to a sharp decline that occurs shortly after the transition to adulthood (103,303). These treatment conditions, optimized for our studies, resulted in a ~9- $\log_2$-fold induction

of the *hsp-70* gene *C12C8.1*, a classical HSF-1 target gene, in *hsf-1*(+) animals treated with HS (Figure E1b, see Appendix E, black bars). As expected, RNAi against *hsf-1* blunted *hsp-70* induction by HS (Figure E1b, see Appendix E, purple bars). The efficiency of our RNAi feeding strategy was assessed by testing the effects of *hsf-1* RNAi on transcription driven by two heat shock protein promoter- GFP reporter worm strains (Figure E1c-d, see Appendix E). HS increases GFP expression, and this effect is dependent on HSF-1 as demonstrated with *hsf-1* RNAi. Using an HSF-1::GFP overexpression worm strain, we also show that HSF-1 protein levels are reduced 80% in response to *hsf-1* RNAi treatment (Figure E1e-d, see Appendix E). Overall, these data validate our HS treatment conditions and RNAi feeding strategy.

Cluster analysis performed on biological replicate RNA-seq samples revealed conserved patterns of expression induced by each treatment condition (Figure E2, see Appendix E). We normalized each condition to the *hsf-1*(+);-HS control in order to determine fold changes in relative RNA abundance (Figure E3, see Appendix E). A complete list of the significant genes altered in response to each condition, after normalization to the control, is provided in Tables E1, E2, and E3 (see Appendix E). Volcano plot analyses show that while a limited group of genes for each comparison have a $\log_2$-fold change of 6 or higher, the majority of genes have a $\log_2$ -fold change of approximately 4 or less (Figure E4a-c, see Appendix E). As growth temperature and HSF-1 expression levels can affect the rate of development in the worm (304), we verified that our observed gene expression changes were not simply due to a change in the rate of development between each treatment condition. To do this, we analyzed several genes that are known to be differentially expressed during development and molting, including

abu-11, *wrt-2*, *his-24*, *lin-29*, *abu-10*, *abu6*, *pqn-47*, *pin-42*, *ptr-3*, *abu-8*, *abu-7*, and *sdz-37* (305), and detected no significant expression differences in these genes across treatment groups (Figure E5, see Appendix E). Overall, our data indicate that the worms in our four treatment conditions are developmentally synchronous to one another, and that the biological replicates for each condition share a similar expression profile, thus validating our experimental conditions.

Next, to visualize total HS-dependent vs. -independent gene expression regulated by HSF-1, we constructed a Venn diagram with the differentially expressed genes for each condition which were determined to be statistically significant as compared to the *hsf-1*(+);-HS control (Figure E6, see Appendix E). The shaded areas of the Venn diagram correspond to HS-dependent and -independent processes regulated by HSF-1 (as indicated by the red and pink shaded areas in Figure E6, respectively), and these are the transcripts that we have focused our subsequent analyses on. Altogether, we found that 942 genes are significantly regulated by HSF-1 during HS (Figure E6, see Appendix E, red shaded area), and that 2,436 genes are significantly regulated by HSF-1 independently of HS (Figure E6, see Appendix E, pink shaded area), highlighting that HSF-1 regulates both HS-dependent and -independent transcriptional processes. Interestingly, only 4 genes are significantly regulated by HS independently of HSF-1. HSF-1 is thus not only an essential transcriptional regulator for a majority of the genes altered by HS, but global RNA expression analysis supports a gene-regulatory role for HSF-1 under both heat stress and non-stress conditions. A greater number of gene changes that depend on HSF-1 are independent of heat stress, thus highlighting the important role of HSF-1 in regulating gene expression under non-stress conditions.

Genes that are regulated by HSF-1 in response to HS

Genes that are normally upregulated by HSF-1 in response to HS

To determine whether HSF-1 can affect gene expression in both a positive and negative fashion, we separated out the positively vs. negatively regulated genes and analyzed them by Venn diagram. We find that 654 transcripts are normally upregulated by HSF-1 upon HS (Figure 6.1a, dark blue). We next examined these 654 genes in more depth. The top 15 genes in this category are listed in Table 6.1 (a complete list of the 654 significantly upregulated genes is provided in Table E1, see Appendix E). Included in the top 15 upregulated transcripts are 3 *hsp-70* family genes and 6 *hsp-16* family genes, all with $\log_2$-fold changes greater than 6. The presence of chaperone genes in our top 15 hits was expected, and gave us confidence in our experimental strategy. Aside from chaperone genes, there are a number of non-chaperones included in the top 15 most upregulated genes, including the nucleosome remodeling factor complex member *nurf-1* (306), the predicted collagen gene *col-149*, and various genes of unknown function (Table 6.1). Therefore, the top 15 genes regulated by HSF-1 under HS conditions include 9 *hsp* genes and 6 genes with diverse functions.

We then further examined the induction characteristics of the top 15 HSF-1-dependent genes induced by HS. The $\log_2$-fold changes for a subset of these genes are plotted (Figure E7a, see Appendix E, black bars) and compared to the expression of the same genes in the presence of HS but in the absence of *hsf-1* (Figure E7a, see Appendix E, purple bars). The fact that *hsf-1* RNAi completely eliminates HS-inducibility of these genes highlights their dependency on HSF-1. Independent quantitative RT-PCR (qRT-

PCR) for the same subset of highly induced genes (Figure E7b, see Appendix E) validates our RNA-seq data.

In order to better visualize the global patterns of transcript upregulation by HSF-1 in response to HS, we constructed a heat map of the 654 significantly upregulated genes (Figure 6.1b, lane 1). Interestingly, and consistent with the data for a set of the top 15 upregulated genes (Figure E7a-b, see Appendix E), genes that are normally upregulated by HSF-1 upon HS are either unchanged or downregulated under HS conditions upon *hsf-1* knockdown on a global level (Figure 6.1b, lane 2). The fact that many of the 654 HS-induced genes that require HSF-1 are downregulated upon *hsf-1* knockdown implies that HSF-1 may play a role in the basal regulation of these genes, which is then enhanced upon HS. Together, these data demonstrate the HSF-1 dependency of most HS-induced genes.

To identify the various functional processes normally upregulated by HSF-1 during HS, we used the Database for Annotation, Visualization, and Integrated Discovery (DAVID) classification tool to define the top 5 gene ontology terms for all of the 654 genes found to be significantly upregulated (Figure 6.1c). The complete output from DAVID can be found in Table E3 (see Appendix E). Surprisingly, the top functional category, with an enrichment score of 97, contains genes involved in cuticle structure. The next four categories, all with enrichment scores under 12, include genes involved in translation, the response to stress, the regulation of growth, and amine catabolic processes. We thus find that the largest functional category of genes regulated by HS is not the expected heat stress-responsive gene-set, but instead genes associated with forming cuticle structure.

We next tested the effects of a cuticle collagen gene, *col-123*, on induction of the HSR by measuring *hsp-70* promoter activity in p*hsp-70*::GFP worms (Figure E8a-c, see Appendix E). We see that *col-123* RNAi decreases HS-induced *hsp-70* promoter activity, and may control tissue-specific regulation of the HSR. Testing the effects of other collagen genes on regulation of the HSR may provide insight into a signaling role for collagens in coordinating stress responses.

Genes that are normally downregulated by HSF-1 in response to HS

We next examined the genes separated out from the Venn diagram analysis to be normally downregulated by HSF-1 upon HS (Figure 6.2). We find that there are 288 transcripts in this group (Figure 6.2a, dark purple). The top 15 genes normally downregulated by HSF-1 upon HS are listed in Table 6.2 (a complete list of the 288 significantly downregulated genes is provided in Table E1, see Appendix E). There are a variety of distinct transcripts downregulated by HSF-1 during HS. The gene with the highest $\log_2$-fold decrease (-3.71) is *acs-2,* which encodes an acyl-CoA synthetase. This enzyme participates in breakdown of fatty acids into acyl-CoA in the mitochondria to allow for β-oxidation, thus increasing fat consumption (307). Another downregulated gene is *dct-1,* which encodes a protein that has pro-apoptotic activity (308). The tetraspanin family member *tsp-1* is also downregulated. The tetraspanin family of proteins is required for epithelial integrity in the worm and regulates cuticle formation (309). Other downregulated genes include *fbxa-66* and *fbxa-21,* which encode FboxA proteins with unknown functions; *nep-26,* which encodes a zinc metallopeptidase that negatively regulates signaling peptides (310); *glc-1,* which encodes a subunit of a glutamate-gated chloride channel (311); and *delm-2,* which encodes an ortholog of an acid-sensing ion

channel family member (312). There are also multiple transcripts of unknown function in this gene group. Therefore, the top 15 genes normally downregulated by HSF-1 under HS conditions include genes with a diverse set of functions.

We then further studied the top 15 genes that are normally downregulated by HSF-1 upon HS. The $\log_2$-fold changes of a subset of the top 15 HSF-1-dependent genes repressed by HS are plotted (Figure E9a, see Appendix E, black bars), and these data are compared to the expression of the same genes in the presence of HS but in the absence of *hsf-1* (Figure E9a, see Appendix E, purple bars). Interestingly, we found that all of the genes that are downregulated by HS in the presence of HSF-1 are upregulated by HS in the absence of HSF-1. One way this could occur is if HSF-1 normally suppresses the expression of these genes, and HS-activated HSF-1 suppresses them even further. To verify our RNA-seq data, we performed independent qRT-PCR for the same subset of highly downregulated genes, and found that the qRT-PCR data was consistent with our RNA-seq data (Figure E9b, see Appendix E).

To visualize the patterns of transcripts that are normally downregulated by HSF-1 upon HS, we constructed a heat map to visualize the $\log_2$-fold changes of the 288 significantly downregulated genes (Figure 6.2b, lane 1). As a comparison, the expression of the same transcripts under HS conditions upon *hsf-1* knockdown is shown (Figure 6.2b, lane 2). As with the data for the top downregulated genes (Figure E9a-b, see Appendix E), many of the 288 genes that are normally downregulated by HSF-1 under HS conditions are conversely upregulated by HS in the absence of HSF-1. Thus, HS can have completely opposite effects on gene expression depending on the presence or absence of HSF-1.

Upon DAVID analysis of gene ontology terms for the repressed genes, the top 5 functional categories all had enrichment scores of 4 or lower. These functional categories include genes that encode proteins with kinase activity, ion binding activity, transcription, ATP-binding activity, and reproductive development (Figure 6.2c). The complete output from DAVID can be found in Table E3 (see Appendix E). Overall, these results show that a diverse group of genes are normally suppressed by HSF-1 during HS.

Genes that are regulated by HSF-1 independently of HS

Genes that are normally upregulated by HSF-1 independently of HS

While HSF-1 has been historically studied for its role in regulating responses elicited by HS, HSF-1 also has functions that are independent of HS including roles in development, metabolism, and longevity (110,111,138,297). To identify processes upregulated by HSF-1 independently of HS, we examined the 1,353 genes from the Venn diagram that we determined to be downregulated in response to *hsf-1* RNAi independently of HS, suggesting that they are normally upregulated by HSF-1 (Figure 6.3a, light purple). In order to gain insight into the normal HSF-1-regulatory role of these HS-independent genes, we reversed our data comparison [control vs. *hsf-1*(-);-HS] to obtain the fold change, as this gene group is shown to be downregulated in response to *hsf-1* RNAi and would thus normally be upregulated by HSF-1.

The top 15 genes that are normally upregulated by HSF-1 under non-stress conditions are listed in Table 6.3 (a complete list of the significantly upregulated genes is provided in Table E2, see Appendix E). Surprisingly, a group of vitellogenin lipid transporter transcripts (*vit*-1, -3,-4, and -5) are among the top 15 genes. Vitellogenins are made in the intestine of late larval/early adult hermaphrodites and are taken up by the germ cells

to provide nourishment to embryos (313). Other top upregulated genes include *acdh-1,* which encodes a short chain acyl-CoA dehydrogenase and may play a role in energy production (314,315); *K11G9.3,* which is predicted to be an ortholog of human butyrylcholinesterase; *folt-2,* which encodes a folate transporter (316); *ilys-5,* which is predicted to have lysozyme activity; *ZC266.1,* which is predicted to have G-protein coupled receptor activity; *fat-7*, which encodes a fatty acid desaturase (317); *K10B2.2,* which is predicted to have carboxypeptidase activity; *Y52E8A.4*, which encodes the ortholog to a major facilitator superfamily; *ugt-22,* which encodes the ortholog of a polypeptide predicted to have transferase activity; and two genes with unknown function. Therefore, a diverse set of genes, including vitellogenins and others, are normally upregulated by HSF-1 independently of HS.

We then further characterized the induction characteristics of the top 15 genes that are normally upregulated by HSF-1 independently of heat stress. The $\log_2$-fold changes of a subset of these top 15 genes are plotted (Figure E10a, see Appendix E, orange bars), and are compared to the expression of the same genes in the presence of HS and absence of *hsf-1* (Figure E10a, see Appendix E, purple bars). This data shows that HS does not affect the expression of these genes in the absence of *hsf-1*. The expression of these mRNAs was also verified with qRT-PCR, and the results are consistent with the RNA-seq data (Figure E10b, see Appendix E).

To investigate a HS-independent role for HSF-1 in the induction of gene expression on a global level, we generated a heat map of all 1,353 genes found via Venn diagram to be normally upregulated by HSF-1 in the absence of HS (Figure 6.3b, lane 1). As a comparison, genes that are normally upregulated by HSF-1 in the presence of HS are

plotted (Figure 6.3b, lane 2). The transcripts in this group that are normally upregulated by HSF-1 in the absence of HS remain upregulated or unchanged in the presence of HS, verifying the heat stress-independent induction of this gene group.

We next used DAVID to determine the top 5 functional processes that are normally upregulated by HSF-1 independently of HS. We found that cuticle structure was again the gene category with the highest enrichment score (9.7), as was also the case for the genes that are upregulated by HSF-1 during HS (Figure 6.3c). This indicates that HSF-1 may regulate the basal expression of genes involved in cuticle structure, and that these genes are then further induced upon HS. Other functional processes, with enrichment scores between 4-10, include genes that encode proteins involved in the mitochondrial envelope, acyl-CoA dehydrogenase activity, peptidase activity, and oxidoreductase activity. The complete output from DAVID can be found in Table E4 (see Appendix E). The mitochondrial envelope, acyl-CoA dehydrogenase activity, peptidase activity, and oxidoreductase activity are all processes that can be linked to metabolism, further substantiating a functional role for HSF-1 in regulating this process.

Genes that are normally downregulated by HSF-1 independently of HS

We next examined the 1,083 genes from the Venn diagram that we determined to be upregulated in response to *hsf-1* RNAi independently of HS, suggesting that they are normally downregulated by HSF-1 (Figure 6.4a, light blue). We reversed our data comparison [control vs *hsf-1*(-);-HS] to obtain the fold change, as this gene group is shown to be upregulated in response to *hsf-1* RNAi and would thus normally be downregulated by HSF-1. The top 15 genes in this category are listed in Table 6.4 (a complete list of the significantly downregulated genes is provided in Table E2, see Appendix E). There are a

variety of transcript types in this list, including *T22F3.11,* which is an mRNA that encodes the ortholog of the human solute carrier family 17; *eol-1,* which regulates olfactory learning (318); *BO348.2,* which encodes an ortholog of human lipopolysaccharide-induced TNF factor; *col-158,* which encodes a structural constituent of the cuticle; *fbxa-163* and *T08E11.1,* which encode proteins that contain F-box motifs predicted to be important for protein-protein interactions; *clec-174* and *clec-13*, which encode carbohydrate binding proteins; *srg-31,* which encodes a protein involved in embryo development; *clec-60,* which encodes a protein involved in the immune response; *B0507.8,* which encodes an ortholog of human cingulin-like 1; *clec-13,* which is predicted to have carbohydrate binding activity; *F22F12.1,* which encodes an ortholog of human GRB10 interacting GYF protein 2; and *Y47H10A.5* and *ZK355.8,* which both have unknown functions. Overall, we find that a diverse set of mRNAs are normally downregulated by HSF-1 independently of HS, indicating that HSF-1 may normally suppress a variety of cellular processes in a HS-independent manner.

The induction characteristics of the top 15 genes in this category were then analyzed. The $\log_2$-fold changes from the RNA-seq data for a subset these genes are plotted (Figure E10c, see Appendix E, orange bars), and are compared to the expression of the same genes in the presence of HS in the absence of *hsf-1* (Figure E10c, see Appendix E, purple bars). The expression of these mRNAs was also verified with qRT-PCR, and the results are consistent with the RNA-seq data (Figure E10d, see Appendix E). Altogether, these data confirm that HS does not affect the expression of these genes in the absence of *hsf-1*.

To investigate a HS-independent role for HSF-1 in the suppression of gene expression, we constructed a heat map of all 1,083 genes found via Venn diagram to be normally suppressed by *hsf-1* in the absence of HS (Figure 6.4b, lane 1). As a comparison, the expression patterns of the same transcripts suppressed by *hsf-1* in the presence of HS are shown (Figure 6.4b, lane 2). The transcripts in this group that are significantly downregulated by HSF-1 in the absence of HS remain downregulated or unchanged by HSF-1 in the presence of HS, further verifying that regulation of this subset of genes by HSF-1 is independent of HS.

We next used DAVID to determine the functional processes that are normally downregulated by HSF-1 independently of HS. Genes involved in cell cycle processes were most abundant, with an enrichment score of 19, followed by genes involved in epithelium development, regulation of growth, genitalia development, and cell migration, all with enrichment scores under 6 (Figure 6.4c). The complete output from DAVID can be found in Table E4 (see Appendix E). Cell cycle processes, epithelium development, regulation of growth, genitalia development, and cell migration are all processes that can be linked to development, thus confirming a HS-independent role for HSF-1 in development.

Discussion

Regulation of gene expression by HSF-1

C. elegans is a useful model organism for identifying regulatory processes that are shared between species. While the transcription factor HSF-1 has classically been studied as a factor that is responsive to cytoplasmic proteotoxic stress, it is becoming increasingly evident that this transcription factor also has major non-stress-induced roles in

coordinating gene expression. With the RNA-sequencing experiments performed here, we confirm that HSF-1 can regulate gene expression under both heat-stress and non-stress conditions. In addition to genes that are classically stress-responsive, such as chaperones, our work shows that HSF-1 also regulates sets of genes involved in a variety of cellular processes including metabolism, development, and longevity.

Cuticle structure genes are normally upregulated by HSF-1 via HS-dependent and -independent mechanisms

A surprising result of our study is that genes controlling cuticle structure comprise the largest gene ontology group that is upregulated by HSF-1 in both a HS-dependent and -independent manner. The *C. elegans* cuticle is an exoskeletal structure that creates a barrier between the animal and the environment, provides body shape, and allows movement via attachment to muscle. Many of the genes in the cuticle structure category are collagens, structural proteins that form an extracellular matrix composing the exoskeleton, or cuticle, of the nematode. There are ~154 distinct collagen genes in *C. elegans*, and they are expressed in a tissue-specific fashion and at distinct temporal times (319). Cuticle structure is controlled by enzymes involved in collagen processing, and the polymerization pattern is dictated by actin filaments that are organized in specific patterns around the body of the worm. In humans, collagens comprise about one-third of all expressed protein (320). Aside from the structural role of collagens, these genes can also participate in signal transduction (321-323). Collagen genes were recently found to be upregulated by SKN-1, the *C. elegans* oxidative stress-responsive transcription factor (324). In future work, it will be interesting to test whether collagen can act to relay signals to stress-specific transcription factors including SKN-1 and HSF-1.

Roles for HSF-1 in regulating metabolism and development in a HS-independent manner

Although HSF-1 has classically been studied as a transcription factor that responds to HS and cytoplasmic proteotoxic stress, HSF-1 has recently been gaining importance as a transcription factor that is involved in non-stress processes including development and metabolism (325,326). In mice, HSF family members have been documented to be involved in diverse developmental processes, including oogenesis, spermatogenesis, and corticogenesis (327). HSF-1 in the worm has also been shown to be regulated by insulin/IGF-1, TGF-β, and cGMP signaling to control development (328). The finding that mammalian HSF1 can be regulated by SIRT1, a deacetylase that is under metabolic control, provides evidence that HSF-1 and metabolism are linked (58). This finding is also true for *C. elegans* HSF-1, as the SIRT1 homolog SIR-2.1 regulates the *C. elegans* HSR (329). Additionally, the insulin-like signaling regulators DDL-1/2 have been linked to HSF-1 regulation (135). Here, we show that under non-stress conditions, HSF-1 upregulates a number of genes involved in developmental and metabolic processes. Therefore, our work further highlights the links between HSF-1 and these non-stress processes.

Network analysis identifies a nuclear hormone receptor as a common link between processes regulated by HSF-1 upon HS

To determine how the genes regulated by HSF-1 during HS may interact with each other, we performed network analysis using genes associated with the top GO-terms as determined by DAVID. We used the MiMI plugin to integrate data from protein interaction databases (including gene ontology databases, MeSH, and PubMed) to allow for the creation of interaction networks using the network-building software Cytoscape. This

analysis enabled us to identify interacting partners shared by at least two genes regulated by HSF-1 during HS. The transcripts induced by HSF-1 during HS are shown in red, while the transcripts downregulated by HSF-1 during HS are shown in blue, with the intensity of color correlating to the fold change. Genes that are not colored were not found to be affected by HSF-1 during HS in our dataset, but are neighbors shared by at least two genes that were affected.

We found network linkages between the processes of cuticle structure formation, translation, the response to stress, protein kinase activity, and transcription (Figure 6.5a). Interestingly, the nuclear hormone receptor *nhr-111* is a common link between several of the HS-regulated processes that require HSF-1, including cuticle structure, translation, and the response to stress. Nuclear hormone receptors comprise a class of ligand-gated transcription factors that bind to small molecule metabolites such as fatty acids, vitamins, and steroids to directly regulate gene transcription (330). They are thus well-poised to coordinate metabolism, development, reproduction, and homeostasis across diverse tissues. *nhr-111* is broadly expressed in *C. elegans* and is located in eight head neurons, the sensory PVD neurons in the posterior lateral body wall, the pharynx, the intestine, the dorsal peri-vulva region, and the somatic gonad precursor cells (331). In future work, it will be interesting to test the role of *nhr-111* and other nuclear hormone receptors in the HSR, and to see if it can contribute towards the coordination of this response across tissues.

Network analysis identifies a tyrosine kinase as a common link between various developmental processes regulated by HSF-1 independently of HS

To uncover *C. elegans* interaction networks associated with processes regulated by HSF-1 independently of HS, we performed network analysis using genes associated with the top GO-terms as determined by DAVID (Figure 6.5b). Network linkages were found for genes involved in the mitochondrial envelope, peptidase activity, oxidoreductase activity, cell cycle processes, and epithelium development. We found that *let-23,* an epidermal growth factor receptor tyrosine kinase (EGF-RTK) (332), is predicted to interact with many of these transcripts. The EGF pathway in *C. elegans* has been linked to multiple developmental pathways (333). This RTK may thus allow for signaling to HSF-1 during non-stress conditions to modulate developmental gene expression. Interestingly, HSF1 null mouse embryonic fibroblasts are defective in both basal and EGF-induced cell migration (334), so the link between HSF-1 and the EGF signaling pathways may be conserved across species. It will thus be worthwhile in future work to test for the involvement of *let-23* in the regulation of HSF-1 activity in *C. elegans*.

HSF-1 impacts aging-regulated gene expression

As HSF-1 has been implicated to play an important role in both aging and disease (335), we analyzed the role of HSF-1 in regulating age-associated transcriptional changes in our data sets (Figure 6.6). By comparing the transcriptome profiles between young and old adult *C. elegans,* a previous study by Budovskaya *et al.* identified 1,254 genes to be differentially regulated upon worm aging (336). A Venn diagram comparison of these 1,254 age-regulated genes with those that we found to be regulated by HSF-1 during HS shows that 174 aging-associated genes overlapped with our dataset (Figure 6.6a). Table

E5 (see Appendix E) lists the genes shared between both datasets. The functional processes regulated by this overlapping gene set were then determined via DAVID analysis. Cuticle structure was the largest functional category, with an enrichment score of 76 (Figure 6.6b). Other gene categories, all with enrichment scores of 5 or lower, include cuticle development, the response to stress, amine catabolic processes, carbohydrate binding, and membrane structure. Network analysis performed the 174 overlapping genes shows that only a small subset of these genes are predicted to interact with each other (Figure 6.6c).

Next, a comparison between aging-associated genes and those we found to be regulated by HSF-1 independently of HS was done. A Venn diagram shows that 275 aging-associated genes overlapped with our dataset (Figure 6.6d), and Table E6 (see Appendix E), lists the genes shared between both data-sets. The functional processes regulated by this gene set was then determined via DAVID analysis. Cuticle structure was again the largest category, with an enrichment score of 9. The other categories, with enrichment scores of 5 or lower, include peptidase activity, C-type lectin, vitamin binding, and lifespan-associated processes (Figure 6.6e). The transcriptional impact of these HSF-1 and aging-regulated genes that are independent of HS was then determined by network generation (Figure 6.6f). Interestingly, the interaction network of aging-associated genes regulated by HSF-1 independently of HS is four-fold larger than the network of aging genes that depend on HS. We thus conclude that HSF-1 may have a role in impacting longevity that can be separated from its role in stress responses.

HSF-1 regulates collagen genes which may affect the aging process

It is interesting that the cuticle structure genes constitute the largest overlap with aging-related genes. In humans, mutations in collagens lead to a large number of heritable human diseases, including rare diseases as well as common ones such as osteoporosis and musculoskeletal diseases (337). Collagens are long-lived proteins known to accumulate damage during aging, leading to a decline in tissue health (338). Also, type I collagens become resistant to proteolysis upon age (339,340), affecting their turnover. Interestingly, mice expressing cleavage-resistant type I collagen go through an accelerated aging process (341). Thus, cellular aging can be affected by the state of the extracellular matrix in mammals.

Recently, collagen production and extracellular matrix remodeling were determined to be essential for longevity in *C. elegans*. Collagen may directly affect signaling processes associated with longevity in *C. elegans*, including signaling through SKN-1 (324,342). We note that HSF-1 was also recently shown to regulate cytoskeletal integrity in a process that can influence stress resistance and longevity in *C. elegans* (343). Thus, the linkage of both the extracellular matrix and the cytoskeleton to HSF-1 may provide a mechanism by which HSF-1 promotes longevity.

Conclusion

Next generation sequencing has allowed us to uncover highly varied roles for *C. elegans* HSF-1 in both HS-dependent and -independent mechanisms, including roles in the regulation of development, cytoprotection, metabolism, and aging (for a model, see Figure E11 in Appendix E). Network analyses show that under HS conditions, the nuclear hormone receptor NHR-111 may allow coordination of the HSF-1 response across

tissues, while under basal conditions, the EGF receptor LET-23 may regulate a similar coordination. These findings warrant further studies in order to further understand the methods of non-cell-autonomous signaling across tissues. A striking result shown here is that multiple genes involved in cuticle structure, including collagen genes, are enriched as HSF-1 targets in HS-dependent and -independent manners. As recent studies link collagen to cytoprotection and longevity, the regulation of collagen expression may be one method by which HSF-1 enhances lifespan. Harnessing the ability of HSF-1 to regulate collagen could thus have broad appeal in the treatment of diseases of aging.

Methods

C. elegans strains and maintenance

The wild-type N2 strain, p*hsp-70*(*C12C8.1*)::GFP (111), p*hsp-16.2*(*Y46H3A.3*)::GFP (344), and EQ73 (HSF-1::GFP) (135) strains were used in this study. Worms were maintained at 23°C on standard NGM plates seeded with *Escherichia coli* OP50 (345-347). A synchronous population of nematodes was obtained by standard 20% hypochlorite treatment, and a 24 hour rotation at 220 rpm in M9 buffer without food.

RNA interference and heat shock conditions

Approximately 4,000 wild-type nematodes were synchronized and placed at the L1 larval stage onto standard NGM plates supplemented with 50 µg/mL ampicillin and 1 mM isopropyl-beta-D-thiogalactopyranoside seeded with either HT115 bacteria containing an empty plasmid (L4440, control), or sequence-verified gene-specific RNAi isolated from the Ahringer RNAi library (146). RNAi bacteria were allowed to induce on the plates overnight at room-temperature. Synchronized animals developed on RNAi plates before being treated at the L4 stage with a 30 minute 33°C HS by submerging the plates in a

water bath. The time and duration of HS was optimized for this experiment (Figure E1 B-D, see Appendix E). Worms were then collected for RNA extraction.

Immunoblotting and quantification

Animals were harvested in Buffer C (20 mM HEPES pH 7.9, 25% Glycerol, 0.42 M NaCl, 1.5 mM MgCl2, 0.2 mM EDTA, and 0.5 mM DTT) with the addition of Halt™ protease inhibitors (Pierce, cat# 78430). Protein was extracted by sonication with a Diagenode Bioruptor 300 for 10 minutes with 30 second pulses. Protein was quantified by Bradford assay, resolved on a 10% SDS-PAGE gel, and transferred to a PVDF membrane. The blot was incubated with an α-GFP polyclonal antibody (Abcam, cat# ab290) at a 1:2500 dilution and with α-Actin (Amersham, cat# JLA20-C) at a 1:750 dilution. Quantification of band intensity was performed using ImageJ Software (v. 1.44; http://imagej.nih.gov/ij/).

RNA preparation for RNA-seq

Total RNA was prepared using TRIzol® reagent (Ambion®, cat# 15596-026) by standard protocols, and then cleaned up on RNeasy columns (QIAgen, cat# 74104). RNA integrity analysis, sample preparation, and RNA-sequencing was performed at the Yale Center for Genome Analysis using the Illumina HiSeq 2000 sequencing system.

RNA-seq data analysis

A quality-control analysis of raw RNA-seq reads was performed using the FastQC program (348). Short reads were aligned to the *C. elegans* reference genome (ws200 release) using Bowtie software (349). The program TopHat was used to discover transcript splicing junctions (350). The program Cufflinks was chosen to assemble the aligned reads, estimate their abundance, and calculate the fragments per kilobase of exon per million fragments mapped (FPKM) values (351). Transcripts that were

differentially expressed in different conditions, compared to the *hsf-1*(+);-HS control, were determined with CuffDiff, which uses the Benjamini-Hochberg correction for multiple testing to obtain the q-value (the FDR-adjusted the p-value) (352). The results were visualized with a dendogram using the program CummeRbund (352). The RNA-seq data has been deposited in NCBI SRA database (Access ID: PRJNA311958).

Volcano plot analysis

Volcano plots were made using GraphPad Prism Software (GraphPad Software, La Jolla California USA, http://www.graphpad.com), where the Y-axis represents the q-value (FDR-corrected p-value) after being adjusted to reflect a $-\log_{10}$ value, and the X-axis represents the $\log_2$-fold change of each mRNA after comparison to the *hsf-1*(+);-HS control.

Venn diagram analysis

Venny 2.0 (353) was used to construct Venn diagrams with the significantly altered mRNAs for each condition (q-value<0.05) as compared to the *hsf-1*(+);-HS control.

Quantitative RT-PCR

qRT-PCR was performed to validate the top hits from our RNA-seq data. An aliquot of the RNA samples that were used for sequencing were reverse transcribed into cDNA using a High Capacity cDNA Reverse Transcription Kit (Applied Biosystems, cat# 4368814) according to the manufacturer's instructions. cDNA was diluted to 50 ng/µl to be used as a template for qRT-PCR which was performed with the Step One Plus Real-time PCR system (Applied Biosystems) using iTaq™ Universal SYBR® Green Supermix (BioRad, cat# 172-5121) according to manufacturer's instructions. Data analysis was performed according to standard calculations using the comparative Ct method (189). Relative

mRNA levels were normalized to *gapdh*, and calculated from two biological replicates and technical triplicates. Primer sequences are available upon request. Statistical analyses were carried out with GraphPad Prism Software (GraphPad Software, La Jolla California USA, http://www.graphpad.com) using ANOVA followed by the Bonferroni post-hoc test. Error bars are representative of standard deviation between independent biological replicates.

Fluorescence microscopy

Animals were anesthetized with 10 mM Levamisole and photographed using an EVOS fluorescence microscope. Image processing was accomplished using Adobe Photoshop© (Adobe Systems Incorporated, San Jose, CA).

Heat map generation

The heat maps were organized using Cluster 3, by organizing the genes into 3 clusters, using K-means and 100 runs, and the Euclidean distance similarity metric (354).

Gene ontology analysis via DAVID

Database for Annotation, Visualization, and Integrated Discovery (DAVID) was used to identify over-represented gene ontology terms using the Functional Annotation Clustering tool and a high classification stringency (355). The enrichment score provided by DAVID takes into account the probability that the members of a gene cluster are present randomly in the gene list. The enrichment score determines biologically significant functional groups by using the p-values for a cluster of genes to determine the geometric mean of that cluster (in negative log scale), where if the geometric mean of the p-values = $1e^{-10}$, then the enrichment score would be 10.

Network analysis with the Cytoscape platform

Network analysis was performed using the MiMI plugin for the Cytoscape platform (356). The MiMI plugin integrates data from protein interaction databases including gene ontology databases, MeSH, and PubMed to allow the creation of interaction networks using the network-building software Cytoscape. Interacting partners shared by at least two mRNAs were identified and used to construct interaction pathways.

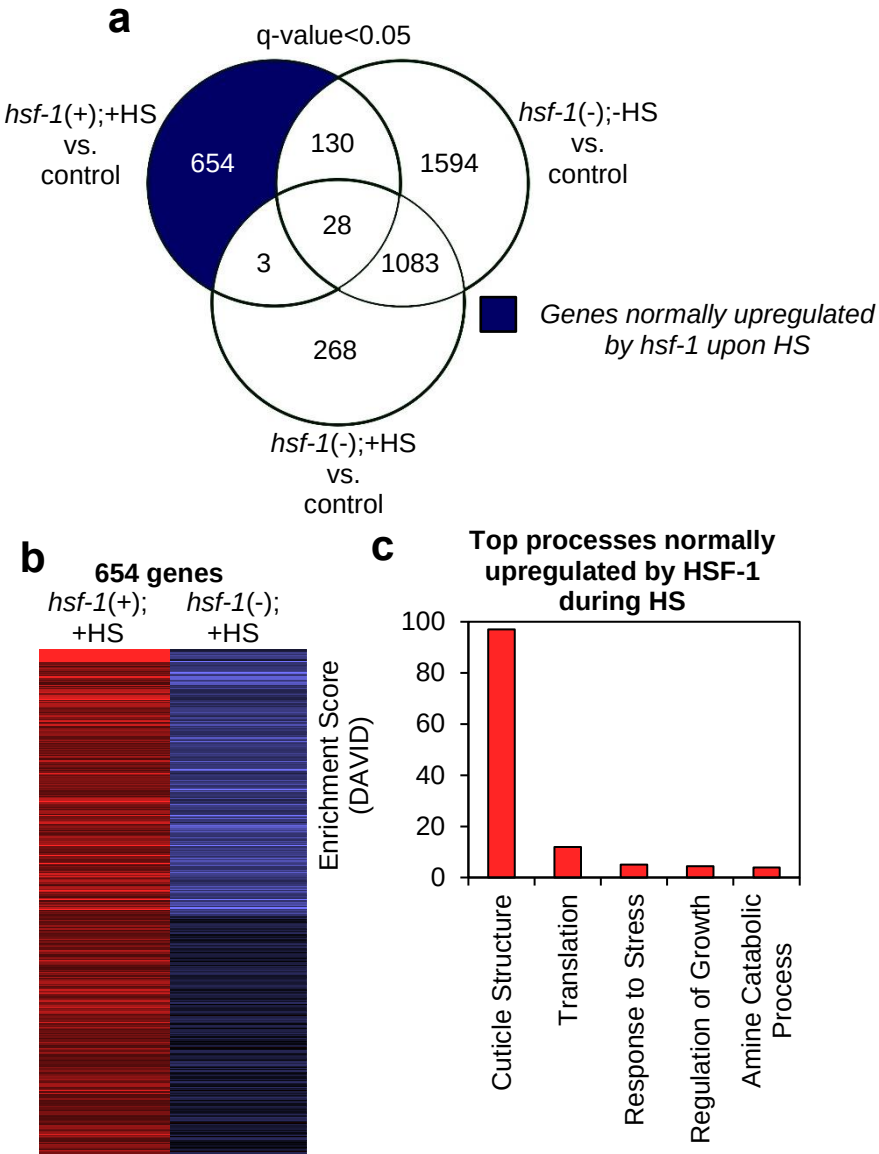

Figure 6.1. Genes that are normally upregulated by HSF-1 in response to HS. (**a**) The Venn diagram shows the overlap among genes that were found to be significantly upregulated (q-value<0.05) for each of the indicated comparisons between samples. The dark blue shaded area includes genes that are normally upregulated by HSF-1 upon HS. The q-value is the FDR-adjusted p-value of the test statistic, as determined by the Benjamini-Hochberg correction for multiple testing. (**b**) Hierarchical clustering of the genes normally upregulated by HSF-1 upon HS. Lane 1 corresponds to the fold change of the 654 genes found in the dark blue section of the Venn diagram in (**a**) in the *hsf-1*(+);+HS vs. control samples. As a comparison, lane 2 corresponds to the fold change of the same genes found in lane 1, but in the *hsf-1*(-);+HS vs. control samples, as determined by RNA-seq. The heat map was organized using Cluster 3 by k-means and Euclidean distance. (**c**) Top processes normally upregulated by HSF-1 during HS. The genes found in the dark blue section of the Venn diagram in (**a**) were classified by Gene Ontology terms that were determined using DAVID.

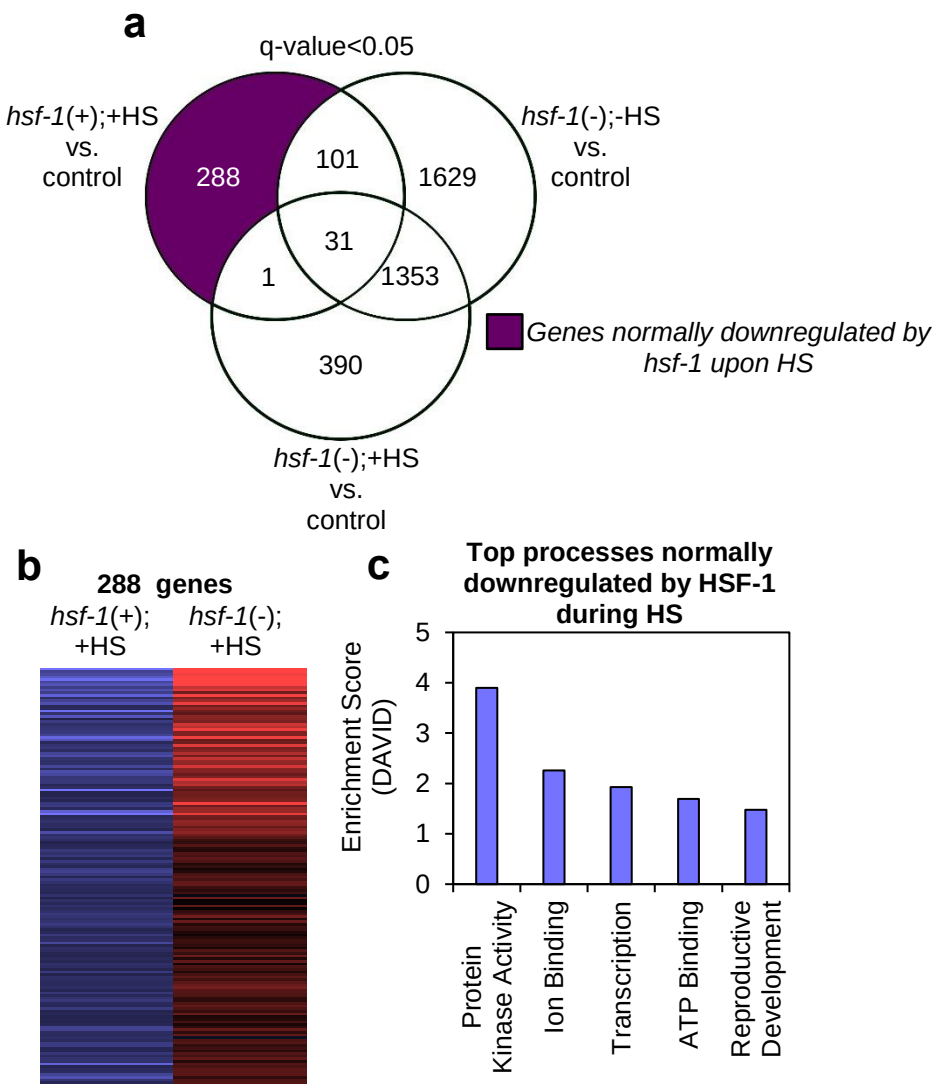

Figure 6.2 Genes that are normally downregulated by HSF-1 in response to HS. (**a**) The Venn diagram shows the overlap among genes that were found to be significantly downregulated (q-value<0.05) for each of the indicated comparisons between samples. The dark purple shaded area includes genes that are normally downregulated by HSF-1 upon HS. The q-value is the FDR-adjusted p-value of the test statistic, as determined by the Benjamini-Hochberg correction for multiple testing. (**b**) Hierarchical clustering of the genes normally downregulated by HSF-1 upon HS. Lane 1 corresponds to the fold change of the 288 genes found in the dark purple section of the Venn diagram in (**a**) in the *hsf-1*(+);+HS vs. control samples. As a comparison, lane 2 corresponds to the fold change of the same genes found in lane 1, but in the *hsf-1*(-);+HS vs control samples, as determined by RNA-seq. The heat map was organized using Cluster 3 by k-means and Euclidean distance. (**c**) Top processes normally downregulated by HSF-1 during HS. The genes found in the dark purple section of the Venn diagram in (**a**) were classified by Gene Ontology terms that were determined using DAVID.

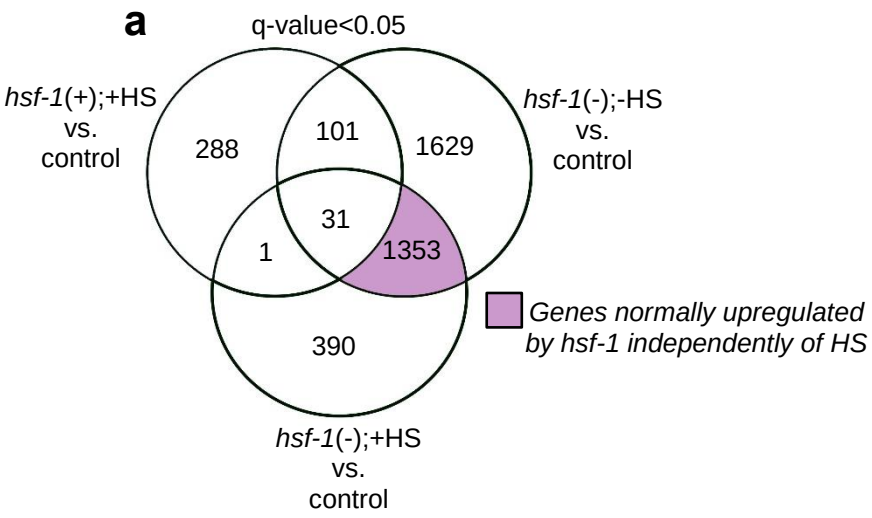

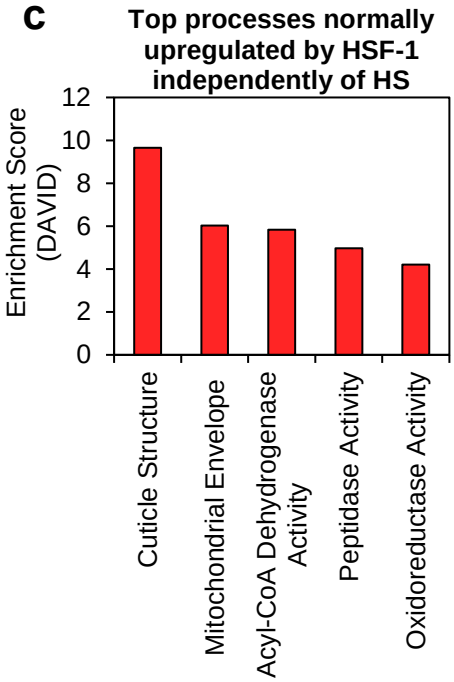

Figure 6.3. Genes that are normally upregulated by HSF-1 independently of HS. (**a**) The Venn diagram shows the overlap among genes that were found to be significantly downregulated (q-value<0.05) for each of the indicated comparisons between samples. The light purple shaded area includes genes that are downregulated upon treatment with *hsf-1* RNAi, and are likely normally induced by HSF-1 independently of heat shock, therefore are referred to as upregulated genes. The q-value is the FDR-adjusted p-value of the test statistic, as determined by the Benjamini-Hochberg correction for multiple testing. (**b**) Hierarchical clustering of the genes normally upregulated by HSF-1 independently of HS. The fold change of genes found in the light purple section of the Venn diagram in (**a**) were determined by RNA-seq to be downregulated in response to *hsf-1* RNAi, and would thus normally be upregulated by HSF-1. Lane 1 corresponds to the fold change of these genes in the control vs. *hsf-1*(-);-HS samples, and as a comparison, lane 2 corresponds to each the fold change of the same genes found in lane 1 but in the control vs. *hsf-1*(-);+HS samples. The heat map was organized using Cluster 3 by k-means and Euclidean distance. (**c**) Top processes normally upregulated by HSF-1 independently of HS. The genes found in the light purple section of the Venn diagram were classified by Gene Ontology terms that were determined using DAVID.

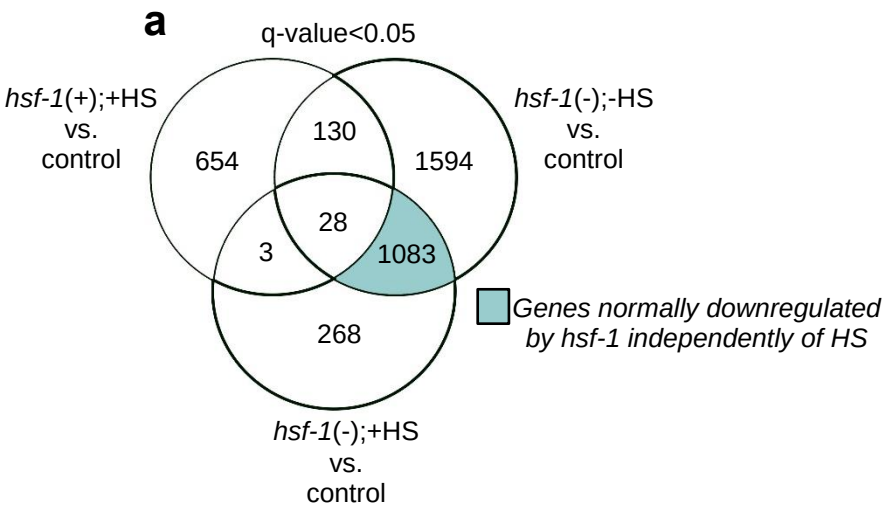

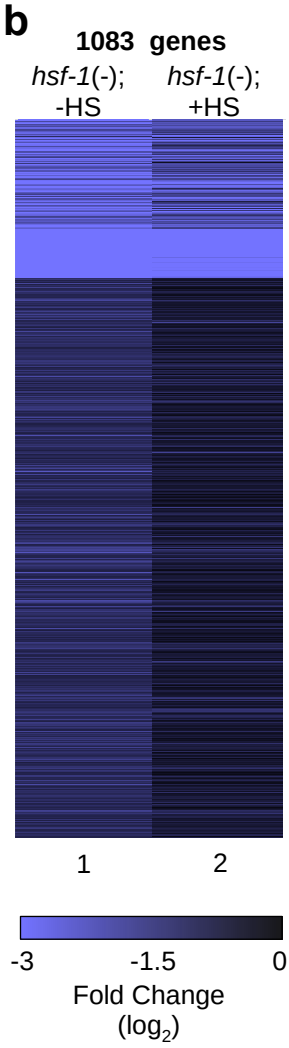

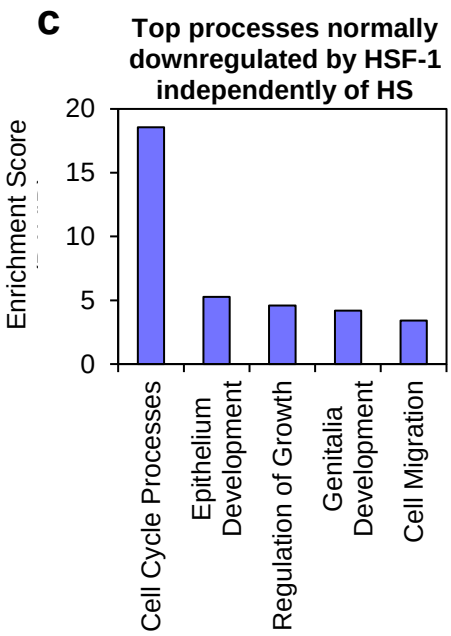

Figure 6.4. Genes that are normally downregulated by HSF-1 independently of HS. (**a**) The Venn diagram shows the overlap among genes that were found to be significantly upregulated (q-value<0.05) for each of the indicated comparisons between samples. The light blue shaded area includes genes that are upregulated upon treatment with *hsf-1* RNAi, and are likely normally suppressed by HSF-1 independently of heat shock, therefore are referred to as downregulated genes. The q-value is the FDR-adjusted p-value of the test statistic, as determined by the Benjamini-Hochberg correction for multiple testing. (**b**) Hierarchical clustering comparing the genes normally suppressed by HSF-1 independently of HS. The fold change of genes found in the light blue section of the Venn diagram in (**a**) were determined by RNA-seq to be upregulated in response to *hsf-1* RNAi, and would thus normally be suppressed by HSF-1. Lane 1 corresponds to the fold change of these genes in the control vs. *hsf-1*(-);-HS samples, and as a comparison, lane 2 corresponds to each the fold change of the same genes found in lane 1 but in the control vs. *hsf-1*(-);+HS samples. The heat map was organized using Cluster 3 by k-means and Euclidean distance. (**c**) Top processes normally downregulated by HSF-1 independently of HS. The genes found in the light blue section of the Venn diagram were classified by Gene Ontology terms that were determined using DAVID.

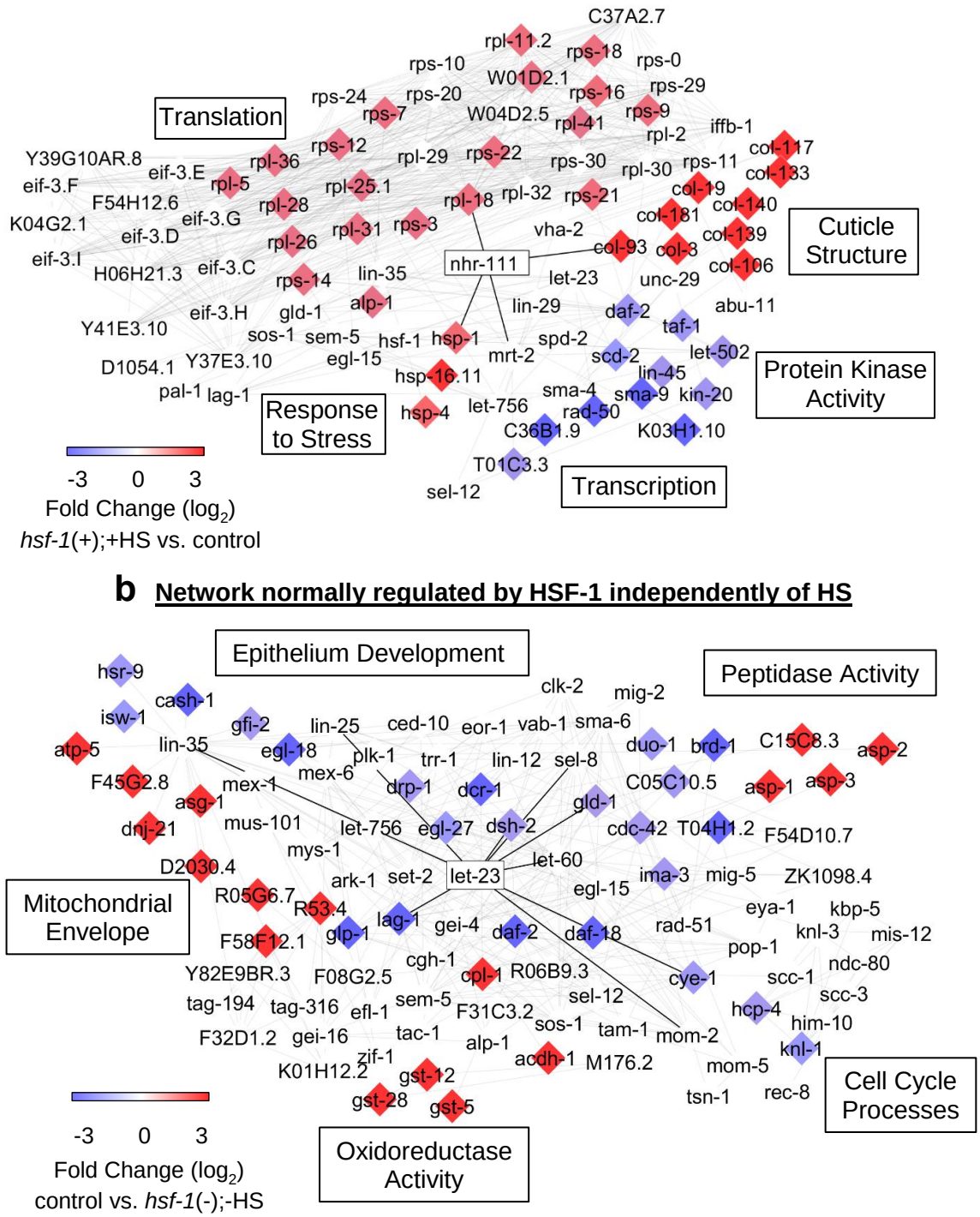

Figure 6.5. Network analyses of the top HSF-1-regulated processes. (**a**) Predicted network regulated by HSF-1 during HS**.** Genes associated with the top 5 induced and suppressed processes in Figure 6.1c and 6.2c were used for analysis. (**b)** Predicted network regulated by HSF-1 independently of HS. Genes associated with the top 5 induced and suppressed processes in Figure 6.3c and 6.4c were used for analysis. For (**a**) and (**b**), the color of each gene corresponds to the degree of HSF-1 regulation of the corresponding transcript. Network analysis was done with MiMI using the Cytoscape platform. The uncolored genes were not affected by HSF-1 during or independently of HS in our dataset, but are neighbors shared by at least two genes that were affected in our dataset.

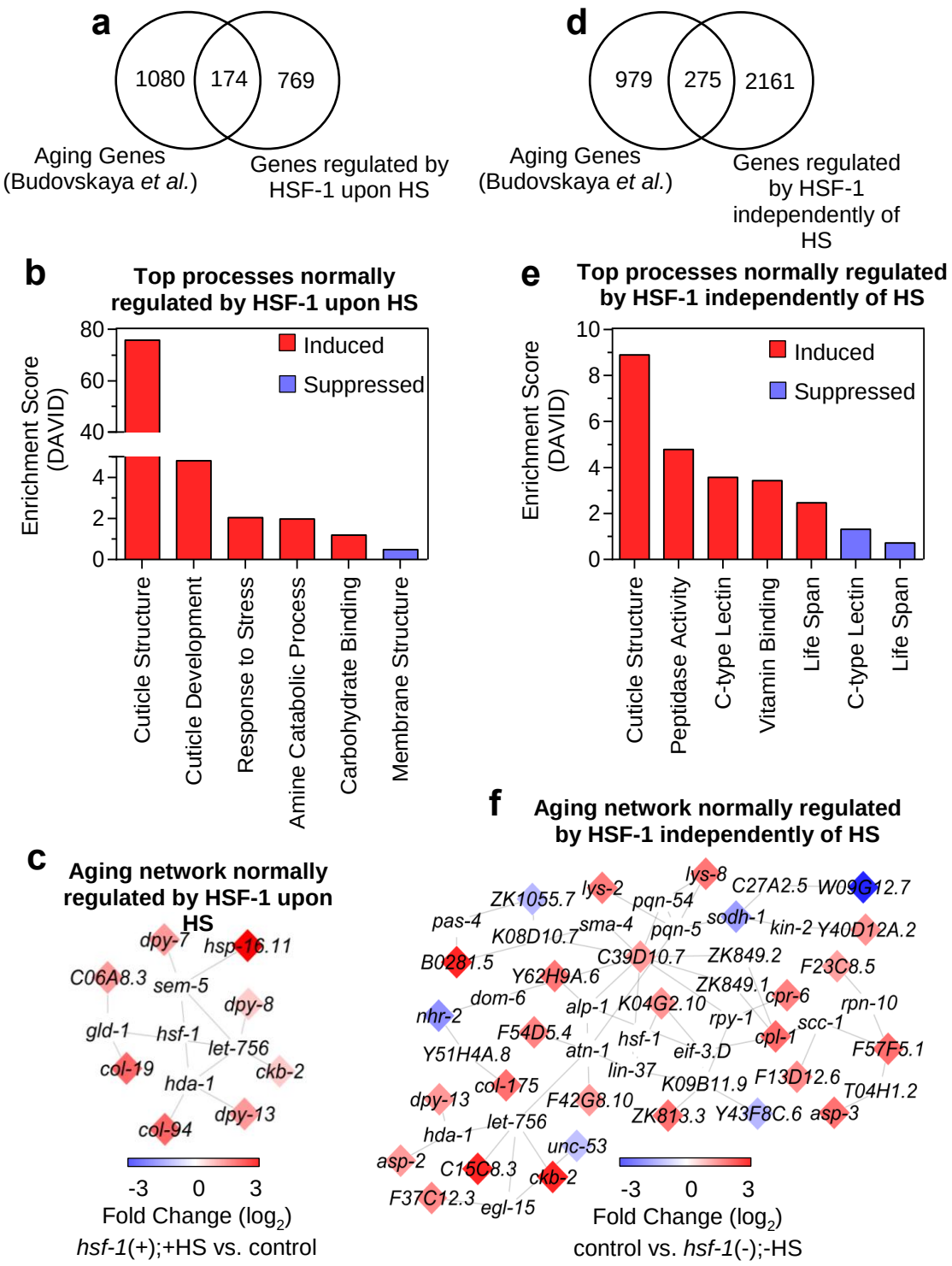

Figure 6.6. Age-regulated genes controlled by HSF-1. (**a**) The Venn diagram shows the overlap among genes that are differentially expressed during aging and regulated by HSF-1 during HS. The Venn diagram was made using genes previously found to be regulated during aging by *Budovskaya et al.* compared to genes we found to be regulated by HSF-1 during HS. (**b**) Cellular processes affected by aging and HSF-1 during HS. Genes shared between the aging dataset and HSF-1-regulated HS-dependent dataset from (**a**) were analyzed with DAVID and the Gene Ontology terms are listed in order of decreasing enrichment. (**c**) Network analysis of the genes regulated by aging and HSF-1 during HS.-

Figure 6.6. Age-regulated genes controlled by HSF-1 (Continued). Network analysis was done with MiMI using the Cytoscape platform and the transcripts listed in Table E6 (see Appendix E). The color of each transcript corresponds to the degree of HSF-1 regulation. Genes that are not colored were not affected by HSF-1 our dataset, but are neighbors shared by at least two genes that were affected in our dataset. (**d**) The Venn diagram shows the overlap among genes that are differentially expressed during aging and regulated by HSF-1 independently of HS. The Venn diagram was made using genes previously found to be regulated during aging by *Budovskaya et al.* compared to genes we found to be regulated by HSF-1 independent of HS. (**e**) Cellular processes affected by aging and HSF-1 independently of HS. Genes shared between the aging dataset and HSF-1-regulated HS-independent dataset from (**c**) were analyzed with DAVID and the Gene Ontology terms are listed in order of decreasing enrichment. (**f**) Network analysis of the genes regulated by aging and HSF-1 independently of HS. Network analysis was done with MiMI using the Cytoscape platform and the transcripts listed in Table E7 (see Appendix E). The color of each transcript corresponds to the degree of HSF-1 regulation. Genes that are not colored were not affected by HSF-1 in our dataset, but are neighbors shared by at least two genes that were affected in our dataset.

Table 6.1. Top 15 genes normally upregulated by HSF-1 upon HS.

	Transcript ID	Gene Name	Fold Change (log_2) *hsf-1*(+);+HS vs control	Description (WormBase)
1	*F44E5.5*	*F44E5.5*	8.06	*F44E5.5* encodes a member of the Hsp70 family of heat shock proteins
2	*F44E5.4*	*F44E5.4*	7.87	*F44E5.4* encodes a member of the Hsp70 family of heat shock proteins
3	*Y46H3A.3*	*hsp-16.2*	7.53	*hsp-16.2* encodes a 16-kD heat shock protein (HSP) that is a member of the hsp16/hsp20/alphaB-crystallin (HSP16) family of heat shock proteins
4	*Y46H3A.2*	*hsp-16.41*	7.41	*hsp-16.41* encodes a 16-kD heat shock protein (HSP) that is a member of the hsp16/hsp20/alphaB-crystallin (HSP16) family of heat shock proteins
5	*T27E4.2*	*hsp-16.11*	7.31	*hsp-16.11* encodes a 16-kD heat shock protein (HSP) that is a member of the hsp16/hsp20/alphaB-crystallin (HSP16) family of heat shock proteins
6	*C12C8.1*	*hsp-70*	7.15	*hsp-70* encodes a heat-shock protein that is a member of the HSP70 family of molecular chaperones
7	*T27E4.8*	*hsp-16.1*	6.9	*hsp-16.1* encodes a 16-kD heat shock protein (HSP) that is a member of the hsp16/hsp20/alphaB-crystallin (HSP16) family of heat shock proteins
8	*T27E4.3*	*hsp-16.48*	6.77	*hsp-16.48* encodes a 16-kD heat shock protein (HSP) that is a member of the hsp16/hsp20/alphaB-crystallin (HSP16) family of heat shock proteins
9	*Y38E10A.13*	*nspe-1*	6.54	*nspe-1* is a nematode-specific peptide that has an unknown function
10	*T27E4.9*	*hsp-16.49*	6.5	*hsp-16.49* encodes a 16-kD heat shock protein (HSP) that is a member of the hsp16/hsp20/alphaB-crystallin (HSP16) family of heat shock proteins
11	*F26H11.2*	*nurf-1*	4.15	*nurf-1* encodes the *C. elegans* ortholog of *Drosophila* NURF301, a component of the NURF chromatin remodeling complex
12	*ZC21.10*	*ZC21.10*	3.84	Unknown function
13	*D2013.8*	*scp-1*	3.68	*scp-1* encodes PTC-related protein that contains a sterol-sensing domain related to human Sterol regulatory element binding protein (SREBP) cleavage activating protein
14	*R107.5*	*R107.5*	3.29	Unknown function
15	*B0024.1*	*col-149*	3.01	*col-149* is predicted to be a structural constituent of the cuticle

Table 6.2. Top 15 genes normally downregulated by HSF-1 upon HS.

	Transcript ID	Gene Name	Fold Change (log_2) *hsf-1*(+);+HS vs control	Description (WormBase)
1	*F28F8.2*	*acs-2*	-3.71	*acs-2* encodes an acyl-CoA synthetase; by homology, ACS-2 is predicted to catalyze conversion of a fatty acid to Acyl-CoA for subsequent beta oxidation
2	*W09G12.7*	*W09G12.7*	-3.28	Unknown function
3	*C07A4.2*	*C07A4.2*	-2.85	Unknown function
4	*C14F5.1*	*dct-1*	-2.84	*dct-1* encodes a protein with similarity to the mammalian BNIP3 proteins that interact with Bcl-2 and the Adenovirus E1B proteins which have been shown to have pro-apoptotic activity
5	*C02F5.8*	*tsp-1*	-2.81	*tsp-1* is a part of the tetraspanin family that encodes an ortholog of a human CD151 molecule
6	*Y54F10BM.11*	*fbxa-66*	-2.63	*fbxa-66* encodes an FboxA protein that has an unknown function
7	*Y119D3B.9*	*fbxa-21*	-2.55	*fbxa-21* encodes an FboxA protein that has an unknown function
8	*K08D9.4*	*K08D9.4*	-2.54	Unknown function
9	*C49G7.7*	*C49G7.7*	-2.52	Unknown function
10	*T12A7.6*	*T12A7.6*	-2.42	Unknown function
11	*F33H12.7*	*F33H12.7*	-2.30	Unknown function
12	*Y47H10A.5*	*Y47H10A.5*	-2.14	Unknown function
13	*ZK970.1*	*nep-26*	-2.12	*nep-26* is a thermolysin-like zinc metallopeptidase found on the surface of cells that negatively regulates small signaling peptides
14	*F11A5.10*	*glc-1*	-2.07	*glc-1* is the alpha subunit of a glutamate-gated chloride channel
15	*C24G7.1*	*delm-2*	-2.06	*delm-2* encodes an ortholog of human acid-sensing ion channel family member 4, and is predicted to have sodium channel activity

Table 6.3. Top 15 genes normally upregulated by HSF-1 independently of HS.

	Transcript ID	Gene Name	Fold Change (log_2) *hsf-1*(-);-HS vs control	Description (WormBase)
1	*C55B7.4*	*acdh-1*	4.62	*acdh-1* encodes a short-chain acyl-CoA dehydrogenase. ACDH-1 is predicted to be a mitochondrial enzyme that catalyzes the first step of fatty acid beta-oxidation, and thus plays a key role in energy production
2	*F59D8.1*	*vit-3*	3.52	*vit-3* encodes a vitellogenin, a precursor of the lipid-binding protein related to vertebrate vitellogenins and mammalian ApoB-100, a core LDL particle constituent
3	*F59D8.2*	*vit-4*	3.47	*vit-4* is involved in embryo development and is predicted to have lipid transporter activity
4	*C04F6.1*	*vit-5*	3.39	*vit-5* encodes a vitellogenin, a lipid-binding protein precursor related to vertebrate vitellogenins and mammalian ApoB-100, a core LDL particle constituent
5	*K09F5.2*	*vit-1*	3.38	*vit-1* is predicted to have lipid transporter activity
6	*Y40H7A.10*	*Y40H7A.10*	3.37	Unknown function
7	*K11G9.3*	*K11G9.3*	3.15	*K11G9.3* encodes an ortholog of human butyrylcholinesterase
8	*F37B4.7*	*folt-2*	3.06	*folt-2* encodes a putative folate transporter and is orthologous to the human folate transporters SLC19A1, SLC19A2, and SLC19A3
9	*F22A3.6*	*ilys-5*	2.99	*ilys-5* is involved in embryo development and is predicted to have lysozyme activity
10	*ZC266.1*	*ZC266.1*	2.76	*ZC266.1* is predicted to have G-protein coupled receptor activity
11	*F10D2.9*	*fat-7*	2.64	*fat-7* encodes an essential delta-9 fatty acid desaturase that is required for the synthesis of monounsaturated fatty acids
12	*K10B2.2*	*K10B2.2*	2.55	*K10B2.2* encodes an ortholog of human cathepsin A and is predicted to have carboxypeptidase activity
13	*Y52E8A.4*	*Y52E8A.4*	2.46	*Y52E8A.4* encodes an ortholog of human major facilitator superfamily domain containing 11
14	*C08F11.8*	*ugt-22*	2.44	*ugt-22* encodes an ortholog of human UDP glucuronosyltransferase 1 family polypeptide, and is predicted to have transferase activity
15	*F54F7.2*	*F54F7.2*	2.44	Unknown function

Table 6.4. Top 15 genes normally regulated by HSF-1 independently of HS.

	Transcript ID	Gene Name	Fold Change (log_2) *hsf-1*(-);-HS vs control	Description (WormBase)
1	*T22F3.11*	*T22F3.11*	-5.85	*T22F3.11* encodes an ortholog of human solute carrier family 17
2	*T26F2.3*	*eol-1*	-5.38	*eol-1* is required in the URX sensory neurons for inhibition of olfactory learning
3	*B0348.2*	*B0348.2*	-5.32	*B0348.2* encodes an ortholog of human lipopolysaccharide-induced TNF factor
4	*Y47H10A.5*	*Y47H10A.5*	-5.17	Unknown function
5	*D2023.7*	*col-158*	-5.17	*col-158* is predicted to be a structural constituent of the cuticle
6	*C08E3.6*	*fbxa-163*	-4.95	*fbxa-163* encodes a protein containing an F-box, a motif predicted to mediate protein-protein interactions
7	*F07E5.9*	*F07E5.9*	-4.90	Unknown function
8	*Y46C8AL.2*	*clec-174*	-4.89	*clec-174* is predicted to have carbohydrate binding activity
9	*T07H8.5*	*srg-31*	-4.84	*srg-31* is involved in embryo development and is predicted to have transmembrane signaling receptor activity
10	*ZK666.6*	*clec-60*	-4.81	*clec-60* appears to play a role in the innate immune response to some bacterial pathogens
11	*B0507.8*	*B0507.8*	-4.64	*B0507.8* encodes an ortholog of human cingulin-like 1
12	*ZK355.8*	*ZK355.8*	-4.60	Unknown function
13	*H16D19.1*	*clec-13*	-4.50	*clec-13* is predicted to have carbohydrate binding activity
14	*T08E11.1*	*T08E11.1*	-4.37	*T08E11.1* encodes a protein containing an F-box motif predicted to mediate protein-protein interactions
15	*F22G12.1*	*F22G12.1*	-4.35	*F22G12.1* encodes an ortholog of human GRB10 interacting GYF protein 2

CHAPTER 7. HSF-1 IS A REGULATOR OF MIRNA EXPRESSION IN *CAENORHABDITIS ELEGANS*

Authored by: Jessica Brunquell, Feng Cheng and Sandy D. Westerheide

Accepted with Revisions to PLOS ONE

All experiments were performed by J. Brunquell. J. Brunquell performed miRNA extraction for miRNA-sequencing, RNA-sequencing, RNAi verification, and fluorescent imaging. F. Cheng contributed to data analyses, normalization of the sequencing data, and dendogram clustering of the samples. J. Brunquell, F. Cheng, and S.D. Westerheide participated in design of the study. The manuscript was written by J. Brunquell and S.D. Westerheide.

Abstract

The ability of an organism to sense and adapt to environmental stressors is essential for proteome maintenance and survival. The highly-conserved heat shock response is a survival mechanism employed by all organisms, including the nematode *Caenorhabditis elegans*, upon exposure to environmental extremes. Transcriptional control of the metazoan heat shock response is mediated by the heat shock transcription factor HSF-1. In addition to regulating global stress-responsive genes to promote stress-resistance and survival, HSF-1 has recently been shown to regulate stress-independent functions in controlling development, metabolism, and longevity. However, the indirect role of HSF-1 in coordinating stress-dependent and -independent processes through post-transcriptional regulation is largely unknown. MicroRNAs (miRNAs) have recently

emerged as a class of post-transcriptional regulators that control gene expression through translational repression or mRNA degradation. To determine the role of HSF-1 in regulating miRNA expression, we have performed high-throughput small RNA-sequencing in *C. elegans* grown in the presence and absence of *hsf-1* RNAi followed by treatment with or without heat shock. This has allowed us to uncover the miRNAs regulated by HSF-1 via heat-dependent and -independent mechanisms. Integrated miRNA/mRNA target-prediction analyses suggest HSF-1 as a post-transcriptional regulator of development, metabolism, and longevity through regulating miRNA expression. This provides new insight into the possible mechanism by which HSF-1 controls these processes. We have also uncovered oxidative stress response factors and insulin-like signaling factors as a common link between processes affected by HSF-1-regulated miRNAs in stress-dependent and -independent mechanisms, respectively. This may provide a role for miRNAs in regulating cross-talk between various stress responses. Our work therefore uncovers an interesting potential role for HSF-1 in post-transcriptionally controlling gene expression in *C. elegans*, and suggests a mechanism for cross-talk between stress responses.

Introduction

The ability of an organism to adapt to proteotoxic stressors is essential for long-term survival. The mammalian heat shock factor HSF1 is a highly-conserved transcription factor that protects against extreme environmental conditions through induction of the cytoprotective heat shock response (HSR) (66). Activation of the HSR is triggered by proteotoxic stressors including heat, heavy metals, and infection (163). Upon exposure to stress, HSF1 transcribes heat shock protein genes (*hsps*) which encode molecular

chaperones that mediate the refolding or degradation of damaged proteins (294,295). HSF1 is thus an important mediator of the response to heat stress and proteome maintenance.

The *C. elegans* HSR is highly-conserved and mediated by the HSF1 homolog HSF-1. Studies in *C. elegans* have demonstrated a role for HSF-1 outside of its classic role in regulating the HSR by demonstrating HSF-1 as a regulator of development, metabolism, and longevity (110,111,314,325,357). HSF-1 has also been shown to be a regulator of global mRNA expression in both stress-dependent and -independent processes (357). However, the post-transcriptional role for HSF-1 in controlling stress-dependent and -independent gene expression is largely unknown.

MicroRNAs (miRNAs) are a family of small, non-coding, and conserved RNA molecules that elicit complex mechanisms of genetic control through the post-transcriptional modulation of gene expression. The primary function of miRNAs is in the silencing of gene expression through complimentary base pairing to the 3' UTR of target mRNAs leading to their degradation or translational repression (98,99). The regulation of gene expression by miRNAs is suggested to be vast. There are over 1,000 miRNAs in the human genome and over 250 miRNAs in the *C. elegans* genome, and many miRNAs are predicted to have hundreds of putative mRNA targets (358). Thus, miRNAs are important post-transcriptional regulators of global gene expression in multiple organisms.

Studies in *C. elegans* have been useful for determining the biological outcomes associated with changes in miRNA expression (359). For example, miRNAs have been shown to control various physiological process including the control of stress responses, development, and longevity, in the nematode (360-363). Interestingly, these miRNA-

regulated processes are also known to be regulated by HSF-1. However, the role of HSF-1 in coordinating miRNA expression to regulate these overlapping biological processes is unclear.

In this study, we examined the genome-wide role of HSF-1 in regulating miRNA expression to affect biological processes in *C. elegans*. We performed high-throughput small-RNA sequencing in *C. elegans* grown in the presence and absence of *hsf-1* RNAi followed by treatment with or without heat shock (HS). We have found that HSF-1 controls miRNA expression during and independently of heat stress. The biological processes predicted to be impacted by HSF-1-regulated miRNAs include development, metabolism, and longevity. Additionally, integrated miRNA/mRNA target prediction analyses have uncovered oxidative stress response factors and insulin-like signaling factors as a common link between processes affected by HSF-1 regulated miRNAs in stress-dependent and -independent mechanisms, respectively. Overall, this work highlights miRNAs as important HSF-1 targets that may have biological implications in regulating development, metabolism, and longevity, and in cross-talk between stress responses.

Results

Uncovering the genome-wide regulation of miRNA expression by HSF-1 in HS-dependent and -independent mechanisms

Experimental design used for miRNA-sequencing

To uncover the post-transcriptional role of HSF-1 in regulating mRNA expression through controlling miRNA abundance, we utilized miRNA-sequencing to characterize the HSF-1 regulatory miRNA network in both HS-dependent and -independent mechanisms in *C. elegans* (Figure 7.1). Synchronous L1 larval stage nematodes were fed empty vector (EV)

control RNAi [*hsf-1*(+)] or *hsf-1* RNAi [*hsf-1*(-)] until the L4 larval stage prior to treatment with or without a 30 minute 33°C heat shock in biological duplicates (Figure 7.1a). miRNA-seq was performed on the Illumina Hi-Seq 2000 platform and analyzed by miRDeep2 in order to identify miRNA read counts for each treatment condition. This experimental set-up thus allows for the determination of the genome-wide miRNAs regulated by HSF-1.

Validation of experimental treatment conditions

To validate our RNAi and HS treatment conditions, we assessed HS-inducible *hsp* promoter activity and mRNA expression in response to treatment with or without *hsf-1* RNAi (Figure F1, see Appendix F) (357). The promoter activity of the HSF-1 target genes *hsp-70* and *hsp-16.2* were determined using *hsp* promoter fusion constructs, and we have determined that *hsp* promoter activity is induced upon HS and that this induction is dependent on HSF-1 (Figure F1a-d, see Appendix F). Additionally, *hsps* constitute a majority of the top protein-coding genes induced by HS, and all are dependent on HSF-1, as determined by an mRNA-seq experiment performed in parallel to this miRNA-seq study (Figure F1e, see Appendix F) (357). These data thus verify that the HS conditions used for this study induce global *hsp* mRNA expression while demonstrating the efficiency of our *hsf-1* RNAi treatment conditions used for miRNA-seq.

Next, we validated the biological replicates used for miRNA-seq by determining similarities between experimental duplicates for each experimental treatment condition (Figure F2, see Appendix F). Similarities between biological duplicates were first analyzed with Cluster analysis. The data shows that experimental duplicates clustered together, indicating high similarity between replicates (Figure F2a, see Appendix F). Linear regression analysis of each treatment condition validates similarities between miRNA-seq

reads for each replicate, with each condition having R^2 values above 0.94 (Figure F2b-e, see Appendix F). Overall, these data validate our biological replicates by showing a conserved pattern of expression between duplicates for each experimental condition.

HSF-1 alters global miRNA abundance during and independently of HS

To determine relative miRNA abundance, we normalized each treatment condition to the *hsf-1*(+);-HS control, and significantly altered miRNAs were uncovered using the Benjamini-Hochberg correction for multiple testing (Figure 7.1b). A complete list of the significantly altered miRNAs, and their fold change for each experimental condition relative to the *hsf-1*(+);-HS control, is provided in Tables F1, F2, and F3 (see Appendix F). The resulting global miRNA expression profiles for each treatment condition were plotted in order to visualize miRNA distribution patterns between experimental conditions (Figure F3, see Appendix F). In the presence and absence of HS, *hsf-1* RNAi alters global miRNA distribution, suggesting HSF-1 as a regulator of miRNA expression during and independently of HS in *C. elegans*.

Venn diagrams separate miRNAs regulated by HSF-1 during and independently of HS

To further examine the role of HSF-1 in regulating miRNA expression in HS-dependent and -independent mechanisms, Venn diagrams were made using the miRNAs listed in Table F1 (Figure 7.1c). The shaded regions of the Venn diagrams correspond to miRNAs regulated by *hsf-1* upon HS (Figure 7.1c, blue shading), and miRNAs regulated by *hsf-1* independently of HS (Figure 7.1c, yellow shading). Through Venn diagram analysis, we have found that a total of 22 miRNAs are regulated by HSF-1 in a HS-dependent manner, and that 7 miRNAs are regulated by HSF-1 in a HS-independent manner. Overall, this method of Venn diagram analysis separates the miRNAs regulated by HSF-1 during and

independently of heat stress, and our preceding analyses focus on these HSF-1-regulated miRNAs.

HSF-1 regulates miRNA expression during HS

miRNAs normally upregulated by HSF-1 during HS

We were next interested in further examining the miRNAs normally regulated by HSF-1 during HS (Figure 7.2). By separating out the upregulated vs. downregulated miRNAs via Venn diagram, we have determined that 10 miRNAs are normally upregulated by HSF-1 upon HS (Figure F4a, blue shading, see Appendix F). The log_2-fold changes of these 10 miRNAs obtained from the sequencing data are plotted in the presence and absence of HSF-1 during HS (Figure F4.b, blue and grey bars, respectively, see Appendix F). We considered a miRNA to normally be upregulated by HSF-1 during HS if a significant difference existed between the *hsf-1*(+);+HS and *hsf-1*(-);+HS treatment conditions as determined by the Benjamini-Hochberg correction for multiple testing. After taking these parameters into account, 6 miRNAs were determined to normally be upregulated by HSF-1 during HS (Figure F4.c, see Appendix F). Through this method of data analysis, we found that *miR-784, miR-231, miR-86, miR-53*, *miR-47,* and *miR-34* are normally upregulated by HSF-1 during HS.

Next, we determined the known functions of the miRNAs we found to normally be upregulated by HSF-1 upon HS. The description according to WormBase, along with the log_2-fold change of each miRNA, is listed (Table 7.1, upregulated). While the functions of *miR-784, miR-231, miR-86, miR-53*, and *miR-47* are currently unknown, *miR-34* encodes a microRNA that is highly-conserved with orthologues in *Drosophila,* mouse, and human (364). In *C. elegans*, *miR-34* is highly expressed upon aging (360). Although a deletion

of *miR-34* does not significantly impact *C. elegans* lifespan (360), loss of *miR-34* in *Drosophila* does accelerate aging and brain degeneration (364). Induction of *miR-34* by HSF-1 during HS may thus be one method of controlling aging-associated processes.

To uncover potential mRNA targets of the miRNAs we found to be regulated by HSF-1 upon HS, we performed integrated prediction-based analysis by comparing predicted mRNA targets to genes we previously determined to be regulated by HSF-1 upon HS via mRNA-seq (Figure 7.2a) (357). We used mirWIP as our primary prediction tool, as this program reduces false positives by considering multiple characteristics of miRNA target binding such as structural accessibility of target sequences, total free energy, and base-pairing (365). For miRNAs not yet in the mirWIP database, we used TargetScan to predict mRNA targets. In order to generate a consolidated and accurate HSF-1-regulated miRNA/mRNA network, we compared the predicted mRNA targets to genes we previously determined by mRNA-seq, performed in parallel to this study, to be regulated by HSF-1 (357). Due to the inhibitory nature of miRNAs on target mRNA expression, predicted mRNA targets were inversely correlated to the mRNA-seq data. The resulting integrated miRNA/mRNA prediction output predicted to be suppressed by HSF-1 upon HS is shown in Figure 7.2b. Overall, 62 potential mRNA targets are predicted to be downregulated by the miRNAs that we determined to normally be upregulated by HSF-1 upon HS.

Next, we used the database for annotation, visualization, and integrated discovery (DAVID) to uncover the biological processes predicted to be suppressed by the miRNAs upregulated by HSF-1 during HS (Figure 7.2c). The category with the largest enrichment score (2.33) is cell fate commitment, followed by signal transduction, protein kinase

activity, signaling cascade, and development, all with enrichment scores between 2.21-1.12. These processes encompass developmental and signaling pathways, which are likely the main physiological processes suppressed by HSF-1-regulated miRNAs during HS.

miRNAs normally downregulated by HSF-1 during HS

We were next interested in examining the miRNAs normally downregulated by HSF-1 during HS (Figure 7.2d-e). By separating out the upregulated vs. downregulated miRNAs via Venn diagram, we determined that 12 miRNAs are normally downregulated by HSF-1 upon HS (Figure F5a, blue shading, see Appendix F). The $\log_2$-fold change of these 12 miRNAs are plotted in the presence and absence of HSF-1 during HS (Figure Fb, blue bars and grey bars, respectively, see Appendix F). We considered a miRNA to normally be downregulated by HSF-1 during HS if a significant difference existed between the *hsf-1*(+);+HS and *hsf-1*(-);+HS treatment conditions as determined by the Benjamini-Hochberg correction for multiple testing. After taking these parameters into account, 2 miRNAs were determined to normally be downregulated by HSF-1 during HS (Figure F5c, see Appendix F). Through this method of data analysis, we found that *miR-48* and *miR-228* are normally downregulated by HSF-1 upon HS.

We were next interested in determining the known functions of the miRNAs we found to normally be downregulated by HSF-1 upon HS. The description according to WormBase, along with the $\log_2$-fold change of each miRNA, is listed (Table 7.1, downregulated). *miR-228* is upregulated in aging worms, and a *miR-228* deletion has been shown to increase longevity and heat stress resistance (361,366). *miR-48* belongs to the *let-7* miRNA family that is well-known to control developmental timing events at the

larval-to-adult transition, and mutations in *miR-48* can result in developmental timing defects (367,368). Thus, HSF-1 may normally suppress *miR-228* and *miR-48* expression during HS to promote longevity and stress resistance, and to control developmental timing events during stress conditions.

To uncover potential mRNA targets of the miRNAs we found to be downregulated by HSF-1 upon HS, we again used the prediction tools mirWIP and TargetScan followed by an integrated miRNA/mRNA analysis (Figure 7.2d). We compared the predicted mRNA targets to genes we previously determined by mRNA-seq, performed in parallel to this study, to be upregulated by HSF-1 during HS (357). Overall, 31 potential mRNA targets are predicted to be upregulated by the miRNAs that we determined to normally be downregulated by HSF-1 upon HS

Next, we used DAVID to uncover the biological processes predicted to be induced by HSF-1-regulated miRNAs during HS (Figure 7.2e). The category with the largest enrichment score (1.57) is cuticle collagen, followed by reproduction and signaling, with enrichment scores of 1.28 and 1.23, respectively. These processes encompass aging and signaling associated pathways, which are likely the main physiological processes induced by HSF-1-regulated miRNAs during HS.

HSF-1 regulates miRNA expression independently of HS

miRNAs normally upregulated by HSF-1 independently of HS

To uncover a HS-independent role for HSF-1 in regulating miRNA expression, we next focused on the miRNAs normally regulated by HSF-1 independently of HS (Figure 7.3). By separating out the upregulated vs. downregulated miRNAs via Venn diagram, we determined that 2 miRNAs are downregulated in response to *hsf-1* RNAi independently

of HS, thus these miRNAs would normally be upregulated by HSF-1 (Figure F6a, yellow shading, see Appendix F). The log_2-fold change of these 2 miRNAs are plotted in the absence of HSF-1 and in the presence and absence of HS (Figure F6b, grey and yellow bars, respectively, see Appendix F). To determine the normal regulatory role of HSF-1 on miRNA expression, we reversed our data comparison (control vs. indicated treatment conditions). We considered a miRNA to be regulated by HSF-1 independently of HS if no significant difference existed between the *hsf-1*(-);+HS and *hsf-1*(-);-HS treatment conditions using the Benjamini-Hochberg correction for multiple testing. After taking these parameters into account, 1 miRNA was determined to normally be upregulated by HSF-1 independently of HS (Figure F6c, see Appendix F). Through this method of data analysis, we found that *miR-72* is normally upregulated by HSF-1 independently of HS.

Next, we determined the known functions of the miRNA we found to normally be upregulated by HSF-1 independently of HS. The description according to WormBase, along with the log_2-fold change of each miRNA, is listed (Table 2, upregulated). We again reversed our data comparison [control vs. *hsf-1*(-);-HS] in order to represent the normal degree of HSF-1 regulation on miRNA expression. However, the function of *miR-72* is unknown, thus warranting future studies regarding *miR-72*.

To uncover potential mRNA targets of the miRNAs regulated by HSF-1 independently of HS, we performed integrated prediction-based analysis by comparing predicted mRNA targets to genes we previously determined to be regulated by HSF-1 independently of HS via mRNA-seq (Figure 7.3a) (357). Due to the inhibitory nature of miRNAs on target mRNA expression, predicted mRNA targets were inversely correlated to the mRNA-seq data. The resulting integrated miRNA/mRNA prediction output predicted to be suppressed

by HSF-1 independently of HS is shown in Figure 7.3b. Overall, 101 potential mRNA targets are predicted to be downregulated by HSF-1-regulated miRNAs independently of HS.

We next used DAVID to uncover the biological processes predicted to be suppressed by HSF-1-regulated miRNAs independently of HS (Figure 7.3c). The category with the largest enrichment score (3.48) is growth, followed by development, cuticle collagen, epithelium development, and cytoskeleton organization with enrichment scores between 2.63-2.19. These processes all contribute to development, which is likely the main process suppressed by HSF-1-regulated miRNAs independently of HS.

miRNAs normally downregulated by HSF-1 independently of HS

We were next interested in determining a HS-independent role for HSF-1 in downregulating miRNA expression (Figure 7.3d-e). By separating out the upregulated vs. downregulated miRNAs via Venn diagram, we have determined that 5 miRNAs are upregulated in response to *hsf-1* RNAi independently of HS, thus these miRNAs would normally be downregulated by HSF-1 (Figure F7a, yellow shading, see Appendix F). The $\log_2$-fold change of these 5 miRNAs are plotted in the absence of HSF-1 and in the presence and absence of HS (Figure F7b, grey and yellow bars, respectively, see Appendix F). To determine the normal regulatory role of HSF-1 on miRNA expression, we reversed our data comparison (control vs. indicated treatment conditions). We considered a miRNA to be regulated by HSF-1 independently of HS if no significant difference existed between the *hsf-1*(-);+HS and *hsf-1*(-);-HS treatment conditions using the Benjamini-Hochberg correction for multiple testing. After taking these parameters into account, 3 miRNAs were determined to normally be downregulated by HSF-1

independently of HS (Figure F7c, see Appendix F). Through this method of data analysis, we have determined that *miR-239b*, *miR-1820*, and *miR-228* are normally downregulated by HSF-1 independently of HS.

Next, we determined the known functions of the miRNAs we found to normally be downregulated by HSF-1 independently of HS. The description according to WormBase, along with the $\log_2$-fold change of each miRNA, is listed (Table 7.2, downregulated). We again reversed our data comparison [control vs. *hsf-1*(-);-HS] in order to represent the normal degree of HSF-1 regulation. *miR-239b* is known to be highly upregulated upon aging, and mutants lacking *miR-239a/b* exhibit an increased lifespan and resistance to stress (360,369). One mechanism utilized by *miR-239b* to control longevity is through regulation of the insulin-like signaling pathway. *miR-239b* functions upstream of *daf-16* to control the expression of the *daf-16* target genes *age-1* and *pdk-1* (360). Another miRNA we found to normally be downregulated by HSF-1 independently of HS is *miR-1820.* Although the function of *miR-1820* is currently unknown, dauer worms show increased expression of *miR-1820* suggesting a possible link to metabolism and longevity (370). *miR-228* is another miRNA downregulated by HSF-1 independently of HS, however this miRNA is also downregulated by HSF-1 during HS. *miR-228* is thus likely an important HSF-1 target that may be regulated by HSF-1 to regulate longevity in both a stress-dependent and -independent fashion. Overall, we have determined that HSF-1 normally suppresses *miR-239b*, *miR-1820*, and *miR-228,* which may regulate longevity and metabolic processes independently of HS.

To uncover potential mRNA targets of the miRNAs downregulated by HSF-1 independently of HS, we used the prediction tools mirWIP and TargetScan followed by

integrated miRNA/mRNA analysis (Figure 7.3d). We compared the predicted mRNA targets to genes we previously determined by mRNA-seq, performed in parallel to this study, to be upregulated by HSF-1 independently of HS (357). Overall, 39 potential mRNA targets are predicted to be induced by HSF-1-regulated miRNAs independently of HS.

We next used DAVID to uncover the biological processes predicted to be induced by HSF-1-regulated miRNAs independently of HS (Figure 7.3e). The category with the largest enrichment score (0.83) is signaling, followed by ion binding and development, with enrichment scores between 0.5-0.28. These processes encompass developmental and signaling processes, which are likely the main processes induced by HSF-1-regulated miRNAs independently of HS.

Discussion

HSF-1 post-transcriptionally regulates gene expression by controlling miRNA abundance

miRNAs are emerging as a group of post-transcriptional modulators of gene expression that often function through translational repression or mRNA degradation. We show here that HSF-1 controls the expression of miRNAs, suggesting a post-transcriptional role for HSF-1 in regulating gene expression. Interestingly, the number of mRNAs predicted to be post-transcriptionally suppressed by HSF-1 during HS is twice as large as those predicted to be induced by HSF-1 during HS. Similarly, the number of mRNAs predicted to be post-transcriptionally suppressed by HSF-1 independently of HS is three times as large as those predicted to be induced by HSF-1 independently of HS. Overall, these data suggest that miRNAs may primarily be utilized by HSF-1 to suppress gene expression.

Global biological processes impacted during HS by HSF-1-regulated miRNAs

Oxidative stress response factors link miRNA/mRNA networks regulated by HSF-1 during HS

To determine a broad impact for HSF-1 in post-transcriptionally regulating gene expression during HS, the network-building software Cytoscape and the Agilent literature search tool were used to build an interaction network with the integrated miRNA/mRNA network that we determined to be regulated by HSF-1 upon HS (Figure 7.4). Predicted mRNA targets were overlaid with the expression changes obtained from mRNA-seq, performed in parallel to this study (357), where blue corresponds to negative regulation and red corresponds to positive regulation by HSF-1 upon HS. Uncolored mRNA genes were not affected in our dataset but are neighbors shared by at least two genes that were affected. This method of network generation thus allows for the determination of a broad network of genes predicted to be post-transcriptionally regulated by HSF-1 during HS.

To uncover important links between the induced and suppressed networks, we grouped together the upregulated and downregulated interaction groups to visualize connecting mRNAs (Figure 7.4, represented as bold connecting lines). We have identified the oxidative stress response factors *mdt-15*, *skn-1*, and *aip-1* as a link between the induced and suppressed networks regulated by HSF-1 upon HS. *miR-34*, a miRNA induced by HSF-1 upon HS, is predicted to suppress *mdt-15*. In *C. elegans*, MDT-15 is an evolutionary conserved subunit of a mediator complex that is required for the SKN-1-mediated oxidative stress response (371). The downregulation of *mdt-15* by *miR-34* may therefore be one method of suppressing the oxidative stress response during a heat stress. This may be advantageous for heat stress survival, as the oxidative stress

response has been shown to impair the HSR (372-374). We also see that *miR-48*, a miRNA we identified to be suppressed by HSF-1 upon HS, may result in upregulation of *aip-1*, a known SKN-1 and HSF-1 target gene (110,375). *Aip-1* is a component of the proteasome that functions to increase the accessibility of a protein substrate to the proteasome, ultimately assisting in adaptation to proteotoxic stressors (376). Overall, these data suggest that the ability of HSF-1 to control miRNA expression upon heat stress may be one method utilized by organisms to regulate stress-specific gene expression that may confer stress-specific adaptation.

Cytoprotection, development, metabolism, and longevity are predicted to be impacted during HS by HSF-1-regulated miRNAs

Next, DAVID was used to determine the globally enriched biological processes impacted by the miRNAs regulated by HSF-1 during HS (Figure F8, see Appendix F). Induction of *miR-784, miR-231, miR-86, miR-53, miR-47,* and *miR-34* by HSF-1 during HS is predicted to have the largest impact on the suppression of genes encoding proteins involved in the regulation of transcription and behavior, as these processes have enrichment scores of 5.49 and 4.93, respectively (Figure F8a, see Appendix F). Other suppressed processes in this category, with enrichment scores between 4.29-2.7, include the regulation of intracellular signaling, phosphorylation, reproductive behavior, RNA-metabolic processes, cytoskeletal organization, enzyme linked receptor signaling, post-embryonic development, fatty acid metabolic processes, cell death, epithelium development, and aging. These biological processes encompass development, metabolism, and longevity, which are likely the main physiological processes normally suppressed during HS by HSF-1-regulated miRNAs.

We next determined the top biological processes upregulated in response to suppression of *miR-48* and *miR-228* by HSF-1 during HS (Figure F8b). The induction of genes encoding proteins involved in cellular homeostasis and reproductive behavior constitute the top induced processes with enrichment scores of 2.71 and 2.01, respectively. Other induced processes in this category, with enrichment scores between 1.68 and 1.41, include genes encoding proteins involved in cuticle formation and post-embryonic development. These processes can be linked to cytoprotection, thus cytoprotective processes are normally induced by HSF-1-regulated miRNAs during HS.

Global biological processes impacted independently of HS by HSF-1-regulated miRNAs

Insulin-like signaling factors link miRNA/mRNA networks regulated by HSF-1 independently of HS

To determine a broad impact for HSF-1 in post-transcriptionally regulating gene expression independently of HS, we again used the software Cytoscape and the Agilent literature search tool to build an interaction network with the integrated miRNA/mRNA network we determined to be regulated by HSF-1 independently of HS (Figure 7.5). Predicted mRNA targets were overlaid with the expression changes obtained from mRNA-seq, performed in parallel to this study (357), where blue corresponds to negative regulation and red corresponds to positive regulation by HSF-1 independently of HS. Uncolored genes were not affected in our dataset, but are neighbors shared by at least two genes that were affected. This method of network generation thus allows for the determination of a broad network of genes predicted to be post-transcriptionally regulated by HSF-1 independently of HS.

To uncover important linkages between the induced and suppressed networks, we grouped upregulated and downregulated processes in order to visualize connecting mRNAs (Figure 7.5, represented as bold connecting lines). Interestingly, we uncovered the insulin-like signaling factors *daf-16* and *dao-4* as a link between the induced and suppressed miRNAs regulated by HSF-1 independently of HS. We identified *miR-72*, a miRNA we show to normally be induced by HSF-1 independently of HS, as a *daf-16* suppressor. Controlling *daf-16* may be one mechanism utilized by HSF-1 to fine-tune metabolism and longevity independently of HS. The *daf-16* target gene *dao-4* is predicted to be upregulated in response to suppression of *miR-1820* and *miR-228* by HSF-1. HSF-1 has previously been linked to having a non-stress role in controlling metabolism, where caloric restriction, metabolic factors, and insulin-like signaling factors have been linked to HSF-1 and the HSR (72,110,135,377,378). Recent studies suggest that the insulin-like signaling factor and FOXO transcription factor DAF-16 has a stress-independent role in controlling HSF-1-mediated lifespan extension (379). Overall, these data suggest that HSF-1-regulated miRNA networks may be connected through insulin-like signaling factors to control metabolism and lifespan in a heat-stress independent fashion.

Development, metabolism, and longevity are predicted to be impacted by HSF-1-regulated miRNAs independently of HS

Next, DAVID was used to determine the globally enriched biological processes impacted by the miRNAs regulated by HSF-1 independently of HS (Figure F9, see Appendix F). Induction of *miR-72* by HSF-1 is predicted to have the largest impact on suppressing genes encoding proteins involved in the regulation of post-embryonic development and cell migration, as these processes have enrichment scores of 13.68 and 10.14,

respectively (Figure F9a, see Appendix F). Other suppressed processes in this category, with enrichment scores between 8.28-2.48, include the regulation of phosphorylation, sex differentiation, apoptosis, growth, epithelium development, axis specification, cell adhesion, reproductive development, behavior, aging, neuron development, cuticle development, and RNA metabolic processes. These processes are involved in development, further supporting our previous work suggesting HSF-1 as a global regulator of developmental processes independently of HS (357).

We next determined the biological processes upregulated in response to suppression of *miR-1820* and *miR-228* by HSF-1 independently of HS (Figure F9b, see Appendix F). Each upregulated process has a relatively low enrichment score (under 1.02), suggesting that suppression of biological processes is the primary role of HSF-1-regulated miRNAs. However, the most highly upregulated processes are phosphate metabolic processes and growth, with enrichment scores of 1.02 and 0.74, respectively. The other induced process in this category, with an enrichment score of 0.61, is epithelium development. Overall, genes encoding proteins involved in regulating developmental processes may be induced by HSF-1-regulated miRNAs independently of HS.

HSF-1 may impact longevity through the post-transcriptional control of collagen and cytoskeletal genes

In this study, we show that cuticle processes are enriched by HSF-1 upon HS and suppressed by HSF-1 independently of HS. Collagen genes, which encode cuticle proteins, were recently shown to impact lifespan and to be regulated by HSF-1 during and independently of HS (380). The oxidative stress factor SKN-1 may also regulate the expression of specific collagen genes to control longevity, supporting a role for collagen

genes in regulating longevity during stress (380). These data suggest a post-transcriptional role for HSF-1 in regulating specific cuticle collagen genes, further supporting our previous work suggesting HSF-1 as a regulator of collagen gene expression. Ultimately, the regulation of collagens may influence aging and longevity during stressors.

Cytoskeletal organization may be another process impacted by HSF-1-regulated miRNAs, and may be one method to promote cytoprotection and longevity during HS. HSF-1 was recently shown to regulate genes that control cytoskeletal stability which extended lifespan and promoted stress resistance in *C. elegans* (343). Thus, these data suggest HSF-1 may post-transcriptionally control cytoskeletal processes and ultimately influence longevity.

Conclusion

The miRNA-sequencing experiment performed in this study has allowed us to uncover a possible post-transcriptional role for HSF-1 in regulating heat stress-dependent and -independent processes in *C. elegans*. During HS, HSF-1 is predicted to post-transcriptionally promote specific genes encoding proteins involved in cytoprotection and development, while suppressing other genes encoding proteins involved in development, metabolism, and longevity. Independently of HS, HSF-1 is predicted to post-transcriptionally promote specific genes encoding proteins involved in development and metabolism, while suppressing other genes encoding proteins involved in development, metabolism, and longevity. Integrated miRNA/mRNA network analyses point to HSF-1-regulated miRNAs as a link between the oxidative stress response and the insulin-like signaling pathway to HSF-1-regulated processes, suggesting a mechanism for cross-talk

between stress responses (For a model, see Figure 7.6). Additionally, this work further highlights a role for HSF-1 in regulating the expression of cuticle collagen genes which may control longevity. Overall, our work has uncovered a potential role for HSF-1 in post-transcriptionally controlling gene expression in *C. elegans*, and suggests a mechanism for cross-talk between stress responses.

Methods

C. elegans maintenance

Wild-type N2 worms were maintained at 23°C on standard NGM plates seeded with *Escherichia coli* OP50 (345). Age synchronization was accomplished by standard 20% hypochlorite treatment, and a 24-hour rotation at 220 rpm in M9 buffer without food.

RNA interference and heat shock treatment

RNAi was carried out using standard plates supplemented with 50 µg/mL ampicillin and 1 mM isopropyl-beta-ɒ-thiogalactopyranoside seeded with HT115 bacteria containing an empty plasmid (L4440, empty vector control) or sequence-verified *hsf-1* RNAi isolated from the Ahringer RNAi library (146). Bacteria were allowed to induce on the RNAi plates overnight at room-temperature prior to plating synchronous L1 larval stage worms. Worms remained on RNAi plates until the L4 larval-stage before being heat shocked by submerging plates in a 33°C water bath for 30 minutes. The time and duration of heat shock was previously optimized for our studies (357).

miRNA preparation for miRNA-seq

miRNA was prepared from biological duplicates using TRIzol reagent (Life Technologies, *cat#* 15596-026) following the manufacturer's protocol, and then cleaned up on miRNeasy columns (Qiagen, *cat.#* 217004) with on-column DNA digestion. Sample integrity,

preparation, and sequencing was performed at the Yale Center for Genome Analysis (West Haven, CT) using the Illumina Hi-Seq 2000 sequencing system. The miRNA-seq data has been deposited in the BioProject repository (Bio Project ID: PRJNA357087).

miRNA-sequencing data analysis

The miRDeep2 software package was used to identify known miRNAs from the miRNA-sequencing data (381). Low quality reads, and reads shorter than 18 nucleotides, were removed to obtain clean reads after adapter trimming. The unique sequences were mapped to the *C. elegans* reference genome (WS200) with the read aligner Bowtie2 using default parameters (382). Alignments with no mismatches in the first 18 nucleotides of a read sequence, up to two mismatches after 18 nucleotides, and reads that did not map more than five times to the genome, were the miRNAs used in our analyses.

Volcano plot generation

Volcano plots were made in Excel, where the Y-axis represents the $-\log_{10}$ q-value (FDR-adjusted p-value), and the X-axis represents the $\log_2$-fold change of each miRNA after normalization to the *hsf-1*(+);-HS control.

miRNA-seq data normalization and statistical analysis

The fold change of each miRNA was obtained by averaging the reads of the *hsf-1*(+);-HS control and normalizing each corresponding miRNA, for each treatment condition, to the control prior to transforming into $\log_2$ values. miRNAs that did not have reads in each biological replicate were removed from subsequent analyses. The Benjamini-Hochberg correction for multiple testing was then used to determine significantly altered miRNAs between each treatment condition.

Computational target prediction and network visualization

mirWIP was used as a primary tool for determining miRNA/mRNA target predictions (365). For miRNAs not yet listed in the mirWIP database, TargetScan was used to predicted miRNA/mRNA interactions (383). To consolidate the predicted mRNA targets, the output from mirWIP or TargetScan was compared to corresponding mRNA-seq data, performed in parallel to this miRNA-seq experiment. The mRNA-seq data is available in the NCBI SRA database (Access ID: PRJNA311958) (357). The network building software Agilent was then used to determine interacting partners shared between at least two predicted mRNA targets, and the miRNA/mRNA interaction network was generated using Cytoscape (v3.1.1) (384).

Gene ontology analysis

The Database for Annotation, Visualization, and Integrated Discovery (DAVID) was used to determine over-represented gene ontology terms associated with the predicted miRNA/mRNA networks (385). The Functional Annotation Clustering tool was then used to group gene ontology terms. The significance of each group was determined with the enrichment score, as provided by DAVID, which uses p-values for a cluster of genes to determine the geometric mean of that cluster in a negative log scale.

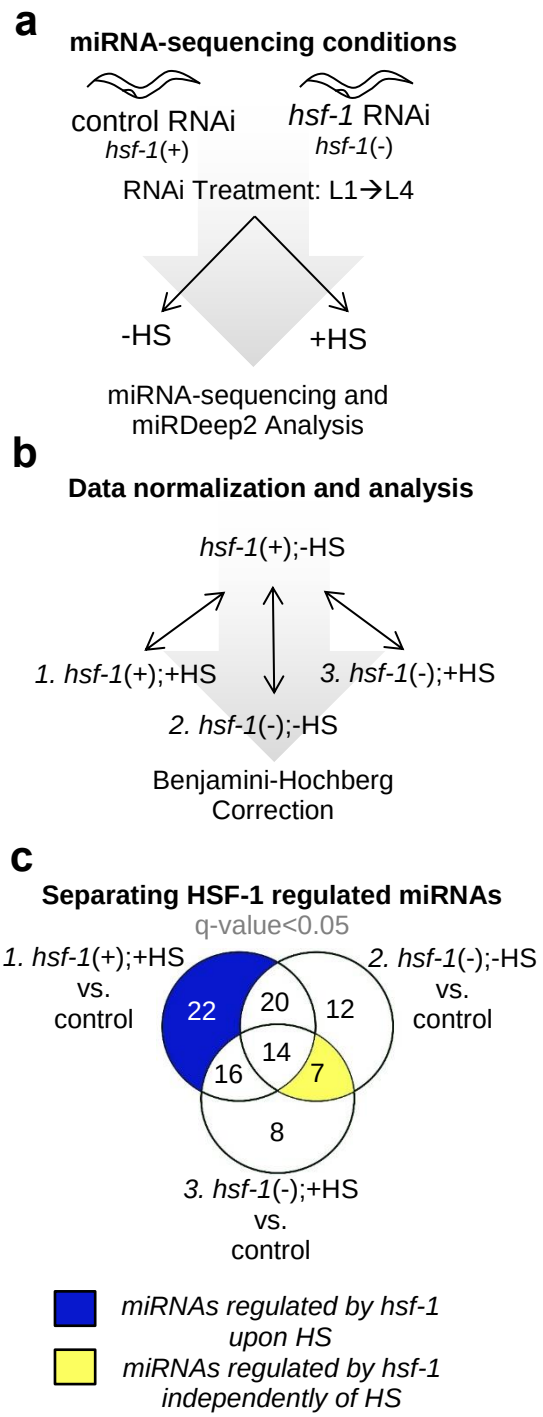

Figure 7.1. Scheme for miRNA-sequencing experimental setup and data normalization. (**a**) Schematic depicting miRNA-sequencing conditions. miRNA samples were generated from wild-type (N2) *C. elegans* treated with the four indicated conditions, where "*hsf-1*(+)" refers to worms treated with control (empty vector) RNAi, and "*hsf-1*(-)" refers to worms treated with hsf-1 RNAi. Synchronous worms were given RNAi from the L1 larval stage to the L4 larval stage. At the L4 larval stage, worms were left untreated (-HS) or given a 30 minute 33°C heat shock (+HS). miRNA-sequencing was performed in biological duplicates on the Illumina Hi-Seq 2000 platform and analyzed using miRDeep2. (**b**) Scheme for data normalization. Each treatment condition was compared relative to the empty vector control [*hsf-1*(+);-HS] to determine the relative fold change in expression of each miRNA. The Benjamini-Hochberg correction test was used to identify all differentially expressed genes compared relative to the *hsf-1*(+);-HS control, and also between treatment conditions. (**c**) Separating miRNAs regulated by HSF-1 during and independently of HS. The Venn diagram shows the total number of miRNAs that were found to be significantly altered (q-value<0.05), as compared to the *hsf-1*(+);-HS control, for each of the indicated comparisons between samples. The q-value is the FDR-adjusted p-value of the test statistic, as determined by the Benjamini-Hochberg correction for multiple testing.

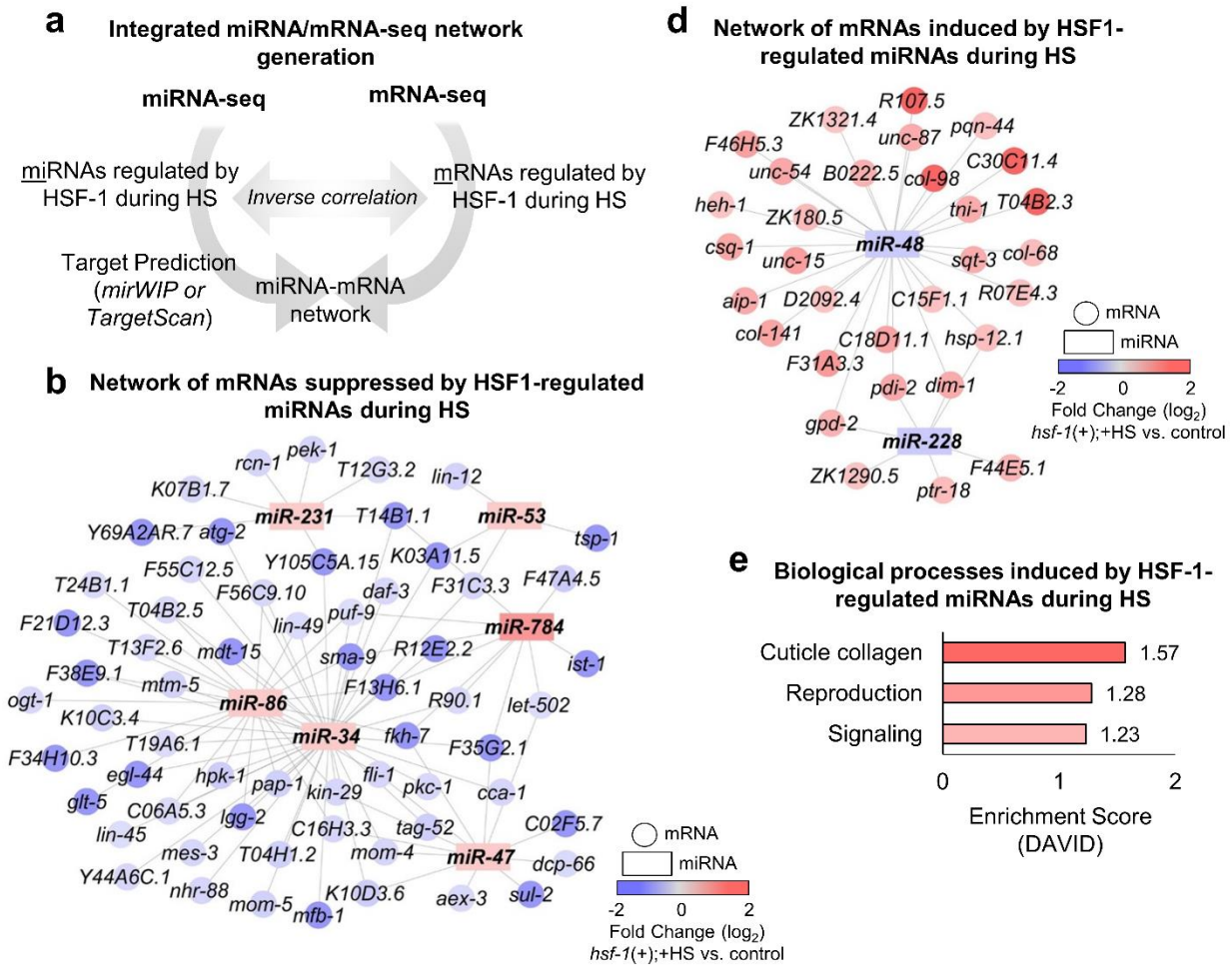

Figure 7.2. Networks and biological processes impacted by HSF-1-regulated miRNAs during HS. (**a**) Schematic depicting integrated miRNA/mRNA network generation. The miRNAs determined via miRNA-seq to be regulated by HSF-1 during HS were run through the target prediction tools mirWIP or TargetScan to uncover predicted mRNA targets. Due to the inhibitory nature of miRNAs, predicted mRNA targets were inversely correlated to mRNAs found to be regulated by HSF-1 during HS via mRNA-seq performed in parallel to this study. (**b**) Predicted network suppressed by HSF-1-regulated miRNAs upon HS. The miRNAs that we found to normally be induced by HSF-1 during HS via miRNA-seq (rectangles) were compared to mRNAs previously determined to normally be suppressed by HSF-1 during HS via mRNA-seq (circles). (**c**) Biological processes predicted to be suppressed by HSF-1-regulated miRNAs during HS. DAVID was used to uncover biological processes predicted to be suppressed by HSF-1 upon HS using the network in (**b**). (**d**) Predicted network induced by HSF-1-regulated miRNAs upon HS. The miRNAs that we found to normally be suppressed by HSF-1 during HS via miRNA-seq (rectangles) were compared to mRNAs previously determined to normally be induced by HSF-1 via mRNA-seq (circles). (**e**) Biological processes predicted to be induced by HSF-1-regulated miRNAs during HS. DAVID was used to uncover biological processes predicted to be induced by HSF-1 upon HS using the network in (**d**).

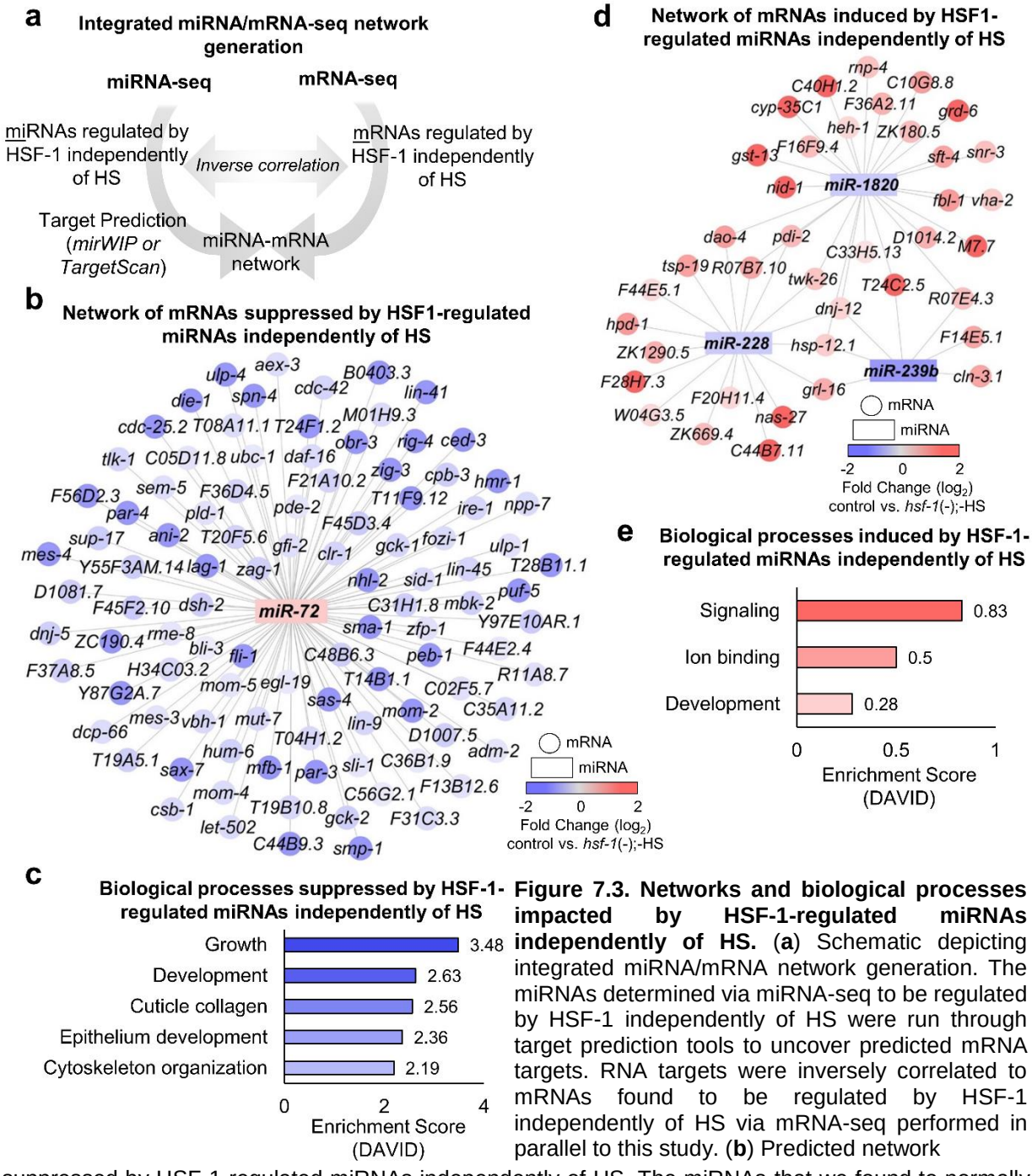

Figure 7.3. Networks and biological processes impacted by HSF-1-regulated miRNAs independently of HS. (**a**) Schematic depicting integrated miRNA/mRNA network generation. The miRNAs determined via miRNA-seq to be regulated by HSF-1 independently of HS were run through target prediction tools to uncover predicted mRNA targets. RNA targets were inversely correlated to mRNAs found to be regulated by HSF-1 independently of HS via mRNA-seq performed in parallel to this study. (**b**) Predicted network suppressed by HSF-1-regulated miRNAs independently of HS. The miRNAs that we found to normally be induced by HSF-1 independently of HS via miRNA-seq (rectangles) were compared to mRNAs previously determined to normally be suppressed by HSF-1 independently of HS via mRNA-seq (circles). (**c**) Biological processes predicted to be suppressed by HSF-1-regulated miRNAs independently of HS. DAVID was used to uncover biological processes predicted to be suppressed by HSF-1 independently of HS using the network in (**b**). (**d**) Predicted network induced by HSF-1-regulated miRNAs independently of HS. The miRNAs that we found to normally be suppressed by HSF-1 independently of HS via miRNA-seq (rectangles) were compared to mRNAs previously determined to normally be induced by HSF-1 independently of HS via mRNA-seq (circles). (**e**) Biological processes predicted to be induced by HSF-1-regulated miRNAs independently of HS. DAVID was used to uncover biological processes predicted to be induced by HSF-1 independently of HS using the network in (**d**).

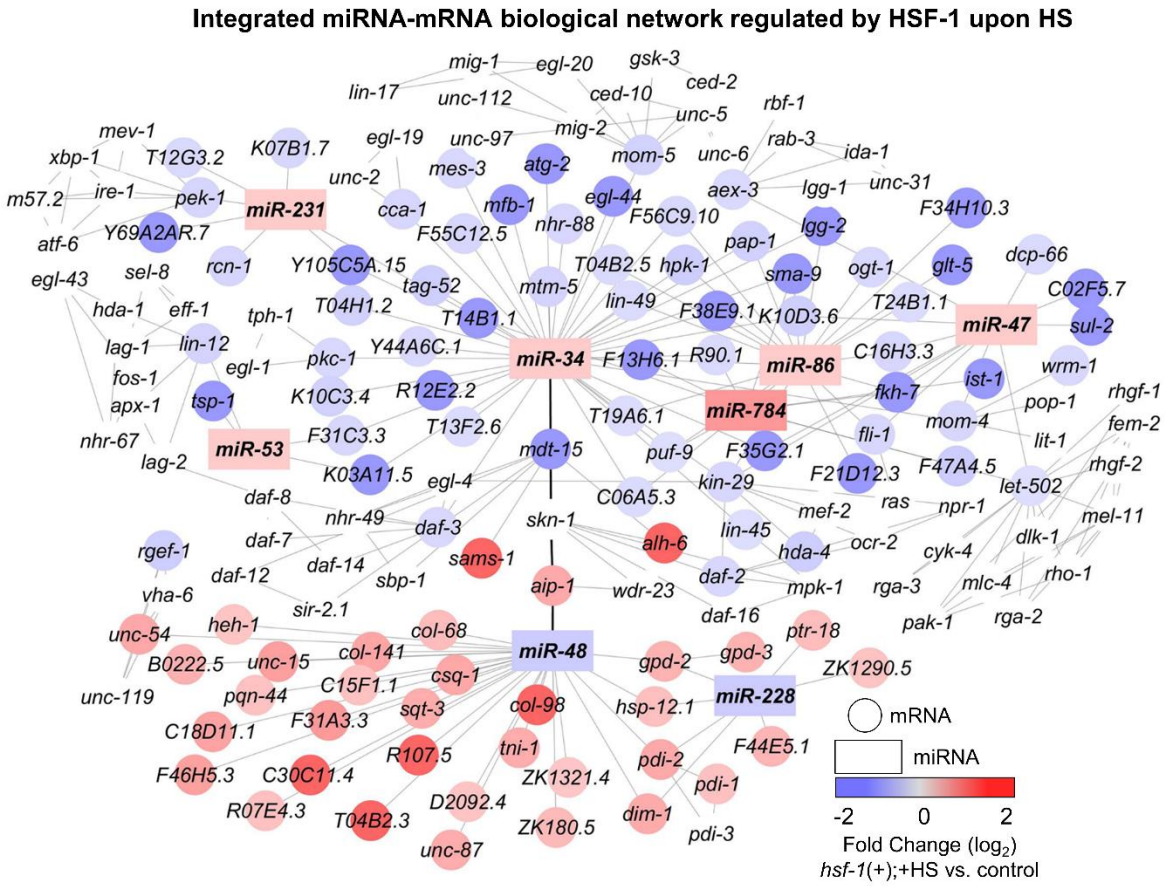

Figure 7.4. Integrated target prediction analysis uncovers miRNA/mRNA interaction networks regulated by HSF-1 during HS. The miRNAs (rectangles) that we determined to be regulated by HSF-1 during HS were used for target prediction analysis carried out by mirWIP or TargetScan. The mRNA targets (circles) were consolidated by comparing the predicted mRNAs to those determined by mRNA-sequencing, performed in parallel to miRNA sequencing, to be regulated by HSF-1 during HS. Interactions were predicted using the Agilent literature search tool, and network generation was done with Cytoscape. Transcripts that are not colored were not affected in our dataset, but are neighbors shared by at least two transcripts that were affected. The color of each miRNA or mRNA corresponds to the degree of HSF-1 regulation, where red represents induction and blue represents suppression. Bold connecting lines represent connections between upregulated and downregulated clusters.

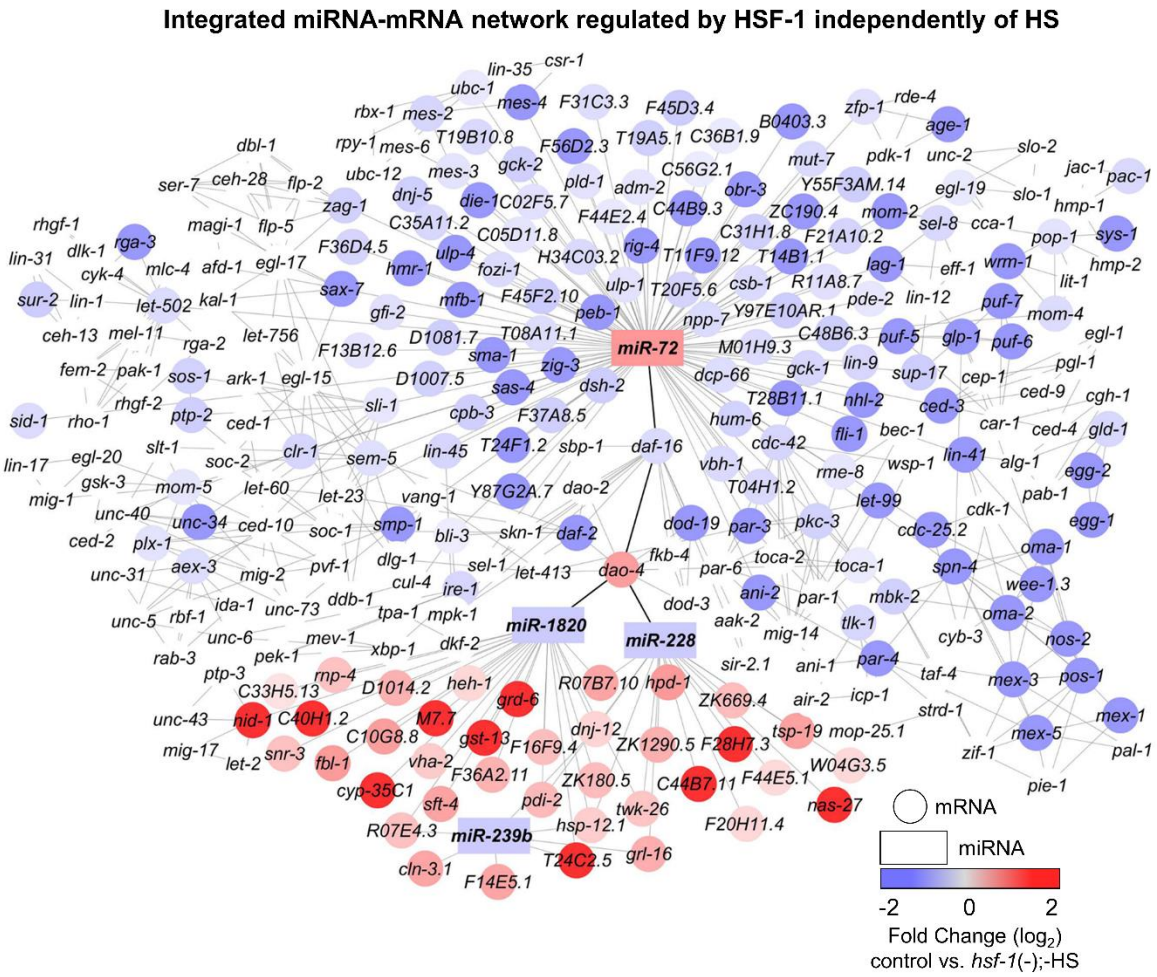

Figure 7.5. Integrated target prediction analysis uncovers miRNA/mRNA interaction networks regulated by HSF-1 independently of HS. The miRNAs (rectangles) that we determined to be regulated by HSF-1 independently of HS were used for target prediction analysis carried out by mirWIP or TargetScan. The mRNA targets (circles) were consolidated by comparing the predicted mRNAs to those determined by mRNA-sequencing, performed in parallel to miRNA sequencing, to be regulated by HSF-1 independently of HS. Interactions were predicted using the Agilent literature search tool, and network generation was done with Cytoscape. Transcripts that are not colored were not affected in our dataset, but are neighbors shared by at least two transcripts that were affected. The color of each miRNA or mRNA corresponds to the degree of HSF-1 regulation, where red represents induction and blue represents suppression. Bold connecting lines represent connections between upregulated and downregulated clusters.

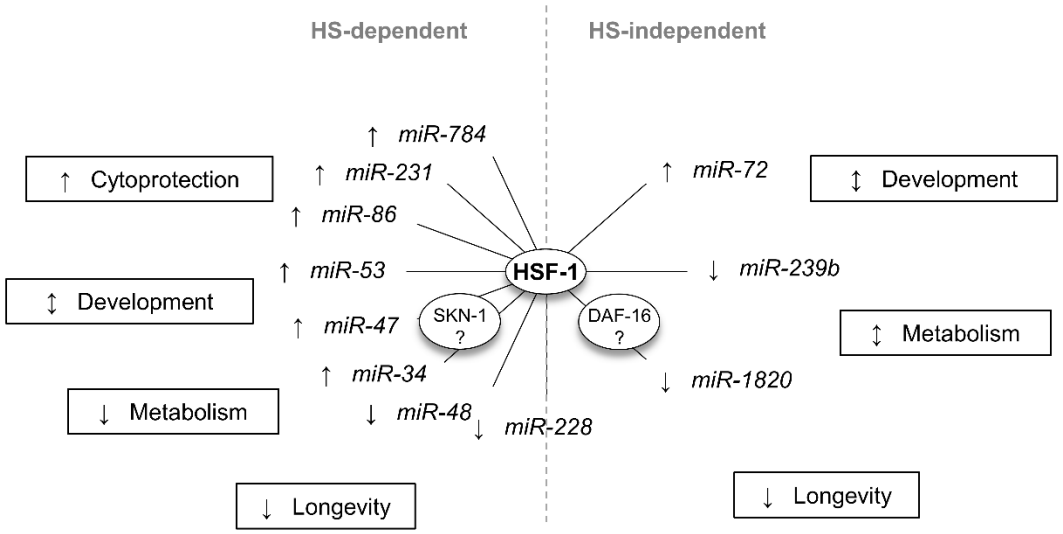

Figure 7.6. A model for heat stress-dependent and -independent processes controlled by HSF-1-regulated miRNAs. HSF-1 controls miRNA expression during and independently of HS. During HS, HSF-1 is predicted to post-transcriptionally regulate genes involved in cytoprotection, development, metabolism, and longevity. These processes may be connected through the oxidative stress response transcription factor SKN-1. Independently of HS, HSF-1 is predicted to post-transcriptionally regulate genes involved in development, metabolism, and longevity. These processes may be connected through the insulin-like signaling transcription factor DAF-16. This work highlights a possible role for HSF-1 in post-transcriptionally regulating gene expression and various biological processes, and provides a possible mechanism for cross-talk between stress responses.

Table 7.1. miRNAs normally regulated by HSF-1 upon HS.

miRNA	Fold Change (log_2) *hsf-1*(+);+HS vs. control	Description (WormBase)
Normally upregulated by *hsf-1* upon heat shock		
miR-784	1.35	*miR-784* is expressed in head neurons and the vulva, however the precise function of *miR-784* is unknown.
miR-231	0.67	*miR-231* may have a potential ortholog in *C. briggsae*. *miR-231* is strongly expressed at all stages of development in wild-type worms, however the precise function of *miR-231* is unknown.
miR-86	0.58	*miR-86* is conserved in the nematode *C. briggsae*. *mir-86* is strongly expressed at all developmental stages in wild-type worms, however the precise function of *miR-86* is unknown.
miR-53	0.38	*miR-53* is expressed constitutively throughout development, however the precise function is unknown.
miR-47	0.22	*miR-47* is conserved in *C. briggsae*. *mir-47* is expressed constitutively throughout development, however the precise function of *miR-47* is unknown.
miR-34	0.15	*miR-34* is conserved in *C. briggsae, Drosophila,* and humans. *mir-34* can regulate adult lifespan along with resistance to heat and oxidative stress. *miR-34* functions via negative regulation of autophagy.
Normally downregulated by *hsf-1* upon heat shock		
miR-228	-0.13	*miR-228* appears to be conserved in *C. briggsae*. *miR-228* belongs to the *miR-124* family of microRNAs along with human *miR-124a-1, miR-124a-2, miR-124-a-3*, m*iR-183,* and *Drosophila miR-268.* *miR-228* is upregulated during aging, and a deletion of *miR-228* increases longevity and stress resistance.
miR-48	-0.13	*miR-48* belongs to the *let-7* family of microRNAs. *miR-48* can act with other *let-7* family members to control developmental timing events.

The log_2-fold change of each miRNA is listed along with a description adapted from WormBase.

Table 7.2. miRNAs normally regulated by HSF-1 independently of HS

miRNA	Fold Change (log_2) control vs. *hsf-1*(-);-HS	Description (WormBase)
Normally upregulated by *hsf-1* independently of heat shock		
miR-72	0.12	*miR-72* is a member of the *mir-31* microRNA family that includes human *miR-31.* However, the precise function of *miR-72* is unknown.
Normally downregulated by *hsf-1* independently of heat shock		
miR-239b	-5.70	*miR-239b* is highly upregulated during aging. Deletion of *miR-239* can result in lifespan extension, while overexpression can lead to a reduction in lifespan.
miR-1820	-0.57	*mir-1820* is upregulated in dauer worms.
miR-228	-0.11	*miR-228* appears to be conserved in *C. briggsae*. *miR-228* belongs to the *miR-124* family of microRNAs along with human *miR-124a-1, miR-124a-2, miR-124-a-3*, m*iR-183,* and *Drosophila miR-268. miR-228* is upregulated during aging, and a deletion of *miR-228* increases longevity and stress resistance.

The log_2-fold change of each miRNA is listed along with a description adapted from WormBase.

CHAPTER 8. CONCLUSIONS AND FUTURE DIRECTIONS

Conclusions

Summary: Compound, genetic, and environmental regulation and transcriptional targets of HSF-1 in C. elegans

In these studies, we have uncovered compound, genetic, and environmental regulators of the HSR in *C. elegans,* while also identifying genome-wide HSF-1 targets. Our data suggest that treatment with the DNA-synthesis inhibitor Fluorodeoxyuridine, and the compounds caffeine and coffee, activate the HSR in an HSF-1-dependent manner and lead to an increase in proteostasis in a *C. elegans* Huntington's disease model. Also, we have uncovered that the nematode protein LST-3 is the ancestor of mammalian cell cycle and apoptosis regulator CCAR2. Mammalian CCAR2 negatively regulates the prolongevity factor SIRT1 and the HSR, and we have determined that this regulation is conserved in *C. elegans* and mediated by LST-3. Using *C. elegans* as a model has also allowed us to determine the negative impact LST-3 has on longevity, proteostasis, and fitness, suggesting that enhancing Sir-2.1 activity and the HSR would be beneficial for these processes. Furthermore, we have determined the global impact of HSF-1 in regulating transcriptional processes during and independently of HS by globally profiling HSF-1 mRNA and miRNA targets. Interestingly, we uncovered a large role for HSF-1 in regulating collagen gene expression during and independently of HS. These studies have uncovered regulators of the HSR in *C. elegans*, and have determined stress-dependent

and independent roles for HSF-1 in regulating longevity, transcription, proteostasis, and cytoprotection. Modulating the HSR thus promotes thermotolerance and longevity and may be beneficial for diseases of protein dysfunction (for a model, see Figure 8.1).

Modulating the HSR to promote longevity and healthy aging

A global increase in life expectancy has also resulted in an increase of age-associated diseases. Aging is currently thought to be the largest risk factor for many fatal diseases, including neurodegenerative disorders and cancer (386). Increasing longevity is therefore only beneficial when health, and the ability to handle stress, is also promoted during the aging process. Identifying the molecular events that impact natural cellular defense mechanisms may therefore uncover therapeutic targets to prevent chronic diseases of aging.

The HSR is a cellular defense mechanism that protects against stressors by promoting cryoprotection and longevity. Aging is associated with attenuation of the HSR in mammalian and non-mammalian systems (112,387-389). It has also been suggested that small-molecule intervention of the HSR may promote protection against age-associated diseases such as neurodegenerative diseases (163). Thus, uncovering HSR modulators may assist in preventing diseases of aging and protein dysfunction.

Fluorodeoxyuridine, coffee, and caffeine treatment may protect against aging-related diseases through activation of the HSR

The studies performed here provide insight into compound activation of the HSR via treatment with Fluorodeoxyuridine, and coffee and caffeine, in *C. elegans*. The problem with existing HSR modulators is bioavailability and toxicity (127). However, Fluorodeoxyuridine, coffee, and caffeine are currently bioavailable and approved for

consumption by the population, thus these compounds may overcome current boundaries for existing HSR activators. It will be interesting to see if future studies in mammals will also associate Fluorodeoxyuridine, coffee, and caffeine treatment as beneficial therapies for aging-related disorders through activation of the HSR.

Enhancing sirtuin activity to promote longevity

Another mechanism thought to be beneficial for enhancing longevity is through enhancement of the prolongevity factor SIRT1. The HSR is enhanced by SIRT1, as SIRT1 prevents attenuation of the HSR by promoting increased transcription of *hsp* genes (58). SIRT1 has numerous interacting partners, including the cell cycle and apoptosis regulator CCAR2 (73,192). CCAR2 negatively regulates SIRT1 activity by preventing substrate binding through competitive inhibition (77). Our lab has recently uncovered CCAR2 as a negative regulator of the HSR, possibly through its inhibitory interaction with SIRT1 (67). By using *C. elegans* as a model organism, we have shown that negative regulation of the HSR by CCAR2 is conserved and negatively impacts proteostasis, fitness, and longevity. Thus, uncovering inhibitors of CCAR2 may enhance SIRT1 activity and ultimately promote longevity and healthy aging in a mammalian system.

A role for HSF-1 in promoting longevity through the induction of collagen gene expression

The HSR is not only essential for regulating stress-dependent process in promoting adaptation and survival during stressful insults, but is also required for the stress-independent process such as longevity and development. Using next generation sequencing, we uncovered a novel role for HSF-1 in regulating collagen gene expression during and independently of HS in *C. elegans*. Collagen has been implicated to play a

role in modulating disease states and longevity (380,390,391). Thus, it will be interesting to further examine the relationship between collagen, HSF-1, and longevity.

Future Study 1: Collagens as Modulators of the HSR and Longevity

Rationale: Collagen genes are regulated by HSF-1 during and independently of HS and may impact longevity

HSF-1 has been uncovered as the master regulator of the HSR, but also as a developmental and lifespan regulating transcription factor. Our next generation sequencing data has led to the hypothesis that HSF-1 controls the expression of a variety of collagen genes in a HS-dependent and -independent manner (357). Our preliminary studies show that knockdown of the collagen gene, *col-123*, results in enhancement of *hsp-70* promoter activity in a tissue specific manner (357). We expect that other collagen genes will also modulate *hsp-70* promoter activity and the HSR. Regulation of collagen gene expression by HSF-1 may therefore ultimately impact proteostasis and longevity, which are two areas the HSR is known to promote.

In *C. elegans*, collagen genes are major constituents of the cuticle of the worm. In humans, collagens are long-lived proteins that can accumulate during the aging process, ultimately leading to a decline in tissue health. Collagens are also known to be involved in numerous diseases including osteoporosis and musculoskeletal diseases. Interestingly, collagen is also associated with aging, as mice expressing cleavage-resistant type I collagen experience an accelerated aging process. Also, collagen production was determined to be essential for longevity in *C. elegans* (380). Thus, regulation of collagen genes by HSF-1, and regulation of the HSR by collagens, may be one mechanism utilized by HSF-1 to promote longevity.

AIM 1: Uncovering collagen genes as modulators of the HSR

Our interest is in further determining the role HSF-1 in regulating collagen gene expression, and assessing how collagen genes affect the HSR and aging. By performing RNA-seq, we found 85 collagen genes to be regulated by HSF-1 during HS, while 32 collagen genes were found to be regulated by HSF-1 independently of HS (Table 8.1 and 8.2, respectively) (357). The known *C. elegans* HSF-1 binding site (TTCnnGAA) was identified in the promoters of these select collagen genes. Of the 85 collagen genes found to be regulated by HSF-1 during HS via RNA-seq, 59 have known HSF-1-binding sites in their promoters. Of the 32 collagen genes found to be regulated by HSF-1 independently of HS via RNA-seq, 22 have known HSF-1-binding sites in their promoters. Due to our interest in determining a direct role for HSF-1 in regulating collagen gene expression, our studies will focus on the collagen genes we found to be regulated by HSF-1 during and independently of HS, and that also contain known HSF-1 binding sites in their promoters.

To determine which of the collagens regulated by HSF-1 would also affect the HSR, a small-scale genetic RNAi screen will be performed using a worm construct with the *hsp-70* promoter fused to GFP, and fluorescence will be used as a marker for induction of the HSR (Figure 8.2). Collagen RNAi's would first be isolated from our RNAi library, and each clone would be sequence verified. Next, worms would be fed control, and collagen gene-specific RNAi's, through-out their larval stages. Once the last larval stage is reached, worms would be left untreated or given a minor 33°C 30-minute HS. Fluorescence intensity would then be measured and used to determine which collagen genes affect the HSR. To verify the RNAi screen, qRT-PCR would also be performed to measure *hsp-70* mRNA expression in wild-type worms in response to collagen RNAi treatment, and in the

presence and absence of HS. This experimental set-up would thus allow for the determination of the specific collagen genes that influence induction of the HSR, and which collagen genes should be assessed for future studies.

AIM 2: Determining a direct role for HSF-1 in regulating collagen gene expression

We would next be interested in determining a direct role for HSF-1 in regulating collagen gene expression. Chromatin immunoprecipitation (ChIP) would be performed to assess HSF-1-binding to the promoters of the collagen genes determined from AIM1 to regulate the HSR (Figure 8.3). Using a worm construct that contains HSF-1 tagged GFP that has been generated by the CRISPR/Cas9 system, ChIP would be performed using a ChIP-grade GFP antibody alongside an IgG antibody as a control. Next, qRT-PCR would be performed probing for HSF-1 binding to collagen gene promoters. This experimental set-up would thus further establish a direct role for HSF-1 in regulating collagen production by measuring the binding of HSF-1 to collagen gene promoters.

AIM 3: Uncovering a role for HSF-1-regulated collagen genes in modulating longevity, healthy aging, and proteostasis

The effects of collagen gene expression on proteostasis, healthspan, and longevity would next be assessed (Figure 8.4). First, lifespan assays would performed in wild-type worms using RNAi knockdown of the collagen genes determined from AIMS 1 and 2 to affect the HSR and be regulated by HSF-1. However, measuring lifespan is not a complete representation of aging, thus healthspan assays would also be done throughout the aging process. These healthspan assays include measuring pharyngeal pumping, movement, brood size, and body length. To measure proteostasis, polyglutamine aggregation would be observed in an aging *C. elegans* Huntington's disease in response to collagen RNAi

treatment. As another measure of proteostasis, the ability of wild-type worms to respond to a lethal heat-stress in response to collagen RNAi treatment would also be performed. These experiments would thus allow for the determination of the role of collagen genes in modulating longevity, healthy aging, and proteostasis in *C. elegans*.

Next, the role of HSF-1 in regulating proteostasis and healthy aging through the modulation of collagen gene expression would be determined. First, an HSF-1 null *C. elegans* strain would be generated using CRISPR/Cas9 technology. This strain would then be used in parallel to a wild-type strain for all longevity and proteostasis studies. To examine proteostasis in the Huntington's disease model, the CRISPR generated HSF-1 null worm strain would be crossed to the Huntington's disease model strain. This design would allow for the determination of the role of HSF-1 in regulating collagen gene expression to modulate longevity, healthy aging, and proteostasis.

Conclusion: Manipulating collagen gene expression may be one mechanism utilized by HSF-1 to promote longevity during and independently of heat-stress

Uncovering a role for collagen-mediated modulation of the HSR is a novel and interesting concept that may lead to future mammalian studies linking the HSR to increasing longevity through collagen production. This may have impacts in uncovering therapies to increase collagen production to promote healthy aging, proteostasis, and longevity through modulation of the HSR.

Future Study 2: Uncovering a Sirtuin/HSF-1 longevity-associated network

Rationale: Modulating sirtuin activity enhances the HSR and promotes longevity

SIRT1 belongs to a conserved family of deacetylases known to promote longevity. Mammalian cells have seven sirtuin family members, SIRT1-7, whereas *C. elegans* have

four, Sir-2.1-2.4 (280). The most actively studied sirtuin is SIRT1, which corresponds to Sir-2.1 in *C. elegans*. Enhancing the activity of SIRT1 enhances longevity in mammalian and *C. elegans* systems (392,393). Thus, uncovering modulators of SIRT1 activity is an active area of research with the underlying goal being to promote health and longevity.

SIRT1 promotes the mammalian HSR and is required for many longevity-promoting pathways (58,280). The HSR is enhanced by SIRT1 via deacetylation of the DNA-binding domain of HSF-1, resulting in enhanced *hsp-70* gene expression (58). Among enhancement of the HSR, SIRT1 is also implicated as a mediator of the numerous health benefits obtained by caloric restriction (280). Using *C. elegans* as a model organism, our lab has shown that the ability of caloric restriction to work through SIRT1 to enhance the HSR and fitness is conserved (72). In the studies performed here, we have uncovered that modulating Sir-2.1 activity promotes stress-resistance, fitness, longevity, and proteostasis. Altogether, our studies suggest that regulation of the HSR by modulating SIRT1 activity is conserved and may impact longevity and healthy aging.

AIM 1. Determine the genome-wide targets of Sir-2.1 during and independently of heat- stress

Our lab has previously established a role for Sir-2.1 in enhancing the *C. elegans* HSR. To gain insight into the genome-wide role of Sir-2.1 in regulating the HSR, RNA-sequencing would be performed in control worms, and a Sir-2.1 deletion strain generated by CRISPR/Cas9 technology, and worms would either be left untreated or given a minor 30 minute 33°C heat-stress (Figure 8.5a). After RNA-sequencing is completed and the data is analyzed as shown in Figure 8.5b, Venn diagrams would be used to compare each experimental condition (Figure 8.5c). This would allow for the separation of genes

regulated by Sir-2.1 during heat-stress and independently of heat-stress. Overall, this experimental design would allow for the determination of the genome-wide role of Sir-2.1 in regulating gene expression during and independently of heat-stress.

AIM 2. Determine the global HSF-1/Sir-2.1 network

To determine the HSF-1/Sir-2.1 regulated network, the genes found in AIM 1 to be regulated by Sir-2.1 during and independently of heat-stress would be compared to genes we previously determined to be regulated by HSF-1 (Figure 8.6). This would allow for the identification of an HSF-1/Sir-2.1 regulated network on a genome-wide scale.

The biological processes affected by the HSF-1/Sir-2.1 network would next be assessed. The list of genes determined to be regulated by HSF-1/Sir-2.1 in AIM 1 would be run through the Database for Annotation, Visualization, and Integrated Discovery tool. This method of analyses would uncover enriched cellular processes affected by the HSF-1/Sir-2.1 network. Based on our previous studies, we expect that longevity would be one of the top processes regulated by this network of genes, and would further confirm a role for both HSF-1 and Sir-2.1 in regulating longevity.

AIM 3. Determine the role of HSF-1/Sir-2.1 regulated genes in modulating the HSR and longevity

The impact of genes regulated by HSF-1 and Sir-2.1 during and independently of heat-stress would next be assessed for effects on the HSR and longevity (Figure 8.7). An RNAi screen would be performed for the genes found to be associated with HSF-1 and Sir-2.1, and their impacts on the HSR and longevity would be determined. First, the induction of the HSR in response to RNAi knockdown of all HSF-1/Sir-2.1 regulated genes would be done with a worm construct containing the *hsp-70* promoter fused to GFP. First, RNAi's

would be isolated from our RNAi library, and each clone would be sequence verified. Worms would then be fed control, and gene-specific RNAi's, through-out their larval stages. Once the last larval stage is reached, worms would be left untreated or given a minor 33°C 30-minute HS. Fluorescence intensity would then be measured and used to determine which collagen genes affect the HSR. To verify the RNAi screen, qRT-PCR would also be performed to measure *hsp-70* mRNA expression in wild-type worms in response to gene-specific RNAi treatment, and in the presence and absence of HS. This experimental set-up would determine the impact of the genes involved in the HSF-1/Sir-2.1 network on the HSR.

Next, lifespan assays would be performed to determine effects on longevity. Worms would be fed control or gene-specific RNAi corresponding to the genes found in AIM 2 to be regulated by Sir-2.1 and HSF-1. To maintain the parental population, approximately 200 worms/condition would be transferred to fresh plates daily until progeny production ceased. Dead/live worms would be scored every other day until no survivors remained. This experimental design would therefore assess the impact of genes associated with the HSF-1/Sir-2.1 network on regulating longevity.

Conclusion: Identifying a role for Sir-2.1 in regulating longevity during and independently of heat-stress

Uncovering a role for the genetic targets of HSF-1 and Sir-2.1 will not only lead to the identification of novel targets in an important longevity-associated pathway, but may also lead to future studies linking sirtuins to the HSR and longevity. This work may also have future impacts determining genes essential for longevity and their roles in mammalian systems.

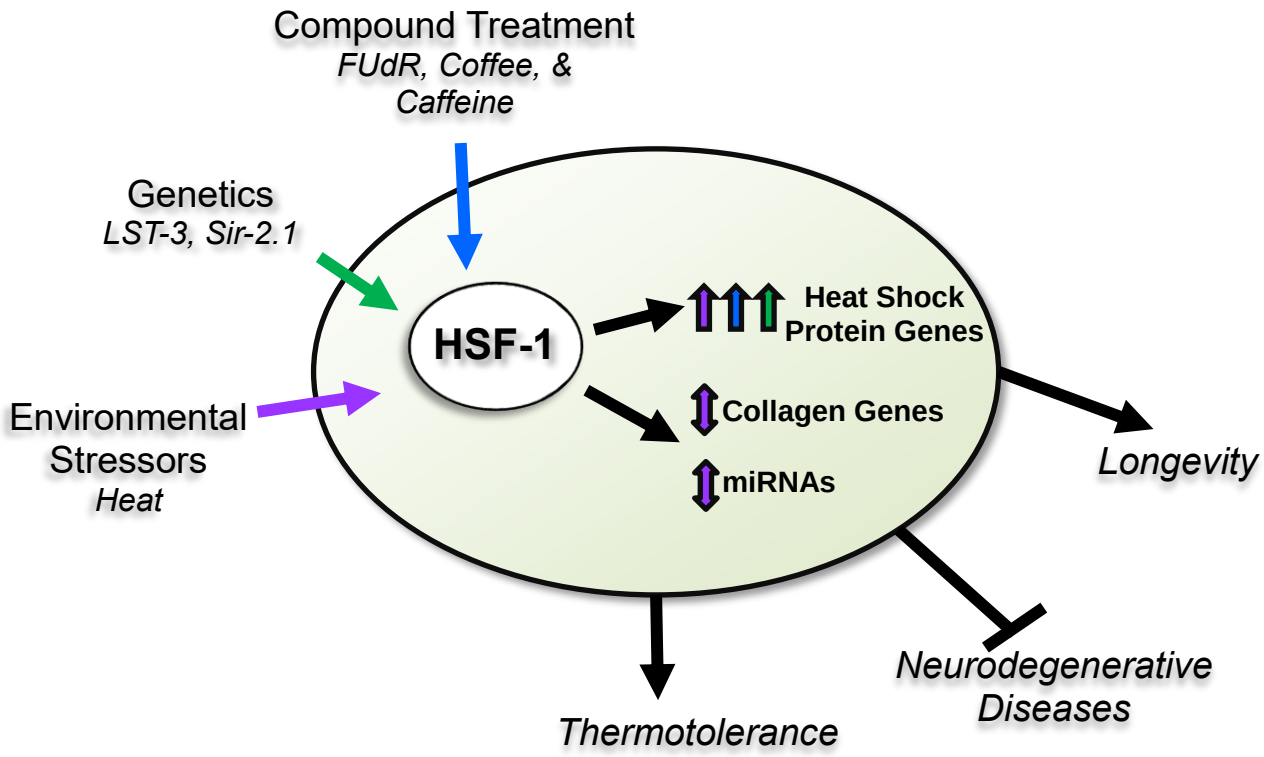

Figure 8.1. Modulating the HSR to promote thermotolerance and longevity, and to prevent neurodegenerative diseases. In these studies, we have uncovered environmental, compound, and genetic regulators of the HSR, and have determined global HSF-1 mRNA/miRNA targets. We have found that enhancing the HSR upon treatment with FUdR, coffee, and caffeine, or through enhancing Sir-2.1 activity, protects against polyglutamine aggregate formation in a *C. elegans* Huntington's disease model. These data suggest that compound intervention of the HSR may be beneficial for neurodegenerative diseases. Additionally, enhancing Sir-2.1 activity promotes longevity and thermotolerance. Similarly, we have uncovered HSF-1 as a regulator of collagen gene expression and miRNA expression, and have predicted these targets to play a role in regulating longevity. Overall, we have found that enhancing the HSR through genetic intervention, compound treatment, and environmental stress may promote longevity, thermotolerance, and may be beneficial for aggregate-associated neurodegenerative disorders.

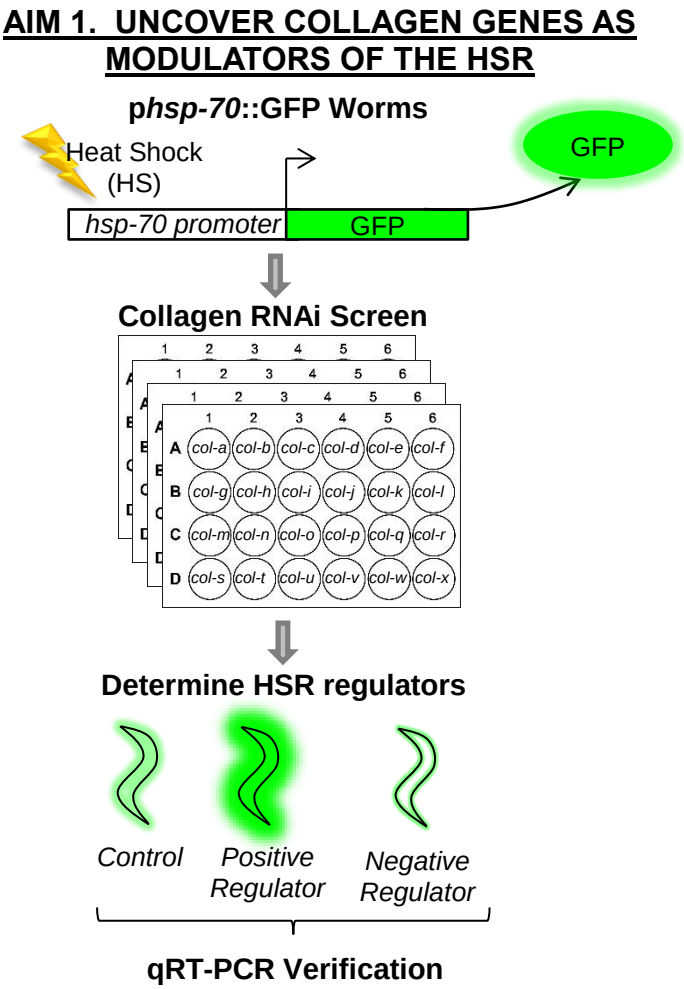

Figure 8.2. Uncovering collagens as modulators of the HSR. A *C. elegans* promoter fusion construct containing a *hsp-70* promoter fused to GFP (p*hsp-70*::GFP) will be used to assess activation of the HSR. Collagen RNAi's that we previously determined to be regulated by HSF-1 during and independently of HS, and that contain HSF-1 binding sites in their promoters, will be isolated from an RNAi library and fed to p*hsp-70*::GFP worms from their L2 larval stage to the L4 larval stage and left untreated or given a minor HS. Fluorescence will then be measured for each collagen RNAi and compared to the control to determine positive or negative regulation of the HSR.

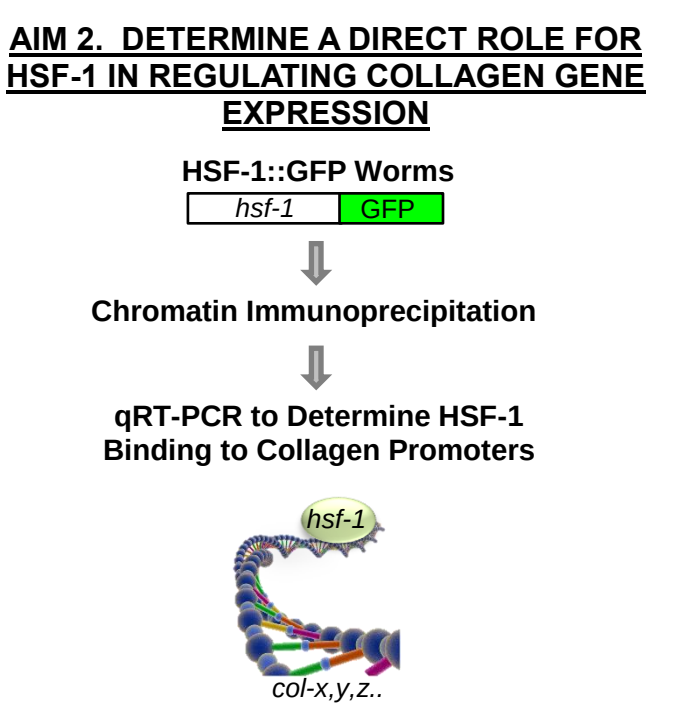

Figure 8.3. Determine HSF-1 binding to collagen gene promoters. A worm strain containing HSF-1 fused to GFP under the control of its own endogenous promoter will be fed collagen RNAi's determined from AIM 1 to regulate the HSR prior to performing ChIP followed by qRT-PCR to determine HSF-1 binding to collagen gene promoters.

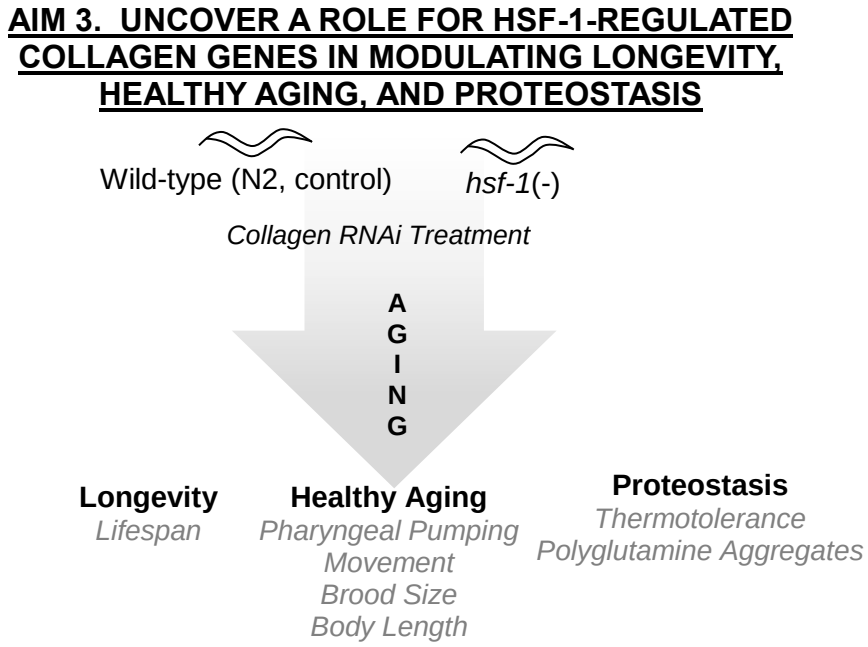

Figure 8.4. The role of HSF-1-regulated collagen genes in controlling longevity, healthy aging, and proteostasis. The collagen genes determined from AIMS 1 and 2 to be regulated by HSF-1 and influence the HSR will be assessed in wild-type worms (N2), and a CRISPR generated *hsf-1* null worm [*hsf-1*(-)] for their effects on lifespan, healthy aging, and proteostasis.

Table 8.1. Collagen genes regulated by HSF-1- during HS.

Gene ID	log_2 Fold *hsf-1*(+);+HS vs. control	Description
col-149	3.01	Function unknown.
col-143	2.55	Function unknown.
col-80	2.44	Function unknown.
col-129	2.43	Function unknown.
col-140	2.40	Function unknown.
col-139	2.37	Function unknown.
col-169	2.37	Function unknown.
col-147	2.35	Function unknown.
col-142	2.34	Function unknown.
col-93	2.32	Function unknown.
col-160	2.30	Function unknown.
col-170	2.29	Function unknown.
col-159	2.22	Function unknown.
col-19	2.17	*col-19* encodes a member of the collagen superfamily containing collagen triple helix repeats (20 copies) that is required for normal structure of the alae; expressed during the L2-to-dauer and L4-to-adult molts with strongest expression in adult animals.
col-124	2.17	Function unknown.
col-81	2.16	Function unknown.
col-94	2.14	Function unknown.
col-122	2.13	Function unknown.
col-92	2.11	Function unknown.
col-20	2.11	*col-20* encodes a collagen; its expression pattern and mutant phenotypes are unknown.
col-179	2.08	Function unknown.
col-178	2.07	Function unknown.
col-7	2.06	*col-7* encodes a member of the collagen superfamily containing collagen triple helix repeats (20 copies); expressed during the L2-to-dauer molt and the L4-to-adult molt.
col-146	2.06	Function unknown.
col-62	2.03	Function unknown.
col-181	2.02	*col-181* is homologous to the human gene PRO ALPHA 1(I) COLLAGEN (COL1A1; OMIM:120150)
col-167	2.02	Function unknown.
col-168	2.01	Function unknown.
col-127	2.01	Function unknown.
col-98	1.99	Function unknown.
col-8	1.99	Function unknown.
col-126	1.99	Function unknown.
col-184	1.99	Function unknown.

Table 8.1. (Continued)

col-101	1.98	col-101 encodes a cuticle collagen; loss of col-101 via large-scale RNAi screens results in animals that are pale and slow growing.
col-144	1.91	Function unknown.
col-117	1.89	Function unknown.
col-3	1.88	col-3 encodes a collagen protein that affects body morphogenesis
col-10	1.88	Function unknown.
col-133	1.84	Function unknown.
col-106	1.82	col-106 encodes a predicted cuticular collagen.
col-125	1.74	Function unknown.
col-180	1.64	Function unknown.
col-145	1.62	Function unknown.
col-107	1.59	Function unknown.
col-157	1.59	Function unknown.
col-71	1.54	Function unknown.
col-12	1.53	col-12 encodes a member of the collagen superfamily containing collagen triple helix repeats (20 copies); expressed throughout development but expression peaks after each larval molt when new cuticle is being secreted and deposited
col-88	1.53	Function unknown.
col-166	1.50	Function unknown.
col-38	1.50	col-38 encodes a member of the collagen superfamily containing collagen triple helix repeats (20 copies) required for normal body morphology.
col-138	1.47	Function unknown.
col-66	1.47	Function unknown.
col-48	1.47	col-48 encodes a cuticle collagen.
col-130	1.46	Function unknown.
col-17	1.45	col-17 encodes a collagen which is expressed in all developmental stages except eggs
col-13	1.44	col-13 encodes a collagen which is expressed in all stages of development
col-63	1.44	Function unknown.
col-104	1.44	Function unknown.
col-175	1.41	Function unknown.
col-96	1.39	Function unknown.
col-152	1.39	Function unknown.
col-77	1.38	col-77 encodes a cuticular collagen; as loss of col-77 activity via RNAi screens results in no obvious defects
col-156	1.38	Function unknown.
col-141	1.38	Function unknown.
col-161	1.37	Function unknown.
col-65	1.34	Function unknown.
col-73	1.33	Function unknown.
col-60	1.32	Function unknown.
col-46	1.29	col-46 encodes a cuticle collagen.

Table 8.1. (Continued)

col-162	1.28	Function unknown.
col-154	1.28	Function unknown.
col-120	1.28	Function unknown.
col-97	1.26	*col-97* encodes a cuticular collagen; loss of *col-97* activity via large-scale RNAi screens results in defects in body morphology and locomotion.
col-91	1.23	*col-91* encodes a cuticle collagen; loss of *col-91* via large-scale RNAi results in no obvious defects.
col-58	1.18	Function unknown.
col-14	1.17	*col-14* encodes a collagen protein that affects vulval morphology in a large-scale RNAi screen; mRNA expressed in embryos and transcript levels peak during each larval stage.
col-49	1.16	*col-49* encodes a cuticle collagen.
col-89	1.13	Function unknown.
col-34	1.09	*col-34* encodes a cuticle collagen protein and is a critical component of male tail cuticle organization affecting ray morphology.
col-155	1.08	Function unknown.
col-150	1.07	Function unknown.
col-137	1.05	Function unknown.
col-109	1.03	*col-109* encodes a cuticular collagen; loss of *col-109* via large-scale RNAi screens results in no obvious defects.
col-68	1.02	Function unknown.
col-118	1.02	Function unknown.

Table 8.2. Collagen genes regulated by HSF-1 independently of HS.

Gene ID	log2 Fold *hsf-1*(-);-HS vs. control	Description
col-135	2.52	Function unknown.
col-68	1.87	Function unknown.
col-120	1.79	Function unknown.
col-88	1.71	Function unknown.
col-175	1.62	Function unknown.
col-60	1.54	Function unknown.
col-138	1.51	Function unknown.
col-63	1.49	Function unknown.
col-49	1.49	*col-49* encodes a cuticle collagen.
col-71	1.48	Function unknown.
col-182	1.45	Function unknown.
col-38	1.42	*col-38* encodes a member of the collagen superfamily containing collagen triple helix repeats (20 copies) required for normal body morphology.
col-77	1.39	*col-77* encodes a cuticular collagen; as loss of *col-77* activity via RNAi screens results in no obvious defects
col-91	1.22	*col-91* encodes a cuticle collagen; loss of *col-91* via large-scale RNAi results in no obvious defects.
col-170	1.22	Function unknown.
col-130	1.17	Function unknown.
col-162	1.16	Function unknown.
col-76	1.13	Function unknown.
col-161	1.09	Function unknown.
col-65	1.08	Function unknown.
col-104	1.07	Function unknown.
col-73	0.97	Function unknown.
col-137	0.95	Function unknown.
col-61	0.95	Function unknown.
col-97	0.94	*col-97* encodes a cuticular collagen; loss of *col-97* activity via large-scale RNAi screens results in defects in body morphology and locomotion.
col-133	0.93	Function unknown.
col-58	0.90	Function unknown.
col-96	0.89	Function unknown.
col-123	-4.37	*col-123* is homologous to the human gene A TYPE IV COLLAGEN (COL6A1; OMIM:303631)
col-84	-4.95	*col-84* encodes a nematode cuticular collagen; RNAi experiments that target *col-84* (as well as neighboring genes) result in defects in embryonic and larval development
col-158	-5.00	Function unknown.
col-185	-5.79	Function unknown.

AIM 1. Determine the genome-wide targets of Sir-2.1 during and independently of heat- stress

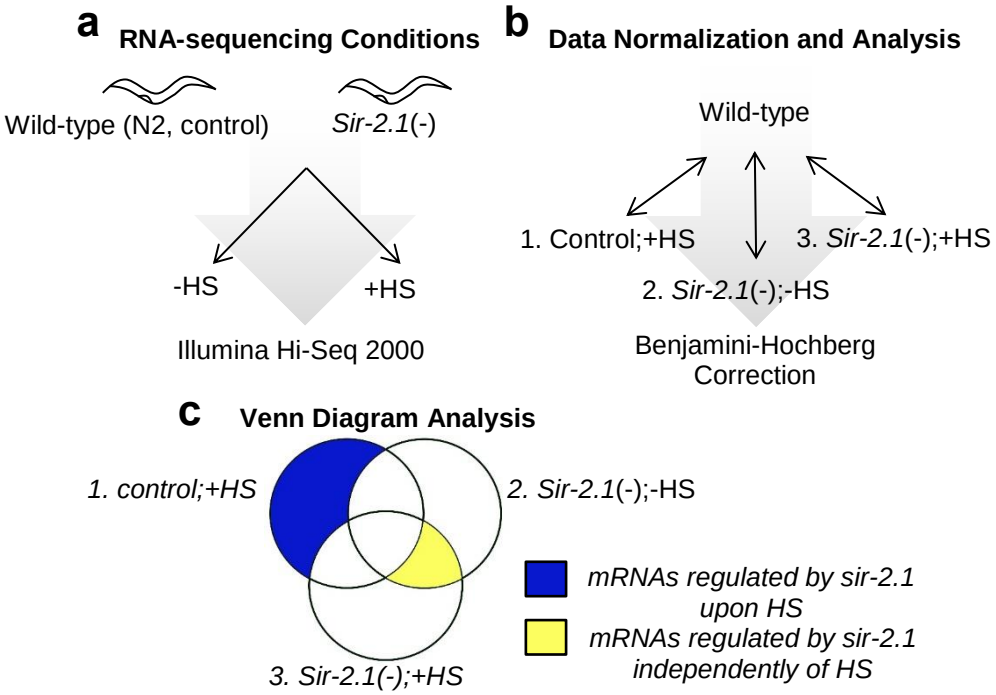

Figure 8.5. Determining genome-wide Sir-2.1 targets. (**a**) Schematic for RNA-sequencing conditions. RNA samples from wild-type L4 larval worms will be generated in two biological replicates under the four indicated conditions. "*sir-2.1*(+)" refers to worms that will be treated with empty vector control RNAi, and "*sir-2.1*(-)" refers to worms that will be treated with *sir-2.1* RNAi. "-HS" indicates worms that will be left at growth temperature, while "+HS" indicates worms that will be treated with a 33°C 30 minute HS. RNA-sequencing would be performed on the Illumina Hi-Seq 2000 platform. (**b**) Schematic of data normalization. Each experimental treatment condition will be normalized relative to the untreated control. Differentially expressed mRNAs will then be determined using the Benjamini-Hochberg correction for multiple testing. (**c**) Separating Sir-2.1 regulated mRNAs. A Venn diagram will be used to compare each treatment condition in order to separate mRNAs regulated by Sir-2.1 during and independently of HS.

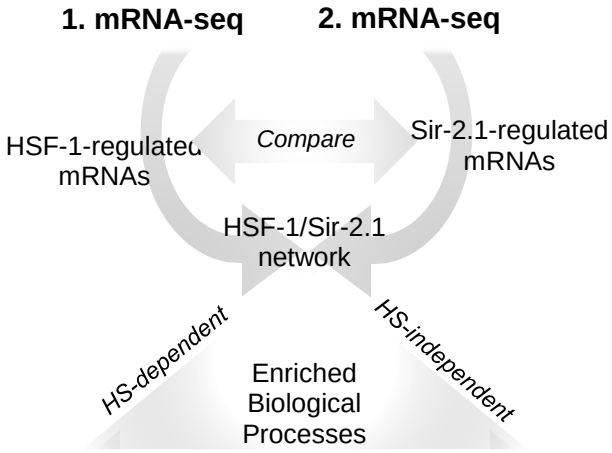

Figure 8.6. Determining HSF-1/Sir-2.1 regulated networks. The mRNAs found from AIM 1 to be regulated by Sir-2.1 during and independently of HS will be compared to those we previously found to be regulated by HSF-1 during and independently of HS. These mRNAs will then be run through the Database for Annotation, Visualization, and Integration tool to determine enriched biological processes influenced by the HSF-1/Sir-2.1 network.

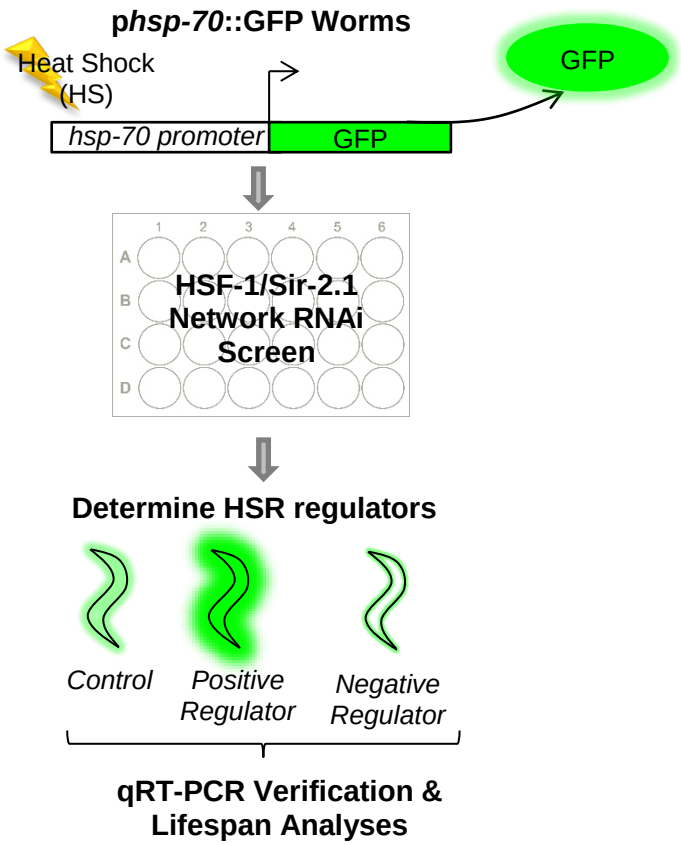

Figure 8.7. Determine a role for the HSF-1/Sir-2.1 network in regulating the HSR and longevity. A *C. elegans* promoter fusion construct containing a *hsp-70* promoter fused to GFP (p*hsp-70*::GFP) will be used to assess activation of the HSR. RNAi's of genes we found to be regulated by HSF-1/Sir-2.1 will be isolated from an RNAi library and fed to p*hsp-70*::GFP worms from their L1 larval stage to the L4 larval stage and left untreated or given a minor HS. Fluorescence will then be measured for each RNAi and compared to the control to determine positive or negative regulation of the HSR. qRT-PCR will then be done to confirm regulation, followed by lifespan analyses to determine the effects of modulating the HSF-1/Sir-2.1 network on lifespan.

REFERENCES

1. De Maio, A., Santoro, M. G., Tanguay, R. M., and Hightower, L. E. (2012) Ferruccio Ritossa's scientific legacy 50 years after his discovery of the heat shock response: a new view of biology, a new society, and a new journal. *Cell Stress Chaperones* **17**, 139-143
2. Ritossa, F. (1996) Discovery of the heat shock response. *Cell Stress Chaperones* **1**, 97-98
3. Ritossa, F. (1962) New Puffing Pattern Induced by Temperature Shock and Dnp in Drosophila. *Experientia* **18**, 571-&
4. Tissieres, A., Mitchell, H. K., and Tracy, U. M. (1974) Protein synthesis in salivary glands of Drosophila melanogaster: relation to chromosome puffs. *J Mol Biol* **84**, 389-398
5. Lewis, M., Helmsing, P. J., and Ashburner, M. (1975) Parallel changes in puffing activity and patterns of protein synthesis in salivary glands of Drosophila. *Proc Natl Acad Sci U S A* **72**, 3604-3608
6. Spradling, A., Pardue, M. L., and Penman, S. (1977) Messenger RNA in heat-shocked Drosophila cells. *J Mol Biol* **109**, 559-587
7. Greene, J. M., Larin, Z., Taylor, I. C., Prentice, H., Gwinn, K. A., and Kingston, R. E. (1987) Multiple basal elements of a human hsp70 promoter function differently in human and rodent cell lines. *Mol Cell Biol* **7**, 3646-3655
8. Mosser, D. D., Theodorakis, N. G., and Morimoto, R. I. (1988) Coordinate changes in heat shock element-binding activity and HSP70 gene transcription rates in human cells. *Mol Cell Biol* **8**, 4736-4744
9. Wu, B. J., Kingston, R. E., and Morimoto, R. I. (1986) Human HSP70 promoter contains at least two distinct regulatory domains. *Proc Natl Acad Sci U S A* **83**, 629-633
10. Parker, C. S., and Topol, J. (1984) A Drosophila RNA polymerase II transcription factor binds to the regulatory site of an hsp 70 gene. *Cell* **37**, 273-283
11. Wiederrecht, G., Shuey, D. J., Kibbe, W. A., and Parker, C. S. (1987) The Saccharomyces and Drosophila heat shock transcription factors are identical in size and DNA binding properties. *Cell* **48**, 507-515
12. Goldenberg, C. J., Luo, Y., Fenna, M., Baler, R., Weinmann, R., and Voellmy, R. (1988) Purified human factor activates heat shock promoter in a HeLa cell-free transcription system. *J Biol Chem* **263**, 19734-19739
13. Eggers, D. K., Welch, W. J., and Hansen, W. J. (1997) Complexes between nascent polypeptides and their molecular chaperones in the cytosol of mammalian cells. *Molecular biology of the cell* **8**, 1559-1573
14. Frydman, J., Nimmesgern, E., Ohtsuka, K., and Hartl, F. U. (1994) Folding of nascent polypeptide chains in a high molecular mass assembly with molecular chaperones. *Nature* **370**, 111-117
15. Saibil, H. R., Zheng, D., Roseman, A. M., Hunter, A. S., Watson, G. M., Chen, S., Auf Der Mauer, A., O'Hara, B. P., Wood, S. P., Mann, N. H., Barnett, L. K., and Ellis, R. J. (1993) ATP induces large quaternary rearrangements in a cage-like chaperonin structure. *Curr Biol* **3**, 265-273

16. Gragerov, A. I., Martin, E. S., Krupenko, M. A., Kashlev, M. V., and Nikiforov, V. G. (1991) Protein aggregation and inclusion body formation in Escherichia coli rpoH mutant defective in heat shock protein induction. *FEBS Lett* **291**, 222-224
17. Kerner, M. J., Naylor, D. J., Ishihama, Y., Maier, T., Chang, H. C., Stines, A. P., Georgopoulos, C., Frishman, D., Hayer-Hartl, M., Mann, M., and Hartl, F. U. (2005) Proteome-wide analysis of chaperonin-dependent protein folding in Escherichia coli. *Cell* **122**, 209-220
18. Mayer, M. P. (2010) Gymnastics of molecular chaperones. *Mol Cell* **39**, 321-331
19. Mayer, M. P., and Bukau, B. (2005) Hsp70 chaperones: cellular functions and molecular mechanism. *Cell Mol Life Sci* **62**, 670-684
20. Mayer, M. P. (2013) Hsp70 chaperone dynamics and molecular mechanism. *Trends Biochem Sci* **38**, 507-514
21. Zhu, X., Zhao, X., Burkholder, W. F., Gragerov, A., Ogata, C. M., Gottesman, M. E., and Hendrickson, W. A. (1996) Structural analysis of substrate binding by the molecular chaperone DnaK. *Science* **272**, 1606-1614
22. Goloubinoff, P., and De Los Rios, P. (2007) The mechanism of Hsp70 chaperones: (entropic) pulling the models together. *Trends Biochem Sci* **32**, 372-380
23. Ben-Zvi, A. P., and Goloubinoff, P. (2001) Review: mechanisms of disaggregation and refolding of stable protein aggregates by molecular chaperones. *J Struct Biol* **135**, 84-93
24. Fan, C. Y., Lee, S., and Cyr, D. M. (2003) Mechanisms for regulation of Hsp70 function by Hsp40. *Cell Stress Chaperones* **8**, 309-316
25. Slepenkov, S. V., and Witt, S. N. (2002) The unfolding story of the Escherichia coli Hsp70 DnaK: is DnaK a holdase or an unfoldase? *Mol Microbiol* **45**, 1197-1206
26. Diamant, S., and Goloubinoff, P. (1998) Temperature-controlled activity of DnaK-DnaJ-GrpE chaperones: protein-folding arrest and recovery during and after heat shock depends on the substrate protein and the GrpE concentration. *Biochemistry* **37**, 9688-9694
27. Kriehuber, T., Rattei, T., Weinmaier, T., Bepperling, A., Haslbeck, M., and Buchner, J. (2010) Independent evolution of the core domain and its flanking sequences in small heat shock proteins. *FASEB J* **24**, 3633-3642
28. de Jong, W. W., Leunissen, J. A., and Voorter, C. E. (1993) Evolution of the alpha-crystallin/small heat-shock protein family. *Mol Biol Evol* **10**, 103-126
29. Raman, B., and Rao, C. M. (1994) Chaperone-like activity and quaternary structure of alpha-crystallin. *J Biol Chem* **269**, 27264-27268
30. van Montfort, R. L., Basha, E., Friedrich, K. L., Slingsby, C., and Vierling, E. (2001) Crystal structure and assembly of a eukaryotic small heat shock protein. *Nat Struct Biol* **8**, 1025-1030
31. Van Montfort, R., Slingsby, C., and Vierling, E. (2001) Structure and function of the small heat shock protein/alpha-crystallin family of molecular chaperones. *Adv Protein Chem* **59**, 105-156
32. Ghosh, J. G., Shenoy, A. K., Jr., and Clark, J. I. (2006) N- and C-Terminal motifs in human alphaB crystallin play an important role in the recognition, selection, and solubilization of substrates. *Biochemistry* **45**, 13847-13854
33. Carver, J. A., Aquilina, J. A., Truscott, R. J., and Ralston, G. B. (1992) Identification by 1H NMR spectroscopy of flexible C-terminal extensions in bovine lens alpha-crystallin. *FEBS Lett* **311**, 143-149
34. Leroux, M. R., Melki, R., Gordon, B., Batelier, G., and Candido, E. P. (1997) Structure-function studies on small heat shock protein oligomeric assembly and interaction with unfolded polypeptides. *J Biol Chem* **272**, 24646-24656
35. Andley, U. P., Mathur, S., Griest, T. A., and Petrash, J. M. (1996) Cloning, expression, and chaperone-like activity of human alphaA-crystallin. *J Biol Chem* **271**, 31973-31980

36. Morris, A. M., Treweek, T. M., Aquilina, J. A., Carver, J. A., and Walker, M. J. (2008) Glutamic acid residues in the C-terminal extension of small heat shock protein 25 are critical for structural and functional integrity. *FEBS J* **275**, 5885-5898
37. Damberger, F. F., Pelton, J. G., Harrison, C. J., Nelson, H. C., and Wemmer, D. E. (1994) Solution structure of the DNA-binding domain of the heat shock transcription factor determined by multidimensional heteronuclear magnetic resonance spectroscopy. *Protein Sci* **3**, 1806-1821
38. Harrison, C. J., Bohm, A. A., and Nelson, H. C. (1994) Crystal structure of the DNA binding domain of the heat shock transcription factor. *Science* **263**, 224-227
39. Vuister, G. W., Kim, S. J., Orosz, A., Marquardt, J., Wu, C., and Bax, A. (1994) Solution structure of the DNA-binding domain of Drosophila heat shock transcription factor. *Nat Struct Biol* **1**, 605-614
40. Fernandes, M., Xiao, H., and Lis, J. T. (1994) Fine structure analyses of the Drosophila and Saccharomyces heat shock factor--heat shock element interactions. *Nucleic Acids Res* **22**, 167-173
41. Peteranderl, R., and Nelson, H. C. (1992) Trimerization of the heat shock transcription factor by a triple-stranded alpha-helical coiled-coil. *Biochemistry* **31**, 12272-12276
42. Rabindran, S. K., Haroun, R. I., Clos, J., Wisniewski, J., and Wu, C. (1993) Regulation of heat shock factor trimer formation: role of a conserved leucine zipper. *Science* **259**, 230-234
43. Westwood, J. T., and Wu, C. (1993) Activation of Drosophila heat shock factor: conformational change associated with a monomer-to-trimer transition. *Mol Cell Biol* **13**, 3481-3486
44. Eastmond, D. L., and Nelson, H. C. (2006) Genome-wide analysis reveals new roles for the activation domains of the Saccharomyces cerevisiae heat shock transcription factor (Hsf1) during the transient heat shock response. *J Biol Chem* **281**, 32909-32921
45. Soncin, F., and Calderwood, S. K. (1996) Reciprocal effects of pro-inflammatory stimuli and anti-inflammatory drugs on the activity of heat shock factor-1 in human monocytes. *Biochem Biophys Res Commun* **229**, 479-484
46. Green, M., Schuetz, T. J., Sullivan, E. K., and Kingston, R. E. (1995) A heat shock-responsive domain of human HSF1 that regulates transcription activation domain function. *Mol Cell Biol* **15**, 3354-3362
47. Newton, E. M., Knauf, U., Green, M., and Kingston, R. E. (1996) The regulatory domain of human heat shock factor 1 is sufficient to sense heat stress. *Mol Cell Biol* **16**, 839-846
48. Xu, Y. M., Huang, D. Y., Chiu, J. F., and Lau, A. T. (2012) Post-translational modification of human heat shock factors and their functions: a recent update by proteomic approach. *Journal of proteome research* **11**, 2625-2634
49. Budzynski, M. A., Puustinen, M. C., Joutsen, J., and Sistonen, L. (2015) Uncoupling Stress-Inducible Phosphorylation of Heat Shock Factor 1 from Its Activation. *Mol Cell Biol* **35**, 2530-2540
50. Soncin, F., Zhang, X., Chu, B., Wang, X., Asea, A., Ann Stevenson, M., Sacks, D. B., and Calderwood, S. K. (2003) Transcriptional activity and DNA binding of heat shock factor-1 involve phosphorylation on threonine 142 by CK2. *Biochem Biophys Res Commun* **303**, 700-706
51. Murshid, A., Chou, S. D., Prince, T., Zhang, Y., Bharti, A., and Calderwood, S. K. (2010) Protein kinase A binds and activates heat shock factor 1. *PloS one* **5**, e13830
52. Holmberg, C. I., Hietakangas, V., Mikhailov, A., Rantanen, J. O., Kallio, M., Meinander, A., Hellman, J., Morrice, N., MacKintosh, C., Morimoto, R. I., Eriksson, J. E., and Sistonen, L. (2001) Phosphorylation of serine 230 promotes inducible transcriptional activity of heat shock factor 1. *The EMBO journal* **20**, 3800-3810

53. Dayalan Naidu, S., Sutherland, C., Zhang, Y., Risco, A., de la Vega, L., Caunt, C. J., Hastie, C. J., Lamont, D. J., Torrente, L., Chowdhry, S., Benjamin, I. J., Keyse, S. M., Cuenda, A., and Dinkova-Kostova, A. T. (2016) Heat Shock Factor 1 Is a Substrate for p38 Mitogen-Activated Protein Kinases. *Mol Cell Biol* **36**, 2403-2417
54. Kim, S. A., Yoon, J. H., Lee, S. H., and Ahn, S. G. (2005) Polo-like kinase 1 phosphorylates heat shock transcription factor 1 and mediates its nuclear translocation during heat stress. *J Biol Chem* **280**, 12653-12657
55. Wang, X., Khaleque, M. A., Zhao, M. J., Zhong, R., Gaestel, M., and Calderwood, S. K. (2006) Phosphorylation of HSF1 by MAPK-activated protein kinase 2 on serine 121, inhibits transcriptional activity and promotes HSP90 binding. *J Biol Chem* **281**, 782-791
56. Xavier, I. J., Mercier, P. A., McLoughlin, C. M., Ali, A., Woodgett, J. R., and Ovsenek, N. (2000) Glycogen synthase kinase 3beta negatively regulates both DNA-binding and transcriptional activities of heat shock factor 1. *J Biol Chem* **275**, 29147-29152
57. Zelin, E., and Freeman, B. C. (2015) Lysine deacetylases regulate the heat shock response including the age-associated impairment of HSF1. *Journal of molecular biology* **427**, 1644-1654
58. Westerheide, S. D., Anckar, J., Stevens, S. M., Jr., Sistonen, L., and Morimoto, R. I. (2009) Stress-inducible regulation of heat shock factor 1 by the deacetylase SIRT1. *Science* **323**, 1063-1066
59. Voellmy, R., and Boellmann, F. (2007) Chaperone regulation of the heat shock protein response. *Adv Exp Med Biol* **594**, 89-99
60. Abravaya, K., Myers, M. P., Murphy, S. P., and Morimoto, R. I. (1992) The human heat shock protein hsp70 interacts with HSF, the transcription factor that regulates heat shock gene expression. *Genes Dev* **6**, 1153-1164
61. Zou, J., Guo, Y., Guettouche, T., Smith, D. F., and Voellmy, R. (1998) Repression of heat shock transcription factor HSF1 activation by HSP90 (HSP90 complex) that forms a stress-sensitive complex with HSF1. *Cell* **94**, 471-480
62. Ananthan, J., Goldberg, A. L., and Voellmy, R. (1986) Abnormal proteins serve as eukaryotic stress signals and trigger the activation of heat shock genes. *Science* **232**, 522-524
63. Mifflin, L. C., and Cohen, R. E. (1994) Characterization of denatured protein inducers of the heat shock (stress) response in Xenopus laevis oocytes. *J Biol Chem* **269**, 15710-15717
64. Kelley, P. M., and Schlesinger, M. J. (1978) The effect of amino acid analogues and heat shock on gene expression in chicken embryo fibroblasts. *Cell* **15**, 1277-1286
65. Ellis, R. J., and Hartl, F. U. (1996) Protein folding in the cell: competing models of chaperonin function. *FASEB J* **10**, 20-26
66. Vihervaara, A., and Sistonen, L. (2014) HSF1 at a glance. *Journal of cell science* **127**, 261-266
67. Raynes, R., Pombier, K. M., Nguyen, K., Brunquell, J., Mendez, J. E., and Westerheide, S. D. (2013) The SIRT1 modulators AROS and DBC1 regulate HSF1 activity and the heat shock response. *PloS one* **8**, e54364
68. Michan, S., and Sinclair, D. (2007) Sirtuins in mammals: insights into their biological function. *Biochem J* **404**, 1-13
69. Viswanathan, M., and Tissenbaum, H. A. (2013) C. elegans sirtuins. *Methods Mol Biol* **1077**, 39-56
70. Fritze, C. E., Verschueren, K., Strich, R., and Easton Esposito, R. (1997) Direct evidence for SIR2 modulation of chromatin structure in yeast rDNA. *The EMBO journal* **16**, 6495-6509

71. Yeung, F., Hoberg, J. E., Ramsey, C. S., Keller, M. D., Jones, D. R., Frye, R. A., and Mayo, M. W. (2004) Modulation of NF-kappaB-dependent transcription and cell survival by the SIRT1 deacetylase. *The EMBO journal* **23**, 2369-2380
72. Raynes, R., Leckey, B. D., Jr., Nguyen, K., and Westerheide, S. D. (2012) Heat shock and caloric restriction have a synergistic effect on the heat shock response in a sir2.1-dependent manner in Caenorhabditis elegans. *The Journal of biological chemistry* **287**, 29045-29053
73. Kim, J. E., Chen, J., and Lou, Z. (2008) DBC1 is a negative regulator of SIRT1. *Nature* **451**, 583-586
74. Kokkola, T., Suuronen, T., Molnar, F., Maatta, J., Salminen, A., Jarho, E. M., and Lahtela-Kakkonen, M. (2014) AROS has a context-dependent effect on SIRT1. *FEBS Lett* **588**, 1523-1528
75. Kim, E. J., Kho, J. H., Kang, M. R., and Um, S. J. (2007) Active regulator of SIRT1 cooperates with SIRT1 and facilitates suppression of p53 activity. *Mol Cell* **28**, 277-290
76. Brunquell, J., Yuan, J., Erwin, A., Westerheide, S. D., and Xue, B. (2014) DBC1/CCAR2 and CCAR1 Are Largely Disordered Proteins that Have Evolved from One Common Ancestor. *BioMed research international* **2014**, 418458
77. Kang, H., Suh, J. Y., Jung, Y. S., Jung, J. W., Kim, M. K., and Chung, J. H. (2011) Peptide switch is essential for Sirt1 deacetylase activity. *Mol Cell* **44**, 203-213
78. Yuan, J., Luo, K., Liu, T., and Lou, Z. (2012) Regulation of SIRT1 activity by genotoxic stress. *Genes Dev* **26**, 791-796
79. Zannini, L., Buscemi, G., Kim, J. E., Fontanella, E., and Delia, D. (2012) DBC1 phosphorylation by ATM/ATR inhibits SIRT1 deacetylase in response to DNA damage. *J Mol Cell Biol* **4**, 294-303
80. Zheng, H., Yang, L., Peng, L., Izumi, V., Koomen, J., Seto, E., and Chen, J. (2013) hMOF acetylation of DBC1/CCAR2 prevents binding and inhibition of SirT1. *Mol Cell Biol* **33**, 4960-4970
81. Hubbard, B. P., Loh, C., Gomes, A. P., Li, J., Lu, Q., Doyle, T. L., Disch, J. S., Armour, S. M., Ellis, J. L., Vlasuk, G. P., and Sinclair, D. A. (2013) Carboxamide SIRT1 inhibitors block DBC1 binding via an acetylation-independent mechanism. *Cell cycle* **12**, 2233-2240
82. Eisen, M. B., Spellman, P. T., Brown, P. O., and Botstein, D. (1998) Cluster analysis and display of genome-wide expression patterns. *Proc Natl Acad Sci U S A* **95**, 14863-14868
83. Gasch, A. P., Spellman, P. T., Kao, C. M., Carmel-Harel, O., Eisen, M. B., Storz, G., Botstein, D., and Brown, P. O. (2000) Genomic expression programs in the response of yeast cells to environmental changes. *Molecular biology of the cell* **11**, 4241-4257
84. GuhaThakurta, D., Palomar, L., Stormo, G. D., Tedesco, P., Johnson, T. E., Walker, D. W., Lithgow, G., Kim, S., and Link, C. D. (2002) Identification of a novel cis-regulatory element involved in the heat shock response in Caenorhabditis elegans using microarray gene expression and computational methods. *Genome research* **12**, 701-712
85. Matsuura, H., Ishibashi, Y., Shinmyo, A., Kanaya, S., and Kato, K. (2010) Genome-wide analyses of early translational responses to elevated temperature and high salinity in Arabidopsis thaliana. *Plant & cell physiology* **51**, 448-462
86. Larkindale, J., and Vierling, E. (2008) Core genome responses involved in acclimation to high temperature. *Plant physiology* **146**, 748-761
87. Richmond, C. S., Glasner, J. D., Mau, R., Jin, H., and Blattner, F. R. (1999) Genome-wide expression profiling in Escherichia coli K-12. *Nucleic Acids Res* **27**, 3821-3835
88. Rohlin, L., Trent, J. D., Salmon, K., Kim, U., Gunsalus, R. P., and Liao, J. C. (2005) Heat shock response of Archaeoglobus fulgidus. *Journal of bacteriology* **187**, 6046-6057
89. Tabuchi, Y., Takasaki, I., Wada, S., Zhao, Q. L., Hori, T., Nomura, T., Ohtsuka, K., and Kondo, T. (2008) Genes and genetic networks responsive to mild hyperthermia in human lymphoma U937 cells. *International journal of hyperthermia : the official journal of*

European Society for Hyperthermic Oncology, North American Hyperthermia Group **24**, 613-622
90. Bouche, G., Amalric, F., Caizergues-Ferrer, M., and Zalta, J. P. (1979) Effects of heat shock on gene expression and subcellular protein distribution in Chinese hamster ovary cells. *Nucleic Acids Res* **7**, 1739-1747
91. Lindquist, S. (1980) Varying patterns of protein synthesis in Drosophila during heat shock: implications for regulation. *Dev Biol* **77**, 463-479
92. Fritah, S., Col, E., Boyault, C., Govin, J., Sadoul, K., Chiocca, S., Christians, E., Khochbin, S., Jolly, C., and Vourc'h, C. (2009) Heat-shock factor 1 controls genome-wide acetylation in heat-shocked cells. *Molecular biology of the cell* **20**, 4976-4984
93. Niskanen, E. A., Malinen, M., Sutinen, P., Toropainen, S., Paakinaho, V., Vihervaara, A., Joutsen, J., Kaikkonen, M. U., Sistonen, L., and Palvimo, J. J. (2015) Global SUMOylation on active chromatin is an acute heat stress response restricting transcription. *Genome Biol* **16**, 153
94. Duncan, R., and Hershey, J. W. (1984) Heat shock-induced translational alterations in HeLa cells. Initiation factor modifications and the inhibition of translation. *J Biol Chem* **259**, 11882-11889
95. Vries, R. G., Flynn, A., Patel, J. C., Wang, X., Denton, R. M., and Proud, C. G. (1997) Heat shock increases the association of binding protein-1 with initiation factor 4E. *J Biol Chem* **272**, 32779-32784
96. Shalgi, R., Hurt, J. A., Krykbaeva, I., Taipale, M., Lindquist, S., and Burge, C. B. (2013) Widespread regulation of translation by elongation pausing in heat shock. *Mol Cell* **49**, 439-452
97. Merret, R., Nagarajan, V. K., Carpentier, M. C., Park, S., Favory, J. J., Descombin, J., Picart, C., Charng, Y. Y., Green, P. J., Deragon, J. M., and Bousquet-Antonelli, C. (2015) Heat-induced ribosome pausing triggers mRNA co-translational decay in Arabidopsis thaliana. *Nucleic Acids Res* **43**, 4121-4132
98. Guo, H., Ingolia, N. T., Weissman, J. S., and Bartel, D. P. (2010) Mammalian microRNAs predominantly act to decrease target mRNA levels. *Nature* **466**, 835-840
99. Carthew, R. W., and Sontheimer, E. J. (2009) Origins and Mechanisms of miRNAs and siRNAs. *Cell* **136**, 642-655
100. Das, S., and Bhattacharyya, N. P. (2014) Heat shock factor 1 regulates hsa-miR-432 expression in human cervical cancer cell line. *Biochem Biophys Res Commun* **453**, 461-466
101. Guan, Q., Lu, X., Zeng, H., Zhang, Y., and Zhu, J. (2013) Heat stress induction of miR398 triggers a regulatory loop that is critical for thermotolerance in Arabidopsis. *Plant J* **74**, 840-851
102. Wilmink, G. J., Roth, C. L., Ibey, B. L., Ketchum, N., Bernhard, J., Cerna, C. Z., and Roach, W. P. (2010) Identification of microRNAs associated with hyperthermia-induced cellular stress response. *Cell Stress Chaperones* **15**, 1027-1038
103. Ben-Zvi, A., Miller, E. A., and Morimoto, R. I. (2009) Collapse of proteostasis represents an early molecular event in Caenorhabditis elegans aging. *Proceedings of the National Academy of Sciences of the United States of America* **106**, 14914-14919
104. Labbadia, J., and Morimoto, R. I. (2015) Repression of the Heat Shock Response Is a Programmed Event at the Onset of Reproduction. *Mol Cell* **59**, 639-650
105. Singh, R., Kolvraa, S., Bross, P., Jensen, U. B., Gregersen, N., Tan, Q., Knudsen, C., and Rattan, S. I. (2006) Reduced heat shock response in human mononuclear cells during aging and its association with polymorphisms in HSP70 genes. *Cell Stress Chaperones* **11**, 208-215
106. Tower, J. (2011) Heat shock proteins and Drosophila aging. *Experimental gerontology* **46**, 355-362

107. Starnes, J. W., Choilawala, A. M., Taylor, R. P., Nelson, M. J., and Delp, M. D. (2005) Myocardial heat shock protein 70 expression in young and old rats after identical exercise programs. *The journals of gerontology. Series A, Biological sciences and medical sciences* **60**, 963-969
108. Heydari, A. R., Wu, B., Takahashi, R., Strong, R., and Richardson, A. (1993) Expression of heat shock protein 70 is altered by age and diet at the level of transcription. *Mol Cell Biol* **13**, 2909-2918
109. Liu, A. Y., Lee, Y. K., Manalo, D., and Huang, L. E. (1996) Attenuated heat shock transcriptional response in aging: molecular mechanism and implication in the biology of aging. *Exs* **77**, 393-408
110. Hsu, A. L., Murphy, C. T., and Kenyon, C. (2003) Regulation of aging and age-related disease by DAF-16 and heat-shock factor. *Science* **300**, 1142-1145
111. Morley, J. F., and Morimoto, R. I. (2004) Regulation of longevity in Caenorhabditis elegans by heat shock factor and molecular chaperones. *Molecular biology of the cell* **15**, 657-664
112. Soti, C., and Csermely, P. (2003) Aging and molecular chaperones. *Experimental gerontology* **38**, 1037-1040
113. Shamovsky, I., and Gershon, D. (2004) Novel regulatory factors of HSF-1 activation: facts and perspectives regarding their involvement in the age-associated attenuation of the heat shock response. *Mechanisms of ageing and development* **125**, 767-775
114. Neef, D. W., Jaeger, A. M., and Thiele, D. J. (2011) Heat shock transcription factor 1 as a therapeutic target in neurodegenerative diseases. *Nature reviews. Drug discovery* **10**, 930-944
115. Kakkar, V., Meister-Broekema, M., Minoia, M., Carra, S., and Kampinga, H. H. (2014) Barcoding heat shock proteins to human diseases: looking beyond the heat shock response. *Disease models & mechanisms* **7**, 421-434
116. Hightower, L. E. (1980) Cultured animal cells exposed to amino acid analogues or puromycin rapidly synthesize several polypeptides. *Journal of cellular physiology* **102**, 407-427
117. Lee, Y. J., and Dewey, W. C. (1987) Induction of heat shock proteins in Chinese hamster ovary cells and development of thermotolerance by intermediate concentrations of puromycin. *Journal of cellular physiology* **132**, 1-11
118. Jinn, T. L., Chiu, C. C., Song, W. W., Chen, Y. M., and Lin, C. Y. (2004) Azetidine-induced accumulation of class I small heat shock proteins in the soluble fraction provides thermotolerance in soybean seedlings. *Plant & cell physiology* **45**, 1759-1767
119. Van Rijn, J., Wiegant, F. A., Van den Berg, J., and Van Wijk, R. (2000) Heat shock response by cells treated with azetidine-2-carboxylic acid. *International journal of hyperthermia : the official journal of European Society for Hyperthermic Oncology, North American Hyperthermia Group* **16**, 305-318
120. Jones, K. A., and Findly, R. C. (1986) Induction of heat shock proteins by canavanine in Tetrahymena. No change in ATP levels measured in vivo by NMR. *J Biol Chem* **261**, 8703-8707
121. Winklhofer, K. F., Reintjes, A., Hoener, M. C., Voellmy, R., and Tatzelt, J. (2001) Geldanamycin restores a defective heat shock response in vivo. *J Biol Chem* **276**, 45160-45167
122. Sittler, A., Lurz, R., Lueder, G., Priller, J., Lehrach, H., Hayer-Hartl, M. K., Hartl, F. U., and Wanker, E. E. (2001) Geldanamycin activates a heat shock response and inhibits huntingtin aggregation in a cell culture model of Huntington's disease. *Human molecular genetics* **10**, 1307-1315
123. Kim, H. R., Kang, H. S., and Kim, H. D. (1999) Geldanamycin induces heat shock protein expression through activation of HSF1 in K562 erythroleukemic cells. *IUBMB life* **48**, 429-433

124. Griffin, T. M., Valdez, T. V., and Mestril, R. (2004) Radicicol activates heat shock protein expression and cardioprotection in neonatal rat cardiomyocytes. *American journal of physiology. Heart and circulatory physiology* **287**, H1081-1088
125. Brunquell, J., Bowers, P., and Westerheide, S. D. (2014) Fluorodeoxyuridine enhances the heat shock response and decreases polyglutamine aggregation in an HSF-1-dependent manner in Caenorhabditis elegans. *Mechanisms of ageing and development* **141-142**, 1-4
126. Kim, H. J., Joo, H. J., Kim, Y. H., Ahn, S., Chang, J., Hwang, K. B., Lee, D. H., and Lee, K. J. (2011) Systemic analysis of heat shock response induced by heat shock and a proteasome inhibitor MG132. *PloS one* **6**, e20252
127. West, J. D., Wang, Y., and Morano, K. A. (2012) Small molecule activators of the heat shock response: chemical properties, molecular targets, and therapeutic promise. *Chemical research in toxicology* **25**, 2036-2053
128. Riddle, D. L., Blumenthal, T., Meyer, B. J., and Priess, J. R. (1997) Introduction to C. elegans.
129. Harrington, A. J., Hamamichi, S., Caldwell, G. A., and Caldwell, K. A. (2010) C. elegans as a model organism to investigate molecular pathways involved with Parkinson's disease. *Dev Dyn* **239**, 1282-1295
130. Chen, F., Mackerell, A. D., Jr., Luo, Y., and Shapiro, P. (2008) Using Caenorhabditis elegans as a model organism for evaluating extracellular signal-regulated kinase docking domain inhibitors. *J Cell Commun Signal* **2**, 81-92
131. Hosono, R. (1978) Sterilization and growth inhibition of Caenorhabditis elegans by 5-fluorodeoxyuridine. *Experimental gerontology* **13**, 369-374
132. Mitchell, D. H., Stiles, J. W., Santelli, J., and Sanadi, D. R. (1979) Synchronous growth and aging of Caenorhabditis elegans in the presence of fluorodeoxyuridine. *J Gerontol* **34**, 28-36
133. Gandhi, S., Santelli, J., Mitchell, D. H., Stiles, J. W., and Sanadi, D. R. (1980) A simple method for maintaining large, aging populations of Caenorhabditis elegans. *Mechanisms of ageing and development* **12**, 137-150
134. Bijnsdorp, I. V., Comijn, E. M., Padron, J. M., Gmeiner, W. H., and Peters, G. J. (2007) Mechanisms of action of FdUMP[10]: metabolite activation and thymidylate synthase inhibition. *Oncol Rep* **18**, 287-291
135. Chiang, W. C., Ching, T. T., Lee, H. C., Mousigian, C., and Hsu, A. L. (2012) HSF-1 regulators DDL-1/2 link insulin-like signaling to heat-shock responses and modulation of longevity. *Cell* **148**, 322-334
136. Prahlad, V., Cornelius, T., and Morimoto, R. I. (2008) Regulation of the cellular heat shock response in Caenorhabditis elegans by thermosensory neurons. *Science* **320**, 811-814
137. van Oosten-Hawle, P., Porter, R. S., and Morimoto, R. I. (2013) Regulation of organismal proteostasis by transcellular chaperone signaling. *Cell* **153**, 1366-1378
138. Morton, E. A., and Lamitina, T. (2013) Caenorhabditis elegans HSF-1 is an essential nuclear protein that forms stress granule-like structures following heat shock. *Aging cell* **12**, 112-120
139. Van Raamsdonk, J. M., and Hekimi, S. (2011) FUdR causes a twofold increase in the lifespan of the mitochondrial mutant gas-1. *Mechanisms of ageing and development* **132**, 519-521
140. Davies, S. K., Leroi, A. M., and Bundy, J. G. (2012) Fluorodeoxyuridine affects the identification of metabolic responses to daf-2 status in Caenorhabditis elegans. *Mechanisms of ageing and development* **133**, 46-49
141. Aitlhadj, L., and Sturzenbaum, S. R. (2010) The use of FUdR can cause prolonged longevity in mutant nematodes. *Mechanisms of ageing and development* **131**, 364-365

142. Morley, J. F., Brignull, H. R., Weyers, J. J., and Morimoto, R. I. (2002) The threshold for polyglutamine-expansion protein aggregation and cellular toxicity is dynamic and influenced by aging in Caenorhabditis elegans. *Proc Natl Acad Sci U S A* **99**, 10417-10422
143. Angeli, S., Klang, I., Sivapatham, R., Mark, K., Zucker, D., Bhaumik, D., Lithgow, G. J., and Andersen, J. K. (2013) A DNA synthesis inhibitor is protective against proteotoxic stressors via modulation of fertility pathways in Caenorhabditis elegans. *Aging (Albany NY)* **5**, 759-769
144. Feldman, N., Kosolapov, L., and Ben-Zvi, A. (2014) Fluorodeoxyuridine Improves Caenorhabditis elegans Proteostasis Independent of Reproduction Onset. *PloS one* **9**, e85964
145. Hajdu-Cronin, Y. M., Chen, W. J., and Sternberg, P. W. (2004) The L-type cyclin CYL-1 and the heat-shock-factor HSF-1 are required for heat-shock-induced protein expression in Caenorhabditis elegans. *Genetics* **168**, 1937-1949
146. Kamath, R. S., Fraser, A. G., Dong, Y., Poulin, G., Durbin, R., Gotta, M., Kanapin, A., Le Bot, N., Moreno, S., Sohrmann, M., Welchman, D. P., Zipperlen, P., and Ahringer, J. (2003) Systematic functional analysis of the Caenorhabditis elegans genome using RNAi. *Nature* **421**, 231-237
147. Cunha, R. A., and Agostinho, P. M. (2010) Chronic caffeine consumption prevents memory disturbance in different animal models of memory decline. *Journal of Alzheimer's disease : JAD* **20 Suppl 1**, S95-116
148. Eskelinen, M. H., and Kivipelto, M. (2010) Caffeine as a protective factor in dementia and Alzheimer's disease. *Journal of Alzheimer's disease : JAD* **20 Suppl 1**, S167-174
149. Ascherio, A., Zhang, S. M., Hernan, M. A., Kawachi, I., Colditz, G. A., Speizer, F. E., and Willett, W. C. (2001) Prospective study of caffeine consumption and risk of Parkinson's disease in men and women. *Annals of neurology* **50**, 56-63
150. Hameleers, P. A., Van Boxtel, M. P., Hogervorst, E., Riedel, W. J., Houx, P. J., Buntinx, F., and Jolles, J. (2000) Habitual caffeine consumption and its relation to memory, attention, planning capacity and psychomotor performance across multiple age groups. *Human psychopharmacology* **15**, 573-581
151. Paganini-Hill, A., Kawas, C. H., and Corrada, M. M. (2007) Non-alcoholic beverage and caffeine consumption and mortality: the Leisure World Cohort Study. *Preventive medicine* **44**, 305-310
152. Santos, C., Lunet, N., Azevedo, A., de Mendonca, A., Ritchie, K., and Barros, H. (2010) Caffeine intake is associated with a lower risk of cognitive decline: a cohort study from Portugal. *Journal of Alzheimer's disease : JAD* **20 Suppl 1**, S175-185
153. Lublin, A., Isoda, F., Patel, H., Yen, K., Nguyen, L., Hajje, D., Schwartz, M., and Mobbs, C. (2011) FDA-approved drugs that protect mammalian neurons from glucose toxicity slow aging dependent on cbp and protect against proteotoxicity. *PloS one* **6**, e27762
154. Sutphin, G. L., Bishop, E., Yanos, M. E., Moller, R. M., and Kaeberlein, M. (2012) Caffeine extends life span, improves healthspan, and delays age-associated pathology in Caenorhabditis elegans. *Longevity & healthspan* **1**, 9
155. Bridi, J. C., Barros, A. G., Sampaio, L. R., Ferreira, J. C., Antunes Soares, F. A., and Romano-Silva, M. A. (2015) Lifespan Extension Induced by Caffeine in Caenorhabditis elegans is Partially Dependent on Adenosine Signaling. *Frontiers in aging neuroscience* **7**, 220
156. Dostal, V., Roberts, C. M., and Link, C. D. (2010) Genetic mechanisms of coffee extract protection in a Caenorhabditis elegans model of beta-amyloid peptide toxicity. *Genetics* **186**, 857-866
157. Gidalevitz, T., Prahlad, V., and Morimoto, R. I. (2011) The stress of protein misfolding: from single cells to multicellular organisms. *Cold Spring Harb Perspect Biol* **3**

158. Frydman, J. (2001) Folding of newly translated proteins in vivo: the role of molecular chaperones. *Annual review of biochemistry* **70**, 603-647
159. Hartl, F. U., Bracher, A., and Hayer-Hartl, M. (2011) Molecular chaperones in protein folding and proteostasis. *Nature* **475**, 324-332
160. Satyal, S. H., Schmidt, E., Kitagawa, K., Sondheimer, N., Lindquist, S., Kramer, J. M., and Morimoto, R. I. (2000) Polyglutamine aggregates alter protein folding homeostasis in Caenorhabditis elegans. *Proc Natl Acad Sci U S A* **97**, 5750-5755
161. Muchowski, P. J. (2002) Protein misfolding, amyloid formation, and neurodegeneration: a critical role for molecular chaperones? *Neuron* **35**, 9-12
162. Muchowski, P. J., and Wacker, J. L. (2005) Modulation of neurodegeneration by molecular chaperones. *Nature reviews. Neuroscience* **6**, 11-22
163. Westerheide, S. D., and Morimoto, R. I. (2005) Heat shock response modulators as therapeutic tools for diseases of protein conformation. *J Biol Chem* **280**, 33097-33100
164. Lee, B. S., Chen, J., Angelidis, C., Jurivich, D. A., and Morimoto, R. I. (1995) Pharmacological modulation of heat shock factor 1 by antiinflammatory drugs results in protection against stress-induced cellular damage. *Proc Natl Acad Sci U S A* **92**, 7207-7211
165. Westerheide, S. D., Bosman, J. D., Mbadugha, B. N., Kawahara, T. L., Matsumoto, G., Kim, S., Gu, W., Devlin, J. P., Silverman, R. B., and Morimoto, R. I. (2004) Celastrols as inducers of the heat shock response and cytoprotection. *J Biol Chem* **279**, 56053-56060
166. Jurivich, D. A., Sistonen, L., Sarge, K. D., and Morimoto, R. I. (1994) Arachidonate is a potent modulator of human heat shock gene transcription. *Proc Natl Acad Sci U S A* **91**, 2280-2284
167. Torok, Z., Tsvetkova, N. M., Balogh, G., Horvath, I., Nagy, E., Penzes, Z., Hargitai, J., Bensaude, O., Csermely, P., Crowe, J. H., Maresca, B., and Vigh, L. (2003) Heat shock protein coinducers with no effect on protein denaturation specifically modulate the membrane lipid phase. *Proc Natl Acad Sci U S A* **100**, 3131-3136
168. Coburn, C., and Gems, D. (2013) The mysterious case of the C. elegans gut granule: death fluorescence, anthranilic acid and the kynurenine pathway. *Frontiers in genetics* **4**, 151
169. Oba, S., Nagata, C., Nakamura, K., Fujii, K., Kawachi, T., Takatsuka, N., and Shimizu, H. (2010) Consumption of coffee, green tea, oolong tea, black tea, chocolate snacks and the caffeine content in relation to risk of diabetes in Japanese men and women. *The British journal of nutrition* **103**, 453-459
170. Fredholm, B. B., Battig, K., Holmen, J., Nehlig, A., and Zvartau, E. E. (1999) Actions of caffeine in the brain with special reference to factors that contribute to its widespread use. *Pharmacological reviews* **51**, 83-133
171. Farah, A., and Donangelo, C. M. (2006) Phenolic compounds in coffee. *Brazilian Journal of Plant Physiology* **18**, 23-36
172. Houessou, J. K., Benac, C., Delteil, C., and Camel, V. (2005) Determination of polycyclic aromatic hydrocarbons in coffee brew using solid-phase extraction. *Journal of agricultural and food chemistry* **53**, 871-879
173. Moeenfard, M., Erny, G. L., and Alves, A. (2016) Variability of some diterpene esters in coffee beverages as influenced by brewing procedures. *Journal of food science and technology* **53**, 3916-3927
174. Trinh, K., Andrews, L., Krause, J., Hanak, T., Lee, D., Gelb, M., and Pallanck, L. (2010) Decaffeinated coffee and nicotine-free tobacco provide neuroprotection in Drosophila models of Parkinson's disease through an NRF2-dependent mechanism. *The Journal of neuroscience : the official journal of the Society for Neuroscience* **30**, 5525-5532
175. Higgins, L. G., Cavin, C., Itoh, K., Yamamoto, M., and Hayes, J. D. (2008) Induction of cancer chemopreventive enzymes by coffee is mediated by transcription factor Nrf2.

Evidence that the coffee-specific diterpenes cafestol and kahweol confer protection against acrolein. *Toxicology and applied pharmacology* **226**, 328-337
176. Elmenhorst, D., Meyer, P. T., Matusch, A., Winz, O. H., and Bauer, A. (2012) Caffeine occupancy of human cerebral A1 adenosine receptors: in vivo quantification with 18F-CPFPX and PET. *Journal of nuclear medicine : official publication, Society of Nuclear Medicine* **53**, 1723-1729
177. Nehlig, A., Daval, J. L., and Debry, G. (1992) Caffeine and the central nervous system: mechanisms of action, biochemical, metabolic and psychostimulant effects. *Brain research. Brain research reviews* **17**, 139-170
178. Shi, D., Nikodijevic, O., Jacobson, K. A., and Daly, J. W. (1993) Chronic caffeine alters the density of adenosine, adrenergic, cholinergic, GABA, and serotonin receptors and calcium channels in mouse brain. *Cellular and molecular neurobiology* **13**, 247-261
179. Tatum, M. C., Ooi, F. K., Chikka, M. R., Chauve, L., Martinez-Velazquez, L. A., Steinbusch, H. W., Morimoto, R. I., and Prahlad, V. (2015) Neuronal serotonin release triggers the heat shock response in C. elegans in the absence of temperature increase. *Curr Biol* **25**, 163-174
180. van Oosten-Hawle, P., and Morimoto, R. I. (2014) Transcellular chaperone signaling: an organismal strategy for integrated cell stress responses. *The Journal of experimental biology* **217**, 129-136
181. Ashrafi, K., Chang, F. Y., Watts, J. L., Fraser, A. G., Kamath, R. S., Ahringer, J., and Ruvkun, G. (2003) Genome-wide RNAi analysis of Caenorhabditis elegans fat regulatory genes. *Nature* **421**, 268-272
182. Schroeder, L. K., Kremer, S., Kramer, M. J., Currie, E., Kwan, E., Watts, J. L., Lawrenson, A. L., and Hermann, G. J. (2007) Function of the Caenorhabditis elegans ABC transporter PGP-2 in the biogenesis of a lysosome-related fat storage organelle. *Molecular biology of the cell* **18**, 995-1008
183. Roh, H. C., Collier, S., Guthrie, J., Robertson, J. D., and Kornfeld, K. (2012) Lysosome-related organelles in intestinal cells are a zinc storage site in C. elegans. *Cell metabolism* **15**, 88-99
184. Chen, X., Barclay, J. W., Burgoyne, R. D., and Morgan, A. (2015) Using C. elegans to discover therapeutic compounds for ageing-associated neurodegenerative diseases. *Chemistry Central journal* **9**, 65
185. Calamini, B., and Morimoto, R. I. (2012) Protein homeostasis as a therapeutic target for diseases of protein conformation. *Current topics in medicinal chemistry* **12**, 2623-2640
186. Balch, W. E., Morimoto, R. I., Dillin, A., and Kelly, J. W. (2008) Adapting proteostasis for disease intervention. *Science* **319**, 916-919
187. Neef, D. W., Turski, M. L., and Thiele, D. J. (2010) Modulation of heat shock transcription factor 1 as a therapeutic target for small molecule intervention in neurodegenerative disease. *PLoS Biol* **8**, e1000291
188. McCall, A. L., Millington, W. R., and Wurtman, R. J. (1982) Blood-brain barrier transport of caffeine: dose-related restriction of adenine transport. *Life sciences* **31**, 2709-2715
189. Bookout, A. L., and Mangelsdorf, D. J. (2003) Quantitative real-time PCR protocol for analysis of nuclear receptor signaling pathways. *Nucl Recept Signal* **1**, e012
190. Schneider, C. A., Rasband, W. S., and Eliceiri, K. W. (2012) NIH Image to ImageJ: 25 years of image analysis. *Nature methods* **9**, 671-675
191. Zack, G. W., Rogers, W. E., and Latt, S. A. (1977) Automatic measurement of sister chromatid exchange frequency. *The journal of histochemistry and cytochemistry : official journal of the Histochemistry Society* **25**, 741-753
192. Zhao, W., Kruse, J. P., Tang, Y., Jung, S. Y., Qin, J., and Gu, W. (2008) Negative regulation of the deacetylase SIRT1 by DBC1. *Nature* **451**, 587-590

193. Li, Z., Chen, L., Kabra, N., Wang, C., Fang, J., and Chen, J. (2009) Inhibition of SUV39H1 methyltransferase activity by DBC1. *J Biol Chem* **284**, 10361-10366
194. Chini, C. C., Escande, C., Nin, V., and Chini, E. N. (2010) HDAC3 is negatively regulated by the nuclear protein DBC1. *J Biol Chem* **285**, 40830-40837
195. Sundararajan, R., Chen, G., Mukherjee, C., and White, E. (2005) Caspase-dependent processing activates the proapoptotic activity of deleted in breast cancer-1 during tumor necrosis factor-alpha-mediated death signaling. *Oncogene* **24**, 4908-4920
196. Anantharaman, V., and Aravind, L. (2008) Analysis of DBC1 and its homologs suggests a potential mechanism for regulation of sirtuin domain deacetylases by NAD metabolites. *Cell cycle* **7**, 1467-1472
197. Park, S. H., Riley, P. t., and Frisch, S. M. (2013) Regulation of anoikis by deleted in breast cancer-1 (DBC1) through NF-kappaB. *Apoptosis* **18**, 949-962
198. Rishi, A. K., Zhang, L., Boyanapalli, M., Wali, A., Mohammad, R. M., Yu, Y., Fontana, J. A., Hatfield, J. S., Dawson, M. I., Majumdar, A. P., and Reichert, U. (2003) Identification and characterization of a cell cycle and apoptosis regulatory protein-1 as a novel mediator of apoptosis signaling by retinoid CD437. *J Biol Chem* **278**, 33422-33435
199. Kim, J. H., Yang, C. K., Heo, K., Roeder, R. G., An, W., and Stallcup, M. R. (2008) CCAR1, a key regulator of mediator complex recruitment to nuclear receptor transcription complexes. *Mol Cell* **31**, 510-519
200. Yu, E. J., Kim, S. H., Heo, K., Ou, C. Y., Stallcup, M. R., and Kim, J. H. (2011) Reciprocal roles of DBC1 and SIRT1 in regulating estrogen receptor alpha activity and co-activator synergy. *Nucleic acids research* **39**, 6932-6943
201. Marchler-Bauer, A., Lu, S., Anderson, J. B., Chitsaz, F., Derbyshire, M. K., DeWeese-Scott, C., Fong, J. H., Geer, L. Y., Geer, R. C., Gonzales, N. R., Gwadz, M., Hurwitz, D. I., Jackson, J. D., Ke, Z., Lanczycki, C. J., Lu, F., Marchler, G. H., Mullokandov, M., Omelchenko, M. V., Robertson, C. L., Song, J. S., Thanki, N., Yamashita, R. A., Zhang, D., Zhang, N., Zheng, C., and Bryant, S. H. (2011) CDD: a Conserved Domain Database for the functional annotation of proteins. *Nucleic acids research* **39**, D225-229
202. Bycroft, M., Hubbard, T. J., Proctor, M., Freund, S. M., and Murzin, A. G. (1997) The solution structure of the S1 RNA binding domain: a member of an ancient nucleic acid-binding fold. *Cell* **88**, 235-242
203. Hubbard, B. P., Loh, C., Gomes, A. P., Li, J., Lu, Q., Doyle, T. L., Disch, J. S., Armour, S. M., Ellis, J. L., Vlasuk, G. P., and Sinclair, D. A. (2013) Carboxamide SIRT1 inhibitors block DBC1 binding via an acetylation-independent mechanism. *Cell Cycle* **12**
204. Alber, T. (1992) Structure of the leucine zipper. *Curr Opin Genet Dev* **2**, 205-210
205. Nin, V., Escande, C., Chini, C. C., Giri, S., Camacho-Pereira, J., Matalonga, J., Lou, Z., and Chini, E. N. (2012) Role of Deleted in Breast Cancer 1 (DBC1) Protein in SIRT1 Deacetylase Activation Induced by Protein Kinase A and AMP-activated Protein Kinase. *J Biol Chem* **287**, 23489-23501
206. Aravind, L., and Koonin, E. V. (2000) SAP - a putative DNA-binding motif involved in chromosomal organization. *Trends Biochem Sci* **25**, 112-114
207. Neukirch, S., Goriely, A., and Hausrath, A. C. (2008) Chirality of coiled coils: elasticity matters. *Phys Rev Lett* **100**, 038105
208. Chini, C. C., Escande, C., Nin, V., and Chini, E. N. (2013) DBC1 (Deleted in Breast Cancer 1) modulates the stability and function of the nuclear receptor Rev-erbalpha. *Biochem J* **451**, 453-461
209. Waterhouse, R. M., Tegenfeldt, F., Li, J., Zdobnov, E. M., and Kriventseva, E. V. (2013) OrthoDB: a hierarchical catalog of animal, fungal and bacterial orthologs. *Nucleic acids research* **41**, D358-365
210. Oates, M. E., Romero, P., Ishida, T., Ghalwash, M., Mizianty, M. J., Xue, B., Dosztanyi, Z., Uversky, V. N., Obradovic, Z., Kurgan, L., Dunker, A. K., and Gough, J. (2013)

D(2)P(2): database of disordered protein predictions. *Nucleic acids research* **41**, D508-516
211. Chen, J. W., Romero, P., Uversky, V. N., and Dunker, A. K. (2006) Conservation of intrinsic disorder in protein domains and families: II. functions of conserved disorder. *Journal of proteome research* **5**, 888-898
212. Daughdrill, G. W., Narayanaswami, P., Gilmore, S. H., Belczyk, A., and Brown, C. J. (2007) Dynamic behavior of an intrinsically unstructured linker domain is conserved in the face of negligible amino acid sequence conservation. *J Mol Evol* **65**, 277-288
213. Brown, C. J., Johnson, A. K., and Daughdrill, G. W. (2010) Comparing models of evolution for ordered and disordered proteins. *Molecular biology and evolution* **27**, 609-621
214. Wrabl, J. O., Gu, J., Liu, T., Schrank, T. P., Whitten, S. T., and Hilser, V. J. (2011) The role of protein conformational fluctuations in allostery, function, and evolution. *Biophys Chem* **159**, 129-141
215. Brown, C. J., Johnson, A. K., Dunker, A. K., and Daughdrill, G. W. (2011) Evolution and disorder. *Curr Opin Struct Biol* **21**, 441-446
216. Jeong, C. S., and Kim, D. (2012) Coevolved residues and the functional association for intrinsically disordered proteins. *Pac Symp Biocomput*, 140-151
217. Chemes, L. B., Glavina, J., Alonso, L. G., Marino-Buslje, C., de Prat-Gay, G., and Sanchez, I. E. (2012) Sequence evolution of the intrinsically disordered and globular domains of a model viral oncoprotein. *PloS one* **7**, e47661
218. Mahani, A., Henriksson, J., and Wright, A. P. (2013) Origins of Myc proteins--using intrinsic protein disorder to trace distant relatives. *PloS one* **8**, e75057
219. Borcherds, W., Kashtanov, S., Wu, H., and Daughdrill, G. W. (2013) Structural divergence is more extensive than sequence divergence for a family of intrinsically disordered proteins. *Proteins* **81**, 1686-1698
220. Peng, Z., Oldfield, C. J., Xue, B., Mizianty, M. J., Dunker, A. K., Kurgan, L., and Uversky, V. N. (2014) A creature with a hundred waggly tails: intrinsically disordered proteins in the ribosome. *Cellular and molecular life sciences : CMLS* **71**, 1477-1504
221. Dunker, A. K., Lawson, J. D., Brown, C. J., Williams, R. M., Romero, P., Oh, J. S., Oldfield, C. J., Campen, A. M., Ratliff, C. M., Hipps, K. W., Ausio, J., Nissen, M. S., Reeves, R., Kang, C., Kissinger, C. R., Bailey, R. W., Griswold, M. D., Chiu, W., Garner, E. C., and Obradovic, Z. (2001) Intrinsically disordered protein. *J Mol Graph Model* **19**, 26-59
222. Iakoucheva, L. M., Brown, C. J., Lawson, J. D., Obradovic, Z., and Dunker, A. K. (2002) Intrinsic disorder in cell-signaling and cancer-associated proteins. *Journal of molecular biology* **323**, 573-584
223. Uversky, V. N., Oldfield, C. J., and Dunker, A. K. (2005) Showing your ID: intrinsic disorder as an ID for recognition, regulation and cell signaling. *J Mol Recognit* **18**, 343-384
224. Xue, B., Oldfield, C. J., Van, Y. Y., Dunker, A. K., and Uversky, V. N. (2012) Protein intrinsic disorder and induced pluripotent stem cells. *Mol Biosyst* **8**, 134-150
225. Sun, X., Xue, B., Jones, W. T., Rikkerink, E., Dunker, A. K., and Uversky, V. N. (2011) A functionally required unfoldome from the plant kingdom: intrinsically disordered N-terminal domains of GRAS proteins are involved in molecular recognition during plant development. *Plant Mol Biol* **77**, 205-223
226. Wood, M., Rae, G. M., Wu, R. M., Walton, E. F., Xue, B., Hellens, R. P., and Uversky, V. N. (2013) Actinidia DRM1--an intrinsically disordered protein whose mRNA expression is inversely correlated with spring budbreak in kiwifruit. *PloS one* **8**, e57354
227. Hegyi, H., and Gerstein, M. (2001) Annotation transfer for genomics: measuring functional divergence in multi-domain proteins. *Genome research* **11**, 1632-1640
228. Hsu, W. L., Oldfield, C., Meng, J., Huang, F., Xue, B., Uversky, V. N., Romero, P., and Dunker, A. K. (2012) Intrinsic protein disorder and protein-protein interactions. *Pac Symp Biocomput*, 116-127

229. Ispolatov, I., Yuryev, A., Mazo, I., and Maslov, S. (2005) Binding properties and evolution of homodimers in protein-protein interaction networks. *Nucleic acids research* **33**, 3629-3635
230. Altschul, S. F., Gish, W., Miller, W., Myers, E. W., and Lipman, D. J. (1990) Basic local alignment search tool. *Journal of molecular biology* **215**, 403-410
231. Camacho, C., Coulouris, G., Avagyan, V., Ma, N., Papadopoulos, J., Bealer, K., and Madden, T. L. (2009) BLAST+: architecture and applications. *BMC Bioinformatics* **10**, 421
232. Magrane, M., and Consortium, U. (2011) UniProt Knowledgebase: a hub of integrated protein data. *Database (Oxford)* **2011**, bar009
233. Xue, B., Brown, C. J., Dunker, A. K., and Uversky, V. N. (2013) Intrinsically disordered regions of p53 family are highly diversified in evolution. *Biochimica et biophysica acta* **1834**, 725-738
234. Xue, B., Dunbrack, R. L., Williams, R. W., Dunker, A. K., and Uversky, V. N. (2010) PONDR-FIT: a meta-predictor of intrinsically disordered amino acids. *Biochimica et biophysica acta* **1804**, 996-1010
235. Romero, P., Obradovic, Z., Li, X., Garner, E. C., Brown, C. J., and Dunker, A. K. (2001) Sequence complexity of disordered protein. *Proteins* **42**, 38-48
236. Schlessinger, A., Punta, M., Yachdav, G., Kajan, L., and Rost, B. (2009) Improved disorder prediction by combination of orthogonal approaches. *PloS one* **4**, e4433
237. Ishida, T., and Kinoshita, K. (2008) Prediction of disordered regions in proteins based on the meta approach. *Bioinformatics* **24**, 1344-1348
238. Deng, X., Eickholt, J., and Cheng, J. (2009) PreDisorder: ab initio sequence-based prediction of protein disordered regions. *BMC Bioinformatics* **10**, 436
239. Xue, B., Oldfield, C. J., Dunker, A. K., and Uversky, V. N. (2009) CDF it all: consensus prediction of intrinsically disordered proteins based on various cumulative distribution functions. *FEBS letters* **583**, 1469-1474
240. Mizianty, M. J., Stach, W., Chen, K., Kedarisetti, K. D., Disfani, F. M., and Kurgan, L. (2010) Improved sequence-based prediction of disordered regions with multilayer fusion of multiple information sources. *Bioinformatics* **26**, i489-496
241. Kozlowski, L. P., and Bujnicki, J. M. (2012) MetaDisorder: a meta-server for the prediction of intrinsic disorder in proteins. *BMC Bioinformatics* **13**, 111
242. Vucetic, S., Brown, C. J., Dunker, A. K., and Obradovic, Z. (2003) Flavors of protein disorder. *Proteins* **52**, 573-584
243. Peng, K., Radivojac, P., Vucetic, S., Dunker, A. K., and Obradovic, Z. (2006) Length-dependent prediction of protein intrinsic disorder. *BMC Bioinformatics* **7**, 208
244. Obradovic, Z., Peng, K., Vucetic, S., Radivojac, P., Brown, C. J., and Dunker, A. K. (2003) Predicting intrinsic disorder from amino acid sequence. *Proteins* **53 Suppl 6**, 566-572
245. Peng, K., Vucetic, S., Radivojac, P., Brown, C. J., Dunker, A. K., and Obradovic, Z. (2005) Optimizing long intrinsic disorder predictors with protein evolutionary information. *J Bioinform Comput Biol* **3**, 35-60
246. Prilusky, J., Felder, C. E., Zeev-Ben-Mordehai, T., Rydberg, E. H., Man, O., Beckmann, J. S., Silman, I., and Sussman, J. L. (2005) FoldIndex: a simple tool to predict whether a given protein sequence is intrinsically unfolded. *Bioinformatics* **21**, 3435-3438
247. Dosztanyi, Z., Csizmok, V., Tompa, P., and Simon, I. (2005) IUPred: web server for the prediction of intrinsically unstructured regions of proteins based on estimated energy content. *Bioinformatics* **21**, 3433-3434
248. Campen, A., Williams, R. M., Brown, C. J., Meng, J., Uversky, V. N., and Dunker, A. K. (2008) TOP-IDP-scale: a new amino acid scale measuring propensity for intrinsic disorder. *Protein Pept Lett* **15**, 956-963
249. He, B., Wang, K., Liu, Y., Xue, B., Uversky, V. N., and Dunker, A. K. (2009) Predicting intrinsic disorder in proteins: an overview. *Cell Res* **19**, 929-949

250. Cheng, Y., Oldfield, C. J., Meng, J., Romero, P., Uversky, V. N., and Dunker, A. K. (2007) Mining alpha-helix-forming molecular recognition features with cross species sequence alignments. *Biochemistry* **46**, 13468-13477
251. Mohan, A., Oldfield, C. J., Radivojac, P., Vacic, V., Cortese, M. S., Dunker, A. K., and Uversky, V. N. (2006) Analysis of molecular recognition features (MoRFs). *Journal of molecular biology* **362**, 1043-1059
252. Oldfield, C. J., Cheng, Y., Cortese, M. S., Romero, P., Uversky, V. N., and Dunker, A. K. (2005) Coupled folding and binding with alpha-helix-forming molecular recognition elements. *Biochemistry* **44**, 12454-12470
253. Hsu, W. L., Oldfield, C. J., Xue, B., Meng, J., Huang, F., Romero, P., Uversky, V. N., and Dunker, A. K. (2013) Exploring the binding diversity of intrinsically disordered proteins involved in one-to-many binding. *Protein science : a publication of the Protein Society* **22**, 258-273
254. Gypas, F., Tsaousis, G. N., and Hamodrakas, S. J. (2013) mpMoRFsDB: a database of molecular recognition features in membrane proteins. *Bioinformatics* **29**, 2517-2518
255. Kotta-Loizou, I., Tsaousis, G. N., and Hamodrakas, S. J. (2013) Analysis of Molecular Recognition Features (MoRFs) in membrane proteins. *Biochimica et biophysica acta* **1834**, 798-807
256. Malaney, P., Pathak, R. R., Xue, B., Uversky, V. N., and Dave, V. (2013) Intrinsic Disorder in PTEN and its Interactome Confers Structural Plasticity and Functional Versatility. *Sci Rep* **3**, 2035
257. Xue, B., Dunker, A. K., and Uversky, V. N. (2010) Retro-MoRFs: Identifying Protein Binding Sites by Normal and Reverse Alignment and Intrinsic Disorder Prediction. *Int J Mol Sci* **11**, 3725-3747
258. Coelho Ribeiro Mde, L., Espinosa, J., Islam, S., Martinez, O., Thanki, J. J., Mazariegos, S., Nguyen, T., Larina, M., Xue, B., and Uversky, V. N. (2013) Malleable ribonucleoprotein machine: protein intrinsic disorder in the Saccharomyces cerevisiae spliceosome. *PeerJ* **1**, e2
259. Xue, B., Dunker, A. K., and Uversky, V. N. (2012) Orderly order in protein intrinsic disorder distribution: disorder in 3500 proteomes from viruses and the three domains of life. *J Biomol Struct Dyn* **30**, 137-149
260. Oldfield, C. J., Cheng, Y., Cortese, M. S., Brown, C. J., Uversky, V. N., and Dunker, A. K. (2005) Comparing and combining predictors of mostly disordered proteins. *Biochemistry* **44**, 1989-2000
261. Uversky, V. N., Gillespie, J. R., and Fink, A. L. (2000) Why are "natively unfolded" proteins unstructured under physiologic conditions? *Proteins* **41**, 415-427
262. Dunker, A. K., Obradovic, Z., Romero, P., Garner, E. C., and Brown, C. J. (2000) Intrinsic protein disorder in complete genomes. *Genome Inform Ser Workshop Genome Inform* **11**, 161-171
263. Soding, J., Biegert, A., and Lupas, A. N. (2005) The HHpred interactive server for protein homology detection and structure prediction. *Nucleic acids research* **33**, W244-248
264. Kallberg, M., Wang, H. P., Wang, S., Peng, J., Wang, Z. Y., Lu, H., and Xu, J. B. (2012) Template-based protein structure modeling using the RaptorX web server. *Nat Protoc* **7**, 1511-1522
265. Roy, A., Kucukural, A., and Zhang, Y. (2010) I-TASSER: a unified platform for automated protein structure and function prediction. *Nat Protoc* **5**, 725-738
266. Benkert, P., Tosatto, S. C., and Schomburg, D. (2008) QMEAN: A comprehensive scoring function for model quality assessment. *Proteins* **71**, 261-277
267. Tamura, K., Peterson, D., Peterson, N., Stecher, G., Nei, M., and Kumar, S. (2011) MEGA5: molecular evolutionary genetics analysis using maximum likelihood, evolutionary

distance, and maximum parsimony methods. *Molecular biology and evolution* **28**, 2731-2739
268. Rogozin, I. B., Makarova, K. S., Wolf, Y. I., and Koonin, E. V. (2004) Computational approaches for the analysis of gene neighbourhoods in prokaryotic genomes. *Brief Bioinform* **5**, 131-149
269. De, S., Teichmann, S. A., and Babu, M. M. (2009) The impact of genomic neighborhood on the evolution of human and chimpanzee transcriptome. *Genome research* **19**, 785-794
270. Poyatos, J. F., and Hurst, L. D. (2007) The determinants of gene order conservation in yeasts. *Genome biology* **8**, R233
271. Engstrom, P. G., Ho Sui, S. J., Drivenes, O., Becker, T. S., and Lenhard, B. (2007) Genomic regulatory blocks underlie extensive microsynteny conservation in insects. *Genome research* **17**, 1898-1908
272. Dawson, D. A., Akesson, M., Burke, T., Pemberton, J. M., Slate, J., and Hansson, B. (2007) Gene order and recombination rate in homologous chromosome regions of the chicken and a passerine bird. *Molecular biology and evolution* **24**, 1537-1552
273. Becker, J., and Craig, E. A. (1994) Heat-shock proteins as molecular chaperones. *Eur J Biochem* **219**, 11-23
274. Hendrick, J. P., and Hartl, F. U. (1993) Molecular chaperone functions of heat-shock proteins. *Annu Rev Biochem* **62**, 349-384
275. Hartl, F. U. (1996) Molecular chaperones in cellular protein folding. *Nature* **381**, 571-579
276. Jolly, C., and Morimoto, R. I. (2000) Role of the heat shock response and molecular chaperones in oncogenesis and cell death. *J Natl Cancer Inst* **92**, 1564-1572
277. Ebrahimi-Fakhari, D., Saidi, L. J., and Wahlster, L. (2013) Molecular chaperones and protein folding as therapeutic targets in Parkinson's disease and other synucleinopathies. *Acta neuropathologica communications* **1**, 79
278. Liu, D. J., Hammer, D., Komlos, D., Chen, K. Y., Firestein, B. L., and Liu, A. Y. (2014) SIRT1 knockdown promotes neural differentiation and attenuates the heat shock response. *Journal of cellular physiology* **229**, 1224-1235
279. Raychaudhuri, S., Loew, C., Korner, R., Pinkert, S., Theis, M., Hayer-Hartl, M., Buchholz, F., and Hartl, F. U. (2014) Interplay of acetyltransferase EP300 and the proteasome system in regulating heat shock transcription factor 1. *Cell* **156**, 975-985
280. Raynes, R., Brunquell, J., and Westerheide, S. D. (2013) Stress Inducibility of SIRT1 and Its Role in Cytoprotection and Cancer. *Genes & cancer* **4**, 172-182
281. Bonkowski, M. S., and Sinclair, D. A. (2016) Slowing ageing by design: the rise of NAD+ and sirtuin-activating compounds. *Nature reviews. Molecular cell biology* **17**, 679-690
282. Tomita, T., Hamazaki, J., Hirayama, S., McBurney, M. W., Yashiroda, H., and Murata, S. (2015) Sirt1-deficiency causes defective protein quality control. *Scientific reports* **5**, 12613
283. Viswanathan, M., and Guarente, L. (2011) Regulation of Caenorhabditis elegans lifespan by sir-2.1 transgenes. *Nature* **477**, E1-2
284. Mouchiroud, L., Houtkooper, R. H., Moullan, N., Katsyuba, E., Ryu, D., Canto, C., Mottis, A., Jo, Y. S., Viswanathan, M., Schoonjans, K., Guarente, L., and Auwerx, J. (2013) The NAD(+)/Sirtuin Pathway Modulates Longevity through Activation of Mitochondrial UPR and FOXO Signaling. *Cell* **154**, 430-441
285. Schmeisser, K., Mansfeld, J., Kuhlow, D., Weimer, S., Priebe, S., Heiland, I., Birringer, M., Groth, M., Segref, A., Kanfi, Y., Price, N. L., Schmeisser, S., Schuster, S., Pfeiffer, A. F., Guthke, R., Platzer, M., Hoppe, T., Cohen, H. Y., Zarse, K., Sinclair, D. A., and Ristow, M. (2013) Role of sirtuins in lifespan regulation is linked to methylation of nicotinamide. *Nature chemical biology* **9**, 693-700
286. Cascella, R., Evangelisti, E., Zampagni, M., Becatti, M., D'Adamio, G., Goti, A., Liguri, G., Fiorillo, C., and Cecchi, C. (2014) S-linolenoyl glutathione intake extends life-span and

stress resistance via Sir-2.1 upregulation in Caenorhabditis elegans. *Free radical biology & medicine* **73**, 127-135
287. Gertz, M., Fischer, F., Nguyen, G. T., Lakshminarasimhan, M., Schutkowski, M., Weyand, M., and Steegborn, C. (2013) Ex-527 inhibits Sirtuins by exploiting their unique NAD+-dependent deacetylation mechanism. *Proceedings of the National Academy of Sciences of the United States of America* **110**, E2772-2781
288. Qin, B., Minter-Dykhouse, K., Yu, J., Zhang, J., Liu, T., Zhang, H., Lee, S., Kim, J., Wang, L., and Lou, Z. (2015) DBC1 functions as a tumor suppressor by regulating p53 stability. *Cell reports* **10**, 1324-1334
289. Yoo, A. S., Bais, C., and Greenwald, I. (2004) Crosstalk between the EGFR and LIN-12/Notch pathways in C. elegans vulval development. *Science* **303**, 663-666
290. Viswanathan, M., Kim, S. K., Berdichevsky, A., and Guarente, L. (2005) A role for SIR-2.1 regulation of ER stress response genes in determining C. elegans life span. *Developmental cell* **9**, 605-615
291. Barstead, R. J., and Moerman, D. G. (2006) C. elegans deletion mutant screening. *Methods in molecular biology* **351**, 51-58
292. Mukhopadhyay, A., Deplancke, B., Walhout, A. J., and Tissenbaum, H. A. (2008) Chromatin immunoprecipitation (ChIP) coupled to detection by quantitative real-time PCR to study transcription factor binding to DNA in Caenorhabditis elegans. *Nature protocols* **3**, 698-709
293. Anckar, J., and Sistonen, L. (2007) Heat shock factor 1 as a coordinator of stress and developmental pathways. *Adv Exp Med Biol* **594**, 78-88
294. Parsell, D. A., and Lindquist, S. (1993) The function of heat-shock proteins in stress tolerance: degradation and reactivation of damaged proteins. *Annu Rev Genet* **27**, 437-496
295. Young, J. C., Agashe, V. R., Siegers, K., and Hartl, F. U. (2004) Pathways of chaperone-mediated protein folding in the cytosol. *Nat Rev Mol Cell Biol* **5**, 781-791
296. Garigan, D., Hsu, A. L., Fraser, A. G., Kamath, R. S., Ahringer, J., and Kenyon, C. (2002) Genetic analysis of tissue aging in Caenorhabditis elegans: a role for heat-shock factor and bacterial proliferation. *Genetics* **161**, 1101-1112
297. Walker, G. A., Thompson, F. J., Brawley, A., Scanlon, T., and Devaney, E. (2003) Heat shock factor functions at the convergence of the stress response and developmental pathways in Caenorhabditis elegans. *FASEB J* **17**, 1960-1962
298. Minsky, N., and Roeder, R. G. (2015) Direct link between metabolic regulation and the heat-shock response through the transcriptional regulator PGC-1alpha. *Proc Natl Acad Sci U S A* **112**, E5669-5678
299. Peng, Z. Y., Serkova, N. J., Kominsky, D. J., Brown, J. L., and Wischmeyer, P. E. (2006) Glutamine-mediated attenuation of cellular metabolic dysfunction and cell death after injury is dependent on heat shock factor-1 expression. *JPEN. Journal of parenteral and enteral nutrition* **30**, 373-378; discussion 379
300. Prahlad, V., Cornelius, T., and Morimoto, R. I. (2008) Regulation of the cellular heat shock response in Caenorhabditis elegans by thermosensory neurons. *Science* **sas320**, 811-814
301. Consortium, C. e. S. (1998) Genome sequence of the nematode C. elegans: a platform for investigating biology. *Science* **282**, 2012-2018
302. Kaletta, T., and Hengartner, M. O. (2006) Finding function in novel targets: C. elegans as a model organism. *Nature reviews. Drug discovery* **5**, 387-398
303. Labbadia, J., and Morimoto, R. I. (2015) Repression of the Heat Shock Response Is a Programmed Event at the Onset of Reproduction. *Molecular Cell*

304. Klass, M. R. (1977) Aging in the nematode Caenorhabditis elegans: major biological and environmental factors influencing life span. *Mechanisms of ageing and development* **6**, 413-429
305. Hendriks, G. J., Gaidatzis, D., Aeschimann, F., and Grosshans, H. (2014) Extensive oscillatory gene expression during C. elegans larval development. *Mol Cell* **53**, 380-392
306. Andersen, E. C., Lu, X., and Horvitz, H. R. (2006) C. elegans ISWI and NURF301 antagonize an Rb-like pathway in the determination of multiple cell fates. *Development* **133**, 2695-2704
307. Van Gilst, M. R., Hadjivassiliou, H., Jolly, A., and Yamamoto, K. R. (2005) Nuclear hormone receptor NHR-49 controls fat consumption and fatty acid composition in C. elegans. *PLoS Biol* **3**, e53
308. Pinkston-Gosse, J., and Kenyon, C. (2007) DAF-16/FOXO targets genes that regulate tumor growth in Caenorhabditis elegans. *Nature genetics* **39**, 1403-1409
309. Moribe, H., Yochem, J., Yamada, H., Tabuse, Y., Fujimoto, T., and Mekada, E. (2004) Tetraspanin protein (TSP-15) is required for epidermal integrity in Caenorhabditis elegans. *Journal of cell science* **117**, 5209-5220
310. Turner, A. J., Isaac, R. E., and Coates, D. (2001) The neprilysin (NEP) family of zinc metalloendopeptidases: genomics and function. *BioEssays : news and reviews in molecular, cellular and developmental biology* **23**, 261-269
311. Ghosh, R., Andersen, E. C., Shapiro, J. A., Gerke, J. P., and Kruglyak, L. (2012) Natural variation in a chloride channel subunit confers avermectin resistance in C. elegans. *Science* **335**, 574-578
312. Han, L., Wang, Y., Sangaletti, R., D'Urso, G., Lu, Y., Shaham, S., and Bianchi, L. (2013) Two novel DEG/ENaC channel subunits expressed in glia are needed for nose-touch sensitivity in Caenorhabditis elegans. *The Journal of neuroscience : the official journal of the Society for Neuroscience* **33**, 936-949
313. Spieth, J., Denison, K., Kirtland, S., Cane, J., and Blumenthal, T. (1985) The C. elegans vitellogenin genes: short sequence repeats in the promoter regions and homology to the vertebrate genes. *Nucleic Acids Res* **13**, 5283-5295
314. Murphy, C. T., McCarroll, S. A., Bargmann, C. I., Fraser, A., Kamath, R. S., Ahringer, J., Li, H., and Kenyon, C. (2003) Genes that act downstream of DAF-16 to influence the lifespan of Caenorhabditis elegans. *Nature* **424**, 277-283
315. Van Gilst, M. R., Hadjivassiliou, H., and Yamamoto, K. R. (2005) A Caenorhabditis elegans nutrient response system partially dependent on nuclear receptor NHR-49. *Proc Natl Acad Sci U S A* **102**, 13496-13501
316. Balamurugan, K., Ashokkumar, B., Moussaif, M., Sze, J. Y., and Said, H. M. (2007) Cloning and functional characterization of a folate transporter from the nematode Caenorhabditis elegans. *American journal of physiology. Cell physiology* **293**, C670-681
317. Watts, J. L., and Browse, J. (2000) A palmitoyl-CoA-specific delta9 fatty acid desaturase from Caenorhabditis elegans. *Biochem Biophys Res Commun* **272**, 263-269
318. Shen, Y., Zhang, J., Calarco, J. A., and Zhang, Y. (2014) EOL-1, the homolog of the mammalian Dom3Z, regulates olfactory learning in C. elegans. *The Journal of neuroscience : the official journal of the Society for Neuroscience* **34**, 13364-13370
319. Johnstone, I. L. (2000) Cuticle collagen genes. Expression in Caenorhabditis elegans. *Trends Genet* **16**, 21-27
320. Di Lullo, G. A., Sweeney, S. M., Korkko, J., Ala-Kokko, L., and San Antonio, J. D. (2002) Mapping the ligand-binding sites and disease-associated mutations on the most abundant protein in the human, type I collagen. *J Biol Chem* **277**, 4223-4231
321. Fu, H. L., Valiathan, R. R., Arkwright, R., Sohail, A., Mihai, C., Kumarasiri, M., Mahasenan, K. V., Mobashery, S., Huang, P., Agarwal, G., and Fridman, R. (2013) Discoidin domain

receptors: unique receptor tyrosine kinases in collagen-mediated signaling. *J Biol Chem* **288**, 7430-7437
322. Munger, J. S., and Sheppard, D. (2011) Cross talk among TGF-beta signaling pathways, integrins, and the extracellular matrix. *Cold Spring Harb Perspect Biol* **3**, a005017
323. Seeger-Nukpezah, T., and Golemis, E. A. (2012) The extracellular matrix and ciliary signaling. *Current opinion in cell biology* **24**, 652-661
324. Ewald, C. Y., Landis, J. N., Abate, J. P., Murphy, C. T., and Blackwell, T. K. (2014) Dauer-independent insulin/IGF-1-signalling implicates collagen remodelling in longevity. *Nature*
325. Seo, K., Choi, E., Lee, D., Jeong, D. E., Jang, S. K., and Lee, S. J. (2013) Heat shock factor 1 mediates the longevity conferred by inhibition of TOR and insulin/IGF-1 signaling pathways in C. elegans. *Aging Cell* **12**, 1073-1081
326. Steinkraus, K. A., Smith, E. D., Davis, C., Carr, D., Pendergrass, W. R., Sutphin, G. L., Kennedy, B. K., and Kaeberlein, M. (2008) Dietary restriction suppresses proteotoxicity and enhances longevity by an hsf-1-dependent mechanism in Caenorhabditis elegans. *Aging Cell* **7**, 394-404
327. Akerfelt, M., Morimoto, R. I., and Sistonen, L. (2010) Heat shock factors: integrators of cell stress, development and lifespan. *Nat Rev Mol Cell Biol* **11**, 545-555
328. Barna, J., Princz, A., Kosztelnik, M., Hargitai, B., Takacs-Vellai, K., and Vellai, T. (2012) Heat shock factor-1 intertwines insulin/IGF-1, TGF-beta and cGMP signaling to control development and aging. *BMC developmental biology* **12**, 32
329. Raynes, R., Leckey, B. D., Jr., Nguyen, K., and Westerheide, S. D. (2012) Heat Shock and Caloric Restriction have a Synergistic Effect on the Heat Shock Response in a sir2.1-dependent Manner in Caenorhabditis elegans. *The Journal of biological chemistry*, 287(234):29045-29053
330. Taubert, S., Ward, J. D., and Yamamoto, K. R. (2011) Nuclear hormone receptors in nematodes: evolution and function. *Molecular and cellular endocrinology* **334**, 49-55
331. Weber, K. P., Alvaro, C. G., Baer, G. M., Reinert, K., Cheng, G., Clever, S., and Wightman, B. (2012) Analysis of C. elegans NR2E nuclear receptors defines three conserved clades and ligand-independent functions. *BMC Evol Biol* **12**, 81
332. Aroian, R. V., Koga, M., Mendel, J. E., Ohshima, Y., and Sternberg, P. W. (1990) The let-23 gene necessary for Caenorhabditis elegans vulval induction encodes a tyrosine kinase of the EGF receptor subfamily. *Nature* **348**, 693-699
333. Yu, S., and Driscoll, M. (2011) EGF signaling comes of age: promotion of healthy aging in C. elegans. *Experimental gerontology* **46**, 129-134
334. O'Callaghan-Sunol, C., and Sherman, M. Y. (2006) Heat shock transcription factor (HSF1) plays a critical role in cell migration via maintaining MAP kinase signaling. *Cell cycle* **5**, 1431-1437
335. Anckar, J., and Sistonen, L. (2011) Regulation of HSF1 function in the heat stress response: implications in aging and disease. *Annual review of biochemistry* **80**, 1089-1115
336. Budovskaya, Y. V., Wu, K., Southworth, L. K., Jiang, M., Tedesco, P., Johnson, T. E., and Kim, S. K. (2008) An elt-3/elt-5/elt-6 GATA transcription circuit guides aging in C. elegans. *Cell* **134**, 291-303
337. Myllyharju, J., and Kivirikko, K. I. (2004) Collagens, modifying enzymes and their mutations in humans, flies and worms. *Trends Genet* **20**, 33-43
338. Toyama, B. H., and Hetzer, M. W. (2013) Protein homeostasis: live long, won't prosper. *Nat Rev Mol Cell Biol* **14**, 55-61
339. Hamlin, C. R., and Kohn, R. R. (1971) Evidence for progressive, age-related structural changes in post-mature human collagen. *Biochim Biophys Acta* **236**, 458-467
340. Hamlin, C. R., and Kohn, R. R. (1972) Determination of human chronological age by study of a collagen sample. *Experimental gerontology* **7**, 377-379

341. Vafaie, F., Yin, H., O'Neil, C., Nong, Z., Watson, A., Arpino, J. M., Chu, M. W., Wayne Holdsworth, D., Gros, R., and Pickering, J. G. (2014) Collagenase-resistant collagen promotes mouse aging and vascular cell senescence. *Aging Cell* **13**, 121-130
342. Shin, H., Lee, H., Fejes, A. P., Baillie, D. L., Koo, H. S., and Jones, S. J. (2011) Gene expression profiling of oxidative stress response of C. elegans aging defective AMPK mutants using massively parallel transcriptome sequencing. *BMC Res Notes* **4**, 34
343. Baird, N. A., Douglas, P. M., Simic, M. S., Grant, A. R., Moresco, J. J., Wolff, S. C., Yates, J. R., 3rd, Manning, G., and Dillin, A. (2014) HSF-1-mediated cytoskeletal integrity determines thermotolerance and life span. *Science* **346**, 360-363
344. Link, C. D., Cypser, J. R., Johnson, C. J., and Johnson, T. E. (1999) Direct observation of stress response in Caenorhabditis elegans using a reporter transgene. *Cell Stress Chaperones* **4**, 235-242
345. Brenner, S. (1974) The genetics of Caenorhabditis elegans. *Genetics* **77**, 71-94
346. Stiernagle, T. (2006) Maintenance of C. elegans. *WormBook : the online review of C. elegans biology*, 1-11
347. Hirsh, D., Oppenheim, D., and Klass, M. (1976) Development of the reproductive system of Caenorhabditis elegans. *Dev Biol* **49**, 200-219
348. Andrews, S. (2010) FastQC: a quality control tool for high throughput sequence data.
349. Langmead, B. (2010) Aligning short sequencing reads with Bowtie. *Current protocols in bioinformatics / editoral board, Andreas D. Baxevanis ... [et al.]* **Chapter 11**, Unit 11 17
350. Trapnell, C., Pachter, L., and Salzberg, S. L. (2009) TopHat: discovering splice junctions with RNA-Seq. *Bioinformatics* **25**, 1105-1111
351. Trapnell, C., Williams, B. A., Pertea, G., Mortazavi, A., Kwan, G., van Baren, M. J., Salzberg, S. L., Wold, B. J., and Pachter, L. (2010) Transcript assembly and quantification by RNA-Seq reveals unannotated transcripts and isoform switching during cell differentiation. *Nature biotechnology* **28**, 511-515
352. Trapnell, C., Roberts, A., Goff, L., Pertea, G., Kim, D., Kelley, D. R., Pimentel, H., Salzberg, S. L., Rinn, J. L., and Pachter, L. (2012) Differential gene and transcript expression analysis of RNA-seq experiments with TopHat and Cufflinks. *Nat Protoc* **7**, 562-578
353. Oliveros, J. C. ((2007-2015)) An interactive tool for comparing lists with Venn's diagrams. in *Venny*
354. de Hoon, M. J., Imoto, S., Nolan, J., and Miyano, S. (2004) Open source clustering software. *Bioinformatics* **20**, 1453-1454
355. Dennis, G., Jr., Sherman, B. T., Hosack, D. A., Yang, J., Gao, W., Lane, H. C., and Lempicki, R. A. (2003) DAVID: Database for Annotation, Visualization, and Integrated Discovery. *Genome Biol* **4**, P3
356. Gao, J., Ade, A. S., Tarcea, V. G., Weymouth, T. E., Mirel, B. R., Jagadish, H. V., and States, D. J. (2009) Integrating and annotating the interactome using the MiMI plugin for cytoscape. *Bioinformatics* **25**, 137-138
357. Brunquell, J., Morris, S., Lu, Y., Cheng, F., and Westerheide, S. D. (2016) The genome-wide role of HSF-1 in the regulation of gene expression in Caenorhabditis elegans. *BMC genomics* **17**, 559
358. Friedlander, M. R., Lizano, E., Houben, A. J., Bezdan, D., Banez-Coronel, M., Kudla, G., Mateu-Huertas, E., Kagerbauer, B., Gonzalez, J., Chen, K. C., LeProust, E. M., Marti, E., and Estivill, X. (2014) Evidence for the biogenesis of more than 1,000 novel human microRNAs. *Genome Biol* **15**, R57
359. Alvarez-Garcia, I., and Miska, E. A. (2005) MicroRNA functions in animal development and human disease. *Development* **132**, 4653-4662
360. de Lencastre, A., Pincus, Z., Zhou, K., Kato, M., Lee, S. S., and Slack, F. J. (2010) MicroRNAs both promote and antagonize longevity in C. elegans. *Curr Biol* **20**, 2159-2168

361. Lucanic, M., Graham, J., Scott, G., Bhaumik, D., Benz, C. C., Hubbard, A., Lithgow, G. J., and Melov, S. (2013) Age-related micro-RNA abundance in individual C. elegans. *Aging (Albany NY)* **5**, 394-411
362. Nehammer, C., Podolska, A., Mackowiak, S. D., Kagias, K., and Pocock, R. (2015) Specific microRNAs regulate heat stress responses in Caenorhabditis elegans. *Sci Rep* **5**, 8866
363. Lee, R. C., Feinbaum, R. L., and Ambros, V. (1993) The C. elegans heterochronic gene lin-4 encodes small RNAs with antisense complementarity to lin-14. *Cell* **75**, 843-854
364. Liu, N., Landreh, M., Cao, K., Abe, M., Hendriks, G. J., Kennerdell, J. R., Zhu, Y., Wang, L. S., and Bonini, N. M. (2012) The microRNA miR-34 modulates ageing and neurodegeneration in Drosophila. *Nature* **482**, 519-523
365. Hammell, M., Long, D., Zhang, L., Lee, A., Carmack, C. S., Han, M., Ding, Y., and Ambros, V. (2008) mirWIP: microRNA target prediction based on microRNA-containing ribonucleoprotein-enriched transcripts. *Nature methods* **5**, 813-819
366. Smith-Vikos, T., de Lencastre, A., Inukai, S., Shlomchik, M., Holtrup, B., and Slack, F. J. (2014) MicroRNAs mediate dietary-restriction-induced longevity through PHA-4/FOXA and SKN-1/Nrf transcription factors. *Curr Biol* **24**, 2238-2246
367. Li, M., Jones-Rhoades, M. W., Lau, N. C., Bartel, D. P., and Rougvie, A. E. (2005) Regulatory mutations of mir-48, a C. elegans let-7 family MicroRNA, cause developmental timing defects. *Developmental cell* **9**, 415-422
368. Abbott, A. L., Alvarez-Saavedra, E., Miska, E. A., Lau, N. C., Bartel, D. P., Horvitz, H. R., and Ambros, V. (2005) The let-7 MicroRNA family members mir-48, mir-84, and mir-241 function together to regulate developmental timing in Caenorhabditis elegans. *Developmental cell* **9**, 403-414
369. Miska, E. A., Alvarez-Saavedra, E., Abbott, A. L., Lau, N. C., Hellman, A. B., McGonagle, S. M., Bartel, D. P., Ambros, V. R., and Horvitz, H. R. (2007) Most Caenorhabditis elegans microRNAs are individually not essential for development or viability. *PLoS genetics* **3**, e215
370. Ahmed, R., Chang, Z., Younis, A. E., Langnick, C., Li, N., Chen, W., Brattig, N., and Dieterich, C. (2013) Conserved miRNAs are candidate post-transcriptional regulators of developmental arrest in free-living and parasitic nematodes. *Genome biology and evolution* **5**, 1246-1260
371. Goh, G. Y., Martelli, K. L., Parhar, K. S., Kwong, A. W., Wong, M. A., Mah, A., Hou, N. S., and Taubert, S. (2014) The conserved Mediator subunit MDT-15 is required for oxidative stress responses in Caenorhabditis elegans. *Aging Cell* **13**, 70-79
372. Adachi, M., Liu, Y., Fujii, K., Calderwood, S. K., Nakai, A., Imai, K., and Shinomura, Y. (2009) Oxidative stress impairs the heat stress response and delays unfolded protein recovery. *PloS one* **4**, e7719
373. Spiro, Z., Arslan, M. A., Somogyvari, M., Nguyen, M. T., Smolders, A., Dancso, B., Nemeth, N., Elek, Z., Braeckman, B. P., Csermely, P., and Soti, C. (2012) RNA interference links oxidative stress to the inhibition of heat stress adaptation. *Antioxidants & redox signaling* **17**, 890-901
374. Crombie, T. A., Tang, L., Choe, K. P., and Julian, D. (2016) Inhibition of the oxidative stress response by heat stress in Caenorhabditis elegans. *The Journal of experimental biology*
375. Ferguson, A. A., Springer, M. G., and Fisher, A. L. (2010) skn-1-Dependent and -independent regulation of aip-1 expression following metabolic stress in Caenorhabditis elegans. *Mol Cell Biol* **30**, 2651-2667
376. Stanhill, A., Haynes, C. M., Zhang, Y., Min, G., Steele, M. C., Kalinina, J., Martinez, E., Pickart, C. M., Kong, X. P., and Ron, D. (2006) An arsenite-inducible 19S regulatory particle-associated protein adapts proteasomes to proteotoxicity. *Mol Cell* **23**, 875-885

377. Volovik, Y., Moll, L., Marques, F. C., Maman, M., Bejerano-Sagie, M., and Cohen, E. (2014) Differential regulation of the heat shock factor 1 and DAF-16 by neuronal nhl-1 in the nematode C. elegans. *Cell reports* **9**, 2192-2205
378. Dai, S., Tang, Z., Cao, J., Zhou, W., Li, H., Sampson, S., and Dai, C. (2015) Suppression of the HSF1-mediated proteotoxic stress response by the metabolic stress sensor AMPK. *The EMBO journal* **34**, 275-293
379. Douglas, P. M., Baird, N. A., Simic, M. S., Uhlein, S., McCormick, M. A., Wolff, S. C., Kennedy, B. K., and Dillin, A. (2015) Heterotypic Signals from Neural HSF-1 Separate Thermotolerance from Longevity. *Cell reports* **12**, 1196-1204
380. Ewald, C. Y., Landis, J. N., Porter Abate, J., Murphy, C. T., and Blackwell, T. K. (2015) Dauer-independent insulin/IGF-1-signalling implicates collagen remodelling in longevity. *Nature* **519**, 97-101
381. Friedlander, M. R., Chen, W., Adamidi, C., Maaskola, J., Einspanier, R., Knespel, S., and Rajewsky, N. (2008) Discovering microRNAs from deep sequencing data using miRDeep. *Nature biotechnology* **26**, 407-415
382. Langmead, B., and Salzberg, S. L. (2012) Fast gapped-read alignment with Bowtie 2. *Nature methods* **9**, 357-359
383. Jan, C. H., Friedman, R. C., Ruby, J. G., and Bartel, D. P. (2011) Formation, regulation and evolution of Caenorhabditis elegans 3'UTRs. *Nature* **469**, 97-101
384. Cline, M. S., Smoot, M., Cerami, E., Kuchinsky, A., Landys, N., Workman, C., Christmas, R., Avila-Campilo, I., Creech, M., Gross, B., Hanspers, K., Isserlin, R., Kelley, R., Killcoyne, S., Lotia, S., Maere, S., Morris, J., Ono, K., Pavlovic, V., Pico, A. R., Vailaya, A., Wang, P. L., Adler, A., Conklin, B. R., Hood, L., Kuiper, M., Sander, C., Schmulevich, I., Schwikowski, B., Warner, G. J., Ideker, T., and Bader, G. D. (2007) Integration of biological networks and gene expression data using Cytoscape. *Nat Protoc* **2**, 2366-2382
385. Huang da, W., Sherman, B. T., and Lempicki, R. A. (2009) Systematic and integrative analysis of large gene lists using DAVID bioinformatics resources. *Nat Protoc* **4**, 44-57
386. Kennedy, B. K., Berger, S. L., Brunet, A., Campisi, J., Cuervo, A. M., Epel, E. S., Franceschi, C., Lithgow, G. J., Morimoto, R. I., Pessin, J. E., Rando, T. A., Richardson, A., Schadt, E. E., Wyss-Coray, T., and Sierra, F. (2014) Geroscience: linking aging to chronic disease. *Cell* **159**, 709-713
387. Calderwood, S. K., Murshid, A., and Prince, T. (2009) The shock of aging: molecular chaperones and the heat shock response in longevity and aging--a mini-review. *Gerontology* **55**, 550-558
388. Arslan, M. A., Csermely, P., and Soti, C. (2006) Protein homeostasis and molecular chaperones in aging. *Biogerontology* **7**, 383-389
389. Soti, C., and Csermely, P. (2000) Molecular chaperones and the aging process. *Biogerontology* **1**, 225-233
390. Li, Y. S., Xiao, W. F., and Luo, W. (2016) Cellular aging towards osteoarthritis. *Mechanisms of ageing and development*
391. Heljasvaara, R., Aikio, M., Ruotsalainen, H., and Pihlajaniemi, T. (2016) Collagen XVIII in tissue homeostasis and dysregulation - Lessons learned from model organisms and human patients. *Matrix biology : journal of the International Society for Matrix Biology*
392. Purushotham, A., Schug, T. T., and Li, X. (2009) SIRT1 performs a balancing act on the tight-rope toward longevity. *Aging (Albany NY)* **1**, 669-673
393. Imai, S. (2007) Is Sirt1 a miracle bullet for longevity? *Aging Cell* **6**, 735-737

APPENDIX A: SUPPORTING FIGURES FOR CHAPTER 2. FLUORODEOXYURIDINE ENHANCES THE HEAT SHOCK RESPONSE AND DECREASES POLYGLUTAMINE AGGREGATION IN AN HSF-1-DEPENDENT MANNER IN *CAENORHABDITIS ELEGANS*

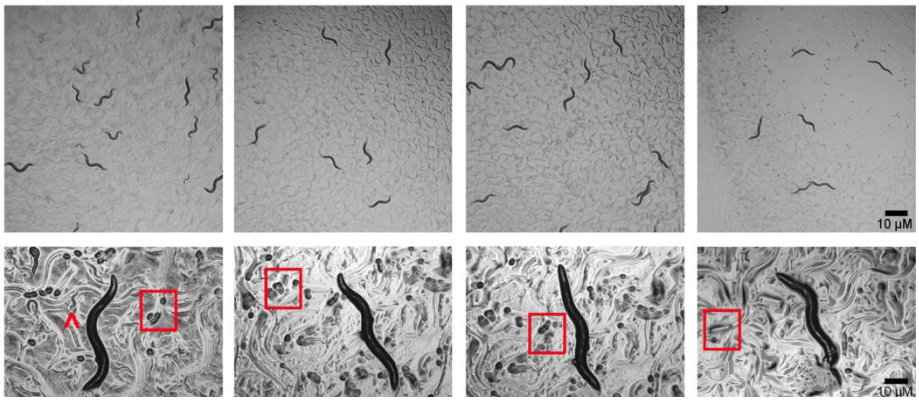

FUdR (µM)	-	25	100	200
Stage Administered	-	L1	L4/YA	L4/YA

Figure A1. Treatment with 25 µM of FUdR from L1 to day 3 does not affect worm growth while still inhibiting egg hatching similarly to 100 µM or 200 µM of FUdR from the L4 stage to day 3 of adulthood. Images are representative of day 3 nematodes given 25 µM of FUdR at the L1 stage until day 3 of adulthood, or 100 µM or 200 µM of FUdR given at the L4 stage until day 3 of adulthood. Nematodes that were not grown in the presence of FUdR were picked to new plates daily. The box outline contains eggs that have not hatched, while the ^ points to a larval nematode.

APPENDIX B: SUPPORTING FIGURES AND TABLES FOR CHAPTER 3. COFFEE EXTRACT AND CAFFEINE ENHANCE THE HEAT SHOCK RESPONSE AND PROMOTE PROTEOSTASIS IN AN HSF-1-DEPENDENT MANNER IN *CAENORHABDITIS ELEGANS*

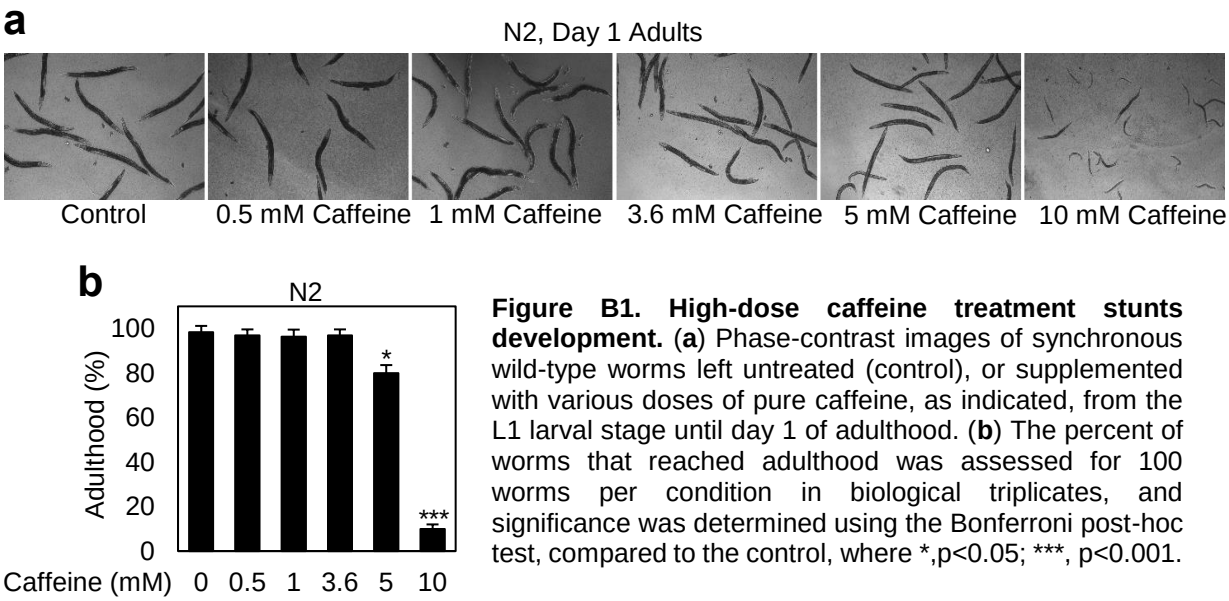

Figure B1. High-dose caffeine treatment stunts development. (**a**) Phase-contrast images of synchronous wild-type worms left untreated (control), or supplemented with various doses of pure caffeine, as indicated, from the L1 larval stage until day 1 of adulthood. (**b**) The percent of worms that reached adulthood was assessed for 100 worms per condition in biological triplicates, and significance was determined using the Bonferroni post-hoc test, compared to the control, where *,$p<0.05$; ***, $p<0.001$.

APPENDIX C: SUPPORTING FIGURES AND TABLES FOR CHAPTER 4. DBC1/CCAR2 AND CCAR1 HAVE EVOLVED FROM ONE COMMON ANCESTOR

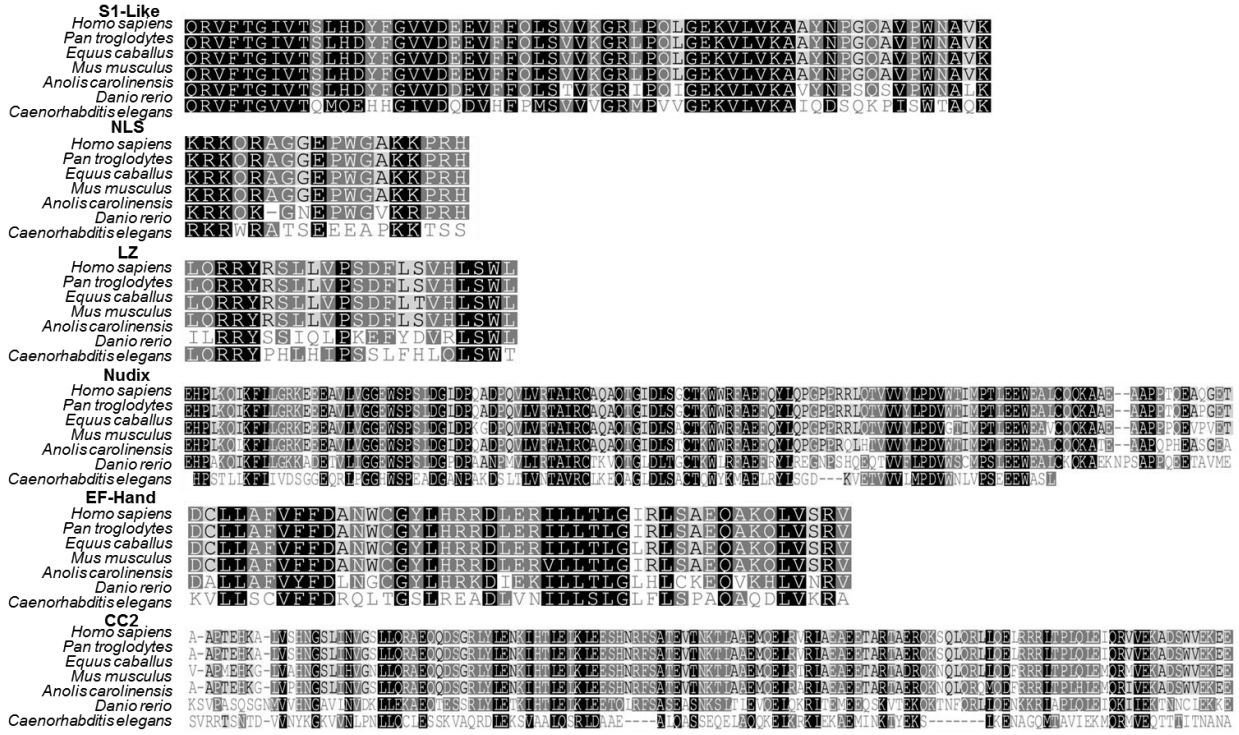

Figure C1. Sequence alignment of CCAR2 domains from various species.

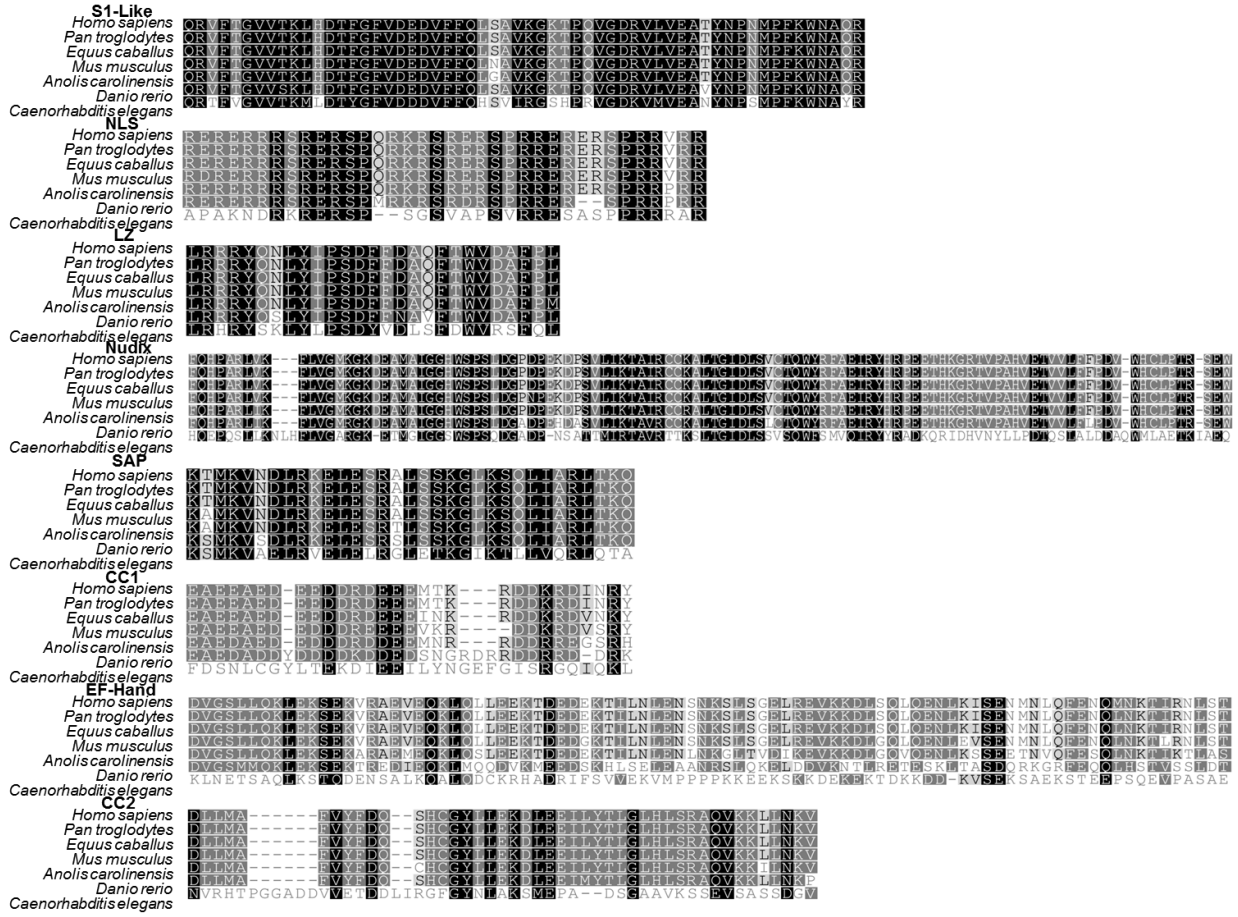

Figure C2. Sequence alignment of CCAR1 domains from various species.

```
hDBC1  481   NAETPEATTQQETDTDLPEAPPPPLEPAVIARPGCVNLSLHGIVEDRRPKER-ISFEVMV
hCCAR1 721   -----------YILPDEPAIIVHPNWAAKSGKFDCSIMSLSVLLDYRLEDNKEHSFEVSL
                        .* *     *  .*  .: .*  :**  ::: *  .::  **** :
hDBC1        LAELFLEMLQRDFGYRVYKMLLSLPEKVVSPPEPEKEEAAKEEATKEEEAIKEEVVKEPK
hCCAR1       FAELFNEMLQRDFGVRIYKSLLSLPEKED---KKEKDKKSKKDERKDKKEERDDETDEPK
             :**** ******** *:** *******     : **:: :*::  *:::  ::: ..***
hDBC1        DEAQNEGPATESEAPLKEDGLLPKPLSSGGEEEEKPRGEASEDLCEMALDPELLLLRDDG
hCCAR1       PKRRKSGDDKDKKEDRDERKKEDKRKDDSKDDDETEEDNNQDEYDPMEAEEAEDEEDDRD
              : ::.*  .:.:   .*     *  ... :::*. ..: .::   *  :       * .
hDBC1        EEEFAGAKLEDSEVRSVASNQSEMEFSSLQDMPKELDPSAVLPLDCLLAFVFFDANWCGY
hCCAR1       EEEMTKRDDKRDINRYCKERPS-------KDKEKEKTQMITINRDLLMAFVYFDQSHCGY
             ***::  . : .  *   .. *       :*  **     .:  * *:***:** . ***
hDBC1        LHRRDLERILLTLGIRLSAEQAKQLVSRVVTQNICQYRSLQYSRQEGLDGGLP---EEVL
hCCAR1       LLEKDLEEILYTLGLHLSRAQVKKLLNKVVLRESCFYRKLTDTSKDEENHEESESLQEDM
             * .:***.** ***::**  *.*:*:.:** :: * **.*  : ::  :   .   :* :
hDBC1        FGNLDLLPPPGKSTKPGAAPTEHKALVSHNGSLINVGSLLQRAEQQDSGRLYLENKIHTL
hCCAR1       LGNRLLLPTP-TVKQESKDVEENVGLIVYNGAMVDVGSLLQKLEKSEKVRAEVEQKLQLL
             :**  ***.* . .: .    *: .*: :**::::******: *:.:. *  :*:*:: *
hDBC1        ELKLEESHNRFSATEVTNKTLAAEMQELRVRLAEAEETARTAERQKSQLQRLLQELRRRL
hCCAR1       EEKTDEDEKTILNLENSNKSLSGELREVKKDLSQLQENLKISENMNLQFENQMNKTIRNL
             * * :*..: :   * :**:*:.*::*::  *:: :*. : :*. : *::. :::  *.*
hDBC1        TPLQLEIQRVVEKADSWVEKEEPAPSN-----      923
hCCAR1       STVMDEIHTVLKKDNVKNEDKDQKSKENGASV     1150
             :.:  **: *::* :   *.::  ..:
```

Figure C3. Alignment of the C-terminal domain between human DBC1 (hDBC1, CCAR2) and human CCAR1 (hCCAR1).

Figure C4. Sequence alignment between zebrafish CCAR1 (Uniprot ID: F1QV66) and *C. elegans* CCAR1 (Uniprot ID: G5EFJ2).

Figure C5. Sequence alignment between zebrafish CCAR1 (Uniprot ID: F1QV66) and zebrafish CCAR2 (Uniprot ID: E9QH28).

Table C1. All CCAR2, CCAR1, and LST-3 sequences used in this study and their Uniprot IDs.

Species	CCAR2	CCAR1	LST-3
Homo sapiens **(Human)**	Q8N163	Q8IX12	—
Pongo abelii **(Orangutan)**	Q5R8S0	H2NAQ9	—
Pan troglodytes **(Chimpanzee)**	H2QVV3	H2Q1Z8	—
Macaca mulatta **(Rhesus Monkey)**	F6RJW4	F6TNW6	—
Nomascus leucogenys **(Gibbon)**	G1S0U2	G1RM48	—
Gorilla gorilla gorilla **(Lowland Gorilla)**	G3QJ10	G3QJY0	—
Rattus norvegicus **(Rat)**	D3ZG47	F1LM55	—
Mus musculus **(Mouse)**	Q8VDP4	Q8CH18	—
Pteropus alecto **(Black flying fox)**	L5L6J0	L5KGF7	—
Spermophilus tridecemlineatus **(Ground squirrel)**	I3MHS6	I3LYS6	—
Mustela putorius furo **(European domestic ferret)**	M3XWK6	M3XZT2	—
Cavia porcellus **(Guinea pig)**	H0VI64	H0V2G0	—
Otolemur garnettii **(Garnett's greater bushbaby)**	H0X308	H0X8T3	—
Sarcophilus harrisii **(Tasmanian devil)**	G3X2S1	G3VZQ7	—
Myotis lucifugus **(Little brown bat)**	G1P531	G1NV87	—
Felis catus **(Cat)**	M3W4H2	M3WHD5	—
Canis familiaris **(Dog)**	E2RKJ1	E2QS34	—
Ailuropoda melanoleuca **(Giant panda)**	G1L8L0	G1MI35	—
Loxodonta africana **(African elephant)**	G3TKV2	G3SXP2	—
Bos taurus **(Bovine)**	E1B9H3	Q17R04	—
Bos mutus **(Wild yak)**	L8INM1	L8HXX6	—
Equus caballus **(Horse)**	F6VJ81	F6XN96	—
Oryctolagus cuniculus **(Rabbit)**	G1T501	G1T536	—
Anolis carolinensis **(Green anole)**	H9GUP4	H9GFZ8	—
Pelodiscus sinensis **(Chinese softshell turtle)**	K7GJ39	K7FC21	—
Takifugu rubripes **(Japanese pufferfish)**	H2UA38	H2UA36	—
Latimeria chalumnae **(West Indian ocean coelacanth)**	H3ATA1	H3B750	—
Danio rerio **(Zebrafish)**	E7FGT1	F1QV66	—
Sus scrofa **(Pig)**	F1RMA3	—	—
Macaca fascicularis **(Crab-eating macaque)**	G7PCV6	—	—

Table C1. (Continued)

***Cricetulus griseus* (Chinese hamster)**	G3GUY5	—	—
***Callithrix jacchus* (White-tufted-ear marmoset)**	—	F7I8T1	—
***Tupaia chinensis* (Chinese tree shrew)**	—	L9JR90	—
***Monodelphis domestica* (Gray short-tailed opossum)**	—	F6VYZ1	—
***Myotis davidii* (David's myotis)**	—	L5M3R6	—
***Ornithorhynchus anatinus* (Duckbill platypus)**	—	F6V6B0	—
***Columba livia* (Domestic pigeon)**	—	R7VNX9	—
***Gallus gallus* (Chicken)**	—	F1P4X5	—
***Taeniopygia guttata* (Zebra finch)**	—	H0Z024	—
***Meleagris gallopavo* (Common turkey)**	—	G1MYH8	—
***Xenopus laevis* (African clawed frog)**	—	Q641G3	—
***Xenopus tropicalis* (Western clawed frog)**	—	F6RQZ6	—
***Gasterosteus aculeatus* (Three-spined stickleback)**	—	G3NYR2	—
***Xiphophorus maculatus* (Southern platyfish)**	—	M3ZKQ0	—
***Tetraodon nigroviridis* (Spotted green pufferfish)**	—	H3CTD1	—
***Oreochromis niloticus* (Nile tilapia)**	—	I3KPZ5	—
***Chelonia mydas* (Green sea-turtle)**	—	M7CHZ7	—
***Apis mellifera* (Honeybee)**	—	H9KE07	—
***Nasonia vitripennis* (Parasitic wasp)**	—	K7J0P2	—
***Culex quinquefasciatus* (Southern house mosquito)**	—	B0XGS6	—
***Bombyx mori* (Silk moth)**	—	H9JSF9	—
***Pediculus humanus subsp. corporis* (Body louse)**	—	E0W1T1	—
***Camponotus floridanus* (Florida carpenter ant)**	—	E1ZZH2	—
***Harpegnathos saltator* (Jumping ant)**	—	E2BXL7	—
***Acromyrmex echinatior* (Panamanian leafcutter ant)**	—	F4WLM0	—
***Crassostrea gigas* (Pacific oyster)**	—	K1QFN3	—
***Strongylocentrotus purpuratus* (Purple sea urchin)**	—	H3JG74	—
***Schistosoma japonicum* (Blood fluke)**	—	C1LHT1	—
***Loa loa* (Eye worm)**		E1FKS7	
Caenorhabditis briggsae	—	—	A8XU29
***Caenorhabditis brenneri* (Nematode worm)**	—	—	G0P9M6
Caenorhabditis elegans	—	—	G5EFJ2

APPENDIX D: SUPPORTING FIGURES AND TABLES FOR CHAPTER 5: LST-3 IS A NEGATIVE REGULATOR OF SIR-2.1 AND THE HEAT SHOCK RESPONSE IN *CAENORHABDITIS ELEGANS*

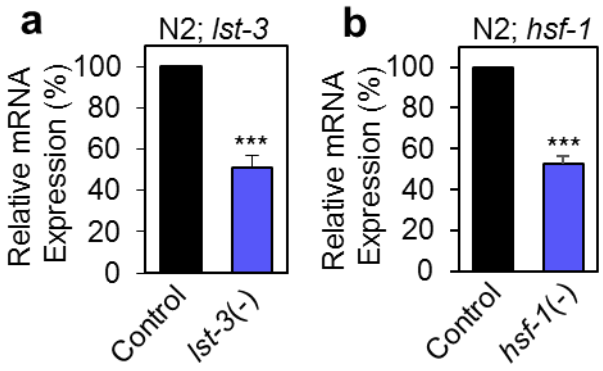

Figure D1. *lst-3* and *hsf-1* mRNA levels are decreased roughly 50% in response to RNAi treatment. (**a**) qRT-PCR was used to measure *lst-3* mRNA expression in synchronous wild-type (N2) worms fed control RNAi or *lst-3* RNAi [*lst-3*(-)] from the L1 larval stage to the L4 larval stage. (**b**) qRT-PCR was used to measure *hsf-1* mRNA expression in synchronous wild-type (N2) worms fed control RNAi or *hsf-1* RNAi [*hsf-1*(-)] from the L1 larval stage to the L4 larval stage. For (**a-b**), significance was determined using the Bonferroni post-hoc test where *** p< 0.001.

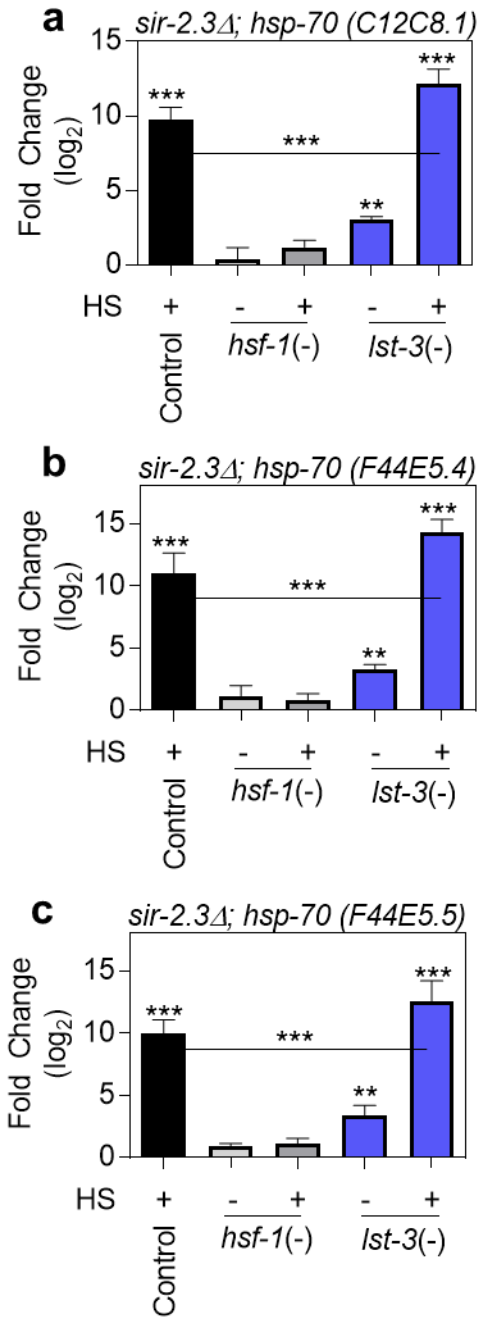

Figure D2. *lst-3* RNAi enhances a family of *hsp-70* mRNAs in a *sir-2.3*-independent manner upon HS. (**a-c**) qRT-PCR was used to measure the expression of the *hsp-70* family members *C12C8.1*, *F44E5.5*, and *F44E5.4* in synchronous *sir-2.3Δ* (RB654) worms fed control RNAi, *hsf-1* RNAi [*hsf-1*(-)], or *lst-3* RNAi [*lst-3*(-)] from the L1 larval stage to the L4 larval stage prior to treatment with or without a 15 minute 33°C HS followed by a 15 minute recovery. For (**a-c**), significance was determined using the Bonferroni post-hoc test where ** p< 0.01, *** p< 0.001.

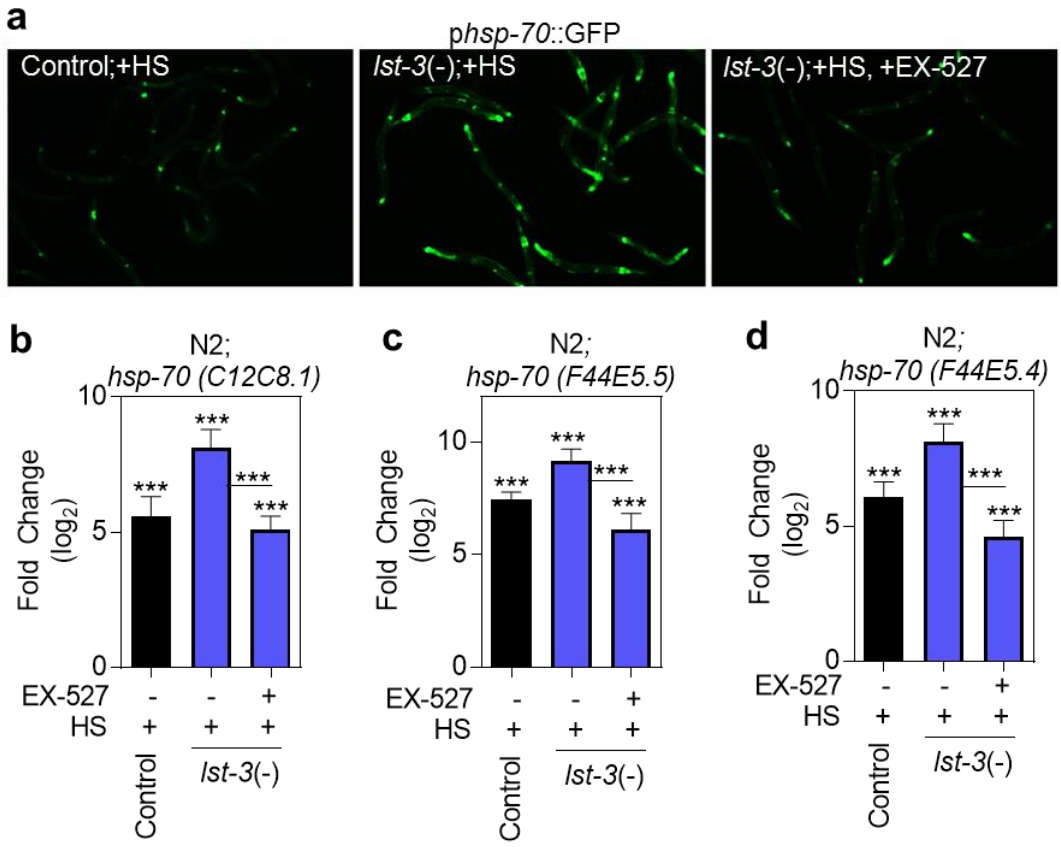

Figure D3. The ability of *lst-3* RNAi to enhance *hsp-70* promoter activity and mRNA expression during HS is dependent on the deacetylase activity of Sir-2.1. (**a**) p*hsp-70*::GFP worms were fed control RNAi, or *lst-3* RNAi [*lst-3*(-)] in combination with 1 µM EX-527 (Sir-2.1 inhibitor) from the L1 larval stage to the L4 larval stage prior to treatment with or without a 15 minute HS followed by a 6 hour recovery. (**b-d**) Wild-type (N2) worms were fed control RNAi, or *lst-3* RNAi [*lst-3*(-)] in combination with 1 µM EX-527 from the L1 larval stage to the L4 larval stage prior to treatment with or without a 15 minute HS followed by a 15 minute recovery. For (**b-d**), significance was determined using the Bonferroni post-hoc test where *** p< 0.001.

APPENDIX E: SUPPORTING FIGURES AND TABLES FOR CHAPTER 6. THE GENOME-WIDE ROLE OF HSF-1 IN THE REGULATION OF GENE EXPRESSION IN *CAENORHABDITIS ELEGANS*

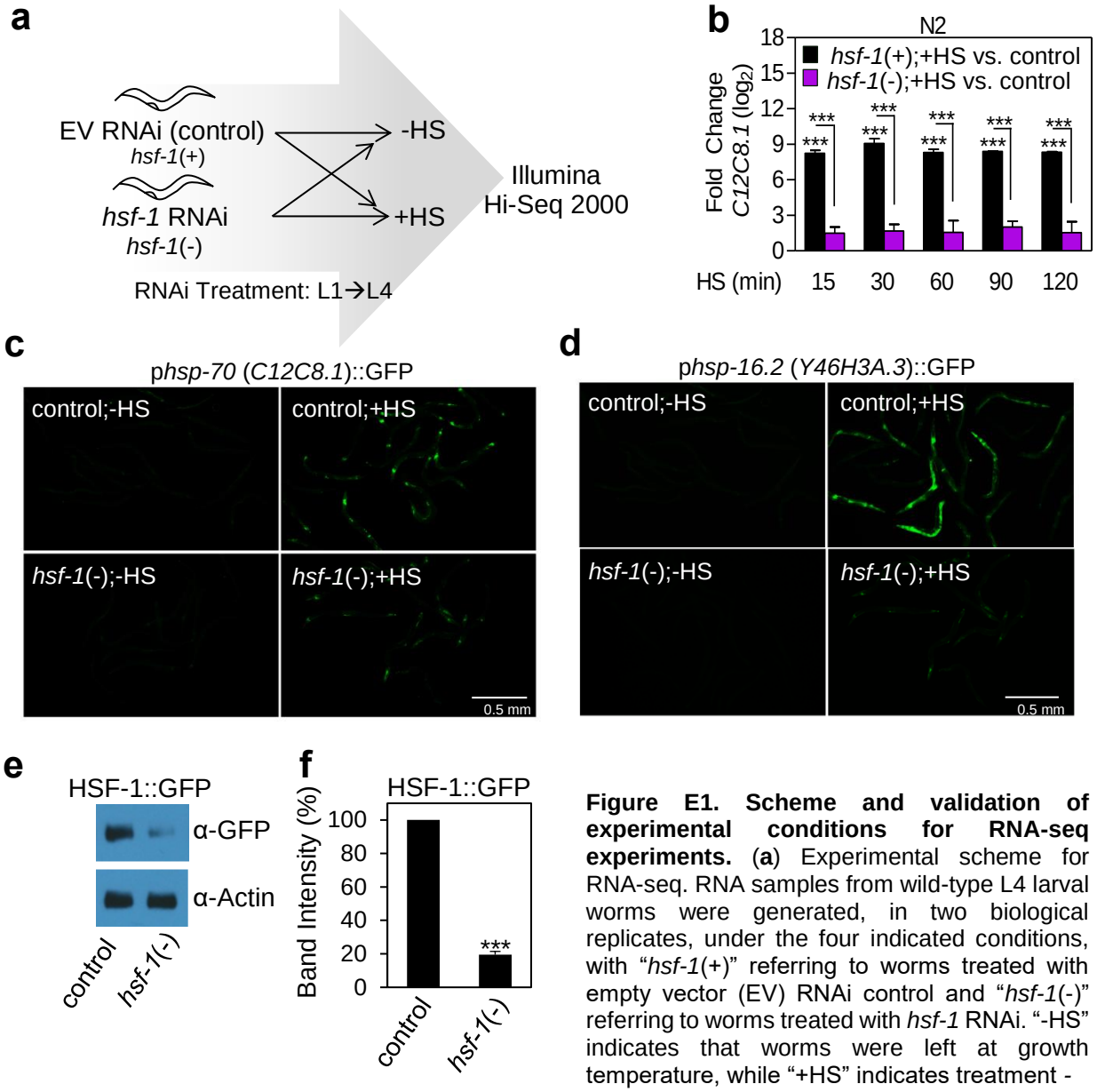

Figure E1. Scheme and validation of experimental conditions for RNA-seq experiments. (**a**) Experimental scheme for RNA-seq. RNA samples from wild-type L4 larval worms were generated, in two biological replicates, under the four indicated conditions, with "*hsf-1*(+)" referring to worms treated with empty vector (EV) RNAi control and "*hsf-1*(-)" referring to worms treated with *hsf-1* RNAi. "-HS" indicates that worms were left at growth temperature, while "+HS" indicates treatment -

Figure E1. Scheme and validation of experimental conditions for RNA-seq experiments (Continued). with a 30 minute 33°C heat shock. RNA-sequencing was performed on the Illumina Hi-Seq 2000 platform. (**b**) *C12C8.1* (*hsp-70*) mRNA is robustly induced by a 33°C HS over a 15-120 minute time window. Synchronous wild-type (N2) L1 nematodes were treated with RNAi against *hsf-1* or with an empty vector (EV) control, indicated as *hsf-1*(-) or *hsf-1*(+), respectively. At the L4 larval stage, worms were either left at growth temperature or treated with a 33°C HS for the indicated times before RNA extraction. *hsp-70* mRNA levels were quantified with qRT-PCR and the results represent the average fold change from a set of biological duplicates and technical triplicates. (**c-d**) *hsf-1* RNAi decreases HS-induced *hsp* promoter activity. Fluorescent images of synchronous p*hsp-70*::GFP or p*hsp-16.2*::GFP worms fed EV RNAi (control) or *hsf-1* RNAi from the L1 larval stage to the L4 larval stage prior to treatment with or without a 33°C 30 minute heat shock (HS) followed by a 12 hour recovery. (**e-f**) *hsf-1* RNAi decreases HSF-1 protein abundance. A transgenic worm strain containing GFP tagged HSF-1 under the control of its own endogenous promoter (HSF-1::GFP) was given the same RNAi feeding strategy in (**c-d**) prior to protein extraction and immunoblotting for GFP or actin (as a control). Image J was then used to quantify the band intensity of the immunoblot in (**e**). For (**b**) and (**f**), significance was determined using the Bonferroni post-hoc test where *** p< 0.001.

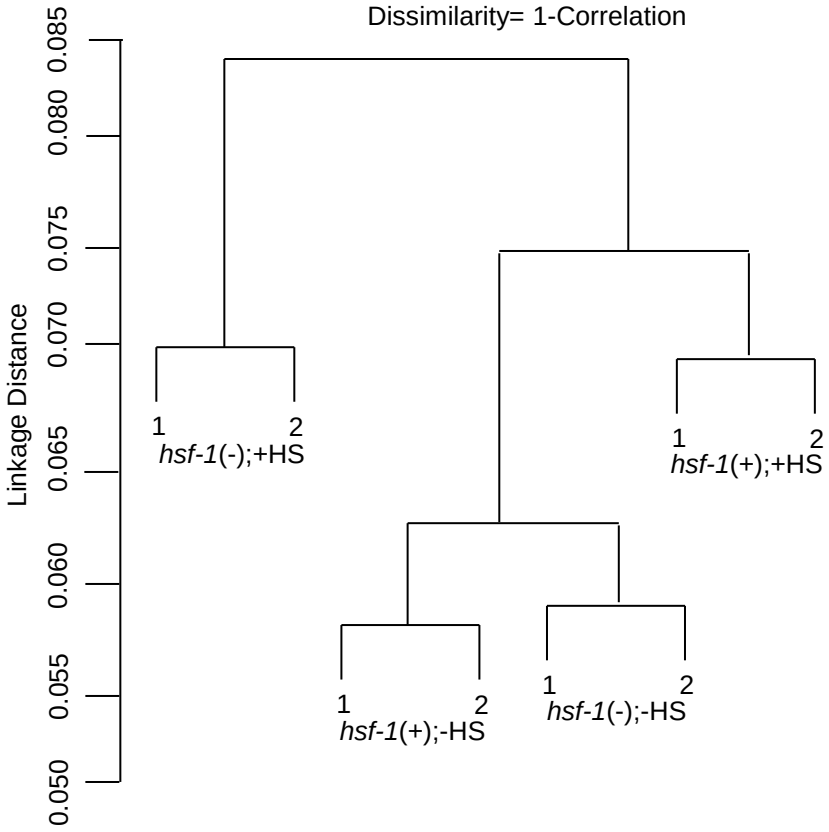

Figure E2. Dendogram clustering of the biological duplicates for each RNA-seq condition reveals conserved alignment between replicates. The dendogram was generated with the program CummeRbund to provide insight into the relationships between different conditions. Significant differentially expressed genes used to draw the dendrograms are based on Jensen-Shannon distances.

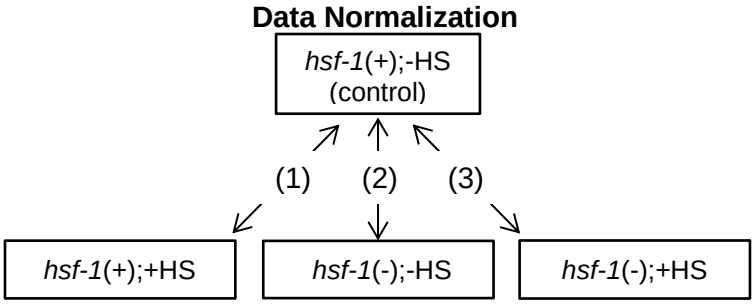

Figure E3. Scheme for RNA-seq data normalization. Each treatment condition was compared relative to the *hsf-1*(+);-HS control in order to determine fold changes in mRNA expression.

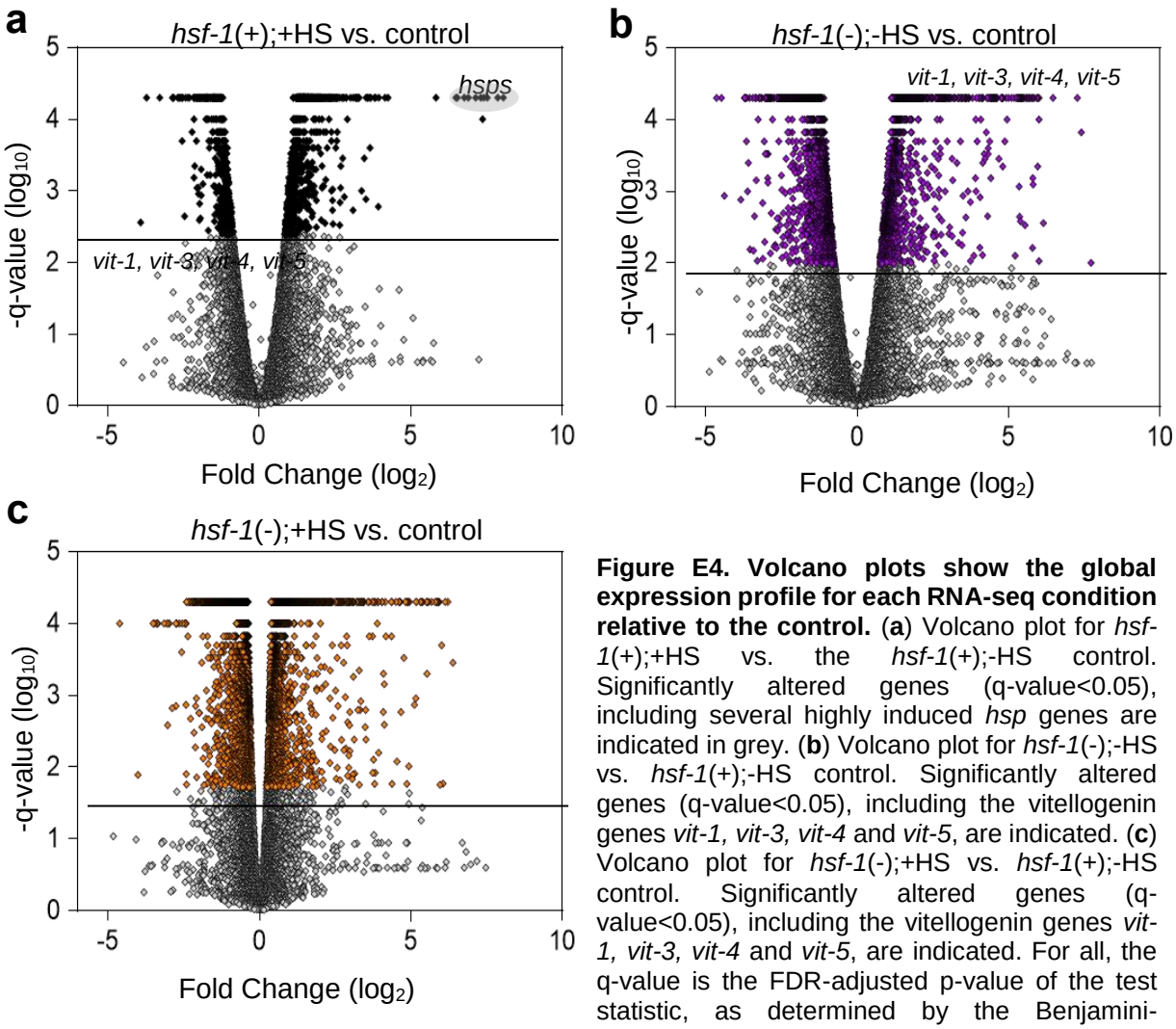

Figure E4. Volcano plots show the global expression profile for each RNA-seq condition relative to the control. (**a**) Volcano plot for *hsf-1*(+);+HS vs. the *hsf-1*(+);-HS control. Significantly altered genes (q-value<0.05), including several highly induced *hsp* genes are indicated in grey. (**b**) Volcano plot for *hsf-1*(-);-HS vs. *hsf-1*(+);-HS control. Significantly altered genes (q-value<0.05), including the vitellogenin genes *vit-1, vit-3, vit-4* and *vit-5*, are indicated. (**c**) Volcano plot for *hsf-1*(-);+HS vs. *hsf-1*(+);-HS control. Significantly altered genes (q-value<0.05), including the vitellogenin genes *vit-1, vit-3, vit-4* and *vit-5*, are indicated. For all, the q-value is the FDR-adjusted p-value of the test statistic, as determined by the Benjamini-Hochberg correction for multiple testing.

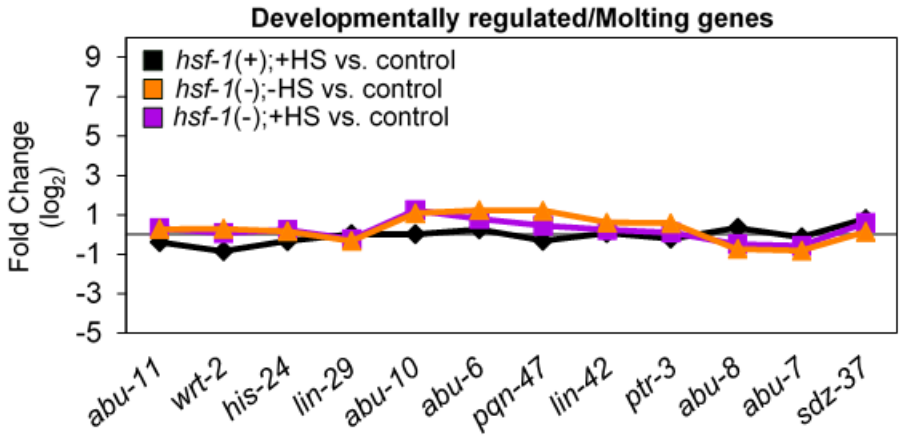

Figure E5. Genes regulated by development and molting share a similar expression profile between each RNA-seq treatment condition. The $\log_2$ fold change from our RNA-seq data for the indicated transcripts that are known to oscillate during development shows that no significant expression profile changes occur between datasets, indicating that treatment with *hsf-1* RNAi and/or HS did not affect the synchronicity of worms between our treatment conditions.

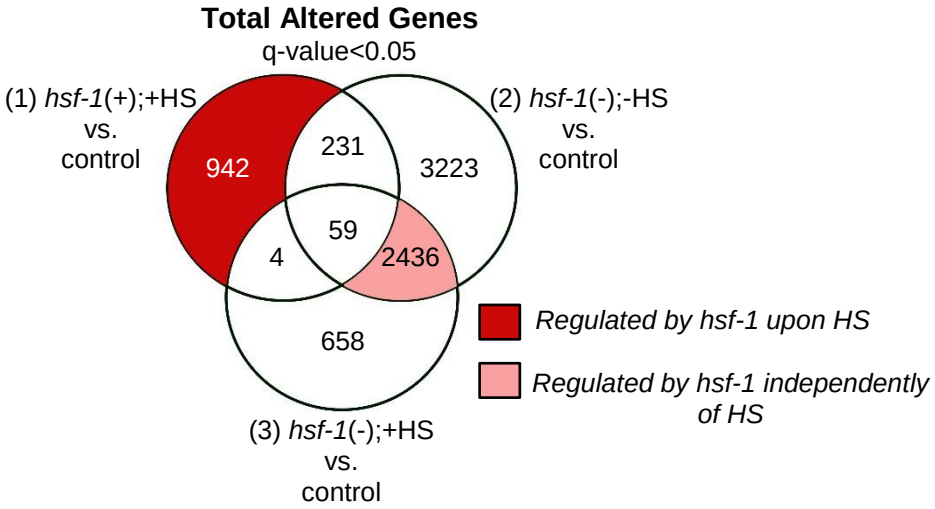

Figure E6. The Venn diagram shows the total number of genes that were found to be significantly altered (q-value<0.05) for each of the indicated comparisons between samples. The q-value is the FDR-adjusted p-value of the test statistic, as determined by the Benjamini-Hochberg correction for multiple testing. The red area of the Venn diagram indicates genes that are regulated by HSF-1 upon HS, whereas the pink portion of the Venn diagram indicates genes that are regulated by HSF-1 independently of HS.

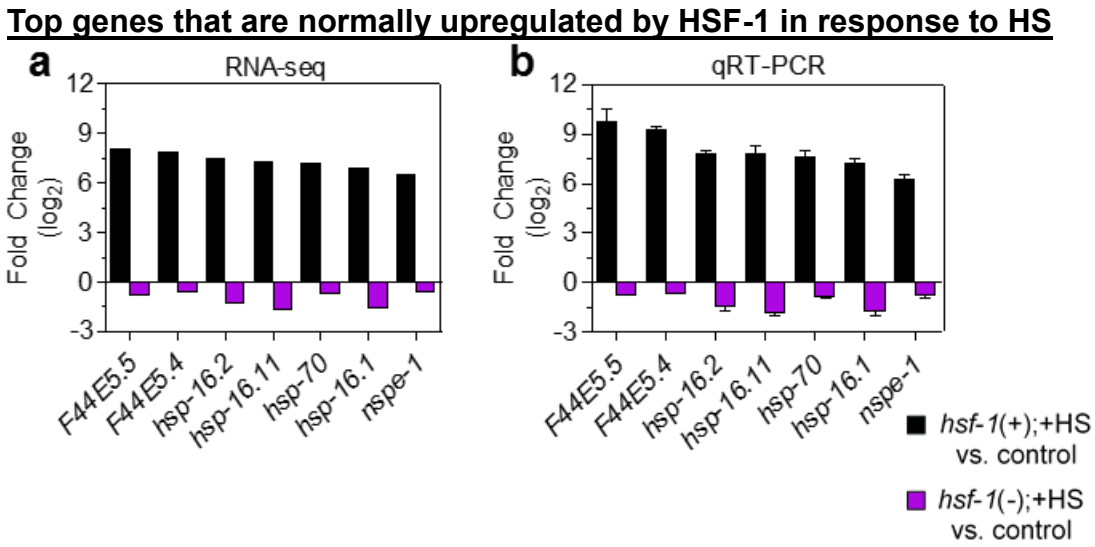

Figure E7. Validation of top RNA-seq hits for genes normally upregulated by HSF-1 during HS via qRT-PCR. (**a**) Fold changes of a subset of the top 15 upregulated genes as measured by RNA-seq analysis. (**b**) Validation of the same genes in (**a**) as measured by qRT-PCR analysis.

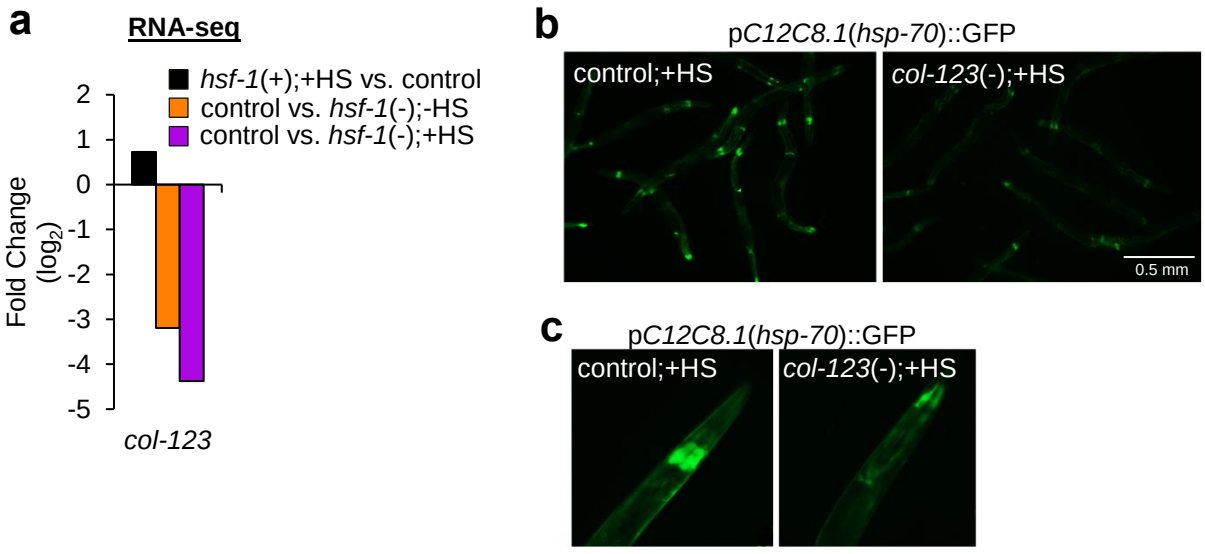

Figure E8. Collagen genes may control tissue specific regulation of the HSR. To verify that the presence of cuticle collagen genes in our dataset was not due to developmental timing differences between our treatment conditions, we tested the effects of *col-123* on induction of the HSR. (**a**) The $\log_2$ fold change of *col-123* mRNA expression based on RNA-seq data between each treatment condition. (**b**) Fluorescent images of synchronous p*hsp-70*::GFP worms fed EV RNAi (control) or *col-123* RNAi [*col-123*(-)] from the L1 larval stage to the L4 larval stage prior to treatment with or without a 33°C 30 minute heat shock (HS) followed by a 12 hour recovery. (**c**) The anterior of p*hsp-70*::GFP worms given the same treatment conditions as in (**b**) shows a decrease and shift in *hsp-70* promoter activity in response to treatment with *col-123* RNAi as compared to the control.

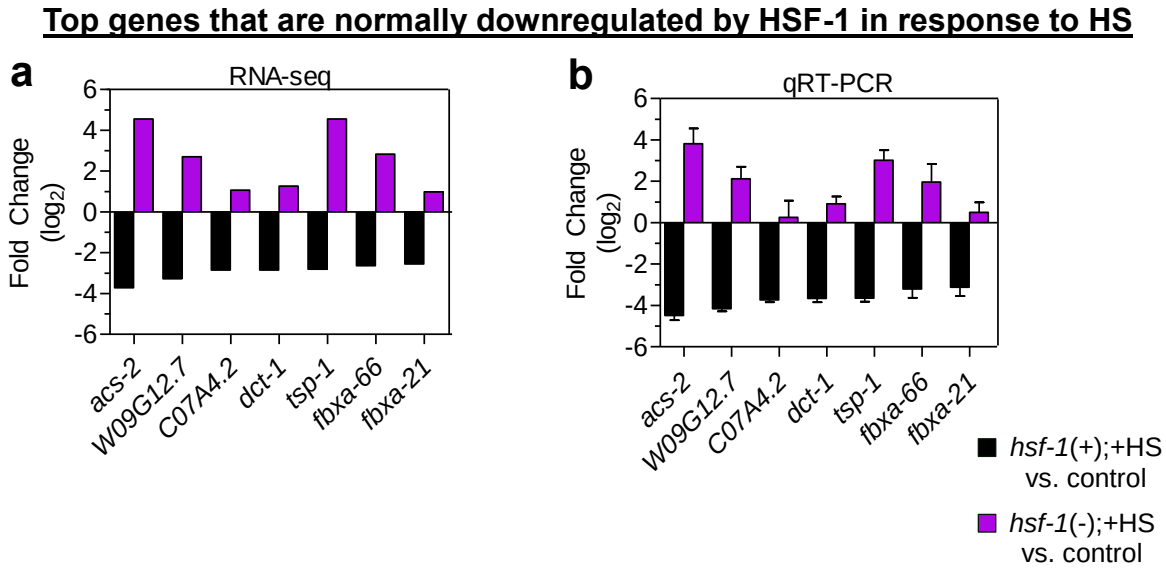

Figure E9. Validation of top RNA-seq hits for genes normally downregulated by HSF-1 during HS via qRT-PCR. (**a**) Fold changes of a subset of the top 15 downregulated genes as measured by RNA-seq analysis. (**b**) Validation of the same genes in (**b**) as measured by qRT-PCR analysis.

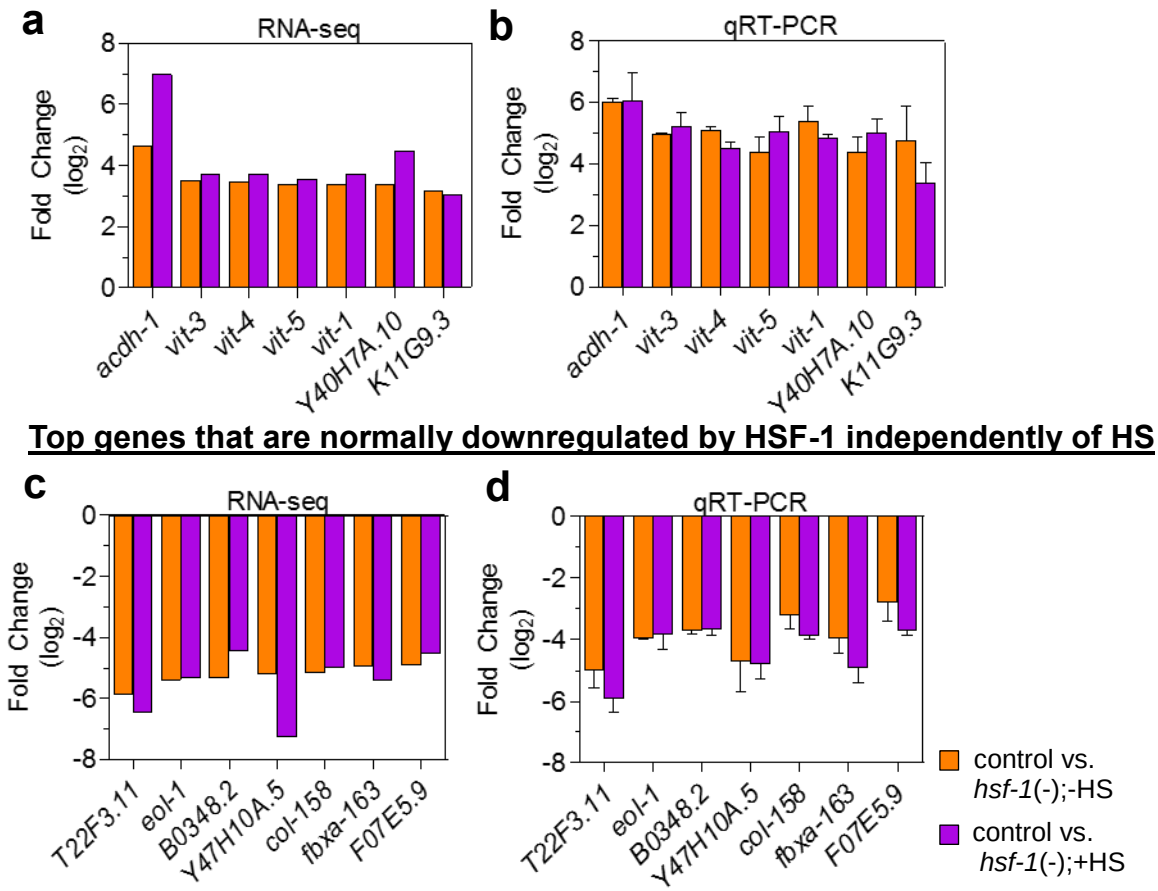

Figure E10. Validation of the top RNA-seq hits for genes normally regulated by HSF-1 independently of HS via qRT-PCR. (**a**) Fold changes of a subset of the top 15 normally upregulated genes as measured by RNA-seq analysis. (**b**) Validation of the same genes in (**a**) as measured by qRT-PCR analysis. (**c**) Fold changes of a subset of the top 15 downregulated genes as measured by RNA-seq analysis. (**d**) Validation of the same genes in (**c**) as measured by qRT-PCR analysis. For (**a-d**) the data comparison was reversed [control vs. *hsf-1*(-);-HS or +HS] to obtain the fold change of these genes, in order to gain insight into the normal HSF-1-regulatory role of these HS-independent genes.

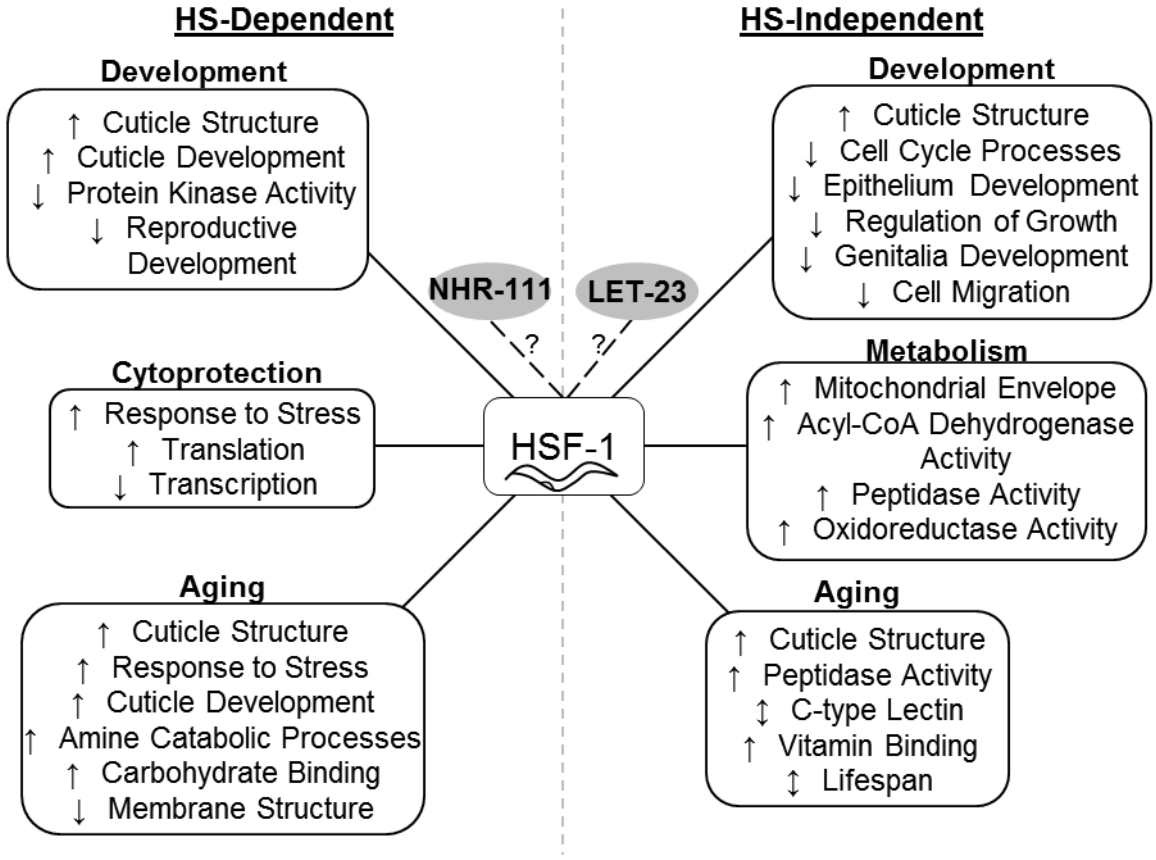

Figure E11. A model for major HSF-1 regulated processes in HS-dependent and -independent mechanisms. HSF-1 regulates a variety of processes during HS, but also has unique roles outside of the HSR. During HS, HSF-1 regulates development, cytoprotection, and aging, which may be regulated by the nuclear hormone receptor NHR-111. These processes are likely affected in order to promote survival to stress. The functions of HSF-1 outside of stress include roles in regulating development, metabolism, and aging, which may be regulated by a transmembrane tyrosine kinase LET-23. This highlights a role for HSF-1 in regulating both HS-dependent and –independent processes in *C. elegans*.

Table E1. Significantly altered genes in the *hsf-1*(+);+HS treatment condition compared to the control.

Gene Name	log_2 Fold
F44E5.5	8.06
F44E5.4	7.87
hsp-16.2	7.53
hsp-16.41	7.41
R11A5.3	7.37
hsp-16.11	7.31
hsp-70	7.15
hsp-16.1	6.90
hsp-16.48	6.77
nspe-1	6.54
hsp-16.49	6.50
MTCE.7	5.84
fil-2	4.26
nurf-1	4.15
MTCE.33	3.95
Y53F4B.8	3.94
ZC21.10	3.84
col-102	3.81
scp-1	3.68
nspe-7	3.66
F18E3.13	3.66
col-36	3.60
grl-23	3.57
F18E3.11	3.53
col-85	3.52
col-50	3.47
col-51	3.38
R107.5	3.30
linc-6	3.29
col-40	3.27
C13A2.12	3.23
F22F7.8	3.21
F19B2.5	3.21
F59C12.4	3.18
col-2	3.11
his-51	3.10
col-149	3.01
col-37	2.91
cut-1	2.88
Y43F8B.2	2.87
pqn-75	2.81

Gene Name	log_2 Fold
F41C3.2	2.79
fbxa-151	2.77
C45B2.8	2.76
Y48E1B.8	2.75
grl-20	2.70
col-183	2.69
fbxa-18	2.67
K02E2.8	2.67
fbxa-78	2.66
grl-25	2.61
F47B7.7	2.58
F08G2.5	2.58
ZC250.4	2.57
his-50	2.57
lips-15	2.56
col-143	2.55
T20D4.7	2.54
comt-5	2.53
dgat-2	2.53
C13G3.1	2.49
col-43	2.48
col-176	2.47
T20B6.3	2.44
col-80	2.44
M01G12.8	2.43
col-129	2.43
unc-23	2.42
M04G7.1	2.42
M162.5	2.42
col-140	2.40
Y47D3B.6	2.39
Y54G9A.4	2.39
Y39F10A.1	2.39
cut-2	2.37
col-139	2.37
col-169	2.37
C52D10.1	2.37
his-38	2.36
col-147	2.35
col-142	2.34

Gene Name	log_2 Fold
T10C6.15	2.33
col-93	2.32
col-103	2.31
F59C6.18	2.31
col-160	2.30
F49E12.9	2.29
col-170	2.29
T04B2.3	2.25
C30C11.4	2.25
his-28	2.25
cnc-4	2.25
F53B3.6	2.24
col-159	2.22
flp-33	2.21
his-21	2.20
col-119	2.19
F46F2.3	2.18
Y94H6A.10	2.18
col-19	2.17
col-124	2.17
col-81	2.16
col-94	2.14
fat-5	2.13
col-122	2.13
ugt-63	2.13
T01G5.1	2.12
C29G2.6	2.11
col-92	2.11
col-20	2.11
col-179	2.08
T27F6.8	2.08
F10D7.3	2.07
linc-44	2.07
col-178	2.07
K08D12.6	2.07
col-7	2.06
col-146	2.06
Y38E10A.28	2.05
Y71G12B.18	2.05

Gene Name	log_2 Fold
Y53F4B.23	2.03
col-62	2.03
col-95	2.03
col-181	2.02
cysl-2	2.02
col-167	2.02
aqp-8	2.01
col-168	2.01
nlp-25	2.01
col-127	2.01
col-98	1.99
col-8	1.99
col-126	1.99
col-184	1.99
col-101	1.98
nhr-114	1.98
F42A8.1	1.96
myo-2	1.96
Y41C4A.11	1.96
K01C8.1	1.95
F45D11.3	1.94
T28C12.4	1.94
nspc-6	1.94
C02E7.6	1.94
nspc-3	1.94
vap-1	1.93
his-53	1.93
nspc-2	1.93
his-7	1.93
C52D10.3	1.92
col-144	1.91
nspc-7	1.90
dpy-3	1.90
C30E1.9	1.89
Y37E11B.7	1.89
F45D11.4	1.89
col-117	1.89
C08E8.10	1.89
F08D12.2	1.89

Table E1 (Continued)

Gene Name	log_2 Fold
pepm-1	1.89
tni-3	1.89
col-3	1.88
col-10	1.88
his-6	1.87
F45D11.2	1.86
clh-4	1.85
F41E6.12	1.85
fbxa-72	1.85
col-133	1.84
K01D12.9	1.84
T21B6.3	1.84
dnj-13	1.83
R05H10.1	1.82
col-106	1.82
B0457.6	1.82
C03G6.17	1.81
nhr-53	1.81
F07C6.6	1.80
C53C9.2	1.80
fbxa-88	1.80
nspc-5	1.80
T10G3.3	1.80
mdt-26	1.80
F08F3.4	1.79
his-5	1.78
nspc-4	1.78
his-18	1.78
W09G12.9	1.77
his-27	1.77
ttll-12	1.76
T20D4.10	1.76
sptl-2	1.76
R07E3.4	1.76
twk-42	1.76
his-19	1.75
unc-95	1.75
col-54	1.75
twk-16	1.75
F13E9.12	1.75
fipr-9	1.74
col-125	1.74

Gene Name	log_2 Fold
dpy-5	1.74
inx-18	1.73
W08F4.5	1.73
B0238.12	1.73
Y39B6A.21	1.73
ins-33	1.72
myo-1	1.72
Y59E9AR.1	1.72
srh-71	1.71
his-40	1.71
mua-6	1.71
ech-7	1.70
alh-6	1.70
his-22	1.70
nac-1	1.70
fbxa-54	1.69
math-14	1.69
B0454.5	1.69
Y47G6A.33	1.69
K09C4.5	1.69
F41B4.1	1.68
C49G7.3	1.68
F43C9.1	1.68
T25B9.1	1.67
K09C6.9	1.67
nspc-9	1.67
pgp-1	1.67
col-45	1.66
Y38C1AA.9	1.66
C05C8.7	1.65
K01A11.1	1.65
msp-58	1.65
F11E6.3	1.64
phat-3	1.64
T10B5.8	1.64
decr-1.1	1.64
msp-51	1.64
tdo-2	1.64
twk-33	1.64

Gene Name	log_2 Fold
arrd-14	1.64
gale-1	1.64
C53D6.7	1.64
col-180	1.64
dpy-4	1.64
ins-27	1.64
Y17G9A.2	1.63
F39D8.7	1.62
sams-1	1.62
col-145	1.62
his-49	1.62
pqn-94	1.62
C02E7.7	1.61
mxl-3	1.61
Y49G5A.1	1.61
W03F9.1	1.61
W02D9.10	1.60
nlp-26	1.60
Y71D11A.3	1.60
math-15	1.60
ZC116.1	1.60
nspc-14	1.60
C39D10.8	1.59
col-107	1.59
ldh-1	1.59
nlp-34	1.59
nspc-1	1.59
sup-9	1.59
col-157	1.59
C18D4.6	1.58
hmit-1.2	1.58
F41D9.2	1.58
F36A2.3	1.57
C39B5.5	1.57
kin-15	1.56
F08D12.3	1.56
far-2	1.56
his-52	1.55
F31A3.3	1.55
Y67H2A.9	1.55
R12E2.6	1.55

Gene Name	log_2 Fold
fipr-10	1.55
cdd-1	1.54
col-71	1.54
K01A6.7	1.54
F29C6.1	1.54
dpy-13	1.54
gst-24	1.54
sqt-1	1.54
haao-1	1.53
kvs-5	1.53
C14B4.2	1.53
srx-58	1.53
col-12	1.53
col-88	1.53
hsp-4	1.53
C47E8.11	1.53
C45B2.2	1.52
T19C4.1	1.52
far-1	1.52
fipr-7	1.52
fipr-5	1.51
aqp-7	1.51
F13C5.5	1.51
col-166	1.50
fipr-4	1.50
C56E6.2	1.50
cor-1	1.50
Y50D4B.6	1.50
T12D8.9	1.50
col-38	1.50
H05L03.3	1.50
R12E2.14	1.49
daf-21	1.49
tatn-1	1.49
Y53H1B.2	1.49
F56H9.2	1.49
srp-2	1.48
Y54E10A.17	1.48
unc-15	1.48
bli-6	1.48
T22F7.4	1.48

Table E1 (Continued)

Gene Name	log_2 Fold
msp-55	1.48
F58G6.3	1.48
Y37A1B.7	1.47
col-138	1.47
F57H12.6	1.47
C54D10.10	1.47
fkb-4	1.47
col-66	1.47
C31B8.8	1.47
mlc-2	1.47
col-48	1.47
R09E12.9	1.46
grsp-1	1.46
ZK1307.1	1.46
hrg-4	1.46
grd-13	1.46
col-130	1.46
rol-1	1.46
lgc-34	1.46
Y15E3A.4	1.45
col-17	1.45
F40A3.2	1.45
F46H5.3	1.45
grl-27	1.44
col-13	1.44
F23D12.11	1.44
chw-1	1.44
D1005.2	1.44
gly-8	1.44
col-63	1.44
col-104	1.44
grd-3	1.43
C48D1.7	1.42
Y43C5A.7	1.42
ZC449.5	1.42
C18B2.3	1.42
R102.2	1.42
crt-1	1.42
sodh-2	1.42
C18D11.1	1.42
M03B6.1	1.42

Gene Name	log_2 Fold
rol-8	1.42
B0507.3	1.41
dur-1	1.41
Y9C9A.8	1.41
dpy-9	1.41
T21G5.2	1.41
col-175	1.41
col-33	1.40
F21F8.11	1.40
C36C5.12	1.40
C11H1.9	1.40
sdz-6	1.40
fipr-6	1.40
R12C12.10	1.40
W02B3.4	1.40
mup-2	1.39
nspc-12	1.39
cyp-14A5	1.39
col-96	1.39
nspc-19	1.39
srr-4	1.39
K09H9.8	1.39
col-152	1.39
fat-6	1.38
col-77	1.38
his-61	1.38
col-156	1.38
rol-6	1.38
col-141	1.38
K08E7.8	1.38
cah-4	1.37
T06E6.10	1.37
tnt-2	1.37
F41E7.2	1.37
col-161	1.37
ahcy-1	1.37
T25F10.6	1.37
fipr-21	1.37
T21F4.1	1.36
srp-1	1.36
F37H8.5	1.36

Gene Name	log_2 Fold
C50A2.3	1.36
F52B11.2	1.36
best-21	1.36
K12B6.11	1.36
nas-9	1.36
F53F1.4	1.35
nspc-15	1.35
atgp-2	1.35
hsp-1	1.35
mtp-18	1.35
set-18	1.35
nspc-10	1.35
nspb-1	1.35
Y47D7A.13	1.34
csq-1	1.34
elo-8	1.34
nspc-13	1.34
best-14	1.34
msp-53	1.34
ram-2	1.34
lgc-45	1.34
col-65	1.34
Y47D7A.15	1.34
ugt-13	1.33
VF13D12L.3	1.33
col-73	1.33
msp-42	1.33
flu-2	1.33
R13D11.4	1.33
dao-2	1.33
dpy-7	1.33
F25E5.8	1.33
C06A8.3	1.32
nlp-30	1.32
gyg-1	1.32
ZK546.7	1.32
F36D1.7	1.32
col-60	1.32
upb-1	1.32
perm-2	1.32

Gene Name	log_2 Fold
ndx-1	1.32
unc-54	1.32
K08A2.1	1.31
his-3	1.31
pdi-2	1.31
Y50E8A.12	1.31
aip-1	1.30
F18E3.12	1.30
gcsh-1	1.30
lgc-26	1.30
Y43F8B.1	1.30
Y73F4A.1	1.29
Y71H2AM.15	1.29
F45D3.3	1.29
ZK909.3	1.29
sqt-2	1.29
T28A11.6	1.29
fipr-8	1.29
dim-1	1.29
C05D9.3	1.29
Y71F9B.13	1.29
col-46	1.29
best-17	1.28
col-162	1.28
tni-1	1.28
pck-1	1.28
col-154	1.28
K02E7.6	1.28
ZK84.1	1.28
Y39D8A.1	1.28
K03E5.2	1.28
lpr-6	1.28
aldo-1	1.28
tag-18	1.28
col-120	1.28
F32A5.4	1.28
T05C1.3	1.27
pfn-3	1.27
ttr-59	1.27
unc-87	1.27

Table E1 (Continued)

Gene Name	log_2 Fold
osm-11	1.27
ZK896.3	1.27
F22E5.1	1.27
sqt-3	1.26
Y59E9AR.7	1.26
col-97	1.26
dpy-18	1.26
ZK1058.9	1.25
tsp-8	1.25
C36C5.5	1.25
nrf-5	1.25
Y37D8A.5	1.25
pmt-2	1.25
F31D4.8	1.24
pho-14	1.24
Y51A2D.18	1.24
sqrd-1	1.24
C23H5.15	1.24
ugt-45	1.23
cpn-3	1.23
rps-21	1.23
R13H4.2	1.23
C51E3.9	1.23
col-91	1.23
swt-7	1.23
F47B3.3	1.23
F17C8.9	1.23
T13F3.6	1.23
Y48C3A.18	1.23
F38B7.2	1.23
mlc-3	1.22
C45B2.1	1.22
dpy-2	1.22
msp-59	1.22
ost-1	1.21
nspc-16	1.21
ttr-18	1.21
rpl-34	1.21
T05E7.1	1.21
Y45F10B.13	1.21
F09E10.1	1.21
pqn-60	1.21
osm-7	1.21
ptps-1	1.21
rps-16	1.21
lon-2	1.21
Y71H2B.4	1.20
B0205.13	1.20
his-58	1.20
B0222.5	1.20
ZK185.3	1.20
F20A1.1	1.20
F08D12.7	1.20
ugt-60	1.20
H40L08.2	1.19
tnt-4	1.19
Y53G8B.1	1.19
T09B4.8	1.19
act-1	1.19
pcbd-1	1.19
gpd-3	1.19
F41F3.3	1.18
tag-320	1.18
F22F4.5	1.18
col-58	1.18
C14F11.6	1.18
rla-1	1.18
R05D7.1	1.18
rpl-11.2	1.17
grl-15	1.17
gpd-2	1.17
F36A2.7	1.17
T22B7.7	1.17
kel-8	1.17
act-2	1.17
col-14	1.17
F57G8.5	1.17
F49F1.1	1.17
F36H9.4	1.17
rps-9	1.16
fip-5	1.16
D1086.1	1.16
M03B6.2	1.16
col-49	1.16
F28H1.4	1.16
C49F5.7	1.16
ZC328.2	1.16
C01B10.3	1.15
perm-4	1.15
rncs-1	1.15
nlp-31	1.15
F44E5.1	1.15
Y19D10B.6	1.14
F25E2.2	1.14
rpl-18	1.14
F22F7.1	1.14
R05F9.6	1.14
lec-5	1.14
mlc-1	1.14
rps-18	1.14
F46C8.8	1.14
gst-27	1.14
Y57A10A.23	1.14
R13A5.10	1.13
rps-13	1.13
his-35	1.13
C31C9.2	1.13
col-89	1.13
T02B11.3	1.13
gpx-5	1.13
Y47G6A.21	1.13
unc-52	1.13
T04G9.4	1.13
mec-5	1.13
rps-22	1.12
T06E4.5	1.12
nspc-20	1.12
CC8.2	1.12
ttr-6	1.12
nlp-27	1.12
F19F10.3	1.12
mec-7	1.12
F20G2.2	1.11
atf-8	1.11
C29F5.1	1.11
rps-7	1.11
B0228.7	1.11
lev-11	1.11
ttr-10	1.11
ubq-2	1.10
lec-2	1.10
rps-14	1.10
catp-3	1.10
rps-27	1.10
dpy-10	1.10
C26F1.1	1.10
rps-26	1.09
dpy-8	1.09
rpl-33	1.09
ZK180.5	1.09
unc-27	1.09
col-34	1.09
msp-19	1.08
col-155	1.08
elo-5	1.08
brp-1	1.08
ttr-16	1.08
spp-14	1.08
C11E4.7	1.08
ttr-20	1.08
gstk-1	1.08
Y82E9BR.13	1.08
mrpl-17	1.07
rpl-31	1.07
F49C12.6	1.07
cnc-3	1.07
R07E5.4	1.07
F20A1.10	1.07
rpl-5	1.07
col-150	1.07
elo-2	1.07

Table E1 (Continued)

Gene Name	log_2 Fold
F54D5.16	1.07
R12E2.15	1.07
C04G6.2	1.06
rpl-28	1.06
rrn-2.1	1.06
rpl-21	1.06
B0034.1	1.06
Y1A5A.1	1.06
hsp-3	1.06
ndk-1	1.06
T01H8.2	1.06
cpg-9	1.06
clec-146	1.06
twk-34	1.06
F45H10.3	1.05
immp-1	1.05
rps-3	1.05
rps-12	1.05
gst-1	1.05
col-137	1.05
F29C4.2	1.05
cpn-4	1.05
pvf-1	1.05
T04A11.1	1.04
aldo-2	1.04
Y105C5B.5	1.04
C33A12.19	1.04
aat-5	1.04
F58E6.13	1.04
ttr-31	1.04
mboa-3	1.03
msp-81	1.03
fbxa-61	1.03
F37C4.5	1.03
rpl-36	1.03
col-109	1.03
pat-4	1.03
C42D4.3	1.03
H06A10.1	1.03
C54E4.5	1.03

Gene Name	log_2 Fold
F36H9.5	1.03
C16A3.10	1.02
cpin-1	1.02
Y37A1A.2	1.02
col-68	1.02
cyp-29A2	1.02
F40H3.2	1.02
col-118	1.02
W01D2.1	1.02
ubl-1	1.02
ptr-18	1.02
spp-17	1.02
fmo-3	1.02
sti-1	1.01
K10H10.4	1.01
nhr-31	1.01
F58F12.1	1.01
F26E4.6	1.01
fkb-3	1.01
ZC239.6	1.00
gst-36	1.00
tba-1	1.00
F14B8.4	1.00
gln-1	1.00
gst-13	1.00
bli-2	1.00
ras-2	1.00
hsp-12.1	1.00
lin-33	1.00
D1054.8	1.00
F53F8.4	0.99
har-1	0.99
gst-26	0.99
lips-10	0.99
K02E11.10	0.99
C46C11.3	0.99
rpl-25.1	0.99
alp-1	0.99
T28H10.2	0.99
rpl-26	0.98
inx-12	0.98
eif-3.J	0.98

Gene Name	log_2 Fold
umps-1	0.98
fip-2	0.98
mif-2	0.98
cyn-5	0.98
B0457.2	0.98
T19B10.2	0.98
F58G6.9	0.98
his-41	0.98
F13D12.3	0.98
K05C4.2	0.98
grsp-4	0.97
Y51F10.7	0.97
Y37D8A.2	0.97
elks-1	0.97
cnc-8	0.97
mec-12	0.97
tag-174	0.97
K11H12.7	0.97
F26G1.5	0.97
Y38H8A.3	0.97
F53F10.3	0.97
F16B4.4	0.97
msp-57	0.96
pfk-1	0.96
cdo-1	0.96
pdi-1	0.96
ZK909.6	0.96
cls-2	0.96
R07E4.3	0.96
Y54G2A.18	0.95
odc-1	0.95
sucl-1	0.95
F45H10.2	0.95
F15B9.8	0.95
pqn-44	0.95
H42K12.3	0.95
C33G8.4	0.95
C15F1.1	0.95
sdz-24	0.95
Y54G11A.17	0.94

Gene Name	log_2 Fold
E01G4.3	0.94
C44C1.1	0.94
gst-42	0.94
C41H7.1	0.94
ncx-2	0.93
myo-3	0.93
nkat-3	0.93
Y51H7C.13	0.93
F58A6.9	0.93
mrps-28	0.93
nlp-24	0.93
fkb-5	0.93
M02D8.1	0.93
grd-10	0.93
aagr-4	0.92
rpl-41	0.92
ife-2	0.92
far-6	0.92
F07A11.2	0.92
ckb-2	0.92
pat-12	0.92
ifa-1	0.92
D2092.4	0.92
Y59C2A.1	0.91
ZK1290.5	0.91
eef-1B.1	0.90
sucl-2	0.90
Y54G2A.45	0.90
heh-1	0.89
Y22D7AL.10	0.89
ugt-44	0.89
R12E2.7	0.89
dhs-9	0.89
prdx-3	0.88
mbf-1	0.88
asg-2	0.88
cdr-4	0.88
ZK1321.4	0.88
Y39G8B.1	0.88
gst-20	0.87

Table E1 (Continued)

Gene Name	log_2 Fold
F20D1.3	0.87
prdx-6	0.87
B0491.5	0.87
cct-1	0.86
F09B12.3	0.86
Y55F3AM.13	0.86
T05B11.1	0.86
pah-1	0.85
F34D10.4	-0.84
C27A12.6	-0.87
ZK863.4	-0.88
ego-1	-0.89
Y32F6A.4	-0.89
polk-1	-0.89
nrde-2	-0.90
cpt-1	-0.90
nfm-1	-0.90
ppk-2	-0.91
prg-2	-0.91
let-502	-0.91
puf-9	-0.91
acy-3	-0.91
swsn-7	-0.91
F17C11.4	-0.91
lipl-2	-0.91
lin-45	-0.92
T01C3.3	-0.92
cyb-2.2	-0.92
F16D3.4	-0.92
toe-2	-0.92
duo-3	-0.92
cpsf-2	-0.92
sax-1	-0.92
F20D12.2	-0.93
syx-17	-0.93
let-413	-0.93
nhx-2	-0.93
M163.1	-0.93
T19A6.1	-0.94
fbxa-215	-0.94
F19F10.9	-0.95

Gene Name	log_2 Fold
cul-5	-0.95
C06A5.3	-0.95
T24B1.1	-0.95
ZK550.2	-0.95
T13F2.6	-0.96
ZC239.22	-0.96
D1046.3	-0.96
rga-4	-0.96
C56C10.11	-0.96
M03C11.8	-0.96
C17H12.2	-0.96
R10E8.8	-0.97
nhr-90	-0.97
K09H11.7	-0.97
kin-20	-0.97
clec-218	-0.97
lin-49	-0.97
ztf-15	-0.97
imp-3	-0.98
mtk-1	-0.98
F10D11.2	-0.98
R90.1	-0.98
Y71F9AL.10	-0.98
daao-1	-0.98
plc-3	-0.99
F40F12.7	-0.99
T04B2.5	-0.99
lin-23	-0.99
tps-2	-0.99
atg-9	-0.99
F46F11.1	-0.99
Y42H9AR.4	-0.99
pgp-5	-0.99
nhr-176	-1.00
W03F9.4	-1.00
dcp-66	-1.00
K02D7.1	-1.00
smc-5	-1.00
C25A1.5	-1.01
tag-253	-1.01

Gene Name	log_2 Fold
T03E6.8	-1.01
K09H11.1	-1.01
T12G3.2	-1.01
cpr-1	-1.01
hlh-30	-1.01
F18F11.5	-1.01
F21A3.11	-1.02
smk-1	-1.02
bath-12	-1.02
aex-3	-1.02
R09H10.5	-1.02
Y50D7A.8	-1.03
mig-1	-1.03
F15A8.6	-1.03
T10E9.2	-1.03
mes-3	-1.03
wrm-1	-1.04
crml-1	-1.04
cam-1	-1.04
C13F10.6	-1.04
C31C9.6	-1.04
F49C12.7	-1.04
F13B12.6	-1.04
Y44A6C.1	-1.04
C18A11.1	-1.04
clec-54	-1.04
F56C9.10	-1.04
tax-6	-1.04
ogt-1	-1.04
mys-4	-1.04
dhs-18	-1.04
hrdl-1	-1.04
F17C11.10	-1.05
pkc-1	-1.05
tre-1	-1.05
daf-3	-1.05
amx-1	-1.05
ppm-2	-1.05
zip-12	-1.05
tat-2	-1.06
ZK822.5	-1.06
lem-3	-1.06

Gene Name	log_2 Fold
icl-1	-1.06
F14H3.6	-1.06
daf-2	-1.06
mbk-1	-1.06
fli-1	-1.06
Y105C5A.1	-1.07
T01E8.1	-1.07
K09F6.9	-1.07
mel-26	-1.07
evl-14	-1.07
ZC376.6	-1.07
ZK632.2	-1.07
hum-1	-1.08
taf-1	-1.08
Y19D10A.16	-1.08
F31C3.3	-1.08
mom-4	-1.08
K03H1.5	-1.08
F33G12.6	-1.09
K07B1.7	-1.09
nhr-88	-1.09
clec-4	-1.09
C17E4.3	-1.09
C34D10.1	-1.09
kin-29	-1.09
T01D3.6	-1.09
F02H6.2	-1.09
fnci-1	-1.10
sox-2	-1.10
T02B5.3	-1.10
F22H10.2	-1.10
F02H6.3	-1.10
oac-20	-1.10
asm-2	-1.10
nhr-117	-1.11
K12B6.9	-1.11
C06G8.3	-1.11
gck-1	-1.11
F55C12.5	-1.11
cca-1	-1.11

Table E1 (Continued)

Gene Name	log_2 Fold
C16H3.3	-1.12
pek-1	-1.12
T04C4.1	-1.12
plc-2	-1.12
F55H12.3	-1.12
C30G12.6	-1.12
xpg-1	-1.12
msi-1	-1.12
Y58A7A.4	-1.13
F28B3.5	-1.13
B0001.2	-1.13
nhr-96	-1.13
csnk-1	-1.13
maco-1	-1.13
math-45	-1.13
rcn-1	-1.13
glo-4	-1.13
Y55F3BR.2	-1.14
Y38C1AA.6	-1.15
gon-4	-1.15
T28B8.1	-1.15
rev-1	-1.15
C10C5.5	-1.15
mans-1	-1.15
math-27	-1.16
acs-17	-1.16
C06A5.1	-1.16
DH11.2	-1.16
nhr-99	-1.16
C53A3.2	-1.16
K02C4.3	-1.16
nhr-134	-1.17
Y82E9BR.19	-1.17
eri-7	-1.17
cec-2	-1.17
Y97E10AR.1	-1.17
rabx-5	-1.18
mtm-5	-1.18
F07B7.12	-1.19
ccch-1	-1.19
F43C11.7	-1.19
scd-2	-1.19
M106.2	-1.19
cyp-13A2	-1.19
lin-12	-1.20
nhr-112	-1.20
ZK809.5	-1.20
daf-5	-1.20
K09F6.10	-1.20
sid-1	-1.20
C38C3.4	-1.20
F32D8.12	-1.21
egrh-1	-1.21
frpr-11	-1.21
crtc-1	-1.21
imp-1	-1.22
C30G4.7	-1.22
F47B8.4	-1.22
C34D4.10	-1.22
mom-5	-1.22
C53A5.6	-1.23
del-5	-1.23
ugt-51	-1.23
F16B3.3	-1.23
T04H1.2	-1.23
pap-1	-1.23
cyp-37B1	-1.23
pamn-1	-1.24
K10C3.4	-1.24
atg-18	-1.24
C18D4.8	-1.25
irld-53	-1.25
gad-3	-1.25
rde-1	-1.25
C33D9.5	-1.25
R166.6	-1.25
Y57A10A.1	-1.25
dpf-6	-1.26
fbxa-124	-1.26
F28A12.4	-1.27
F13C5.1	-1.27
clec-7	-1.27
C13E3.1	-1.27
C10C5.4	-1.27
C26E1.2	-1.27
Y6G8.2	-1.28
K07B1.8	-1.28
F47B10.9	-1.28
T09E11.11	-1.28
atg-13	-1.29
Y7A9C.1	-1.29
K10D3.6	-1.29
let-23	-1.29
M04C3.1	-1.29
fmo-1	-1.30
Y19D10B.4	-1.30
F56E10.1	-1.30
Y69A2AR.12	-1.30
T23B12.6	-1.30
C27H5.4	-1.30
C34F6.5	-1.31
C44H9.4	-1.31
tag-52	-1.31
K02D10.4	-1.31
C17E4.20	-1.32
hda-4	-1.32
gem-4	-1.32
dve-1	-1.32
F56C9.8	-1.32
olrn-1	-1.32
T28F4.5	-1.33
C36B1.9	-1.33
Y75B8A.28	-1.34
M02E1.1	-1.34
ace-2	-1.35
Y32F6B.1	-1.35
F47H4.2	-1.35
hpk-1	-1.35
D1086.5	-1.35
rgef-1	-1.35
ets-4	-1.36
rad-50	-1.36
C06A6.2	-1.36
gon-2	-1.36
R05D3.12	-1.36
ndnf-1	-1.36
aakg-1	-1.37
C03B1.7	-1.37
F42G2.2	-1.37
F11E6.11	-1.38
D2030.2	-1.39
F47A4.5	-1.39
nhl-2	-1.40
F53B2.8	-1.40
ZK896.5	-1.40
C08F11.13	-1.40
nhr-206	-1.41
oac-6	-1.41
C04G6.6	-1.41
C02F5.7	-1.42
Y20C6A.1	-1.43
glt-5	-1.43
sma-9	-1.43
pef-1	-1.43
oac-14	-1.43
nhr-128	-1.43
atg-11	-1.43
catp-7	-1.44
F13H6.1	-1.44
F28C1.3	-1.45
K03A11.5	-1.45
F53H2.3	-1.45
C35E7.4	-1.45
C06B3.6	-1.45
Y70C5A.3	-1.45
R05G6.10	-1.46
atg-2	-1.46
T14B1.1	-1.46
attf-5	-1.46
pgp-2	-1.46
mdt-15	-1.46
Y71H2B.8	-1.47

Table E1 (Continued)

Gene Name	log_2 Fold
spp-2	-1.48
Y105C5A.15	-1.49
F16A11.1	-1.49
F35G2.1	-1.49
sul-2	-1.50
nhr-59	-1.50
egl-44	-1.50
C52E2.4	-1.50
R193.2	-1.51
set-15	-1.51
nhr-56	-1.51
F34H10.3	-1.52
C32D5.6	-1.53
best-5	-1.53
T01H10.8	-1.53
F38E9.1	-1.54
T28H10.3	-1.54
btb-21	-1.56
C23H4.6	-1.57
C03A7.12	-1.58
F10E9.12	-1.59
Y71H2AM.3	-1.59
C34D10.2	-1.61
F16G10.15	-1.61
Y43F8B.9	-1.62
ubc-8	-1.64
Y32B12C.5	-1.64
nhx-6	-1.66
R07E4.1	-1.67
ist-1	-1.68
btb-1	-1.68
C52E2.5	-1.68
T28F4.4	-1.70
F21D12.3	-1.70
F26A1.13	-1.70
C50F7.5	-1.70
clec-47	-1.70
C03A7.13	-1.71
C04E7.3	-1.72
fbxa-24	-1.72
lgg-2	-1.72
gcl-1	-1.73
gld-2	-1.73
ugt-54	-1.75
irg-2	-1.75
ugt-4	-1.77
sma-10	-1.77
Y51A2D.13	-1.78
coel-1	-1.79
lys-3	-1.79
tsp-2	-1.80
T16G1.7	-1.82
clec-223	-1.84
mfb-1	-1.85
F53F4.8	-1.85
pho-9	-1.88
Y69A2AR.7	-1.89
W03D8.8	-1.90
F57C12.6	-1.90
F07C4.12	-1.91
gbh-2	-1.92
C03A7.2	-1.93
C44H9.5	-1.94
clec-2	-1.96
ZC443.3	-1.96
T24C4.4	-1.96
nhr-83	-1.97
K03H1.10	-1.97
F18G5.6	-1.98
math-38	-2.00
Y94H6A.2	-2.00
M01B2.13	-2.00
R12E2.2	-2.04
T19C4.5	-2.04
cpt-3	-2.05
C06B3.7	-2.05
C24G7.1	-2.06
K08F9.1	-2.07
glc-1	-2.07
nep-26	-2.12
npr-20	-2.12
Y47H10A.5	-2.14
T05E12.3	-2.15
F25B3.5	-2.15
fkh-7	-2.15
ech-9	-2.16
F26A1.14	-2.21
F33H12.7	-2.30
dod-3	-2.34
T12A7.6	-2.42
ugt-18	-2.46
C49G7.7	-2.52
Y43F8B.23	-2.54
K08D9.4	-2.54
fbxa-21	-2.55
nep-14	-2.60
fbxa-66	-2.63
ftn-1	-2.68
tsp-1	-2.81
dct-1	-2.84
C07A4.2	-2.85
W09G12.7	-3.28
acs-2	-3.71
srh-2	-3.90

Table E2. Significantly altered genes in the hsf-1(-);-HS treatment condition compared to the control.

Gene Name	log_2 Fold
rab-11.2	6.39
col-36	6.21
grl-23	6.13
K10G4.13	6.05
col-85	6.02
ZK863.10	5.96
col-50	5.93
col-51	5.92
col-102	5.88
T22F3.11	5.85
col-2	5.84
C13A2.12	5.80
col-40	5.69
col-37	5.59
col-84	5.53
col-183	5.53
grl-20	5.51
T26F2.3	5.38
grl-25	5.36
cut-1	5.32
B0348.2	5.32
Y47H10A.5	5.17
col-158	5.17
grl-9	5.16
F56F11.1	5.11
fbxa-163	4.95
col-185	4.93
F07E5.9	4.90
clec-174	4.89
sri-70	4.87
srg-31	4.84
clec-60	4.81
Y75B8A.39	4.77
ZK355.3	4.67
B0507.8	4.64
Y50E8A.19	4.61
ZK355.8	4.60
C17H1.6	4.54
clec-13	4.50
ZK228.10	4.38
T08E11.1	4.37

Gene Name	log_2 Fold
C25F9.2	4.36
F22G12.1	4.35
sri-36	4.17
col-43	4.16
grl-3	4.12
W08D2.11	4.12
B0284.2	4.09
F10A3.1	4.08
clec-15	4.05
F42C5.3	4.04
T05H10.3	3.94
sdz-35	3.92
dod-20	3.92
fbxa-165	3.89
dct-3	3.84
C25F9.16	3.82
F13E9.9	3.80
Y39B6A.24	3.78
W07B8.4	3.77
col-163	3.77
ZK666.13	3.74
W08A12.4	3.73
C17H1.4	3.72
anr-30	3.63
fbxa-161	3.63
grl-17	3.58
F09C12.2	3.52
H39E23.3	3.50
oac-24	3.49
C25F9.11	3.45
fat-5	3.44
C54D10.12	3.43
fbxa-30	3.40
F33H12.7	3.36
hsf-1	3.36
F57G4.1	3.35
F22E5.7	3.32
C08E8.4	3.31
col-45	3.30
Y26D4A.3	3.30
ZK185.4	3.29

Gene Name	log_2 Fold
F57G4.11	3.26
ugt-15	3.25
fbxa-158	3.23
col-123	3.19
C17H1.8	3.14
C23H5.12	3.13
tbb-6	3.11
F23B2.10	3.10
C54D10.14	3.10
Y40C5A.3	3.09
C10F3.7	3.08
Y37H2A.14	3.08
Y82E9BL.3	3.07
B0563.9	3.04
F22E5.6	2.99
srh-195	2.98
ver-1	2.98
arrd-11	2.97
C49G7.12	2.97
C23G10.11	2.96
C54D10.8	2.95
F01G10.4	2.95
clec-42	2.95
W02A2.9	2.94
F08G2.5	2.94
ZC196.6	2.91
wrt-7	2.91
clec-71	2.89
B0284.1	2.89
jmjd-3.3	2.87
F15D4.5	2.87
cnc-9	2.85
C50F7.5	2.85
R03H10.6	2.85
F16B4.6	2.83
F49H6.5	2.80
sri-39	2.78
clec-61	2.78
F07C4.12	2.76
W09C3.3	2.73
dmd-10	2.70

Gene Name	log_2 Fold
F26D11.13	2.70
F46A8.1	2.69
acs-2	2.69
Y17D7C.2	2.69
C17H1.14	2.67
B0507.10	2.66
H02F09.3	2.66
math-15	2.63
fmo-2	2.60
ZC47.11	2.59
W01C9.2	2.58
C17H1.7	2.58
bro-1	2.56
K11H12.6	2.56
C30H6.12	2.54
B0462.5	2.54
F15B9.6	2.52
B0507.7	2.51
R07C12.1	2.49
arrd-9	2.48
E02H4.4	2.43
C38D9.2	2.41
F26F2.1	2.41
B0507.6	2.38
F59C12.4	2.36
F46A8.7	2.36
Y6E2A.5	2.34
C15C7.4	2.34
clec-167	2.33
F18E3.12	2.33
F46A8.13	2.32
C28G1.2	2.32
Y6G8.5	2.32
Y58A7A.5	2.31
T28F3.5	2.30
F44G3.10	2.29
ZK896.1	2.28
C08E3.1	2.27
skr-5	2.25
Y71G12B.32	2.22

Table E2 (Continued)

Gene Name	log_2 Fold
B0507.3	2.22
dsl-3	2.20
ZC239.14	2.20
C15H11.16	2.18
Y34F4.2	2.16
C17H1.5	2.15
F53H2.1	2.15
C06E7.88	2.14
oac-14	2.12
hot-5	2.11
W02D7.11	2.10
rrf-2	2.10
F18E3.11	2.10
clec-17	2.10
F53F4.4	2.07
tsp-2	2.07
F56D2.3	2.07
math-10	2.07
ZC196.2	2.06
Y9C9A.16	2.05
Y6E2A.4	2.05
zip-6	2.05
T24E12.5	2.03
T08B6.2	2.03
M28.8	2.02
fbxa-162	2.01
fbxa-164	2.01
Y43B11AL.1	1.97
F20G2.5	1.96
best-1	1.96
fbxa-144	1.95
C31B8.4	1.95
zip-10	1.94
T19C9.8	1.94
C08E3.13	1.93
Y17G9B.1	1.92
tsp-1	1.92
srw-86	1.92
T26H5.8	1.90
bath-46	1.90
K08D9.6	1.90

Gene Name	log_2 Fold
fkh-5	1.89
F59B1.10	1.89
T10D4.15	1.88
irg-1	1.88
fbxa-135	1.88
Y105C5B.7	1.87
srbc-20	1.87
best-2	1.86
Y57G11B.1	1.86
F54B8.4	1.85
C17H1.10	1.85
Y71G12B.2	1.84
F53E10.5	1.84
fbxa-166	1.83
sodh-1	1.82
Y54G2A.36	1.81
mtl-1	1.78
C54D2.1	1.78
sip-1	1.77
F37D6.3	1.77
daf-7	1.76
Y34F4.6	1.76
gcy-15	1.76
C17F4.3	1.75
F46C5.1	1.75
lea-1	1.75
Y75B7AL.2	1.75
linc-123	1.74
math-37	1.74
pgp-8	1.74
F10C2.7	1.74
ilys-2	1.72
oac-18	1.72
nlp-18	1.72
clec-82	1.72
K05C4.8	1.71
F43C11.8	1.71
F53B2.8	1.71
Y51B9A.9	1.71
F07G11.4	1.70

Gene Name	log_2 Fold
col-41	1.70
mxl-3	1.70
W03D2.6	1.70
C18G1.6	1.70
bath-47	1.69
B0294.1	1.69
F18E3.13	1.69
cpt-3	1.69
Y43F8B.25	1.68
F35E12.4	1.68
Y39H10B.3	1.68
K09H11.11	1.68
F25D1.4	1.67
T06E6.15	1.67
trpl-5	1.67
col-33	1.67
valv-1	1.67
grsp-3	1.67
B0205.13	1.66
B0403.3	1.66
twk-31	1.65
F53C3.6	1.64
H43E16.1	1.64
F08A8.5	1.63
fbxc-19	1.63
srr-2	1.62
fbxc-23	1.61
ZC449.5	1.61
K10G4.5	1.60
Y48G8AR.2	1.60
clec-106	1.60
ZC190.10	1.60
C06E4.8	1.60
Y46G5A.20	1.59
ZC376.1	1.59
Y37H2B.1	1.58
B0238.13	1.57
F19B10.13	1.56
Y51H4A.25	1.55
ceh-62	1.54

Gene Name	log_2 Fold
C10C5.2	1.54
C44B12.6	1.54
lipl-3	1.53
C46G7.5	1.53
dpf-6	1.53
ZK596.1	1.53
tts-1	1.52
ZK402.1	1.52
arf-1.1	1.52
F57B9.3	1.51
F47B8.4	1.51
T22F3.10	1.50
Y41C4A.11	1.49
C25F9.12	1.49
Y19D10A.11	1.49
F25D1.3	1.49
Y47H9C.1	1.48
F26G5.1	1.47
ckr-1	1.47
far-7	1.47
F55F3.4	1.46
hpo-38	1.46
F46F3.3	1.45
linc-72	1.45
T19D12.4	1.44
R03H10.7	1.44
T10C6.7	1.44
R11E3.2	1.43
zip-7	1.43
fbxa-115	1.42
fbxa-48	1.42
C25F9.6	1.42
cpg-1	1.41
rnt-1	1.41
sptf-2	1.40
T23F4.3	1.40
fog-3	1.39
lin-41	1.39
phg-1	1.39
C44H9.7	1.39
fbxa-54	1.38

Table E2 (Continued)

Gene Name	log_2 Fold
C23H4.6	1.38
C02B8.3	1.38
R07C12.4	1.38
fbxa-59	1.38
clec-81	1.38
C01A2.6	1.38
Y105C5A.13	1.37
T08E11.8	1.37
M01H9.2	1.37
Y46H3A.5	1.37
puf-5	1.37
dpy-1	1.36
C09G5.7	1.36
K09C6.9	1.36
pho-14	1.36
mesp-1	1.36
T24E12.1	1.35
pgp-1	1.35
M151.3	1.35
lrx-1	1.35
B0554.5	1.35
T28B11.1	1.35
F17B5.1	1.34
gst-24	1.34
Y43F8B.15	1.34
clec-72	1.34
F22B3.4	1.34
flp-33	1.33
C34H4.2	1.33
srz-85	1.32
Y71A12B.19	1.32
cyd-1	1.32
C23H5.15	1.32
Y37D8A.5	1.32
K08D10.9	1.32
gem-4	1.32
T05F1.9	1.32
nas-3	1.31
puf-7	1.31
cpg-2	1.30

Gene Name	log_2 Fold
egg-1	1.30
math-14	1.30
set-12	1.29
clec-76	1.29
K10D11.3	1.29
puf-3	1.28
meg-2	1.28
cpb-1	1.28
C46C2.3	1.28
K10G4.3	1.28
puf-10	1.27
dgat-2	1.27
meg-1	1.27
C27H2.2	1.27
rme-2	1.27
M01G12.8	1.26
hacd-1	1.25
tyr-5	1.25
col-95	1.25
linc-17	1.25
Y53G8AL.4	1.24
cysl-2	1.24
col-176	1.24
T11F9.1	1.24
C06A5.8	1.24
T24D1.3	1.24
nhr-57	1.24
Y52B11A.14	1.24
skr-15	1.23
Y73B3A.13	1.23
Y9C9A.8	1.23
gln-5	1.23
C08F11.3	1.23
C03G6.17	1.23
F53G2.2	1.22
T02G6.1	1.22
F25E5.8	1.22
tth-1	1.22
twk-14	1.22
F08F3.9	1.21

Gene Name	log_2 Fold
T12G3.1	1.21
C39F7.1	1.21
Y22D7AL.15	1.21
T26H5.9	1.21
F11E6.6	1.21
C34B7.1	1.21
K02D3.1	1.20
D1007.19	1.20
sru-40	1.20
F28F8.7	1.20
F40F12.9	1.19
Y2H9A.6	1.19
mltn-1	1.19
Y55F3AM.10	1.19
F20G4.2	1.18
gly-14	1.18
W05F2.3	1.18
C50A2.3	1.18
ncs-6	1.18
dod-19	1.18
F26G1.10	1.18
C17C3.5	1.17
fbxa-151	1.17
C29A12.2	1.17
fbxa-25	1.17
B0024.4	1.17
F59B10.4	1.17
ift-74	1.16
T11F9.10	1.16
bath-26	1.16
Y54G9A.4	1.16
F23D12.2	1.16
Y39A3A.4	1.16
F53G12.4	1.15
fbxa-141	1.15
let-99	1.15
fbxa-95	1.15
pqn-82	1.15
cnp-3	1.15
K01F9.2	1.15

Gene Name	log_2 Fold
T23B3.6	1.14
cdc-25.2	1.14
pie-1	1.14
egg-6	1.13
ztf-14	1.13
F54F7.6	1.13
nhr-21	1.13
pos-1	1.12
C36C9.1	1.12
M151.7	1.12
C41G7.8	1.12
arrd-3	1.12
F46A8.11	1.12
C04B4.2	1.12
puf-6	1.11
C25E10.5	1.11
set-28	1.11
oma-1	1.11
Y47G7B.2	1.11
fbxa-78	1.11
ZK1055.7	1.10
C45H4.14	1.10
C01G8.1	1.10
wdr-5.3	1.10
M02E1.2	1.10
ZK858.10	1.10
cyp-35B1	1.09
cgt-1	1.09
F21F8.11	1.09
Y54G2A.10	1.08
T05F1.2	1.08
pgp-5	1.08
F21C10.10	1.08
cin-4	1.08
math-38	1.08
str-7	1.07
M01F1.9	1.07
Y53G8AL.1	1.07
gst-3	1.07
zig-4	1.07

Table E2 (Continued)

Gene Name	log_2 Fold
mex-1	1.07
M116.2	1.06
gln-6	1.06
ptc-2	1.06
F58G11.4	1.06
cyp-34A10	1.06
tba-7	1.06
C16C8.12	1.06
fbxa-24	1.06
chs-1	1.06
clec-87	1.05
oac-57	1.05
C39H7.2	1.05
F25E2.1	1.05
lip-1	1.05
cav-2	1.05
fkb-7	1.05
R12C12.5	1.04
bath-21	1.04
F52D1.2	1.04
syx-2	1.04
T09B4.1	1.04
puf-11	1.03
ced-3	1.03
C06B8.2	1.03
daf-18	1.03
tbc-4	1.03
F22B7.9	1.03
C40A11.8	1.03
Y39A1A.9	1.03
F28E10.5	1.03
C39D10.2	1.03
F25A2.1	1.02
rnp-8	1.02
mex-5	1.01
R09A8.1	1.01
spn-4	1.01
K11D12.9	1.01
F10D7.3	1.01
C14B4.2	1.01
C28G1.5	1.01
T27F6.8	1.01

Gene Name	log_2 Fold
F14H12.2	1.00
BE0003N10.3	1.00
math-50	1.00
nhr-6	1.00
F31F6.2	1.00
Y54G2A.32	1.00
ham-1	1.00
Y116F11B.10	0.99
C24G7.1	0.99
acd-2	0.99
dhs-15	0.99
gpd-1	0.99
T06D4.1	0.99
clh-3	0.99
F15D3.8	0.98
C44B7.6	0.98
Y45G5AM.3	0.98
srp-8	0.98
hmit-1.2	0.98
Y37D8A.4	0.98
K08D10.14	0.98
flh-1	0.98
C38D4.7	0.98
oma-2	0.98
M01B2.6	0.98
M01G12.9	0.97
his-58	0.97
F59C6.18	0.97
Y41G9A.5	0.97
F59H5.1	0.97
fbxc-20	0.97
cdt-2	0.97
ZK637.6	0.97
ins-19	0.97
gyg-2	0.97
Y59A8B.21	0.97
trcs-1	0.96
flr-4	0.96
C14A6.16	0.96

Gene Name	log_2 Fold
bath-19	0.96
lips-15	0.96
mex-6	0.96
R07A4.2	0.96
C33B4.4	0.95
F58E2.3	0.95
ZC15.10	0.95
Y20F4.8	0.95
nhr-7	0.95
math-20	0.95
F47H4.2	0.94
ZK673.4	0.94
clec-75	0.94
C44C1.6	0.94
Y17G7B.21	0.94
B0205.14	0.94
Y37D8A.16	0.94
H05L03.3	0.94
ceh-91	0.94
cyp-33C8	0.94
lec-11	0.94
wee-1.3	0.94
F41C3.2	0.93
oac-29	0.93
hpo-24	0.93
acly-2	0.93
F38A5.7	0.93
K11H12.11	0.93
mrp-4	0.93
K06A9.1	0.93
xtr-1	0.93
C35C5.8	0.93
egg-4	0.92
T26F2.2	0.92
Y82E9BR.25	0.92
Y38H6C.9	0.92
wago-5	0.92
lex-1	0.92
Y36E3A.2	0.92
sqv-5	0.92

Gene Name	log_2 Fold
oac-47	0.92
Y22D7AL.9	0.91
polq-1	0.91
Y38C1AA.9	0.91
CE7X_3.2	0.91
hrde-1	0.91
T20F5.4	0.91
T14B1.1	0.91
hsp-17	0.91
B0393.6	0.91
R02F2.4	0.91
K08D8.4	0.91
Y56A3A.16	0.90
cyp-13A5	0.90
peb-1	0.90
Y37E11B.3	0.90
pup-2	0.90
egg-3	0.90
ZC239.22	0.90
perm-1	0.90
ceh-37	0.90
F59H6.3	0.90
rig-4	0.90
Y49G5B.1	0.90
Y37B11A.2	0.89
C36A4.5	0.89
ptr-2	0.89
R102.5	0.89
T01C8.2	0.89
C06E1.1	0.89
T02G5.11	0.89
Y55D9A.2	0.89
glp-1	0.89
C09E7.8	0.89
rfc-3	0.89
F54E12.2	0.89
smp-1	0.89
Y32B12B.4	0.88
Y102A11A.9	0.88
pme-1	0.88

Table E2 (Continued)

Gene Name	log_2 Fold
szy-4	0.88
gei-12	0.88
ZC204.12	0.88
C34E10.8	0.88
vab-1	0.88
fog-1	0.88
fbxa-121	0.88
kgb-1	0.88
Y54G11A.4	0.88
oac-58	0.88
sox-4	0.88
C13A2.3	0.88
tpxl-1	0.88
C30G12.1	0.88
B0393.3	0.88
pme-6	0.88
mex-3	0.88
spsb-2	0.88
myo-2	0.87
gld-3	0.87
tbx-36	0.87
dna-2	0.87
F11E6.7	0.87
C50F4.9	0.87
ora-1	0.87
hmit-1.1	0.87
C29F9.4	0.87
T22F7.4	0.87
T02B5.1	0.87
ZK1053.4	0.87
T13H5.6	0.87
ZC190.4	0.87
F59C6.14	0.86
tdc-1	0.86
E01G4.5	0.86
F44F1.4	0.86
Y34F4.4	0.86
mnp-1	0.86
abi-1	0.86
apx-1	0.86
Y50D4A.6	0.86
nlp-2	0.86
F21F3.3	0.86
inx-22	0.86
nspc-19	0.86
ugt-16	0.86
lon-2	0.86
del-10	0.85
Y60A3A.8	0.85
fbxa-199	0.85
F11A5.9	0.85
F49F1.5	0.85
K10G6.5	0.85
fbxa-3	0.85
his-40	0.85
bath-4	0.85
pef-1	0.85
clec-233	0.84
Y110A2AL.3	0.84
ZK384.4	0.84
C01B4.7	0.84
T26H5.10	0.84
lrg-1	0.84
rga-3	0.84
hke-4.1	0.84
lys-3	0.84
oac-31	0.84
K01G5.3	0.84
C39E9.10	0.84
F55A4.4	0.84
ZC47.8	0.83
gar-3	0.83
W02F12.3	0.83
Y57A10A.31	0.83
ugt-18	0.83
K03H4.2	0.83
C09H10.5	0.83
maco-1	0.83
Y73B3A.1	0.83
vhp-1	0.83
sma-1	0.83
vap-1	0.83
flp-19	0.83
fbxa-209	0.83
K02F6.7	0.83
egg-5	0.83
C41D11.4	0.83
Y22D7AR.2	0.83
R09A1.3	0.83
F16H6.10	0.83
M02D8.6	0.83
clec-91	0.83
C08G5.7	0.83
mod-5	0.83
ZC443.4	0.82
col-54	0.82
F14H3.5	0.82
srr-6	0.82
C27D9.1	0.82
gld-4	0.82
C05C10.5	0.82
fbxa-88	0.82
Y87G2A.7	0.82
tat-3	0.82
Y48G1BM.6	0.82
F12A10.8	0.82
Y39E4B.5	0.82
Y34F4.1	0.82
rhy-1	0.82
rog-1	0.82
cya-1	0.82
pzf-1	0.82
pad-2	0.82
hmbx-1	0.82
F44E7.5	0.81
egal-1	0.81
F52D2.12	0.81
acs-13	0.81
K09F6.10	0.81
ttx-1	0.81
egg-2	0.81
Y102A11A.3	0.81
fbxa-98	0.81
mca-1	0.81
nspc-17	0.81
nipi-3	0.81
Y48G1BL.6	0.81
F27D9.2	0.81
K08F11.1	0.81
T11F9.12	0.81
dyf-3	0.81
B0035.6	0.81
spd-2	0.81
dyf-17	0.81
F11C7.6	0.80
dpy-6	0.80
unc-71	0.80
Y48E1B.8	0.80
Y65A5A.2	0.80
mcm-3	0.80
set-3	0.80
Y71F9AR.2	0.80
F42A6.3	0.80
K01A2.9	0.80
M04C3.2	0.80
cul-6	0.80
lag-1	0.80
Y110A7A.4	0.80
Y70G10A.3	0.80
hpl-1	0.80
twk-33	0.80
zig-3	0.80
aqp-7	0.80
T13F2.6	0.80
mre-11	0.80
K08D8.12	0.80
C47G2.7	0.80
Y57G11C.51	0.80
C25F9.5	0.80

Table E2 (Continued)

Gene Name	log_2 Fold
age-1	0.80
Y38H8A.3	0.79
Y43F8C.3	0.79
sas-6	0.79
ttm-4	0.79
C14B1.7	0.79
F59A6.5	0.79
clc-1	0.79
F49E2.5	0.79
his-38	0.79
rskn-1	0.79
igcm-1	0.79
F48G7.2	0.79
mei-2	0.79
D1044.6	0.79
Y17G7B.13	0.79
ZK177.1	0.79
Y71H2AM.14	0.79
daf-2	0.79
unc-34	0.79
F22F7.8	0.78
Y71A12C.2	0.78
pvf-1	0.78
C49G7.7	0.78
fbxa-60	0.78
bath-1	0.78
R11H6.2	0.78
glt-5	0.78
pri-2	0.78
best-24	0.78
K10C8.1	0.78
com-1	0.78
lrr-1	0.78
B0238.9	0.78
mom-2	0.78
C06A1.4	0.78
nop-1	0.78
gpd-4	0.78
trr-1	0.77
C39H7.4	0.77

Gene Name	log_2 Fold
par-3	0.77
Y46H3C.7	0.77
glct-6	0.77
klf-1	0.77
rom-1	0.77
AC8.9	0.77
xpc-1	0.77
ergo-1	0.77
hmg-20	0.77
skr-3	0.77
nhr-2	0.77
klp-19	0.77
aakg-5	0.77
K01A12.4	0.77
ptc-1	0.77
skpt-1	0.77
scl-2	0.77
C52A10.2	0.77
fsn-1	0.77
C42D8.1	0.77
F28B3.4	0.77
mcm-5	0.76
gadr-6	0.76
C05G5.2	0.76
T08B2.11	0.76
mel-28	0.76
vrk-1	0.76
C01F1.6	0.76
pitr-3	0.76
Y41D4B.4	0.76
Y51F10.2	0.76
magu-2	0.76
mes-1	0.76
ZK418.13	0.76
H02I12.5	0.76
fbxc-2	0.76
hpo-42	0.76
T24B8.7	0.75
skr-4	0.75
rin-1	0.75
plk-3	0.75
tag-89	0.75

Gene Name	log_2 Fold
aat-5	0.75
rod-1	0.75
tir-1	0.75
fbxa-150	0.75
myo-1	0.75
F07A11.2	0.75
die-1	0.75
scc-1	0.75
flp-27	0.75
atm-1	0.75
K10D3.10	0.75
tftc-1	0.75
C45B11.2	0.75
C34B4.2	0.75
ZC190.5	0.75
math-24	0.75
lpin-1	0.75
vps-39	0.75
hpo-11	0.74
T01D3.1	0.74
zwl-1	0.74
ani-2	0.74
F09A5.2	0.74
snf-6	0.74
scav-2	0.74
hex-4	0.74
C27C12.3	0.74
1-Apr	0.74
Y41C4A.8	0.74
cku-70	0.74
Y43F8B.14	0.74
ulp-4	0.74
T22D1.5	0.74
W02G9.4	0.74
fbxa-11	0.74
math-42	0.74
F33H2.5	0.74
K10C3.4	0.74
elt-2	0.73
prg-1	0.73
nac-1	0.73
flh-2	0.73

Gene Name	log_2 Fold
Y53F4B.45	0.73
K11D2.1	0.73
nmy-2	0.73
F28B3.1	0.73
C50B6.3	0.73
C14C11.2	0.73
lst-1	0.73
F27E5.9	0.73
npp-14	0.73
T24F1.2	0.73
F29G9.2	0.73
VY35H6BL.1	0.73
spd-5	0.73
rsa-2	0.73
Y46G5A.43	0.73
F19B2.5	0.73
fli-1	0.73
C34C12.2	0.72
polg-1	0.72
gana-1	0.72
Y53F4B.13	0.72
W02D9.10	0.72
sys-1	0.72
C44B9.3	0.72
cyp-36A1	0.72
C27D9.2	0.72
hcp-1	0.72
nas-9	0.72
Y54G2A.21	0.72
Y68A4A.13	0.72
fbxa-107	0.72
Y116F11B.6	0.72
R08E3.2	0.71
C04F12.1	0.71
mop-25.3	0.71
nlp-14	0.71
ksr-2	0.71
syd-9	0.71
R102.2	0.71

Table E2 (Continued)

Gene Name	log_2 Fold
Y45G12C.16	0.71
mei-1	0.71
F01D5.5	0.71
C01G6.3	0.71
dgtr-1	0.71
kel-8	0.71
H11E01.2	0.71
swt-1	0.71
B0281.3	0.71
nep-1	0.71
MTCE.33	0.71
ZK863.8	0.71
lec-7	0.71
F13H8.1	0.71
nhr-178	0.70
F49F1.1	0.70
Y17G7B.20	0.70
mes-4	0.70
capg-2	0.70
T19C4.1	0.70
srh-2	0.70
T27A3.7	0.70
H31G24.3	0.70
fbxc-5	0.70
ugt-8	0.70
isw-1	0.70
F10E9.3	0.70
clk-2	0.70
cdh-10	0.70
dgk-4	0.70
Y56A3A.36	0.70
F39B2.1	0.70
Y57A10A.1	0.70
dod-6	0.70
srw-85	0.70
C39E9.7	0.70
sgo-1	0.70
F25E5.4	0.70
Y50D4C.5	0.70
F59E12.1	0.70

Gene Name	log_2 Fold
math-39	0.70
C39E9.12	0.70
cyb-3	0.70
aap-1	0.70
nos-2	0.70
F28C6.2	0.70
swsn-4	0.70
C25A1.1	0.70
knl-1	0.70
obr-3	0.69
Y54G2A.19	0.69
K07B1.8	0.69
F54D5.5	0.69
F58D5.5	0.69
fbxa-182	0.69
W03A5.1	0.69
EEED8.2	0.69
T01C3.3	0.69
F26G1.1	0.69
his-48	0.69
igdb-1	0.69
H11L12.1	0.69
duox-2	0.69
tlp-1	0.69
F15D4.2	0.69
dpy-26	0.69
1-Sep	0.69
wrm-1	0.69
tyr-1	0.69
C33D9.13	0.69
par-4	0.69
H14E04.1	0.69
his-72	0.69
lin-36	0.69
B0511.12	0.69
F55A11.7	0.69
ape-1	0.69
Y76B12C.6	0.69
arid-1	0.69
best-17	0.69
chs-2	0.69

Gene Name	log_2 Fold
nhl-2	0.69
C48B4.7	0.69
C05A9.2	0.69
F54D5.9	0.69
F19C7.2	0.69
F32D1.7	0.69
C17D12.5	0.68
drp-1	0.68
B0507.2	0.68
cebp-1	0.68
mpst-5	0.68
F13C5.5	0.68
otpl-3	0.68
W09G12.9	0.68
C29F9.3	0.68
secs-1	0.68
mcm-7	0.68
Y53H1B.2	0.68
ppw-1	0.68
lat-1	0.68
nekl-1	0.68
cdt-1	0.68
W02G9.10	0.68
nspc-12	0.68
C07E3.3	0.68
pes-5	0.68
T04F8.7	0.68
exc-4	0.68
smc-4	0.68
C13B7.6	0.68
crn-2	0.68
C25D7.12	0.68
T08D2.3	0.68
rig-3	0.68
aka-1	0.67
srsx-34	0.67
C27F2.7	0.67
efa-6	0.67
Y111B2A.3	0.67
tag-120	0.67
hmr-1	0.67
Y75B8A.25	0.67

Gene Name	log_2 Fold
cyk-4	0.67
Y48G1C.1	0.67
bir-2	0.67
Y43F8B.24	0.67
tol-1	0.67
set-2	0.67
tag-278	0.67
hmp-1	0.67
K11D2.4	0.67
T04F3.2	0.67
F35D2.3	0.67
mfb-1	0.66
H21P03.2	0.66
cogc-3	0.66
ikke-1	0.66
pqn-20	0.66
Y69A2AR.32	0.66
fbxa-61	0.66
ptr-13	0.66
sas-4	0.66
cec-2	0.66
K11H3.8	0.66
Y54G2A.73	0.66
F08F3.8	0.66
W09D6.1	0.66
rfc-1	0.66
ugt-25	0.66
F45F2.11	0.66
gras-1	0.66
sup-26	0.66
F29G9.1	0.66
clec-146	0.66
wrn-1	0.66
swsn-9	0.66
Y48G1BL.5	0.66
Y39A3CR.3	0.66
R02D5.3	0.66
K07H8.9	0.66
lin-24	0.66

Table E2 (Continued)

Gene Name	log_2 Fold
T04D3.5	0.66
Y54F10BM.9	0.66
sax-7	0.66
ZK1290.14	0.66
F28C6.4	0.66
gmeb-4	0.65
D1043.1	0.65
fbn-1	0.65
athp-2	0.65
H04D03.3	0.65
rcor-1	0.65
ife-5	0.65
Y73B6BL.12	0.65
C37C3.9	0.65
nspc-3	0.65
ugt-13	0.65
C36B1.13	0.65
pck-1	0.65
nspc-15	0.65
acs-19	0.65
swsn-7	0.65
tag-52	0.65
F52H3.4	0.65
srgp-1	0.65
H04M03.3	0.65
C48D1.5	0.65
C30F12.3	0.65
K11G9.5	0.65
W03F9.2	0.65
F45F2.10	0.65
Y57G11C.5	0.65
F45D3.4	0.65
Y97E10AR.1	0.65
igeg-1	0.65
M116.5	0.65
rom-4	0.64
dom-3	0.64
ZK973.1	0.64
F14F9.8	0.64

Gene Name	log_2 Fold
Y67H2A.10	0.64
nhr-23	0.64
F32A7.5	0.64
sur-2	0.64
viln-1	0.64
osta-3	0.64
T27A1.2	0.64
ets-6	0.64
mat-2	0.64
F14D7.2	0.64
R03H10.2	0.64
C06A1.12	0.64
sas-5	0.64
duo-1	0.64
C41H7.4	0.64
F30F8.10	0.64
lec-8	0.64
M04F3.5	0.64
npp-21	0.64
scl-3	0.64
ifp-1	0.64
F52B11.5	0.64
Y38E10A.14	0.64
Y110A7A.9	0.64
ebp-2	0.64
Y39A3CL.1	0.64
rrc-1	0.64
Y52B11A.11	0.64
Y48A6C.1	0.64
nhl-1	0.64
Y41E3.1	0.63
F52C12.1	0.63
sup-17	0.63
T16G1.4	0.63
nhr-15	0.63
gei-14	0.63
Y48G1C.10	0.63
Y38F2AR.6	0.63
hsp-12.3	0.63

Gene Name	log_2 Fold
lin-13	0.63
R13H4.5	0.63
anr-34	0.63
dsh-2	0.63
unc-17	0.63
cpsf-4	0.63
F46B6.5	0.63
shc-2	0.63
srr-4	0.63
zim-1	0.63
pak-2	0.63
H10D18.5	0.63
gon-1	0.63
R01H10.7	0.63
mdt-28	0.63
rabx-5	0.63
gon-4	0.63
F25D7.4	0.63
F13G3.6	0.63
let-756	0.63
R11D1.1	0.63
Y50D4C.3	0.63
aly-1	0.63
met-1	0.63
rilp-1	0.63
Y39B6A.43	0.62
his-45	0.62
T23B5.3	0.62
tag-343	0.62
ZC250.4	0.62
mboa-3	0.62
nprl-3	0.62
K06A5.1	0.62
unc-40	0.62
nasp-2	0.62
enu-3	0.62
ubxn-6	0.62
nspc-14	0.62
gon-14	0.62
npr-28	0.62
athp-1	0.62
C17E4.3	0.62

Gene Name	log_2 Fold
hlh-2	0.62
Y71F9B.13	0.62
nlp-16	0.62
C49A9.3	0.62
F57H12.5	0.62
top-2	0.62
C27F2.8	0.62
rbr-2	0.62
drsh-1	0.62
Y48G8AL.10	0.62
smc-6	0.62
C08F8.3	0.62
ect-2	0.62
pdf-1	0.61
egrh-1	0.61
C40H1.8	0.61
set-14	0.61
dcr-1	0.61
epg-6	0.61
T24H10.4	0.61
trcs-2	0.61
best-13	0.61
sygl-1	0.61
F59A7.5	0.61
cpb-3	0.61
W09G12.7	0.61
ZC317.7	0.61
Y51A2D.7	0.61
C31H1.8	0.61
daam-1	0.61
glh-2	0.61
odd-2	0.61
dvc-1	0.61
dhhc-1	0.61
C41C4.18	0.61
math-41	0.61
F44G3.2	0.61
zyg-9	0.60
F56F11.4	0.60
H05L14.2	0.60
F33H2.3	0.60

Table E2 (Continued)

Gene Name	log_2 Fold
flcn-1	0.60
svop-1	0.60
nspc-9	0.60
B0336.5	0.60
deps-1	0.60
C41H7.5	0.60
C16C8.11	0.60
C34C6.2	0.60
cpg-4	0.60
C48B6.3	0.60
tbc-2	0.60
eps-8	0.60
hyl-1	0.60
ptp-2	0.60
aqp-8	0.60
F14B4.2	0.60
K06B9.4	0.60
F23H11.4	0.60
Y55F3AM.14	0.60
hcp-4	0.60
egl-18	0.60
F35F11.2	0.60
D1081.7	0.60
W02B8.2	0.60
nhr-231	0.60
C02F12.5	0.60
lin-54	0.60
jmjc-1	0.60
F37A8.5	0.60
R13D7.2	0.60
fbxa-67	0.60
Y10G11A.90	0.60
T24D1.2	0.60
unc-26	0.60
Y53F4B.9	0.60
F35G12.4	0.60
M57.1	0.59
K05F1.1	0.59
Y104H12D.2	0.59
CC8.2	0.59

Gene Name	log_2 Fold
T19A5.1	0.59
F15A8.6	0.59
kca-1	0.59
arrd-13	0.59
cpna-5	0.59
snf-11	0.59
alx-1	0.59
R07E3.4	0.59
mbk-2	0.59
dct-17	0.59
C13G3.1	0.59
max-1	0.59
klp-15	0.59
zen-4	0.59
orc-1	0.59
T07D1.2	0.59
smg-9	0.59
K11D12.12	0.59
Y19D10A.4	0.59
ugt-43	0.59
gck-2	0.59
pqn-15	0.59
B0432.7	0.59
M60.4	0.59
dnj-5	0.59
F55H2.5	0.59
gna-2	0.59
swp-1	0.59
dmd-6	0.59
brd-1	0.59
D1007.5	0.59
slr-2	0.59
B0212.3	0.59
ztf-6	0.59
hpo-4	0.58
F31D4.5	0.58
H06I04.1	0.58
R08E3.1	0.58
cye-1	0.58
glna-1	0.58
dmsr-2	0.58
scrm-1	0.58

Gene Name	log_2 Fold
rde-4	0.58
nhr-3	0.58
pig-1	0.58
C06G4.1	0.58
B0432.8	0.58
ZC328.2	0.58
cpr-3	0.58
zag-1	0.58
igeg-2	0.58
C28A5.1	0.58
riok-1	0.58
mbtr-1	0.58
C27D8.4	0.58
hoe-1	0.58
poml-4	0.58
asd-1	0.58
F14F9.4	0.58
cdl-1	0.58
gpdh-1	0.57
farl-11	0.57
xpo-1	0.57
sqrd-1	0.57
F55G1.15	0.57
cnk-1	0.57
F54D10.5	0.57
Y82E9BR.23	0.57
spe-5	0.57
nspd-6	0.57
rict-1	0.57
pptr-2	0.57
C09D4.4	0.57
C42C1.8	0.57
C55B6.1	0.57
ZC477.5	0.57
hum-6	0.57
sam-10	0.57
mtm-9	0.57
F33H2.2	0.57
B0041.11	0.57
mys-2	0.57
egl-27	0.57

Gene Name	log_2 Fold
pqn-62	0.57
R02D3.8	0.57
ckk-1	0.57
ceh-21	0.57
unc-53	0.57
Y51F10.4	0.57
F40F8.4	0.57
C49C8.5	0.57
hst-1	0.57
osm-11	0.57
T04C4.1	0.57
F30F8.1	0.57
D2096.11	0.57
pkc-3	0.57
hcp-3	0.57
panl-2	0.57
R06C7.2	0.57
F35C11.5	0.57
chaf-2	0.57
T19B4.5	0.56
K10D3.4	0.56
cyp-34A2	0.56
F17C11.7	0.56
icp-1	0.56
larp-5	0.56
siah-1	0.56
mig-5	0.56
ifd-2	0.56
try-1	0.56
sos-1	0.56
gad-1	0.56
Y55F3AM.6	0.56
Y48C3A.18	0.56
Y17G7B.10	0.56
pif-1	0.56
ssl-1	0.56
T02B11.4	0.56
sqv-6	0.56
Y54F10BM.1	0.56
hsr-9	0.56

Table E2 (Continued)

Gene Name	log_2 Fold
Y51H7C.3	0.56
czw-1	0.56
bre-3	0.56
nspc-13	0.56
lin-37	0.56
Y55F3BR.2	0.56
C31E10.6	0.56
mpst-6	0.56
snet-1	0.56
C50E3.13	0.56
ceh-38	0.56
klp-16	0.56
T20F5.6	0.56
utx-1	0.56
msh-5	0.56
M04F3.6	0.56
eri-9	0.56
deg-3	0.56
wnk-1	0.55
kin-18	0.55
kle-2	0.55
mlh-1	0.55
atx-3	0.55
C34C12.7	0.55
sin-3	0.55
gadr-5	0.55
Y54F10AM.11	0.55
tat-2	0.55
F52D2.7	0.55
ZK131.11	0.55
air-1	0.55
T07F8.4	0.55
Y43E12A.3	0.55
tbc-9	0.55
exoc-8	0.55
sago-2	0.55
F19F10.11	0.55
spc-1	0.55
C18B2.4	0.55
dog-1	0.55

Gene Name	log_2 Fold
hpo-16	0.55
rde-11	0.55
C18H2.2	0.55
chtl-1	0.55
clec-90	0.55
Y65B4BL.4	0.55
Y71F9AR.3	0.55
B0205.9	0.55
F35G12.5	0.55
comt-3	0.55
cdh-4	0.55
nlp-9	0.55
sup-35	0.55
F53F8.5	0.55
F25E5.1	0.55
T01C3.9	0.54
F54D11.2	0.54
F30A10.3	0.54
Y55B1AR.2	0.54
tim-1	0.54
lin-49	0.54
mig-22	0.54
btf-1	0.54
F16B4.2	0.54
B0524.6	0.54
C44B7.10	0.54
hda-10	0.54
F59A3.4	0.54
F21A10.2	0.54
fncm-1	0.54
Y116A8C.13	0.54
flt-1	0.54
plrg-1	0.54
smgl-2	0.54
ceh-100	0.54
sydn-1	0.54
ctns-1	0.54
ZK418.7	0.54
nprl-2	0.54
R06A4.2	0.54

Gene Name	log_2 Fold
pcn-1	0.54
F33E11.2	0.54
nfyb-1	0.54
Y73B6BL.4	0.54
evl-18	0.54
K07D4.9	0.54
T01D3.3	0.54
Y73B3A.4	0.54
aly-2	0.54
capg-1	0.54
W01A8.5	0.54
ubc-18	0.54
F36D4.5	0.54
cdc-25.1	0.54
rad-26	0.54
usp-48	0.54
fbxc-45	0.54
tag-77	0.54
F13A7.14	0.54
C52A10.1	0.54
nud-2	0.54
mes-2	0.54
F17C11.10	0.54
C47D12.2	0.54
ZC239.13	0.54
F09A5.4	0.53
daf-19	0.53
pqn-85	0.53
F45D11.16	0.53
C33C12.9	0.53
Y57G11C.36	0.53
Y58A7A.4	0.53
H19M22.3	0.53
let-418	0.53
Y82E9BR.13	0.53
fdps-1	0.53
F09C8.2	0.53
cdc-42	0.53
mrt-1	0.53
unc-5	0.53

Gene Name	log_2 Fold
W02B3.4	0.53
Y106G6G.4	0.53
C34B7.2	0.53
Y48C3A.12	0.53
Y39B6A.42	0.53
D2096.7	0.53
C27A12.6	0.53
C24H12.5	0.53
nhr-31	0.53
C06A5.1	0.53
rnf-1	0.53
cpn-1	0.53
Y39D8A.1	0.53
spe-41	0.53
clr-1	0.53
gmn-1	0.53
Y37E11B.2	0.53
lin-45	0.53
plk-1	0.53
T05E8.3	0.53
rep-1	0.53
Y62E10A.14	0.53
R07E4.5	0.53
clp-3	0.53
ztf-28	0.53
T03F1.7	0.53
F53B3.5	0.53
K10D11.6	0.53
T04A11.1	0.53
Y56A3A.28	0.53
scc-3	0.53
T12G3.7	0.53
Y69H2.7	0.53
F38B7.2	0.53
K10C8.3	0.52
wapl-1	0.52
M02B7.2	0.52
asfl-1	0.52
aat-9	0.52
tps-1	0.52

Table E2 (Continued)

Gene Name	log_2 Fold
dpy-21	0.52
Y17G9B.9	0.52
lem-3	0.52
Y73B3B.5	0.52
bath-42	0.52
acs-4	0.52
cash-1	0.52
akt-1	0.52
pis-1	0.52
xnd-1	0.52
ctg-2	0.52
src-1	0.52
eak-7	0.52
Y71H2B.5	0.52
set-5	0.52
pqn-41	0.52
rpa-1	0.52
unc-22	0.52
ttll-5	0.52
ire-1	0.52
vps-37	0.52
T21C9.13	0.52
msh-6	0.52
C38C10.2	0.52
Y69A2AR.1	0.52
F08F3.6	0.52
ubc-25	0.52
lig-1	0.52
zif-1	0.52
gck-1	0.52
crml-1	0.52
F21D5.1	0.52
Y37H9A.3	0.52
C50F2.2	0.51
srap-1	0.51
Y71H2AM.2	0.51
C36B1.11	0.51
twk-34	0.51
W05F2.7	0.51
thoc-3	0.51
Y71H2AM.15	0.51
pgp-9	0.51
cls-1	0.51
syp-1	0.51
F57B10.9	0.51
Y50D4C.6	0.51
lin-9	0.51
Y22D7AR.6	0.51
ifet-1	0.51
fbxa-123	0.51
rbg-3	0.51
R04D3.3	0.51
Y73B3A.3	0.51
nfya-2	0.51
H18N23.2	0.51
spe-29	0.51
prom-1	0.51
C14C11.7	0.51
dhc-1	0.51
K11G12.6	0.51
C06A5.3	0.51
smg-8	0.51
bub-1	0.51
top-3	0.51
cls-3	0.51
K06G5.1	0.51
klp-11	0.51
tag-115	0.51
cyn-4	0.51
dut-1	0.51
lev-1	0.51
ubc-23	0.51
Y48A5A.1	0.51
Y6B3B.4	0.51
edc-3	0.51
wago-1	0.51
Y59C2A.3	0.51
W02D7.6	0.51
spat-1	0.50
nspc-16	0.50
zip-5	0.50
tlk-1	0.50
Y65B4BR.1	0.50
Y58A7A.3	0.50
C02F12.8	0.50
Y34D9A.3	0.50
plst-1	0.50
hda-1	0.50
sdc-1	0.50
T08B6.9	0.50
C32D5.11	0.50
rae-1	0.50
Y2H9A.4	0.50
F39G3.5	0.50
pmp-3	0.50
tftc-3	0.50
dnj-8	0.50
ppfr-1	0.50
ehs-1	0.50
sorb-1	0.50
rcq-5	0.50
F36G3.1	0.50
Y6D1A.1	0.50
daf-25	0.50
far-8	0.50
car-1	0.50
cah-4	0.50
F10C2.4	0.50
brf-1	0.50
R03G5.6	0.50
Y48E1C.2	0.50
unc-76	0.50
C05C10.2	0.50
set-9	0.50
zyg-11	0.50
klp-7	0.50
Y67D8B.4	0.50
ghi-1	0.50
npp-3	0.50
ima-2	0.50
phf-10	0.50
lst-4	0.50
W05H7.1	0.50
Y40D12A.1	0.50
cyp-31A3	0.50
M01E5.3	0.50
C32D5.3	0.50
nlg-1	0.50
cand-1	0.50
Y111B2A.24	0.50
C27C7.1	0.50
mab-20	0.50
C18F10.7	0.50
itsn-1	0.50
F42G9.6	0.50
T05G5.9	0.50
rbc-2	0.50
spr-5	0.50
dbr-1	0.49
lin-53	0.49
ttn-1	0.49
tnt-3	0.49
attf-6	0.49
C39F7.5	0.49
B0261.7	0.49
cdk-2	0.49
C10G11.7	0.49
pab-2	0.49
T23H2.3	0.49
T04A8.7	0.49
C36E8.4	0.49
hex-3	0.49
F52C12.3	0.49
sptl-2	0.49
tep-1	0.49
F26H9.2	0.49
smgl-1	0.49
ced-5	0.49
fhod-1	0.49
H11E01.3	0.49
gld-1	0.49
sax-2	0.49

Table E2 (Continued)

Gene Name	log_2 Fold
H05C05.2	0.49
hse-5	0.49
bath-28	0.49
M4.1	0.49
C27B7.2	0.49
C35A11.2	0.49
ubxn-4	0.49
M57.2	0.49
hpo-20	0.49
flp-9	0.49
C14A4.12	0.49
F08B12.4	0.49
pqn-89	0.49
imb-2	0.49
T10H10.2	0.49
B0024.13	0.49
wrb-1	0.49
cogc-8	0.49
emr-1	0.49
daz-1	0.49
F52C9.1	0.49
T02B11.3	0.49
ric-8	0.49
F49E2.2	0.49
ZK809.5	0.49
R07C12.2	0.49
Y45G5AM.7	0.48
H03A11.2	0.48
wht-7	0.48
C50F4.1	0.48
haf-2	0.48
F49E8.7	0.48
npp-8	0.48
gpa-16	0.48
F45D3.3	0.48
dnj-14	0.48
bath-29	0.48
C14A4.11	0.48
dlk-1	0.48
spe-15	0.48
tag-218	0.48

Gene Name	log_2 Fold
F45D3.2	0.48
aho-3	0.48
T19B10.8	0.48
M01G5.1	0.48
Y69A2AL.2	0.48
phf-15	0.48
K09D9.1	0.48
bath-43	0.48
Y48G1C.12	0.48
thoc-2	0.48
unc-57	0.48
C49F5.6	0.48
F55A3.7	0.48
set-25	0.48
C08B11.8	0.48
rad-51	0.48
Y22D7AL.7	0.48
C54D10.13	0.48
cyp-31A5	0.48
sel-8	0.48
Y53G8B.2	0.48
ess-2	0.48
D2096.12	0.48
Y77E11A.7	0.48
cdh-7	0.48
ave-1	0.48
mdt-6	0.48
F52H3.2	0.48
taf-6.1	0.48
glh-3	0.48
sop-2	0.48
pac-1	0.48
T07D4.2	0.48
F47B8.2	0.48
tli-1	0.48
clp-2	0.48
T04H1.2	0.48
jmjd-2	0.48
sop-3	0.47
Y41E3.7	0.47
C53C9.2	0.47

Gene Name	log_2 Fold
F58F9.3	0.47
mdt-30	0.47
Y82E9BL.18	0.47
nrd-1	0.47
orc-2	0.47
T08G11.1	0.47
Y24D9B.1	0.47
nca-2	0.47
Y48G1A.2	0.47
bath-13	0.47
Y48A6B.10	0.47
Y67D8C.9	0.47
cmk-1	0.47
F53H1.4	0.47
H34C03.2	0.47
swsn-1	0.47
Y50D7A.2	0.47
K07H8.1	0.47
kin-4	0.47
F45D11.15	0.47
ZK1025.1	0.47
F07C6.4	0.47
mdt-27	0.47
Y39G10AR.9	0.47
npl-4.1	0.47
dkf-2	0.47
vps-11	0.47
C41H7.3	0.47
M01B12.4	0.47
gei-17	0.47
K09H9.7	0.47
pitr-1	0.47
zfp-2	0.47
F40F8.11	0.47
vbh-1	0.47
C05C8.7	0.47
plk-2	0.47
dnc-4	0.47
vps-35	0.47
csb-1	0.47

Gene Name	log_2 Fold
sel-10	0.46
K10B4.3	0.46
F33H1.4	0.46
rabn-5	0.46
C25H3.11	0.46
mut-7	0.46
set-24	0.46
csk-1	0.46
C50E3.5	0.46
puf-8	0.46
dkf-1	0.46
npp-9	0.46
noca-1	0.46
D2045.2	0.46
pqn-31	0.46
W08G11.3	0.46
dur-1	0.46
fbxa-157	0.46
trim-9	0.46
wip-1	0.46
M01A10.1	0.46
K03B4.2	0.46
M01H9.3	0.46
T05F1.4	0.46
cab-1	0.46
cil-1	0.46
pqn-21	0.46
sdc-2	0.46
cyb-2.1	0.46
ZK688.5	0.46
dcaf-1	0.46
vps-4	0.46
T12C9.7	0.46
vacl-14	0.46
cdc-6	0.46
tbp-1	0.46
cyp-34A4	0.46
ppfr-2	0.46
kcc-1	0.46
W03G9.3	0.46
F01G4.4	0.46

Table E2 (Continued)

Gene Name	log_2 Fold
Y69A2AR.22	0.46
daf-16	0.46
mys-1	0.45
orc-3	0.45
Y76A2B.4	0.45
F59E12.9	0.45
F59A7.8	0.45
fozi-1	0.45
inft-2	0.45
lsy-12	0.45
B0353.1	0.45
C34C6.7	0.45
smg-3	0.45
nra-1	0.45
npp-7	0.45
Y43F8C.6	0.45
F33E11.3	0.45
Y37A1A.2	0.45
him-6	0.45
Y67D2.2	0.45
hmp-2	0.45
ztf-8	0.45
Y37E11AM.2	0.45
cogc-5	0.45
B0304.2	0.45
F55A3.3	0.45
klp-20	0.45
sid-1	0.45
K06B9.2	0.45
ZC308.4	0.45
mig-38	0.45
Y87G2A.1	0.45
cki-1	0.45
clp-4	0.45
snx-14	0.45
Y102A11A.2	0.45
ncr-1	0.45
F53F4.12	0.45
col-103	0.45
tyr-4	0.45

Gene Name	log_2 Fold
pdfr-1	0.45
F25H2.6	0.45
fnci-1	0.45
abts-4	0.45
fer-1	0.45
C25A8.5	0.45
flp-18	0.45
R05H10.3	0.45
Y105E8A.14	0.45
T09F3.5	0.45
C50C3.2	0.45
F49C12.9	0.45
E01A2.6	0.45
panl-3	0.45
nars-1	0.45
pbrm-1	0.45
F58G11.3	0.45
rba-1	0.45
T04C9.1	0.45
C30F12.4	0.45
Y38F2AR.13	0.45
Y54E2A.8	0.45
C16A11.3	0.45
pqn-47	0.45
B0403.5	0.45
tag-341	0.45
ccpp-1	0.44
K04G7.1	0.44
pgl-3	0.44
Y65B4A.1	0.44
mom-4	0.44
rsks-1	0.44
atf-6	0.44
npp-19	0.44
K01A2.10	0.44
cyb-1	0.44
H40L08.1	0.44
Y73B3A.21	0.44
let-502	0.44
lem-2	0.44

Gene Name	log_2 Fold
Y54E10A.12	0.44
rmd-1	0.44
ceh-20	0.44
pqe-1	0.44
ztf-23	0.44
T28H10.3	0.44
K12D12.5	0.44
Y54F10AR.1	0.44
linc-6	0.44
ttr-26	0.44
swsn-6	0.44
F54D1.6	0.44
Y42H9AR.4	0.44
F20C5.3	0.44
pdr-1	0.44
C37A2.8	0.44
C35D10.7	0.44
klp-18	0.44
F36A2.13	0.44
aex-3	0.44
T01E8.1	0.44
clec-86	0.44
C14B1.3	0.44
prp-3	0.44
C16C10.1	0.44
W07E11.1	0.44
him-18	0.44
ifd-1	0.44
W03G9.2	0.44
chd-1	0.44
Y54E2A.4	0.44
tcc-1	0.44
sac-1	0.44
Y67D2.6	0.44
T23G11.7	0.44
D1081.9	0.43
F39E9.7	0.43
gei-6	0.43
MTCE.7	0.43
T08A11.1	0.43

Gene Name	log_2 Fold
ZK524.4	0.43
dcp-66	0.43
C25G4.2	0.43
K12H6.2	0.43
W07A8.2	0.43
szy-20	0.43
Y65B4BL.3	0.43
acs-16	0.43
M110.3	0.43
sms-1	0.43
nhx-5	0.43
R04F11.3	0.43
mrp-7	0.43
rsd-2	0.43
ing-3	0.43
unc-69	0.43
cec-10	0.43
rrf-3	0.43
F31C3.3	0.43
rsd-6	0.43
hum-7	0.43
F45D11.14	0.43
let-526	0.43
F30B5.4	0.43
F54B3.1	0.43
max-2	0.43
ccr-4	0.43
C33A12.19	0.43
cyl-1	0.43
rec-8	0.43
K07H8.2	0.43
nhr-5	0.43
fkh-9	0.43
C06B8.7	0.43
wsp-1	0.43
him-17	0.43
C10G11.6	0.43
C06A5.6	0.43
cul-2	0.42
mon-2	0.42
npl-4.2	0.42
npp-4	0.42

Table E2 (Continued)

Gene Name	log_2 Fold
cyb-2.2	0.42
F14B8.5	0.42
T25D10.4	0.42
ima-1	0.42
cas-2	0.42
Y73F8A.24	0.42
attf-3	0.42
tbc-14	0.42
fbxa-156	0.42
nfx-1	0.42
F28H6.4	0.42
otub-2	0.42
Y82E9BR.21	0.42
Y57A10A.25	0.42
pad-1	0.42
fbxc-43	0.42
lam-2	0.42
R05D11.9	0.42
C27A12.9	0.42
C38H2.2	0.42
ZK813.4	0.42
F15E6.3	0.42
bath-44	0.42
K02B12.5	0.42
clec-205	0.42
C14F11.6	0.42
moa-2	0.42
hda-2	0.42
Y54G11A.1	0.42
F08F8.10	0.42
fbxa-79	0.42
F33H1.3	0.42
Y73F4A.2	0.42
eea-1	0.42
M70.4	0.42
Y47D3A.29	0.42
dcap-1	0.42
crn-1	0.42
selb-1	0.42
mel-11	0.42
lin-15B	0.41
Y47G6A.29	0.41
arrd-7	0.41
F10E7.11	0.41
tbc-15	0.41
F58G1.2	0.41
tmd-2	0.41
bath-41	0.41
tsp-12	0.41
mak-1	0.41
M01E11.3	0.41
mrck-1	0.41
uba-1	0.41
T28F3.4	0.41
ZK484.3	0.41
atgp-2	0.41
F01G12.6	0.41
gap-3	0.41
nhr-48	0.41
sem-5	0.41
ced-2	0.41
hda-6	0.41
T09B9.4	0.41
R10F2.6	0.41
swt-6	0.41
dpf-5	0.41
F53F4.14	0.41
him-10	0.41
spr-2	0.41
C35C5.6	0.41
F26F2.7	0.41
C04G6.4	0.41
seu-1	0.41
lgl-1	0.41
tag-232	0.41
C26G2.2	0.41
C25F9.4	0.41
pqm-1	0.41
F54A3.6	0.41
K05F1.10	0.41
T10B11.8	0.41
F07H5.10	0.41
E01G4.3	0.41
F20D12.2	0.41
col-119	0.41
K01G5.9	0.41
Y44E3A.6	0.41
hmg-11	0.41
T09F5.12	0.41
C36E8.1	0.41
ZK616.5	0.41
fbxa-27	0.41
clec-62	0.41
K08A2.1	0.41
Y54G2A.26	0.40
W03A5.4	0.40
set-21	0.40
C18H9.3	0.40
cpsf-1	0.40
F22G12.5	0.40
F54D10.3	0.40
ntl-9	0.40
ubxn-3	0.40
K08A2.4	0.40
sbp-1	0.40
fzy-1	0.40
unc-94	0.40
dpl-1	0.40
rad-54	0.40
bet-1	0.40
T12A7.2	0.40
lin-26	0.40
pme-5	0.40
F42H10.6	0.40
unc-80	0.40
F08F8.9	0.40
clp-7	0.40
Y52B11A.9	0.40
C07A4.2	0.40
jmjd-1.2	0.40
cdh-1	0.40
zim-2	0.40
unc-23	0.40
C01G5.5	0.40
set-30	0.40
egl-9	0.40
Y73B3B.1	0.40
F59A3.2	0.40
T03F1.12	0.40
cid-1	0.40
gen-1	0.40
Y73B6BL.27	0.40
R11A8.7	0.40
sinh-1	0.40
ncx-2	0.40
hpo-3	0.40
tag-65	0.40
mog-3	0.40
gfi-2	0.40
rha-1	0.40
ttm-5	0.40
wdfy-2	0.40
ZC504.3	0.40
B0019.2	0.40
ZC262.7	0.40
R74.8	0.39
F25E2.3	0.39
R119.1	0.39
K04C2.3	0.39
ncl-1	0.39
Y41C4A.9	0.39
F34H10.3	0.39
mep-1	0.39
B0303.11	0.39
W05F2.4	0.39
F37D6.2	0.39
F55F8.9	0.39
F36D3.1	0.39
F37A4.1	0.39
B0412.3	0.39
F27C1.2	0.39
inx-21	0.39
thoc-1	0.39

Table E2 (Continued)

Gene Name	log_2 Fold
pqn-51	0.39
Y40C5A.1	0.39
ketn-1	0.39
let-765	0.39
ptr-8	0.39
Y51F10.10	0.39
taf-1	0.39
T05F1.11	0.39
F35G12.12	0.39
cbp-1	0.39
mcm-6	0.39
vps-33.1	0.39
fbxa-192	0.39
W04D2.6	0.39
Y50D7A.8	0.39
R148.4	0.39
C41H7.6	0.39
C49C3.9	0.39
eftu-2	0.39
cul-3	0.39
tat-4	0.39
tbc-20	0.39
emb-5	0.38
ric-19	0.38
F46B6.4	0.38
btbd-10	0.38
mage-1	0.38
M163.1	0.38
F55A11.8	0.38
dph-1	0.38
F43G6.3	0.38
F19B10.10	0.38
bmk-1	0.38
nasp-1	0.38
ubc-15	0.38
mel-47	0.38
C02F5.7	0.38
pqn-96	0.38
nspc-20	0.38
tag-30	0.38
hcp-2	0.38
K08F4.1	0.38

Gene Name	log_2 Fold
hpo-40	0.38
clec-88	0.38
sto-1	0.38
sec-8	0.38
zfp-1	0.38
cpna-1	0.38
unc-61	0.38
Y82E9BR.18	0.38
cec-6	0.38
snrp-200	0.38
C23H3.3	0.38
pat-3	0.38
M05B5.2	0.38
myo-3	0.38
Y71G10AR.4	0.38
tes-1	0.38
K09F6.9	0.38
wdr-5.1	0.38
B0261.1	0.38
mmaa-1	0.38
Y48G1C.11	0.37
C09G9.1	0.37
eri-5	0.37
Y106G6H.5	0.37
csn-6	0.37
F59E12.11	0.37
DC2.8	0.37
ulp-1	0.37
Y69A2AR.28	0.37
xpo-2	0.37
tpa-1	0.37
exc-5	0.37
T25B9.6	0.37
dgn-1	0.37
F47A4.5	0.37
mcm-2	0.37
emb-27	0.37
W06B4.2	0.37

Gene Name	log_2 Fold
Y69A2AR.31	0.37
nspc-10	0.37
exos-4.2	0.37
C56E6.2	0.37
mog-4	0.37
ula-1	0.37
eri-3	0.37
K08D8.3	0.37
C56C10.11	0.37
dpf-3	0.37
sun-1	0.37
M01F1.8	0.37
R06F6.8	0.37
M01F1.4	0.37
F10D7.5	0.37
fbxa-63	0.37
Y37E11AL.3	0.37
T13H5.8	0.37
arx-2	0.37
lam-1	0.37
fbxa-66	0.37
F13E9.1	0.37
F25E5.5	0.37
rskd-1	0.37
sap-49	0.37
C14B1.9	0.37
wve-1	0.37
Y39G8B.9	0.37
mdt-8	0.37
mut-15	0.37
Y105E8A.8	0.37
F58B3.6	0.37
sulp-2	0.37
spdl-1	0.37
egl-26	0.37
B0454.9	0.37
pfn-1	0.37
pld-1	0.37
C08H9.3	0.36
ztf-9	0.36

Gene Name	log_2 Fold
spas-1	0.36
pop-1	0.36
T05B9.1	0.36
Y92H12A.5	0.36
fem-2	0.36
F10D11.2	0.36
spr-4	0.36
haf-3	0.36
lin-65	0.36
set-16	0.36
ced-4	0.36
T07E3.4	0.36
ubxn-1	0.36
F13E6.4	0.36
W03F11.4	0.36
air-2	0.36
C31C9.2	0.36
F13B12.6	0.36
tat-5	0.36
Y94H6A.3	0.36
pyp-1	0.36
rab-8	0.36
F14E5.2	0.36
gei-8	0.36
catp-8	0.36
lin-40	0.36
bre-4	0.36
Y53G8AM.8	0.36
fbxa-4	0.36
F20A1.10	0.36
M04D5.3	0.36
trpa-2	0.36
fbxa-53	0.36
T23F2.3	0.36
plx-1	0.36
gls-1	0.36
ztf-15	0.36
ifb-2	0.36
ubh-2	0.36
Y54E10A.6	0.36
F53H1.3	0.36

Table E2 (Continued)

Gene Name	log_2 Fold
ulp-5	0.36
smc-3	0.36
bicd-1	0.36
F34D10.4	0.36
lin-5	0.36
Y44E3A.4	0.36
hop-1	0.36
F10B5.2	0.36
hpo-22	0.36
mes-3	0.36
rap-1	0.36
set-26	0.35
cup-5	0.35
C49A9.9	0.35
M02B1.3	0.35
W04A8.1	0.35
coel-1	0.35
pms-2	0.35
clec-5	0.35
lgc-34	0.35
Y48E1C.1	0.35
T03F6.3	0.35
B0432.6	0.35
F44B9.8	0.35
dpy-28	0.35
ccz-1	0.35
F22B5.4	0.35
T16G12.6	0.35
F55D12.5	0.35
K03E6.7	0.35
F17C11.11	0.35
ced-7	0.35
T23G7.3	0.35
hmg-4	0.35
Y119D3B.14	0.35
evl-14	0.35
cdf-2	0.35
Y34D9A.7	0.35
K07A3.3	0.35
C42C1.4	0.35
C07H6.4	0.35

Gene Name	log_2 Fold
Y11D7A.7	0.35
R07B7.2	0.35
ZC434.8	0.35
F52H3.6	0.35
ash-2	0.35
egrh-3	0.35
T26A5.2	0.35
F14B8.6	0.35
F09F7.7	0.35
flp-16	0.35
ZK1067.3	0.34
math-18	0.34
F25B5.6	0.34
Y15E3A.4	0.34
F25B4.5	0.34
acl-12	0.34
hum-4	0.34
lit-1	0.34
unc-59	0.34
W03D8.10	0.34
prp-8	0.34
T08B6.4	0.34
R10H1.1	0.34
C05D11.8	0.34
F32D1.6	0.34
pisy-1	0.34
W03C9.2	0.34
T21B6.3	0.34
hpr-17	0.34
mpk-1	0.34
pme-2	0.34
lsl-1	0.34
F10C1.8	0.34
arx-3	0.34
Y50D4A.1	0.34
E04F6.9	0.34
dcar-1	0.34
mus-101	0.34
Y110A2AR.1	0.34
snt-4	0.34
dpf-7	0.34

Gene Name	log_2 Fold
cpr-4	0.34
sbt-1	0.34
mek-1	0.34
frl-1	0.34
rnp-1	0.34
catp-6	0.34
cki-2	0.34
sdc-3	0.34
C50D2.7	0.34
pghm-1	0.34
ifg-1	0.34
T05E7.3	0.34
zip-4	0.34
C06E1.9	0.34
K09H9.2	0.34
npp-10	0.34
Y59E9AL.36	0.34
pha-4	0.34
ida-1	0.34
H25P19.1	0.34
F18A1.7	0.34
ubr-1	0.33
sut-2	0.33
W05F2.6	0.33
rgs-7	0.33
adm-2	0.33
Y50D7A.3	0.33
T21B10.3	0.33
T05A7.6	0.33
K09E4.2	0.33
Y75B8A.13	0.33
C32E8.3	0.33
mys-4	0.33
F57H12.6	0.33
ZK930.1	0.33
mom-5	0.33
F36A2.2	0.33
mtm-3	0.33
C17D12.7	0.33
F25H5.5	0.33
K08E4.3	0.33

Gene Name	log_2 Fold
Y92H12A.4	0.33
ZK938.1	0.33
tag-53	0.33
gex-3	0.33
mig-14	0.33
W01C8.5	0.33
R17.2	0.33
smg-2	0.33
F52C12.4	0.33
unc-68	0.33
coh-4	0.33
Y39B6A.37	0.33
C04G2.8	0.33
cyh-1	0.33
frm-7	0.33
taf-2	0.33
nab-1	0.33
hpo-27	0.33
ztf-18	0.33
F53C3.13	0.33
Y40B1B.8	0.33
F53H1.1	0.33
rnp-5	0.33
T02G5.12	0.33
efl-1	0.33
num-1	0.33
Y47G6A.25	0.32
prx-10	0.32
tars-1	0.32
Y119C1A.1	0.32
pde-2	0.32
fkb-8	0.32
tat-1	0.32
D2030.8	0.32
ani-3	0.32
egl-3	0.32
cls-2	0.32
prp-38	0.32
M02B7.5	0.32
taf-8	0.32
T08A11.2	0.32

Table E2 (Continued)

Gene Name	log_2 Fold
C13F10.6	0.32
D2096.1	0.32
C18E9.9	0.32
Y39G10AR.18	0.32
rnr-2	0.32
sli-1	0.32
F58B3.7	0.32
ptp-3	0.32
C56A3.8	0.32
cyld-1	0.32
Y37E3.1	0.32
T24B8.3	0.32
hcf-1	0.32
math-40	0.32
pqn-65	0.32
wrt-10	0.32
pct-1	0.32
E03H4.8	0.32
ZK1010.5	0.32
suds-3	0.32
Y54F10AR.2	0.32
F20A1.1	0.32
ppw-2	0.32
vglu-2	0.32
C13F10.4	0.32
rme-8	0.32
lst-2	0.32
htp-3	0.32
har-2	0.32
C13C4.5	0.32
F58D2.2	0.32
grsp-2	0.32
F48E8.4	0.32
eor-1	0.32
C41D11.3	0.31
ZC443.3	0.31
sand-1	0.31
ogt-1	0.31
Y71H2B.2	0.31
dpff-1	0.31

Gene Name	log_2 Fold
F11G11.5	0.31
pry-1	0.31
C17E4.6	0.31
such-1	0.31
ima-3	0.31
C49C3.7	0.31
jac-1	0.31
mix-1	0.31
T28D9.4	0.31
spe-39	0.31
klp-4	0.31
let-711	0.31
lsy-2	0.31
prp-21	0.31
pmr-1	0.31
snx-3	0.31
F26F4.5	0.31
C49G7.10	0.31
cids-1	0.31
H14A12.3	0.31
C43E11.12	0.31
dnj-25	0.31
nhr-49	0.31
chd-7	0.31
gcn-2	0.31
F17C11.2	0.31
fic-1	0.31
gly-9	0.31
mig-15	0.31
nstp-4	0.31
sel-2	0.31
F32B5.7	0.30
Y67D8A.2	0.30
mlk-1	0.30
C38D4.4	0.30
tbx-2	0.30
mdf-2	0.30
hda-3	0.30
jhdm-1	0.30
B0361.8	0.30
wago-2	0.30
R07E5.1	0.30

Gene Name	log_2 Fold
C36A4.4	0.30
R02D3.4	0.30
pph-4.2	0.30
mtm-6	0.30
F13B12.1	0.30
K07E3.1	0.30
Y92H12BL.1	0.30
Y37H9A.1	0.30
ubc-1	0.30
swsn-2.2	0.30
C18E3.5	0.30
R10H10.7	0.30
apd-3	0.30
wago-4	0.30
W06B4.1	0.30
gex-2	0.30
ldh-1	0.30
vps-18	0.30
let-858	0.30
mtk-1	0.30
T09F3.2	0.30
ego-2	0.30
F15D3.6	0.29
pnc-1	0.29
arl-8	0.29
T12B3.4	0.29
F36D3.4	0.29
F32B5.4	0.29
ZC239.6	0.29
T22C1.6	0.29
Y105E8A.23	0.29
sma-5	0.29
uba-2	0.29
agef-1	0.29
T10D4.3	0.29
egl-19	0.29
hgrs-1	0.29
unc-37	0.29
F18A1.6	0.29
M03C11.8	0.29

Gene Name	log_2 Fold
Y92H12BR.7	0.29
vps-16	0.29
F22G12.4	0.29
swan-2	0.29
Y79H2A.3	0.29
cdtl-7	0.29
nipa-1	0.29
jamp-1	0.29
pkc-1	0.29
lact-3	0.29
aspm-1	0.29
epc-1	0.29
Y48G1C.8	0.29
T02C12.2	0.29
jph-1	0.29
gst-22	0.29
clh-6	0.29
Y45G5AL.1	0.29
C24G6.8	0.29
F44E2.4	0.29
F10C5.2	0.28
taf-6.2	0.28
F57C9.1	0.28
C33G8.4	0.28
xrn-1	0.28
msh-2	0.28
epi-1	0.28
rde-2	0.28
Y47D9A.1	0.28
F41G3.6	0.28
C15C6.2	0.28
nfm-1	0.28
F56D12.6	0.28
vha-7	0.28
H28O16.2	0.28
Y66D12A.15	0.28
btb-16	0.28
pfs-2	0.28
ubc-16	0.28
toca-1	0.28

Table E2 (Continued)

Gene Name	log_2 Fold
ZK1067.2	0.28
acl-9	0.28
F48E8.6	0.28
nhr-66	0.28
atg-7	0.28
cul-1	0.28
T07A9.14	0.28
syx-18	0.28
F47B3.7	0.28
mafr-1	0.28
C46C2.2	0.28
wdr-23	0.27
R02D3.3	0.27
prl-1	0.27
C36B1.9	0.27
F14H3.6	0.27
cyk-3	0.27
C56E6.9	0.27
exoc-7	0.27
eri-1	0.27
Y48G10A.2	0.27
R07E5.7	0.27
smg-6	0.27
Y77E11A.2	0.27
mog-1	0.27
K08E4.6	0.27
ppk-3	0.27
F54D8.6	0.27
rhi-1	0.27
tbc-3	0.27
Y106G6D.7	0.27
F08G5.1	0.27
tsg-101	0.27
arp-1	0.27
cyp-31A2	0.27
C18H7.11	0.27
F46F11.9	0.26
tag-325	0.26
Y67H2A.7	0.26
mat-3	0.26

Gene Name	log_2 Fold
pgs-1	0.26
pqn-27	0.26
Y17G9B.5	0.26
C41G7.3	0.26
T26A8.1	0.26
C33F10.11	0.26
K08F9.4	0.26
dod-22	0.26
sym-4	0.26
ZC376.6	0.26
skih-2	0.26
ymel-1	0.26
egl-21	0.26
C56G2.1	0.26
F35A5.1	0.26
Y97E10C.1	0.25
D2023.6	0.25
C01G5.6	0.25
usp-5	0.25
F52B5.3	0.25
W08F4.3	0.25
M03B6.2	0.25
C34D10.2	0.25
lbp-1	0.25
abt-2	0.25
C27A12.2	0.25
C32E8.5	0.25
dhs-13	0.25
M88.5	0.25
bli-3	0.25
mdt-17	0.25
suf-1	0.25
T11G6.5	0.24
hlh-30	0.24
nsf-1	0.24
snap-29	0.24
sel-11	0.24
ndc-80	0.24
lin-42	0.24
T23B12.4	0.24
ain-1	0.24

Gene Name	log_2 Fold
Y48G8AL.5	0.24
tag-196	0.24
ify-1	0.24
plc-4	0.24
npp-11	0.24
Y71H2AM.11	-0.24
elo-2	-0.24
W07G4.5	-0.24
cup-2	-0.24
ska-1	-0.25
Y48G10A.1	-0.25
msp-45	-0.25
mrpl-19	-0.25
K02F3.9	-0.25
cdc-7	-0.25
ZK632.11	-0.25
fbxa-210	-0.25
C54G4.9	-0.25
inx-17	-0.25
mif-3	-0.25
Y7A5A.1	-0.25
C02D5.4	-0.26
ZC434.4	-0.26
vps-26	-0.26
vps-22	-0.26
mdt-19	-0.26
Y38F2AR.3	-0.26
vha-9	-0.26
dnj-10	-0.26
F40E10.6	-0.26
apm-1	-0.26
rnh-2	-0.26
Y39G10AR.32	-0.26
C11D2.4	-0.26
msp-64	-0.26
wah-1	-0.26
K07C5.2	-0.26
dhs-24	-0.26

Gene Name	log_2 Fold
mrpl-41	-0.26
F26A1.1	-0.26
Y73B3A.2	-0.26
fln-2	-0.27
F13H10.3	-0.27
pkc-2	-0.27
nxf-2	-0.27
B0280.9	-0.27
pde-6	-0.27
sti-1	-0.27
mboa-2	-0.27
C33H5.13	-0.27
M05D6.6	-0.27
Y51H4A.7	-0.27
Y106G6A.1	-0.27
C31H5.6	-0.27
D1046.3	-0.27
nlp-33	-0.27
mecr-1	-0.27
Y53F4B.18	-0.27
F07F6.8	-0.27
spp-15	-0.27
col-118	-0.28
Y119C1B.5	-0.28
T20B12.3	-0.28
spp-2	-0.28
F54A3.5	-0.28
F29B9.8	-0.28
cec-1	-0.28
Y51H4A.15	-0.28
gop-2	-0.28
blmp-1	-0.28
Y71G12B.6	-0.28
K12H4.3	-0.28
F01F1.11	-0.28
fgt-1	-0.28
rabs-5	-0.28
F30F8.9	-0.28
ZC239.15	-0.28
col-34	-0.28

Table E2 (Continued)

Gene Name	log_2 Fold
dve-1	-0.29
C28C12.12	-0.29
K07C5.3	-0.29
mrps-14	-0.29
glo-4	-0.29
E03H12.5	-0.29
Y47G6A.7	-0.29
msp-142	-0.29
Y62E10A.6	-0.29
F45H10.3	-0.29
C01F6.9	-0.29
M04B2.4	-0.29
F44G4.1	-0.29
F10G2.1	-0.29
C44C10.9	-0.29
Y66D12A.9	-0.29
C34B2.5	-0.29
E02H1.2	-0.29
C30G12.6	-0.29
C01B10.11	-0.29
ZK742.2	-0.29
F55A12.2	-0.29
prmt-7	-0.29
plc-2	-0.29
idhb-1	-0.29
ZK686.2	-0.29
T03D8.6	-0.29
C31H1.5	-0.29
ZC317.6	-0.29
col-170	-0.29
phip-1	-0.29
Y54G11A.2	-0.29
F59F4.1	-0.30
F08B4.7	-0.30
tpst-1	-0.30
F58H1.3	-0.30
M142.5	-0.30
F33D4.4	-0.30
Y18D10A.16	-0.30
F42G2.2	-0.30

Gene Name	log_2 Fold
Y32F6A.4	-0.30
M02H5.8	-0.30
cah-3	-0.30
F35B3.4	-0.30
acdh-7	-0.30
Y55B1AL.2	-0.30
dnc-2	-0.30
F59D6.3	-0.30
mett-10	-0.30
B0303.7	-0.30
C53A3.2	-0.30
B0361.6	-0.30
hda-5	-0.30
mrpl-4	-0.30
sec-22	-0.30
lon-8	-0.30
dhhc-3	-0.30
T08D2.1	-0.30
btb-20	-0.30
ugt-58	-0.30
ctl-3	-0.31
msp-33	-0.31
T21C9.4	-0.31
C24D10.6	-0.31
tag-304	-0.31
klf-3	-0.31
Y48A6B.3	-0.31
C14H10.1	-0.31
T28B4.1	-0.31
T06D8.7	-0.31
Y54G2A.23	-0.31
F48C1.6	-0.31
T05A7.1	-0.31
F29A7.6	-0.31
F10C1.9	-0.31
pxd-1	-0.31
rpl-41	-0.31
ykt-6	-0.31
Y38C1AA.14	-0.31
ugt-6	-0.31

Gene Name	log_2 Fold
Y55F3BR.11	-0.31
C49F8.3	-0.31
lron-7	-0.31
Y53G8AR.6	-0.31
bed-3	-0.31
T10E9.1	-0.31
Y40C5A.4	-0.31
apm-3	-0.31
F58F12.1	-0.31
T17H7.7	-0.32
vars-1	-0.32
vab-19	-0.32
col-133	-0.32
rpb-11	-0.32
npp-23	-0.32
pcyt-1	-0.32
dsbn-1	-0.32
clk-1	-0.32
F48A9.1	-0.32
emb-1	-0.32
T27A10.6	-0.32
dylt-1	-0.32
dnj-19	-0.32
T13F2.2	-0.32
C35B1.5	-0.32
F15E6.6	-0.32
msp-19	-0.32
Y47D3A.21	-0.32
T28D6.7	-0.32
pqn-70	-0.32
ZK353.9	-0.32
Y71F9B.2	-0.32
ccdc-47	-0.32
ZK643.2	-0.32
K01D12.15	-0.32
R144.6	-0.32
K07C5.4	-0.32
ubl-1	-0.32
T28D9.1	-0.32
lipl-1	-0.32

Gene Name	log_2 Fold
Y57E12AL.3	-0.32
mrpl-46	-0.32
JC8.2	-0.32
T13H5.4	-0.32
nhr-122	-0.32
T24C4.5	-0.32
hif-1	-0.32
col-96	-0.33
C18B2.5	-0.33
K02B7.3	-0.33
T02H6.11	-0.33
K11H3.3	-0.33
K09C4.10	-0.33
hint-1	-0.33
W04C9.4	-0.33
F53A9.8	-0.33
F53B6.4	-0.33
bmy-1	-0.33
sars-2	-0.33
nra-4	-0.33
C48E7.7	-0.33
C06G3.6	-0.33
ZK792.5	-0.33
F39E9.10	-0.33
mboa-6	-0.33
C05D10.4	-0.33
F49H12.5	-0.33
rpl-30	-0.33
ska-3	-0.33
C06A6.4	-0.33
K02B12.7	-0.33
rpl-10	-0.33
R151.10	-0.33
C07H6.2	-0.33
C27A7.6	-0.33
F54C4.4	-0.33
lec-3	-0.33
W09C5.1	-0.33
fbxa-203	-0.33
Y45F10C.2	-0.33
otub-3	-0.33

Table E2 (Continued)

Gene Name	log_2 Fold
F37B12.1	-0.33
F09E8.2	-0.33
T11G6.4	-0.33
F44E5.1	-0.33
ceh-93	-0.33
upb-1	-0.33
R10E4.1	-0.33
mrpl-47	-0.33
prx-6	-0.33
C05D11.9	-0.33
syp-2	-0.33
tag-18	-0.33
dnj-30	-0.33
F22F4.4	-0.33
Y69E1A.2	-0.33
M02D8.1	-0.33
F36A2.14	-0.33
lars-2	-0.33
rbd-1	-0.33
F35C8.5	-0.34
gst-20	-0.34
vps-45	-0.34
C46A5.6	-0.34
F53A9.1	-0.34
kbp-5	-0.34
ZK1225.4	-0.34
ran-4	-0.34
Y73E7A.6	-0.34
R07E5.13	-0.34
Y105E8A.11	-0.34
K07F5.15	-0.34
F43G6.8	-0.34
T22C1.5	-0.34
ZK822.5	-0.34
ftr-1	-0.34
K07H8.3	-0.34
F18G5.6	-0.34
fbxa-101	-0.34
gpc-2	-0.34
ZK1307.1	-0.34
lgg-1	-0.34
smc-5	-0.34
C05C12.4	-0.34
fmo-1	-0.34
skr-16	-0.34
mrpl-18	-0.34
C13F10.7	-0.34
F40A3.2	-0.34
gei-13	-0.34
ttr-14	-0.34
R12E2.11	-0.34
nxt-1	-0.34
T10F2.5	-0.34
exos-7	-0.34
Y71G12B.17	-0.34
F56A8.3	-0.34
W04G3.5	-0.34
stdh-1	-0.34
dhs-28	-0.34
T27E7.1	-0.34
C37C3.2	-0.34
F28H7.8	-0.34
R10E4.9	-0.34
moma-1	-0.34
dnc-3	-0.34
K02E2.6	-0.34
C45G9.13	-0.34
ugt-64	-0.34
cct-4	-0.34
Y54G2A.45	-0.35
B0035.16	-0.35
dnc-5	-0.35
Y20C6A.1	-0.35
K01G5.5	-0.35
abcf-1	-0.35
rpia-1	-0.35
C10C5.5	-0.35
pinn-1	-0.35
T12B3.3	-0.35
clec-50	-0.35
acl-7	-0.35
C46C2.7	-0.35
hpo-17	-0.35
cct-5	-0.35
nhr-203	-0.35
dld-1	-0.35
pars-1	-0.35
tpra-1	-0.35
atg-13	-0.35
srf-3	-0.35
C32F10.8	-0.35
bir-1	-0.35
cyp-31A1	-0.35
Y47G6A.26	-0.35
cyn-9	-0.35
pat-12	-0.35
T21C9.9	-0.35
F42G10.1	-0.35
F46A9.1	-0.35
F32A11.1	-0.35
madf-5	-0.35
pes-22	-0.35
mrps-35	-0.35
fut-8	-0.35
F59B1.8	-0.35
R13H9.6	-0.35
lap-1	-0.35
mrpl-36	-0.35
mec-12	-0.35
Y71H10B.1	-0.35
vha-10	-0.35
C08F11.12	-0.35
rpl-11.1	-0.35
gld-2	-0.35
T08B2.12	-0.35
R09B3.3	-0.35
smn-1	-0.35
pgp-3	-0.35
K01C8.7	-0.35
C11E4.7	-0.35
mdt-20	-0.35
C49H3.4	-0.35
Y54E5A.5	-0.35
sel-9	-0.35
C17E4.11	-0.35
K07G5.6	-0.36
Y73B6BL.31	-0.36
ttr-41	-0.36
vha-14	-0.36
C50F2.5	-0.36
F22H10.3	-0.36
clec-170	-0.36
F26E4.6	-0.36
cysl-3	-0.36
F45F2.9	-0.36
D1054.3	-0.36
col-131	-0.36
F55F3.2	-0.36
rpl-23	-0.36
F15B9.8	-0.36
H28O16.1	-0.36
Y38A10A.2	-0.36
prdx-2	-0.36
ucr-1	-0.36
Y49E10.18	-0.36
K01A2.5	-0.36
ooc-5	-0.36
F16B3.3	-0.36
F10A3.17	-0.36
B0286.3	-0.36
rnf-5	-0.36
F48D6.4	-0.36
F20H11.4	-0.36
let-23	-0.36
W02D9.4	-0.36
ttr-31	-0.36
lap-2	-0.36
tnt-2	-0.36
B0491.5	-0.36
atf-5	-0.36
F55A3.2	-0.36
F55G11.4	-0.36
ctl-1	-0.36

Table E2 (Continued)

Gene Name	log_2 Fold
heh-1	-0.36
C06G1.1	-0.36
C41H7.1	-0.36
mnat-1	-0.36
C41D11.9	-0.36
Y48G1C.6	-0.36
E03H12.7	-0.36
immt-1	-0.36
C47A4.1	-0.36
sir-2.1	-0.37
Y39B6A.1	-0.37
got-1.2	-0.37
ril-1	-0.37
F44E2.10	-0.37
R07B7.8	-0.37
C16A11.7	-0.37
F13D12.5	-0.37
F28C6.8	-0.37
fbxa-64	-0.37
trx-3	-0.37
mans-2	-0.37
fbxc-47	-0.37
sfxn-2	-0.37
Y53C12A.3	-0.37
xbp-1	-0.37
cyp-37B1	-0.37
F15G9.1	-0.37
kin-5	-0.37
ned-8	-0.37
Y50D4A.5	-0.37
K11G12.5	-0.37
nhr-210	-0.37
Y51H1A.3	-0.37
tag-321	-0.37
mrps-18B	-0.37
gna-1	-0.37
C41D11.5	-0.37
pcp-3	-0.37
F21D5.5	-0.37
F33H2.6	-0.37
hut-1	-0.37
ivd-1	-0.37

Gene Name	log_2 Fold
T20D3.2	-0.37
atg-16.1	-0.37
Y17D7B.4	-0.37
T15B12.1	-0.37
B0250.5	-0.37
hpo-34	-0.37
F10D11.6	-0.37
nhr-256	-0.37
K10D11.5	-0.37
T04F3.3	-0.37
K09C6.7	-0.37
Y110A7A.6	-0.37
nhr-100	-0.37
ptr-14	-0.37
C28A5.6	-0.37
cep-1	-0.37
sqt-2	-0.37
K01C8.1	-0.37
M28.5	-0.37
ZK856.5	-0.37
T23B12.11	-0.37
C33H5.17	-0.37
Y4C6B.7	-0.37
T23F6.3	-0.37
F36H12.9	-0.37
pfn-2	-0.37
pamn-1	-0.37
F36D4.2	-0.37
swt-7	-0.38
F15D3.7	-0.38
T13G4.4	-0.38
F09E5.14	-0.38
F33D11.10	-0.38
C34B2.10	-0.38
ath-1	-0.38
F09E5.2	-0.38
ZK637.2	-0.38
C05C8.1	-0.38
ZK1320.11	-0.38
T28A8.5	-0.38
F56C11.6	-0.38
fard-1	-0.38

Gene Name	log_2 Fold
K06H7.2	-0.38
cpi-2	-0.38
asp-5	-0.38
K01D12.7	-0.38
C35D10.13	-0.38
F26G1.5	-0.38
F53A2.7	-0.38
F20G2.2	-0.38
T16G12.8	-0.38
chch-3	-0.38
Y71H2AR.1	-0.38
C14F11.4	-0.38
fbxa-206	-0.38
F25B4.7	-0.38
C30F8.3	-0.38
F42A9.8	-0.38
tni-1	-0.38
pdhb-1	-0.38
Y60A3A.14	-0.38
C18E9.2	-0.38
K11D9.3	-0.38
dad-1	-0.38
F41C3.11	-0.38
hsp-60	-0.38
Y54G2A.52	-0.38
F40F9.5	-0.38
F21D5.7	-0.38
nduf-5	-0.38
josd-1	-0.38
Y76B12C.3	-0.38
T19C4.5	-0.38
syx-7	-0.38
Y37E11AM.3	-0.38
tram-1	-0.38
C26D10.6	-0.38
Y25C1A.13	-0.38
ZK795.2	-0.38
ZK287.7	-0.38
nkat-3	-0.39
C45B2.2	-0.39

Gene Name	log_2 Fold
msp-71	-0.39
rpb-9	-0.39
atp-5	-0.39
C17G10.7	-0.39
K09H9.8	-0.39
Y25C1A.14	-0.39
K11G9.2	-0.39
M01A8.2	-0.39
gst-7	-0.39
cpt-6	-0.39
sqt-1	-0.39
rpl-12	-0.39
abu-12	-0.39
C48B4.8	-0.39
K10C2.1	-0.39
fbxa-211	-0.39
C34B2.8	-0.39
C44C10.11	-0.39
rps-22	-0.39
Y16B4A.2	-0.39
R53.4	-0.39
C51E3.6	-0.39
bath-5	-0.39
stc-1	-0.39
C01H6.6	-0.39
F14H3.12	-0.39
F25H8.1	-0.39
R107.5	-0.39
col-145	-0.39
D1046.2	-0.39
tag-260	-0.39
toc-1	-0.39
rpb-4	-0.39
dhs-20	-0.39
C10C5.3	-0.39
F46G10.4	-0.39
C56G2.3	-0.39
Y67H2A.5	-0.39
B0280.11	-0.39
F59E11.5	-0.39
Y37B11A.3	-0.39
C15B12.1	-0.39

Table E2 (Continued)

Gene Name	log_2 Fold
F08A8.2	-0.39
nstp-1	-0.39
vha-4	-0.39
glna-3	-0.39
idh-1	-0.39
F10E7.5	-0.39
ttr-34	-0.39
C26F1.3	-0.39
fkb-5	-0.39
ric-4	-0.39
nhr-13	-0.39
rpl-15	-0.40
C25H3.10	-0.40
fbxa-167	-0.40
T04B8.5	-0.40
F14D2.11	-0.40
ZC477.3	-0.40
lin-44	-0.40
snx-27	-0.40
Y50D4B.3	-0.40
M88.7	-0.40
sptl-1	-0.40
vha-15	-0.40
W03C9.5	-0.40
C18G1.9	-0.40
tag-344	-0.40
lbp-3	-0.40
C27F2.4	-0.40
F28C1.3	-0.40
C34E7.4	-0.40
F40G9.17	-0.40
hhat-1	-0.40
C25F6.1	-0.40
F08G5.3	-0.40
snu-23	-0.40
vha-17	-0.40
T09B4.8	-0.40
cyc-1	-0.40
col-113	-0.40
dnj-12	-0.40
pfd-2	-0.40
Y95B8A.2	-0.40

Gene Name	log_2 Fold
B0280.13	-0.40
nhr-115	-0.40
cyp-37A1	-0.40
osr-1	-0.40
acl-13	-0.40
dif-1	-0.40
sec-10	-0.40
cutl-26	-0.40
F55F8.3	-0.40
dhp-1	-0.40
gly-19	-0.40
cpr-1	-0.40
stl-1	-0.40
gst-27	-0.40
T01D3.6	-0.40
fbxa-80	-0.40
cpin-1	-0.40
C28D4.4	-0.41
vha-8	-0.41
C14C6.5	-0.41
ZK1098.3	-0.41
T06A4.3	-0.41
Y69E1A.5	-0.41
F20D1.1	-0.41
sfxn-1.5	-0.41
icln-1	-0.41
F32B6.10	-0.41
F25H5.7	-0.41
C30B5.4	-0.41
F37H8.3	-0.41
EEED8.16	-0.41
emb-8	-0.41
C37A2.7	-0.41
exos-9	-0.41
cyp-33C9	-0.41
F40F12.3	-0.41
memb-2	-0.41
rpoa-12	-0.41
inx-16	-0.41
ZK550.6	-0.41
mans-3	-0.41
tag-170	-0.41

Gene Name	log_2 Fold
T01H8.2	-0.41
R07E5.4	-0.41
ZK180.6	-0.41
C17H12.3	-0.41
jmjd-5	-0.41
mfap-1	-0.41
C48B4.11	-0.41
C27F2.9	-0.41
T01H10.8	-0.41
AC3.5	-0.41
apc-10	-0.41
K11H12.1	-0.41
K11H12.4	-0.41
K10D6.2	-0.41
C34D4.3	-0.41
K07A1.5	-0.41
erd-2	-0.41
T20H4.5	-0.41
btb-4	-0.41
C01B10.9	-0.41
F54D5.16	-0.41
sucl-2	-0.41
D2030.11	-0.41
crn-7	-0.41
col-172	-0.41
W03F8.3	-0.41
msd-2	-0.41
F45H10.2	-0.41
C54C6.6	-0.41
ram-2	-0.42
C24A3.2	-0.42
dhhc-14	-0.42
drr-1	-0.42
ubc-7	-0.42
ZK1320.7	-0.42
eif-3.F	-0.42
gbh-1	-0.42
cdr-7	-0.42
D2030.2	-0.42
ZK546.2	-0.42
Y57G11C.22	-0.42

Gene Name	log_2 Fold
lab-1	-0.42
elt-7	-0.42
smg-5	-0.42
Y49F6C.8	-0.42
col-141	-0.42
B0416.5	-0.42
F14D2.8	-0.42
F54H5.2	-0.42
ucr-2.1	-0.42
fbxa-193	-0.42
nhx-9	-0.42
R03E1.2	-0.42
kmo-1	-0.42
pqbp-1.1	-0.42
mpz-4	-0.42
C48B6.10	-0.42
mrpl-16	-0.42
aat-6	-0.42
Y111B2A.13	-0.42
B0310.2	-0.42
set-1	-0.42
nmgp-1	-0.42
F13B6.2	-0.42
ZK593.3	-0.42
D2030.4	-0.42
D2023.4	-0.42
F37B4.10	-0.42
F02A9.4	-0.42
F22F7.1	-0.42
asb-2	-0.42
lron-8	-0.42
msp-113	-0.42
tps-2	-0.42
col-58	-0.42
pgl-2	-0.42
arl-1	-0.42
Y38F2AR.12	-0.42
C44H9.6	-0.42
spo-7	-0.42
C45G9.5	-0.42

Table E2 (Continued)

Gene Name	log_2 Fold
D1007.4	-0.42
Y62F5A.12	-0.42
hsp-16.11	-0.42
R151.2	-0.43
nhr-96	-0.43
Y67D2.5	-0.43
K05C4.5	-0.43
Y17D7C.3	-0.43
gst-36	-0.43
nhr-204	-0.43
Y53G8AL.2	-0.43
F41C3.5	-0.43
sox-2	-0.43
R02D3.1	-0.43
aly-3	-0.43
lipl-5	-0.43
Y119C1B.10	-0.43
sut-1	-0.43
tag-280	-0.43
ugt-28	-0.43
F18C12.3	-0.43
F59C6.16	-0.43
nhr-108	-0.43
mrpl-12	-0.43
C44F1.1	-0.43
F56C9.8	-0.43
mrpl-11	-0.43
Y39B6A.13	-0.43
acn-1	-0.43
nhr-58	-0.43
C43H6.3	-0.43
adt-1	-0.43
dpy-5	-0.43
ech-4	-0.43
cpt-2	-0.43
asp-4	-0.43
add-2	-0.43
dnj-2	-0.43
nhr-228	-0.43
F48C1.5	-0.43

Gene Name	log_2 Fold
henn-1	-0.43
ZK354.6	-0.43
rpl-27	-0.43
fut-1	-0.43
nuo-2	-0.43
ZK1058.5	-0.43
F22D6.9	-0.43
F09F9.2	-0.44
B0495.9	-0.44
B0334.4	-0.44
Y44A6D.3	-0.44
F55B11.4	-0.44
fbxa-14	-0.44
T25B9.9	-0.44
Y41D4B.11	-0.44
F43D2.6	-0.44
C09H5.7	-0.44
his-11	-0.44
ZK1248.11	-0.44
nhx-3	-0.44
R05D11.4	-0.44
snr-1	-0.44
T13F3.8	-0.44
csn-2	-0.44
ceeh-1	-0.44
F26B1.8	-0.44
T12B3.2	-0.44
gsr-1	-0.44
aman-1	-0.44
F28F5.6	-0.44
dnj-22	-0.44
M02B7.7	-0.44
cyp-13A2	-0.44
Y56A3A.19	-0.44
pbo-1	-0.44
F21D9.2	-0.44
R151.6	-0.44
agt-1	-0.44
T21G5.1	-0.44
hrg-1	-0.44
Y53G8AR.9	-0.44

Gene Name	log_2 Fold
phb-2	-0.44
vhl-1	-0.44
nhr-184	-0.44
F42G8.10	-0.44
Y67D2.3	-0.44
B0285.4	-0.44
F53B2.5	-0.44
ZK792.1	-0.44
nlp-4	-0.44
Y51A2D.14	-0.44
Y57G11C.42	-0.44
gska-3	-0.44
alh-11	-0.44
F29C4.2	-0.44
Y47H10A.4	-0.44
rhr-1	-0.44
ragc-1	-0.45
F32B6.3	-0.45
moag-4	-0.45
ugt-50	-0.45
C30H6.5	-0.45
C30H6.8	-0.45
sur-5	-0.45
C27C12.4	-0.45
W03A5.2	-0.45
unc-62	-0.45
F23D12.11	-0.45
men-1	-0.45
ehbp-1	-0.45
catp-5	-0.45
smd-1	-0.45
tag-320	-0.45
inx-15	-0.45
erv-46	-0.45
cyn-5	-0.45
cyn-12	-0.45
Y47D7A.13	-0.45
qdpr-1	-0.45
gipc-1	-0.45
trx-4	-0.45
nhr-143	-0.45

Gene Name	log_2 Fold
ZK1248.19	-0.45
tag-146	-0.45
pas-2	-0.45
T09A5.5	-0.45
C23H3.5	-0.45
R09E10.6	-0.45
K11B4.2	-0.45
best-14	-0.45
Y105C5B.5	-0.45
atad-3	-0.45
B0035.15	-0.45
tatn-1	-0.45
haf-6	-0.45
ncx-7	-0.45
dhs-6	-0.45
Y73B6BL.44	-0.45
F32B5.6	-0.45
C31H2.4	-0.45
B0238.11	-0.45
Y60A3A.9	-0.45
Y22D7AL.10	-0.45
nhr-98	-0.45
scav-1	-0.46
mam-3	-0.46
M153.1	-0.46
ifb-1	-0.46
msd-3	-0.46
R10D12.8	-0.46
rbx-1	-0.46
K08C9.2	-0.46
plc-3	-0.46
col-65	-0.46
K08H2.10	-0.46
C55B7.3	-0.46
rsp-6	-0.46
F55B11.1	-0.46
hgo-1	-0.46
nol-5	-0.46
C01A2.3	-0.46
rmd-3	-0.46

Table E2 (Continued)

Gene Name	log_2 Fold
Y47G6A.3 3	-0.46
amt-4	-0.46
Y11D7A.9	-0.46
F11E6.8	-0.46
ugt-61	-0.46
col-173	-0.46
Y7A9C.1	-0.46
nlp-27	-0.46
F25E2.2	-0.46
T27A3.5	-0.46
lsm-6	-0.46
lgc-44	-0.46
nlp-17	-0.46
aex-6	-0.46
R10D12.13	-0.46
F25B5.3	-0.46
F20D6.6	-0.46
C28H8.14	-0.46
nhr-55	-0.46
gdh-1	-0.46
C18B12.6	-0.46
msd-1	-0.46
rpb-7	-0.46
R07B1.13	-0.46
T06A1.5	-0.46
Y45F3A.1	-0.46
math-35	-0.46
oxy-5	-0.46
R12C12.1	-0.46
C06G3.8	-0.46
pcm-1	-0.46
ras-2	-0.46
C50D2.3	-0.46
B0393.9	-0.47
hsp-12.1	-0.47
M01H9.4	-0.47
mrps-12	-0.47
ant-1.4	-0.47
C33E10.4	-0.47
ugt-29	-0.47
F30A10.9	-0.47

Gene Name	log_2 Fold
C01G5.3	-0.47
T20B12.1	-0.47
mrps-2	-0.47
F49E2.1	-0.47
F42F12.4	-0.47
lbp-2	-0.47
F11F1.6	-0.47
ZK1248.13	-0.47
C15C6.1	-0.47
ZK792.7	-0.47
F33D4.5	-0.47
acs-12	-0.47
T21G5.4	-0.47
ceh-88	-0.47
dct-9	-0.47
F25H9.7	-0.47
ech-8	-0.47
fmo-5	-0.47
nhr-78	-0.47
ahcy-1	-0.47
C44E4.4	-0.47
vha-11	-0.47
rpc-25	-0.47
msp-53	-0.47
pbs-4	-0.47
K08D8.6	-0.47
H23N18.5	-0.47
R04A9.6	-0.47
gfl-1	-0.47
C01A2.5	-0.48
ttr-8	-0.48
ZK1025.3	-0.48
F55C5.2	-0.48
ads-1	-0.48
snr-4	-0.48
C02F5.5	-0.48
mpst-4	-0.48
F33G12.7	-0.48
F32D8.4	-0.48
F57C2.5	-0.48
Y105C5B.9	-0.48
ZK512.4	-0.48

Gene Name	log_2 Fold
ZC434.3	-0.48
K10C9.7	-0.48
K07H8.10	-0.48
hst-2	-0.48
ttr-17	-0.48
flap-1	-0.48
C03H12.1	-0.48
set-22	-0.48
lpd-9	-0.48
ccch-3	-0.48
C47E12.7	-0.48
F54H5.5	-0.48
syp-3	-0.48
C34C12.6	-0.48
F08F8.4	-0.48
Y17G7B.1 2	-0.48
nuo-1	-0.48
W04B5.2	-0.48
asg-1	-0.48
chn-1	-0.48
F26E4.3	-0.48
C55B7.11	-0.48
math-26	-0.48
C13C4.4	-0.48
ZK856.8	-0.48
C26B2.2	-0.48
T09B4.4	-0.48
Y34B4A.7	-0.48
T26E3.4	-0.48
bus-4	-0.48
faah-2	-0.48
ger-1	-0.48
taf-13	-0.48
C14A6.13	-0.48
K12B6.11	-0.48
C14C10.6	-0.49
Y97E10AL. 3	-0.49
C18A3.3	-0.49
F28B4.3	-0.49
his-15	-0.49

Gene Name	log_2 Fold
aps-1	-0.49
ddo-1	-0.49
Y51H7C.1 3	-0.49
T23F2.5	-0.49
hpo-19	-0.49
lsm-1	-0.49
R05G6.10	-0.49
Y71F9AL.1 2	-0.49
F19B10.2	-0.49
F25F8.1	-0.49
Y26E6A.3	-0.49
F33D11.2	-0.49
dpy-4	-0.49
mrps-15	-0.49
R11A8.5	-0.49
apy-1	-0.49
clec-258	-0.49
vha-2	-0.49
Y44A6D.5	-0.49
F27D4.1	-0.49
Y71G12B. 27	-0.49
gss-1	-0.49
asg-2	-0.49
mrpl-9	-0.49
ges-1	-0.49
Y22D7AR. 10	-0.49
acdh-11	-0.49
T14F9.2	-0.49
cpg-9	-0.49
ZK596.2	-0.49
mec-7	-0.49
bra-2	-0.49
pir-1	-0.49
daf-36	-0.49
C54E4.2	-0.49
F55F8.2	-0.49
Y54F10AM .8	-0.49
nhr-101	-0.49

Table E2 (Continued)

Gene Name	log_2 Fold
math-3	-0.49
Y73C8B.3	-0.49
C54G4.2	-0.49
F42G4.6	-0.50
C55A6.12	-0.50
F49C12.12	-0.50
E01B7.2	-0.50
T22C8.3	-0.50
dhfr-1	-0.50
F29B9.11	-0.50
F53E10.6	-0.50
Y47G6A.19	-0.50
F35H8.2	-0.50
kat-1	-0.50
gst-26	-0.50
T02G5.7	-0.50
fib-1	-0.50
cgt-2	-0.50
F59A6.2	-0.50
F36H12.4	-0.50
E04D5.5	-0.50
F52H2.3	-0.50
dnj-7	-0.50
C05G5.1	-0.50
F42A8.1	-0.50
T15H9.2	-0.50
nhr-134	-0.50
dnj-3	-0.50
clec-227	-0.50
C36B7.6	-0.50
K02D10.4	-0.50
gln-3	-0.50
B0272.3	-0.50
C25G4.3	-0.50
msp-51	-0.50
F49E7.2	-0.50
ttr-24	-0.50
F10D11.3	-0.50
clec-49	-0.50
D1044.1	-0.50
T20D3.3	-0.50

Gene Name	log_2 Fold
art-1	-0.50
C25H3.9	-0.50
Y37F4.1	-0.50
Y54F10AM.5	-0.50
aqp-4	-0.50
F53E10.1	-0.50
hyl-2	-0.50
F26B1.5	-0.50
nlp-40	-0.50
fbxa-216	-0.50
F35H10.6	-0.50
ech-5	-0.51
ZC239.17	-0.51
C23G10.7	-0.51
his-26	-0.51
F58E6.13	-0.51
nhr-126	-0.51
dhhc-12	-0.51
F37A4.2	-0.51
tag-124	-0.51
M02F4.3	-0.51
F37F2.2	-0.51
R03D7.2	-0.51
far-5	-0.51
nhr-151	-0.51
EEED8.3	-0.51
mam-1	-0.51
spe-4	-0.51
ZK418.8	-0.51
rps-15	-0.51
F52H2.5	-0.51
F41F3.8	-0.51
F36G9.3	-0.51
clec-84	-0.51
vha-1	-0.51
lips-7	-0.51
D2092.1	-0.51
C06A6.2	-0.51
wrt-5	-0.51
nhr-8	-0.51
che-14	-0.51

Gene Name	log_2 Fold
F39H11.1	-0.51
bus-8	-0.51
Y113G7B.12	-0.51
C28G1.6	-0.51
suca-1	-0.51
Y37E11B.6	-0.51
F55H2.7	-0.51
Y59E9AL.6	-0.51
C27D8.3	-0.51
grd-5	-0.51
gst-1	-0.51
Y71H2B.11	-0.51
Y39E4B.6	-0.51
acdh-8	-0.51
F09E5.3	-0.51
C48B6.2	-0.51
F55C12.4	-0.52
mtss-1	-0.52
F23C8.5	-0.52
odd-1	-0.52
rnp-2	-0.52
R09H10.5	-0.52
hsp-1	-0.52
ZK287.9	-0.52
hst-6	-0.52
C06E2.1	-0.52
fbxa-197	-0.52
cpi-1	-0.52
C08B6.11	-0.52
B0252.1	-0.52
col-174	-0.52
ethe-1	-0.52
C53D6.6	-0.52
gstk-2	-0.52
W02F12.2	-0.52
mel-32	-0.52
spd-3	-0.52
tag-297	-0.52
D1086.17	-0.52
hke-4.2	-0.52
R02F2.9	-0.52

Gene Name	log_2 Fold
T19C3.2	-0.52
dpy-13	-0.52
snr-6	-0.52
C14A4.6	-0.52
C48B4.10	-0.52
del-6	-0.52
eef-1B.2	-0.52
C02E7.6	-0.52
K07H8.5	-0.52
F57B10.14	-0.52
C46A5.1	-0.52
F54D7.7	-0.52
clec-57	-0.52
C35A5.6	-0.52
cco-2	-0.52
vha-13	-0.52
Y71F9B.9	-0.52
ZK1236.5	-0.52
F55H12.3	-0.52
ugt-41	-0.52
asns-2	-0.52
ets-9	-0.52
ugt-39	-0.52
nstp-2	-0.52
K08F4.5	-0.52
T12G3.6	-0.52
F01D4.5	-0.52
F44F1.3	-0.52
B0035.3	-0.53
F53B6.7	-0.53
daf-14	-0.53
ttr-47	-0.53
C10H11.7	-0.53
ZC204.14	-0.53
mif-2	-0.53
dlc-2	-0.53
R05D11.5	-0.53
F25H9.2	-0.53
wrt-6	-0.53
clec-85	-0.53
bah-1	-0.53
C49F5.7	-0.53

Table E2 (Continued)

Gene Name	log_2 Fold
pmp-1	-0.53
T07A9.15	-0.53
nhr-144	-0.53
F38B6.4	-0.53
sucl-1	-0.53
fshr-1	-0.53
vha-19	-0.53
C04E6.7	-0.53
D1053.4	-0.53
W03D8.5	-0.53
T03F7.7	-0.53
har-1	-0.53
Y53C12A.6	-0.53
T20F10.2	-0.53
pept-2	-0.53
chp-1	-0.53
F57B10.8	-0.53
cpr-5	-0.53
K06H7.7	-0.53
R04F11.2	-0.53
mutd-1	-0.53
cey-3	-0.53
C37H5.2	-0.53
Y63D3A.7	-0.53
R10H10.6	-0.53
nspa-5	-0.53
ptr-21	-0.53
ugt-1	-0.53
gpx-2	-0.53
npa-1	-0.53
H12D21.10	-0.53
msp-65	-0.53
rpl-39	-0.53
C35D10.17	-0.53
ttr-3	-0.53
lon-3	-0.53
F54C9.3	-0.53
T25B9.4	-0.53
F13A7.7	-0.53
Y7A9A.79	-0.53
nhx-4	-0.54
rla-2	-0.54
Y57A10A.23	-0.54
C46H11.6	-0.54
blos-4	-0.54
R09F10.5	-0.54
R10E4.3	-0.54
F55G1.9	-0.54
ZK563.5	-0.54
cgr-1	-0.54
cut-2	-0.54
R12C12.7	-0.54
lact-8	-0.54
C04F12.6	-0.54
ZK970.8	-0.54
C15H7.3	-0.54
C47E12.11	-0.54
F45H11.8	-0.54
T07D3.9	-0.54
C55A6.6	-0.54
F39H2.3	-0.54
C17F4.7	-0.54
glrx-10	-0.54
sulp-4	-0.54
Y116A8C.30	-0.54
gspd-1	-0.54
C34E10.10	-0.54
sss-1	-0.54
C43E11.5	-0.54
C08B6.8	-0.54
nuo-4	-0.54
T19B4.3	-0.54
R144.12	-0.54
T14B4.2	-0.54
T15H9.5	-0.54
pas-5	-0.54
F21C3.6	-0.54
cex-1	-0.54
K09E2.3	-0.54
F53F4.10	-0.54
rnh-1.2	-0.54
C17E4.20	-0.54
apc-11	-0.54
C09D4.3	-0.54
ZK105.1	-0.54
Y60A3A.25	-0.55
C16C8.16	-0.55
ddo-3	-0.55
C09D4.1	-0.55
fbxa-189	-0.55
C44C10.3	-0.55
glna-2	-0.55
F22D6.8	-0.55
R07E5.11	-0.55
mboa-7	-0.55
T14B4.3	-0.55
pho-11	-0.55
twk-26	-0.55
nhr-92	-0.55
C06C3.10	-0.55
F42G8.8	-0.55
Y53C12A.11	-0.55
nspa-4	-0.55
gad-3	-0.55
asm-1	-0.55
col-153	-0.55
F21A3.5	-0.55
K12H4.5	-0.55
F42H10.2	-0.55
Y54G2A.49	-0.55
Y47G6A.15	-0.55
acl-5	-0.55
Y71F9AL.9	-0.55
pgrn-1	-0.55
cnc-8	-0.55
R05G6.7	-0.55
pqn-74	-0.55
lec-10	-0.55
F10D2.10	-0.56
twk-25	-0.56
nhr-59	-0.56
K07F5.16	-0.56
vha-16	-0.56
aps-3	-0.56
frh-1	-0.56
ttr-12	-0.56
eif-1.A	-0.56
cut-4	-0.56
K12C11.3	-0.56
C36B1.14	-0.56
K08C7.7	-0.56
T22C8.6	-0.56
ZK688.11	-0.56
F54F3.4	-0.56
mrps-21	-0.56
dlc-1	-0.56
F58D5.2	-0.56
mrps-26	-0.56
acdh-12	-0.56
F55A4.8	-0.56
dpm-1	-0.56
iftb-1	-0.56
mccc-1	-0.56
K06A4.7	-0.56
C35D10.8	-0.56
nhr-153	-0.56
T23C6.4	-0.56
fipr-21	-0.56
app-1	-0.56
K09G1.1	-0.56
C55F2.1	-0.56
F10C1.3	-0.56
nucb-1	-0.56
C03A7.2	-0.56
ZK546.14	-0.56
cdk-4	-0.56
wrt-1	-0.56
ceh-79	-0.56
rps-2	-0.56
MTCE.31	-0.56
ZK686.1	-0.56
T02B11.9	-0.56
glrx-22	-0.56
nuo-6	-0.56

Table E2 (Continued)

Gene Name	log_2 Fold
K02E10.6	-0.56
Y39A1A.14	-0.56
ncs-3	-0.56
col-130	-0.56
F26F4.8	-0.56
gas-1	-0.56
col-48	-0.57
ZK896.5	-0.57
ZK809.8	-0.57
ifa-1	-0.57
M04C9.1	-0.57
gst-42	-0.57
K08D12.3	-0.57
AH6.3	-0.57
H41C03.3	-0.57
F08G12.3	-0.57
nhr-109	-0.57
lpd-5	-0.57
C16C10.4	-0.57
daf-22	-0.57
ttr-30	-0.57
EEED8.13	-0.57
C50F4.4	-0.57
tag-234	-0.57
T21H3.1	-0.57
F17C11.6	-0.57
D1086.5	-0.57
ctb-1	-0.57
clec-10	-0.57
R08C7.8	-0.57
F30A10.2	-0.57
C48B6.4	-0.57
C01H6.4	-0.57
kqt-3	-0.57
K04C1.5	-0.57
F58B3.4	-0.57
F56F4.3	-0.57
ZK856.18	-0.57
tre-2	-0.57
ZK84.5	-0.57
msp-57	-0.58
K01D12.9	-0.58

Gene Name	log_2 Fold
ver-2	-0.58
W03G9.8	-0.58
rnp-4	-0.58
F32B4.2	-0.58
ZK20.4	-0.58
mrps-31	-0.58
F14D7.6	-0.58
acs-3	-0.58
F36F2.1	-0.58
vha-3	-0.58
aos-1	-0.58
msp-52	-0.58
daf-5	-0.58
F57B10.5	-0.58
glrx-21	-0.58
C26E6.12	-0.58
ZC373.5	-0.58
F49E12.12	-0.58
aps-2	-0.58
hil-3	-0.58
F47E1.4	-0.58
ugt-9	-0.58
R08A2.2	-0.58
ttll-15	-0.58
F09F7.4	-0.58
ZK1127.13	-0.58
dnpp-1	-0.58
Y59E9AR.7	-0.58
F31E9.3	-0.58
grl-7	-0.58
T27A3.6	-0.58
F10E9.5	-0.58
hmit-1.3	-0.58
C25H3.3	-0.58
snr-3	-0.58
oig-2	-0.58
K12B6.2	-0.58
C25A1.16	-0.59
C14B9.10	-0.59
C33G3.4	-0.59
ech-3	-0.59

Gene Name	log_2 Fold
Y71H2B.1	-0.59
F54F7.3	-0.59
K04G11.3	-0.59
fbxa-202	-0.59
urm-1	-0.59
phf-30	-0.59
C49A9.6	-0.59
twk-24	-0.59
C18E9.4	-0.59
K08E3.10	-0.59
msp-55	-0.59
F56B3.11	-0.59
ZC239.16	-0.59
dnj-13	-0.59
F09E5.11	-0.59
F09G2.1	-0.59
lpr-7	-0.59
acp-5	-0.59
C49A9.2	-0.59
Y49E10.16	-0.59
ard-1	-0.59
Y53F4B.3	-0.59
lbp-4	-0.59
B0205.12	-0.59
R07E4.3	-0.59
Y39B6A.3	-0.59
F57C12.6	-0.59
T10B11.5	-0.59
Y37A1B.5	-0.59
K04G7.11	-0.59
acdh-4	-0.59
Y65B4BL.6	-0.60
F27C1.3	-0.60
Y44F5A.1	-0.60
cyp-25A3	-0.60
Y73F4A.1	-0.60
grl-5	-0.60
his-70	-0.60
ZK185.5	-0.60
nhx-2	-0.60
nhr-177	-0.60
nhr-36	-0.60

Gene Name	log_2 Fold
kbp-4	-0.60
R12C12.6	-0.60
E02H1.6	-0.60
nhr-232	-0.60
Y69A2AR.21	-0.60
nol-1	-0.60
C47E8.11	-0.60
tiar-3	-0.60
htp-1	-0.60
hsp-43	-0.60
prx-11	-0.60
Y55B1AR.4	-0.60
Y95D11A.1	-0.60
C54G4.3	-0.60
F31F7.1	-0.60
F37C4.4	-0.60
W06A11.4	-0.60
Y19D10B.6	-0.60
B0334.3	-0.60
F18F11.5	-0.60
nhr-106	-0.60
Y51A2B.6	-0.60
T08B1.1	-0.60
R09F10.1	-0.60
T01G5.7	-0.60
ZC374.2	-0.60
best-20	-0.61
W09G12.10	-0.61
his-25	-0.61
C17C3.1	-0.61
K08C9.1	-0.61
pho-1	-0.61
acdh-9	-0.61
T14G8.3	-0.61
F55C10.5	-0.61
T06E4.5	-0.61
Y57G7A.5	-0.61
ZC477.2	-0.61
T05E7.1	-0.61
col-109	-0.61

Table E2 (Continued)

Gene Name	log_2 Fold
F38A5.6	-0.61
mrpl-50	-0.61
Y43D4A.5	-0.61
alh-9	-0.61
T24C12.3	-0.61
C14A11.6	-0.61
ZK1225.5	-0.61
R09B3.2	-0.61
E01G4.6	-0.61
bus-18	-0.61
F16F9.4	-0.61
mrps-7	-0.61
psmd-9	-0.61
K02G10.15	-0.61
T24D3.2	-0.61
lon-1	-0.62
F58F12.4	-0.62
T05B4.14	-0.62
Y37E3.11	-0.62
exos-3	-0.62
F31F4.1	-0.62
F42A9.7	-0.62
M7.8	-0.62
spp-16	-0.62
R193.2	-0.62
T10G3.3	-0.62
F11C1.5	-0.62
elo-6	-0.62
F28E10.4	-0.62
nlt-1	-0.62
irk-3	-0.62
set-15	-0.62
hsp-16.1	-0.62
F54H5.3	-0.62
R11H6.4	-0.62
C04F1.1	-0.62
oac-50	-0.62
tre-1	-0.62
CD4.10	-0.62
R04F11.5	-0.62
F56D5.3	-0.62
col-73	-0.62
F55B11.2	-0.62
M79.2	-0.62
grd-14	-0.62
etf-1	-0.62
F02E9.3	-0.62
Y75B8A.31	-0.62
col-14	-0.62
R09D1.11	-0.62
C47B2.2	-0.63
F09E5.8	-0.63
nlp-47	-0.63
ugt-44	-0.63
M01B2.13	-0.63
B0281.4	-0.63
C35D10.10	-0.63
coq-5	-0.63
F56C4.4	-0.63
F37C4.6	-0.63
Y62E10A.2	-0.63
aco-1	-0.63
C04F12.16	-0.63
C55C2.4	-0.63
fbxa-196	-0.63
nas-7	-0.63
smp-2	-0.63
acs-7	-0.63
Y39A3CL.3	-0.63
ZK1127.5	-0.63
ugt-33	-0.63
F56A8.4	-0.63
tkt-1	-0.64
sulp-7	-0.64
ZK84.2	-0.64
C30B5.6	-0.64
F56F10.1	-0.64
T08G11.2	-0.64
F41F3.3	-0.64
Y47D7A.16	-0.64
ZK180.5	-0.64
F49D11.6	-0.64
T21C9.6	-0.64
dhs-7	-0.64
ZK669.4	-0.64
T10F2.2	-0.64
cyc-2.2	-0.64
hsp-3	-0.64
gon-2	-0.64
F22E5.1	-0.64
dpm-3	-0.64
zip-12	-0.64
T28B8.6	-0.64
D1014.4	-0.64
Y48G1C.13	-0.64
aex-1	-0.64
fbxc-32	-0.64
rpl-22	-0.64
W06D11.3	-0.64
F45H11.5	-0.64
twk-46	-0.64
Y66D12A.13	-0.64
K08D8.5	-0.64
faah-3	-0.64
mdt-11	-0.64
C15F1.1	-0.64
repo-1	-0.65
C43E11.9	-0.65
T05C12.1	-0.65
col-104	-0.65
F23F1.6	-0.65
prx-5	-0.65
K04G2.7	-0.65
ubxn-5	-0.65
ent-4	-0.65
cdo-1	-0.65
gst-12	-0.65
col-175	-0.65
asp-6	-0.65
mrps-24	-0.65
C07E3.9	-0.65
F58A6.5	-0.65
rhr-2	-0.65
gst-6	-0.65
ucr-2.2	-0.65
acs-5	-0.65
ptr-24	-0.65
ZC123.1	-0.65
npr-20	-0.65
C02E7.7	-0.65
nlp-29	-0.65
his-13	-0.65
F34D10.9	-0.65
perm-2	-0.65
fip-5	-0.65
math-32	-0.65
nhr-107	-0.65
Y34B4A.5	-0.65
chhy-1	-0.65
fip-6	-0.65
C04E6.5	-0.65
K02A6.3	-0.65
ddp-1	-0.65
nhr-16	-0.65
F19G12.9	-0.65
Y43F8B.23	-0.65
F26G1.11	-0.65
pdi-2	-0.65
F58F9.7	-0.65
C05C10.3	-0.66
Y48G10A.6	-0.66
C41G11.1	-0.66
try-7	-0.66
F36H5.14	-0.66
ZK795.3	-0.66
C08F11.10	-0.66
F53A9.2	-0.66
nex-3	-0.66
C55A6.11	-0.66
D1007.15	-0.66
T09A5.7	-0.66
col-91	-0.66
F57F4.4	-0.66
B0207.7	-0.66
R53.2	-0.66

Table E2 (Continued)

Gene Name	log_2 Fold
Y39B6A.7	-0.66
lys-1	-0.66
M05B5.4	-0.66
F58D5.6	-0.66
ttr-48	-0.66
T19H5.6	-0.66
F10G8.2	-0.66
ZK84.1	-0.66
Y105E8B.7	-0.66
B0496.1	-0.66
C06H5.6	-0.66
K10D2.5	-0.66
nlp-24	-0.66
K09A11.1	-0.66
his-42	-0.66
Y75B8A.4	-0.66
F59D12.5	-0.66
cuc-1	-0.66
ZC190.8	-0.67
Y58A7A.1	-0.67
mrpl-24	-0.67
sfxn-1.3	-0.67
ttr-44	-0.67
fbxa-70	-0.67
F25H5.8	-0.67
C04G2.5	-0.67
lpd-8	-0.67
W01B11.6	-0.67
F20G2.7	-0.67
K07C11.7	-0.67
vha-6	-0.67
T05F1.13	-0.67
C39B5.5	-0.67
Y57A10A.3	-0.67
mrp-3	-0.67
gpa-7	-0.67
tsp-10	-0.67
F58H1.8	-0.67
ugt-23	-0.67
C28D4.8	-0.67
Y105C5B.18	-0.67
decr-1.1	-0.67
F36A4.5	-0.67
nhr-220	-0.67
F01G10.9	-0.67
ugt-21	-0.67
F10E9.12	-0.67
C07H4.1	-0.67
gst-35	-0.67
ctl-2	-0.67
ZK809.9	-0.67
mai-2	-0.67
Y6G8.2	-0.67
C34B2.9	-0.67
C25E10.8	-0.67
elo-9	-0.67
gfi-1	-0.67
F52A8.5	-0.67
Y43C5B.3	-0.67
Y69E1A.8	-0.68
Y18D10A.21	-0.68
F47B8.8	-0.68
col-38	-0.68
perm-4	-0.68
Y47D7A.7	-0.68
D1086.10	-0.68
K02A11.4	-0.68
tag-173	-0.68
F58B4.5	-0.68
col-97	-0.68
clec-51	-0.68
B0207.2	-0.68
H12D21.5	-0.68
F17H10.2	-0.68
lbp-5	-0.68
C32C4.3	-0.68
W09C3.2	-0.68
acs-1	-0.68
C53H9.3	-0.68
nhr-110	-0.68
T16G1.6	-0.68
C35C5.10	-0.69
mdt-9	-0.69
tni-4	-0.69
pes-9	-0.69
mrpl-32	-0.69
fbxa-224	-0.69
D2062.7	-0.69
tag-345	-0.69
pqn-68	-0.69
Y67H2A.9	-0.69
Y39E4A.3	-0.69
nas-36	-0.69
F16G10.15	-0.69
thn-2	-0.69
ZK512.8	-0.69
H10E21.4	-0.69
C30G12.2	-0.69
glo-3	-0.69
C06A12.3	-0.69
mrpl-51	-0.69
K02E11.10	-0.69
F32B6.4	-0.69
K03B4.6	-0.69
ssp-31	-0.69
C44B7.7	-0.69
asp-2	-0.69
sma-10	-0.69
fbxa-57	-0.69
C24A3.4	-0.69
T11F8.1	-0.69
spe-11	-0.69
W01A8.8	-0.69
D1007.3	-0.69
F37C12.3	-0.69
Y47D7A.6	-0.69
F35H12.5	-0.70
best-23	-0.70
F36H12.3	-0.70
oat-1	-0.70
C35E7.10	-0.70
K04F10.1	-0.70
K08C7.6	-0.70
F26E4.5	-0.70
ZK666.8	-0.70
F36A4.4	-0.70
dct-5	-0.70
best-12	-0.70
zip-3	-0.70
C09B7.2	-0.70
T14B4.5	-0.70
gcst-1	-0.70
B0228.6	-0.70
C01G10.8	-0.70
pps-1	-0.70
tsp-18	-0.70
ZK1128.3	-0.70
K04G2.11	-0.70
lsm-3	-0.70
hrg-4	-0.70
C08H9.2	-0.70
ZK354.3	-0.70
spp-5	-0.70
bli-6	-0.70
C26C6.9	-0.70
lpd-2	-0.70
T01D1.3	-0.70
M04C9.4	-0.70
nhr-168	-0.71
F56F4.4	-0.71
R144.11	-0.71
C01H6.8	-0.71
F07H5.3	-0.71
kbp-2	-0.71
F42A9.3	-0.71
ttr-50	-0.71
snr-7	-0.71
C35E7.9	-0.71
K11D12.13	-0.71
ubl-5	-0.71
gta-1	-0.71
Y106G6H.1	-0.71
Y106G6E.3	-0.71
K09H11.1	-0.71

Table E2 (Continued)

Gene Name	log_2 Fold
F39H12.3	-0.71
R03G8.6	-0.71
C30G12.4	-0.71
C04F12.7	-0.71
K07F5.12	-0.71
ZK1127.4	-0.71
lgc-32	-0.71
T04C12.8	-0.71
W03G9.5	-0.71
T10B10.8	-0.71
T06G6.6	-0.71
F55D12.6	-0.71
C40C9.3	-0.71
C29F3.7	-0.71
ugt-17	-0.71
col-161	-0.71
lsm-8	-0.72
Y67A6A.1	-0.72
R09E10.2	-0.72
nspd-9	-0.72
F11D5.7	-0.72
F53F4.16	-0.72
tut-2	-0.72
MTCE.3	-0.72
C28D4.7	-0.72
acs-22	-0.72
F14B6.6	-0.72
B0545.4	-0.72
M60.2	-0.72
mdt-10	-0.72
ndx-8	-0.72
K09F6.4	-0.72
C46F2.1	-0.72
rpl-29	-0.72
col-63	-0.72
tkr-3	-0.72
C06G8.3	-0.72
fbxa-69	-0.72
lbp-7	-0.72
R186.8	-0.72
F42C5.5	-0.72
gstk-1	-0.72

Gene Name	log_2 Fold
F31D4.9	-0.72
math-45	-0.72
R08B4.3	-0.72
F23C8.8	-0.72
F52H2.6	-0.72
clec-150	-0.72
flu-2	-0.72
H22K11.2	-0.72
W04E12.7	-0.72
col-162	-0.72
F17A9.4	-0.73
F36A2.11	-0.73
lips-9	-0.73
F35E12.10	-0.73
T10E9.6	-0.73
irld-6	-0.73
col-71	-0.73
F23F1.10	-0.73
F34D10.6	-0.73
T22A3.12	-0.73
Y43B11AR.1	-0.73
C28D4.5	-0.73
ZC250.5	-0.73
C07D8.6	-0.73
T10B5.4	-0.73
F35G12.11	-0.73
lys-2	-0.73
cth-2	-0.73
fkb-3	-0.73
ttr-45	-0.73
nspd-4	-0.73
C52E2.5	-0.73
C26B9.5	-0.73
aagr-1	-0.73
clec-230	-0.73
nhr-10	-0.73
C49A9.10	-0.73
ugt-12	-0.73
vps-25	-0.73
hil-2	-0.73
C05C10.7	-0.73

Gene Name	log_2 Fold
ZK858.8	-0.73
elo-5	-0.74
H29C22.1	-0.74
lipl-2	-0.74
clec-117	-0.74
ugt-7	-0.74
ZK265.9	-0.74
bli-2	-0.74
nas-22	-0.74
acdh-5	-0.74
F27E5.1	-0.74
kvs-4	-0.74
snrp-27	-0.74
R12E2.14	-0.74
F49C12.11	-0.74
rpb-8	-0.74
Y51F10.7	-0.74
F59A2.5	-0.74
D1014.2	-0.74
ptps-1	-0.74
ZK673.1	-0.74
msp-63	-0.74
ttr-51	-0.74
fbxa-33	-0.74
fbxc-42	-0.74
ZK1290.5	-0.74
Y42H9AR.2	-0.75
Y47D9A.5	-0.75
C10C5.4	-0.75
mrpl-54	-0.75
pqn-88	-0.75
C29F7.10	-0.75
F20D1.9	-0.75
madf-10	-0.75
ssp-32	-0.75
F59C6.11	-0.75
ZK1248.5	-0.75
F58A6.1	-0.75
cyp-34A9	-0.75
T27C10.8	-0.75
K03H6.2	-0.75

Gene Name	log_2 Fold
nhr-104	-0.75
W05E10.1	-0.75
Y69H2.9	-0.75
Y82E9BR.22	-0.75
nhr-76	-0.75
F12B6.2	-0.75
F11A10.7	-0.75
dmd-8	-0.75
F54D5.12	-0.75
F32A5.3	-0.75
nhr-12	-0.75
col-137	-0.75
clec-54	-0.75
ZK1193.2	-0.75
tin-13	-0.75
C17G10.3	-0.75
ZC581.7	-0.75
F57B1.5	-0.76
F45G2.8	-0.76
F54D1.1	-0.76
T01C3.2	-0.76
clec-151	-0.76
clec-147	-0.76
gpx-6	-0.76
T10E9.3	-0.76
C15H9.9	-0.76
F09C8.1	-0.76
F14H3.3	-0.76
C01B10.10	-0.76
Y87G2A.20	-0.76
F13B12.2	-0.76
M05B5.7	-0.76
hog-1	-0.76
tomm-7	-0.76
C03F11.4	-0.76
decr-1.3	-0.76
R09D1.10	-0.76
F13D12.6	-0.76
R09B5.12	-0.76
acy-4	-0.76

Table E2 (Continued)

Gene Name	log_2 Fold
D2021.4	-0.76
ZK822.2	-0.77
pes-23	-0.77
ZK512.1	-0.77
F22D3.6	-0.77
acox-1	-0.77
B0041.1	-0.77
F52E1.14	-0.77
mlp-1	-0.77
ent-2	-0.77
tag-147	-0.77
C33G8.2	-0.77
F53F1.4	-0.77
F56H1.3	-0.77
F54C1.8	-0.77
ZC477.7	-0.77
C46G7.1	-0.77
ttr-53	-0.77
ile-2	-0.77
C44H9.5	-0.77
F36H9.5	-0.77
irld-57	-0.77
K08E7.8	-0.77
his-37	-0.77
Y11D7A.5	-0.77
F18F11.1	-0.77
fbxa-97	-0.77
C03B1.13	-0.77
ttr-9	-0.77
F23C8.3	-0.77
C23G10.1	-0.77
gut-2	-0.77
C03B1.7	-0.77
T28C6.5	-0.77
C45B11.9	-0.78
Y81G3A.1	-0.78
Y38A10A.7	-0.78
acbp-1	-0.78
T09A5.15	-0.78
Y51H7C.1	-0.78
grl-16	-0.78
nhr-42	-0.78
F10G8.1	-0.78
K08H10.9	-0.78
spl-1	-0.78
C10A4.9	-0.78
F18A1.1	-0.78
ZK265.6	-0.78
C35B1.4	-0.78
ndg-4	-0.78
D1086.7	-0.78
T07D4.5	-0.78
Y40B1B.7	-0.78
F53B7.3	-0.78
F52F12.8	-0.78
R09H10.3	-0.78
C33A12.1	-0.78
F14D7.10	-0.78
F40H6.1	-0.78
mrpl-53	-0.78
F37A8.1	-0.78
ckb-2	-0.78
F59B1.2	-0.79
tomm-22	-0.79
T10B5.7	-0.79
pmp-2	-0.79
fbxa-125	-0.79
K11C4.1	-0.79
nbet-1	-0.79
T22B3.3	-0.79
T04F3.4	-0.79
mec-5	-0.79
C23H4.2	-0.79
Y43F4B.10	-0.79
ZK813.2	-0.79
F19C7.4	-0.79
C03A7.13	-0.79
B0272.4	-0.79
dsc-4	-0.79
tag-261	-0.79
C23H4.4	-0.79
Y71G12B.3	-0.79
F31E9.11	-0.79
R12E2.15	-0.79
W02B12.4	-0.79
lbp-6	-0.80
ZK616.3	-0.80
ZK899.2	-0.80
C16C10.8	-0.80
F55B11.7	-0.80
F59C6.3	-0.80
R06C1.4	-0.80
ZK512.7	-0.80
Y49E10.29	-0.80
C48B4.1	-0.80
F25H5.2	-0.80
F43C11.7	-0.80
tin-10	-0.80
F25G6.8	-0.80
C12D8.9	-0.80
R07E4.1	-0.80
F13H6.3	-0.80
F44A6.4	-0.80
F27C1.1	-0.80
C55C2.3	-0.80
K07E1.1	-0.80
dct-18	-0.80
rol-1	-0.80
skr-7	-0.80
ZC395.10	-0.80
Y57G11C.46	-0.80
Y47D3B.12	-0.80
C02F5.14	-0.80
nhr-136	-0.80
mltn-12	-0.81
C01G12.3	-0.81
F56B3.6	-0.81
nspd-2	-0.81
mrpl-13	-0.81
F40G9.5	-0.81
C07A9.9	-0.81
fpn-1.1	-0.81
Y59H11AM.4	-0.81
nhr-179	-0.81
Y54E2A.9	-0.81
cdr-1	-0.81
abu-15	-0.81
F58H1.6	-0.81
wrt-4	-0.81
C56C10.6	-0.81
syx-6	-0.81
C50F7.3	-0.81
B0554.4	-0.81
efn-4	-0.81
col-60	-0.81
smf-3	-0.81
col-76	-0.81
pfd-4	-0.81
col-138	-0.82
F21A3.4	-0.82
ets-4	-0.82
C28C12.11	-0.82
C14A4.9	-0.82
clec-52	-0.82
F53G12.8	-0.82
F54H12.5	-0.82
mbr-1	-0.82
mpst-3	-0.82
C29E4.12	-0.82
F14B8.4	-0.82
F10E7.6	-0.82
spe-12	-0.82
F36A2.12	-0.82
trap-4	-0.82
T13A10.1	-0.82
prx-3	-0.82
W06D4.2	-0.82
nspd-7	-0.82
nspd-1	-0.82
ZK1251.3	-0.82
D1081.12	-0.82
M03B6.1	-0.82
T01D1.4	-0.82
ugt-52	-0.82
B0035.13	-0.82

Table E2 (Continued)

Gene Name	log_2 Fold
T10E9.8	-0.82
C52E4.7	-0.82
W10G11.2	-0.82
ZC434.7	-0.82
F14H3.4	-0.83
C15C8.3	-0.83
R02E4.3	-0.83
cyp-33E2	-0.83
nhr-237	-0.83
col-77	-0.83
Y23H5B.1	-0.83
C10C6.3	-0.83
fbxa-32	-0.83
ztf-26	-0.83
K07F5.14	-0.83
col-49	-0.83
F22F4.5	-0.83
Y47D3A.13	-0.83
clec-206	-0.83
F39G3.2	-0.83
Y48G8AL.12	-0.83
nhr-142	-0.83
C15A11.2	-0.83
C07D10.5	-0.84
B0207.11	-0.84
F21D5.4	-0.84
H27M09.5	-0.84
ZC412.10	-0.84
fbxa-187	-0.84
MTCE.25	-0.84
ZC376.3	-0.84
T25B9.1	-0.84
F38B2.6	-0.84
mrps-18A	-0.84
spp-1	-0.84
cyp-14A2	-0.84
W08E3.4	-0.84
B0491.7	-0.84
nspd-5	-0.84
T12D8.5	-0.84
linc-19	-0.84

Gene Name	log_2 Fold
linc-4	-0.84
F10E9.11	-0.84
F01F1.2	-0.84
W09D6.4	-0.84
cdr-6	-0.84
C06A8.8	-0.84
acd-5	-0.84
ttr-46	-0.84
ech-6	-0.84
K08E4.7	-0.85
dod-3	-0.85
gst-28	-0.85
MTCE.16	-0.85
Y51B9A.5	-0.85
F55B11.5	-0.85
ret-1	-0.85
peel-1	-0.85
C05D2.8	-0.85
ZK550.2	-0.85
C42D4.1	-0.85
tag-267	-0.85
F07D3.3	-0.85
F46F5.6	-0.85
F44G4.5	-0.85
ZC155.2	-0.85
W10G11.3	-0.85
F43E2.6	-0.85
R12E2.7	-0.85
Y106G6D.8	-0.85
K08C7.1	-0.85
rnh-1.3	-0.85
C06A8.6	-0.85
C26B2.7	-0.85
C32D5.4	-0.85
F09E10.1	-0.85
K07A1.10	-0.86
fipr-6	-0.86
ZK813.7	-0.86
D1022.4	-0.86
C53D6.10	-0.86
F14F7.5	-0.86

Gene Name	log_2 Fold
C47A4.3	-0.86
C08F11.11	-0.86
C24B9.3	-0.86
C39D10.7	-0.86
R07B7.10	-0.86
F14E5.1	-0.86
R13A1.3	-0.86
R102.4	-0.86
ZK354.7	-0.86
cyp-29A2	-0.86
Y45F10C.4	-0.86
ZK622.1	-0.86
F02C9.1	-0.87
C14C11.4	-0.87
T28H11.7	-0.87
F28A10.1	-0.87
cln-3.1	-0.87
spe-10	-0.87
dnj-21	-0.87
rpac-19	-0.87
ZK1098.6	-0.87
pqn-54	-0.87
ttr-15	-0.87
C04F12.12	-0.87
Y69A2AR.3	-0.87
ZK813.1	-0.87
sft-4	-0.87
Y48A6B.7	-0.87
F07A11.5	-0.87
F53F4.18	-0.87
mrps-17	-0.87
C54D10.4	-0.87
klo-2	-0.87
C30G7.4	-0.88
F52F12.5	-0.88
nlp-26	-0.88
D2062.6	-0.88
ZK484.6	-0.88
W09C3.7	-0.88
F13A7.12	-0.88
B0416.4	-0.88

Gene Name	log_2 Fold
mrpl-23	-0.88
pfd-5	-0.88
ZK909.6	-0.88
F53C11.3	-0.88
spe-17	-0.88
ZK228.3	-0.88
D1054.8	-0.88
mrps-33	-0.88
lin-10	-0.89
K01D12.8	-0.89
C47D12.5	-0.89
npax-4	-0.89
R01H2.4	-0.89
btb-21	-0.89
snb-7	-0.89
W01A8.10	-0.89
M04C9.3	-0.89
C23H4.3	-0.89
ZC373.2	-0.89
Y53F4B.36	-0.89
T21E12.5	-0.89
F37E3.3	-0.89
pgp-11	-0.89
EEED8.15	-0.89
F10E9.4	-0.89
AC3.9	-0.90
F21C3.7	-0.90
spds-1	-0.90
T08H10.1	-0.90
B0252.5	-0.90
M153.2	-0.90
nhr-244	-0.90
C29F7.3	-0.90
K04A8.10	-0.90
ZC21.10	-0.90
C49H3.3	-0.90
F55F10.3	-0.90
C01G6.2	-0.90
dhs-21	-0.90
C53B4.3	-0.90
tsp-19	-0.90
pfd-6	-0.90

Table E2 (Continued)

Gene Name	log_2 Fold
B0496.6	-0.90
cyp-33E1	-0.91
C17H12.4	-0.91
msd-4	-0.91
F36H9.2	-0.91
ftn-2	-0.91
T16G12.7	-0.91
Y40D12A.2	-0.91
T28A11.2	-0.91
Y73B3B.3	-0.91
R102.15	-0.91
F40G9.2	-0.91
htas-1	-0.91
ZK973.4	-0.91
nhr-176	-0.91
F17E9.4	-0.91
asm-2	-0.91
irld-8	-0.91
Y22D7AR.7	-0.91
K05F1.8	-0.91
spp-8	-0.92
C55C3.4	-0.92
C53B4.2	-0.92
clec-65	-0.92
F57B1.9	-0.92
K09G1.2	-0.92
C38C6.3	-0.92
D2045.8	-0.92
ZK673.6	-0.92
C10G8.8	-0.92
C29F7.1	-0.92
F54D7.6	-0.92
ZK930.4	-0.92
F58B4.7	-0.92
acs-14	-0.92
ZC416.6	-0.92
D1081.3	-0.92
C03C11.1	-0.93
cpz-1	-0.93
spp-3	-0.93
Y87G2A.2	-0.93

Gene Name	log_2 Fold
C06B3.7	-0.93
C55A6.4	-0.93
C35A11.4	-0.93
C03C10.2	-0.93
Y40C7B.1	-0.93
Y47D3A.32	-0.93
spp-22	-0.93
dhs-25	-0.93
F53F8.3	-0.93
fbxa-74	-0.93
hpo-18	-0.93
Y57G11B.3	-0.93
T06E4.9	-0.93
Y106G6A.4	-0.93
gst-15	-0.93
dao-4	-0.93
C04G6.2	-0.93
W03F8.2	-0.94
T09A12.1	-0.94
C05B5.5	-0.94
F56F3.4	-0.94
W02D9.7	-0.94
C45B2.1	-0.94
W02D9.6	-0.94
W09C3.8	-0.94
F13G11.3	-0.94
ZC412.9	-0.94
F47B10.9	-0.94
T20D4.5	-0.94
R12C12.9	-0.95
F44E2.9	-0.95
C17H12.8	-0.95
F37C12.18	-0.95
trap-2	-0.95
C28C12.1	-0.95
inx-9	-0.95
R102.11	-0.95
F17B5.8	-0.95
F02H6.3	-0.95
T13F2.9	-0.95

Gene Name	log_2 Fold
F35H10.2	-0.95
Y71H2B.8	-0.95
mocs-1	-0.95
twk-37	-0.95
T04B2.7	-0.95
C06A6.7	-0.95
mtl-2	-0.95
T28A11.6	-0.95
F08F1.4	-0.95
E01G6.3	-0.95
F45E4.6	-0.95
K07G5.5	-0.95
F57C2.4	-0.96
C16C8.20	-0.96
R09E10.1	-0.96
col-110	-0.96
F33D11.7	-0.96
F56G4.7	-0.96
F08A8.4	-0.96
clec-232	-0.96
T24C4.4	-0.96
fbxa-51	-0.96
C25B8.8	-0.96
Y23H5B.8	-0.96
wrt-8	-0.96
Y69E1A.4	-0.96
F16C3.4	-0.96
F55C10.4	-0.96
F36A4.2	-0.96
dct-11	-0.96
sup-10	-0.96
ssp-37	-0.96
dpyd-1	-0.96
clec-223	-0.96
C10A4.4	-0.96
K02B12.2	-0.96
clec-166	-0.96
F46F5.11	-0.96
C50F4.10	-0.97
col-182	-0.97
afmd-1	-0.97
aqp-10	-0.97

Gene Name	log_2 Fold
K07A1.6	-0.97
C46C2.5	-0.97
T04F8.2	-0.97
cyp-25A2	-0.97
W02B12.1	-0.97
clec-236	-0.97
col-61	-0.97
Y62H9A.3	-0.97
Y51A2D.18	-0.97
D1054.11	-0.97
M162.7	-0.97
F33D4.7	-0.97
fbl-1	-0.97
pcp-2	-0.97
R05D7.2	-0.97
elp-1	-0.97
D2062.5	-0.97
hpd-1	-0.97
R06A10.5	-0.97
F20D6.5	-0.98
fbxa-190	-0.98
nhr-112	-0.98
nsy-7	-0.98
irld-7	-0.98
lys-8	-0.98
F46A9.2	-0.98
F25B4.8	-0.98
F21D5.3	-0.98
maoc-1	-0.98
F58G6.9	-0.98
F34D10.8	-0.98
Y119D3B.13	-0.99
Y69A2AR.27	-0.99
best-7	-0.99
gbh-2	-0.99
T16G1.7	-0.99
C07A4.3	-0.99
C24D10.2	-0.99
B0563.5	-0.99
gcsh-1	-0.99

Table E2 (Continued)

Gene Name	log_2 Fold
dhs-3	-0.99
F44D12.6	-0.99
ser-7	-0.99
Y47D7A.15	-0.99
F58A4.12	-0.99
C23H4.7	-0.99
msra-1	-1.00
C10G8.4	-1.00
Y39H10B.2	-1.00
ttr-40	-1.00
C34B2.3	-1.00
T11B7.1	-1.00
F36H9.4	-1.00
linc-15	-1.00
Y38F2AR.10	-1.00
nuc-1	-1.00
fipr-13	-1.00
gpx-7	-1.00
Y62H9A.15	-1.00
fbxa-83	-1.00
W05H9.3	-1.01
K07A1.4	-1.01
haao-1	-1.01
C31H1.2	-1.01
ZK1240.5	-1.01
mig-1	-1.01
C05C12.6	-1.01
C18A3.7	-1.01
Y37D8A.19	-1.01
pmt-2	-1.01
C34G6.3	-1.01
asp-1	-1.01
M7.12	-1.01
F07F6.2	-1.01
hsp-16.48	-1.01
F59A6.12	-1.01
F42A9.6	-1.01
F53H4.2	-1.01
T25B9.2	-1.01
C27D6.3	-1.01
C25H3.17	-1.02
Y73F8A.14	-1.02
Y14H12A.1	-1.02
T28A11.16	-1.02
K08F9.1	-1.02
C05D12.2	-1.02
hrg-3	-1.02
Y46G5A.14	-1.02
ttr-35	-1.02
K04G2.10	-1.02
linc-36	-1.02
C46C11.2	-1.02
hrg-6	-1.02
C40H1.2	-1.03
ZK813.3	-1.03
ZK1240.9	-1.03
Y69H2.3	-1.03
lys-5	-1.03
Y38H6C.15	-1.03
F54H12.7	-1.03
C04E12.2	-1.03
gpx-1	-1.03
nhr-263	-1.03
cpt-4	-1.04
F55B11.3	-1.04
clec-210	-1.04
F32H5.1	-1.04
T02B11.8	-1.04
cdd-1	-1.04
btb-2	-1.04
F45B8.5	-1.04
T01H3.5	-1.04
Y38E10A.28	-1.04
F30A10.12	-1.04
C01G12.9	-1.04
F43H9.4	-1.04
R09D1.6	-1.04
F40H3.2	-1.04
F55C12.6	-1.04
B0416.11	-1.04
C15H7.2	-1.04
F56D6.13	-1.04
dhs-18	-1.04
Y66H1A.5	-1.05
Y43F8C.13	-1.05
R13A5.10	-1.05
MTCE.23	-1.05
F08G5.6	-1.05
C43G2.3	-1.05
Y32F6B.1	-1.05
comt-2	-1.05
T20D4.3	-1.05
Y70C5A.3	-1.05
C32H11.3	-1.05
F20D6.11	-1.05
C29E4.14	-1.05
T04A8.5	-1.05
ZC376.2	-1.05
C01B10.4	-1.05
trap-3	-1.05
F44A6.5	-1.05
C43H6.1	-1.05
nrf-6	-1.05
B0034.7	-1.05
C05E7.2	-1.06
emo-1	-1.06
C03A7.12	-1.06
B0379.2	-1.06
R105.1	-1.06
C55A6.7	-1.06
irg-3	-1.06
clec-155	-1.06
skr-14	-1.06
lips-6	-1.06
F55D12.2	-1.06
dod-17	-1.07
D1081.11	-1.07
asp-3	-1.07
clec-56	-1.07
ZC449.8	-1.07
Y38F1A.7	-1.07
clec-222	-1.07
C45B11.8	-1.07
alh-12	-1.07
ZK1248.20	-1.07
ZC581.10	-1.07
cpt-5	-1.07
hsp-16.49	-1.07
tag-10	-1.08
C25A8.4	-1.08
dhs-14	-1.08
K02A11.2	-1.08
kin-26	-1.08
C44C1.5	-1.08
Y105E8B.9	-1.08
T02D1.8	-1.08
nhr-147	-1.08
grd-6	-1.08
Y23H5B.12	-1.08
C05D12.3	-1.08
ZK185.3	-1.09
F41H10.2	-1.09
R07H5.9	-1.09
ttr-37	-1.09
dylt-3	-1.09
sesn-1	-1.09
T05C3.6	-1.09
ugt-49	-1.09
amx-3	-1.09
asah-1	-1.09
R08E5.3	-1.10
T12B5.15	-1.10
T22C1.9	-1.10
F38E1.3	-1.10
F18C12.4	-1.10
ZC404.2	-1.10
K07F5.8	-1.10
ZK688.12	-1.10
F55H12.2	-1.11
T18D3.9	-1.11
Y54G9A.9	-1.11
Y53C10A.15	-1.12
F07G6.10	-1.12
R10H10.3	-1.12

Table E2 (Continued)

Gene Name	log_2 Fold
Y62H9A.4	-1.12
F12A10.1	-1.12
F30A10.14	-1.12
sth-1	-1.12
W04A4.2	-1.12
ugt-53	-1.13
lact-4	-1.13
F42G4.5	-1.13
oac-42	-1.13
Y40C7B.3	-1.13
spp-23	-1.13
Y38F2AR.9	-1.13
F35F10.1	-1.13
col-88	-1.13
R12E2.6	-1.13
F23A7.8	-1.13
F54D5.4	-1.13
R04A9.9	-1.14
nspb-2	-1.14
Y119D3B.21	-1.14
Y62H9A.6	-1.14
rap-3	-1.14
cpr-6	-1.14
T28F4.4	-1.14
ssp-33	-1.14
F59F4.2	-1.14
W04E12.2	-1.15
prmt-6	-1.15
F30A10.13	-1.15
mec-3	-1.15
W07B8.1	-1.15
C31H2.14	-1.15
B0207.9	-1.15
M7.7	-1.15
F41F3.1	-1.15
F57F5.1	-1.16
T04G9.7	-1.16
Y47D9A.4	-1.16
pyk-2	-1.16
Y51A2D.13	-1.17
ZK228.4	-1.17
cyp-33E3	-1.17
Y105C5B.17	-1.17
oac-8	-1.17
F58B6.1	-1.17
R11H6.7	-1.17
F29B9.7	-1.17
col-120	-1.17
ugt-46	-1.18
C35B1.8	-1.18
nep-4	-1.18
K08B5.2	-1.18
F41C3.7	-1.18
ugt-26	-1.18
R09D1.8	-1.18
Y45G12C.1	-1.18
twk-6	-1.18
F48E3.4	-1.18
F13H8.12	-1.19
Y59E9AL.8	-1.19
Y57G11C.15	-1.19
acbp-3	-1.19
gst-10	-1.19
Y57A10A.14	-1.19
C52A10.3	-1.19
T05B11.4	-1.19
E02C12.8	-1.19
R04B5.11	-1.19
F46F5.9	-1.20
F49E12.1	-1.20
F56A4.3	-1.20
Y105E8B.5	-1.20
C36C9.10	-1.20
W08E12.4	-1.20
T03F6.10	-1.21
pqn-8	-1.21
C05D12.4	-1.21
C53D6.11	-1.21
H23N18.6	-1.21
Y53F4B.11	-1.21
C26C6.6	-1.21
W03F11.1	-1.22
F21F8.4	-1.22
F23F12.3	-1.22
cah-5	-1.22
nid-1	-1.22
Y105C5B.20	-1.22
T12B5.14	-1.22
Y39B6A.21	-1.22
H20E11.2	-1.22
dhs-2	-1.22
trap-1	-1.23
K08F4.13	-1.23
T13F3.6	-1.23
C02C2.4	-1.23
oac-6	-1.23
clec-66	-1.23
col-68	-1.24
C27H5.4	-1.24
C04H5.7	-1.24
pho-9	-1.24
F22G12.7	-1.24
clec-8	-1.24
D1054.10	-1.24
T24A6.20	-1.25
C18D4.8	-1.25
math-48	-1.25
frpr-11	-1.25
try-3	-1.25
W08E12.3	-1.26
K07E12.2	-1.26
F36A4.3	-1.26
ZK418.2	-1.26
spp-17	-1.26
C14A6.6	-1.26
C47G2.6	-1.26
Y57G11C.14	-1.26
F23A7.4	-1.26
ZK616.1	-1.27
T25E12.16	-1.27
ZK686.5	-1.27
F13H10.1	-1.27
F55G11.8	-1.27
frm-9	-1.27
C08F11.13	-1.27
F23F12.13	-1.27
C17E7.12	-1.28
col-152	-1.28
C44B7.11	-1.28
cyp-35A4	-1.28
F01D5.2	-1.29
C31G12.1	-1.29
E04F6.15	-1.29
T19H5.7	-1.29
ugt-32	-1.29
nep-15	-1.29
F33D11.1	-1.30
T05E12.6	-1.30
F16H6.7	-1.30
K02E7.6	-1.30
R12E2.8	-1.30
F28H7.3	-1.31
T20D4.11	-1.31
ttr-36	-1.31
grd-2	-1.31
fbxa-175	-1.31
lys-4	-1.32
crn-6	-1.32
C05B5.9	-1.32
F22H10.2	-1.32
W02D7.4	-1.32
gst-5	-1.32
ech-1	-1.33
aat-4	-1.33
F58G6.3	-1.33
C04E7.5	-1.34
F13H8.3	-1.34
ugt-47	-1.34
F25D1.5	-1.34
fbxa-180	-1.34
gst-4	-1.34

Table E2 (Continued)

Gene Name	log_2 Fold
C04E12.5	-1.34
anr-33	-1.35
nas-20	-1.35
C17B7.5	-1.35
oac-10	-1.35
F40A3.7	-1.35
ZK1240.8	-1.35
grl-27	-1.35
C52E12.6	-1.35
D1086.3	-1.35
Y57G11C.40	-1.36
F12E12.11	-1.36
F41E6.1	-1.36
C48D1.7	-1.36
ttr-49	-1.36
gst-13	-1.36
ZC395.5	-1.37
T22F3.7	-1.37
R04E5.2	-1.37
K04F1.9	-1.37
fbxa-178	-1.37
ZK822.8	-1.37
Y102E9.5	-1.38
F15A4.2	-1.38
C35A5.3	-1.38
inx-8	-1.38
K12H4.7	-1.38
cutl-18	-1.39
Y50E8A.1	-1.39
T28F4.6	-1.39
ugt-62	-1.39
sdz-27	-1.39
F26F12.4	-1.39
T09E11.11	-1.39
D1086.11	-1.40
F10E7.3	-1.40
C34F6.5	-1.40
snf-4	-1.40
K10C2.3	-1.40
Y4C6A.4	-1.40
cpl-1	-1.41
W03D8.8	-1.41
cbl-1	-1.41
ceeh-2	-1.41
efn-3	-1.42
C01B10.44	-1.42
clec-97	-1.42
Y27F2A.8	-1.42
Y57G11C.52	-1.42
C05B5.12	-1.42
ugt-5	-1.43
clec-186	-1.43
pcp-1	-1.43
linc-61	-1.44
ugt-51	-1.44
str-168	-1.44
R09D1.9	-1.44
F07C6.6	-1.44
ugt-54	-1.44
C35A5.5	-1.44
gst-33	-1.45
Y73F8A.15	-1.45
T01G5.8	-1.45
K09H11.4	-1.45
F49B2.4	-1.45
F31D5.1	-1.45
pho-13	-1.46
nas-27	-1.46
ZK287.3	-1.47
H20E11.3	-1.47
F22E12.3	-1.47
fipr-23	-1.47
gst-30	-1.47
T20D4.4	-1.48
B0563.10	-1.48
T28F4.5	-1.48
Y62H9A.5	-1.48
Y19D10A.16	-1.49
C55C3.8	-1.49
C09B8.5	-1.49
B0454.8	-1.49
Y39A1A.2	-1.50
T25B9.12	-1.50
E02H9.7	-1.50
C01B4.6	-1.50
M01G12.14	-1.51
nas-21	-1.51
nspa-8	-1.51
calu-1	-1.51
nep-14	-1.52
F26C11.1	-1.52
W03F9.4	-1.52
C14E2.12	-1.52
Y32F6A.5	-1.52
F58G6.7	-1.53
Y39F10A.3	-1.53
C32D5.6	-1.54
lact-1	-1.54
clec-209	-1.54
hsd-2	-1.54
F15H9.8	-1.55
linc-84	-1.55
C14C6.2	-1.55
Y38F1A.6	-1.55
H06H21.8	-1.55
cyp-25A1	-1.56
F56A4.2	-1.56
Y43F8B.9	-1.57
clec-3	-1.57
Y57G11B.5	-1.58
Y54G2A.3	-1.58
W02H3.1	-1.58
C53D6.5	-1.58
C17G1.2	-1.59
F14H12.7	-1.59
K07H8.7	-1.59
T20D4.10	-1.60
cyp-35A5	-1.60
bas-1	-1.60
ttr-42	-1.60
E02C12.6	-1.60
dct-16	-1.61
F53F4.8	-1.62
Y73B6BL.288	-1.63
fbxa-92	-1.63
irld-35	-1.63
cyp-35C1	-1.63
dod-24	-1.63
pgp-2	-1.63
D1054.18	-1.63
F54B11.11	-1.64
hsp-16.2	-1.65
H12D21.3	-1.65
R08F11.4	-1.65
C18A11.4	-1.65
D1086.20	-1.65
B0416.10	-1.65
lips-14	-1.65
F56D6.12	-1.66
F56D6.17	-1.67
F45D11.1	-1.67
T24C2.5	-1.67
F18E2.1	-1.67
skr-10	-1.68
F42A10.7	-1.68
fbxa-91	-1.68
clec-4	-1.68
F49C12.7	-1.69
cyp-35A2	-1.69
tbh-1	-1.69
W08E12.2	-1.69
F48G7.8	-1.69
F22G12.8	-1.70
ftn-1	-1.70
C08A9.11	-1.70
C33G8.3	-1.71
fipr-22	-1.71
ugt-4	-1.71
Y40H7A.11	-1.71
clec-118	-1.72
ech-9	-1.72
clec-218	-1.73

Table E2 (Continued)

Gene Name	log_2 Fold
K09E3.6	-1.73
F22H10.6	-1.75
F17A2.13	-1.76
Y57G11C.41	-1.76
cyp-35A3	-1.76
F07E5.7	-1.76
dhs-23	-1.76
R10E4.6	-1.76
irld-53	-1.77
nhr-68	-1.77
F01D5.3	-1.78
col-135	-1.78
T16G12.1	-1.80
pmp-5	-1.80
clec-28	-1.81
sri-40	-1.81
cdr-4	-1.82
clec-7	-1.82
F28A12.4	-1.83
Y105C5B.15	-1.83
T28A11.19	-1.84
T02B5.3	-1.85
K07A1.13	-1.85
clec-26	-1.86
F08A8.3	-1.86
B0281.5	-1.86
fut-5	-1.86
cat-4	-1.86
F41C6.4	-1.86
F35F10.6	-1.87
C44B7.5	-1.88
str-144	-1.90
Y17D7B.2	-1.91
F15E11.15	-1.91
clec-160	-1.91
ugt-30	-1.92
fbxa-84	-1.93
F55G11.2	-1.93
Y94H6A.10	-1.95
K09A9.8	-1.99

Gene Name	log_2 Fold
F25C8.1	-1.99
R07C3.13	-2.00
Y19D10B.7	-2.01
F15E11.13	-2.01
K10C2.8	-2.03
C32H11.4	-2.05
catp-2	-2.07
npr-13	-2.08
clec-53	-2.09
srh-237	-2.09
ugt-10	-2.11
C23H5.8	-2.12
C05D9.12	-2.12
F15E11.12	-2.14
spp-4	-2.15
C36C5.5	-2.16
Y40C7B.4	-2.16
srh-70	-2.17
hsp-16.41	-2.19
gba-4	-2.19
Y43D4A.2	-2.21
C42D4.2	-2.24
asm-3	-2.28
W06G6.20	-2.28
F22E5.8	-2.29
F15E11.1	-2.34
F15E11.14	-2.34
vit-2	-2.37
nhx-6	-2.41
Y19D10B.4	-2.42
ZK742.3	-2.42
K10C2.7	-2.42
oac-32	-2.43
F54F7.2	-2.44
ugt-22	-2.44
oac-20	-2.46
Y52E8A.4	-2.46
K10B2.2	-2.55
clec-2	-2.58
fat-7	-2.64
F48G7.5	-2.73
F35F10.5	-2.76

Gene Name	log_2 Fold
ZC266.1	-2.76
clec-190	-2.89
T05E12.3	-2.99
ilys-5	-2.99
clec-31	-3.04
folt-2	-3.06
K11G9.3	-3.15
Y40H7A.10	-3.37
vit-1	-3.38
vit-5	-3.39
vit-4	-3.47
vit-3	-3.52
Y40H7A.147	-4.01
acdh-1	-4.62

Table E3. Significantly altered genes in the hsf-1(-);+HS treatment condition compared to the control.

Gene Name	log_2 Fold
rab-11.2	7.72
col-108	7.40
Y47H10A.5	7.27
T22F3.11	6.47
Y60C6A.1	6.15
col-37	6.00
F11D11.3	6.00
ZK863.10	6.00
clec-101	5.96
col-183	5.95
col-51	5.94
col-85	5.85
col-164	5.81
ZK355.3	5.80
F33H12.7	5.80
col-185	5.79
grl-25	5.77
grl-9	5.73
col-2	5.67
col-72	5.66
grl-20	5.60
col-50	5.56
Y75B8A.39	5.54
Y40C5A.3	5.50
col-44	5.47
grl-23	5.43
cut-1	5.42
col-40	5.40
ZK638.1	5.39
fbxa-163	5.38
grl-19	5.37
C13A2.12	5.36
col-35	5.35
T26F2.3	5.33
col-36	5.31
hsf-1	5.29
srg-31	5.26
B0563.9	5.22
col-102	5.18
ZK355.8	5.09
col-158	5.00

Gene Name	log_2 Fold
col-84	4.95
T08E11.1	4.92
grd-7	4.88
grl-3	4.81
dct-3	4.80
clec-60	4.80
F49H12.12	4.79
col-114	4.79
F42C5.3	4.75
clec-174	4.68
B0507.8	4.62
F22G12.1	4.61
col-45	4.59
acs-2	4.56
tsp-1	4.55
sdz-35	4.52
F07E5.9	4.51
C25F9.2	4.49
grl-17	4.46
B0284.1	4.43
B0348.2	4.42
M6.11	4.41
W07B8.4	4.40
col-123	4.37
col-43	4.35
R05A10.1	4.33
clec-13	4.32
T23F1.5	4.31
W08A12.4	4.31
C08E8.4	4.28
F07G11.1	4.26
F10A3.1	4.22
fbxa-165	4.19
tyr-3	4.16
cnc-9	4.14
C53A5.9	4.14
Y37H2A.14	4.13
fbxa-30	4.11
C54D10.8	4.08
dmd-10	4.06
C54D10.14	4.05

Gene Name	log_2 Fold
C11D2.2	4.05
Y39B6A.24	4.01
B0284.2	3.96
C50F7.5	3.94
grd-9	3.93
R07C12.1	3.91
K01D12.10	3.90
Y71H2AR.2	3.85
F57G4.11	3.81
ins-35	3.74
ZK285.2	3.74
tsp-2	3.69
W01C9.2	3.68
B0462.5	3.67
F09C12.2	3.66
W02A2.9	3.62
F26D11.13	3.59
C54D10.12	3.58
pgp-8	3.58
clec-15	3.58
C49G7.12	3.55
fbxa-158	3.53
F49H6.5	3.49
ZK896.1	3.48
C38D9.2	3.47
B0284.5	3.46
T24E12.5	3.46
B0507.10	3.45
F15D4.5	3.45
F22E5.6	3.41
B0507.6	3.38
tbb-6	3.35
F15B9.6	3.35
K08D9.6	3.33
C17H1.7	3.32
fbxa-161	3.29
dod-20	3.24
col-33	3.21
W09C3.3	3.18
zip-6	3.15

Gene Name	log_2 Fold
E02H4.4	3.14
F23B2.10	3.13
F53F4.4	3.13
H02F09.3	3.07
clec-71	3.05
skr-5	3.05
Y9C9A.16	3.03
C25F9.11	3.01
R03H10.6	3.01
F46A8.1	2.98
C17H1.10	2.97
fbxa-162	2.94
F46C5.1	2.93
T19D12.4	2.92
rrf-2	2.91
F26F2.1	2.90
C49G7.7	2.89
C23H5.12	2.89
T14B1.1	2.86
F07C4.12	2.85
ugt-27	2.84
fbxa-66	2.83
ZC239.14	2.81
F53B2.8	2.80
W09G12.8	2.79
C17H1.5	2.79
cpt-3	2.78
C44B12.6	2.77
F55F3.4	2.76
R11E3.2	2.75
wrt-7	2.74
fmo-2	2.74
Y34F4.2	2.74
C06E7.88	2.73
B0507.7	2.71
W09G12.7	2.70
Y6E2A.5	2.70
Y43F8B.15	2.69
T06E6.15	2.69
T28F3.5	2.69
jmjd-3.3	2.69

Table E3 (Continued)

Gene Name	log_2 Fold
C10C5.2	2.68
Y6E2A.4	2.68
srw-71	2.68
gem-4	2.64
B0403.3	2.64
mod-5	2.63
C24G7.1	2.61
Y26D4A.3	2.61
W07A12.4	2.61
oac-24	2.60
F14H12.2	2.60
clec-167	2.58
oac-14	2.57
C08F11.3	2.57
fbxa-135	2.57
fbxa-144	2.56
fbxa-138	2.55
F32G8.2	2.54
tsp-6	2.53
F20D6.2	2.52
F08A8.5	2.51
lys-3	2.49
F07G11.4	2.48
F20G2.5	2.48
B0238.13	2.45
F47B8.4	2.43
F01D4.8	2.39
srr-6	2.38
C23H4.6	2.33
C25F9.12	2.33
Y58A7A.5	2.32
K07E8.2	2.32
K03D3.2	2.32
Y43F8B.25	2.32
best-2	2.32
K07B1.8	2.30
fat-5	2.28
F16B4.6	2.28
cut-6	2.26
dsl-3	2.25
fbxa-199	2.24
T21D12.7	2.23

Gene Name	log_2 Fold
pgp-5	2.20
kin-6	2.20
Y38H8A.8	2.19
Y71G12B.2	2.19
Y105C5A.1 271	2.19
K08D10.9	2.18
ugt-14	2.18
dos-3	2.18
bath-47	2.17
bro-1	2.17
F47H4.2	2.17
F44F1.4	2.13
F54B8.4	2.12
Y110A2AL. 4	2.12
T28B11.1	2.12
C06E4.8	2.11
F44G3.10	2.10
F59B1.10	2.10
F53G2.2	2.10
Y55F3BR.7	2.10
irg-2	2.09
gpx-8	2.09
F31E3.2	2.07
trpl-5	2.07
mtl-1	2.07
F08G2.5	2.05
M01G12.9	2.05
F56D2.3	2.05
C23G10.11	2.04
lin-41	2.04
ZC443.2	2.04
F43C11.8	2.04
acdh-2	2.03
fbxc-23	2.02
C44H9.7	2.02
Y2H9A.6	2.02
pef-1	2.02
inx-20	2.01
numr-1	2.01
gst-3	1.99

Gene Name	log_2 Fold
btb-12	1.99
tbc-4	1.99
K10G4.3	1.98
W02G9.10	1.97
puf-10	1.97
M28.8	1.97
C31B8.4	1.97
ptc-2	1.96
best-1	1.96
clec-61	1.95
F28F8.7	1.94
F08F3.9	1.94
F48B9.1	1.94
C13A2.3	1.93
meg-2	1.93
M01B2.13	1.93
clec-17	1.91
B0024.4	1.91
T08E11.8	1.91
dpy-1	1.89
F57B9.3	1.88
irg-1	1.88
C13A2.1	1.87
ZK596.1	1.87
Y6G8.5	1.87
Y71G12B.3 2	1.86
clec-47	1.85
oac-29	1.85
Y73B3A.13	1.85
W03D2.6	1.84
K01G12.3	1.84
nhr-21	1.84
T21D12.11	1.84
Y52B11A.1 1	1.83
Y46H3C.7	1.83
twk-32	1.83
ZK177.1	1.83
rnt-1	1.82
C08E3.1	1.82
cdc-25.2	1.81

Gene Name	log_2 Fold
zig-3	1.80
fkb-7	1.80
F28E10.5	1.80
zig-4	1.79
T02G5.11	1.79
K03H4.2	1.79
col-116	1.79
F26F12.3	1.79
EEED8.4	1.79
R09A8.1	1.79
ins-4	1.78
srp-8	1.78
Y47H9C.1	1.78
math-37	1.77
rog-1	1.77
Y59A8B.21	1.77
set-12	1.77
ceh-86	1.76
Y105E8A.2 9	1.76
fbxa-25	1.75
tat-2	1.75
K09F6.10	1.75
F22B3.4	1.74
srw-86	1.74
daf-2	1.74
F26G5.1	1.74
F58E2.3	1.74
wdr-5.3	1.74
Y43F8B.12	1.73
syx-2	1.73
linc-84	1.73
fbxa-48	1.73
fbxa-59	1.72
C41D11.4	1.71
K10C3.4	1.70
Y57A10A.1	1.70
bath-26	1.70
Y51B9A.9	1.70
tts-1	1.70
C04G6.6	1.69
dex-1	1.68

Table E3 (Continued)

Gene Name	log_2 Fold
daf-18	1.67
nekl-1	1.67
F35E12.4	1.67
ZC443.3	1.67
C08E3.13	1.67
C34C6.2	1.67
zip-10	1.67
peb-1	1.66
mex-3	1.66
nhr-2	1.65
ulp-4	1.65
F26A1.14	1.64
flh-1	1.64
puf-6	1.64
bath-21	1.64
Y58A7A.4	1.64
ceh-37	1.64
Y73B3A.4	1.64
daf-7	1.63
Y105C5A.13	1.63
C34B7.1	1.62
far-7	1.62
cpr-3	1.62
F28B3.4	1.62
egg-1	1.61
xpc-1	1.61
T06D4.1	1.61
ptr-13	1.61
C14A6.16	1.60
maco-1	1.60
hsp-12.6	1.60
Y55F3AM.14	1.60
col-176	1.59
unc-34	1.59
hpo-24	1.58
F54E2.4	1.58
rig-4	1.58
ced-3	1.58
T01D3.3	1.57
clec-82	1.57

Gene Name	log_2 Fold
F34D10.4	1.57
oac-34	1.57
fbxa-53	1.56
Y49G5B.1	1.56
tyr-5	1.56
T24B8.7	1.55
egl-18	1.55
T09B4.1	1.55
sys-1	1.55
T28C6.10	1.55
gon-4	1.55
F19B10.13	1.54
Y56A3A.16	1.54
hot-5	1.54
igcm-1	1.54
math-38	1.54
chs-1	1.54
gld-4	1.53
srw-85	1.53
Y17G7B.21	1.53
sma-1	1.53
nhl-2	1.51
1-Apr	1.51
ZC443.4	1.51
F53H2.3	1.51
F37A8.5	1.51
puf-5	1.50
C46C2.3	1.50
sodh-1	1.50
Y65B4BL.3	1.50
R08E3.2	1.50
ZC239.22	1.50
F29G9.1	1.50
K11H12.9	1.49
H43E16.1	1.48
C49F5.6	1.48
fbxa-24	1.48
C27H2.2	1.48
cec-2	1.48
fbxa-127	1.48
C44B9.3	1.47
T13F2.6	1.47

Gene Name	log_2 Fold
linc-72	1.47
apx-1	1.47
oma-1	1.46
Y116F11B.10	1.46
F58D5.5	1.46
Y53G8AL.1	1.46
clec-233	1.46
let-99	1.45
cah-1	1.45
T04F3.2	1.45
gei-12	1.45
C17E4.3	1.45
gln-5	1.45
tdc-1	1.45
Y22D7AR.2	1.45
C50B6.3	1.45
linc-56	1.44
B0205.14	1.44
fbxa-166	1.44
puf-7	1.44
math-15	1.44
Y34F4.4	1.44
par-4	1.44
F54E12.2	1.43
C16C8.12	1.43
F34H10.3	1.43
C48D1.5	1.43
lip-1	1.43
polq-1	1.43
T04F8.7	1.43
F42H10.5	1.43
ugt-8	1.43
sqv-5	1.42
Y37B11A.2	1.42
F59A6.5	1.42
oac-56	1.42
M03A1.3	1.42
nhr-6	1.42
cpg-1	1.42
cpb-1	1.42

Gene Name	log_2 Fold
T08D2.8	1.42
T05F1.2	1.41
swt-3	1.41
dpy-6	1.41
rod-1	1.41
tbc-14	1.41
egg-6	1.41
gap-3	1.40
mltn-1	1.40
tth-1	1.40
inx-22	1.40
rhy-1	1.40
C27D9.1	1.40
F14H3.5	1.40
cdk-2	1.40
T12G3.1	1.40
F14F9.4	1.39
pqn-20	1.39
T04C4.1	1.39
C33D9.13	1.39
dhs-16	1.39
cya-1	1.38
age-1	1.38
glt-5	1.38
duox-2	1.38
cdh-10	1.37
arid-1	1.37
Y39H10A.4	1.37
exc-4	1.37
pos-1	1.37
Y105E8A.25	1.37
tba-7	1.36
K03H1.10	1.36
sam-10	1.36
ceh-39	1.36
flcn-1	1.36
fbxa-60	1.36
frm-3	1.35
Y54F10BM.1	1.35
daam-1	1.35

Table E3 (Continued)

Gene Name	log_2 Fold
cebp-1	1.35
C04B4.2	1.35
F31D4.5	1.35
clec-72	1.35
F07B7.12	1.35
B0554.5	1.34
rom-1	1.34
Y76B12C.11	1.34
math-50	1.34
egg-2	1.34
tag-199	1.34
B0212.3	1.34
Y76B12C.6	1.34
wrm-1	1.34
K08D8.4	1.33
olrn-1	1.33
K09F6.9	1.33
ncs-6	1.33
ZK809.5	1.33
gap-1	1.33
mex-5	1.33
F09E5.10	1.33
twk-2	1.33
pad-2	1.33
trcs-1	1.32
C04E7.3	1.32
hpo-11	1.32
fli-1	1.32
Y48A6C.1	1.32
cpg-2	1.32
dod-19	1.32
H05L14.2	1.32
die-1	1.32
F43D2.2	1.32
nep-1	1.32
cbp-1	1.32
C06A5.1	1.32
C34D10.2	1.32
C36B1.9	1.32
rabx-5	1.31
linc-17	1.31

Gene Name	log_2 Fold
swsn-7	1.31
crml-1	1.31
C29F9.3	1.31
T01C3.3	1.31
C28G1.5	1.30
egg-3	1.30
Y102A11A.9	1.30
pqn-15	1.30
set-2	1.30
Y34D9A.7	1.30
snf-6	1.30
C07E3.3	1.30
fbxa-150	1.30
mes-3	1.30
R102.5	1.30
Y39A1A.9	1.29
cul-6	1.29
T24D1.3	1.29
pup-2	1.29
F19C7.2	1.29
fbxa-182	1.29
tag-343	1.29
lin-13	1.29
T05F1.9	1.29
spd-5	1.29
trr-1	1.29
lat-1	1.29
ptc-1	1.29
F20C5.3	1.29
egl-2	1.28
Y48G1C.10	1.28
F39B2.1	1.28
vrk-1	1.28
nhr-25	1.28
T28H10.3	1.28
plst-1	1.28
C27A12.6	1.27
sip-1	1.27
M04C3.2	1.27
C34E10.8	1.27

Gene Name	log_2 Fold
C37C3.9	1.27
dct-1	1.27
rbc-2	1.26
Y60A3A.8	1.26
srap-1	1.26
mex-6	1.26
W03F11.5	1.26
sptf-2	1.26
fncm-1	1.26
C06A1.4	1.26
nhr-23	1.26
R03G5.6	1.26
ztf-20	1.26
cyb-2.2	1.26
Y48G1BL.6	1.26
K11H3.8	1.25
mfb-1	1.25
egg-4	1.25
F54D1.6	1.25
Y55F3BR.2	1.25
Y50D4C.5	1.25
fog-3	1.25
F11E6.7	1.25
smp-1	1.25
F17C11.10	1.25
Y39E4B.5	1.25
zag-1	1.25
sid-1	1.25
tftc-1	1.24
T21C9.13	1.24
F02H6.2	1.24
Y105C5A.1	1.24
F54D5.5	1.24
puf-11	1.24
hum-6	1.24
Y57A10A.31	1.24
F47B8.2	1.24
spn-4	1.24
Y54G2A.19	1.24
hex-3	1.24
glp-1	1.24

Gene Name	log_2 Fold
swt-1	1.24
T08B2.11	1.23
T05E7.3	1.23
Y48G1C.1	1.23
Y82E9BR.19	1.23
Y67H2A.10	1.23
vps-39	1.23
M04F3.6	1.23
C05D11.8	1.22
gst-41	1.22
smk-1	1.22
cyp-13A5	1.22
C49G7.10	1.22
F31F6.2	1.22
Y20F4.4	1.22
pac-1	1.22
M151.7	1.22
dgk-4	1.22
Y71H2AM.2	1.22
rskn-1	1.22
tbc-15	1.22
H41C03.1	1.22
ptr-2	1.22
C06E1.1	1.22
pqn-47	1.21
ZC239.1	1.21
C44H9.4	1.21
lig-1	1.21
ksr-2	1.21
lex-1	1.21
ptr-10	1.21
F35C11.5	1.21
F16H6.10	1.21
cil-1	1.20
gld-3	1.20
igdb-1	1.20
mtk-1	1.20
F55A3.7	1.20
sru-40	1.20
R03H10.7	1.20

Table E3 (Continued)

Gene Name	log_2 Fold
perm-1	1.20
unc-103	1.20
Y111B2A.9	1.20
capg-2	1.20
ZC190.4	1.20
unc-77	1.20
gpa-16	1.20
C01F1.6	1.20
par-3	1.20
Y42H9AR.4	1.20
C05C10.2	1.20
sur-2	1.19
Y97E10AR.1	1.19
fbxa-115	1.19
C13F10.6	1.19
Y47G7B.2	1.19
atm-1	1.19
flh-3	1.19
sup-17	1.19
Y102A11A.3	1.19
pme-1	1.19
meg-1	1.19
puf-3	1.19
fox-1	1.19
dpy-21	1.18
C09F9.2	1.18
max-1	1.18
pak-2	1.18
oac-57	1.18
Y54G2A.11	1.18
clec-81	1.18
nos-2	1.18
C06A5.8	1.18
flh-2	1.18
Y54G11A.1	1.18
T04H1.2	1.18
ham-1	1.18
T28B4.4	1.18
R10E4.11	1.17
tlp-1	1.17

Gene Name	log_2 Fold
T08A11.1	1.17
kin-4	1.17
T23B3.6	1.17
F52H3.4	1.17
Y38H6C.9	1.17
C16C8.2	1.17
cdh-1	1.17
rme-2	1.17
Y43F8C.6	1.17
imp-1	1.17
grl-22	1.17
polg-1	1.17
C36C9.1	1.17
Y73B3B.1	1.17
F26A1.13	1.17
ergo-1	1.17
mys-4	1.17
K02C4.3	1.16
ztf-15	1.16
plx-1	1.16
Y48A6B.10	1.16
C36B1.11	1.16
clr-1	1.16
ZK1055.7	1.16
Y22D7AL.9	1.16
lea-1	1.16
aakg-1	1.16
M01G5.1	1.16
fozi-1	1.16
C42D8.1	1.16
C13E3.1	1.16
dcp-66	1.16
sos-1	1.15
F26G1.1	1.15
Y71H2AM.3	1.15
Y54G2A.36	1.15
pha-4	1.15
Y47G6A.29	1.15
T26H5.9	1.15
flt-1	1.15
lin-49	1.15

Gene Name	log_2 Fold
F15A8.6	1.15
srd-53	1.14
sta-2	1.14
R12C12.5	1.14
ubc-23	1.14
acd-2	1.14
H11L12.1	1.14
Y56A3A.28	1.14
Y50D7A.2	1.14
clec-76	1.14
mei-2	1.14
acly-2	1.14
dcr-1	1.14
Y6B3B.4	1.14
mig-38	1.14
F56E10.1	1.14
ZK637.6	1.14
sax-7	1.14
C06B8.7	1.14
ZK973.1	1.13
egg-5	1.13
C10G11.6	1.13
M4.1	1.13
unc-71	1.13
gon-1	1.13
bath-19	1.13
C05A9.2	1.13
fbxa-141	1.13
W05F2.3	1.13
spsb-1	1.13
C33D9.5	1.13
igeg-2	1.13
puf-8	1.13
ppt-1	1.13
athp-2	1.13
Y41D4B.4	1.13
oma-2	1.12
rig-3	1.12
Y17D7C.2	1.12
cyb-2.1	1.12
pab-2	1.12
szy-4	1.12

Gene Name	log_2 Fold
F31C3.3	1.12
gln-6	1.12
C11H1.5	1.12
ubc-8	1.12
Y48G1BM.6	1.12
F52D2.12	1.12
T11F9.12	1.12
plx-2	1.12
F18A1.7	1.12
tat-3	1.12
gon-14	1.11
Y51A2D.15	1.11
F12A10.8	1.11
sydn-1	1.11
H34C03.2	1.11
R02F2.4	1.11
Y50D7A.11	1.11
tbx-36	1.11
W01A11.7	1.11
ZK970.7	1.11
F13E6.4	1.11
Y44E3A.4	1.11
T07C12.12	1.11
rga-3	1.11
Y41G9A.5	1.10
chs-2	1.10
C14A4.12	1.10
str-7	1.10
F13D2.1	1.10
Y50D7A.8	1.10
F33H2.5	1.10
Y48G1BL.5	1.10
cyp-34A2	1.10
egrh-1	1.10
Y38F2AR.6	1.10
hlh-2	1.10
epg-6	1.09
fil-2	1.09
lag-1	1.09
vps-11	1.09
mre-11	1.09

Table E3 (Continued)

Gene Name	log_2 Fold
far-3	1.09
sas-4	1.09
T19B10.8	1.09
tsg-101	1.09
F45D3.2	1.09
zim-2	1.09
gst-24	1.09
lec-11	1.08
csb-1	1.08
gck-4	1.08
fbxa-95	1.08
F47D12.9	1.08
F20C5.6	1.08
mom-4	1.08
dpf-6	1.08
cyp-23A1	1.08
F21A10.2	1.08
F45D3.4	1.08
rad-50	1.08
cpb-3	1.08
mbk-2	1.08
cash-1	1.08
rad-26	1.08
Y105E8A.24	1.08
hop-1	1.08
C05G5.2	1.08
pqn-62	1.08
Y58A7A.3	1.07
mel-28	1.07
gcl-1	1.07
F36A2.13	1.07
F16B4.2	1.07
srgp-1	1.07
rrf-3	1.07
ttm-4	1.07
M106.2	1.07
C17H12.6	1.07
F44E2.4	1.07
F13B6.1	1.07
har-2	1.07
ZC308.4	1.07

Gene Name	log_2 Fold
D1044.6	1.07
tftc-3	1.07
gyg-2	1.07
C34B7.2	1.07
C09E7.8	1.07
F11A5.9	1.07
panl-2	1.07
mel-26	1.07
C23H5.15	1.07
ulp-1	1.07
com-1	1.07
rbg-3	1.06
Y48C3A.12	1.06
evl-14	1.06
wee-1.3	1.06
chk-2	1.06
T26H5.10	1.06
sup-35	1.06
ZC449.5	1.06
swsn-9	1.06
plk-3	1.06
lsy-12	1.06
C06A5.3	1.06
Y43F8C.3	1.06
evl-18	1.06
sdc-3	1.06
ifet-1	1.06
cyh-1	1.06
lin-12	1.06
sqv-6	1.05
ceh-38	1.05
M01F1.9	1.05
T22D1.5	1.05
sel-8	1.05
sem-5	1.05
atg-9	1.05
unc-53	1.05
Y73B3A.1	1.05
C36A4.5	1.05
ztf-6	1.05
hmr-1	1.05
ubc-25	1.05

Gene Name	log_2 Fold
fnci-1	1.05
F57B10.9	1.05
sas-5	1.05
bath-30	1.05
aka-1	1.04
B0511.12	1.04
cdh-7	1.04
K02B12.5	1.04
K03A11.5	1.04
C02B8.6	1.04
brd-1	1.04
pqn-21	1.04
toca-1	1.04
T19C3.3	1.04
wnk-1	1.04
F46B6.5	1.04
let-765	1.04
gck-1	1.04
chd-7	1.04
cyp-35B1	1.03
scc-3	1.03
dnj-5	1.03
ZK1025.1	1.03
npp-14	1.03
tol-1	1.03
bet-1	1.03
cdh-3	1.03
C49C3.9	1.03
Y37E11AM.2	1.03
egal-1	1.03
cgh-1	1.03
K10B4.3	1.03
lrp-1	1.03
C39F7.5	1.03
E03H4.8	1.03
K06A9.1	1.03
anoh-2	1.03
bath-42	1.03
R04F11.3	1.03
lin-36	1.03
F13E9.1	1.03

Gene Name	log_2 Fold
daf-12	1.03
Y71F9AR.3	1.03
T08D2.3	1.02
F21C10.7	1.02
D1043.1	1.02
spr-4	1.02
pap-1	1.02
vhp-1	1.02
M04F3.5	1.02
sgo-1	1.02
F35G2.1	1.02
W02B8.2	1.02
mesp-1	1.02
H02I12.5	1.02
nhr-41	1.02
F59H5.1	1.02
zyg-11	1.02
vet-2	1.01
egl-15	1.01
F30F8.10	1.01
F10D11.2	1.01
H03A11.2	1.01
ace-2	1.01
met-1	1.01
lin-45	1.01
mcm-3	1.01
Y53F4B.13	1.01
F36H2.3	1.01
nhr-211	1.01
mom-5	1.01
frm-8	1.01
Y54G2A.21	1.01
ess-2	1.01
pme-6	1.01
T23F4.2	1.01
F18E3.12	1.01
clec-90	1.01
kgb-1	1.01
tim-1	1.00
F47G3.1	1.00
ubc-1	1.00
F44E7.5	1.00

Table E3 (Continued)

Gene Name	log_2 Fold
C31H1.8	1.00
C35A11.2	1.00
zyg-9	1.00
clh-4	1.00
C06A5.6	1.00
smc-6	1.00
odd-2	1.00
dna-2	1.00
Y48G1C.8	1.00
knl-1	1.00
lrg-1	1.00
xbx-5	1.00
B0205.13	1.00
czw-1	1.00
isw-1	1.00
mys-1	1.00
1-Sep	1.00
K08D10.1	1.00
trcs-2	1.00
srh-71	0.99
swsn-4	0.99
let-502	0.99
rpm-1	0.99
scav-2	0.99
pdk-1	0.99
clec-87	0.99
F14D7.2	0.99
phf-10	0.99
cin-4	0.99
clp-2	0.99
ceh-91	0.99
otpl-3	0.99
C14B1.9	0.99
daf-19	0.99
smc-4	0.99
hum-1	0.99
lin-9	0.99
dpy-26	0.99
C29F9.4	0.98
B0393.3	0.98
kin-18	0.98
ZC317.7	0.98

Gene Name	log_2 Fold
C27F2.8	0.98
lem-3	0.98
rev-1	0.98
Y87G2A.7	0.98
F47A4.5	0.98
cdt-1	0.98
egl-27	0.98
aex-3	0.98
viln-1	0.98
K09D9.1	0.98
unc-68	0.98
unc-80	0.98
M70.5	0.98
pdfr-1	0.98
msi-1	0.98
Y119C1A.1	0.98
cgt-1	0.97
nmy-2	0.97
Y22D7AL.15	0.97
pqn-65	0.97
ugt-24	0.97
ZK154.5	0.97
ced-7	0.97
M57.1	0.97
asfl-1	0.97
Y75B8A.28	0.97
oac-31	0.97
pld-1	0.97
atg-18	0.97
pop-1	0.97
pho-14	0.97
mes-4	0.97
R05D3.12	0.97
hmg-20	0.97
C13F10.4	0.97
Y75B8A.3	0.97
pad-1	0.96
M01E11.3	0.96
M01E5.3	0.96
Y92H12A.4	0.96

Gene Name	log_2 Fold
Y55F3AM.6	0.96
Y17G7B.13	0.96
nop-1	0.96
clec-91	0.96
mex-1	0.96
T05E8.3	0.96
C48B6.3	0.96
cogc-5	0.96
T09F5.12	0.96
hlh-30	0.96
lam-2	0.96
orc-1	0.96
pis-1	0.96
ZK484.4	0.96
hex-4	0.95
csnk-1	0.95
pkc-1	0.95
C08G5.7	0.95
dhc-1	0.95
hcp-1	0.95
cpg-4	0.95
hsr-9	0.95
C16C8.11	0.95
gex-3	0.94
tes-1	0.94
Y55D9A.2	0.94
fmi-1	0.94
ZC376.6	0.94
cbn-1	0.94
Y111B2A.3	0.94
F28H6.4	0.94
hmbx-1	0.94
F13B12.6	0.94
T19B4.5	0.94
K06A5.1	0.94
R11D1.1	0.94
rde-2	0.94
tag-294	0.94
K11D12.9	0.94
F01G4.4	0.94
math-24	0.94

Gene Name	log_2 Fold
adpr-1	0.94
best-13	0.93
fbxa-98	0.93
mdt-15	0.93
taf-1	0.93
F09C8.2	0.93
ntl-9	0.93
tag-77	0.93
scc-1	0.93
grd-4	0.93
cye-1	0.93
dlg-1	0.93
sox-4	0.93
Y55F3BL.2	0.93
F14H3.6	0.93
M60.4	0.93
src-1	0.93
Y55F3AM.10	0.93
Y92H12A.5	0.93
Y54F10AR.1	0.93
ZK863.4	0.92
lin-59	0.92
C36E8.1	0.92
duo-1	0.92
fbxa-107	0.92
tir-1	0.92
eri-9	0.92
sli-1	0.92
C14B1.7	0.92
C35D10.7	0.92
C41H7.4	0.92
ccpp-1	0.92
abi-1	0.92
F02E8.4	0.92
F59E12.1	0.92
tag-278	0.92
C56G2.1	0.92
bus-1	0.92
efa-6	0.92
R10H10.7	0.92

Table E3 (Continued)

Gene Name	log_2 Fold
fbxa-11	0.92
smg-2	0.92
egl-19	0.92
smg-1	0.92
R11A8.7	0.92
Y82E9BL.18	0.92
T23B12.6	0.92
F33H1.4	0.92
C39H7.4	0.91
lpin-1	0.91
C30F12.4	0.91
F33G12.6	0.91
C31C9.7	0.91
capg-1	0.91
rga-4	0.91
R07E3.6	0.91
mig-15	0.91
C01G8.1	0.91
W06B4.1	0.91
farl-11	0.91
mrp-2	0.91
Y53F4B.45	0.91
B0507.2	0.91
C26G2.2	0.91
pitr-1	0.91
Y65A5A.2	0.91
F16A11.1	0.91
daz-1	0.91
set-14	0.91
C05C10.5	0.91
set-26	0.91
him-18	0.91
B0393.6	0.90
K02F6.7	0.90
rme-8	0.90
dct-17	0.90
set-9	0.90
F52C12.4	0.90
Y48G1C.11	0.90
ani-2	0.90

Gene Name	log_2 Fold
ima-3	0.90
ketn-1	0.90
C04F12.1	0.90
vbh-1	0.90
D1081.7	0.90
rcor-1	0.90
dnj-8	0.89
adm-2	0.89
D1007.5	0.89
ppfr-1	0.89
ifd-2	0.89
let-653	0.89
mcm-7	0.89
gck-2	0.89
haf-2	0.89
alx-1	0.89
cku-80	0.89
spc-1	0.89
ima-1	0.89
pkc-3	0.89
drp-1	0.89
sea-2	0.89
npp-21	0.89
C18H7.11	0.89
rcq-5	0.88
F33E11.3	0.88
nrd-1	0.88
vglu-3	0.88
T10B11.7	0.88
Y69A2AL.2	0.88
rfc-1	0.88
C02F5.7	0.88
hcf-1	0.88
Y56A3A.7	0.88
rde-1	0.88
atg-2	0.88
R17.2	0.88
K03H1.11	0.88
W06E11.1	0.88
fic-1	0.88
B0205.1	0.88
abt-2	0.88

Gene Name	log_2 Fold
F27E5.9	0.87
Y62E10A.14	0.87
nasp-2	0.87
bli-3	0.87
set-5	0.87
mes-2	0.87
F23H11.4	0.87
obr-3	0.87
F45F2.10	0.87
aakg-5	0.87
athp-1	0.87
gcy-28	0.87
F56C9.10	0.87
fbxa-215	0.87
M03C11.8	0.87
Y15E3A.5	0.87
ctg-2	0.87
bet-2	0.87
mcm-5	0.87
T08G11.1	0.86
gcy-12	0.86
ZK688.5	0.86
gfi-2	0.86
F29G9.2	0.86
mig-5	0.86
emb-5	0.86
C06G4.1	0.86
ain-2	0.86
ZK131.11	0.86
R05D3.2	0.86
ubr-1	0.86
eea-1	0.86
rtel-1	0.86
tlk-1	0.86
F42G9.6	0.86
ntl-4	0.85
mec-15	0.85
gmeb-1	0.85
Y32H12A.8	0.85
dsh-2	0.85
skpt-1	0.85

Gene Name	log_2 Fold
rec-8	0.85
cdc-42	0.85
C27A12.2	0.85
hcp-4	0.85
R09A1.3	0.85
ani-1	0.85
zfp-1	0.85
F22B7.9	0.85
F10C2.4	0.85
B0464.6	0.84
prg-1	0.84
cogc-3	0.84
ced-5	0.84
tep-1	0.84
C06B3.6	0.84
K08F4.1	0.84
C25F9.5	0.84
mom-2	0.84
C09D4.4	0.84
F36D4.5	0.84
dig-1	0.84
hda-3	0.84
gras-1	0.84
D2030.8	0.84
F49E2.5	0.84
mtm-3	0.84
cyp-31A2	0.84
gls-1	0.84
Y45G5AM.3	0.84
D2096.12	0.84
ego-1	0.84
ire-1	0.83
hda-2	0.83
T20F5.6	0.83
R01H10.7	0.83
toe-2	0.83
M02B7.5	0.83
T26A8.4	0.83
F45F2.11	0.83
mut-7	0.83
mus-101	0.83

Table E3 (Continued)

Gene Name	log_2 Fold
cdc-6	0.83
B0205.9	0.83
set-16	0.83
Y37D8A.16	0.83
R12E2.2	0.83
tam-1	0.83
ZK524.4	0.83
ogt-1	0.82
mat-2	0.82
sac-1	0.82
dpy-28	0.82
Y65B4BL.1	0.82
B0261.7	0.82
Y17G7B.20	0.82
T11G6.5	0.82
fsn-1	0.82
hrdl-1	0.82
attf-6	0.82
R02D3.8	0.81
msh-6	0.81
F52B5.3	0.81
T24F1.2	0.81
W04D2.4	0.81
F38A5.7	0.81
Y47D3A.29	0.81
Y54E2A.4	0.81
gei-6	0.81
clec-88	0.81
tag-325	0.81
larp-5	0.81
lem-2	0.81
nasp-1	0.81
T24D1.2	0.81
M01H9.3	0.80
epi-1	0.80
rad-51	0.80
abt-4	0.80
msh-2	0.80
F55C12.5	0.80
F20D12.2	0.80
pgp-9	0.80
nfx-1	0.80

Gene Name	log_2 Fold
T19A5.1	0.80
C17H12.2	0.80
rpa-1	0.80
ptp-2	0.79
unc-94	0.79
npp-7	0.79
uri-1	0.79
tat-5	0.79
gna-2	0.79
C01G6.5	0.79
ubxn-3	0.78
pct-1	0.78
lpr-5	0.78
edc-3	0.78
mon-2	0.78
ikke-1	0.78
F45D3.3	0.78
F11A10.5	0.78
ttll-5	0.78
M05D6.2	0.78
gld-1	0.78
plk-1	0.78
C32D5.3	0.78
C25A1.5	0.77
exoc-8	0.77
clec-180	0.77
F55H12.2	0.77
daf-16	0.77
hgrs-1	0.77
rap-1	0.76
top-2	0.76
pde-2	0.75
pptr-2	0.75
klp-18	0.75
ama-1	0.75
C10G8.8	-0.73
mtss-1	-0.75
clec-48	-0.75
faah-3	-0.76
acs-5	-0.76
fkb-6	-0.76
mrpl-50	-0.76

Gene Name	log_2 Fold
Y54G2A.45	-0.76
mlp-1	-0.77
F53B7.3	-0.77
K07C5.4	-0.77
D1086.6	-0.77
grd-14	-0.77
Y53G8AL.2	-0.77
dnj-12	-0.77
Y97E10AL.3	-0.77
heh-1	-0.77
cct-7	-0.77
ZK795.3	-0.78
T23B3.5	-0.78
msp-49	-0.78
mdt-11	-0.78
mdt-9	-0.78
C14C6.5	-0.78
Y25C1A.13	-0.78
umps-1	-0.79
T09B4.8	-0.79
tag-267	-0.79
tag-18	-0.79
asg-1	-0.79
C48E7.7	-0.79
C05C8.1	-0.79
aps-3	-0.79
ldh-1	-0.79
C01H6.4	-0.79
B0454.5	-0.80
acs-14	-0.80
tba-4	-0.80
ZK484.5	-0.80
ucr-1	-0.80
gas-1	-0.80
glrx-10	-0.80
Y58A7A.1	-0.81
W07G4.5	-0.81
rps-29	-0.81
mrpl-47	-0.81
fkb-3	-0.81
hpo-19	-0.81

Gene Name	log_2 Fold
ZK669.4	-0.81
rpia-1	-0.81
lpd-5	-0.81
ubl-5	-0.81
H29C22.1	-0.81
F53B6.4	-0.81
dnj-19	-0.81
D1086.10	-0.82
gln-2	-0.82
E04A4.5	-0.82
Y69E1A.5	-0.82
pgp-2	-0.82
F08G5.6	-0.82
aat-6	-0.82
tag-174	-0.82
Y38C1AA.14	-0.82
nuc-1	-0.82
ugt-23	-0.82
nduf-7	-0.82
ZC239.16	-0.82
B0491.5	-0.83
mecr-1	-0.83
C17H12.8	-0.83
Y39A1A.14	-0.83
F10C1.9	-0.83
F10E9.4	-0.83
ZK632.9	-0.83
asns-2	-0.83
T12B3.2	-0.83
aco-1	-0.83
grd-5	-0.83
cct-5	-0.83
cdo-1	-0.83
ssp-16	-0.84
F58H1.8	-0.84
F56A8.3	-0.84
spp-14	-0.84
catp-3	-0.84
acdh-11	-0.84
par-5	-0.84
K08D12.3	-0.84

Table E3 (Continued)

Gene Name	log_2 Fold
F54D5.7	-0.84
K09E2.3	-0.84
F26B1.8	-0.84
mrpl-24	-0.84
R53.2	-0.84
ugt-6	-0.84
lsm-1	-0.84
ZC376.2	-0.84
atp-5	-0.85
C04G2.8	-0.85
F42A9.6	-0.85
F44G4.2	-0.85
dhs-18	-0.85
F43C11.7	-0.85
M162.7	-0.85
rpl-41	-0.85
R09B3.2	-0.85
F56F10.1	-0.85
F35H10.6	-0.85
nuo-6	-0.85
art-1	-0.85
C30H6.8	-0.85
F35D11.4	-0.85
acs-22	-0.85
T21G5.4	-0.85
sqt-2	-0.85
F55B11.2	-0.85
R12E2.13	-0.85
W10G11.19	-0.85
snrp-27	-0.86
F47B8.8	-0.86
isp-1	-0.86
F54C9.3	-0.86
sptl-2	-0.86
F15D3.7	-0.86
R02F2.9	-0.86
Y67D2.3	-0.86
snr-3	-0.86
pes-23	-0.86
C29F3.7	-0.86
rps-13	-0.86

Gene Name	log_2 Fold
ZK84.1	-0.87
wrt-4	-0.87
ivd-1	-0.87
Y51H1A.3	-0.87
F10E9.5	-0.87
C25H3.9	-0.87
nspc-13	-0.87
grd-6	-0.87
W04G3.5	-0.87
spl-1	-0.87
ugt-44	-0.87
Y43F8C.5	-0.87
ZK180.5	-0.87
msp-78	-0.87
gipc-1	-0.88
tdo-2	-0.88
mrpl-16	-0.88
F38B7.3	-0.88
vha-2	-0.88
hpo-15	-0.88
sdhd-1	-0.88
M153.1	-0.88
C43E11.5	-0.88
trx-4	-0.88
M88.7	-0.89
ssq-4	-0.89
T24C12.3	-0.89
C04G2.9	-0.89
cpt-4	-0.89
T06G6.6	-0.89
R09B3.3	-0.89
F42C5.5	-0.89
nhr-109	-0.89
lec-10	-0.89
F37H8.3	-0.89
col-96	-0.89
msp-77	-0.89
Y54F10AM.5	-0.89
Y105E8A.11	-0.89
R151.2	-0.90

Gene Name	log_2 Fold
asp-5	-0.90
Y62E10A.13	-0.90
col-58	-0.90
T20H4.5	-0.90
pcp-2	-0.90
F27D4.1	-0.90
C15H11.1	-0.90
C15F1.1	-0.90
cyn-2	-0.90
sur-5	-0.90
rpl-33	-0.90
rpl-26	-0.90
rpl-30	-0.91
ram-2	-0.91
C35C5.10	-0.91
his-59	-0.91
msp-50	-0.91
Y39B6A.3	-0.91
cpi-1	-0.91
Y39E4A.3	-0.91
tin-9.1	-0.91
ZK858.8	-0.91
W06D4.2	-0.91
rpl-43	-0.91
gta-1	-0.91
rpl-38	-0.91
nlp-28	-0.92
C50F2.5	-0.92
C01G10.8	-0.92
drr-1	-0.92
nrf-6	-0.92
unc-23	-0.92
Y62E10A.2	-0.92
dhs-14	-0.92
Y71H2B.4	-0.92
clec-10	-0.92
sucl-2	-0.92
acdh-4	-0.92
B0457.2	-0.92
C47B2.9	-0.92
lbp-4	-0.92

Gene Name	log_2 Fold
F53F4.16	-0.92
R05G6.7	-0.92
afmd-1	-0.93
glrx-22	-0.93
rhr-1	-0.93
ugt-7	-0.93
F20H11.4	-0.93
rpl-31	-0.93
cpt-5	-0.93
grl-16	-0.93
F08F3.4	-0.93
ZK1127.13	-0.93
dhs-9	-0.93
mig-1	-0.93
cgt-2	-0.93
T01D1.3	-0.93
col-133	-0.93
C52B11.5	-0.93
rps-3	-0.93
clec-65	-0.93
cpr-1	-0.93
kat-1	-0.94
tag-261	-0.94
erd-2	-0.94
Y105C5B.9	-0.94
Y19D10A.16	-0.94
nlp-27	-0.94
B0228.7	-0.94
gst-42	-0.94
nlp-24	-0.94
col-97	-0.94
Y57A10A.23	-0.94
gst-7	-0.94
C42D4.1	-0.94
Y81G3A.1	-0.94
R08A2.2	-0.94
lpd-8	-0.94
hda-5	-0.94
C05C12.5	-0.94
best-21	-0.94

Table E3 (Continued)

Gene Name	log_2 Fold
E03H12.7	-0.95
F28F5.6	-0.95
hpo-8	-0.95
gln-3	-0.95
Y71H2AR.1	-0.95
ver-2	-0.95
col-61	-0.95
R04A9.9	-0.95
col-137	-0.95
C53B4.3	-0.95
R05F9.6	-0.95
sss-1	-0.95
rps-26	-0.95
Y50D4B.6	-0.95
F38B7.2	-0.95
F09E5.11	-0.95
msp-45	-0.95
Y17D7B.4	-0.95
rab-19	-0.95
F08D12.7	-0.95
F20D6.6	-0.96
clec-83	-0.96
K09H9.8	-0.96
Y43F4B.10	-0.96
nspc-20	-0.96
dod-17	-0.96
rps-30	-0.96
asp-6	-0.96
sft-4	-0.96
rnp-4	-0.96
mbf-1	-0.96
B0491.7	-0.96
Y71F9B.9	-0.96
cco-1	-0.96
rrn-2.1	-0.96
D1014.4	-0.96
C47D12.5	-0.96
T08H10.3	-0.96
T04F3.3	-0.96
R53.4	-0.96
col-73	-0.97

Gene Name	log_2 Fold
C01G10.14	-0.97
hpd-1	-0.97
ZK616.3	-0.97
lon-1	-0.97
grsp-1	-0.97
F34D10.9	-0.97
F42H11.1	-0.97
F16F9.4	-0.97
W09C5.8	-0.97
ugt-63	-0.97
Y63D3A.7	-0.97
nlp-30	-0.97
his-60	-0.97
T04A8.13	-0.97
K08C7.6	-0.97
ZK1240.5	-0.97
elo-9	-0.97
F53F4.10	-0.97
Y50D4A.5	-0.97
W01A8.8	-0.97
nlp-31	-0.97
Y37E11B.6	-0.97
F23C8.5	-0.97
Y105C5B.5	-0.98
lpd-9	-0.98
upb-1	-0.98
F31D4.8	-0.98
F44A6.4	-0.98
Y43B11AR.1	-0.98
mel-32	-0.98
nspc-14	-0.98
ttr-47	-0.98
ZK856.5	-0.98
K02A11.4	-0.98
ZK265.6	-0.98
mrps-28	-0.98
C01B10.10	-0.98
D1086.17	-0.98
F27E5.1	-0.98
ZK899.2	-0.98
R04F11.5	-0.98

Gene Name	log_2 Fold
ndg-4	-0.98
dlc-1	-0.98
F22H10.2	-0.98
K07A1.5	-0.98
R07E3.4	-0.98
E02H1.6	-0.98
ttr-48	-0.99
rpl-34	-0.99
sqt-1	-0.99
Y87G2A.20	-0.99
B0250.5	-0.99
nbet-1	-0.99
C34B2.8	-0.99
aqp-4	-0.99
K08F4.5	-0.99
F58D5.2	-0.99
C55C3.4	-0.99
ril-1	-0.99
ubq-2	-0.99
rps-19	-0.99
F36A4.4	-0.99
C35D10.17	-0.99
AC3.9	-0.99
T21G5.2	-0.99
R06B10.1	-0.99
F45G2.8	-0.99
F13G3.10	-0.99
ubl-1	-0.99
C27H5.4	-0.99
rps-12	-0.99
clec-150	-0.99
C34D4.2	-0.99
acdh-5	-1.00
W03D8.5	-1.00
ugt-52	-1.00
acdh-9	-1.00
ttr-41	-1.00
D2023.4	-1.00
H22K11.2	-1.00
F59A2.5	-1.00
Y69A2AR.21	-1.00

Gene Name	log_2 Fold
D1086.7	-1.00
F40F12.3	-1.00
cyn-5	-1.00
F57B10.14	-1.00
MTCE.33	-1.01
lact-1	-1.01
tba-9	-1.01
C55B7.3	-1.01
C26F1.1	-1.01
ins-33	-1.01
C07D8.6	-1.01
lbp-3	-1.01
his-53	-1.01
chch-3	-1.01
nspc-15	-1.01
daf-22	-1.01
cyn-7	-1.01
F55E10.6	-1.01
chw-1	-1.01
K07H8.5	-1.01
Y43C5B.3	-1.01
F59D6.3	-1.01
his-70	-1.01
pgrn-1	-1.01
Y67H2A.5	-1.01
apy-1	-1.01
dpy-5	-1.01
kbp-4	-1.01
acox-1	-1.01
cln-3.1	-1.02
C33H5.13	-1.02
K08C9.2	-1.02
aldo-2	-1.02
R12C12.1	-1.02
F54F7.3	-1.02
rmd-3	-1.02
C26B9.5	-1.02
nkat-3	-1.02
F32B6.10	-1.02
ssq-1	-1.02
C16C10.8	-1.02
clec-4	-1.02

Table E3 (Continued)

Gene Name	log_2 Fold
nspc-3	-1.02
rps-23	-1.02
mlc-2	-1.03
F35C8.5	-1.03
F36A2.3	-1.03
rps-16	-1.03
acdh-8	-1.03
tap-1	-1.03
T11F8.1	-1.03
rpl-36	-1.03
T01B11.2	-1.03
Y51A2D.18	-1.03
F10D2.10	-1.03
hsp-12.1	-1.03
rpl-28	-1.03
C26B2.2	-1.03
Y45F10C.2	-1.03
K01D12.15	-1.03
C30G7.4	-1.03
ceh-88	-1.03
F28E10.4	-1.03
C48B6.10	-1.03
R09E10.2	-1.03
daao-1	-1.04
T27E7.1	-1.04
gstk-1	-1.04
F41G3.18	-1.04
K01C8.1	-1.04
ard-1	-1.04
T27E4.7	-1.04
Y62H9A.4	-1.04
ZK1010.8	-1.04
asp-2	-1.04
ZC376.3	-1.04
ZC449.8	-1.04
T06A1.5	-1.04
C39D10.7	-1.04
klo-2	-1.04
F52H2.6	-1.04
F20G2.2	-1.04
F41F3.3	-1.04
C35A5.3	-1.04
C02B10.6	-1.04
T04B2.7	-1.04
mrpl-12	-1.04
mrps-12	-1.05
C16A11.7	-1.05
acl-1	-1.05
his-19	-1.05
C28D4.8	-1.05
T09A5.15	-1.05
msp-40	-1.05
rps-14	-1.05
Y102A5C.36	-1.05
R12E2.7	-1.05
C25A8.4	-1.05
K07G5.5	-1.05
Y47D3B.12	-1.05
F42G8.10	-1.05
Y48A6B.3	-1.05
rps-15	-1.05
F36H12.10	-1.05
alh-6	-1.05
ZK512.4	-1.05
F21C3.6	-1.06
C35D10.8	-1.06
ssq-2	-1.06
ddp-1	-1.06
nlp-29	-1.06
Y54G2A.49	-1.06
F13H6.3	-1.06
C16A3.10	-1.06
F25H5.2	-1.06
F36H12.5	-1.06
fbxa-92	-1.06
F23F1.10	-1.06
Y71G12B.27	-1.06
C05D11.5	-1.06
F54A3.5	-1.06
F43G6.17	-1.06
rps-18	-1.06
Y105C5A.25	-1.06
cnc-4	-1.06
cyp-37B1	-1.06
Y71H2AM.5	-1.07
rps-9	-1.07
ZK930.6	-1.07
nspc-19	-1.07
mec-5	-1.07
W01D2.1	-1.07
col-104	-1.07
Y45F3A.1	-1.07
frh-1	-1.07
pho-1	-1.07
dnj-21	-1.07
ZC196.5	-1.07
C15H7.3	-1.07
Y57A10A.3	-1.07
dpy-13	-1.07
moag-4	-1.07
ZK795.2	-1.08
C29E4.12	-1.08
F23H11.5	-1.08
ugt-4	-1.08
R12E2.15	-1.08
ZK686.1	-1.08
C35B1.5	-1.08
ant-1.3	-1.08
ugt-33	-1.08
clec-49	-1.08
fbl-1	-1.08
dnpp-1	-1.08
T27A3.5	-1.08
bli-2	-1.08
fbxa-202	-1.08
F23F12.12	-1.08
C15B12.1	-1.08
pfd-2	-1.08
msp-10	-1.08
H32K16.2	-1.08
col-65	-1.08
glrx-21	-1.08
trap-4	-1.08
rps-22	-1.08
dpy-4	-1.08
T09A5.7	-1.08
grd-2	-1.08
ZC395.10	-1.09
fbxa-91	-1.09
gcst-1	-1.09
F09E5.8	-1.09
rpb-8	-1.09
nep-4	-1.09
tkt-1	-1.09
col-161	-1.09
F14D7.6	-1.09
F37F2.2	-1.09
maoc-1	-1.09
ger-1	-1.09
W04B5.1	-1.09
T02G5.7	-1.09
twk-26	-1.09
T10C6.10	-1.09
Y54E2A.9	-1.10
Y82E9BR.3	-1.10
rps-25	-1.10
gst-12	-1.10
E01G4.7	-1.10
F43G9.8	-1.10
gst-26	-1.10
F59A6.2	-1.10
F07F6.1	-1.10
ZC190.8	-1.10
atp-4	-1.10
sti-1	-1.10
col-8	-1.10
F52E1.14	-1.10
F22F7.1	-1.10
E03H12.5	-1.10
clec-85	-1.10
K08C7.1	-1.10
snr-7	-1.10
tmem-135	-1.10
F45H10.3	-1.10

Table E3 (Continued)

Gene Name	log_2 Fold
Y69E1A.2	-1.10
ethe-1	-1.10
ant-1.4	-1.10
F44A6.5	-1.10
mrpl-41	-1.10
spe-4	-1.10
T22A3.12	-1.10
F46F2.3	-1.10
msp-71	-1.11
Y56A3A.19	-1.11
Y18D10A.21	-1.11
ttr-46	-1.11
F40G9.5	-1.11
F25G6.8	-1.11
F36F2.1	-1.11
rpl-23	-1.11
R13A1.3	-1.11
R04F11.2	-1.11
F18F11.1	-1.11
T02H6.11	-1.11
C25E10.8	-1.11
C05D12.3	-1.12
nep-20	-1.12
F58F12.1	-1.12
col-184	-1.12
mpst-3	-1.12
F33D11.2	-1.12
F35C11.3	-1.12
H27M09.5	-1.12
cTel55X.1	-1.12
F22D3.4	-1.12
nhr-193	-1.12
F56B3.11	-1.12
fat-6	-1.12
daf-21	-1.12
ech-9	-1.12
F46A9.1	-1.13
B0272.3	-1.13
K04G2.10	-1.13
rps-21	-1.13
C10H11.7	-1.13
ZC373.5	-1.13
Y53F4B.23	-1.13
C08F11.12	-1.13
K12H4.5	-1.13
C10C5.4	-1.13
D2062.6	-1.13
F37E3.3	-1.13
acs-1	-1.13
F53C3.1	-1.13
ttr-45	-1.13
K08E4.7	-1.13
col-76	-1.13
T10E9.6	-1.13
F44E5.1	-1.14
C35A5.6	-1.14
R05D7.1	-1.14
Y62H9A.3	-1.14
F45E4.6	-1.14
Y41E3.22	-1.14
scrm-8	-1.14
mrps-18A	-1.14
mif-2	-1.14
spe-10	-1.14
F42A9.7	-1.14
C08A9.10	-1.14
F23C8.3	-1.14
Y40D12A.2	-1.14
dao-4	-1.14
K06H7.8	-1.14
mrpl-32	-1.15
B0035.13	-1.15
T12D8.5	-1.15
T01C3.2	-1.15
ddo-3	-1.15
K01D12.9	-1.15
C35E7.10	-1.15
ZK354.3	-1.15
F17C11.6	-1.15
amt-4	-1.15
R07B7.10	-1.15
T05F1.11	-1.15
msp-36	-1.15
T22D1.11	-1.16
erv-46	-1.16
ttr-53	-1.16
his-37	-1.16
F58A6.1	-1.16
F12B6.2	-1.16
R12C12.10	-1.16
msp-56	-1.16
Y59E9AL.6	-1.16
col-162	-1.16
H25K10.1	-1.16
C34F11.2	-1.16
gst-27	-1.16
C32C4.3	-1.16
fipr-4	-1.16
ZK1251.5	-1.17
msp-142	-1.17
F17E9.4	-1.17
F36A2.7	-1.17
kvs-4	-1.17
F33D4.7	-1.17
T13F3.8	-1.17
col-106	-1.17
Y38F1A.1	-1.17
col-130	-1.17
W08D2.9	-1.18
C46C11.2	-1.18
nspd-3	-1.18
C28D4.7	-1.18
T08G11.2	-1.18
C46H11.6	-1.18
F29C6.1	-1.18
F26E4.6	-1.18
spe-11	-1.18
Y66H1A.5	-1.18
F13E9.13	-1.18
nspc-1	-1.18
F42G8.8	-1.18
T05C12.1	-1.18
Y106G6H.1	-1.18
T05B11.4	-1.18
F43E2.6	-1.18
C28C12.1	-1.18
Y45F10C.4	-1.19
R05D7.7	-1.19
F26B1.1	-1.19
mrps-7	-1.19
ZK484.6	-1.19
C04E12.2	-1.19
ent-2	-1.19
C29F7.3	-1.19
Y95D11A.1	-1.19
swt-7	-1.19
Y23H5B.1	-1.19
R11.1	-1.19
flu-2	-1.19
ugt-53	-1.19
M04C9.3	-1.19
F32A5.3	-1.19
R09H10.3	-1.19
frm-9	-1.19
elo-2	-1.19
cyp-29A2	-1.20
K09C6.8	-1.20
T21H3.1	-1.20
C33A12.19	-1.20
Y119D3B.21	-1.20
F14E5.1	-1.20
C40H1.2	-1.20
nspc-16	-1.20
fbxa-72	-1.20
C56C10.6	-1.20
har-1	-1.21
W08F4.5	-1.21
Y44A6D.5	-1.21
ttr-51	-1.21
srx-58	-1.21
C55A6.4	-1.21
F25H9.7	-1.21
cpg-9	-1.21
Y82E9BR.22	-1.21

Table E3 (Continued)

Gene Name	log_2 Fold
F29B9.11	-1.21
F25H5.8	-1.21
ZK84.2	-1.21
lipl-2	-1.22
C17D12.5	-1.22
his-7	-1.22
ttr-37	-1.22
cyc-2.2	-1.22
mrpl-23	-1.22
T25B9.1	-1.22
W05E10.1	-1.22
C33G8.2	-1.22
tag-281	-1.22
oat-1	-1.22
col-170	-1.22
W08E12.8	-1.22
fipr-21	-1.22
col-91	-1.22
F37C4.6	-1.22
T01H8.2	-1.22
F10E7.6	-1.22
F14B8.4	-1.22
pdi-2	-1.22
Y43F8B.2	-1.22
T11F8.4	-1.23
F10E9.11	-1.23
nhr-114	-1.23
ZC581.7	-1.23
F54D5.16	-1.23
mrpl-54	-1.23
dct-9	-1.23
Y50E8A.12	-1.23
F11C1.1	-1.23
msd-2	-1.23
Y116A8C.30	-1.23
Y57G11C.15	-1.23
D1022.4	-1.23
F07H5.3	-1.23
C28D4.5	-1.23
Y43C5B.2	-1.24

Gene Name	log_2 Fold
T14G8.3	-1.24
T08H10.1	-1.24
nspc-18	-1.24
Y73F4A.1	-1.24
F45H10.2	-1.24
idh-1	-1.24
R05D7.2	-1.24
acr-11	-1.24
W03F9.1	-1.24
C15H9.9	-1.24
T10B5.7	-1.24
F45H11.5	-1.24
clec-52	-1.24
Y54G2A.23	-1.25
F07C6.6	-1.25
F36D1.7	-1.25
aqp-10	-1.25
F13A7.7	-1.25
F08A8.4	-1.25
C23H4.7	-1.25
C25H3.17	-1.25
C05C10.7	-1.25
fipr-10	-1.25
mrpl-13	-1.25
pfd-6	-1.25
trap-2	-1.25
ZK909.6	-1.25
lbp-5	-1.25
F01F1.2	-1.25
R02F2.6	-1.25
gst-6	-1.25
T23B7.2	-1.25
R10E9.3	-1.25
cyp-14A2	-1.25
C34B2.3	-1.25
mrps-21	-1.25
D1086.3	-1.25
F58H1.6	-1.25
K06A4.7	-1.25
oac-50	-1.25
wrt-5	-1.26
gst-36	-1.26

Gene Name	log_2 Fold
Y32F6A.5	-1.26
Y62H9A.15	-1.26
K11C4.1	-1.26
pmt-2	-1.26
M04C9.4	-1.26
fipr-6	-1.26
K02E11.10	-1.26
T09B4.4	-1.26
nspc-9	-1.26
B0272.4	-1.26
irld-8	-1.26
msd-1	-1.26
C26C6.9	-1.27
hsp-16.2	-1.27
C02F5.5	-1.27
Y40B1B.7	-1.27
rpl-29	-1.27
F13D12.6	-1.27
F23B12.1	-1.27
cnc-8	-1.27
cpz-1	-1.27
fbxb-36	-1.27
nid-1	-1.27
msd-3	-1.27
D2030.4	-1.27
nurf-1	-1.27
Y47D3A.13	-1.28
ZK688.12	-1.28
col-179	-1.28
rla-2	-1.28
msra-1	-1.28
M02E1.3	-1.28
C34B2.9	-1.28
ahcy-1	-1.28
C07E3.9	-1.28
acbp-3	-1.28
F57B1.5	-1.28
T02E1.7	-1.29
tin-10	-1.29
F37C12.3	-1.29
ttr-44	-1.29
hil-2	-1.29

Gene Name	log_2 Fold
spe-12	-1.29
Y54G2A.41	-1.29
lbp-7	-1.29
F48D6.4	-1.29
C17H12.11	-1.29
F42G4.6	-1.29
C49H3.3	-1.29
ZK84.5	-1.29
Y51H7C.13	-1.29
B0496.1	-1.30
B0218.5	-1.30
asg-2	-1.30
C53D6.10	-1.30
C33G8.3	-1.30
C04G2.5	-1.30
H06I04.5	-1.30
ech-1	-1.30
T13A10.1	-1.30
F32B6.4	-1.30
K10D2.5	-1.30
W09D6.4	-1.30
F29C4.2	-1.30
R08B4.3	-1.30
C26B2.7	-1.31
aip-1	-1.31
H09G03.1	-1.31
K08E7.8	-1.31
Y53C10A.15	-1.31
gst-28	-1.31
msp-81	-1.31
fipr-13	-1.31
C43H6.1	-1.31
ZK1307.1	-1.31
crt-1	-1.31
irg-3	-1.31
decr-1.1	-1.31
T16G12.7	-1.31
C44C1.5	-1.31
C32E8.4	-1.31
Y51H7C.1	-1.31

Table E3 (Continued)

Gene Name	log_2 Fold
Y59H11AM.1	-1.31
C01B4.6	-1.31
K07A1.10	-1.32
dhs-3	-1.32
K12C11.5	-1.32
Y54G11A.17	-1.32
C04F12.7	-1.32
nspd-4	-1.32
F52B11.2	-1.32
msp-38	-1.32
nhr-143	-1.32
F49E12.10	-1.32
ZK822.2	-1.32
R105.1	-1.32
ZK666.8	-1.32
ugt-49	-1.32
mtp-18	-1.32
lsm-6	-1.33
K10C2.7	-1.33
ugt-21	-1.33
spp-5	-1.33
T23F6.3	-1.33
F54D7.6	-1.33
ftn-2	-1.33
C01B10.4	-1.33
F23D12.11	-1.33
ugt-26	-1.33
C01G12.3	-1.33
Y37A1B.5	-1.33
rpl-39	-1.33
nspd-5	-1.33
thn-2	-1.33
msp-152	-1.34
D2062.7	-1.34
Y57G7A.5	-1.34
F14F7.4	-1.34
C14A4.6	-1.34
daf-36	-1.34
AH6.3	-1.34
ttr-35	-1.34

Gene Name	log_2 Fold
Y39B6A.34	-1.34
aat-4	-1.34
B0207.11	-1.34
H12D21.5	-1.34
W03F9.4	-1.34
F59A3.13	-1.34
pyk-2	-1.34
haao-1	-1.34
F11D5.7	-1.35
math-32	-1.35
mrpl-36	-1.35
tsp-18	-1.35
F54D1.1	-1.35
alh-12	-1.35
K04G2.11	-1.35
Y71A12B.23	-1.35
C02E7.6	-1.35
pfd-5	-1.35
F46A9.2	-1.35
C03C10.2	-1.35
F57G8.5	-1.35
C45B2.1	-1.36
msp-64	-1.36
C46C2.5	-1.36
ugt-54	-1.36
Y47G6A.33	-1.36
Y57G11B.3	-1.36
D1005.4	-1.36
mai-2	-1.36
fbxa-196	-1.36
B0416.11	-1.36
C01G6.2	-1.36
decr-1.3	-1.36
F07F6.2	-1.36
Y22D7AL.10	-1.36
C10C6.3	-1.36
T02B11.8	-1.36
Y69A2AR.8	-1.36
Y43F8C.13	-1.36
T19B4.3	-1.36

Gene Name	log_2 Fold
K11D12.13	-1.36
amx-3	-1.36
C47A4.5	-1.36
ugt-46	-1.36
clec-223	-1.37
M7.7	-1.37
F27C1.1	-1.37
F54D5.4	-1.37
T19H5.7	-1.37
C31G12.1	-1.37
F32H5.1	-1.37
ZC21.10	-1.37
MTCE.3	-1.37
linc-15	-1.37
C50D2.3	-1.37
F58B4.5	-1.37
R11H6.4	-1.37
hsp-4	-1.38
nspc-10	-1.38
C34G6.3	-1.38
ZK622.1	-1.38
F54D7.7	-1.38
rpl-22	-1.38
ttr-36	-1.38
cuc-1	-1.38
clec-57	-1.38
tag-344	-1.38
R08E5.1	-1.38
gale-1	-1.38
ZK813.7	-1.38
kin-15	-1.38
mrps-17	-1.38
rpac-19	-1.38
C48D1.9	-1.38
col-77	-1.39
dnj-13	-1.39
btb-21	-1.39
F40G9.2	-1.39
ZK1248.20	-1.39
F52F12.8	-1.39
C04G2.12	-1.39
R160.3	-1.39

Gene Name	log_2 Fold
C50E10.1	-1.39
T28B8.6	-1.39
ZK265.9	-1.39
F21F8.4	-1.39
pqn-68	-1.39
F28H1.5	-1.39
cpr-6	-1.40
sth-1	-1.40
tsp-10	-1.40
nspc-7	-1.40
T25B9.2	-1.40
B0496.6	-1.40
spp-8	-1.40
fip-5	-1.40
F56A4.3	-1.40
cco-2	-1.40
hsp-3	-1.40
skr-14	-1.40
dpm-3	-1.40
F58F12.4	-1.40
acbp-1	-1.40
F18C12.4	-1.40
K09H9.9	-1.41
ugt-51	-1.41
C49F5.7	-1.41
Y1A5A.1	-1.41
F56H9.2	-1.41
F39D8.7	-1.41
C18E9.4	-1.41
C18G1.3	-1.41
msp-33	-1.41
F19G12.9	-1.41
C35A11.4	-1.41
Y39E4B.11	-1.41
F58A6.5	-1.41
ech-7	-1.41
T03F6.10	-1.42
C28G1.10	-1.42
C06A6.7	-1.42
ttr-15	-1.42
C44B7.11	-1.42
C02E7.7	-1.42

Table E3 (Continued)

Gene Name	log_2 Fold
Y38H6C.15	-1.42
F59C6.3	-1.42
col-38	-1.42
fpn-1.2	-1.42
Y47G6A.26	-1.42
C03C11.1	-1.42
F30A10.13	-1.42
F58B4.7	-1.43
C04F12.12	-1.43
Y69E1A.8	-1.43
F52F12.5	-1.43
F07G6.10	-1.43
dnj-7	-1.43
C08F11.10	-1.43
ZK228.3	-1.43
ZK686.5	-1.43
bli-6	-1.43
trap-1	-1.43
tag-320	-1.43
nspd-10	-1.43
C02C2.4	-1.43
Y69A2AR.23	-1.44
ddo-1	-1.44
F36F12.7	-1.44
C52E4.7	-1.44
C32D5.4	-1.44
fipr-7	-1.44
Y69H2.3	-1.44
C17G10.3	-1.45
ZK512.8	-1.45
col-182	-1.45
F53G12.8	-1.45
rmo-1	-1.45
C34D4.3	-1.45
Y71H2B.1	-1.45
R07E4.3	-1.45
F13G11.3	-1.45
cdr-6	-1.45
zip-3	-1.45
msp-52	-1.45
nspc-4	-1.45

Gene Name	log_2 Fold
F28H7.3	-1.45
T24C2.5	-1.45
mrps-24	-1.46
lys-2	-1.46
trap-3	-1.46
F13E9.12	-1.46
Y48G1C.13	-1.46
F22E5.1	-1.46
F41F3.1	-1.46
R09E10.1	-1.46
ZC262.10	-1.46
lbp-6	-1.46
Y106G6E.3	-1.46
ncx-7	-1.46
tin-13	-1.47
T12B5.14	-1.47
D1054.11	-1.47
ceh-63	-1.47
his-46	-1.47
emo-1	-1.47
ZK185.3	-1.47
C47A4.3	-1.47
elo-8	-1.47
T02B11.9	-1.47
linc-44	-1.47
C39B5.5	-1.47
C14B9.10	-1.47
scp-1	-1.48
ZC250.5	-1.48
C30G12.2	-1.48
F59B1.2	-1.48
cbs-2	-1.48
C33A12.1	-1.48
dhs-25	-1.48
tomm-22	-1.48
T10G3.3	-1.48
Y47D9A.3	-1.48
asp-1	-1.48
F23F12.3	-1.48
col-71	-1.48
C03B1.13	-1.48

Gene Name	log_2 Fold
R102.3	-1.49
C54G4.3	-1.49
col-49	-1.49
F55B11.3	-1.49
nas-20	-1.49
mrps-10	-1.49
ZC416.6	-1.49
C44B7.7	-1.49
Y42H9AR.2	-1.49
F10E9.2	-1.49
F40H3.2	-1.49
mtl-2	-1.49
col-63	-1.49
C49F5.9	-1.49
pho-13	-1.49
cbl-1	-1.49
oac-10	-1.49
C07A4.3	-1.49
C33C12.7	-1.49
ZK945.6	-1.49
F07A11.5	-1.50
nlp-26	-1.50
F53F1.4	-1.50
ZK930.4	-1.50
T20D4.7	-1.50
F46F5.6	-1.50
nspd-7	-1.50
R03D7.5	-1.50
Y69H2.9	-1.50
Y71G12B.3	-1.50
cpr-5	-1.50
T22E5.1	-1.50
F36H12.4	-1.50
R10H10.3	-1.50
F58A6.9	-1.50
F36H9.2	-1.50
Y51F10.7	-1.51
prmt-6	-1.51
C08F11.11	-1.51
M7.12	-1.51
F28H7.4	-1.51

Gene Name	log_2 Fold
dct-18	-1.51
K09C4.1	-1.51
hsp-16.49	-1.51
ech-6	-1.51
col-138	-1.51
T04F3.4	-1.51
F56B3.6	-1.51
T06E4.10	-1.51
F35F10.5	-1.52
nspc-5	-1.52
K08C9.1	-1.52
ZK354.7	-1.52
R13A5.10	-1.52
fbxa-183	-1.52
F25B4.8	-1.52
C04F12.6	-1.52
ZC477.2	-1.52
immp-1	-1.52
Y14H12A.1	-1.53
F15H9.1	-1.53
best-7	-1.53
C35B1.4	-1.53
fipr-8	-1.53
F45D11.1	-1.54
F56F4.4	-1.54
Y62H9A.6	-1.54
clec-166	-1.54
mrps-33	-1.54
lys-8	-1.54
col-60	-1.54
F17B5.8	-1.54
calu-1	-1.54
C09B8.5	-1.54
T20D4.10	-1.54
msp-113	-1.54
gst-1	-1.55
clec-54	-1.55
bas-1	-1.55
hsp-16.48	-1.55
F53H4.2	-1.55
T24A6.20	-1.55
B0252.5	-1.56

Table E3 (Continued)

Gene Name	log_2 Fold
sdz-6	-1.56
clec-227	-1.56
C04G2.3	-1.56
W09C3.7	-1.56
F46F5.9	-1.56
hsp-1	-1.56
R09E12.9	-1.56
linc-61	-1.57
C50F4.10	-1.57
R04B5.11	-1.57
F13H8.3	-1.57
ssp-37	-1.57
hsp-16.1	-1.57
H01G02.4	-1.58
C47E8.1	-1.58
pho-7	-1.58
ceeh-2	-1.58
ZK287.3	-1.58
dhs-2	-1.58
D1054.8	-1.58
C26C6.6	-1.58
Y51B9A.5	-1.58
ZK1098.6	-1.58
ZC477.7	-1.58
C18A3.7	-1.58
F22F4.5	-1.58
dylt-3	-1.59
F08F1.4	-1.59
nas-27	-1.59
R12E2.14	-1.59
C55C2.3	-1.59
C45B11.8	-1.59
hpo-18	-1.59
C35E7.9	-1.59
smf-3	-1.59
F21A3.4	-1.60
asp-3	-1.60
ugt-62	-1.60
twk-6	-1.60
Y53F4B.36	-1.60
perm-2	-1.60
F44E2.9	-1.60

Gene Name	log_2 Fold
pqn-63	-1.60
peel-1	-1.60
perm-4	-1.61
snb-7	-1.61
F26F12.8	-1.61
W03D8.3	-1.61
M162.5	-1.61
msp-57	-1.61
F54C1.8	-1.61
C05D12.4	-1.61
Y23H5B.12	-1.61
C55C3.8	-1.62
cyp-34A9	-1.62
Y38F1A.7	-1.62
Y48G8AL.12	-1.62
pfd-4	-1.62
F19B2.5	-1.62
C50F7.3	-1.62
col-175	-1.62
C55A6.7	-1.62
ZK813.3	-1.62
C45B11.9	-1.62
F57F5.1	-1.62
W04H10.1	-1.63
urm-1	-1.63
dsc-4	-1.63
W09C3.8	-1.63
Y38E10A.28	-1.63
T28H11.7	-1.63
F38E1.3	-1.63
Y54G9A.9	-1.63
C04G6.2	-1.63
rol-1	-1.63
Y38F2AR.10	-1.63
R02C2.7	-1.64
Y37E11AL.12	-1.64
linc-6	-1.64
ZC155.2	-1.64
F10D11.3	-1.64

Gene Name	log_2 Fold
Y67A6A.1	-1.64
Y69E1A.4	-1.64
msp-59	-1.64
ZK813.2	-1.65
C53H9.3	-1.65
K06A4.6	-1.65
W03F11.1	-1.65
T20B6.3	-1.65
hsp-16.11	-1.65
F32B4.2	-1.65
F36H12.3	-1.65
F36H9.4	-1.65
msp-65	-1.65
F49E12.1	-1.65
C04E6.5	-1.66
C12D8.9	-1.66
R04E5.2	-1.66
F33D11.7	-1.66
W10G11.2	-1.66
clec-66	-1.66
F37C12.18	-1.66
ptps-1	-1.67
F48E3.4	-1.67
F56F3.4	-1.67
C14C11.4	-1.67
W02D9.6	-1.67
W08E3.4	-1.67
B0205.12	-1.67
ZK287.9	-1.67
ZK1248.5	-1.67
K07A1.4	-1.68
gst-10	-1.68
C28C12.11	-1.68
gpx-7	-1.68
cpl-1	-1.68
fbxa-180	-1.68
sdz-27	-1.68
Y37D8A.19	-1.68
Y54G2A.24	-1.68
htas-1	-1.68
ZK849.6	-1.68
H20E11.3	-1.68

Gene Name	log_2 Fold
F55G11.8	-1.69
W03D8.8	-1.69
C40H1.7	-1.69
gpx-1	-1.69
R186.8	-1.69
msp-19	-1.69
H06H21.8	-1.69
lact-4	-1.69
T22B3.3	-1.69
T06E4.12	-1.69
dhs-7	-1.69
ZC262.1	-1.69
tsp-19	-1.69
F10D11.4	-1.69
E02C12.6	-1.69
math-48	-1.70
Y47G6A.15	-1.70
Y34B4A.5	-1.70
F41H10.2	-1.70
F36D1.4	-1.70
ZK1290.5	-1.70
ZK1251.3	-1.71
W02D9.7	-1.71
K09H11.4	-1.71
ZC373.2	-1.71
R08E5.3	-1.71
F36A2.12	-1.71
ZK813.1	-1.71
Y62E10A.3	-1.71
Y22D7AR.10	-1.71
Y39H10B.2	-1.71
F55D12.6	-1.71
col-88	-1.71
ssp-31	-1.72
dhhc-12	-1.72
M02G9.4	-1.72
F10G8.2	-1.72
tag-10	-1.72
F38A5.6	-1.72
T01H3.5	-1.73
C46F2.1	-1.73

Table E3 (Continued)

Gene Name	log_2 Fold
C38C3.7	-1.73
ugt-32	-1.73
spe-17	-1.74
gst-5	-1.74
mpst-4	-1.74
Y51H7C.8	-1.74
T22C1.9	-1.74
cyp-35A4	-1.74
R107.5	-1.74
F21D5.3	-1.74
F36A4.3	-1.74
F43C1.5	-1.74
nspb-3	-1.74
F36A2.11	-1.75
pcp-1	-1.75
Y73F8A.15	-1.75
F10C1.3	-1.75
cyp-33E3	-1.76
F10G7.12	-1.76
clec-97	-1.76
C14A6.13	-1.76
T05C3.6	-1.76
ugt-17	-1.76
C03A7.12	-1.76
D1081.12	-1.76
T13F2.9	-1.76
T02D1.8	-1.77
fbxa-125	-1.77
ZK970.8	-1.77
cdd-1	-1.77
R102.4	-1.78
F31E9.11	-1.78
C24D10.2	-1.78
col-120	-1.79
F07E5.7	-1.79
F56D6.17	-1.79
F59A6.12	-1.79
cah-5	-1.79
Y106G6A.4	-1.79
W04A4.2	-1.79
nspc-6	-1.79
clec-117	-1.79

Gene Name	log_2 Fold
cyp-25A2	-1.80
F55C5.2	-1.80
Y105E8B.5	-1.80
gcsh-1	-1.80
F38B2.6	-1.80
K09G1.2	-1.80
catp-2	-1.80
F31D4.9	-1.81
Y38F2AR.9	-1.81
Y45G12C.1	-1.81
K12H4.7	-1.81
F08A8.3	-1.81
T24D3.2	-1.81
W07B8.1	-1.81
dod-24	-1.82
ttr-9	-1.82
K04F1.9	-1.82
hsp-16.41	-1.82
D1014.2	-1.82
C10G8.4	-1.82
B0207.9	-1.83
Y4C6A.4	-1.83
C55C2.4	-1.83
W10G11.3	-1.83
F26C11.1	-1.83
T09A12.1	-1.83
nspc-2	-1.83
C18D4.8	-1.83
K07A1.6	-1.83
ZK673.6	-1.84
Y59E9AR.7	-1.84
H23N18.6	-1.84
rnh-1.3	-1.84
clec-186	-1.84
Y47D7A.15	-1.84
clec-222	-1.84
ugt-5	-1.85
C23H4.3	-1.85
snb-6	-1.85
D1054.10	-1.85

Gene Name	log_2 Fold
nspb-2	-1.85
asah-1	-1.85
T05E7.1	-1.86
K11C4.14	-1.86
spp-23	-1.86
col-68	-1.87
B0379.2	-1.87
K02E7.6	-1.87
F39G3.2	-1.87
dct-11	-1.87
hrg-1	-1.88
C15C8.3	-1.88
Y57G11C.14	-1.88
inx-8	-1.88
best-11	-1.89
ZK973.4	-1.89
msd-4	-1.89
F30A10.12	-1.89
D1086.11	-1.90
F59F4.2	-1.90
fipr-5	-1.90
nspd-1	-1.90
his-21	-1.90
C43G2.3	-1.90
F36A4.2	-1.91
clec-210	-1.91
gst-4	-1.91
F23F12.13	-1.91
nspd-2	-1.91
F18E2.1	-1.92
F15A4.2	-1.92
ZC581.10	-1.92
btb-2	-1.92
F30A10.14	-1.92
Y67H2A.9	-1.92
D1081.10	-1.92
F57C2.4	-1.93
F56D6.13	-1.93
col-70	-1.93
ZK546.7	-1.93
C17E7.12	-1.94

Gene Name	log_2 Fold
T16G12.1	-1.94
Y102E9.5	-1.94
C53B4.2	-1.94
nlp-25	-1.94
T04G9.7	-1.95
C27D6.3	-1.95
F55F10.3	-1.95
Y57A10B.7	-1.95
msp-53	-1.96
msp-55	-1.96
R11H6.7	-1.96
fipr-9	-1.97
Y69A2AR.3	-1.97
Y43D4A.2	-1.97
F42F12.4	-1.98
F44G4.5	-1.98
dhs-21	-1.98
F54H12.7	-1.98
F25D1.5	-1.99
sfxn-1.3	-1.99
F35H10.2	-1.99
spp-3	-1.99
nspd-9	-1.99
fbxa-84	-1.99
Y52E8A.4	-1.99
Y41C4A.18	-2.00
ZK418.2	-2.00
ZK228.4	-2.00
F56D6.12	-2.00
D1054.18	-2.00
F55B11.5	-2.00
Y57G11C.40	-2.01
M05B5.7	-2.01
K10C2.3	-2.01
gst-13	-2.01
Y47D3A.32	-2.01
B0034.7	-2.02
W05B10.3	-2.02
R08F11.4	-2.02
F42A9.3	-2.02

Table E3 (Continued)

Gene Name	log_2 Fold
T05E12.6	-2.02
Y105C5B.15	-2.02
F28A10.7	-2.03
comt-5	-2.03
B0563.10	-2.03
F44D12.6	-2.03
D2062.4	-2.04
F40H6.1	-2.04
cut-2	-2.04
T02B5.3	-2.05
clec-209	-2.05
F41E6.1	-2.05
cyp-35A3	-2.05
Y59E9AR.1	-2.05
Y57G11B.5	-2.06
E02H9.7	-2.07
W02D7.4	-2.07
F56A4.2	-2.07
W03F8.2	-2.08
clec-56	-2.08
B0281.5	-2.08
ttr-56	-2.08
Y39G8C.2	-2.08
str-144	-2.09
Y73F8A.14	-2.09
F42A10.7	-2.10
T25E4.1	-2.10
Y47D3B.6	-2.10
rncs-1	-2.10
fat-7	-2.10
F55G11.2	-2.11
elo-6	-2.11
C18A11.4	-2.11
ttr-40	-2.11
ssp-32	-2.11
C32H11.3	-2.12
F21C3.7	-2.12
Y105C5B.18	-2.12
C15H7.4	-2.12
B0041.1	-2.12
C47E8.10	-2.12
ugt-30	-2.13
srh-70	-2.13
Y119D3B.13	-2.13
C17G1.2	-2.13
C52E12.6	-2.13
ttr-12	-2.14
Y37E11B.7	-2.14
F37A8.1	-2.14
Y71G12B.18	-2.15
F38A5.8	-2.15
K08F4.13	-2.15
ZK616.1	-2.15
Y57G11C.52	-2.15
spp-17	-2.15
ssp-33	-2.15
E04F6.15	-2.16
msp-58	-2.17
Y53F4B.11	-2.18
ugt-47	-2.19
abu-1	-2.19
clec-160	-2.19
irld-35	-2.20
C14A6.6	-2.20
nspe-5	-2.21
Y62H9A.5	-2.21
K07H8.7	-2.22
cyp-25A1	-2.22
C26B2.8	-2.22
tbh-1	-2.22
D1081.3	-2.22
irld-53	-2.23
ttr-49	-2.23
D1081.11	-2.23
K07E12.2	-2.23
ckb-2	-2.24
linc-36	-2.24
elo-5	-2.25
F25C8.1	-2.25
F22F7.8	-2.25
ZC373.3	-2.27
F28A12.4	-2.27
K03B4.6	-2.27
F49C12.7	-2.27
F22G12.8	-2.28
R05D3.5	-2.28
R12E2.6	-2.28
K01D12.8	-2.30
cyp-35A2	-2.31
Y39B6A.21	-2.32
R09D1.11	-2.33
R09D1.6	-2.33
F41C6.4	-2.33
F49E12.9	-2.34
pqn-54	-2.35
clec-190	-2.35
K07F5.8	-2.35
clec-8	-2.35
msp-51	-2.36
T06E4.14	-2.37
dct-16	-2.37
C15H11.13	-2.38
C36C9.10	-2.38
T13F3.6	-2.38
C48D1.7	-2.38
K12B6.11	-2.39
F58G6.9	-2.39
sri-40	-2.39
hrg-4	-2.39
ttr-42	-2.40
cdr-4	-2.40
T12B5.15	-2.40
F29B9.7	-2.40
Y54G2A.3	-2.40
cyp-35A5	-2.41
Y38F1A.6	-2.41
F10G8.1	-2.42
T19H5.6	-2.42
F15E11.15	-2.43
T06E4.8	-2.44
F22H10.6	-2.44
Y47D9A.4	-2.45
dhs-23	-2.47
clec-229	-2.47
C27F2.6	-2.48
C04E7.5	-2.48
C04H5.7	-2.49
C45B2.8	-2.50
F54B11.11	-2.50
ugt-22	-2.51
col-135	-2.52
C47E8.11	-2.52
C14C6.2	-2.52
R07C3.13	-2.53
K10B2.2	-2.54
T06E4.9	-2.55
F09E10.1	-2.55
asm-3	-2.58
efn-3	-2.58
Y105C5B.17	-2.58
msp-42	-2.59
F53F4.18	-2.60
F15E11.13	-2.61
C36C5.5	-2.61
Y19D10B.7	-2.61
F58G6.7	-2.62
lys-4	-2.63
clec-7	-2.63
Y69A2AR.27	-2.64
T25E12.16	-2.66
lips-14	-2.66
cyp-35C1	-2.67
C17C3.9	-2.69
Y40H7A.11	-2.70
K07A1.13	-2.74
C17B7.4	-2.74
gba-4	-2.75
F15E11.12	-2.80
C32H11.4	-2.82
folt-2	-2.84
srh-237	-2.84
C44B7.5	-2.85

Table E3 (Continued)

Gene Name	log_2 Fold
F44E7.3	-2.86
F23A7.4	-2.86
C14E2.12	-2.88
clec-53	-2.90
hrg-3	-2.92
F58G6.3	-2.93
F13H8.12	-2.94
W08E12.2	-2.95
C42D4.2	-2.96
oac-32	-2.96
F15E11.1	-2.97
oac-20	-2.97
F15E11.14	-2.98
K05F1.8	-3.00
F01D5.3	-3.00
pmp-5	-3.02
K10C2.8	-3.04
K11G9.3	-3.04
C05B5.12	-3.05
spp-4	-3.05
clec-118	-3.07
C31H1.2	-3.11
Y73B6A.3	-3.12
R11A5.3	-3.15
grl-27	-3.18
nhr-68	-3.22
C23H5.8	-3.25
nspe-7	-3.27
clec-26	-3.30
F23A7.8	-3.34
E01G6.3	-3.34
clec-218	-3.36
F28A10.1	-3.39
K02E2.8	-3.43
Y94H6A.10	-3.44
F22E5.8	-3.54
vit-5	-3.55
T05E12.3	-3.60
C36C5.12	-3.62
F54F7.2	-3.65
linc-1	-3.66
vit-3	-3.69
vit-1	-3.72
vit-4	-3.72
Y53F4B.8	-3.84
ZC266.1	-4.39
Y40H7A.10	-4.48
ilys-5	-4.64
acdh-1	-6.98

Table E4. DAVID output of the processes enriched by HSF-1 in a HS-dependent manner.

Annotation Cluster 1	Enrichment Score: 96.97	GO Term/Keyword	Count	P-Value	Benjamini
	INTERPRO	Collagen triple helix repeat	101	3.70E-103	1.90E-100
	INTERPRO	Nematode cuticle collagen, N-terminal	92	2.00E-100	5.20E-98
	GOTERM_MF_FAT	structural constituent of cuticle	94	1.60E-89	4.60E-87
Annotation Cluster 2	**Enrichment Score: 11.87**	**GO Term/Keyword**	**Count**	**P-Value**	**Benjamini**
	SP_PIR_KEYWORDS	ribosomal protein	25	1.60E-15	9.10E-14
	KEGG_PATHWAY	Ribosome	28	3.30E-15	1.60E-13
	GOTERM_CC_FAT	ribosome	30	3.50E-13	3.50E-11
	SP_PIR_KEYWORDS	ribonucleoprotein	24	1.30E-12	4.40E-11
	GOTERM_MF_FAT	structural constituent of ribosome	30	6.30E-12	5.90E-10
	GOTERM_CC_FAT	ribonucleoprotein complex	30	3.00E-10	1.50E-08
	GOTERM_BP_FAT	translation	32	1.90E-09	4.60E-07
Annotation Cluster 3	**Enrichment Score: 5.32**	**GO Term/Keyword**	**Count**	**P-Value**	**Benjamini**
	GOTERM_BP_FAT	collagen and cuticulin-based cuticle development	15	4.00E-06	3.20E-04
	GOTERM_BP_FAT	protein-based cuticle development	15	5.20E-06	3.60E-04
	GOTERM_BP_FAT	cuticle development	15	5.20E-06	3.60E-04
Annotation Cluster 4	**Enrichment Score: 5.01**	**GO Term/Keyword**	**Count**	**P-Value**	**Benjamini**
	GOTERM_BP_FAT	endoplasmic reticulum unfolded protein response	7	4.40E-07	7.10E-05
	GOTERM_BP_FAT	ER-nuclear signaling pathway	7	4.40E-07	7.10E-05
	GOTERM_BP_FAT	response to endoplasmic reticulum stress	7	4.40E-07	7.10E-05
	GOTERM_BP_FAT	cellular response to unfolded protein	7	1.80E-06	2.20E-04
	GOTERM_BP_FAT	response to unfolded protein	7	3.30E-06	3.20E-04
	GOTERM_BP_FAT	response to protein stimulus	7	3.30E-06	3.20E-04
	GOTERM_BP_FAT	response to organic substance	7	4.50E-04	9.90E-03
	GOTERM_BP_FAT	cellular response to stress	8	1.00E-01	5.20E-01
Annotation Cluster 5	**Enrichment Score: 4.55**	**GO Term/Keyword**	**Count**	**P-Value**	**Benjamini**
	INTERPRO	Heat shock protein Hsp70	6	1.30E-05	1.70E-03
	INTERPRO	Heat shock protein 70	6	1.30E-05	1.70E-03
	INTERPRO	Heat shock protein 70, conserved site	6	2.20E-05	2.20E-03
	PIR_SUPERFAMILY	PIRSF002581:chaperone HSP70	5	1.80E-04	1.50E-02
Annotation Cluster 6	**Enrichment Score: 4.44**	**GO Term/Keyword**	**Count**	**P-Value**	**Benjamini**
	GOTERM_BP_FAT	regulation of growth	105	1.80E-05	1.10E-03
	GOTERM_BP_FAT	positive regulation of growth	101	3.90E-05	1.60E-03
	GOTERM_BP_FAT	positive regulation of growth rate	93	5.00E-05	1.90E-03
	GOTERM_BP_FAT	regulation of growth rate	93	5.10E-05	1.80E-03
Annotation Cluster 7	**Enrichment Score: 3.92**	**GO Term/Keyword**	**Count**	**P-Value**	**Benjamini**

Table E4 (Continued)

	GOTERM_BP_FAT	cellular amino acid catabolic process	8	3.10E-05	1.40E-03
	GOTERM_BP_FAT	amine catabolic process	8	8.40E-05	2.50E-03
	GOTERM_BP_FAT	organic acid catabolic process	8	2.90E-04	6.90E-03
	GOTERM_BP_FAT	carboxylic acid catabolic process	8	2.90E-04	6.90E-03
Annotation Cluster 8	**Enrichment Score: 3.85**	**GO Term/Keyword**	**Count**	**P-Value**	**Benjamini**
	GOTERM_CC_FAT	endoplasmic reticulum lumen	7	9.90E-07	2.40E-05
	SP_PIR_KEYWORDS	endoplasmic reticulum	8	8.60E-04	1.10E-02
	GOTERM_CC_FAT	endoplasmic reticulum part	8	3.20E-03	5.20E-02
Annotation Cluster 9	**Enrichment Score: 3.53**	**GO Term/Keyword**	**Count**	**P-Value**	**Benjamini**
	GOTERM_BP_FAT	actin cytoskeleton organization	10	2.10E-05	1.10E-03
	GOTERM_BP_FAT	actin filament-based process	10	3.10E-05	1.50E-03
	GOTERM_BP_FAT	cytoskeleton organization	12	4.10E-02	3.00E-01
Annotation Cluster 10	**Enrichment Score: 3.45**	**GO Term/Keyword**	**Count**	**P-Value**	**Benjamini**
	GOTERM_BP_FAT	growth	76	1.30E-04	3.70E-03
	GOTERM_BP_FAT	post-embryonic development	92	2.80E-04	7.20E-03
	GOTERM_BP_FAT	larval development	90	5.20E-04	1.00E-02
	GOTERM_BP_FAT	nematode larval development	89	8.20E-04	1.50E-02
Annotation Cluster 11	**Enrichment Score: 3.05**	**GO Term/Keyword**	**Count**	**P-Value**	**Benjamini**
	GOTERM_BP_FAT	actomyosin structure organization	6	2.10E-04	5.50E-03
	GOTERM_BP_FAT	myofibril assembly	6	2.10E-04	5.50E-03
	GOTERM_BP_FAT	cellular component assembly involved in morphogenesis	6	2.10E-04	5.50E-03
	GOTERM_BP_FAT	striated muscle cell differentiation	6	3.80E-04	8.70E-03
	GOTERM_BP_FAT	striated muscle cell development	6	3.80E-04	8.70E-03
	GOTERM_BP_FAT	muscle cell development	6	5.00E-04	1.00E-02
	GOTERM_BP_FAT	muscle cell differentiation	6	1.30E-03	2.20E-02
	GOTERM_BP_FAT	cellular component morphogenesis	6	5.10E-01	9.70E-01
Annotation Cluster 12	**Enrichment Score: 2.7**	**GO Term/Keyword**	**Count**	**P-Value**	**Benjamini**
	INTERPRO	Glutathione S-transferase/chloride channel, C-terminal	8	1.30E-03	6.30E-02
	INTERPRO	Glutathione S-transferase, N-terminal	8	1.30E-03	6.30E-02
	INTERPRO	Glutathione S-transferase, C-terminal	7	5.00E-03	1.90E-01
Annotation Cluster 13	**Enrichment Score: 2.7**	**GO Term/Keyword**	**Count**	**P-Value**	**Benjamini**
	GOTERM_BP_FAT	molting cycle, collagen and cuticulin-based cuticle	20	2.00E-03	3.10E-02
	GOTERM_BP_FAT	molting cycle, protein-based cuticle	20	2.00E-03	3.10E-02
	GOTERM_BP_FAT	molting cycle	20	2.10E-03	3.20E-02
Annotation Cluster 14	**Enrichment Score: 2.68**	**GO Term/Keyword**	**Count**	**P-Value**	**Benjamini**
	GOTERM_BP_FAT	cellular macromolecular complex assembly	11	7.40E-04	1.40E-02

Table E4 (Continued)

	GOTERM_BP_FAT	cellular macromolecular complex subunit organization	11	2.10E-03	3.20E-02
	GOTERM_BP_FAT	macromolecular complex assembly	12	2.50E-03	3.50E-02
	GOTERM_BP_FAT	macromolecular complex subunit organization	12	4.90E-03	6.20E-02
Annotation Cluster 15	**Enrichment Score: 2.56**	**GO Term/Keyword**	**Count**	**P-Value**	**Benjamini**
	INTERPRO	Thioredoxin-like	8	1.20E-04	8.90E-03
	GOTERM_BP_FAT	cell redox homeostasis	9	2.50E-03	3.60E-02
	GOTERM_BP_FAT	homeostatic process	11	1.00E-02	1.10E-01
	GOTERM_BP_FAT	cellular homeostasis	9	1.90E-02	1.70E-01
Annotation Cluster 16	**Enrichment Score: 2.43**	**GO Term/Keyword**	**Count**	**P-Value**	**Benjamini**
	GOTERM_BP_FAT	aging	19	3.70E-03	4.80E-02
	GOTERM_BP_FAT	determination of adult life span	19	3.70E-03	4.80E-02
	GOTERM_BP_FAT	multicellular organismal aging	19	3.70E-03	4.80E-02
Annotation Cluster 17	**Enrichment Score: 2.34**	**GO Term/Keyword**	**Count**	**P-Value**	**Benjamini**
	PIR_SUPERFAMILY	PIRSF036514:alpha-crystallin-related small heat shock protein	5	9.40E-04	5.20E-02
	INTERPRO	Alpha crystallin/Heat shock protein	5	1.10E-03	5.90E-02
	INTERPRO	Heat shock protein Hsp20	5	1.40E-03	6.30E-02
	GOTERM_BP_FAT	response to heat	5	1.80E-02	1.70E-01
	GOTERM_BP_FAT	response to temperature stimulus	5	7.80E-02	4.50E-01
Annotation Cluster 18	**Enrichment Score: 2.08**	**GO Term/Keyword**	**Count**	**P-Value**	**Benjamini**
	GOTERM_CC_FAT	endoplasmic reticulum lumen	7	9.90E-07	2.40E-05
	GOTERM_CC_FAT	organelle lumen	9	1.60E-01	6.50E-01
	GOTERM_CC_FAT	intracellular organelle lumen	9	1.60E-01	6.50E-01
	GOTERM_CC_FAT	membrane-enclosed lumen	9	1.90E-01	6.90E-01
Annotation Cluster 19	**Enrichment Score: 1.84**	**GO Term/Keyword**	**Count**	**P-Value**	**Benjamini**
	UP_SEQ_FEATURE	cross-link:Glycyl lysine isopeptide (Lys-Gly) (interchain with G-Cter in ubiquitin)	4	5.00E-03	3.60E-01
	SP_PIR_KEYWORDS	isopeptide bond	4	1.60E-02	9.70E-02
	SP_PIR_KEYWORDS	ubl conjugation	4	3.80E-02	2.00E-01
Annotation Cluster 20	**Enrichment Score: 1.84**	**GO Term/Keyword**	**Count**	**P-Value**	**Benjamini**
	SP_PIR_KEYWORDS	nucleosome core	6	1.50E-04	2.60E-03
	INTERPRO	Histone core	6	2.60E-04	1.70E-02
	GOTERM_CC_FAT	nucleosome	6	4.50E-03	6.20E-02
	GOTERM_BP_FAT	nucleosome organization	6	5.80E-03	7.00E-02
	GOTERM_BP_FAT	nucleosome assembly	6	5.80E-03	7.00E-02
	GOTERM_BP_FAT	chromatin assembly	6	5.80E-03	7.00E-02
	GOTERM_CC_FAT	protein-DNA complex	6	6.90E-03	7.30E-02
	SP_PIR_KEYWORDS	chromosomal protein	6	8.90E-03	6.90E-02
	GOTERM_BP_FAT	protein-DNA complex assembly	6	1.10E-02	1.20E-01
	INTERPRO	Histone-fold	5	1.50E-02	3.60E-01

Table E4 (Continued)

	GOTERM_BP_FAT	DNA packaging	6	1.80E-02	1.70E-01
	GOTERM_BP_FAT	chromatin assembly or disassembly	6	4.80E-02	3.30E-01
	GOTERM_CC_FAT	chromatin	6	5.30E-02	3.30E-01
	GOTERM_BP_FAT	chromatin organization	7	1.20E-01	5.80E-01
	GOTERM_CC_FAT	chromosomal part	6	1.60E-01	6.70E-01
	GOTERM_CC_FAT	chromosome	6	4.00E-01	9.10E-01
	GOTERM_BP_FAT	chromosome organization	7	4.20E-01	9.40E-01
Annotation Cluster 21	**Enrichment Score: 1.83**	**GO Term/Keyword**	**Count**	**P-Value**	**Benjamini**
	GOTERM_MF_FAT	oxidoreductase activity, acting on single donors with incorporation of molecular oxygen	5	7.40E-03	4.10E-01
	SP_PIR_KEYWORDS	dioxygenase	4	1.10E-02	7.90E-02
	GOTERM_MF_FAT	oxidoreductase activity, acting on single donors with incorporation of molecular oxygen, incorporation of two atoms of oxygen	4	3.80E-02	6.30E-01
Annotation Cluster 22	**Enrichment Score: 1.82**	**GO Term/Keyword**	**Count**	**P-Value**	**Benjamini**
	INTERPRO	Pyridoxal phosphate-dependent transferase, major region, subdomain 1	6	5.40E-03	1.90E-01
	GOTERM_MF_FAT	pyridoxal phosphate binding	8	1.10E-02	4.00E-01
	GOTERM_MF_FAT	vitamin B6 binding	8	1.10E-02	4.00E-01
	GOTERM_MF_FAT	vitamin binding	9	7.90E-02	7.90E-01
Annotation Cluster 23	**Enrichment Score: 1.61**	**GO Term/Keyword**	**Count**	**P-Value**	**Benjamini**
	UP_SEQ_FEATURE	site:Lowers pKa of C-terminal Cys of second active site	3	6.60E-03	3.70E-01
	SP_PIR_KEYWORDS	Redox-active center	4	7.60E-03	6.80E-02
	GOTERM_MF_FAT	protein disulfide isomerase activity	3	1.10E-02	3.30E-01
	GOTERM_MF_FAT	intramolecular oxidoreductase activity, transposing S-S bonds	3	1.10E-02	3.30E-01
	GOTERM_MF_FAT	intramolecular oxidoreductase activity, interconverting keto- and enol-groups	3	1.10E-02	3.30E-01
	UP_SEQ_FEATURE	domain:Thioredoxin 1	3	1.30E-02	5.30E-01
	UP_SEQ_FEATURE	domain:Thioredoxin 2	3	1.30E-02	5.30E-01
	INTERPRO	Disulphide isomerase	3	1.40E-02	3.70E-01
	UP_SEQ_FEATURE	site:Contributes to redox potential value	3	2.10E-02	6.00E-01
	PIR_SUPERFAMILY	PIRSF001487:protein disulfide-isomerase	3	2.20E-02	6.10E-01
	INTERPRO	Thioredoxin-like subdomain	3	8.10E-02	8.00E-01
	GOTERM_MF_FAT	intramolecular oxidoreductase activity	3	1.40E-01	9.00E-01
	INTERPRO	Thioredoxin, conserved site	3	1.70E-01	9.40E-01
	INTERPRO	Thioredoxin domain	3	2.00E-01	9.60E-01
Annotation Cluster 24	**Enrichment Score: 1.56**	**GO Term/Keyword**	**Count**	**P-Value**	**Benjamini**
	GOTERM_BP_FAT	alcohol catabolic process	6	1.20E-02	1.30E-01

Table E4 (Continued)

	GOTERM_BP_FAT	cellular carbohydrate catabolic process	6	1.40E-02	1.40E-01
	GOTERM_BP_FAT	glycolysis	5	1.40E-02	1.40E-01
	GOTERM_BP_FAT	carbohydrate catabolic process	7	2.40E-02	2.10E-01
	SP_PIR_KEYWORDS	glycolysis	4	3.00E-02	1.70E-01
	GOTERM_BP_FAT	monosaccharide catabolic process	5	3.50E-02	2.80E-01
	GOTERM_BP_FAT	hexose catabolic process	5	3.50E-02	2.80E-01
	GOTERM_BP_FAT	glucose catabolic process	5	3.50E-02	2.80E-01
	GOTERM_BP_FAT	glucose metabolic process	5	1.20E-01	5.70E-01
Annotation Cluster 25	**Enrichment Score: 1.51**	**GO Term/Keyword**	**Count**	**P-Value**	**Benjamini**
	GOTERM_CC_FAT	actin cytoskeleton	6	1.00E-02	9.40E-02
	GOTERM_CC_FAT	myosin complex	5	1.10E-02	9.40E-02
	GOTERM_MF_FAT	motor activity	5	2.60E-01	9.60E-01
Annotation Cluster 26	**Enrichment Score: 1.26**	**GO Term/Keyword**	**Count**	**P-Value**	**Benjamini**
	SMART	DoH	3	1.50E-02	6.70E-01
	INTERPRO	DOMON	3	3.20E-02	5.30E-01
	GOTERM_MF_FAT	dopamine beta-monooxygenase activity	3	5.90E-02	7.60E-01
	INTERPRO	DOMON related	3	6.30E-02	7.40E-01
	GOTERM_BP_FAT	histidine family amino acid metabolic process	3	7.00E-02	4.30E-01
	GOTERM_BP_FAT	histidine family amino acid catabolic process	3	7.00E-02	4.30E-01
	GOTERM_BP_FAT	histidine catabolic process	3	7.00E-02	4.30E-01
	GOTERM_BP_FAT	histidine metabolic process	3	7.00E-02	4.30E-01
	GOTERM_MF_FAT	oxidoreductase activity, acting on paired donors, with incorporation or reduction of molecular oxygen, reduced ascorbate as one donor, and incorporation of one atom of oxygen	3	9.80E-02	8.20E-01
Annotation Cluster 27	**Enrichment Score: 1.08**	**GO Term/Keyword**	**Count**	**P-Value**	**Benjamini**
	SP_PIR_KEYWORDS	actin-binding	6	1.10E-02	7.90E-02
	GOTERM_MF_FAT	actin binding	6	1.70E-01	9.30E-01
	GOTERM_MF_FAT	cytoskeletal protein binding	6	3.10E-01	9.80E-01
Annotation Cluster 28	**Enrichment Score: 1**	**GO Term/Keyword**	**Count**	**P-Value**	**Benjamini**
	INTERPRO	Troponin	3	5.90E-03	1.80E-01
	GOTERM_BP_FAT	defecation	4	1.70E-01	6.90E-01
	GOTERM_BP_FAT	excretion	4	1.90E-01	7.20E-01
	GOTERM_BP_FAT	secretion	4	5.30E-01	9.70E-01
Annotation Cluster 29	**Enrichment Score: 0.95**	**GO Term/Keyword**	**Count**	**P-Value**	**Benjamini**
	GOTERM_MF_FAT	oxidoreductase activity, acting on heme group of donors, oxygen as acceptor	3	1.10E-01	8.50E-01
	GOTERM_MF_FAT	oxidoreductase activity, acting on heme group of donors	3	1.10E-01	8.50E-01

Table E4 (Continued)

	GOTERM_MF_FAT	heme-copper terminal oxidase activity	3	1.10E-01	8.50E-01
	GOTERM_MF_FAT	cytochrome-c oxidase activity	3	1.10E-01	8.50E-01
Annotation Cluster 30	**Enrichment Score: 0.9**	**GO Term/Keyword**	**Count**	**P-Value**	**Benjamini**
	GOTERM_BP_FAT	negative regulation of multicellular organismal process	7	1.20E-01	5.80E-01
	GOTERM_BP_FAT	negative regulation of multicellular organism growth	7	1.20E-01	5.80E-01
	GOTERM_BP_FAT	negative regulation of growth	7	1.30E-01	6.00E-01
Annotation Cluster 31	**Enrichment Score: 0.88**	**GO Term/Keyword**	**Count**	**P-Value**	**Benjamini**
	GOTERM_MF_FAT	hydrogen ion transmembrane transporter activity	7	7.00E-02	7.90E-01
	GOTERM_MF_FAT	monovalent inorganic cation transmembrane transporter activity	7	7.90E-02	8.10E-01
	KEGG_PATHWAY	Oxidative phosphorylation	8	4.10E-01	7.80E-01
Annotation Cluster 32	**Enrichment Score: 0.85**	**GO Term/Keyword**	**Count**	**P-Value**	**Benjamini**
	GOTERM_BP_FAT	oviposition	17	6.50E-02	4.10E-01
	GOTERM_BP_FAT	reproductive behavior in a multicellular organism	17	7.10E-02	4.30E-01
	GOTERM_BP_FAT	reproductive behavior	17	7.80E-02	4.50E-01
	GOTERM_BP_FAT	behavior	21	1.20E-01	5.70E-01
	GOTERM_BP_FAT	reproductive process in a multicellular organism	19	4.20E-01	9.40E-01
	GOTERM_BP_FAT	multicellular organism reproduction	19	4.20E-01	9.40E-01
Annotation Cluster 33	**Enrichment Score: 0.82**	**GO Term/Keyword**	**Count**	**P-Value**	**Benjamini**
	INTERPRO	Uncharacterised protein family UPF0376	4	8.10E-02	8.10E-01
	PIR_SUPERFAMILY	PIRSF015697:UCP015697	4	2.10E-01	1.00E+00
	INTERPRO	Protein of unknown function DUF19	4	2.10E-01	9.60E-01
Annotation Cluster 34	**Enrichment Score: 0.78**	**GO Term/Keyword**	**Count**	**P-Value**	**Benjamini**
	SMART	LIM	3	7.60E-02	7.60E-01
	SP_PIR_KEYWORDS	LIM domain	3	2.30E-01	6.70E-01
	INTERPRO	Zinc finger, LIM-type	3	2.60E-01	9.90E-01
Annotation Cluster 35	**Enrichment Score: 0.74**	**GO Term/Keyword**	**Count**	**P-Value**	**Benjamini**
	UP_SEQ_FEATURE	domain:GST N-terminal	3	1.30E-01	9.90E-01
	UP_SEQ_FEATURE	domain:GST C-terminal	3	1.40E-01	9.90E-01
	PIR_SUPERFAMILY	PIRSF000503:glutathione transferase	3	3.30E-01	1.00E+00
Annotation Cluster 36	**Enrichment Score: 0.73**	**GO Term/Keyword**	**Count**	**P-Value**	**Benjamini**
	INTERPRO	Concanavalin A-like lectin/glucanase, subgroup	5	4.40E-02	6.20E-01
	SMART	GLECT	3	4.80E-02	7.00E-01
	INTERPRO	Galectin, carbohydrate recognition domain	3	1.80E-01	9.50E-01
	SP_PIR_KEYWORDS	Lectin	4	7.00E-01	9.70E-01
	GOTERM_MF_FAT	sugar binding	4	8.40E-01	1.00E+00

Table E4 (Continued)

Annotation Cluster 37	Enrichment Score: 0.64	GO Term/Keyword	Count	P-Value	Benjamini
	SP_PIR_KEYWORDS	calcium binding	3	1.20E-02	8.40E-02
	SP_PIR_KEYWORDS	EF hand	4	5.50E-02	2.50E-01
	SP_PIR_KEYWORDS	myosin	3	1.10E-01	4.10E-01
	COG_ONTOLOGY	Signal transduction mechanisms / Cytoskeleton / Cell division and chromosome partitioning / General function prediction only	3	1.90E-01	7.50E-01
	SMART	EFh	3	2.40E-01	9.20E-01
	UP_SEQ_FEATURE	domain:EF-hand 1	3	2.60E-01	1.00E+00
	UP_SEQ_FEATURE	domain:EF-hand 2	3	2.60E-01	1.00E+00
	SP_PIR_KEYWORDS	motor protein	3	3.90E-01	8.20E-01
	INTERPRO	EF-Hand type	4	5.50E-01	1.00E+00
	INTERPRO	Calcium-binding EF-hand	3	6.10E-01	1.00E+00
	INTERPRO	EF-HAND 2	3	7.60E-01	1.00E+00
	INTERPRO	EF-HAND 1	3	8.70E-01	1.00E+00
Annotation Cluster 38	**Enrichment Score: 0.54**	**GO Term/Keyword**	**Count**	**P-Value**	**Benjamini**
	INTERPRO	Tubulin/FtsZ, GTPase domain	3	9.10E-02	8.30E-01
	INTERPRO	Tubulin/FtsZ, 2-layer sandwich domain	3	9.10E-02	8.30E-01
	INTERPRO	Tubulin, conserved site	3	1.00E-01	8.50E-01
	INTERPRO	Tubulin	3	1.00E-01	8.50E-01
	GOTERM_BP_FAT	protein polymerization	3	1.40E-01	6.20E-01
	SP_PIR_KEYWORDS	microtubule	3	5.00E-01	8.90E-01
	GOTERM_BP_FAT	microtubule-based movement	3	5.20E-01	9.70E-01
	GOTERM_CC_FAT	microtubule	3	6.60E-01	9.80E-01
	GOTERM_MF_FAT	GTPase activity	4	7.30E-01	1.00E+00
	GOTERM_CC_FAT	microtubule cytoskeleton	3	8.20E-01	1.00E+00
	GOTERM_BP_FAT	microtubule-based process	3	9.70E-01	1.00E+00
Annotation Cluster 39	**Enrichment Score: 0.52**	**GO Term/Keyword**	**Count**	**P-Value**	**Benjamini**
	SP_PIR_KEYWORDS	neuropeptide	4	9.20E-02	3.60E-01
	GOTERM_BP_FAT	neuropeptide signaling pathway	4	3.00E-01	8.60E-01
	GOTERM_BP_FAT	G-protein coupled receptor protein signaling pathway	5	1.00E+00	1.00E+00
Annotation Cluster 40	**Enrichment Score: 0.41**	**GO Term/Keyword**	**Count**	**P-Value**	**Benjamini**
	SMART	IG	3	1.30E-01	8.10E-01
	INTERPRO	Immunoglobulin I-set	3	3.70E-01	1.00E+00
	INTERPRO	Immunoglobulin subtype	3	3.90E-01	1.00E+00
	INTERPRO	Immunoglobulin-like fold	3	6.70E-01	1.00E+00
	INTERPRO	Immunoglobulin-like	3	7.10E-01	1.00E+00
Annotation Cluster 41	**Enrichment Score: 0.38**	**GO Term/Keyword**	**Count**	**P-Value**	**Benjamini**
	GOTERM_CC_FAT	proteinaceous extracellular matrix	3	3.80E-01	9.10E-01
	GOTERM_CC_FAT	extracellular matrix	3	3.90E-01	9.10E-01

Table E4 (Continued)

	GOTERM_CC_FAT	extracellular region part	3	4.90E-01	9.50E-01
Annotation Cluster 42	**Enrichment Score: 0.33**	**GO Term/Keyword**	**Count**	**P-Value**	**Benjamini**
	SP_PIR_KEYWORDS	potassium	3	2.70E-01	7.10E-01
	GOTERM_MF_FAT	potassium ion binding	3	4.70E-01	1.00E+00
	GOTERM_MF_FAT	alkali metal ion binding	3	8.20E-01	1.00E+00
Annotation Cluster 43	**Enrichment Score: 0.32**	**GO Term/Keyword**	**Count**	**P-Value**	**Benjamini**
	GOTERM_BP_FAT	nucleotide biosynthetic process	7	4.50E-01	9.50E-01
	GOTERM_BP_FAT	nucleobase, nucleoside and nucleotide biosynthetic process	7	5.00E-01	9.60E-01
	GOTERM_BP_FAT	nucleobase, nucleoside, nucleotide and nucleic acid biosynthetic process	7	5.00E-01	9.60E-01
Annotation Cluster 44	**Enrichment Score: 0.27**	**GO Term/Keyword**	**Count**	**P-Value**	**Benjamini**
	GOTERM_MF_FAT	serine-type endopeptidase inhibitor activity	5	4.50E-01	1.00E+00
	GOTERM_MF_FAT	endopeptidase inhibitor activity	5	5.20E-01	1.00E+00
	GOTERM_MF_FAT	peptidase inhibitor activity	5	5.70E-01	1.00E+00
	GOTERM_MF_FAT	enzyme inhibitor activity	5	6.20E-01	1.00E+00
Annotation Cluster 45	**Enrichment Score: 0.21**	**GO Term/Keyword**	**Count**	**P-Value**	**Benjamini**
	GOTERM_BP_FAT	nucleoside triphosphate biosynthetic process	4	5.30E-01	9.70E-01
	GOTERM_BP_FAT	ribonucleoside triphosphate biosynthetic process	4	5.30E-01	9.70E-01
	GOTERM_BP_FAT	purine ribonucleoside triphosphate biosynthetic process	4	5.30E-01	9.70E-01
	GOTERM_BP_FAT	purine nucleoside triphosphate biosynthetic process	4	5.30E-01	9.70E-01
	GOTERM_BP_FAT	purine nucleoside triphosphate metabolic process	4	5.40E-01	9.70E-01
	GOTERM_BP_FAT	ribonucleoside triphosphate metabolic process	4	5.40E-01	9.70E-01
	GOTERM_BP_FAT	purine ribonucleoside triphosphate metabolic process	4	5.40E-01	9.70E-01
	GOTERM_BP_FAT	nucleoside triphosphate metabolic process	4	5.50E-01	9.70E-01
	GOTERM_BP_FAT	purine ribonucleotide biosynthetic process	4	6.20E-01	9.90E-01
	GOTERM_BP_FAT	purine ribonucleotide metabolic process	4	6.40E-01	9.90E-01
	GOTERM_BP_FAT	ribonucleotide biosynthetic process	4	6.40E-01	9.90E-01
	GOTERM_BP_FAT	ribonucleotide metabolic process	4	6.70E-01	9.90E-01
	GOTERM_BP_FAT	ATP biosynthetic process	3	7.40E-01	1.00E+00
	GOTERM_BP_FAT	ATP metabolic process	3	7.50E-01	1.00E+00
	GOTERM_BP_FAT	purine nucleotide biosynthetic process	4	8.00E-01	1.00E+00
	GOTERM_BP_FAT	purine nucleotide metabolic process	4	8.20E-01	1.00E+00
Annotation Cluster 46	**Enrichment Score: 0.17**	**GO Term/Keyword**	**Count**	**P-Value**	**Benjamini**

Table E4 (Continued)

	SP_PIR_KEYWORDS	transit peptide	4	5.10E-01	8.90E-01
	SP_PIR_KEYWORDS	mitochondrion	5	7.40E-01	9.80E-01
	UP_SEQ_FEATURE	transit peptide:Mitochondrion	4	8.10E-01	1.00E+00
Annotation Cluster 47	**Enrichment Score: 0.15**	**GO Term/Keyword**	**Count**	**P-Value**	**Benjamini**
	GOTERM_BP_FAT	morphogenesis of an epithelium	12	6.80E-01	9.90E-01
	GOTERM_BP_FAT	epithelium development	12	7.00E-01	9.90E-01
	GOTERM_BP_FAT	tissue morphogenesis	12	7.30E-01	1.00E+00
Annotation Cluster 48	**Enrichment Score: 0.15**	**GO Term/Keyword**	**Count**	**P-Value**	**Benjamini**
	INTERPRO	Potassium channel, two pore-domain	3	4.10E-01	1.00E+00
	INTERPRO	Ion transport 2	3	4.80E-01	1.00E+00
	GOTERM_BP_FAT	potassium ion transport	4	8.20E-01	1.00E+00
	GOTERM_MF_FAT	potassium channel activity	4	8.90E-01	1.00E+00
	SP_PIR_KEYWORDS	ionic channel	5	8.90E-01	1.00E+00
	GOTERM_MF_FAT	cation channel activity	4	9.90E-01	1.00E+00
Annotation Cluster 49	**Enrichment Score: 0.13**	**GO Term/Keyword**	**Count**	**P-Value**	**Benjamini**
	GOTERM_CC_FAT	mitochondrial inner membrane	4	6.30E-01	9.80E-01
	GOTERM_CC_FAT	organelle inner membrane	4	6.30E-01	9.80E-01
	GOTERM_BP_FAT	oxidative phosphorylation	3	7.10E-01	9.90E-01
	GOTERM_CC_FAT	mitochondrial membrane	4	7.40E-01	9.90E-01
	GOTERM_CC_FAT	mitochondrial envelope	4	7.50E-01	9.90E-01
	GOTERM_CC_FAT	envelope	5	7.90E-01	9.90E-01
	GOTERM_CC_FAT	organelle envelope	4	8.60E-01	1.00E+00
	GOTERM_CC_FAT	organelle membrane	5	9.40E-01	1.00E+00
Annotation Cluster 50	**Enrichment Score: 0.11**	**GO Term/Keyword**	**Count**	**P-Value**	**Benjamini**
	SMART	TyrKc	4	2.40E-01	9.40E-01
	INTERPRO	Tyrosine protein kinase	4	7.20E-01	1.00E+00
	INTERPRO	Protein kinase, core	4	1.00E+00	1.00E+00
	GOTERM_MF_FAT	protein tyrosine kinase activity	4	1.00E+00	1.00E+00
	GOTERM_BP_FAT	protein amino acid phosphorylation	4	1.00E+00	1.00E+00
	GOTERM_MF_FAT	protein serine/threonine kinase activity	4	1.00E+00	1.00E+00
	GOTERM_MF_FAT	protein kinase activity	4	1.00E+00	1.00E+00
Annotation Cluster 51	**Enrichment Score: 0.09**	**GO Term/Keyword**	**Count**	**P-Value**	**Benjamini**
	SP_PIR_KEYWORDS	gtp-binding	6	5.40E-01	9.10E-01
	GOTERM_MF_FAT	GTP binding	6	9.30E-01	1.00E+00
	GOTERM_MF_FAT	guanyl ribonucleotide binding	6	9.40E-01	1.00E+00
	GOTERM_MF_FAT	guanyl nucleotide binding	6	9.40E-01	1.00E+00
Annotation Cluster 52	**Enrichment Score: 0.04**	**GO Term/Keyword**	**Count**	**P-Value**	**Benjamini**
	KEGG_PATHWAY	MAPK signaling pathway	3	8.70E-01	9.90E-01
	KEGG_PATHWAY	Endocytosis	3	9.20E-01	9.90E-01
	KEGG_PATHWAY	Spliceosome	3	9.90E-01	1.00E+00

Table E4 (Continued)

Annotation Cluster 53	Enrichment Score: 0.03	GO Term/Keyword	Count	P-Value	Benjamini
	GOTERM_BP_FAT	hermaphrodite genitalia development	21	9.00E-01	1.00E+00
	GOTERM_BP_FAT	genitalia development	21	9.10E-01	1.00E+00
	GOTERM_BP_FAT	sex differentiation	21	9.70E-01	1.00E+00
	GOTERM_BP_FAT	reproductive developmental process	21	9.90E-01	1.00E+00
Annotation Cluster 54	**Enrichment Score: 0.02**	**GO Term/Keyword**	**Count**	**P-Value**	**Benjamini**
	SP_PIR_KEYWORDS	nucleotide-binding	23	7.40E-01	9.70E-01
	SP_PIR_KEYWORDS	atp-binding	17	8.20E-01	9.90E-01
	GOTERM_MF_FAT	ATP binding	22	1.00E+00	1.00E+00
	GOTERM_MF_FAT	adenyl ribonucleotide binding	22	1.00E+00	1.00E+00
	GOTERM_MF_FAT	ribonucleotide binding	28	1.00E+00	1.00E+00
	GOTERM_MF_FAT	purine ribonucleotide binding	28	1.00E+00	1.00E+00
	GOTERM_MF_FAT	adenyl nucleotide binding	23	1.00E+00	1.00E+00
	GOTERM_MF_FAT	purine nucleoside binding	23	1.00E+00	1.00E+00
	GOTERM_MF_FAT	purine nucleotide binding	29	1.00E+00	1.00E+00
	GOTERM_MF_FAT	nucleoside binding	23	1.00E+00	1.00E+00
	GOTERM_MF_FAT	nucleotide binding	33	1.00E+00	1.00E+00
Annotation Cluster 55	**Enrichment Score: 0.01**	**GO Term/Keyword**	**Count**	**P-Value**	**Benjamini**
	GOTERM_BP_FAT	cytokinesis	3	9.50E-01	1.00E+00
	GOTERM_BP_FAT	cell division	3	9.90E-01	1.00E+00
	GOTERM_BP_FAT	cell cycle	4	1.00E+00	1.00E+00
	GOTERM_BP_FAT	cell cycle process	3	1.00E+00	1.00E+00
Annotation Cluster 56	**Enrichment Score: 0**	**GO Term/Keyword**	**Count**	**P-Value**	**Benjamini**
	GOTERM_MF_FAT	passive transmembrane transporter activity	7	9.90E-01	1.00E+00
	GOTERM_MF_FAT	channel activity	7	9.90E-01	1.00E+00
	GOTERM_MF_FAT	substrate specific channel activity	6	1.00E+00	1.00E+00
	GOTERM_MF_FAT	ion channel activity	6	1.00E+00	1.00E+00
Annotation Cluster 57	**Enrichment Score: 0**	**GO Term/Keyword**	**Count**	**P-Value**	**Benjamini**
	GOTERM_MF_FAT	metallopeptidase activity	3	1.00E+00	1.00E+00
	GOTERM_MF_FAT	peptidase activity	5	1.00E+00	1.00E+00
	GOTERM_MF_FAT	peptidase activity, acting on L-amino acid peptides	4	1.00E+00	1.00E+00
	GOTERM_BP_FAT	proteolysis	4	1.00E+00	1.00E+00
Annotation Cluster 58	**Enrichment Score: 0**	**GO Term/Keyword**	**Count**	**P-Value**	**Benjamini**
	GOTERM_BP_FAT	protein transport	3	1.00E+00	1.00E+00
	GOTERM_BP_FAT	establishment of protein localization	3	1.00E+00	1.00E+00
	GOTERM_BP_FAT	protein localization	4	1.00E+00	1.00E+00
Annotation Cluster 59	**Enrichment Score: 0**	**GO Term/Keyword**	**Count**	**P-Value**	**Benjamini**
	GOTERM_BP_FAT	phosphorylation	7	1.00E+00	1.00E+00
	GOTERM_BP_FAT	phosphorus metabolic process	7	1.00E+00	1.00E+00

Table E4 (Continued)

	GOTERM_BP_FAT	phosphate metabolic process	7	1.00E+00	1.00E+00
Annotation Cluster 60	**Enrichment Score: 0**	**GO Term/Keyword**	**Count**	**P-Value**	**Benjamini**
	GOTERM_MF_FAT	transition metal ion binding	36	1.00E+00	1.00E+00
	GOTERM_MF_FAT	metal ion binding	46	1.00E+00	1.00E+00
	GOTERM_MF_FAT	cation binding	46	1.00E+00	1.00E+00
	GOTERM_MF_FAT	ion binding	46	1.00E+00	1.00E+00
Annotation Cluster 61	**Enrichment Score: 0**	**GO Term/Keyword**	**Count**	**P-Value**	**Benjamini**
	GOTERM_BP_FAT	regulation of transcription, DNA-dependent	4	1.00E+00	1.00E+00
	GOTERM_BP_FAT	regulation of RNA metabolic process	4	1.00E+00	1.00E+00
	GOTERM_MF_FAT	transcription factor activity	3	1.00E+00	1.00E+00
	GOTERM_MF_FAT	transcription regulator activity	5	1.00E+00	1.00E+00

Table E5. DAVID output of the processes enriched by HSF-1 in a HS-independent manner.

Annotation Cluster 1	Enrichment Score: 9.65	GO Term/Keyword	Count	P-Value	Benjamini
	INTERPRO	Nematode cuticle collagen, N-terminal	34	4.40E-11	3.50E-08
	INTERPRO	Collagen triple helix repeat	38	6.50E-11	2.60E-08
	GOTERM_MF_FAT	structural constituent of cuticle	35	3.80E-09	4.80E-07
Annotation Cluster 2	**Enrichment Score: 6.03**	**GO Term/Keyword**	**Count**	**P-Value**	**Benjamini**
	GOTERM_CC_FAT	mitochondrial envelope	25	2.90E-08	1.30E-06
	GOTERM_CC_FAT	mitochondrial membrane	24	7.50E-08	2.50E-06
	GOTERM_CC_FAT	mitochondrial inner membrane	21	3.10E-07	8.50E-06
	GOTERM_CC_FAT	organelle inner membrane	21	3.80E-07	8.70E-06
	GOTERM_CC_FAT	organelle envelope	25	1.70E-06	3.30E-05
	GOTERM_CC_FAT	envelope	26	3.80E-06	6.50E-05
	GOTERM_CC_FAT	organelle membrane	27	3.40E-04	4.20E-03
Annotation Cluster 3	**Enrichment Score: 5.83**	**GO Term/Keyword**	**Count**	**P-Value**	**Benjamini**
	INTERPRO	Acyl-CoA oxidase/dehydrogenase, central region	11	3.70E-07	4.30E-05
	INTERPRO	Acyl-CoA oxidase/dehydrogenase, type1/2, C-terminal	11	6.10E-07	6.10E-05
	INTERPRO	Acyl-CoA dehydrogenase/oxidase, N-terminal	10	4.20E-06	3.10E-04
	GOTERM_MF_FAT	acyl-CoA dehydrogenase activity	11	4.80E-06	3.70E-04
Annotation Cluster 4	**Enrichment Score: 4.97**	**GO Term/Keyword**	**Count**	**P-Value**	**Benjamini**
	INTERPRO	Peptidase A1	10	3.30E-07	4.40E-05
	INTERPRO	Peptidase aspartic, catalytic	10	3.30E-07	4.40E-05
	GOTERM_MF_FAT	aspartic-type endopeptidase activity	10	3.40E-04	1.20E-02
	GOTERM_MF_FAT	aspartic-type peptidase activity	10	3.40E-04	1.20E-02
Annotation Cluster 5	**Enrichment Score: 4.79**	**GO Term/Keyword**	**Count**	**P-Value**	**Benjamini**
	PIR_SUPERFAMILY	PIRSF001187:Pepsin	7	2.60E-06	8.30E-04
	SP_PIR_KEYWORDS	Aspartyl protease	7	4.60E-06	2.00E-04
	INTERPRO	Peptidase aspartic, active site	7	3.50E-04	1.20E-02
Annotation Cluster 6	**Enrichment Score: 4.58**	**GO Term/Keyword**	**Count**	**P-Value**	**Benjamini**
	INTERPRO	Glutathione S-transferase, N-terminal	14	1.00E-05	6.20E-04
	INTERPRO	Glutathione S-transferase, C-terminal	13	3.50E-05	2.00E-03
	INTERPRO	Glutathione S-transferase/chloride channel, C-terminal	13	5.30E-05	2.50E-03
Annotation Cluster 7	**Enrichment Score: 4.21**	**GO Term/Keyword**	**Count**	**P-Value**	**Benjamini**
	GOTERM_MF_FAT	oxidoreductase activity, acting on NADH or NADPH	11	4.40E-05	2.40E-03
	GOTERM_MF_FAT	NADH dehydrogenase (quinone) activity	9	6.70E-05	3.20E-03
	GOTERM_MF_FAT	NADH dehydrogenase activity	9	6.70E-05	3.20E-03
	GOTERM_MF_FAT	oxidoreductase activity, acting on NADH or NADPH, quinone or similar compound as acceptor	9	6.70E-05	3.20E-03

Table E5 (Continued)

	GOTERM_MF_FAT	NADH dehydrogenase (ubiquinone) activity	9	6.70E-05	3.20E-03
Annotation Cluster 8	**Enrichment Score: 4.08**	**GO Term/Keyword**	**Count**	**P-Value**	**Benjamini**
	SMART	Pept_C1	10	4.80E-07	4.20E-05
	INTERPRO	Peptidase C1A, papain	10	3.70E-05	2.00E-03
	INTERPRO	Peptidase C1A, papain C-terminal	10	6.70E-05	3.00E-03
	GOTERM_MF_FAT	cysteine-type peptidase activity	13	4.00E-02	3.50E-01
Annotation Cluster 9	**Enrichment Score: 3.64**	**GO Term/Keyword**	**Count**	**P-Value**	**Benjamini**
	GOTERM_CC_FAT	ribonucleoprotein complex	31	1.30E-05	1.90E-04
	GOTERM_CC_FAT	ribosome	25	4.80E-05	6.60E-04
	GOTERM_MF_FAT	structural constituent of ribosome	25	1.30E-04	5.00E-03
	GOTERM_BP_FAT	translation	25	3.60E-02	4.20E-01
Annotation Cluster 10	**Enrichment Score: 3.58**	**GO Term/Keyword**	**Count**	**P-Value**	**Benjamini**
	SMART	SapB	8	1.60E-05	7.30E-04
	INTERPRO	Saposin B	8	7.30E-04	2.30E-02
	INTERPRO	Saposin-like type B, 2	6	1.50E-03	3.90E-02
Annotation Cluster 11	**Enrichment Score: 3.35**	**GO Term/Keyword**	**Count**	**P-Value**	**Benjamini**
	UP_SEQ_FEATURE	domain:GST N-terminal	8	9.10E-06	1.80E-03
	UP_SEQ_FEATURE	domain:GST C-terminal	8	1.70E-05	2.30E-03
	GOTERM_MF_FAT	glutathione transferase activity	7	9.20E-04	2.50E-02
	PIR_SUPERFAMILY	PIRSF000503:glutathione transferase	8	3.20E-03	1.90E-01
	GOTERM_MF_FAT	transferase activity, transferring alkyl or aryl (other than methyl) groups	7	3.90E-02	3.50E-01
Annotation Cluster 12	**Enrichment Score: 3.14**	**GO Term/Keyword**	**Count**	**P-Value**	**Benjamini**
	INTERPRO	Acyl-CoA oxidase/dehydrogenase, type 1	7	2.40E-04	9.00E-03
	INTERPRO	Acyl-CoA dehydrogenase, N-terminal	6	1.10E-03	3.00E-02
	INTERPRO	Acyl-CoA dehydrogenase, conserved site	6	1.50E-03	3.90E-02
Annotation Cluster 13	**Enrichment Score: 3.03**	**GO Term/Keyword**	**Count**	**P-Value**	**Benjamini**
	INTERPRO	Pyridoxal phosphate-dependent transferase, major region, subdomain 1	10	2.40E-04	9.40E-03
	GOTERM_MF_FAT	vitamin B6 binding	13	4.90E-04	1.60E-02
	GOTERM_MF_FAT	pyridoxal phosphate binding	13	4.90E-04	1.60E-02
	GOTERM_MF_FAT	vitamin binding	15	1.40E-02	1.60E-01
Annotation Cluster 14	**Enrichment Score: 2.7**	**GO Term/Keyword**	**Count**	**P-Value**	**Benjamini**
	INTERPRO	Cytosolic fatty-acid binding	6	4.60E-04	1.50E-02
	INTERPRO	Calycin	5	2.10E-03	5.20E-02
	PIR_SUPERFAMILY	PIRSF002390:lipid binding protein, FABP type	5	2.90E-03	2.10E-01
	PIR_SUPERFAMILY	PIRSF500199:intracellular lipid-binding protein	4	5.60E-03	2.60E-01
Annotation Cluster 15	**Enrichment Score: 2.46**	**GO Term/Keyword**	**Count**	**P-Value**	**Benjamini**
	SMART	CLECT	23	2.90E-05	8.40E-04
	INTERPRO	C-type lectin-like	22	2.60E-02	3.50E-01

Table E5 (Continued)

	INTERPRO	C-type lectin	23	5.50E-02	5.30E-01
Annotation Cluster 16	**Enrichment Score: 2.34**	**GO Term/Keyword**	**Count**	**P-Value**	**Benjamini**
	GOTERM_BP_FAT	multicellular organismal aging	28	4.60E-03	1.40E-01
	GOTERM_BP_FAT	determination of adult life span	28	4.60E-03	1.40E-01
	GOTERM_BP_FAT	aging	28	4.60E-03	1.40E-01
Annotation Cluster 17	**Enrichment Score: 2.31**	**GO Term/Keyword**	**Count**	**P-Value**	**Benjamini**
	SP_PIR_KEYWORDS	respiratory chain	7	2.60E-03	3.10E-02
	SP_PIR_KEYWORDS	electron transport	8	4.10E-03	4.70E-02
	GOTERM_CC_FAT	respiratory chain	6	1.10E-02	6.10E-02
Annotation Cluster 18	**Enrichment Score: 2.29**	**GO Term/Keyword**	**Count**	**P-Value**	**Benjamini**
	INTERPRO	Peptidase, cysteine peptidase active site	10	3.00E-04	1.10E-02
	GOTERM_MF_FAT	cysteine-type endopeptidase activity	11	1.10E-02	1.60E-01
	GOTERM_MF_FAT	cysteine-type peptidase activity	13	4.00E-02	3.50E-01
Annotation Cluster 19	**Enrichment Score: 2.19**	**GO Term/Keyword**	**Count**	**P-Value**	**Benjamini**
	INTERPRO	Peptidase S10, serine carboxypeptidase	5	1.40E-03	3.70E-02
	GOTERM_MF_FAT	serine-type exopeptidase activity	5	4.20E-03	8.50E-02
	GOTERM_MF_FAT	serine-type carboxypeptidase activity	5	4.20E-03	8.50E-02
	INTERPRO	Peptidase S10, serine carboxypeptidase, active site	4	1.40E-02	2.40E-01
	GOTERM_MF_FAT	carboxypeptidase activity	6	3.20E-02	3.10E-01
Annotation Cluster 20	**Enrichment Score: 2.14**	**GO Term/Keyword**	**Count**	**P-Value**	**Benjamini**
	SMART	LPD_N	4	6.90E-04	1.50E-02
	SMART	VWD	4	1.80E-03	2.30E-02
	INTERPRO	Vitellinogen, superhelical	4	3.90E-03	8.60E-02
	INTERPRO	Vitellinogen, beta-sheet N-terminal	4	3.90E-03	8.60E-02
	INTERPRO	Lipid transport protein, N-terminal	4	3.90E-03	8.60E-02
	INTERPRO	Vitellinogen, open beta-sheet	4	3.90E-03	8.60E-02
	SP_PIR_KEYWORDS	storage protein	4	4.40E-03	4.80E-02
	UP_SEQ_FEATURE	domain:Vitellogenin	4	5.80E-03	3.20E-01
	GOTERM_MF_FAT	nutrient reservoir activity	4	6.60E-03	1.10E-01
	UP_SEQ_FEATURE	domain:VWFD	4	9.70E-03	4.20E-01
	INTERPRO	von Willebrand factor, type D	4	1.00E-02	1.90E-01
	GOTERM_MF_FAT	lipid transporter activity	4	1.40E-01	7.00E-01
	GOTERM_BP_FAT	lipid transport	4	2.10E-01	8.40E-01
Annotation Cluster 21	**Enrichment Score: 2.1**	**GO Term/Keyword**	**Count**	**P-Value**	**Benjamini**
	GOTERM_CC_FAT	prefoldin complex	5	9.40E-04	8.50E-03
	GOTERM_CC_FAT	cytosolic part	6	4.50E-03	3.00E-02
	GOTERM_CC_FAT	cytosol	6	1.20E-01	4.00E-01
Annotation Cluster 22	**Enrichment Score: 2.08**	**GO Term/Keyword**	**Count**	**P-Value**	**Benjamini**
	GOTERM_BP_FAT	fatty acid beta-oxidation	5	2.80E-03	1.10E-01
	GOTERM_BP_FAT	fatty acid catabolic process	5	2.80E-03	1.10E-01
	GOTERM_BP_FAT	fatty acid oxidation	5	4.10E-03	1.40E-01

Table E5 (Continued)

	GOTERM_BP_FAT	lipid oxidation	5	4.10E-03	1.40E-01
	GOTERM_BP_FAT	cellular lipid catabolic process	6	6.40E-03	1.70E-01
	INTERPRO	Acyl-CoA oxidase	4	6.60E-03	1.30E-01
	INTERPRO	Acyl-CoA oxidase, C-terminal	4	1.00E-02	1.90E-01
	PIR_SUPERFAMILY	PIRSF000168:acyl-CoA oxidase	4	1.00E-02	2.90E-01
	GOTERM_MF_FAT	acyl-CoA oxidase activity	4	1.60E-02	1.90E-01
	PIR_SUPERFAMILY	PIRSF000168:Acyl-CoA_oxidase	4	1.70E-02	3.70E-01
	KEGG_PATHWAY	alpha-Linolenic acid metabolism	5	2.30E-02	1.70E-01
	GOTERM_MF_FAT	oxidoreductase activity, acting on the CH-CH group of donors, oxygen as acceptor	4	3.20E-02	3.10E-01
Annotation Cluster 23	**Enrichment Score: 1.89**	**GO Term/Keyword**	**Count**	**P-Value**	**Benjamini**
	GOTERM_BP_FAT	response to endoplasmic reticulum stress	5	2.80E-03	1.10E-01
	GOTERM_BP_FAT	endoplasmic reticulum unfolded protein response	5	2.80E-03	1.10E-01
	GOTERM_BP_FAT	ER-nuclear signaling pathway	5	2.80E-03	1.10E-01
	GOTERM_BP_FAT	cellular response to unfolded protein	5	5.90E-03	1.60E-01
	GOTERM_BP_FAT	response to protein stimulus	5	8.10E-03	1.90E-01
	GOTERM_BP_FAT	response to unfolded protein	5	8.10E-03	1.90E-01
	GOTERM_BP_FAT	response to organic substance	5	1.10E-01	6.90E-01
	GOTERM_BP_FAT	cellular response to stress	5	9.30E-01	1.00E+00
Annotation Cluster 24	**Enrichment Score: 1.86**	**GO Term/Keyword**	**Count**	**P-Value**	**Benjamini**
	PIR_SUPERFAMILY	PIRSF036514:alpha-crystallin-related small heat shock protein	5	7.50E-03	2.60E-01
	INTERPRO	Alpha crystallin/Heat shock protein	5	1.10E-02	2.00E-01
	INTERPRO	Heat shock protein Hsp20	5	1.40E-02	2.30E-01
	GOTERM_BP_FAT	response to heat	6	3.30E-02	4.40E-01
Annotation Cluster 25	**Enrichment Score: 1.85**	**GO Term/Keyword**	**Count**	**P-Value**	**Benjamini**
	GOTERM_BP_FAT	catechol metabolic process	7	8.30E-03	1.90E-01
	GOTERM_BP_FAT	phenol metabolic process	7	8.30E-03	1.90E-01
	GOTERM_BP_FAT	diol metabolic process	7	8.30E-03	1.90E-01
	GOTERM_MF_FAT	oxidoreductase activity, acting on the CH-CH group of donors, NAD or NADP as acceptor	7	9.70E-03	1.50E-01
	GOTERM_BP_FAT	siderophore biosynthetic process from catechol	6	1.50E-02	2.80E-01
	GOTERM_BP_FAT	siderophore biosynthetic process	6	1.50E-02	2.80E-01
	GOTERM_BP_FAT	nonribosomal peptide biosynthetic process	6	1.50E-02	2.80E-01
	GOTERM_BP_FAT	siderophore metabolic process	6	1.50E-02	2.80E-01
	GOTERM_BP_FAT	enterobactin biosynthetic process	6	1.50E-02	2.80E-01
	GOTERM_BP_FAT	enterobactin metabolic process	6	1.50E-02	2.80E-01
	GOTERM_MF_FAT	2,3-dihydro-2,3-dihydroxybenzoate dehydrogenase activity	6	2.30E-02	2.50E-01
	GOTERM_BP_FAT	peptide metabolic process	7	2.40E-02	3.80E-01
	GOTERM_BP_FAT	peptide biosynthetic process	6	2.50E-02	3.80E-01

Table E5 (Continued)

Annotation Cluster 26	Enrichment Score: 1.81	GO Term/Keyword	Count	P-Value	Benjamini
	GOTERM_CC_FAT	membrane-enclosed lumen	20	2.70E-03	2.00E-02
	GOTERM_CC_FAT	organelle lumen	16	3.70E-02	1.60E-01
	GOTERM_CC_FAT	intracellular organelle lumen	16	3.70E-02	1.60E-01
Annotation Cluster 27	**Enrichment Score: 1.79**	**GO Term/Keyword**	**Count**	**P-Value**	**Benjamini**
	GOTERM_MF_FAT	peptidase activity	44	1.10E-02	1.60E-01
	GOTERM_MF_FAT	peptidase activity, acting on L-amino acid peptides	41	1.30E-02	1.60E-01
	GOTERM_BP_FAT	proteolysis	46	3.00E-02	4.20E-01
Annotation Cluster 28	**Enrichment Score: 1.39**	**GO Term/Keyword**	**Count**	**P-Value**	**Benjamini**
	GOTERM_BP_FAT	regulation of growth rate	131	3.40E-02	4.40E-01
	GOTERM_BP_FAT	positive regulation of growth rate	131	3.50E-02	4.40E-01
	GOTERM_BP_FAT	positive regulation of growth	143	3.70E-02	4.30E-01
	GOTERM_BP_FAT	regulation of growth	145	6.10E-02	5.40E-01
Annotation Cluster 29	**Enrichment Score: 1.34**	**GO Term/Keyword**	**Count**	**P-Value**	**Benjamini**
	GOTERM_MF_FAT	ubiquinol-cytochrome-c reductase activity	3	4.60E-02	3.70E-01
	GOTERM_MF_FAT	oxidoreductase activity, acting on diphenols and related substances as donors	3	4.60E-02	3.70E-01
	GOTERM_MF_FAT	oxidoreductase activity, acting on diphenols and related substances as donors, cytochrome as acceptor	3	4.60E-02	3.70E-01
Annotation Cluster 30	**Enrichment Score: 1.31**	**GO Term/Keyword**	**Count**	**P-Value**	**Benjamini**
	GOTERM_BP_FAT	cell redox homeostasis	10	2.50E-02	3.70E-01
	GOTERM_BP_FAT	cellular homeostasis	12	3.50E-02	4.30E-01
	GOTERM_BP_FAT	homeostatic process	12	1.40E-01	7.30E-01
Annotation Cluster 31	**Enrichment Score: 1.29**	**GO Term/Keyword**	**Count**	**P-Value**	**Benjamini**
	SMART	Sm	4	1.80E-02	1.50E-01
	INTERPRO	Like-Sm ribonucleoprotein, eukaryotic and archaea-type, core	4	8.10E-02	6.60E-01
	INTERPRO	Like-Sm ribonucleoprotein, core	4	9.30E-02	7.00E-01
Annotation Cluster 32	**Enrichment Score: 1.28**	**GO Term/Keyword**	**Count**	**P-Value**	**Benjamini**
	INTERPRO	Ctr copper transporter	4	1.40E-02	2.40E-01
	GOTERM_MF_FAT	copper ion transmembrane transporter activity	4	4.10E-02	3.50E-01
	GOTERM_MF_FAT	transition metal ion transmembrane transporter activity	4	7.70E-02	5.00E-01
	GOTERM_MF_FAT	di-, tri-valent inorganic cation transmembrane transporter activity	4	1.60E-01	7.40E-01
Annotation Cluster 33	**Enrichment Score: 1.26**	**GO Term/Keyword**	**Count**	**P-Value**	**Benjamini**
	GOTERM_CC_FAT	mitochondrial intermembrane space	4	7.50E-03	4.40E-02
	GOTERM_CC_FAT	organelle envelope lumen	4	7.50E-03	4.40E-02
	INTERPRO	Zinc finger, Tim10/DDP-type	3	3.30E-02	4.00E-01
	INTERPRO	Mitochondrial inner membrane translocase complex, Tim8/9/10/13-zinc finger-like	3	3.30E-02	4.00E-01

Table E5 (Continued)

	GOTERM_CC_FAT	mitochondrial intermembrane space protein transporter complex	3	3.60E-02	1.60E-01
	GOTERM_BP_FAT	protein import into mitochondrial inner membrane	3	3.70E-02	4.20E-01
	GOTERM_BP_FAT	mitochondrial membrane organization	3	3.70E-02	4.20E-01
	GOTERM_BP_FAT	inner mitochondrial membrane organization	3	3.70E-02	4.20E-01
	UP_SEQ_FEATURE	short sequence motif:Twin CX3C motif	3	4.30E-02	8.90E-01
	GOTERM_BP_FAT	protein localization in mitochondrion	3	1.40E-01	7.40E-01
	GOTERM_BP_FAT	protein targeting to mitochondrion	3	1.40E-01	7.40E-01
	GOTERM_BP_FAT	mitochondrial transport	3	1.80E-01	8.10E-01
	GOTERM_BP_FAT	mitochondrion organization	3	3.80E-01	9.50E-01
	GOTERM_BP_FAT	protein import	3	4.00E-01	9.60E-01
Annotation Cluster 34	**Enrichment Score: 1.23**	**GO Term/Keyword**	**Count**	**P-Value**	**Benjamini**
	GOTERM_MF_FAT	protein disulfide oxidoreductase activity	5	4.50E-02	3.70E-01
	GOTERM_MF_FAT	oxidoreductase activity, acting on sulfur group of donors	6	6.40E-02	4.60E-01
	GOTERM_MF_FAT	disulfide oxidoreductase activity	5	7.20E-02	4.80E-01
Annotation Cluster 35	**Enrichment Score: 1.19**	**GO Term/Keyword**	**Count**	**P-Value**	**Benjamini**
	INTERPRO	Cytochrome P450, E-class, group I	11	1.50E-02	2.40E-01
	INTERPRO	Cytochrome P450	11	1.80E-02	2.80E-01
	INTERPRO	Cytochrome P450, C-terminal region	10	3.60E-02	4.10E-01
	COG_ONTOLOGY	Secondary metabolites biosynthesis, transport, and catabolism	11	3.80E-02	2.10E-01
	SP_PIR_KEYWORDS	Monooxygenase	11	5.20E-02	2.80E-01
	INTERPRO	Cytochrome P450, conserved site	9	8.60E-02	6.70E-01
	SP_PIR_KEYWORDS	heme	12	1.60E-01	5.40E-01
	GOTERM_MF_FAT	heme binding	14	2.60E-01	8.70E-01
	GOTERM_MF_FAT	tetrapyrrole binding	14	2.80E-01	8.80E-01
Annotation Cluster 36	**Enrichment Score: 1.14**	**GO Term/Keyword**	**Count**	**P-Value**	**Benjamini**
	GOTERM_BP_FAT	cotranslational protein targeting to membrane	4	2.40E-02	3.80E-01
	SP_PIR_KEYWORDS	signal recognition particle	3	5.10E-02	2.80E-01
	GOTERM_CC_FAT	signal recognition particle, endoplasmic reticulum targeting	3	5.20E-02	2.10E-01
	GOTERM_MF_FAT	7S RNA binding	3	6.60E-02	4.50E-01
	GOTERM_CC_FAT	signal recognition particle	3	6.90E-02	2.60E-01
	GOTERM_BP_FAT	protein targeting to ER	3	1.10E-01	7.00E-01
	GOTERM_BP_FAT	SRP-dependent cotranslational protein targeting to membrane	3	1.10E-01	7.00E-01
	KEGG_PATHWAY	Protein export	3	2.10E-01	6.00E-01
Annotation Cluster 37	**Enrichment Score: 1.12**	**GO Term/Keyword**	**Count**	**P-Value**	**Benjamini**
	GOTERM_CC_FAT	proton-transporting ATP synthase complex	7	8.80E-04	8.50E-03

Table E5 (Continued)

	GOTERM_CC_FAT	proton-transporting two-sector ATPase complex, proton-transporting domain	6	7.30E-03	4.40E-02
	GOTERM_BP_FAT	hydrogen transport	9	1.30E-02	2.60E-01
	GOTERM_CC_FAT	proton-transporting two-sector ATPase complex	8	2.80E-02	1.40E-01
	GOTERM_BP_FAT	proton transport	8	3.50E-02	4.20E-01
	GOTERM_BP_FAT	ion transmembrane transport	8	3.90E-02	4.20E-01
	GOTERM_BP_FAT	energy coupled proton transport, down electrochemical gradient	7	7.10E-02	5.70E-01
	GOTERM_BP_FAT	ATP synthesis coupled proton transport	7	7.10E-02	5.70E-01
	GOTERM_BP_FAT	ATP biosynthetic process	9	8.50E-02	6.20E-01
	GOTERM_BP_FAT	ATP metabolic process	9	9.70E-02	6.60E-01
	GOTERM_BP_FAT	purine nucleoside triphosphate biosynthetic process	9	1.20E-01	7.00E-01
	GOTERM_BP_FAT	nucleoside triphosphate biosynthetic process	9	1.20E-01	7.00E-01
	GOTERM_BP_FAT	purine ribonucleoside triphosphate biosynthetic process	9	1.20E-01	7.00E-01
	GOTERM_BP_FAT	ribonucleoside triphosphate biosynthetic process	9	1.20E-01	7.00E-01
	GOTERM_BP_FAT	ribonucleotide biosynthetic process	10	1.30E-01	7.20E-01
	GOTERM_BP_FAT	purine nucleoside triphosphate metabolic process	9	1.30E-01	7.30E-01
	GOTERM_BP_FAT	purine ribonucleoside triphosphate metabolic process	9	1.30E-01	7.30E-01
	GOTERM_BP_FAT	ribonucleoside triphosphate metabolic process	9	1.30E-01	7.30E-01
	GOTERM_BP_FAT	nucleoside triphosphate metabolic process	9	1.40E-01	7.40E-01
	GOTERM_BP_FAT	ribonucleotide metabolic process	10	1.50E-01	7.50E-01
	GOTERM_BP_FAT	purine ribonucleotide biosynthetic process	9	2.00E-01	8.40E-01
	GOTERM_BP_FAT	purine ribonucleotide metabolic process	9	2.30E-01	8.60E-01
	GOTERM_BP_FAT	purine nucleotide biosynthetic process	9	4.80E-01	9.80E-01
	GOTERM_BP_FAT	purine nucleotide metabolic process	9	5.20E-01	9.80E-01
Annotation Cluster 38	**Enrichment Score: 1.1**	**GO Term/Keyword**	**Count**	**P-Value**	**Benjamini**
	INTERPRO	Thiolase	3	4.70E-02	4.90E-01
	PIR_SUPERFAMILY	PIRSF000429:Ac-CoA_Ac_transf	3	8.80E-02	8.40E-01
	INTERPRO	Thiolase-like, subgroup	3	1.20E-01	7.70E-01
Annotation Cluster 39	**Enrichment Score: 1.03**	**GO Term/Keyword**	**Count**	**P-Value**	**Benjamini**
	GOTERM_BP_FAT	aromatic amino acid family catabolic process	3	5.40E-02	5.10E-01
	GOTERM_BP_FAT	aromatic compound catabolic process	3	7.20E-02	5.70E-01
	GOTERM_BP_FAT	aromatic amino acid family metabolic process	3	2.10E-01	8.40E-01

Table E5 (Continued)

Annotation Cluster 40	Enrichment Score: 1.02	GO Term/Keyword	Count	P-Value	Benjamini
	GOTERM_BP_FAT	nucleobase, nucleoside, nucleotide and nucleic acid biosynthetic process	16	7.50E-02	5.80E-01
	GOTERM_BP_FAT	nucleobase, nucleoside and nucleotide biosynthetic process	16	7.50E-02	5.80E-01
	GOTERM_BP_FAT	nucleotide biosynthetic process	14	1.60E-01	7.60E-01
Annotation Cluster 41	**Enrichment Score: 0.99**	**GO Term/Keyword**	**Count**	**P-Value**	**Benjamini**
	INTERPRO	Uncharacterised protein family UPF0376	6	4.30E-02	4.60E-01
	PIR_SUPERFAMILY	PIRSF015697:UCP015697	6	1.40E-01	9.30E-01
	INTERPRO	Protein of unknown function DUF19	6	1.80E-01	8.80E-01
Annotation Cluster 42	**Enrichment Score: 0.96**	**GO Term/Keyword**	**Count**	**P-Value**	**Benjamini**
	SP_PIR_KEYWORDS	dioxygenase	4	7.70E-02	3.40E-01
	GOTERM_MF_FAT	oxidoreductase activity, acting on single donors with incorporation of molecular oxygen, incorporation of two atoms of oxygen	4	1.20E-01	6.60E-01
	GOTERM_MF_FAT	oxidoreductase activity, acting on single donors with incorporation of molecular oxygen	4	1.40E-01	7.00E-01
Annotation Cluster 43	**Enrichment Score: 0.93**	**GO Term/Keyword**	**Count**	**P-Value**	**Benjamini**
	SMART	DnaJ	5	1.90E-02	1.40E-01
	INTERPRO	Heat shock protein DnaJ, N-terminal	5	1.20E-01	7.70E-01
	GOTERM_MF_FAT	heat shock protein binding	5	2.80E-01	8.90E-01
	INTERPRO	Molecular chaperone, heat shock protein, Hsp40, DnaJ	4	3.10E-01	9.70E-01
Annotation Cluster 44	**Enrichment Score: 0.93**	**GO Term/Keyword**	**Count**	**P-Value**	**Benjamini**
	INTERPRO	Chaperone DnaJ, C-terminal	3	3.30E-02	4.00E-01
	INTERPRO	Heat shock protein DnaJ	3	1.60E-01	8.60E-01
	INTERPRO	Molecular chaperone, heat shock protein, Hsp40, DnaJ	4	3.10E-01	9.70E-01
Annotation Cluster 45	**Enrichment Score: 0.88**	**GO Term/Keyword**	**Count**	**P-Value**	**Benjamini**
	GOTERM_BP_FAT	growth	113	4.50E-03	1.50E-01
	GOTERM_BP_FAT	nematode larval development	119	3.90E-01	9.60E-01
	GOTERM_BP_FAT	larval development	119	4.00E-01	9.60E-01
	GOTERM_BP_FAT	post-embryonic development	119	4.50E-01	9.70E-01
Annotation Cluster 46	**Enrichment Score: 0.69**	**GO Term/Keyword**	**Count**	**P-Value**	**Benjamini**
	GOTERM_BP_FAT	pyridine nucleotide metabolic process	4	7.00E-02	5.70E-01
	GOTERM_BP_FAT	oxidoreduction coenzyme metabolic process	4	2.10E-01	8.40E-01
	GOTERM_BP_FAT	nicotinamide nucleotide metabolic process	3	2.10E-01	8.40E-01
	GOTERM_BP_FAT	nicotinamide metabolic process	3	2.10E-01	8.40E-01
	GOTERM_BP_FAT	alkaloid metabolic process	3	2.10E-01	8.40E-01
	GOTERM_BP_FAT	cellular amide metabolic process	3	2.60E-01	8.80E-01
	GOTERM_BP_FAT	secondary metabolic process	3	4.30E-01	9.60E-01
Annotation Cluster 47	**Enrichment Score: 0.64**	**GO Term/Keyword**	**Count**	**P-Value**	**Benjamini**

Table E5 (Continued)

	SMART	PTPc	9	1.20E-02	1.30E-01
	INTERPRO	Protein-tyrosine phosphatase, receptor/non-receptor type	9	2.10E-01	9.10E-01
	GOTERM_BP_FAT	protein amino acid dephosphorylation	9	5.80E-01	9.90E-01
	GOTERM_MF_FAT	protein tyrosine phosphatase activity	9	6.20E-01	9.90E-01
	GOTERM_BP_FAT	dephosphorylation	9	6.60E-01	1.00E+00
Annotation Cluster 48	**Enrichment Score: 0.64**	**GO Term/Keyword**	**Count**	**P-Value**	**Benjamini**
	GOTERM_MF_FAT	fatty acid binding	3	1.90E-01	7.70E-01
	GOTERM_MF_FAT	acyl-CoA binding	3	1.90E-01	7.70E-01
	GOTERM_MF_FAT	monocarboxylic acid binding	3	3.30E-01	9.10E-01
Annotation Cluster 49	**Enrichment Score: 0.62**	**GO Term/Keyword**	**Count**	**P-Value**	**Benjamini**
	GOTERM_MF_FAT	nucleotide kinase activity	3	1.10E-01	6.30E-01
	GOTERM_MF_FAT	phosphotransferase activity, phosphate group as acceptor	3	3.00E-01	8.90E-01
	GOTERM_MF_FAT	nucleobase, nucleoside, nucleotide kinase activity	3	4.10E-01	9.50E-01
Annotation Cluster 50	**Enrichment Score: 0.61**	**GO Term/Keyword**	**Count**	**P-Value**	**Benjamini**
	GOTERM_MF_FAT	heme-copper terminal oxidase activity	3	2.50E-01	8.50E-01
	GOTERM_MF_FAT	cytochrome-c oxidase activity	3	2.50E-01	8.50E-01
	GOTERM_MF_FAT	oxidoreductase activity, acting on heme group of donors	3	2.50E-01	8.50E-01
	GOTERM_MF_FAT	oxidoreductase activity, acting on heme group of donors, oxygen as acceptor	3	2.50E-01	8.50E-01
Annotation Cluster 51	**Enrichment Score: 0.54**	**GO Term/Keyword**	**Count**	**P-Value**	**Benjamini**
	GOTERM_BP_FAT	protein targeting	9	1.90E-03	8.60E-02
	GOTERM_BP_FAT	intracellular protein transport	12	3.80E-01	9.50E-01
	GOTERM_BP_FAT	cellular macromolecule localization	12	5.00E-01	9.80E-01
	GOTERM_BP_FAT	cellular protein localization	12	5.00E-01	9.80E-01
	GOTERM_BP_FAT	intracellular transport	12	6.50E-01	1.00E+00
	GOTERM_BP_FAT	protein transport	16	6.60E-01	1.00E+00
	GOTERM_BP_FAT	establishment of protein localization	16	6.90E-01	1.00E+00
	GOTERM_BP_FAT	protein localization	17	9.20E-01	1.00E+00
Annotation Cluster 52	**Enrichment Score: 0.47**	**GO Term/Keyword**	**Count**	**P-Value**	**Benjamini**
	GOTERM_BP_FAT	water-soluble vitamin biosynthetic process	3	3.10E-01	9.10E-01
	GOTERM_BP_FAT	vitamin biosynthetic process	3	3.10E-01	9.10E-01
	GOTERM_BP_FAT	water-soluble vitamin metabolic process	3	3.80E-01	9.50E-01
	GOTERM_BP_FAT	vitamin metabolic process	3	3.80E-01	9.50E-01
Annotation Cluster 53	**Enrichment Score: 0.45**	**GO Term/Keyword**	**Count**	**P-Value**	**Benjamini**
	PIR_SUPERFAMILY	PIRSF000675:tyrosine-protein kinase	5	5.30E-02	6.90E-01
	SMART	TyrKc	6	3.40E-01	8.90E-01
	SP_PIR_KEYWORDS	tyrosine-protein kinase	6	5.00E-01	9.00E-01
	INTERPRO	Tyrosine protein kinase, active site	5	7.40E-01	1.00E+00

Table E5 (Continued)

	INTERPRO	Tyrosine protein kinase	6	8.40E-01	1.00E+00
Annotation Cluster 54	**Enrichment Score: 0.43**	**GO Term/Keyword**	**Count**	**P-Value**	**Benjamini**
	SMART	CHK	3	2.20E-01	7.80E-01
	INTERPRO	CHK kinase-like	3	4.80E-01	1.00E+00
	INTERPRO	Uncharacterised kinase D1044.1	3	5.00E-01	1.00E+00
Annotation Cluster 55	**Enrichment Score: 0.4**	**GO Term/Keyword**	**Count**	**P-Value**	**Benjamini**
	INTERPRO	Acyl-CoA N-acyltransferase	4	1.60E-01	8.60E-01
	INTERPRO	GCN5-related N-acetyltransferase	3	3.50E-01	9.80E-01
	GOTERM_MF_FAT	acetyltransferase activity	4	4.20E-01	9.50E-01
	GOTERM_MF_FAT	N-acetyltransferase activity	3	6.40E-01	9.90E-01
	GOTERM_MF_FAT	N-acyltransferase activity	3	6.60E-01	9.90E-01
Annotation Cluster 56	**Enrichment Score: 0.39**	**GO Term/Keyword**	**Count**	**P-Value**	**Benjamini**
	GOTERM_BP_FAT	positive regulation of multicellular organism growth	24	3.60E-01	9.40E-01
	GOTERM_BP_FAT	positive regulation of multicellular organismal process	24	4.10E-01	9.60E-01
	GOTERM_BP_FAT	regulation of multicellular organism growth	29	4.60E-01	9.70E-01
Annotation Cluster 57	**Enrichment Score: 0.39**	**GO Term/Keyword**	**Count**	**P-Value**	**Benjamini**
	GOTERM_CC_FAT	nucleosome	5	1.20E-01	4.00E-01
	GOTERM_BP_FAT	nucleosome organization	5	1.50E-01	7.50E-01
	GOTERM_BP_FAT	chromatin assembly	5	1.50E-01	7.50E-01
	GOTERM_BP_FAT	nucleosome assembly	5	1.50E-01	7.50E-01
	GOTERM_CC_FAT	protein-DNA complex	5	1.60E-01	4.60E-01
	GOTERM_BP_FAT	protein-DNA complex assembly	5	2.20E-01	8.50E-01
	SP_PIR_KEYWORDS	chromosomal protein	5	2.90E-01	7.40E-01
	GOTERM_BP_FAT	DNA packaging	5	2.90E-01	9.10E-01
	GOTERM_CC_FAT	chromatin	5	4.70E-01	8.80E-01
	GOTERM_BP_FAT	chromatin assembly or disassembly	5	4.70E-01	9.70E-01
	GOTERM_CC_FAT	chromosomal part	5	7.30E-01	9.80E-01
	GOTERM_BP_FAT	cellular macromolecular complex assembly	5	7.90E-01	1.00E+00
	GOTERM_BP_FAT	chromatin organization	5	8.60E-01	1.00E+00
	GOTERM_BP_FAT	cellular macromolecular complex subunit organization	5	8.70E-01	1.00E+00
	GOTERM_CC_FAT	chromosome	5	9.30E-01	1.00E+00
	GOTERM_BP_FAT	macromolecular complex assembly	5	9.40E-01	1.00E+00
	GOTERM_BP_FAT	macromolecular complex subunit organization	5	9.60E-01	1.00E+00
	GOTERM_BP_FAT	chromosome organization	5	9.90E-01	1.00E+00
Annotation Cluster 58	**Enrichment Score: 0.22**	**GO Term/Keyword**	**Count**	**P-Value**	**Benjamini**
	GOTERM_BP_FAT	establishment of nucleus localization	5	4.00E-01	9.60E-01
	GOTERM_BP_FAT	nucleus localization	5	4.00E-01	9.60E-01
	GOTERM_BP_FAT	pronuclear migration	4	5.90E-01	9.90E-01
	GOTERM_BP_FAT	nuclear migration	4	6.20E-01	9.90E-01

Table E5 (Continued)

	GOTERM_BP_FAT	single fertilization	4	6.70E-01	1.00E+00
	GOTERM_BP_FAT	fertilization	4	6.70E-01	1.00E+00
	GOTERM_BP_FAT	establishment of organelle localization	5	8.00E-01	1.00E+00
	GOTERM_BP_FAT	organelle localization	5	8.20E-01	1.00E+00
Annotation Cluster 59	**Enrichment Score: 0.21**	**GO Term/Keyword**	**Count**	**P-Value**	**Benjamini**
	GOTERM_MF_FAT	peroxidase activity	3	5.60E-01	9.90E-01
	GOTERM_MF_FAT	oxidoreductase activity, acting on peroxide as acceptor	3	5.60E-01	9.90E-01
	GOTERM_MF_FAT	antioxidant activity	3	7.80E-01	1.00E+00
Annotation Cluster 60	**Enrichment Score: 0.19**	**GO Term/Keyword**	**Count**	**P-Value**	**Benjamini**
	GOTERM_BP_FAT	alcohol catabolic process	4	4.60E-01	9.70E-01
	GOTERM_BP_FAT	cellular carbohydrate catabolic process	4	4.70E-01	9.70E-01
	GOTERM_BP_FAT	glucose catabolic process	3	6.60E-01	1.00E+00
	GOTERM_BP_FAT	hexose catabolic process	3	6.60E-01	1.00E+00
	GOTERM_BP_FAT	monosaccharide catabolic process	3	6.60E-01	1.00E+00
	GOTERM_BP_FAT	hexose metabolic process	4	8.10E-01	1.00E+00
	GOTERM_BP_FAT	glucose metabolic process	3	8.60E-01	1.00E+00
Annotation Cluster 61	**Enrichment Score: 0.13**	**GO Term/Keyword**	**Count**	**P-Value**	**Benjamini**
	GOTERM_BP_FAT	negative regulation of multicellular organism growth	6	7.30E-01	1.00E+00
	GOTERM_BP_FAT	negative regulation of multicellular organismal process	6	7.30E-01	1.00E+00
	GOTERM_BP_FAT	negative regulation of growth	6	7.50E-01	1.00E+00
Annotation Cluster 62	**Enrichment Score: 0.12**	**GO Term/Keyword**	**Count**	**P-Value**	**Benjamini**
	GOTERM_BP_FAT	phosphate metabolic process	41	7.40E-01	1.00E+00
	GOTERM_BP_FAT	phosphorus metabolic process	41	7.40E-01	1.00E+00
	GOTERM_BP_FAT	phosphorylation	31	7.70E-01	1.00E+00
Annotation Cluster 63	**Enrichment Score: 0.12**	**GO Term/Keyword**	**Count**	**P-Value**	**Benjamini**
	GOTERM_BP_FAT	molting cycle, collagen and cuticulin-based cuticle	15	7.60E-01	1.00E+00
	GOTERM_BP_FAT	molting cycle, protein-based cuticle	15	7.60E-01	1.00E+00
	GOTERM_BP_FAT	molting cycle	15	7.60E-01	1.00E+00
Annotation Cluster 64	**Enrichment Score: 0.11**	**GO Term/Keyword**	**Count**	**P-Value**	**Benjamini**
	SP_PIR_KEYWORDS	Sodium	3	6.80E-01	9.70E-01
	GOTERM_MF_FAT	sodium ion binding	3	7.50E-01	1.00E+00
	SP_PIR_KEYWORDS	Sodium transport	3	8.10E-01	9.90E-01
	GOTERM_BP_FAT	sodium ion transport	3	9.10E-01	1.00E+00
Annotation Cluster 65	**Enrichment Score: 0.09**	**GO Term/Keyword**	**Count**	**P-Value**	**Benjamini**
	INTERPRO	Potassium channel, voltage dependent, Kv, tetramerisation	4	6.40E-01	1.00E+00
	GOTERM_CC_FAT	voltage-gated potassium channel complex	4	7.20E-01	9.80E-01
	GOTERM_CC_FAT	potassium channel complex	4	7.20E-01	9.80E-01
	GOTERM_CC_FAT	cation channel complex	4	7.70E-01	9.90E-01

Table E5 (Continued)

	GOTERM_CC_FAT	ion channel complex	4	8.30E-01	9.90E-01
	GOTERM_MF_FAT	voltage-gated channel activity	5	8.50E-01	1.00E+00
	GOTERM_MF_FAT	voltage-gated ion channel activity	5	8.50E-01	1.00E+00
	GOTERM_MF_FAT	voltage-gated potassium channel activity	4	8.60E-01	1.00E+00
	GOTERM_MF_FAT	voltage-gated cation channel activity	4	8.90E-01	1.00E+00
	GOTERM_CC_FAT	integral to plasma membrane	4	9.10E-01	1.00E+00
	GOTERM_CC_FAT	intrinsic to plasma membrane	4	9.20E-01	1.00E+00
	GOTERM_MF_FAT	gated channel activity	5	1.00E+00	1.00E+00
Annotation Cluster 66	**Enrichment Score: 0.08**	**GO Term/Keyword**	**Count**	**P-Value**	**Benjamini**
	GOTERM_CC_FAT	endoplasmic reticulum membrane	3	7.60E-01	9.90E-01
	GOTERM_CC_FAT	nuclear envelope-endoplasmic reticulum network	3	7.60E-01	9.90E-01
	GOTERM_CC_FAT	endomembrane system	3	9.90E-01	1.00E+00
Annotation Cluster 67	**Enrichment Score: 0.07**	**GO Term/Keyword**	**Count**	**P-Value**	**Benjamini**
	GOTERM_BP_FAT	negative regulation of macromolecule biosynthetic process	3	8.00E-01	1.00E+00
	GOTERM_BP_FAT	negative regulation of cellular biosynthetic process	3	8.10E-01	1.00E+00
	GOTERM_BP_FAT	negative regulation of biosynthetic process	3	8.10E-01	1.00E+00
	GOTERM_BP_FAT	negative regulation of macromolecule metabolic process	3	9.60E-01	1.00E+00
Annotation Cluster 68	**Enrichment Score: 0.07**	**GO Term/Keyword**	**Count**	**P-Value**	**Benjamini**
	GOTERM_BP_FAT	collagen and cuticulin-based cuticle development	5	8.40E-01	1.00E+00
	GOTERM_BP_FAT	cuticle development	5	8.60E-01	1.00E+00
	GOTERM_BP_FAT	protein-based cuticle development	5	8.60E-01	1.00E+00
Annotation Cluster 69	**Enrichment Score: 0.04**	**GO Term/Keyword**	**Count**	**P-Value**	**Benjamini**
	GOTERM_BP_FAT	reproductive cellular process	5	7.80E-01	1.00E+00
	GOTERM_BP_FAT	oogenesis	4	9.70E-01	1.00E+00
	GOTERM_BP_FAT	female gamete generation	4	9.80E-01	1.00E+00
Annotation Cluster 70	**Enrichment Score: 0.03**	**GO Term/Keyword**	**Count**	**P-Value**	**Benjamini**
	GOTERM_BP_FAT	hermaphrodite genitalia development	39	8.90E-01	1.00E+00
	GOTERM_BP_FAT	genitalia development	39	9.00E-01	1.00E+00
	GOTERM_BP_FAT	sex differentiation	40	9.70E-01	1.00E+00
	GOTERM_BP_FAT	reproductive developmental process	42	9.80E-01	1.00E+00
Annotation Cluster 71	**Enrichment Score: 0.03**	**GO Term/Keyword**	**Count**	**P-Value**	**Benjamini**
	GOTERM_MF_FAT	ATPase activity, coupled to transmembrane movement of ions	3	8.10E-01	1.00E+00
	GOTERM_MF_FAT	ATPase activity, coupled to movement of substances	4	9.40E-01	1.00E+00
	GOTERM_MF_FAT	ATPase activity, coupled to transmembrane movement of substances	4	9.40E-01	1.00E+00
	GOTERM_MF_FAT	hydrolase activity, acting on acid anhydrides, catalyzing	4	9.60E-01	1.00E+00

Table E5 (Continued)

		transmembrane movement of substances			
	GOTERM_MF_FAT	ATPase activity, coupled	5	1.00E+00	1.00E+00
	GOTERM_MF_FAT	ATPase activity	5	1.00E+00	1.00E+00
Annotation Cluster 72	**Enrichment Score: 0.02**	**GO Term/Keyword**	**Count**	**P-Value**	**Benjamini**
	SMART	EGF	3	8.70E-01	1.00E+00
	INTERPRO	EGF-like, type 3	3	9.80E-01	1.00E+00
	INTERPRO	EGF-like	3	9.90E-01	1.00E+00
Annotation Cluster 73	**Enrichment Score: 0.02**	**GO Term/Keyword**	**Count**	**P-Value**	**Benjamini**
	SMART	RRM	3	8.80E-01	1.00E+00
	INTERPRO	Nucleotide-binding, alpha-beta plait	3	9.90E-01	1.00E+00
	INTERPRO	RNA recognition motif, RNP-1	3	9.90E-01	1.00E+00
Annotation Cluster 74	**Enrichment Score: 0.01**	**GO Term/Keyword**	**Count**	**P-Value**	**Benjamini**
	INTERPRO	Protein kinase, core	20	9.10E-01	1.00E+00
	GOTERM_BP_FAT	protein amino acid phosphorylation	20	9.80E-01	1.00E+00
	GOTERM_MF_FAT	protein serine/threonine kinase activity	20	9.90E-01	1.00E+00
	GOTERM_MF_FAT	protein kinase activity	21	1.00E+00	1.00E+00
Annotation Cluster 75	**Enrichment Score: 0.01**	**GO Term/Keyword**	**Count**	**P-Value**	**Benjamini**
	GOTERM_BP_FAT	potassium ion transport	6	9.00E-01	1.00E+00
	GOTERM_MF_FAT	potassium channel activity	6	9.20E-01	1.00E+00
	GOTERM_MF_FAT	cation channel activity	7	9.90E-01	1.00E+00
	GOTERM_MF_FAT	substrate specific channel activity	8	1.00E+00	1.00E+00
	GOTERM_MF_FAT	ion channel activity	8	1.00E+00	1.00E+00
	GOTERM_MF_FAT	passive transmembrane transporter activity	8	1.00E+00	1.00E+00
	GOTERM_MF_FAT	channel activity	8	1.00E+00	1.00E+00
Annotation Cluster 76	**Enrichment Score: 0.01**	**GO Term/Keyword**	**Count**	**P-Value**	**Benjamini**
	GOTERM_MF_FAT	enzyme inhibitor activity	4	9.70E-01	1.00E+00
	GOTERM_MF_FAT	endopeptidase inhibitor activity	3	9.90E-01	1.00E+00
	GOTERM_MF_FAT	peptidase inhibitor activity	3	9.90E-01	1.00E+00
Annotation Cluster 77	**Enrichment Score: 0**	**GO Term/Keyword**	**Count**	**P-Value**	**Benjamini**
	GOTERM_BP_FAT	negative regulation of post-embryonic development	3	1.00E+00	1.00E+00
	GOTERM_BP_FAT	negative regulation of vulval development	3	1.00E+00	1.00E+00
	GOTERM_BP_FAT	regulation of post-embryonic development	3	1.00E+00	1.00E+00
	GOTERM_BP_FAT	regulation of vulval development	3	1.00E+00	1.00E+00
Annotation Cluster 78	**Enrichment Score: 0**	**GO Term/Keyword**	**Count**	**P-Value**	**Benjamini**
	GOTERM_BP_FAT	modification-dependent macromolecule catabolic process	3	1.00E+00	1.00E+00
	GOTERM_BP_FAT	modification-dependent protein catabolic process	3	1.00E+00	1.00E+00
	GOTERM_BP_FAT	cellular macromolecule catabolic process	4	1.00E+00	1.00E+00

Table E5 (Continued)

	GOTERM_BP_FAT	proteolysis involved in cellular protein catabolic process	3	1.00E+00	1.00E+00
	GOTERM_BP_FAT	cellular protein catabolic process	3	1.00E+00	1.00E+00
	GOTERM_BP_FAT	protein catabolic process	3	1.00E+00	1.00E+00
Annotation Cluster 79	**Enrichment Score: 0**	**GO Term/Keyword**	**Count**	**P-Value**	**Benjamini**
	SMART	ZnF_C4	3	1.00E+00	1.00E+00
	SMART	HOLI	3	1.00E+00	1.00E+00
	INTERPRO	Zinc finger, nuclear hormone receptor-type	3	1.00E+00	1.00E+00
	INTERPRO	Zinc finger, NHR/GATA-type	3	1.00E+00	1.00E+00
	INTERPRO	Nuclear hormone receptor, ligand-binding, core	3	1.00E+00	1.00E+00
	GOTERM_MF_FAT	steroid hormone receptor activity	3	1.00E+00	1.00E+00
	GOTERM_MF_FAT	ligand-dependent nuclear receptor activity	3	1.00E+00	1.00E+00
Annotation Cluster 80	**Enrichment Score: 0**	**GO Term/Keyword**	**Count**	**P-Value**	**Benjamini**
	GOTERM_BP_FAT	morphogenesis of an epithelium	9	1.00E+00	1.00E+00
	GOTERM_BP_FAT	epithelium development	9	1.00E+00	1.00E+00
	GOTERM_BP_FAT	tissue morphogenesis	9	1.00E+00	1.00E+00
Annotation Cluster 81	**Enrichment Score: 0**	**GO Term/Keyword**	**Count**	**P-Value**	**Benjamini**
	GOTERM_MF_FAT	cation binding	108	1.00E+00	1.00E+00
	GOTERM_MF_FAT	ion binding	108	1.00E+00	1.00E+00
	GOTERM_MF_FAT	metal ion binding	100	1.00E+00	1.00E+00
Annotation Cluster 82	**Enrichment Score: 0**	**GO Term/Keyword**	**Count**	**P-Value**	**Benjamini**
	GOTERM_MF_FAT	adenyl nucleotide binding	47	1.00E+00	1.00E+00
	GOTERM_MF_FAT	purine nucleoside binding	47	1.00E+00	1.00E+00
	GOTERM_MF_FAT	nucleoside binding	47	1.00E+00	1.00E+00
	GOTERM_MF_FAT	purine nucleotide binding	47	1.00E+00	1.00E+00
	GOTERM_MF_FAT	nucleotide binding	56	1.00E+00	1.00E+00
Annotation Cluster 83	**Enrichment Score: 0**	**GO Term/Keyword**	**Count**	**P-Value**	**Benjamini**
	GOTERM_BP_FAT	oviposition	4	1.00E+00	1.00E+00
	GOTERM_BP_FAT	reproductive behavior in a multicellular organism	4	1.00E+00	1.00E+00
	GOTERM_BP_FAT	reproductive behavior	4	1.00E+00	1.00E+00
	GOTERM_BP_FAT	behavior	5	1.00E+00	1.00E+00
Annotation Cluster 84	**Enrichment Score: 0**	**GO Term/Keyword**	**Count**	**P-Value**	**Benjamini**
	GOTERM_MF_FAT	ATP binding	33	1.00E+00	1.00E+00
	GOTERM_MF_FAT	adenyl ribonucleotide binding	33	1.00E+00	1.00E+00
	GOTERM_MF_FAT	ribonucleotide binding	33	1.00E+00	1.00E+00
	GOTERM_MF_FAT	purine ribonucleotide binding	33	1.00E+00	1.00E+00
Annotation Cluster 85	**Enrichment Score: 0**	**GO Term/Keyword**	**Count**	**P-Value**	**Benjamini**
	GOTERM_BP_FAT	regulation of transcription, DNA-dependent	9	1.00E+00	1.00E+00
	GOTERM_BP_FAT	regulation of RNA metabolic process	9	1.00E+00	1.00E+00
	GOTERM_MF_FAT	transcription factor activity	7	1.00E+00	1.00E+00

Table E5 (Continued)

	GOTERM_BP_FAT	regulation of transcription	9	1.00E+00	1.00E+00

Table E6. Aging-related genes regulated by HSF-1 in a HS-dependent manner.

Gene Name	log_2 Fold [*hsf-1*(+);+HS vs. control]
F44E5.5	8.06
F44E5.4	7.87
R11A5.3	7.37
hsp-16.11	7.31
hsp-70	7.15
hsp-16.1	6.90
hsp-16.49	6.50
col-149	3.01
col-143	2.55
col-80	2.44
col-129	2.43
col-140	2.40
col-139	2.37
col-142	2.34
col-93	2.32
col-160	2.30
F49E12.9	2.29
cnc-4	2.25
col-159	2.22
F46F2.3	2.18
col-19	2.17
col-81	2.16
col-94	2.14
col-122	2.13
ugt-63	2.13
col-92	2.11
col-20	2.11
col-179	2.08
col-178	2.07
col-7	2.06
col-146	2.06
col-62	2.03
col-181	2.02
col-168	2.01
col-98	1.99
col-8	1.99
col-126	1.99
col-184	1.99
col-101	1.98
K01C8.1	1.95
col-144	1.91
dpy-3	1.90
col-117	1.89
tni-3	1.89
col-10	1.88
col-133	1.84
col-125	1.74
B0238.12	1.73
C49G7.3	1.68
T25B9.1	1.67
phat-3	1.64
C53D6.7	1.64
col-180	1.64
dpy-4	1.64
sams-1	1.62
col-145	1.62
nlp-26	1.60
col-107	1.59
col-157	1.59
far-2	1.56
dpy-13	1.54
sqt-1	1.54
haao-1	1.53
col-12	1.53
col-88	1.53
col-38	1.50
unc-15	1.48
col-138	1.47
ZK1307.1	1.46
col-130	1.46
col-17	1.45
F46H5.3	1.45
col-13	1.44
col-63	1.44
grd-3	1.43
T21G5.2	1.41
col-175	1.41
fat-6	1.38
col-77	1.38
col-156	1.38
col-141	1.38
tnt-2	1.37
col-161	1.37
T25F10.6	1.37
T21F4.1	1.36
srp-1	1.36
F37H8.5	1.36
csq-1	1.34
flu-2	1.33
dpy-7	1.33
C06A8.3	1.32
col-60	1.32
sqt-2	1.29
dim-1	1.29
col-154	1.28
tag-18	1.28
col-120	1.28
pfn-3	1.27
col-97	1.26
ZK1058.9	1.25
C36C5.5	1.25
pmt-2	1.25
cpn-3	1.23
R13H4.2	1.23
col-91	1.23
T13F3.6	1.23
ttr-18	1.21
T05E7.1	1.21
F09E10.1	1.21
gpd-3	1.19
T22B7.7	1.17
col-14	1.17
fip-5	1.16
C49F5.7	1.16
C01B10.3	1.15
F25E2.2	1.14
lec-5	1.14
ttr-6	1.12
nlp-27	1.12
F20G2.2	1.11

Table E6 (Continued)

Gene Name	log_2 Fold [*hsf-1*(+);+HS vs. control]
lec-2	1.10
catp-3	1.10
dpy-8	1.09
unc-27	1.09
col-34	1.09
col-155	1.08
elo-5	1.08
ttr-16	1.08
ttr-20	1.08
gstk-1	1.08
cnc-3	1.07
elo-2	1.07
C16A3.10	1.02
col-68	1.02
col-118	1.02
ptr-18	1.02
gst-36	1.00
gst-13	1.00
D1054.8	1.00
mif-2	0.98
T19B10.2	0.98
Y37D8A.2	0.97
cnc-8	0.97
F16B4.4	0.97
cdo-1	0.96
R07E4.3	0.96
gst-42	0.94
M02D8.1	0.93
far-6	0.92
ckb-2	0.92
ifa-1	0.92
heh-1	0.89
ugt-44	0.89
ZK1321.4	0.88
F09B12.3	0.86
pah-1	0.85
W09G12.7	-3.28
tsp-1	-2.81
lys-3	-1.79
irg-2	-1.75

Gene Name	log_2 Fold [*hsf-1*(+);+HS vs. control]
fbxa-24	-1.72
C50F7.5	-1.70
T28H10.3	-1.54
best-5	-1.53
dpf-6	-1.26
rde-1	-1.25
DH11.2	-1.16
B0001.2	-1.13
T04C4.1	-1.12
F02H6.2	-1.09
icl-1	-1.06
C18A11.1	-1.04
K02D7.1	-1.00
K09H11.7	-0.97

Table E7. Aging-related genes regulated by HSF-1 in a HS-independent manner.

Gene Name	log_2 Fold [control vs. *hsf-1*(-);+HS]
col-158	5.00
B0507.8	4.62
tsp-1	4.55
B0284.1	4.43
fbxa-30	4.11
C50F7.5	3.94
F15B9.6	3.35
C17H1.7	3.32
H02F09.3	3.07
T19D12.4	2.92
W09G12.7	2.70
lys-3	2.49
T28B11.1	2.12
ZC443.4	1.51
sodh-1	1.50
fbxa-24	1.48
T12G3.1	1.40
fbxa-60	1.36
F20C5.3	1.29
T28H10.3	1.28
ZK1055.7	1.16
Y56A3A.16	1.54
F22E5.6	3.41
dod-19	1.32
F18A1.7	1.12
ugt-8	1.43
T04F3.2	1.45
fbxa-182	1.29
ZC308.4	1.07
vhp-1	1.02
T04C4.1	1.39
ttm-4	1.07
B0238.13	2.45
C49C3.9	1.03
unc-53	1.05
nhr-2	1.65
clec-87	0.99
Y43F8C.6	1.17
clec-91	0.96
dct-17	0.90

Gene Name	log_2 Fold [control vs. *hsf-1*(-);+HS]
cyp-35B1	1.03
tag-278	0.92
clec-88	0.81
tbb-6	3.35
scav-2	0.99
best-13	0.93
zfp-1	0.85
rec-8	0.85
npp-7	0.79
dpf-6	1.08
ntl-9	0.93
str-7	1.10
attf-6	0.82
F29G9.1	1.50
gna-2	0.79
acdh-1	-6.98
Y40H7A.10	-4.48
vit-1	-3.72
F54F7.2	-3.65
vit-5	-3.55
spp-4	-3.05
pmp-5	-3.02
F15E11.1	-2.97
folt-2	-2.84
lips-14	-2.66
lys-4	-2.63
C36C5.5	-2.61
F09E10.1	-2.55
K10B2.2	-2.54
ugt-22	-2.51
Y38F1A.6	-2.41
T13F3.6	-2.38
cyp-35A2	-2.31
elo-5	-2.25
ckb-2	-2.24
tbh-1	-2.22
cyp-25A1	-2.22
clec-160	-2.19
ugt-47	-2.19
elo-6	-2.11

Gene Name	log_2 Fold [control vs. *hsf-1*(-);+HS]
fat-7	-2.10
F42A10.7	-2.10
clec-56	-2.08
Y57G11B.5	-2.06
cyp-35A3	-2.05
T05E12.6	-2.02
gst-13	-2.01
K10C2.3	-2.01
spp-3	-1.99
dhs-21	-1.98
F18E2.1	-1.92
gst-4	-1.91
C15C8.3	-1.88
dct-11	-1.87
col-68	-1.87
T05E7.1	-1.86
clec-186	-1.84
dod-24	-1.82
K12H4.7	-1.81
cyp-25A2	-1.80
col-120	-1.79
R102.4	-1.78
clec-97	-1.76
pcp-1	-1.75
tag-10	-1.72
col-88	-1.71
F36A2.12	-1.71
ZC373.2	-1.71
W02D9.7	-1.71
F55G11.8	-1.69
H20E11.3	-1.68
cpl-1	-1.68
clec-66	-1.66
F49E12.1	-1.65
hsp-16.11	-1.65
F57F5.1	-1.62
ZK813.3	-1.62
col-175	-1.62
pfd-4	-1.62
cyp-34A9	-1.62

Table E7 (Continued)

Gene Name	log_2 Fold [control vs. *hsf-1*(-);+HS]
C05D12.4	-1.61
hpo-18	-1.59
D1054.8	-1.58
hsp-16.1	-1.57
F13H8.3	-1.57
F53H4.2	-1.55
col-60	-1.54
Y62H9A.6	-1.54
col-138	-1.51
ech-6	-1.51
hsp-16.49	-1.51
C08F11.11	-1.51
cpr-5	-1.50
nlp-26	-1.50
cbl-1	-1.49
col-63	-1.49
C30G12.2	-1.48
lbp-6	-1.46
lys-2	-1.46
F28H7.3	-1.45
cdr-6	-1.45
R07E4.3	-1.45
col-38	-1.42
ttr-15	-1.42
C49F5.7	-1.41
fip-5	-1.40
spp-8	-1.40
cpr-6	-1.40
col-77	-1.39
clec-57	-1.38
F32H5.1	-1.37
F54D5.4	-1.37
haao-1	-1.34
ftn-2	-1.33
C44C1.5	-1.31
irg-3	-1.31
ZK1307.1	-1.31
F48D6.4	-1.29
msra-1	-1.28
D1086.3	-1.25

Gene Name	log_2 Fold [control vs. *hsf-1*(-);+HS]
trap-2	-1.25
pfd-6	-1.25
aqp-10	-1.25
clec-52	-1.24
T10B5.7	-1.24
C15H9.9	-1.24
F07H5.3	-1.23
F37C4.6	-1.22
col-91	-1.22
elo-2	-1.19
R09H10.3	-1.19
flu-2	-1.19
C29F7.3	-1.19
Y66H1A.5	-1.18
F15E11.12	-2.80
asp-3	-1.60
lys-8	-1.54
daf-36	-1.34
cnc-8	-1.27
amx-3	-1.36
T25B9.1	-1.22
B0272.3	-1.13
ttr-46	-1.11
clec-222	-1.84
spp-5	-1.33
Y40D12A.2	-1.14
ssp-37	-1.57
thn-2	-1.33
gst-36	-1.26
amt-4	-1.15
clec-49	-1.08
F42G8.10	-1.05
pmt-2	-1.26
col-130	-1.17
Y62H9A.3	-1.14
acs-1	-1.13
C39D10.7	-1.04
col-76	-1.13
C35B1.5	-1.08
C25A8.4	-1.05

Gene Name	log_2 Fold [control vs. *hsf-1*(-);+HS]
F20G2.2	-1.04
Y62H9A.4	-1.04
apy-1	-1.01
F08A8.4	-1.25
pgrn-1	-1.01
daf-22	-1.01
mif-2	-1.14
K01C8.1	-1.04
F13H6.3	-1.06
gstk-1	-1.04
C26B9.5	-1.02
F13D12.6	-1.27
lbp-3	-1.01
C07D8.6	-1.01
F32A5.3	-1.19
Y45F10C.4	-1.19
D1086.7	-1.00
B0281.5	-2.08
K04G2.10	-1.13
nlp-29	-1.06
frh-1	-1.07
lpd-9	-0.98
col-161	-1.09
sqt-1	-0.99
nlp-27	-0.94
ant-1.4	-1.10
asp-2	-1.04
ZK899.2	-0.98
F23C8.5	-0.97
dpy-13	-1.07
ttr-47	-0.98
F37C12.3	-1.29
dpy-4	-1.08
erd-2	-0.94
C04E12.2	-1.19
gst-42	-0.94
C46C11.2	-1.18
sur-5	-0.90
clec-65	-0.93
Y45F10C.2	-1.03

Table E7 (Continued)

Gene Name	log_2 Fold [control vs. *hsf-1*(-);+HS]
R12C12.1	-1.02
ugt-44	-0.87
F56F10.1	-0.85
col-97	-0.94
cpt-4	-0.89
C29F3.7	-0.86
dod-17	-0.96
C42D4.1	-0.94
F27E5.1	-0.98
C31G12.1	-1.37
C17H12.8	-0.83
sqt-2	-0.85
F08G5.6	-0.82
gta-1	-0.91
F37H8.3	-0.89
grd-5	-0.83
Y69E1A.5	-0.82
asg-1	-0.79
T24C12.3	-0.89
cdo-1	-0.83
F44A6.5	-1.10
nuc-1	-0.82
T21H3.1	-1.20
F10E9.5	-0.87
F47B8.8	-0.86
tag-18	-0.79
col-133	-0.93
ugt-23	-0.82
pes-23	-0.86
asp-5	-0.90
C01H6.4	-0.79
ZC376.2	-0.84
acs-5	-0.76
heh-1	-0.77
C14C6.5	-0.78

APPENDIX F: SUPPORTING FIGURES AND TABLES FOR CHAPTER 7. HSF-1 IS A REGULATOR OF MIRNA EXPRESSION IN CAENORHABDITIS ELEGANS

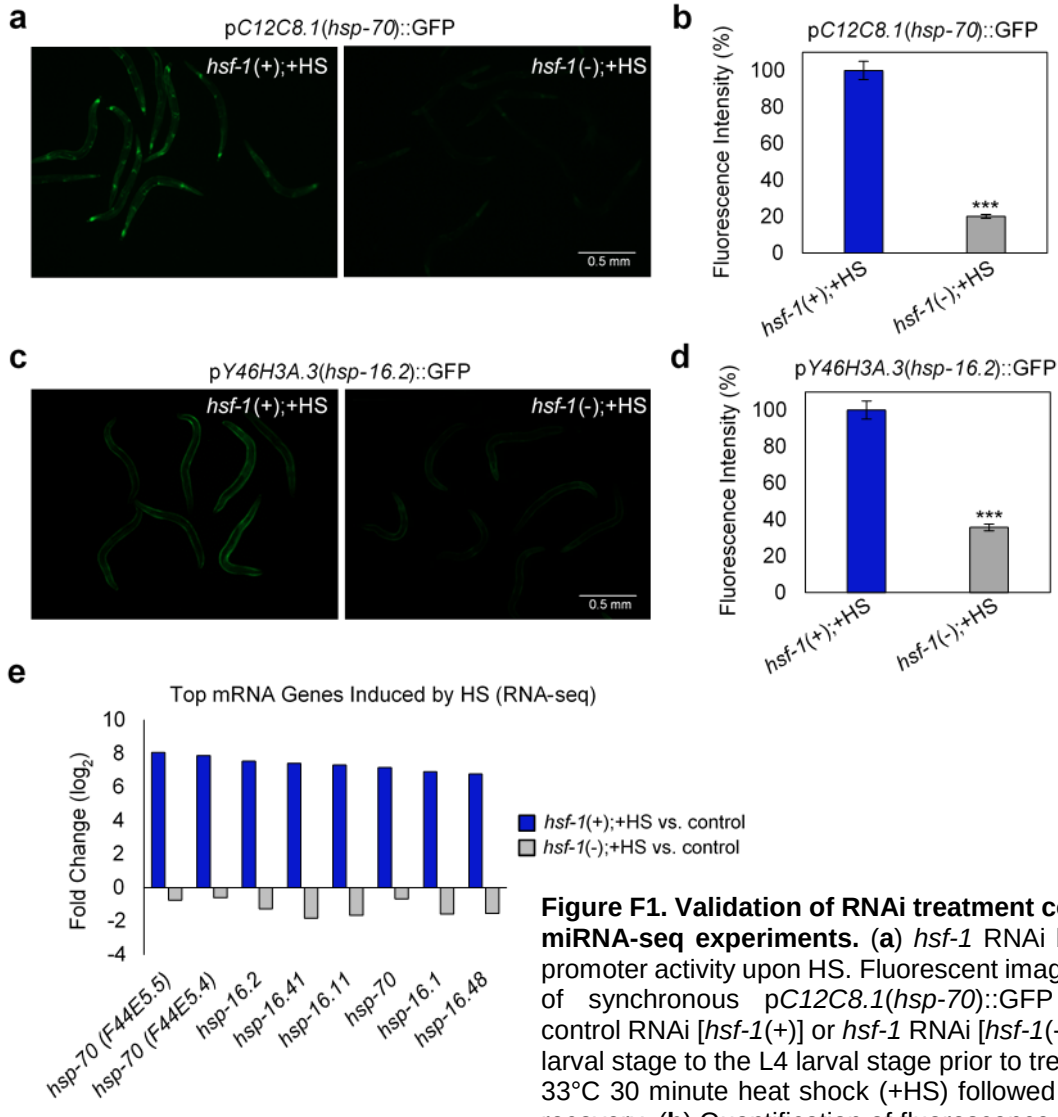

Figure F1. Validation of RNAi treatment conditions for miRNA-seq experiments. (**a**) *hsf-1* RNAi blunts *hsp-70* promoter activity upon HS. Fluorescent images are shown of synchronous p*C12C8.1*(*hsp-70*)::GFP worms fed control RNAi [*hsf-1*(+)] or *hsf-1* RNAi [*hsf-1*(-)] from the L1 larval stage to the L4 larval stage prior to treatment with a 33°C 30 minute heat shock (+HS) followed by a 12 hour recovery. (**b**) Quantification of fluorescence intensity confirms that *hsf-1* RNAi blunts *hsp-70* promoter activity upon HS. Quantification of the fluorescent images in (**a**) demonstrate *hsf-1* RNAi decreases *hsp-70* promoter activity by ~80%. (**c**) *hsf-1* RNAi blunts *hsp-16.2* promoter activity upon HS. Fluorescent images are shown of synchronous p*Y46H3A.3*(*hsp-16.2*)::GFP worms fed control RNAi [*hsf-1*(+)] or *hsf-1* RNAi [*hsf-1*(-)] from the L1 larval stage to the L4 larval stage prior to treatment with a 33°C 30 minute heat shock (+HS) followed by a 12 hour recovery. (**d**) Quantification of fluorescence intensity confirms that *hsf-1* RNAi blunts *hsp-16.2* promoter activity upon HS. Quantification of the fluorescent images in (**c**) demonstrate *hsf-1* RNAi decreases *hsp-16.2* promoter activity ~60%. (**e**) Heat shock protein genes are the top genes induced during a 30 minute 33°C HS. mRNA-seq performed in parallel to miRNA-seq shows that *hsp* genes--

Figure F1. Validation of RNAi treatment conditions for miRNA-seq experiments. (Continued) are the highest induced group of genes in response to HS, and shows these genes are dependent on HSF-1, further validating our experimental conditions. For (**b,d**), error bars represent standard deviation and significance was determined with the Bonferroni post-test where '***';q-value<0.001.

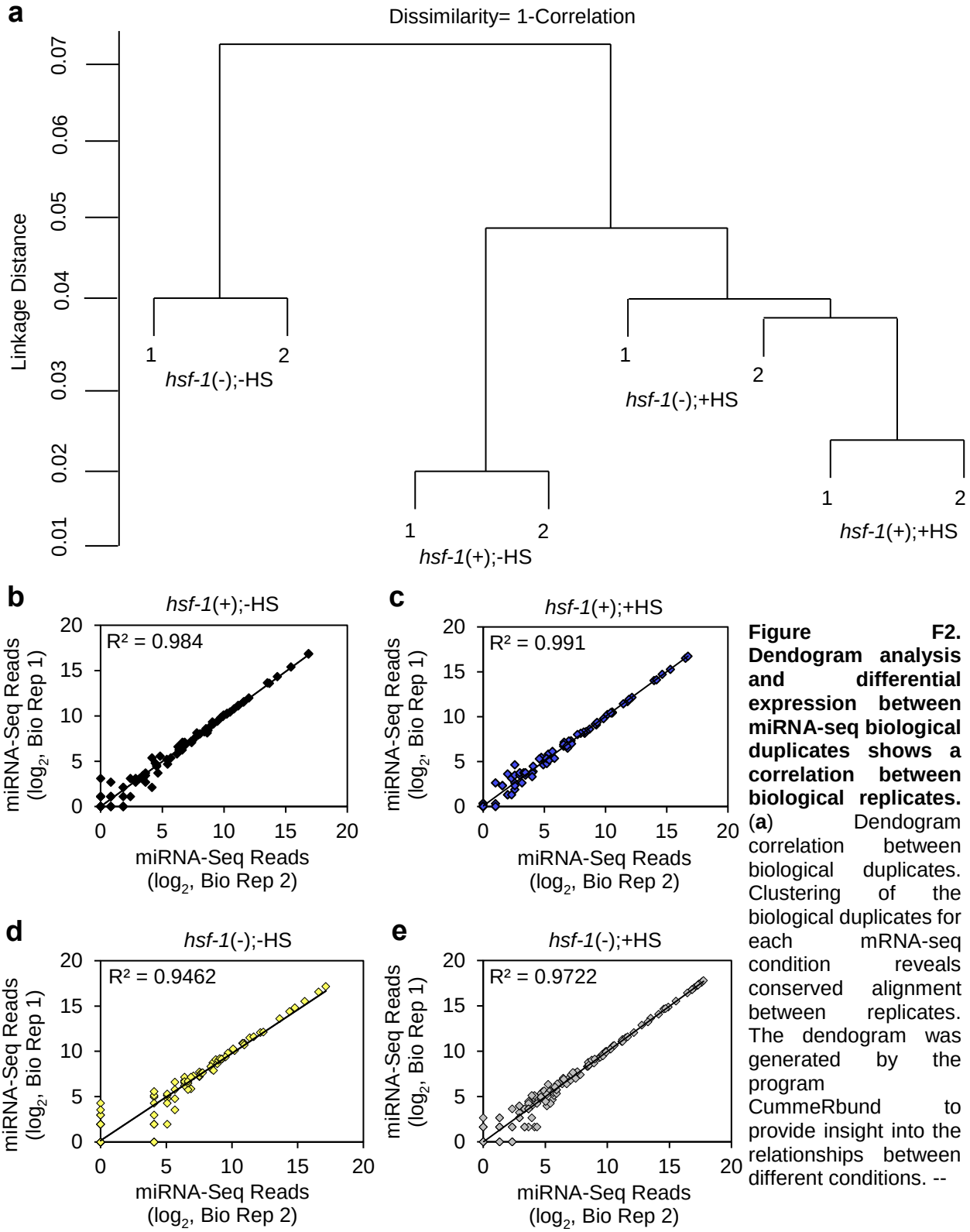

Figure F2. Dendogram analysis and differential expression between miRNA-seq biological duplicates shows a correlation between biological replicates. (**a**) Dendogram correlation between biological duplicates. Clustering of the biological duplicates for each mRNA-seq condition reveals conserved alignment between replicates. The dendogram was generated by the program CummeRbund to provide insight into the relationships between different conditions. --

Figure F2. Dendogram analysis and differential expression between miRNA-seq biological duplicates shows a correlation between biological replicates. (Continued) (**b-e**) Differential expression analysis shows little deviation between biological duplicates. Scatter plots of the miRNA-seq reads for each biological replicate, for each condition, shows similarities between biological duplicates. The x-axis is representative of the reads from the first biological replicate, and the y-axis represents reads from the second biological replicate. The closer the R^2 value is to 1, and the closer each point is to the line, is representative of similarity between replicates.

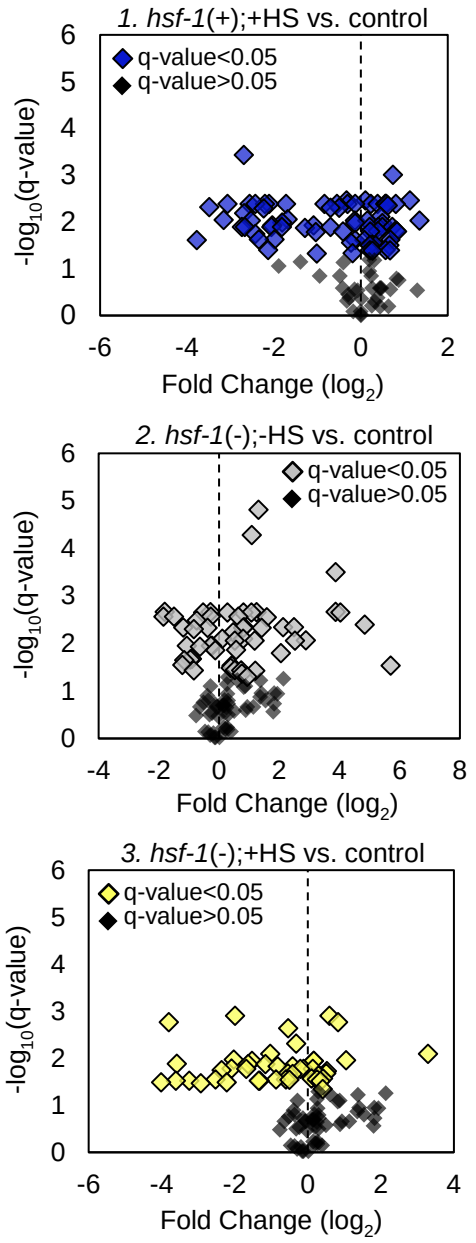

Figure F3. Volcano plots for each miRNA-seq condition relative to the control. Volcano plots show all unchanged (q-value>0.05) and significantly altered (q-value<0.05) miRNAs, relative to the *hsf-1*(+);-HS control. The q-value is the FDR-adjusted p-value of the test statistic as determined by the Benjamini-Hochberg correction for multiple testing.

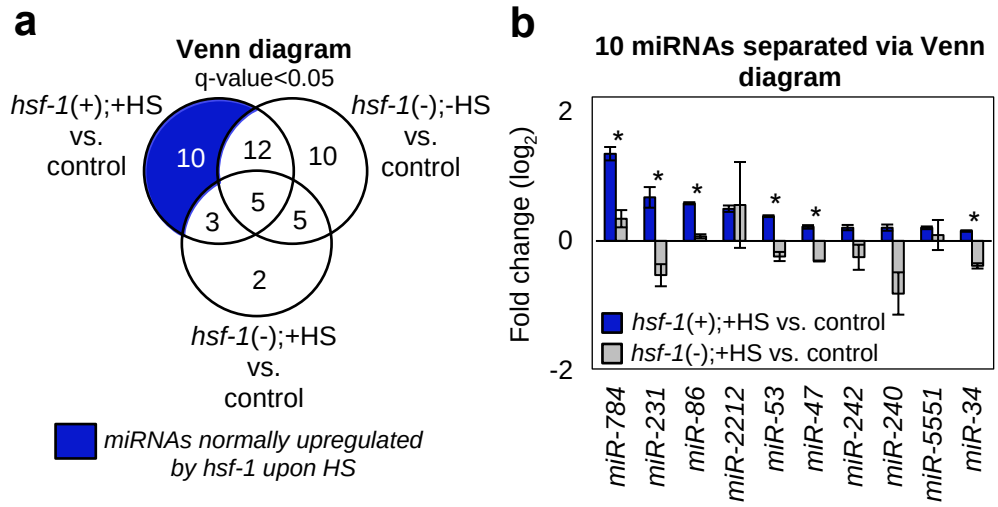

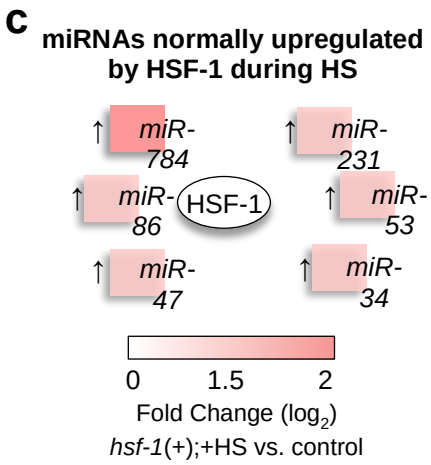

Figure F4. miRNAs normally upregulated by HSF-1 during HS. (**a**) Venn diagram of the miRNAs significantly upregulated as compared to the control. The Venn diagram shows the overlap among miRNAs that were found to be significantly upregulated (q-value<0.05) as compared to the *hsf-1*(+);-HS control for each of the indicated comparisons between samples. The blue shaded region represents miRNAs that are regulated by *hsf-1* during HS. The q-value is the FDR-adjusted p-value of the test statistic as determined by the Benjamini-Hochberg correction for multiple testing (**b**) Relative abundance of the miRNAs normally upregulated by HSF-1 upon HS. The $\log_2$ fold change from the miRNA-seq data, of the miRNAs determined via Venn diagram to be regulated by HSF-1 upon HS as compared to the *hsf-1*(+);-HS control, shows the miRNAs determined to be significantly different compared to each treatment condition. Significance was determined with the Benjamini-Hochberg correction where '*';q-value<0.05. (**c**) miRNAs determined to normally be upregulated by HSF-1 during HS. The miRNAs that had a significant difference between the *hsf-1*(+);+HS and *hsf-1*(-);+HS treatment conditions in (**b**), as determined by the Benjamini-Hochberg correction for multiple testing, are listed.

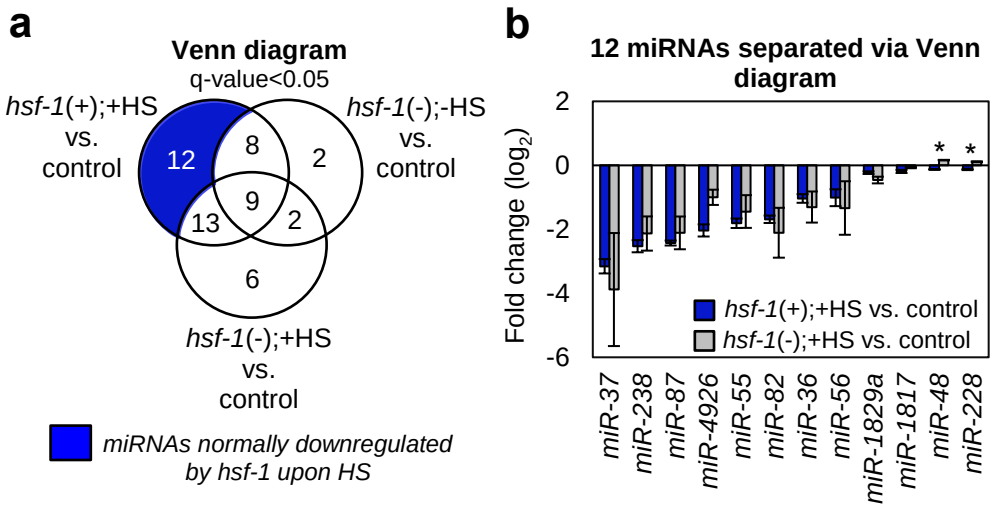

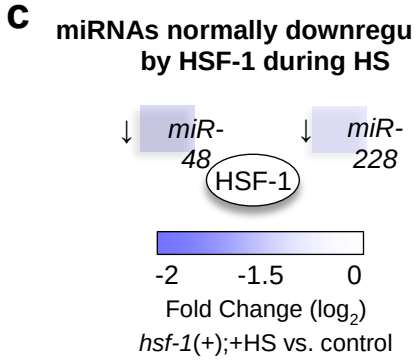

Figure F5. miRNAs normally downregulated by HSF-1 during HS. (**a**) Venn diagram of the miRNAs significantly downregulated compared to the control. The Venn diagram shows the overlap among miRNAs that were found to be significantly downregulated (q-value<0.05) as compared to the *hsf-1*(+);-HS control for each of the indicated comparisons between samples. The blue shaded region represents miRNAs that are normally downregulated by *hsf-1* during HS. The q-value is the FDR-adjusted p-value of the test statistic as determined by the Benjamini-Hochberg correction for multiple testing (**b**) Relative abundance of the miRNAs normally downregulated by HSF-1 upon HS. The $\log_2$ fold change from the miRNA-seq data, of the miRNAs determined via Venn diagram to be regulated by HSF-1 upon HS as compared to the *hsf-1*(+);-HS control, shows the miRNAs determined to be significantly different compared to each treatment condition. Significance was determined with the Benjamini-Hochberg correction where '*';q-value<0.05. (**c**) miRNAs determined to normally be downregulated by HSF-1 during HS. The miRNAs that had a significant difference between the *hsf-1*(+);+HS and *hsf-1*(-);+HS treatment conditions in (**b**) as determined by the Benjamini-Hochberg correction for multiple testing are listed.

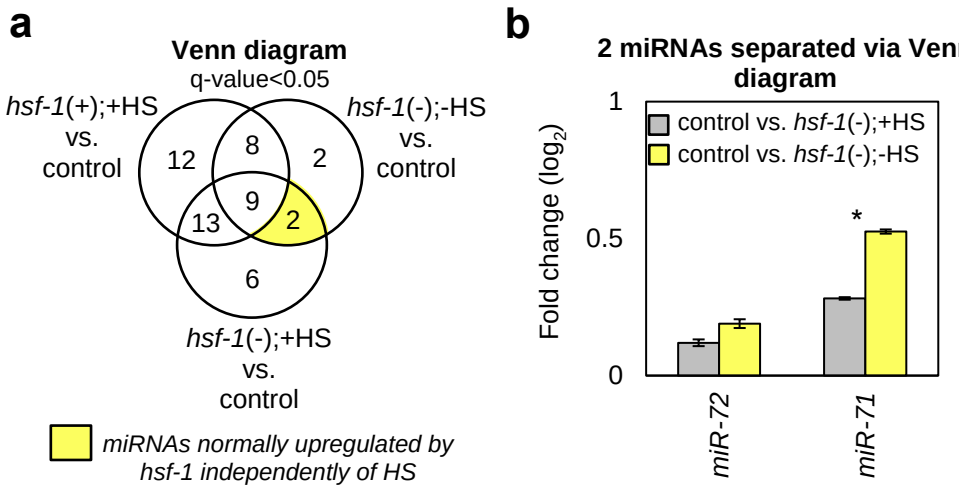

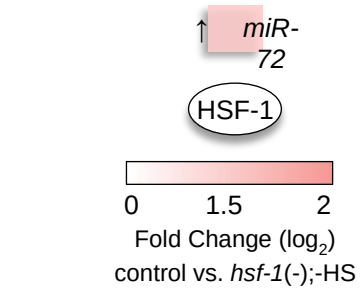

Figure F6. miRNAs normally upregulated by HSF-1 independently of HS. (**a**) Venn diagram of the miRNAs significantly upregulated as compared to the control. The Venn diagram shows the overlap among miRNAs that were found to be significantly downregulated (q-value<0.05) as compared to the *hsf-1*(+);-HS control for each of the indicated comparisons between samples. A miRNA that is downregulated in response to *hsf-1* RNAi is considered to normally be upregulated by HSF-1. The yellow shaded region thus represents miRNAs that are normally upregulated by *hsf-1* independently of HS. The q-value is the FDR-adjusted p-value of the test statistic as determined by the Benjamini-Hochberg correction for multiple testing (**b**) Relative abundance of the miRNAs normally upregulated by HSF-1 independently of HS. The $\log_2$ fold change from the miRNA-seq data, of the miRNAs determined via Venn diagram to be regulated by HSF-1 independently of HS as compared to the *hsf-1*(+);-HS control, shows the miRNAs determined to be significantly different compared to each treatment condition. Significance was determined with the Benjamini-Hochberg correction where '*';q-value<0.05. (**c**) miRNAs determined to normally be upregulated by HSF-1 independently of HS. The miRNAs that did not have a significant difference between the *hsf-1*(-);+HS and *hsf-1*(-);-HS treatment conditions in (**b**), as determined by the Benjamini-Hochberg correction for multiple testing, are listed.

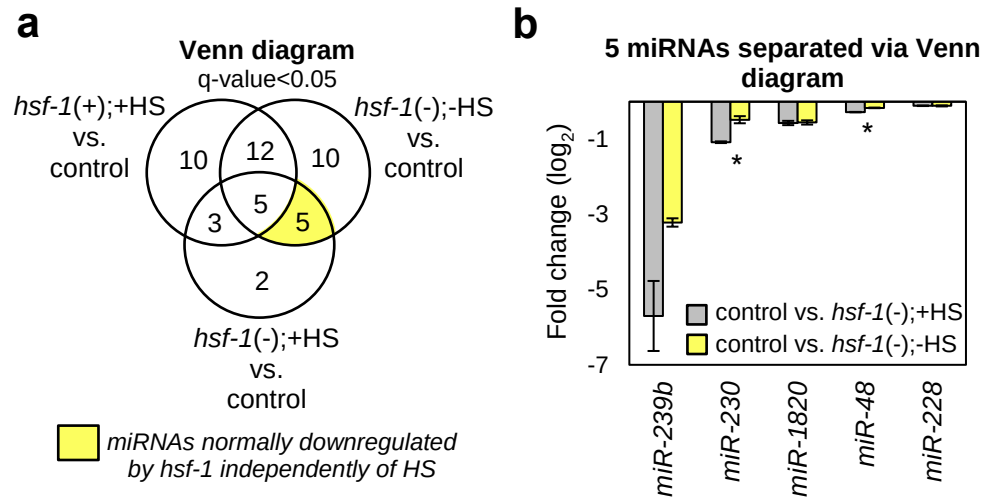

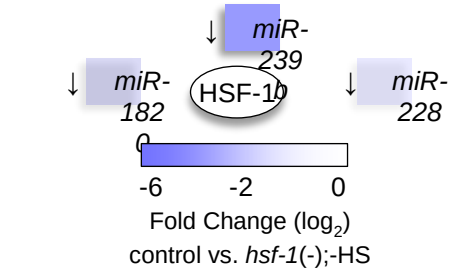

Figure F7. miRNAs normally downregulated by HSF-1 independently of HS. (**a**) Venn diagram of the miRNAs significantly downregulated as compared to the control. The Venn diagram shows the overlap among miRNAs that were found to be significantly upregulated (q-value<0.05) as compared to the *hsf-1*(+);-HS control for each of the indicated comparisons between samples. A miRNA that is upregulated in response to *hsf-1* RNAi is considered to normally be downregulated by HSF-1. The yellow shaded region thus represents miRNAs that are normally downregulated by *hsf-1* independently of HS. The q-value is the FDR-adjusted p-value of the test statistic as determined by the Benjamini-Hochberg correction for multiple testing (**b**) Relative abundance of the miRNAs normally downregulated by HSF-1 independently of HS. The $\log_2$ fold change from the miRNA-seq data, of the miRNAs determined via Venn diagram to be regulated by HSF-1 independently of HS as compared to the *hsf-1*(+);-HS control, shows the miRNAs determined to be significantly different compared to each treatment condition. Significance was determined with the Benjamini-Hochberg correction where '*';q-value<0.05. (**c**) miRNAs determined to normally be downregulated by HSF-1 independently of HS. The miRNAs that did not have a significant difference between the *hsf-1*(+);+HS and *hsf-1*(-);+HS treatment conditions in (**b**), as determined by the Benjamini-Hochberg correction for multiple testing, are listed.

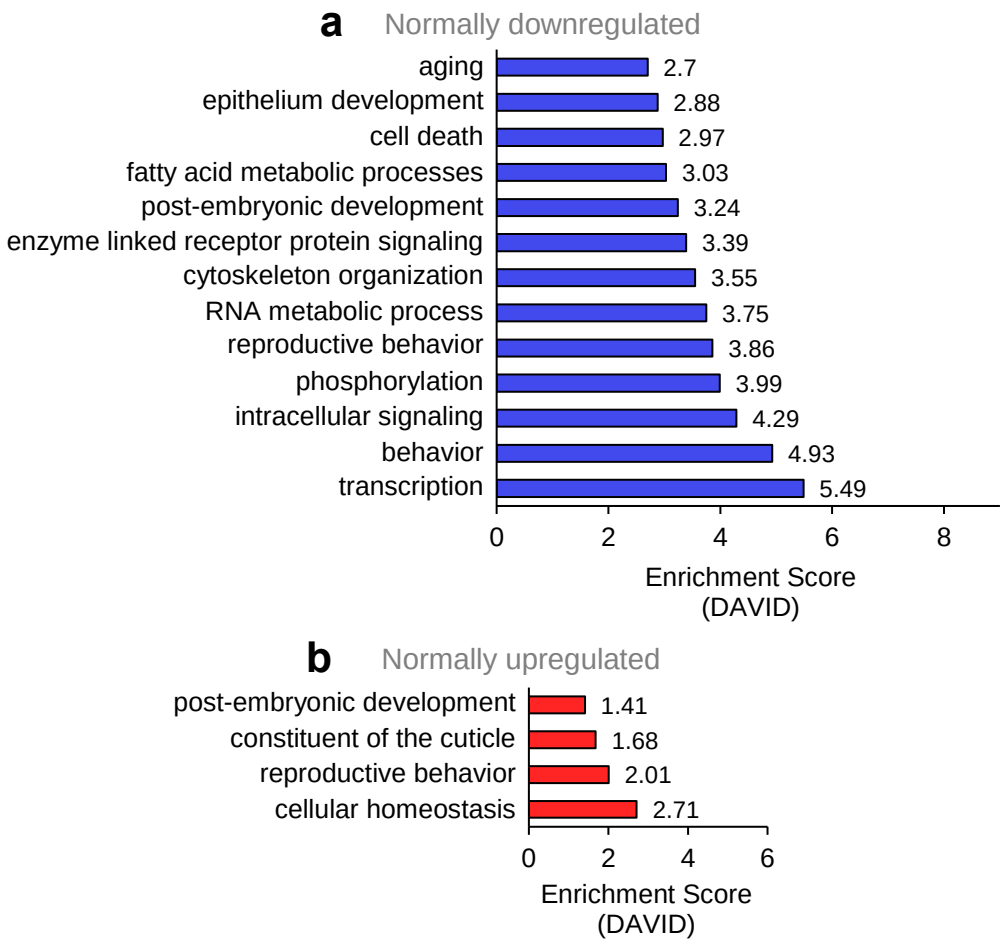

Figure F8. Biological processes enriched by HSF-1-regulated miRNAs during HS. (**a**) Processes normally downregulated by HSF-1-regulated miRNAs during HS. The genes predicted to be suppressed by HSF-1-regulated miRNAs during HS were classified by Gene Ontology terms using DAVID. Processes with an enrichment score>~2.5 are listed. (**b**) Processes normally upregulated by HSF-1-regulated miRNAs during HS. The genes predicted to be induced by HSF-1-regulated miRNAs during HS were classified by Gene Ontology terms using DAVID. The top 4 processes are listed.

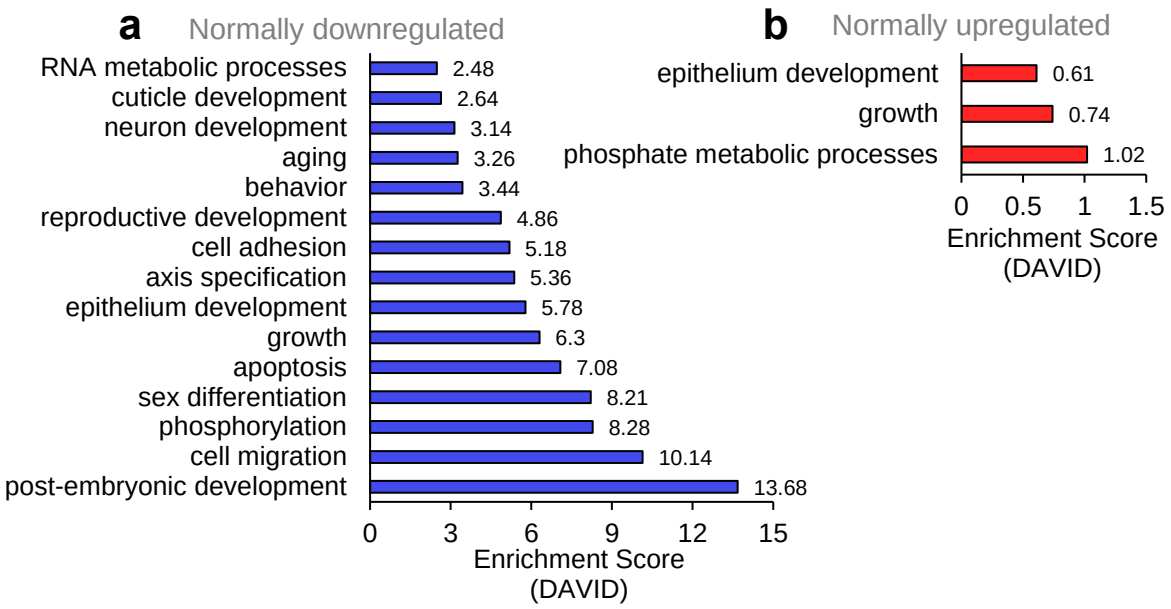

Figure F9. Biological processes enriched by HSF-1-regulated miRNAs independently of HS. (**a**) Processes normally downregulated by HSF-1-regulated miRNAs independently of HS. The genes predicted to be suppressed by HSF-1-regulated miRNAs independently of HS were classified by Gene Ontology terms using DAVID. Processes with an enrichment score>~2.48 are listed. (**b**) Processes normally upregulated by HSF-1-regulated miRNAs independently of HS. The genes predicted to be induced by HSF-1-regulated miRNAs during HS were classified by Gene Ontology terms using DAVID. The top 3 processes are listed.

Table F1. Significantly altered miRNAs in the hsf-1(+);+HS treatment condition compared to the control.

Name	log_2 Fold *hsf-1*(+);+HS vs control
miR-784	1.35
miR-355	1.13
miR-1829c	0.83
miR-62	0.80
miR-794	0.74
miR-46	0.72
miR-5592	0.68
miR-231	0.67
miR-65	0.62
miR-86	0.58
miR-84	0.58
miR-232	0.57
miR-63	0.56
miR-2212	0.50
miR-229	0.50
miR-66	0.45
lin-4	0.40
miR-52	0.39
miR-53	0.38
miR-237	0.34
miR-1022	0.27
miR-4816	0.27
miR-239a	0.23
miR-47	0.22
miR-242	0.21
miR-240	0.21
miR-5551	0.20
miR-34	0.15
miR-80	0.11
miR-259	0.08
miR-228	-0.13
miR-48	-0.13
miR-50	-0.13
miR-241	-0.14
miR-1817	-0.19
miR-1829a	-0.23
let-7	-0.31
miR-57	-0.33
miR-51	-0.41
miR-64	-0.50

Name	log_2 Fold *hsf-1*(+);+HS vs control
miR-61	-0.55
miR-75	-0.70
miR-252	-0.70
miR-83	-0.83
miR-56	-1.01
miR-36	-1.04
miR-58	-1.08
miR-795	-1.29
miR-82	-1.69
miR-2214	-1.72
miR-55	-1.81
miR-90	-1.82
miR-235	-1.99
miR-4926	-2.03
miR-45	-2.06
miR-73	-2.11
miR-74	-2.13
miR-77	-2.21
miR-35	-2.24
miR-4813	-2.34
miR-87	-2.43
miR-44	-2.43
miR-238	-2.53
miR-250	-2.56
miR-42	-2.67
miR-40	-2.69
miR-54	-2.69
miR-39	-2.74
miR-41	-3.07
miR-37	-3.15
miR-246	-3.49
miR-67	-3.78

Table F2. Significantly altered miRNAs in the hsf-1(-);+HS treatment condition compared to the control

Name	log_2 Fold *hsf-1*(-);+HS vs control
miR-239b	3.21
miR-239a	1.02
miR-1830	0.84
miR-84	0.60
miR-1820	0.55
miR-63	0.49
miR-230	0.48
miR-229	0.46
miR-65	0.32
miR-62	0.32
miR-1829c	0.23
miR-236	0.18
miR-48	0.16
miR-66	0.15
miR-228	0.11
miR-241	-0.11
miR-72	-0.19
miR-47	-0.31
miR-34	-0.39
miR-355	-0.43
miR-795	-0.45
miR-75	-0.51
miR-71	-0.53
miR-790	-0.66
miR-83	-0.87
miR-79	-0.95
miR-61	-1.00
miR-90	-1.21
miR-235	-1.46
miR-38	-1.49
miR-2214	-1.58
miR-250	-1.70
miR-74	-1.79
miR-73	-1.97
miR-35	-2.00
miR-77	-2.08
miR-45	-2.30
miR-54	-2.51
miR-41	-2.51
miR-44	-2.93
miR-4813	-3.26
miR-246	-3.33
miR-67	-3.74
miR-39	-3.83
miR-40	-4.53

Table F3. Significantly altered miRNAs in the hsf-1(-);-HS treatment condition compared to the control

Name	log_2 Fold *hsf-1*(-);-HS vs control
miR-239b	5.70
miR-85	4.84
miR-243	4.03
miR-5592	3.88
miR-1020	2.88
miR-4926	2.53
miR-239a	2.49
miR-238	2.13
miR-1	2.05
miR-62	1.59
miR-59	1.41
miR-84	1.31
miR-80	1.25
miR-794	1.21
miR-4816	1.19
miR-46	1.08
miR-230	1.08
miR-355	0.83
lin-4	0.81
miR-1022	0.80
miR-66	0.80
miR-232	0.76
miR-1829b	0.74
miR-63	0.64
miR-1820	0.57
miR-83	0.52
miR-52	0.52
miR-237	0.47
miR-54	0.41
miR-259	0.39
miR-48	0.28
miR-228	0.11
miR-72	-0.12
miR-252	-0.23
let-7	-0.27
miR-51	-0.27
miR-71	-0.28
miR-57	-0.38
miR-77	-0.53
miR-50	-0.63

Name	log_2 Fold *hsf-1*(-);-HS vs control
miR-45	-0.74
miR-4812	-0.83
miR-250	-0.84
miR-246	-0.90
miR-358	-0.92
miR-41	-0.95
miR-58	-1.07
miR-44	-1.16
miR-64	-1.19
miR-75	-1.22
miR-795	-1.49
miR-39	-1.80
miR-42	-1.85

APPENDIX G: EXTENDED PROTOCOLS

Preparing Nematode Growth Medium (NGM) Plates

Purpose: To make agar plates for the maintenance of C. elegans

1. Make the recipe below in a flask that is 2x/per volume of media

NaCl	1.5 g
Bacto-Peptone	1.25 g
Agar	10 g
diH2O	500 mL

**Autoclave a stir bar in the media*

2. Autoclave for 45 minutes and set a hotplate to 55°C
3. Allow NGM to cool to the touch on a hot plate while stirring at medium speed to prevent bubbles
4. Light a flame and sterilely add the following/500 mL of NGM:

Cholesterol (5 mg/mL)	0.5 mL
1 M $CaCl_2$	0.5 mL
1 M $MgSO_4$	0.5 mL
KH_2PO_4, pH 6.0	12.5 mL

5. Fill 100 mM plates with 20 mL or 60 mM plates with 10 mL of liquefied medium
6. Allow to dry for 10 minutes and then flip over to prevent condensation on the plate

C. elegans OP50 Protocol

Purpose: To grow and prepare E. coli as a C. elegans a food source

Day 1. Streak OP50

1. Obtain a glycerol stock of OP50 *E. coli* and keep on ice
2. Using a sterile inoculating loop, scratch off a layer of the frozen stock and spread onto an LB plate with the goal being to spread out the cells to create single colonies
3. Place the plate, lid down, at 37°C overnight

Day 2. Inoculate OP50

1. Determine the amount of OP50 required for the number of plates needed
   **50 mL will become 5 mL which will be enough for 25 100 mM plates*
2. Obtain a flask 2x the volume being made
3. Light a flame, and sterilely add LB to the flask

**Always flame the lid before and after opening a bottle of LB to prevent contamination*

4. Using an inoculating loop, pick a single colony from the plate previously streaked
5. Allow to grow over night in a 37°C shaker 12-16 hours

Day 3: Seeding NGM plates with OP50

1. Place 50 mL of turbid OP50 into a 50 mL conical and centrifuge for 10 minutes at 3,500 rpm
2. Remove enough supernatant to make a 10x stock

   **For 50 mL, leave 5 mL of supernatant*
3. Resuspend the pelleted bacteria by vortexing
4. Light a flame, and sterilely add 200 µL of bacteria to each 100 mM plate and 100 µL of bacteria to each 60 mM plate
5. Using a glass spreader, make a circular bacterial lawn in the center of the plate
6. Allow the plates to remain on the bench over night at room temperature and store at 4°C for up to 1 month

Freezing and Thawing *C. elegans*

Purpose: To preserve C. elegans strains

Freezing:

1. Chunk worms onto standard NGM plates seeded with OP50
2. Allow the worms to propagate for about 5 days until most of the population represents L1 and L2 worms

   **The early larval stages survive upon freezing*
3. Wash the plate with 5 mL of M9
4. Swirl the M9 on the plate and then tilt the plate to allow pooling to one side
5. Collect the worms in a 15 mL conical
6. Pellet the worms for 1 minute at 5,000 rpm
7. Aspirate the M9, and do at least one more 5 mL wash

   *If the liquid is cloudy due to an uptake of OP50 bacteria, do one or more 10 mL washes until clear
8. Aspirate all but 2 mL of M9
9. Re-suspend and distribute 0.5 mL to four 1.8 mL cryovials
10. Add an equal amount 30% glycerol
11. Place the cyrovials in a Styrofoam container at -80˚C over night before transferring to a cryobox

Thawing:

1. Remove a vial from the freezer and allow to thaw completely at room temperature
2. Allow worms to collect at the bottom of the tube, and pipette drops of worms onto a seeded NGM plate
3. After 2-3 days, transfer the surviving animals to separate plates and ensure that they reproduce

***C. elegans* Synchronization via Bleaching**

Purpose: To obtain a synchronous population of worms

Day 1. Synchronizing a Mixed-stage Population

1. Ensure that there are plenty of worms and gravid adults on the plates to be bleach synced
2. Add 5 mL of M9 onto the plate and begin washing the worms off of the plate
3. Transfer the worms to a 15 mL conical tube
   **Do not use a 50 mL conical as the pellet will not be compact*
4. Centrifuge for 1 minute at 5,000 rpm to pellet the worms
5. Aspirate most of the M9 without disturbing the worm pellet
6. Repeat 2-5 until all eggs are detached from the plate
7. Add about 15 mL of 20% alkaline hypochlorite solution to the 15 mL conical

Sterile Water	8.25 mL
1M NaOH	3.75 mL
Bleach	3 mL

8. Mix the tube gently by inverting for approximately 4 minutes
   **Do not bleach for longer than this or you will kill the eggs*
9. Centrifuge for 1 minute at 5000 rpm
10. Aspirate most of the 20% alkaline hypochlorite solution without disturbing the worm pellet
11. Add 15 mL of M9 to the tube and mix well
12. Centrifuge for about 1 minute on high
13. Aspirate most of the M9 without disturbing the worm pellet.
14. Repeat M9 wash 2x
15. Add about 7mL of fresh M9 and agitate to re-suspend the pellet
16. Transfer to a 50 mL flask and place a rotator
17. Let the eggs hatch over night with gentle rocking (24-34 hours)
    **Since there is no food the larvae should be halted at the L1 stage*

Day 2. Plating the Synchronous Worms

1. Check the life stage of the worms, the eggs should be hatched and all worms should at the L1 stage
2. Decant all of the liquid into a 15 mL conical
3. Centrifuge for 1 minute at 5,000 rpm and remove all but 200 µL of M9

**Amount to leave varies on how many plates you will be adding the worms to or how many worms you want/plate*

4. Distribute drops of the concentrated worm pellet onto the top of plates to be used for experiment

   **Ensure that there is enough liquid for each plate that needs worms*

***C. elegans* RNAi Feeding Protocol**

Purpose: To make agar plates that will be used for C. elegans gene knockdown via RNAi feeding

Tip: Make fresh plates prior to each experiment

RNAi Plates

1. Make standard NGM agar in a 1000 mL flask

NaCl	1.5 g
Bacto-Peptone	1.25 g
Agar	10 g
diH2O	500 mL

2. Autoclave for 45 minutes on the liquid cycle with a stir bar in the media
3. Set a hot plate or water bath to 55°C
4. Cool while gently stirring on the hot plate for about 45 minutes

   **Liquid must be cool enough before adding the supplements because heat may cause inactivation of Ampicillin*

5. Light a flame and sterilely add the following/500 mL:

Cholesterol (5mg/ml)	0.5 mL
1M $CaCl_2$	0.5 mL
1M $MgSO_4$	0.5 mL
KH_2PO_4, pH 6.0	12.5 mL
1 mM IPTG (1M stock)	500 µL
50 µg/mL Ampicillin (100 mg/mL stock)	250 µL

6. Fill 100 mM plates with 20 mL and 60 mM plates with 10 mL
7. Allow to dry overnight at room temperature prior to seeding with bacteria

RNAi Bacteria

Day 1. Streaking RNAi bacteria

1. Streak bacteria onto a LB agar plate containing 50 µg/mL Ampicillin and incubate at 37°C overnight

Day 2. Inoculating RNAi bacteria

1. Obtain a sterile flask, fill 50% of the flask with LB supplemented with 50 µg/mL Ampicillin
2. BE VERY STERILE- Inoculate a single colony into the LB-Ampicillin solution

3. Place onto a 37°C shaker between 12-16 hours

Day 3. Seeding RNAi plates

1. Concentrate the bacteria 10x and seed the RNAi plates (200 µl for a 100 mM plate).
2. Allow the bacteria to induce on the plates over night at room temperature.

**Store seeded plates at 4°C in a dark fridge (Ampicillin is light sensitive)*

C. elegans **RNA Extraction**

Purpose: To extract pure RNA from C. elegans using the RNeasy Kit from Qiagen

Prior to performing RNA extraction:

- Set a centrifuge to 4°C
- Spray work area and pipettes with ethanol and RNase away
- Use filter pipette tips and ice at all times

1. To prevent OP50 contamination, pick 10-20 worms to a 20 µl drop of M9 in an RNase-free Eppendorf tube
2. Pellet the worms by brief centrifugation
3. In a fume hood, add 250 µL of Trizol
4. Vortex by hand ~30 sec then vortex at 4°C for 20 minutes until the worms have dissolved
5. In a fume hood, add 150 µL of chloroform
6. Briefly vortex
7. Let tube sit at room temp for 3 mins until layers separate
8. Move to Qiagen RNeasy kit, picks up at step 4 of the protocol for animal cells using spin technology outlined below
9. Ensure ethanol has been added to RPE buffer
10. Transfer the clear aqueous layer of the samples to another tube
11. Add 1 volume of 70% and mix well by pipetting
12. Add all of the lysate to an RNeasy spin column, centrifuge for 15 sec at >8000g or >10,000 rpm, and discard flow through
13. Add 700 µL of buffer RW1 to the column, centrifuge for 15 sec at >8000 g or >10,000 rpm, and discard the flow through
14. Add 500 µL of buffer RPE to the column, centrifuge for 15 sec at >8000 g or >10,000 rpm, and discard the flow through
15. Add 500 µL of buffer RPE to the column, centrifuge for 15 sec at >8000 g or >10,000 rpm, and discard the flow through
16. Move the RNeasy spin column to a new collection tube, centrifuge for 1 min at max speed, and discard the collection tube
17. Place the RNeasy spin column in an RNase free centrifuge tube, add 10-20 µL of RNase-free water directly to the column filter for 1 minute, and centrifuge at max speed to elute the RNA
18. (Optional) Add another 10-20 µL RNase-free water to elute more RNA

19. Proceed immediately to quantification with Nanodrop
20. After quantification, proceed immediately to cDNA synthesis or freeze samples at -80°C

cDNA Synthesis

Purpose: To make cDNA from RNA typically used for qRT-PCR

1. Make up Master Mix in a centrifuge tube

**make half of a reaction more than needed*

Master Mix	1 reaction
10x RT buffer	2.0 µL
25x dNTPs	0.8 µL
10x RT random primers	2.0 µL
RT enzyme	1.0 µL
dH_2O	4.2 µL
Total:	10 µL

2. Transfer 10 µL of MM to a PCR tube
3. Add 10 µL of the appropriate RNA + dH_2O to all sample tubes

**RNA concentration should not exceed 2 µg*

4. Vortex, blip spin, and place into a thermocycler with the following conditions:

Temp	Time
25˚C	10 minutes
37˚C	120 minutes
85˚C	5 minutes
4˚C	Until retrieved

qRT-PCR using SYBR Green

Purpose: To perform transcript level analysis in response to various conditions

-Spray bench and pipettes with ethanol

-Use filter tips and ice for each step

-Label all tubes (1 tube/sample/primer set + 1 MM tube/primer set)

-Thaw SYBR green, primers, and cDNA on ice

1. Add appropriate amount of SYBR green, nuclease free water, and primers to each Master Mix (MM) tube:

Recipe	1 Reaction (3 wells)
SYBR green (with ROX)	33.0 µL
F primer (0.9 µM)	0.66 µL
R primer (0.9 µM)	0.66 µL
DNA template (50 ng/ µL)	3.3 µL
Nuclease free water	28.38 µL
Total:	66 µL

2. Vortex and blip spin the MM
3. Transfer 63 µL of the MM centrifuge tubes
   **Use consistent pipetting techniques*
4. Vortex and blip spin the cDNA and add 3.3 µL to the appropriate tube
5. Vortex and blip spin all samples
6. Obtain a qPCR tray and pipette 20 µL into 3 vertical wells while avoiding bubbles
7. Place a cover on the qPCR tray and centrifuge no short for 6 seconds
8. Hold short for 6 seconds
9. Use suggested cycle settings/thermocycler
10. Analyze the data by the correlative method. The delta Ct is normalized by subtracting the Ct of the gene of interest by the Ct of GAPDH. The delta Ct of the normalized sample is then subtracted from the delta Ct of the control.

C. elegans **Chromatin Immunoprecipitation (%IP method)**

Purpose: To determine the binding of a transcription factor to the promoter of a gene of interest

Day 1. Obtain a synchronous population

1. Bleach synchronize worms-- at least 4 150 mM plates/condition

Day 2. Plating worms

1. Place worms onto NGM or RNAi plates

Day 4. Collection and cross-linking

Worms should be at the last larval (L4) stage

1. Wrap worm plates in parafilm and heat shock at 33°C
   **This protocol has been adapted for heat shocking*
2. After HS, collect the worms with M9 into a 15 mL conical
3. centrifuge at 5,000 rpm for 1 minute and remove the supernatant
4. Re-suspend the pellet in 1 mL of M9 and transfer to a spin column to separate worms from bacteria (Thermo Scientific Cat# 69725). Blip spin to allow bacteria to pass through and clean the worms

**Throughout this step- coat the pipette tip in LB to avoid worm loss from sticking to the pipette tips*

5. Re-suspend worm pellet on top of the filter with 1 mL of 1% formaldehyde
6. Transfer to a 15 mL conical. Centrifuge at 5,000 rpm for 1 minute
7. Using a mortor and pestle, gently 'grind' the worm pellet (20 turns) with intentions of slightly disturbing the cuticle
8. Add 5 mL more of 1% formaldehyde
9. Rock on nutator at room temperature for 10 minutes
10. Snap freeze in liquid nitrogen, and allow to thaw by holding under running water
11. Add 5 mL more of 1% formaldehyde and allow to rock for 10 more minutes
12. Quench the reaction with 125 mM Glycine and incubate on the nutator at RT for an additional 15 minutes
13. Pellet the worms by centrifuging at 5,000 rpm for 1 minute, remove the supernatant, and freeze at -80°C

Day 5. Chromatin shearing and complex formation

1. Thaw the worm pellet, re-suspend in 1 mL cold HLB with the addition of a protease inhibitor cocktail, and transfer to 1.5 mL centrifuge tubes
2. Incubate on ice for 10 minutes
3. Sonicate each tube on high for 10 minutes, 30 seconds on, 30 seconds off using a BioRuptor®

   **This step must be optimized for ~500 bp chromatin shearing. Optimization: Purify the DNA with Qiaquick PCR purification kit (Qiagen). Elute with 50 µl water. Run 5 µL of the input DNA on a 1.5% agarose gel to check the extent of shearing. Most of the DNA fragments should be 200-800 bp*
4. Centrifuge the lysate at 12,000 g at 4°C for 10 minutes
5. Transfer the supernatant to a new tube
6. Keep 100 µL of the supernatant as the INPUT

   **Freeze at -20°C*
7. Aliquot 500 µL to 1 tube/antibody

   *This protocol has been adapted for 2 antibodies, a ChIP antibody and an IgG (negative control) antibody
8. Dilute to 1.5 mL with dilution buffer
9. Add 50 µL of pre-washed salmon sperm DNA/protein-A agarose beads to the diluted supernatant and rotate for 30 minutes at 4°C
10. Pellet the beads by centrifuging 400 g for 2 minutes
11. Transfer the supernatant to fresh tube and discard the beads
12. Add 5 µL of the appropriate ChIP antibody and 0.5 µL of IgG to the supernatant and incubate over night at 4°C on a nutator

    **Antibody amount varies and should be optimized*

Day 6: Immunoprecipitation

1. Add 50 µL of salmon sperm DNA/protein-A agarose beads to each sample and incubate at 4°C for 1 hour on a nutator
2. Centrifuge at 400 g for 3 minutes
3. Wash the beads-AB-TF-DNA complex using 1 mL of WB1 for 3 minutes at 4°C on the nutator shaker
4. Centrifuge at 400 g for 2 minutes and discard the supernatant
5. Repeat steps 4 and 5
6. Wash the beads using 1 mL of WB2 for 3 minutes at °C on the nutator shaker
7. Centrifuge at 400 g for 2 minutes and discard the supernatant
8. Repeat steps 7 and 8
9. Wash the beads with 1 mL of WB3 for 5 minutes at 4°C on the nutator shaker
10. Remove the supernatant
11. Wash the beads 1x using 1 mL of 1xTE
12. Add 500 µL of elution buffer to the beads
13. Rotate 15 min at RT and centrifuge for 1 minute at 2,000 g
14. Transfer the supernatant (protein/DNA complex) to a new tube

-ALL OF THE FOLLOWING STEPS WILL INCLUDE THE INPUT AND IP SAMPLES-

15. Add 2 µL of RNase A (0.5mg/mL)
16. Heat at 65°C for 4-5 hours to reverse crosslink the samples
17. Purify DNA using PCR purification kit according via manufacturer's instructions

**When diluting DNA, keep in mind that IP DNA concentration may be low, while input DNA should be very high. Dilute accordingly.*

Other. qRT-PCR Primer design

Design primers to amplify 75-150 bp in the promoter region of the target gene encompassing the predicted transcription factor binding site.

ChIP Working Solutions			
1% Formaldehyde **Make fresh before each use*	**1xTE**	**Dilution Buffer**	**Elution Buffer**
36 mL of PBS	10 mM Tris-Cl, pH 8	50 mM HEPES-KOH, pH 7.5	1% SDS
1 mL of 37% Formaldehyde	1 mM EDTA in water	150 mM NaCl	0.1M $NaHCO_3$
WB1 –Low Salt	**WB2—High Salt**	**HLB**	**WB3**
50 mM HEPES-KOH, pH 7.5	50 mM HEPES-KOH, pH 7.5	50 mM HEPES-KOH, pH 7.5	50 mM Tris-Cl, pH 8
150 mM NaCl	1 M NaCl	150 mM NaCl	0.25 mM LiCl
1 mM EDTA pH 8	1 mM EDTA pH 8	1 mM EDTA	1 mM EDTA
1% Sodium deoxycholate	1% Sodium deoxycholate	0.1% Sodium deoxycholate	0.5% NP-40
1% Triton X-100	1% Triton X-100	1% Triton X-100	0.5% sodium deoxycholate
0.1% SDS	0.1% SDS	0.1% SDS	--
1 mM Protease inhibitor	1 mM Protease inhibitor	1 mM HALT Protease inhibitor	--

***C. elegans* Immunoprecipitation**

Purpose: To pull down a protein of interest and perform WB analysis to probe for binding partners/PTMs

For solutions, refer to ChIP protocol

Day 1. Obtain a synchronous population

1. Bleach Sync worms-- at least 4 150mM plates/condition

Day 2. Plate worms

1. Place worms into liquid culture or onto plates

Day 4. Worm collection

Worms should be at L4 stage

1. Wrap worm plates in parafilm and heat shock at 33°C for given time points
2. After HS, collect worms with M9 and centrifuge at 5,000 rpm for 1 minute and remove supernatant

3. Re-suspend the pellet in 1 mL of M9 and transfer to a spin column (Thermo Scientific Cat# 69725). Blip spin to allow bacteria to pass through and clean the worms

   **Throughout this step- coat the pipette tip in LB to avoid worm loss from sticking to pipette tips*
4. Pellet the worms by centrifuging at 5000 rpm for 1 minute, remove the supernatant, and freeze at -80°C

Day 5. Chromatin shearing/ antibody-protein complex formation

1. Thaw the worm pellet, re-suspend in 1 mL cold HLB supplemented with a protease inhibitor cocktail, phosphate inhibitors, and the deacetylase inhibitors nicotinimide and TSA, and transfer to 1.5mL centrifuge tubes

   **This procotol has been adapted to examine acetylation*
2. Incubate on ice for 10 minutes
3. Sonicate each tube on high for 10 minutes, 30 seconds on, 30 seconds off using a BioRuptor®

   **Sonication step should be optimized*
4. Centrifuge the lysate at 12,000 g at 4°C for 10 minutes
5. Transfer the supernatant to a new tube
6. Keep 100 µL of the supernatant as the INPUT

   **Freeze at -20°C*
7. Dilute to 1.5 mL with dilution buffer
8. Add 50 µL of prewashed salmon sperm DNA/protein-A agarose beads to the diluted supernatant and rotate for 30 minutes at 4°C
9. Pellet the beads by centrifuging 400 g for 2 minutes
10. Transfer the supernatant to fresh tube and discard the beads
11. Add 5 µL of pull-down antibody to the supernatant and incubate over night at 4°C on nutator

    **Antibody amount varies and should be optimized*

Day 6: Immunoprecipitation

1. Add 50 µL of salmon sperm DNA/protein-A agarose beads to each sample and incubate at 4°C for 1 hour on a nutator
2. Centrifuge 400 g for 3 minutes

   **Save the supernatant and save as 'Supernatant' leaving behind the bead-TF-AB complex*
3. Wash the beads-AB-TF-DNA complex using 1 mL of WB1 for 3 minutes at 4°C on the nutator
4. Centrifuge at 400g for 2 minutes and discard the supernatant
5. Repeat steps 3 and 4
6. Wash the beads using 1 mL of WB2 for 3 minutes at 4°C on the nutator
7. Centrifuge at 400g for 2 minutes and discard the supernatant

8. Repeat steps 6 and 7
9. Wash the beads with 1 mL of WB3 for 5 minutes at 4°C on the nutator
10. Remove the supernatant
11. Wash the beads 1 time using 1 mL of 1xTE
12. Add 25 µL of 1x Laemmli buffer to each sample and boil for 10 minutes and begin immunoblot protocol

C. elegans **Protein Extraction**

Purpose: To obtain protein from C. elegans for Western blotting

Day 1. Obtain a synchronous population

1. Bleach synchronize worms

Day 2. Plate worms

1. Place worms onto NGM or RNAi plates

Day 4. Worm collection

**Worms should be at L4 stage*

1. Wrap worm plates in parafilm and heat shock at 33°C for given time points
2. After HS, collect worms with RT M9 and centrifuge at 5,000 rpm for 1 minute and remove supernatant
3. Re-suspend the pellet in 1 mL of M9 and transfer to a spin column (Thermo Scientific Cat# 69725). Blip spin to allow bacteria to pass through and clean the worms
   **Throughout this step- coat the pipette tip in LB to avoid worm loss from sticking to the pipette tip*
4. Pellet the worms by centrifuging at 5000 rpm for 1 minute, remove the supernatant, and freeze at -80°C

Day 5. Protein Extraction

1. Allow the frozen worm pellet to thaw, re-suspend the pellet in 250µl Buffer C (20mM HEPES pH 7.9, 25% (v/v) glycerol, 0.42M NaCl, 1.5 mM MgCl2, 0.2 mM EDT, and 0.5mM DTT) + Protease inhibitors
2. Sonicate for 15 minutes with 30 second pulsing ON/OFF on high using a BioRuptor®
   **Change water every 5 minutes to keep it ice cold*
3. Centrifuge at 4°C for 10 minutes at 13,000 g
4. Transfer supernatant to new tubes and quantify via Bradford Assay prior to beginning immunoblot protocol

Bradford Assay

Purpose: To determine protein concentrations to use for Western blotting

1. Make up the 1X Bradford reagent by diluting the 5X stock with dIH_2O (1 mL reagent + 4 mL H_2O)
2. Add 1 µL of your protein sample to the appropriate wells of a clear 96 well plate
3. Add the appropriate amount of BSA standard (in 0.5 µL increments) in order to achieve the standard curve
4. For each well, add 200 µL of 1X Bradford reagent using the automated pipette

Read on the plate reader at 595 nm:	1	2	3	4	5	6	7	8	9	10	11	12
A	0 µg BSA	1 µg BSA	2 µg BSA	3 µg BSA	4 µg BSA	5 µg BSA	6 µg BSA	7 µg BSA	8 µg BSA	**Standard**		
B	0 µg BSA	1 µg BSA	2 µg BSA	3 µg BSA	4 µg BSA	5 µg BSA	6 µg BSA	7 µg BSA	8 µg BSA			
C	1	2	3	4	5	6						
D	1	2	3	4	5	6	**Samples 1-6**					
E	1	2	3	4	5	6						

**each experimental sample should be added in triplicate*

Western Blot

Purpose: To identify specific proteins

Day 1. Making gels, transferring, and primary antibody staining

1. Cast the separating gel by pipetting into the Biorad gel apparatus using a P1000 and quickly overlay with 1 mL of hydrated Butanol *(Leave ¼ space for the stacking gel)*
2. Let sit for 30 min
3. After polymerization, remove the Butanol overlay via gravity and rinse with dIH_2O
4. Make up the stacking gel and pipet over the separating gel
5. Insert the comb and let sit to polymerize for at least 30 min

Separating Gel							Stacking Gel	
Component	**6%**	**8%**	**10%**	**12%**	**15%**		**Component**	**4%**
15 M Tris (pH 88)	25 mL	25 mL	25 mL	25 mL	25 mL		1 M Tris (pH 68)	125 mL
40% Acrylamide	15 mL	20 mL	25 mL	30 mL	38 mL		40% Acrylamide	125 mL
10% SDS	100 µL	100 µL	100 µL	100 µL	100 µL		10% SDS	100 µL
10% APS	100 µL	100 µL	100 µL	100 µL	100 µL		10% APS*	100 µL
TEMED	4 µL	4 µL	4 µL	4 µL	4 µL		TEMED*	10 µL
dH_2O	58 mL	53 mL	48 mL	43 mL	35 mL		dH_2O	73 mL
kDa Range:	**60-200**		**16-70**		**12-45**			

6. Place the gel in the electrophoresis chamber, cover with running buffer, remove the comb, and rinse the wells with buffer to remove unpolymerized acrylamide
7. Add Laemmli buffer to aliquoted samples and to empty wells
8. Incubate the protein samples at 95°C for 5 minutes
9. Mix by vortexing, blip spin, and load onto the gel
10. Run the gel at 180V until the dye front has emerged from the gel (about 1 hour)
    **If smaller kDa proteins are being analyzed, the gel may be stopped before the dye front has run off*
11. Remove the stacking layer from the gel
12. Activate a PVDF membrane in 100% methanol or wet a nitrocellulose membrane in a tray filled with dH_2O
13. Fill a large tray with transfer buffer and assemble the blot as shown below:
    **Place the gel so that the marker is on the right. Use 1 piece of thick blotting paper or 2 pieces of thin blotting paper*

Blotting paper
Membrane
Gel
Blotting paper

14. Flip the blot assembly over and place in a semi-dry blotter membrane-side down
15. Set to 10 V and blot for 30 minutes

*Add more time to transfer large kDa proteins or for multiple gels on the blotter

16. Stain with Ponceau S in order to visualize protein bands
17. Rinse the blot with dIH_2O to remove background staining
18. Scan or photograph the blot to confirm equal loading in each lane

**The Ponceau rinses off of nitrocellulose membranes with TBST, for PVDF membranes, add NaOH dropwise into TBST until staining dissipates*

19. Block in 5% non-fat dry milk or BSA, depending on antibody specifications, diluted in TBST at RT for 30 minutes-1 hour
20. Rinse briefly in TBST and proceed to immunostaining
21. Incubate the blot at 4°C ON with primary antibody diluted in 1% milk or BSA

Day 2. Secondary antibody and developing

1. Wash the blot with TBST for 15 min x 5
2. Incubate the blot with secondary antibody diluted in 5% milk in TBST for 2 hours at RT
3. Wash the blot with TBST for 5 min x 5
4. Prepare the ECL reagent according to manufacturer's instructions

**Note: Wash steps and antibody dilutions may vary depending on ECL reagent used. Refer to manufacture's guide for proper handling.*

5. Remove the blot to a transparency sheet in a cassette and quickly pipette 1 mL ECL per blot
6. Incubate for 5 minutes at RT
7. Sandwich the blot between a second transparency and expose to film

Western Blot Working Solutions		
1X SDS Running Buffer	**1X Transfer buffer**	**1X TBST (0.05% Tween)**
100 mL 10X tris/glycine buffer	100 mL 10X tris/glycine buffer	100 mL 10X TBS
895 mL dIH20	100 mL methanol	890 mL dIH2O
5 mL 20% SDS	800 mL dIH2O	5 mL 10% Tween-20

C. elegans RNAi Lifespan Assay Protocol

Purpose: To determine the effect of various conditions on the lifespan of the worm

Day 1. Synchronizing Worms

1. Bleach synchronize worms

Day 2. Plating Worms

1. Plate synchronized worms onto appropriate plates

Day 4. Transferring Worms to Fresh Plates

1. Pick 150 worms/condition to 3 100 mM NGM or RNAi plates for a total of 150 worms/condition

**3 plates are used to make counting the worms easier and to avoid progeny contamination by picking*

Days 5-9. Maintaining a Synchronous Population

1. Pick worms to new plates daily during the reproductive period in order to maintain the same parental generation of worms

Days 10-End. Scoring Worms

1. After the reproductive period, draw 4 separate quadrants on the back of the plate to assist in counting worms. Dead worms are not moving, and remain still even when gently poked with platinum wire. If worms intestines have fallen out, or some worms are lost in the agar, these can be scored as censored. Count live worms every other day until no worms are left

Thermotolerance Assay

Purpose: To determine if various conditions promote survival to a lethal stress

Day 1. Synchronizing Worms

1. Bleach synchronize worms

Day 2. Plating Worms

1. Plate synchronized worms onto appropriate plates

Days 4-5. Transferring Worms to Fresh Plates

1. Each day, transfer 150 worms/condition to 3 100 mM NGM or RNAi plates for a total of 150 worms/condition

Day 6. Thermotolerance Assay

1. [PM] Transfer 100 worms/condition to 1 NGM or RNAi plate
2. Wrap the plate in parafilm and submerge into a water bath with a temperature and time previously determined to kill ~50% of the control population

**This protocol has been adapted for a lethal heat stress*

3. Return the plate to growth temperature and allow the worms to recover over night

Day 7. Scoring Dead/Alive Worms

1. Draw 4 separate quadrants on the back of the plate to assist in counting worms. Dead worms are not moving, and remain still even when gently poked with platinum wire

Thrashing Assay

Purpose: To determine if various conditions affect organismal fitness after a lethal stress

-Perform thrashing assay in parallel to thermotolerance assay

Day 1. Synchronizing Worms

1. Bleach synchronize worms

Day 2. Plating Worms

1. Plate synchronized worms onto appropriate plates

Days 4-5. Transferring Worms to Fresh Plates

1. Each day, transfer 100 worms/condition to 100 mM NGM or RNAi plates

Day 6. Heat Shocking Worms

1. [PM] Transfer 50 worms/condition to 1 NGM or RNAi plate
2. Wrap the plate in parafilm and submerge into a water bath with a temperature and time previously determined to kill ~50% of the control population

**This protocol has been adapted for a lethal heat stress*

3. Return the plate to growth temperature and allow the worms to recover over night

Day 7. Thrashing Assay

1. Pick dead worms, as determined by lack of movement in response to poking with a platinum wire, off of the plate
2. Pick 1 live worm to a drop of M9 on a glass slide
3. Allow ~10 seconds to adjust to the new environment
4. Count thrashes, or a complete worm bend, for 30 seconds for each worm

Polyglutamine Aggregate Assay

Purpose: To determine if various conditions prevent polyglutamine aggregate formation in a Huntington's disease model

Day 1. Synchronizing Worms

1. Bleach synchronize worms

Day 2. Plating Worms

1. Plate synchronized worms onto appropriate plates

Days 4-5. Transferring Worms to Fresh Plates

1. Each day, transfer 50 worms/condition to 100 mM NGM or RNAi plates

Day 6. Heat Shocking Worms

1. [PM] Transfer 50 worms/condition to 1 NGM or RNAi plate
2. Wrap plates to be heat shocked in parafilm and submerge into a water bath with a temperature and time previously determined to induce the heat shock response without killing any worms
3. Return the plate to growth temperature and allow the worms to recover over night

Day 7. Imaging Worms

1. Obtain a clean NGM plate (no bacteria)
2. Place a drop of 1 mM Levamisole onto the NGM plate and allow to dissolve into the agar
3. Pick 5 worms to the Levamisole spot. After 30 seconds, the worms should be paralyzed
4. Place the worms side by side so that the anterior of each worm is aligned
5. Photograph on a low GFP setting in order to visualize punctuate aggregates

Polyglutamine Toxicity Assay

Purpose: To determine if various conditions affect the toxicity associated with polyglutamine aggregates in a C. elegans Huntington's disease model

-Perform polyglutamine toxicity assay in parallel to polyglutamine aggregate assay

Day 1. Synchronizing Worms

1. Bleach synchronize worms

Day 2. Plating Worms

1. Plate synchronized worms onto appropriate plates

Day 4-5. Transferring Worms to Fresh Plates

1. Each day, transfer 50 worms/condition to 100 mM NGM or RNAi plates

Day 6. Heat Shocking Worms

1. [PM] Transfer 50 worms/condition to 1 NGM or RNAi plate
2. Wrap plates to be heat shocked in parafilm and submerge into a water bath with a temperature and time previously determined to induce the heat shock response without killing any worms
3. Return the plate to growth temperature and allow the worms to recover over night

Day 7. Imaging Worms

1. Obtain a NGM plate seeded with bacteria
2. Place an Eppendorf lid labeling sticker on the bottom of the plate
3. Pick 10 worms to the middle of the area outlined by the sticker
4. Allow the worms 3 minutes to move outside of the circle. Worms that do not move are considered paralyzed, whereas worms that move are not paralyzed

APPENDIX H:COPYRIGHT PERMISSION

ELSEVIER LICENSE
TERMS AND CONDITIONS

License Number	4054450308547
License date	Feb 22, 2017
Licensed Content Publisher	Elsevier
Licensed Content Publication	Mechanisms of Ageing and Development
Licensed Content Title	Fluorodeoxyuridine enhances the heat shock response and decreases polyglutamine aggregation in an HSF-1-dependent manner in Caenorhabditis elegans
Licensed Content Author	Jessica Brunquell,Philip Bowers,Sandy D. Westerheide
Licensed Content Date	November–December 2014
Licensed Content Volume	141
Licensed Content Issue	n/a
Licensed Content Pages	4
Start Page	1
End Page	4
Type of Use	reuse in a thesis/dissertation
Portion	full article
Format	both print and electronic
Are you the author of this Elsevier article?	Yes
Will you be translating?	No
Order reference number	
Title of your thesis/dissertation	Uncovering transcriptional activators and targets of HSF-1 in Caenorhabditis elegans
Expected completion date	May 2017
Estimated size (number of pages)	340

BIOMED RESEARCH INTERNATIONAL
COPYRIGHT PERMISSION